

AGARD-CP-244

ADVISORY GROUP FOR AEROSPACE RESEARCH & DEVELOPMENT

7 RUE ANCELLE 92200 NEUILLY SUR SEINE FRANCE

AGARD CONFERENCE PROCEEDINGS No. 244

Aspects of Electromagnetic Wave Scattering in Radio Communications

Edited by A.N. Ince



NORTH ATLANTIC TREATY ORGANIZATION



ON BACK COVER

78 10

Approved for public release;
Distribution Unlimited

AGARD-CP-244

NORTH ATLANTIC TREATY ORGANIZATION ADVISORY GROUP FOR AEROSPACE RESEARCH AND DEVELOPMENT (ORGANISATION DU TRAITE DE L'ATLANTIQUE NORD)

AGARD Conference Proceedings, No. 244

ASPECTS OF ELECTROMAGNETIC WAVE

SCATTERING IN RADIO COMMUNICATIONS.

Edited by

SHAPE Technical Centre

The Hague

Netherlands

700 - 2h

Papers and discussions presented at the Electromagnetic Wave Propagation Panel Symposium held in Cambridge, Massachusetts, USA, 3-7 October, 1977.

400 043

LB

THE MISSION OF AGARD

The mission of AGARD is to bring together the leading personalities of the NATO nations in the fields of science and technology relating to aerospace for the following purposes:

- Exchanging of scientific and technical information;
- Continuously stimulating advances in the aerospace sciences relevant to strengthening the common defence posture;
- Improving the co-operation among member nations in aerospace research and development;
- Providing scientific and technical advice and assistance to the North Atlantic Military Committee in the field of aerospace research and development;
- Rendering scientific and technical assistance, as requested, to other NATO bodies and to member nations in connection with research and development problems in the aerospace field;
- Providing assistance to member nations for the purpose of increasing their scientific and technical potential;
- Recommending effective ways for the member nations to use their research and development capabilities for the common benefit of the NATO community.

The highest authority within AGARD is the National Delegates Board consisting of officially appointed senior representatives from each member nation. The mission of AGARD is carried out through the Panels which are composed of experts appointed by the National Delegates, the Consultant and Exchange Programme and the Aerospace Applications Studies Programme. The results of AGARD work are reported to the member nations and the NATO Authorities through the AGARD series of publications of which this is one.

Participation in AGARD activities is by invitation only and is normally limited to citizens of the NATO nations.

The content of this publication has been reproduced directly from material supplied by AGARD or the authors.

Published September 1978

Copyright © AGARD 1978 All Rights Reserved

ISBN 92-835-0219-1



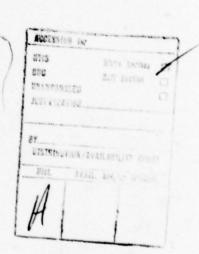
Printed by Technical Editing and Reproduction Ltd Harford House, 7-9 Charlotte St, London, W1P 1HD

THEME

The scattering of electromagnetic waves is of importance in many communication systems and has been intensively studied in the last quarter of a century. Scattering phenomena can be used to advantage to communicate over the horizon, or they may act adversely as in the case of transmission to a terminal in a jungle or heavily urbanised environment. Examples of the former are the VHF (ionoscatter and meteor-burst) and UHF (troposcatter) links which make use of the scatter from inhomogeneities and discontinuities in the ionosphere and troposphere respectively. Examples of adverse effects occur in relatively short range UHF communications to mobile units surrounded by trees or buildings.

In all cases the received signals have a number of common features, namely they are time-dispersive due to multipath and time-varying due to phase, polarisation or attenuation variation. These characteristics severely reduce the performance obtained unless steps are taken to mitigate these effects. This can be done by a suitable choice of modems and by the use of various forms of diversity such as space frequency, time and polarisation. In certain cases, such as in meteor-burst communication, an adaptive rate of transmission can greatly enhance the performance of a system. Most of the systems using a scatter mode of propagation can be made light and transportable. Furthermore, they are relatively inexpensive, easy to operate and are capable of working at almost any latitude. They therefore form a useful alternative to conventional HF and satellite links, especially where modest information rates are concerned, i.e. in so-called "thin-line" communications.

A broad review of the state of the art in scatter communication is considered to be both appropriate and timely. The symposium will therefore be concerned with the theory of scattering and reflection in the troposhere, the ionosphere, from meteor trails, and also scattering from ground environmental hazards such as hills, trees and buildings. Included in the propagation aspect will be the prediction of long and short term signal characteristics and modelling of radio channels using scatter mode of propagation. Consideration will also be given to transmission and signal processing techniques for effective communications over such channels. The symposium is thus designed for geophysicists, communication system planners and designers, and also for the users of such systems.



PROGRAMME COMMITTEE AND MEETING OFFICIALS

PROGRAMME CHAIRMEN

Dr J.H.Blythe

GEC-Marconi Electronics Lab

Great Baddow

Chelmsford CM2 8HM

UK

Dr A.N.Ince

Chief, Communications Division

SHAPE Technical Centre

P.O. Box 174, The Hague

Netherlands

MEMBERS

Dr P.A.Bello

CNR, Inc.

220 Reservoir Street

Needham Heights

Mass. 02194

USA

Dr J.A.Lane

SRC Radio and Space Research Station

Slough

Bucks UK

Dr D.T.Gjessing

Remote Sensing Technology Programme

P.O. Box 25, N-2007 Kjeller

Norway

Dr K. Toman

RADC/ET Hanscom AFB

Mass. 01731

USA

PANEL OFFICERS

CHAIRMAN

DEPUTY CHAIRMAN

Capt de Frégate P.Halley

CNET

Dr H.Albrecht

France

Germany

EXECUTIVE

Cdr D.G.Carruthers **US Navy** AGARD

HOST COORDINATOR

Mr L.W.Roberts Department of Transportation Kendall Square Cambridge, Mass. USA

SESSION CHAIRMEN

SESSION I — SCATTER PROPAGATION OF ELECTROMAGNETIC WAVES

Dr J.H.Blythe

GEC-Marconi Electronics Laboratory Great Baddow, Chelmsford CM2 8HM

UK

SESSION II - TECHNIQUES FOR PROPAGATION MEASUREMENTS AND CHANNEL

SIMULATIONS

Dr P.A.Bello

CNR, Inc.

220 Reservoir Street

Needham Heights Mass. 02194

USA

SESSION III - PROPAGATION HAZARDS FOR COMMUNICATIONS

Dr K. Toman

RADC/ET Hanscom AFB

Mass. 01731

USA

SESSION IV - SYSTEM DESIGNS AND APPLICATIONS

Dr A.N.Ince

SHAPE Technical Centre

P.O.Box 174, The Hague

Netherlands

SESSION V - SIGNAL PROCESSING FOR SCATTER COMMUNICATIONS

Dr D.T.Gjessing

Remote Sensing Technology Programme

P.O. Box 25, N-2007 Kjeller

Norway

SESSION VI - GENERAL DISCUSSION

Dr A.N.Ince

SHAPE Technical Centre

P.O. Box 174, The Hague

Netherlands

EDITOR'S COMMENTS

With a few exceptions the symposium papers have been printed directly from copy furnished by the authors. The promptness of authors who submitted preprints of their papers is gratefully acknowledged. Special thanks go also to all those symposium participants who submitted their questions and comments in writing. The symposium proceedings were very ably recorded by the personnel of the Transportation System Centre, Cambridge, Massachusetts, of the US Department of Transportation. The transcriptions of the tapes and typing of the various papers required a lot of patience and this was demonstrated by my secretaries Miss Lynette King and Miss Lindsay Abraham. The editor apologizes for any changes in meaning or style that may have been made in preparing a printable version of the discussions.

Grateful acknowledgement is made to my colleague Mr I.M.Vogt for his assistance in the preparation of these proceedings.

A.N.INCE

CONTENTS

	Page
THEME	ш
PROGRAMME COMMITTEE AND MEETING OFFICIALS	iv
SESSION CHAIRMEN	
EDITOR'S COMMENTS	vi
REVIEW OF EM SCATTERING IN RADIO COMMUNICATIONS by A.N.Ince	s
	Reference
SESSION I – SCATTER PROPAGATION OF ELECTROMAGNETIC WAVES	
SCATTERING MECHANISMS AND CHANNEL CHARACTERIZATION IN RELATION TO BROAD BAND RADIO COMMUNICATION SYSTEMS by D.T.Gjessing	100 m
ELECTROMAGNETIC WAVE PROPAGATION IN AN INHOMOGENEOUS MEDIUM — A LABORATORY STUDY	
by W.G.Burrows	2
TROPOSPHERIC REFLECTION OF DIFFERENTLY POLARIZED TRANSIENT SIGNALS by X.J.Langenberg	3
TROPOSCATTER APERTURE – MEDIUM COUPLING LOSS by L. Lewin	4
STATISTICS OF TROPOSCATTER CHANNELS WITH RESPECT TO THE APPLICATIONS OF ADAPTIVE EQUALIZING TECHNIQUES by F.Schmitt	5
HF SCATTER FROM OVERDENSE METEOR TRAILS by G.H.Millman	6
TIME AND FREQUENCY SPREAD IN METEOR BURST PROPAGATION PATHS by M.D.Grossi and A.Javed	7
THE EVOLUTION OF SCATTERING EQUATORIAL F-REGION IRREGULARITIES AND RESULTANT EFFECTS ON TRANS-IONOSPHERIC RADIO WAVES by H.E.Whitney, J.Aarons, J.Buchau and E.J.Weber	8
PULSE DELAY AND PULSE DISTORTION BY RANDOM SCATTERING IN THE IONOSPHERE by K.C.Yeh and C.H.Liu	9
THE ATMOSPHERIC SCATTER CHANNEL FOR OPTICAL COMMUNICATIONS OVER-THE-HORIZON by G.C.Mooradian, M.Geller, R.A.Krautwald and D.Stephens	10
SESSION II – TECHNIQUES FOR PROPAGATION MEASUREMENTS AND CHANNEL SIMULATIONS	
RELATIONSHIP BETWEEN MODEM DEVELOPMENT AND CHANNEL CHARACTERIZATION by P.A.Bello	11
WIDEBAND LINE-OF-SIGHT CHANNEL SIMULATION SYSTEM	12

	Referen
TECHNIQUE DE SONDAGE ELECTROMAGNETIQUE PAR ECHANTILLONAGE SPATIO-FREQUENCIEL DES SIGNAUX DE RECEPTION, APPLICATION A	
L'ETUDE DES INHOMOGENEITES DU PLASMA IONOSPHERIQUE par C.Goutelard, J.Caratori et A.Joisel	13
APPLICATION DE LA TECHNIQUE BACKSCATTER AUX PREVISIONS DE TRANSMISSION IONOSPHERIQUES A TRES COURT TERME	
par C.Goutelard, J.Caratori et J.Coatanhay	14
SESSION III – PROPAGATION HAZARDS FOR COMMUNICATION	ONS
CALCULATION OF THE SCATTERING CROSS-SECTION OF PERFECTLY CONDUCTED DIELECTRIC BODIES BY NUMERICAL PERTURBATIONAL METHODS by KD.Becker	ING 15
A SCATTER MODEL FOR LEAFY VEGETATION by A.K.Fung and F.T.Ulaby	16
VHF PROPAGATION PREDICTION WITH PATH PROFILE METHODS by B.K.Lee	17
MULTIPATH CHARACTERISTICS AT UHF IN RURAL IRREGULAR TERRAIN by L. Ladell	18
INTERCEPTION OF SIGNALS TRANSMITTED VIA METEOR TRAILS by A.N.Ince	19
TROPOSPHERIC STRATIFICATION AND ANOMALOUS PROPAGATION by H.T.Dougherty and B.A.Hart	20
SESSION IV – SYSTEM DESIGN AND APPLICATIONS	
A REVIEW OF SCATTER COMMUNICATIONS by A.N.Ince, I.M.Vogt and H.P.Williams	21
DESIGN CONSIDERATIONS FOR DIGITAL TROPOSCATTER COMMUNICATIONS SYSTEMS	
by J.L.Osterholz	22
LEVEL CONTROL IN TROPOSPHERIC SCATTER SYSTEMS by B.S.Skingley	23
THE PERFORMANCE OF METEOR-BURST COMMUNICATIONS AT DIFFERENT FREQUENCIES	
by D.W.Brown and H.P.Williams	24
COMMUNICATIONS VIA METEOR TRAILS by F.J.Sites	25
PROPAGATION MEASUREMENTS ON THE ACE-HIGH TROPOSCATTER SYSTEM by A.N.Ince and I.M.Vogt	26
SESSION V - SIGNAL PROCESSING FOR SCATTER COMMUNICA	TIONS
A REVIEW OF SIGNAL PROCESSING FOR SCATTER COMMUNICATIONS by P.A.Bello	27
MAXIMUM USABLE BANDWIDTH AND FREQUENCY DIVERSITY IN TROPOSCATTER COMMUNICATION	
by R.Valentin	28

	Reference
TROPOSCATTER ANGLE DIVERSITY IN THEORY AND PRACTICE by M.W.Gough, G.C.Rider and R.Larsen	29
by M. W. Google, C.C. Ricer and R. Larsen	•
AN EXPERIMENTAL PROGRAM LEADING TO DEVELOPMENT OF A TACTICAL DIGITAL TROPOSCATTER SYSTEM	
by A.Sherwood, S.Wenglin and J.Wick	30
PROPAGATION MEASUREMENTS ON A TRANSALPINE OVER-THE-HORIZON PATH	
by J.Osterholz, P.T.Nielson, E.Pusone and I.M.Vogt	31
UTILISATION DES CODES PSEUDO ORTHOGONAUX DANS LES CANAUX MULTITRAJETS NON STATIONAIRES	
par F.Chavand, M.Gindre et C.Goutelard	32
AN EXPERIMENTAL MODEM FOR TROPOSCATTER COMMUNICATIONS USING MAXIMUM LIKELIHOOD SEQUENCE ESTIMATION AND ERROR-CORRECTION CODING	
by D.Chase and P.A.Bellow	33
AN EXPERIMENTAL MODEM FOR HF CHANNELS USING SPREAD-SPECTRUM AND BLOCK ENCODING	
by R.E.Schemel and A.N.Ince	34
DISCUSSIONS AND COMMENTS	D

REVIEW OF ELECTROMAGNETIC-WAVE SCATTERING IN RADIO COMMUNICATIONS

by

A. N. Ince
SHAPE Technical Centre,
The Hague,
Netherlands.

1. Introduction

In October 1977 at Cambridge, Massachusetts, USA, The Electromagnetic Wave Propagation Panel of AGARD sponsored the conference the proceedings of which are the subject of this volume. The purpose of the conference was to review the state of the art in scatter communications. Thirty four papers were presented and discussed in five sessions each of which started with a review by a recognized expert in the field.

2. Survey

Investigations into the scattering of electromagnetic waves from irregularities and inhomogenities, both natural and man-made, tend to fall into three categories. These are the study and elucidation of geophysical phenomena, the alleviation of interference between radio systems and thirdly the gathering of information for the design of reliable and economic communication systems. These fields are, of course, all inter-related: indeed, in practically all the forms of scatter communication discussed in the conference, it was the unexpected discovery of scatter propagated signals which led to the recognition and subsequent investigation of the geophysical phenomena. Conversely, studies of the phenomena as such, have greatly helped to provide quantitative information for communications purposes. Papers in Session I addressed the problems which fall into the first category and also reviewed the various scatter mechanism, while in Session III the problems of the second category were discussed; the other sessions concentrated on areas related to the techniques and propagation data necessary for the planning and design of communications systems. The systems which, in one way or another, were the subject of the papers presented were the following:

- 1. HF radio [1.8; 1.9; 2.3; 2.4; 5.8]*
- 2. Ionoscatter [4.1]
- 3. Meteor-burst [1.6; 1.7; 3.5; 4.1; 4.4; 4.5]
- 4. Field Aligned scatter [4.2]
- 5. Troposcatter [1.1; 1.3; 1.4; 1.5; 4.1; 4.2; 4.3; 4.6; 5.2; 5.3; 5.4; 5.5; 5.7]
- 6. Chaff and Needles [4.1]
- Optical scatterings by aerosols [1.10; 4.1]

Fig. 1 provides a convenient overall insight into these systems as far as propagation characteristics are concerned. As is to be expected, scatter systems only come into question at higher radio frequencies where the wavelengths are small enough to be comparable to the size of irregularities in the propagation medium. Thus the lowest frequencies involved in scatter modes of propagation are those at the upper end of the HF band. Fig. 2 shows noise levels over the same frequency range as used in Fig. 1. The need for low noise level locations is clearly highlighted by Fig. 2.

Taken together Figs. 1 and 2 provide a good insight into the possibilities offered by the various scatter systems. However, the channel capacities are not necessarily approximately equal to the inverse of the time spread. This is because the system might be intermittent in operation, as is the case in meteor scatter, or because the system may be using adaptive modems.

As will be seen from above, the systems which were the subject of most of the papers presented were troposcatter and meteor-burst, these being the systems which meet the user requirements most economically and conveniently in terms of range and capacity. The meteor-burst system has, also, the added advantages of providing considerable resistance to interception and jamming and of allowing broadcasting, both of which make it attractive to a certain category of users. Although troposcatter systems have been in use for almost twenty years now the requirement for digitalization has recently created a new impetus for extensive research and development activities both in propagation and in the field of adaptive modem design. The numerous papers presented in meteor-burst is an indication of a revival of interet in this very interesting system which has been neglected in the past and which now appears to be coming into use, a development which may have been prompted

[•] Figures in [] refer to paper numbers in these proceedings.

partly by the progress made in storage and processing techniques.

3. Conclusions

The highlights of the Conference may be summarized as follows:

- 1. Of the six distinct radiowave scatter systems considered in this review, four rely on quite small perturbations on the ambient conditions. The other two, namely meteor burst and chaff, depend on scattering from greatly augmented ionisation and from highly conducting strips respectively. However, from a systems point of view these distinctions are academic. A more practical grouping is into systems involving man-made scatter conditions, i.e. field aligned scatter and chaff or naturally occurring scatter phenomena.
- 2. Both the man-made scattering phenomena would seem to have their major applications in military systems, where they would have the advantage of being capable of being switched on at will in the case of field aligned scatter the system can also be switched off at will. The very special nature of both of these artificially generated scatter systems makes it difficult to forecast the applications to which they may be put in the future. It is worth noting that field aligned scatter also occurs naturally in the auroral zone and communication has often been achieved using frequencies in the VHF bard, but the results achieved so far are too variable to be of practical use.
- 3. In the fairly extensive review of troposcatter systems made in this Conference it is clear that performance predictions still leave something to be desired. Estimates which can be 10 dB or more out are not a cheerful prospect for the designer [Paper 4.1]. It appears that the predictions of the path-loss statistics may be improved by taking into account more details of the meteorological conditions [Papers 1.1 and 4.1]. There is also the need for collecting data on climatic effects for regions where the data does not exist.
- 4. Less obvious, but surely with a certain future in special applications, is the use of meteor burst communications. Regardless of its intermittent nature it allows the transmission of instantaneous data rates of up to hundreds of kilobit/s. Here again there is a need for a more world-wide knowledge of the scatter mechanism in this case a knowledge of the distribution of the radiants of meteors.
- 5. A factor contributing to the large differences between different prediction methods in estimating the performance of a troposcatter link and also to the difference between predicted and measured result, is the so-called aperture-to-medium coupling loss. There were lengthy discussions in the Conference on this topic and these were indicative of the uncertainties that exist in the definition, measurement and scatter mechanisms involved in this loss factor [Paper 1.4]. It is quite clear that the aperture-to-medium coupling loss of an antenna is dependent on the gains of the two antennas used in transmission and also on the separation of the two antennas. On the latter issue it was pointed out, that widely differing results were given in the literature although for the ranges of most practical interest (200-300 kms) all predictions converged to within a few decibels providing that the free-space gain of the antennas are less than 40 to 50 dB. It should be pointed out here that even though the coupling loss increases with antenna gain, the increase in antenna size might still be desirable because multipath delay spread decreases with increasing antenna size.
- 6. A physical laboratory modelling technique discussed in Paper 1.2 seems to lend itself to studies of radio wave propagation in the troposphere. By creating an inhomogeneous gaseous medium (or liquid suspension as suggested in Paper 1.4) through which is propagated a coherent light beam, investigations can be carried out conveniently and economically into the problems outlined in paras (3) and (5) above and into the determination of the significance of the common volume and beambending in relation to the scatter loss and multipath delay spread. Even though it would be impractical to model exactly the atmospheric inhomogeneities in the scattering fluid, it is believed that useful information could well be derived from such a modelling technique.
- 7. Digitalization of tropospheric scatter links requires the use of adaptive modems and bandwidths larger than those needed by equivalent analog systems. Several adaptive modem techniques were described and discussed in the Conference [Papers 4.1; 5.1; 5.4; 5.5; 5.7]. Prototype adaptive modems exist today which allow the transmission of up to about 10 Mega bits/s over typical troposcatter paths. It is evident that more R & D work needs to be undertaken to develop modems which are capable of coping with the maximum expected delay spreads on operational links (including aircraft echoes) and of providing the maximum possible economy in frequency usage. Further studies using multi-level coding and angle diversity are indicated. Power control techniques will also help to reduce interference thus permitting more efficient use to be made of the frequency spectrum [Paper 4.3].
- 8. The use of adaptive equalizer techniques for HF paths seems problematic and uncertain. It appears [Paper 5.8] that the use of the spread-spectrum technique may be a better approach for coping with the multipath problem at HF. This would also have the advantage that the effect of interference and noise of an impulsive nature would be reduced.

- 9. For optimum modem design and comparative evaluation of implemented modems use should be made of path simulators. Different types (software, hardware, synthetic and playback channel simulators) of simulators were described and discussed in Papers 2.1 and 2.2.
- 10. In planning and implementing communication systems the transmission standards to be adopted should be specified taking into account the characteristics of the terminal devices as well as the application for which they are used, the requirements for monitoring and measuring the implemented system, and the network (dedicated and switched) into which it is to be incorporated [Papers 4.1 and 4.2]. It should be borne in mind also that, even though one may wish to specify not only the average channel behaviour but also the statistical distribution of the impairement, the parameters available to the equipment and system designer may not permit the noise/error patterns to be controlled completely, particularly when an existing system is being converted from analog to digital working.

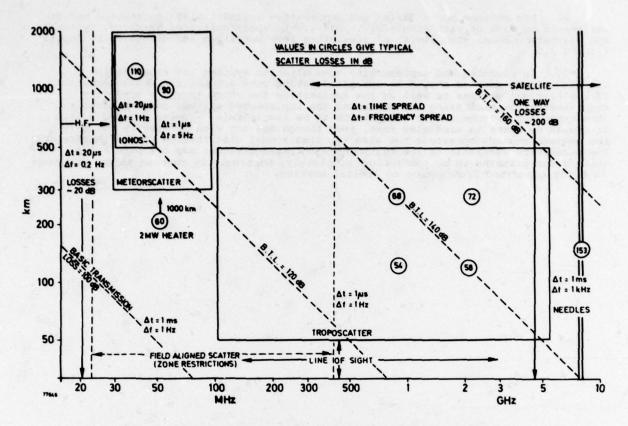


Fig. 1: Typical frequencies and ranges of scatter systems

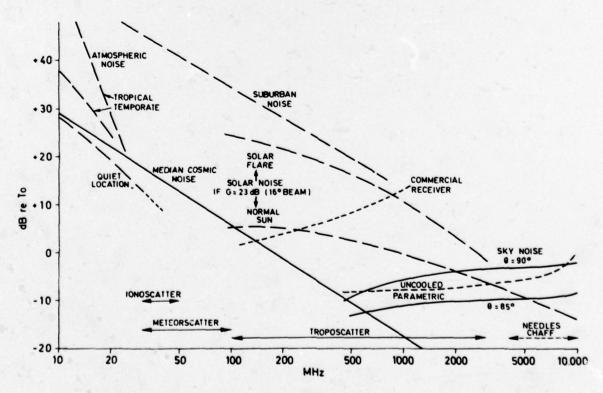


Fig. 2: Noise levels at frequencies involved in scatter systems

SCATTERING MECHANISMS AND CHANNEL CHARACTERIZATION IN RELATION TO BROADBAND RADIO COMMUNICATION SYSTEMS

Dag T. Gjessing

Royal Norwegian Council for Scientific and Industrial Research Remote Sensing Technology Programme P. O. Box 25 - N-2007 Kjeller, Norway

SUMMARY

Many modern communication systems such as systems making use of the spread spectrum mode, of large synchronous time division multiplexing, of package switching in data transmission networks involving computers, are very sensitive to certain properties of the propagation medium (bandwidth, delay spectrum width, etc). With these communication systems in mind, the current review develops in a unified manner some of the more important channel characterization parameters for circuits involving scattering by inhomogeneities in the tropospheric refractive index structure, by topographic irregularities or by rain. Some of the theoretical results, which are derived from first principles, are compared with experimental findings.

1 INTRODUCTION

As the demand for reliable broad band communication circuits increases, so does the need for detailed information about the transmission medium.

The multitude of new demands leads to a very versatile and sophisticated usage of the transmission medium. This, in turn, calls for a very comprehensive description of the medium. The transmission medium constitutes the limiting factor in many interesting and potentially powerful communication techniques of which the following should be mentioned:

- Spread spectrum modulation systems are very sensitive to frequency selective fading, i.e. require a large instantaneous bandwidth. Hence we shall need information about the circuit bandwidth and its variability.
- Large synchronous time division multiplex systems (PCM) set narrow limits with regard to variations in time delay in the system. As a consequence, information about the delay spectrum and its temporal variability is mandatory.
- Data transmission in a network of computers through the package switched broadcast mode requires large bandwidth and control of time delay.
- Congested communication areas makes it important to economize with the frequency spectrum. As a
 consequence of this, we shall need detailed information about the temporal and the spatial variability
 of the parameters characterizing the propagation medium.

With these applications particularly in mind, the current contribution will discuss scattering mechanisms and channel characterization in relation to broadband radio communication systems. We shall discuss four main classes of electromagnetic wave propagation involving scattering phenomena:

- 1 Forward scattering from inhomogeneties in the tropospheric refraction index field leading to overthe-horizon propagation.
- 2 Scattering from irregularities in the troposphere on a line-of-sight path (satellite or terrestrial) leading to reduced bandwidth and limited spatial correlation of field strength.
- 3 Scattering from topographic irregularities on the earth surface giving rise to severe multipath and loss of bandwidth.
- 4 Scattering from rain.

2 BASIC RELATIONSHIPS IN SCATTER PROPAGATION, A BRIEF SURVEY

When discussing the characteristic properties of a scattered (or diffracted) wave in relation to radio communication, it is useful to have a physical understanding of the basic principles involved.

With reference to earlier works (e.g. 1, 2) a brief sketch of some of the more important derivations will be given.

Consider a volume element $dv = dx dy dx = d^3 \hat{f}$ within the scattering volume V, this scattering volume being confined to the spatial region in the troposphere illuminated by the transmitting antenna and "seen" by the receiving antenna. If the permittivity (refractive index squared) within the elementary volume differs by an amount $\Delta \epsilon$ from the average value of the permittivity ϵ_0 , the element of dielectric becomes polarized, giving rise to a dipole moment $d\hat{P} = \Delta \epsilon dv \hat{E}_0$ when under the influence of an electric field \hat{E}_0 . At distance \hat{R} from the scattering element the dipole moment results in a polarization potential $d\pi$ and provided $k^2 \hat{\pi} >> \nabla \nabla \cdot \hat{\pi}$ (which requires $R >> V^{1/3}$), the scattered field strength $\hat{E}_g = k^2 \hat{\pi}$, where \hat{K} is the wave number of the electric field. The scattered field resulting from the integral of elementary scattering elements is then given by

$$E_{a} = \frac{k_{a}^{2}}{4\pi R} \int E_{o}(\hat{r}) \epsilon(\hat{r}, t) e^{-j\hat{K}\cdot\hat{r}} d^{2}\hat{r}$$
(1)

where $\vec{K} = \vec{k}_0 - \vec{k}_B$, \vec{k}_0 and \vec{k}_B being the wave numbers of the incident and the scattered fields, respectively, such that $|K| = (4\pi/\lambda) \sin \theta/2$, where θ , the scattering angle, is the angle between \vec{k}_B and \vec{k}_0 .

Note that (1), which is derived from Maxwell's equation, is perfectly general and does not consider the nature of the refractive-index irregularities described by the function $\epsilon(\hat{r},t)$. This function may be a stochastic one, in which case the refractive-index field is conveniently described by the spatial auto-correlation function of refractive index, or we may be dealing with an ordered variation in ϵ , say a horisontal layer through which the refractive index varies in a systematic fashion expressible as a well-behaved function.

In exactly the same way, $\vec{E}_0(\hat{r})$ describes the spatial variations in the electric field within the scattering volume.

From the basic equation above, we see that there are two limiting cases:

1 If the field $\vec{E}(\vec{r})$ is constant within the scattering volume (or varies slowly in space in comparison with the $\epsilon(\vec{r})$ function), then

$$\vec{E}_{a} = \frac{k^{2} \vec{E}}{4\pi R} \int_{V} e(\vec{r}) e^{-j\vec{K} \cdot \vec{r}} d^{3} \vec{r}$$

which states that the scattered field Es is proportional to the Fourier transform of the spatial variation in refractive index within the scattering volume V.

2 If $\epsilon(\mathring{r})$ is constant within the scattering volume, then the equation tells us that the diffraction field \dot{E}_D is the Fourier transform of the spatial variation in field strength within the scattering volume V.

$$\vec{E}_D = \frac{k^2 \epsilon}{4\pi R} \int_V E(\vec{r}) e^{-j\vec{K} \cdot \vec{r}} d^3 \vec{r}$$

The intermediate conclusions are visualized in Figure 2.1.

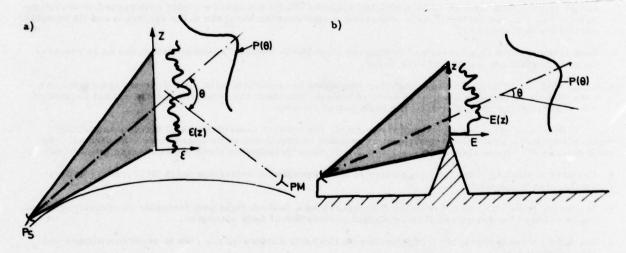


Figure 2.1 a) The scatter field is the Fourier transform of the patial variations in refractive index

b) The diffracted field is the Fourier transform of the spatial variation in the illuminating field E(z)

Now let us concentrate on the scattered field associated with spatial variations in refractive index $\epsilon(\mathbf{r})$.

We shall need information about the scattered power P as a function of scattering angle θ . To obtain this we multiply $\tilde{\mathbf{E}}_{\mathbf{s}}$ by its complex conjugate $\tilde{\mathbf{E}}_{\mathbf{s}}^*$ obtaining the scattering cross-section σ given by

$$\sigma(\theta) = (\pi k^4/2) \Phi(\vec{K}) \tag{2}$$

where $\phi(\vec{K})$ is the spatial "power spectrum" of the refractive-index irregularities such that $\Phi(\vec{K})$ is the Fourier transform of the spatial autocorrelation function of $e(\vec{r})$. The scattering cross-section σ is defined as the mean power in the scattered wave per unit power density of the incident wave in the scattering volume, per unit solid angle in the direction of \vec{k}_{s} , per unit scattering volume.

Note that the power spectrum $\Phi(\vec{K})$ is the Fourier transform of the spatial autocorrelation function of refractive index fluctuations.

Having obtained an expression for the angular power spectrum of the scattered field in terms of the function $\Phi(K)$ describing the spatial variation in refractive index, the questions which arise are the following:

- Does there exist a unique form of the Φ(R) function?
- To what extent does the Φ(R) function vary with time and with geographical location of the scattering volume?

Many forms of the $\Phi(\hat{K})$ function have been suggested. The more important ones are associated with the following names: Obukhoff-Kollmogorov, Booker-Gordon, Bolgiano, Willers-Veisskopf, Norton.

In this brief discussion of the subject, a detailed discussion of the relative merits and justification for the various $\Phi(R)$ functions does not seem justified. There is good justification (1,3) for writing the power spectrum in the form

$$\Phi(\vec{K}) \simeq K^{-n} \tag{3}$$

where n is a number that, depending on the atmospheric conditions, may vary between approximately 2 and 7. Many theories predict n = 11/3. Experiments show (4, 5, 6, 7, 8, 9, 10) that n varies within wide limits. The theoretical value n = 11/3 appears to be close to the median value of the observations.

Based on the refractive index spectrum expressed in the form $\Phi(K) \simeq K^{-n}$ we shall now calculate some of the characteristic parameters of a long-distance forward scatter circuit. There are many such, of which should be mentioned: time-delay spectrum, bandwidth, horisontal and vertical correlation distance of field strength, antenna-to-medium coupling loss.

In this survey we shall concentrate on pulse delay and on bandwidth and limit ourselves to stating the expressions for other important radio circuit parameters in terms of parameters describing the atmospheric structure.

3 CALCULATION OF PULSE DISTORTION AND CHANNEL BANDWIDTH IN TERMS RADIO-METEOROLOGICAL PARAMETERS

Our task is now to calculate the delay spectrum (pulse distortion) and subsequently the bandwidth on the basis of information about the refractive index structure $\epsilon(\vec{r})$ as expressed by its spatial power spectrum $\Phi(K)$, written in the form $\Phi(K) \sim K^{-n}$.

Using wide-beam antennas at either end so that the multipath transmission is governed by the scattering mechanism rather than by the beam geometry, we first seek an expression relating path length 1 and the position in space of the scattering element; i.e. we require an expression relating 1 and the scattering angle θ (see Figure 3.1). If d is the length of the chord between T and R, then simple geometrical calculations give the required results, namely

$$\theta = 2 |(1/d)^2 - 1|^{\frac{1}{2}}$$

If we transmit a short radio pulse, the power that reaches the receiver has travelled through a wide spectrum of different paths.

By substituting for θ in the expression for the angular power spectrum ($P \sim \theta^{-n}$), we get the spectrum relating power and path length. Normalizing this power with respect to the power received via the shortest propagation path 1, namely that determined by the earth's tangent planes, $1_0 = d | 1 + (d/2a)^2 |^{-2}$, (where a is the effective earth radius), the power spectrum takes the form

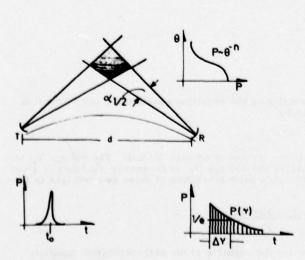


Figure 3. 1 The delay spectrum is determined by the variation in path length

$$|P(1)/P(1_0)| = (4a^2/d^2)^{-n/2}|(1/d) - 1|^{-n/2}$$

Expressing this spectrum in terms of the path length Δl , which is in excess of the minimum path length l_o (i.e. writing $l = l_o + \Delta l$), we find that the power spectrum referred to l_o is given by

$$|P(\Delta 1)/P(1_0)| = |1 + (8a^2/d^3) \Delta 1|^{-n/2}$$

And since $\Delta 1$ = τ C, where C is the velocity of light, the delay spectrum referred to τ_0 (the shortest time delay) is given by

$$|P(r)/P(0)| = |1 + (8a^2 rC/d^3)|^{-n/2}$$
 (4)

The 1/e width of this delay spectrum is then given by

$$\Delta r = (d^3/8a^2C)(e^{2/n} - 1)$$
 (5)

If, on the other hand, the antenna beams are narrow such that the spread in the path length is determined by beam geometry rather than by the $\Phi(K)$ function (i. e. the beams are so narrow that $\Phi(K)$ can be considered constant when θ varies within the scattering volume), then we can find a simple expression

for the delay spectrum in terms of geometrical parameters. Under these conditions the delay spectrum will have a width $\Delta I/C$ given by (11)

$$\Delta \tau = \frac{\mathrm{d}}{2\mathrm{C}} \left(\frac{\mathrm{d}}{\mathrm{a}} \beta + \beta^2 \right)$$

where \$ is the beamwidth.

Having expressed the delay spectrum in terms of radiometeorological parameters, we shall now apply a similar method to calculate the bandwidth of the transmission channel.

To avoid the confusion which often arises when the term "bandwidth" is used in relation to scattering processes, let us define what we mean with bandwidth.

Consider the case where several radio waves having different frequencies are transmitted simultaneously. At the receiver the power at each of these frequencies is measured as a function of time (i. e. we measure $P_{F_1}(t)$, $P_{F_2}(t)$ etc). If we take the instantaneous ratio of power at the various frequencies and integrate the ratio (i. e. we form $\int \frac{P_{F_1}(t)}{P_{F_2}(t)} dt$) then we get information about bandwidth.

On the other hand, if we integrate the signal at either frequency over the appropriate time interval by forming $\frac{\int P_{F_1}(t) dt}{\int P_{F_2}(t) dt}$ we do not obtain information about bandwidth but something which is often referred to as "the wavelength dependence of the scatter circuit".

Forming the $\int \frac{P_{F_1}(t)}{P_{F_2}(t)} dt$ is one way of obtaining information about bandwidth. Another is the following.

As in the case above we transmit a set of radio waves having different frequency. We now make sure that all these frequencies are correlated in amplitude and phase. This is, as an example, achieved by amplitude modulating a carrier, thus obtaining two sidebands 2 f_{AM} apart, if f_{AM} is the frequency of the modulating wave. These sidebands, obviously, are correlated in amplitude and phase. At the receiving end we pick up the two sidebands and correlate one with the other (i.e. we form the cross-correlation function $R_{12}(\tau)$. The more narrow-banded the transmission channel, the poorer is the correlation. (Transmitting many correlated waves spread over a frequency band, we can find the complete autocorrelation function $R(\Delta F)$ in the frequency domain.)

This is very analogous, as we shall see in the following, to the power spectrum of the transmission channel.

By analyzing the first alternative first, we can use the results of simple network theory to obtain a simple approximate result. We know that the response to a delta pulse of a network is known as the impulse response $V(\tau)$ of the network. Furthermore, the Fourier transform of the impulse response is known as the transfer function $F(\omega)$ of the network. By multiplying this transfer function with its complex conjugate, we obtain the power spectrum that we are seeking. From the previous section we obtain the expression for the impulse response by taking the square root of equation 4. Analyzing this function, we find that it closely resembles an exponential function of the form $P(\tau) = \exp(-\alpha \tau)$. The 1/e width of the impulse response is given by

$$\Delta \tau = d^{3}(e^{4/n} - 1)/8aC$$
 (6)

To simplify the Fourier transformation, we assume an exponential impulse response such that $\Delta \tau = 1/\alpha$ (when we introduce only a small error). The Fourier transform of the exponential impulse response $\exp(-\alpha \tau)$ is given by

$$F(\omega) = (\alpha + j\omega)^{-1}$$

The power spectrum is then given by

$$W(\omega) = F(\omega)F^*(\omega)$$
$$= (\alpha^2 + \omega^2)^{-1}$$

Substituting for α as obtained from equation 6 and normalizing the resulting equation for ω = 0, we find that the 1/2 power width of the power spectrum is given by

$$\Delta\omega = 8a^2 \, \text{Cd}^{-3} \, \left(e^{4/n} - 1\right)^{-1} \tag{7}$$

Now let us compute the autocorrelation function in the frequency domain $R(\Delta\omega)$. The voltage V_1 at frequency ω is given by $V_1 = F(\omega) = (\alpha + j\omega)^{-1}$. Similarly, the voltage V_2 at frequency $(\omega + \Delta\omega)$ is given by $V_2 = F(\omega + \Delta\omega) = (\alpha + j(\omega + \Delta\omega))^{-1}$. The normalized complex autocorrelation of these two voltages is then given by

$$R(\Delta\omega) = \frac{\int_{-1}^{\infty} |1/(\alpha + j\omega)| |1/(\alpha - j(\omega + \Delta\omega))| d\omega}{\int_{-1}^{\infty} |1/(\alpha^2 + \omega^2)| d\omega}$$

By solving this integral we get the following expression for the modulus of the autocorrelation function

$$R(\Delta\omega) = |1 + (\Delta\omega/2\alpha)^2|^{-\frac{1}{2}}$$
 (8)

The width of this autocorrelation function is obtained by letting $R(\Delta\omega) = \frac{1}{2}$, thus obtaining

$$\Delta\omega_{12} = 16(3)^{1/2} a^2 Cd^{-3} (e^{4/n} - 1)^{-1}$$
(9)

Note that the width of the autocorrelation in the frequency domain is $2(3)^{\frac{1}{2}}$ times the 1/2-power width of the power spectrum.

A BRIEF SUMMARY CE SOME IMPORTANT CHANNEL CHARACTERIZATION RELATIONSHIPS

We have calculated two of the most important channel parameters, namely pulse distortion and bandwidth, in terms of parameters describing the atmospheric structure. These two important radio-

COMMUNICATION CIRCUIT PARAMETER	RELATION BETWEEN CIRCUIT PARAMETER AND RADIOMET PARAMETER
WIDTH OF DELAY SPECTRIUM	$\Delta \Upsilon = \frac{d^3}{8e^2c} (e^{2/h}-1)$
BANDWIDTH	$\Delta \omega = \frac{8a^2c}{d^3} (e^{4/n}-1)^{-1}$
GAIN LOSS	$G_L = \frac{5Ad^2}{\lambda a^2} (2^{1/n}1) (4^{1/n}-1)^{1/2}$
HORIZONTAL FIELD STRENGTH CORRELATION DISTANCE	$L_{H} = \frac{0.44 \lambda a}{d(41/n_{-1})1/2}$
VERTICAL FIELD STRENGTH CORRELATION DISTANCE	$L_V = \frac{0.44 \lambda}{d(21/n-1)}$
WAVELENGTH DEPENDANCE	$\frac{P(\lambda_1)}{P(\lambda_2)} = \left(\frac{\lambda_1}{\lambda_2}\right)^{n-1}$

meteorological parameters are, as we have seen, n, which gives us information about the spatial spectrum of refractive index fluctuations $(\Phi(K) \cong K^{-n})$ and a, the effective earth radius which gives us information about the bending effect (refraction) of the atmosphere on a radio wave. This effective earth radius is related to the real radius through the following familiar relationship

$$\frac{1}{a} = \frac{1}{R} + \frac{dN}{dZ} \times 10^{-6}$$

where dN/dZ is the rate at which the refractive index decreases with height.

With reference to (1) and (2), a set of relationships which are important in the characterization of a radio channel is given in Table 1.

Table 1 Some relationships characterizing a communication channel

5 RADIOMETEOROLOGICAL PARAMETERS IN RELATION TO RUTINE METEOROLOGICAL OBSERVATIONS

This topic has been considered in some degree of detail in two earlier publications (12, 13). We shall give a summary of the results here. As we have already mentioned, and as will be substantiated in the following section, there are two radiometeorological parameters which are of dominating importance with respect to the characteristic properties of a forward-scatter communication circuit. One is the effective earth radius a, the other is the spectrum slope n of the refractive index irregularity spectrum. We shall now discuss the relationship between purely meteorological factors and the parameters a and n.

A Determination of effective earth radius a from radiosonde measurements

The refractivity N (where $N = (n-1)10^6$, n being the refractive index) is obtained from meteorological parameters by the Debye relationship

$$N = 77 \cdot 6 \frac{P}{T} + 3.73 \times 10^{5} \frac{e}{T^{2}}$$
 (10)

where P is the total pressure in millibars, T the absolute temperature, and e the water vapour pressure in millibars. Thus from knowledge about the vertical profile of P, T, and e as obtained from a conventional radiosonde, we can calculate the refractivity profile.

Knowing the N profile, we can calculate the ray bending from Snell's law (14). We are thus able to calculate the total bending to which a ray is subjected, when propagating from the transmitter to the centre of the scattering volume.

Similarly, we can calculate the bending experienced from the midpath point to the receiver. (In practice, we perform the calculation from the receiver back to the mid-path point). We then know the effective scattering angle, which is the difference between the angle between the earth tangent planes through the transmitter and receiver and the total ray bending.

If d is the distance between the transmitter and receiver, then the angle θ between the tangent planes is given by

$$\theta = \frac{d}{R}$$

where R is the real earth radius. By the same relationship, we then obtain the effective earth radius a using the effective scattering angle

Alternatively, if the refractivity gradient dN/dz is constant through the height interval involved (from ground to scattering volume), then the effective earth radius is given by the simple relationship

$$\frac{1}{a} = \frac{1}{R} + \frac{dN}{da} \times 10^{-6}$$

assuming a near-horisontal direction of the radio beam.

We observe, then, that on the basis of P, T, and e, data from a conventional radiosonde ascent, we can obtain the radiometeorological parameter a appropriate for a given height of the scattering volume (corresponding to a given path length). The solid lines in Figure 5.1 show probability distributions of the ratio a/R based on 230 radio soundings at Sola in south-western Norway during 1966 (2).

For comparison, the dashed line shows the ratio a/R based on 45 radiosonde ascents during October and November 1970 at Maniwaki, near Ottawa, Canada. This line lies intermediate to the Sola curves, but has a slope similar to the Norwegian summer data,

B Determination of spectrum slope n from radiosonde measurements

Here the reader is referred to (12), where an empirical relationship was found between the atmospheric stability (a somewhat modified version of the well-known Väisälä-Brunt frequency v²) and the slope n of the refractive index irregularity spectrum. The conventional Vaisala-Brunt frequency appears as the numerator in the Richardson's number and is normally written as

$$v^2 = \frac{g}{T} \left(\frac{dT}{dz} + \frac{g}{c_p} \right) \tag{11}$$

Here g is the gravitational constant, T the temperature, dT/dz the vertical temperature lapse rate, and c_p the specific heat at constant pressure. We see that the expression within the brackets is a measure of the difference between the actual temperature lapse rate and the adiabatic lapse rate. This expression normally refers to a limited vertical section of the atmosphere.

The correlation of the spectrum slope n with atmospheric parameters describing the dynamic state of the atmosphere was significantly improved when a particular weighting function was placed on the temperature contribution to the stability.

Specifically, by adding a number which is determined by the temperature at the 850 mbar surface (1500 m altitude) to the Väisälä-Brunt frequency, the $n-v^2$ correlation was improved. For our particular purpose therefore, a modified version of v^2 was used:

$$v^2 = \frac{g}{T} \left(\frac{dT}{dz} + 5.50 \times 10^{-3} T_{850} + \frac{g}{c_p} \right)$$
 (12)

Here T, measured in degrees K, and dT/dz, in degrees per 100 m, are average values obtained over the 850 - 400 mbar levels (1.5 to 7 km altitude).

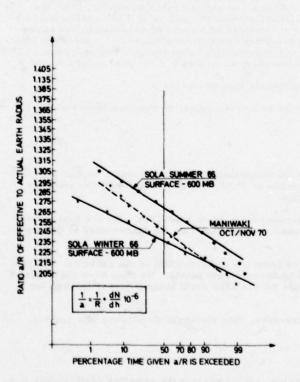


Figure 5. 1 Distributions of the ratio of effective to actual earth radius, based on radiosonde observations at Sola, Norway and Maniwaki, Canada

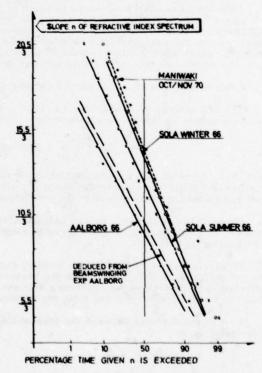


Figure 5.2 Distributions of the slope of the spectrum of refractive index irregularities as deduced from radiosonde observations and beam-swinging experiments

Having obtained v^2 from the results of a temperature profile determined by a conventional radiosonde observation, the spectrum slope n is found, using the expression for the n versus v^2 regression line:

$$n = 40.6 + 708 v^2 \tag{13}$$

Figure 5.2 shows probability distributions of spectrum slope n. The two upper curves are for the radio-sonde station Sola in south-western Norway for summer and winter 1966. These curves correspond to the distributions of Figure 5.1 and form the basis for the calculations to be presented in the following sections. For comparison, Figure 5.2 also shows n distributions for Mainwaki and for Aalborg, northern Denmark, as obtained on the basis of radiosondes. The "predicted" n distribution for Aalborg is compared with that deduced from radio beam-swinging experiments (1, 12).

C Channel characterization statistics on the basis of meteorological data

From the chapter above, we are in a position to calculate the probability distributions for some of the important communication channel parameters.

From the meteorological data as converted to the radiometeorological parameters n and a and presented in Figures 5.1 and 5.2, we are able to calculate channel parameters such as pulse distortion and bandwidth from the list of basic expressions given in Table 1 and derived in chapter 3.

A set of such probability distributions is given in Figures 5.3 and 5.4 (for further details on other channel characterization parameters, the reader is referred to reference 2).

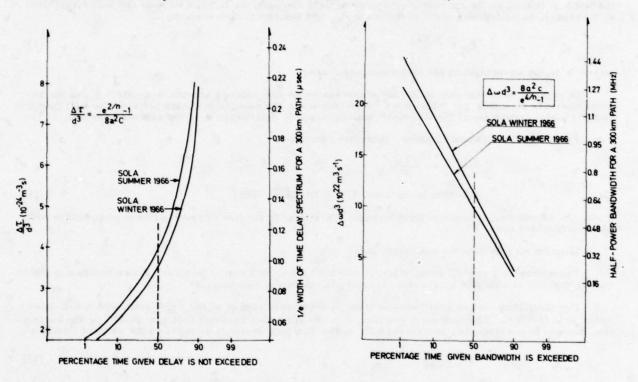


Figure 5. 3 Distributions of the 1/e width Δτ of the time delay spectrum

Figure 5.4 Distributions of the half-power bandwidth $\Delta\omega$

6 FUNDAMENTAL PROPERTIES OF A LINE-OF-SIGHT RADIO PROPAGATION PATH

In the preceding chapter we presented the basic principles and the basic relationships in scatter propagation.

We can make direct use of these also in connection with the line-of-sight problem.

As a consequence of the fact that irregularities in the atmospheric refractive index structure lead to multipath phenomena and delay variations when an electromagnetic wave passes through the irregular transmission medium, we suffer a loss in bandwidth. We shall now give some theoretical results, which are well confirmed experimentally, giving information about the amplitude covariance as a function of frequency separation (i. e. bandwidth properties of the medium).

Before presenting the accurate results of comprehensive calculations, we shall, as in the case of the scattering mechanisms above, give some quantitative results for the purpose of ensuring a physical understanding of the basic physics involved.

Referring to the simple geometrical sketch of Figure 6.1, we see that there are two extreme paths through which the electromagnetic waves can travel from the transmitter T to the receiver R. One is

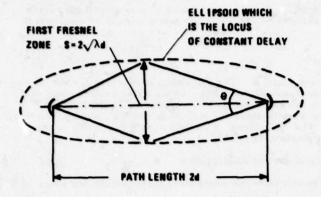


Figure 6. 1 The geometry of line-of-sight propaga-

the shortest direct way from T to R, the other is via a path which is $\lambda/2$ wavelengths longer than the direct route. The result of these two waves is the vector sum of two signals with a 180° difference in phase causing destructive interferences.

To the first order, therefore, we would expect the width • of the angle of arrival spectrum at the receiving point to be given by

$$\tan^{-1} \theta = \frac{\sqrt{\lambda d}}{d}$$

$$\theta \simeq \frac{\sqrt{\lambda d}}{d}$$
(14)

Knowing the angular power spectrum, the beamwidth, the correlation distance in a plane through the point of the receiver normal to the line T-R can be calculated. It can be shown (15) that this spatial correlation of field strength is the Fourier transform of this angular power spectrum.

If this power spectrum is a $\frac{\sin x}{x}$ function, then the Fourier transform is a rectangular function. If the width of this, i.e. the correlation distance of field strength, be L, then we have the following relationship between the half-power width of the beam $\theta_{1/2}$ and the correlation distance L

$$\theta_{1/2} = \frac{0.88 \,\lambda}{L} \tag{15}$$

where \(\) is the wavelength of the electromagnetic wave.

In passing, note that this is the same expression as that relating antenna beamwidth $\theta_{1/2}$ to the antenna aperture diameter L. This is not surprising since the antenna radiation pattern (the $P(\theta)$ function) is the Fourier transform of the illuminating field strength distribution over the antenna aperture.

From equations 14 and 15 above, therefore, we have

$$\frac{0.88\lambda}{L} = \frac{\sqrt{\lambda d}}{d}$$
correlation distance $L = 0.88 \sqrt{\lambda d}$ (16)

Thus, the correlation distance of field strength transverse to the line of propagation is comparable with the first Fresnel zone.

Then let us calculate the bandwidth Aw.

From chapter 3 above, we have learnt that the bandwidth function (autocorrelation function in the frequency domain) is obtained by Fourier transforming the delay spectrum.

For simplicity, let us again assume that the delay spectrum is of the $\frac{\sin x}{x}$ form with a half-power width $\Delta r = (\lambda/2)/C$. The bandwidth function, i. e. the frequency transfer function $P(\Delta F)$ or the correlation function in the frequency domain $R(\Delta F)$, would then be a rectangular function the width of which is

$$\Delta F = \frac{i}{\Delta r} = \frac{2C}{\lambda} \tag{17}$$

= $\frac{1}{2}$ frequency of the electromagnetic wave

These were the approximate results. Then let us present the results of more rigorous calculations.

Referring to Lee and Harp (16) it can be shown that the covariance between waves with different wavenumbers k_1 and k_2 (where $k=2\pi/\lambda$) is given by

$$C_{f}(\rho) = 4\pi^{2}k_{1} k_{2} \int_{0}^{L_{p}} ds \int_{0}^{K_{1}k_{2}} dK \cdot K \cdot \Phi(K) J_{0}(\frac{sK\rho}{L_{p}}) \cdot \sin(\frac{K^{2}s(L_{p}-s)}{2k_{1}L_{p}}) \cdot \sin(\frac{K^{2}s(L_{p}-s)}{2k_{2}L_{p}}) \cdot \dots$$
 (18)

where

i.e.

ρ = spatial separation of receivers between which the correlation is measured

L_ = length of transmission path

s = elementary distance along the path L

K = wavenumber of refractive index irregularities (K = 2π/1 when 1 is the spatial size of the irregularities)

 $\Phi(K)$ = spectrum of refractive index irregularities. This is of the form $\Phi(K) \simeq K^{-n}$, n being an atmospheric parameter which varies with conditions (stability) in the atmosphere (2, 12). The median value of n appears to be close to 4.

Jo = Bessel function of zero order

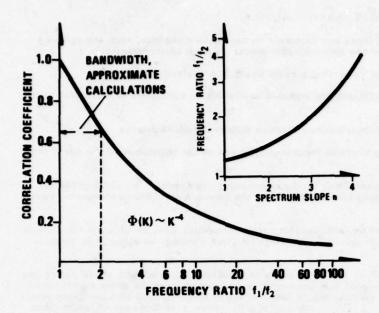


Figure 6.2 Amplitude covariance vs frequency separation f_1/f_2 . The insertion shows the influence on bandwidth of the slope n of the refractive index spectrum $(\Phi(K) \simeq K^{-n})$. Bandwidth is defined as λ_1/λ_2 for correlation coefficient = $\frac{1}{2}$

As we shall see in the following, this covariance function is generalized to include covariances in both space and frequency, and indirectly in time.

For the Kolmogorov spectrum $\Phi(K)$ is of the form $\Phi(K) \simeq K^{-11/3}$.

The frequency covariance function for this spectrum is plotted in Figure 6.2 for $\rho = 0$.

As an insertion in the figure giving the frequency covariance function $R(\Delta F)$, a diagram illustrating the relationship between bandwidth and atmospheric structure is given (after A Kjelaas). Note that the structure parameter is the familiar n parameter $(\Phi(K) \simeq K^{-n})$.

Finally, the spatial correlation properties of the electromagnetic field will be subjected to comprehensive calculations.

In the same way as above where we considered waves with different frequency in a multipath environment, multipath causes waves to interfere in such a way as to produce an interferrogram in a plane normal to the direction of propagation. Correlating then the field strength at different points in the mentioned plane, a covariance function which decreases with increasing spatial separation is observed.

We now use the same basic expression as above (equation 18) and we use one frequency only, thus putting $k_1 = k_2$. The expression for the amplitude covariance between waves at different points in space with orthogonal separation ρ relative to the direction of propagation is then

$$C(\rho) = 4\pi^{2} k^{2} \int_{0}^{L_{p}} ds \int_{0}^{k} dK \cdot K \cdot \Phi(K) J_{0}(\frac{sK\rho}{L_{p}}) \cdot \sin^{2}(\frac{Ks(L_{p}-s)}{2kL_{p}}) \dots$$
 (19)

This function is plotted in Figure 6.3.

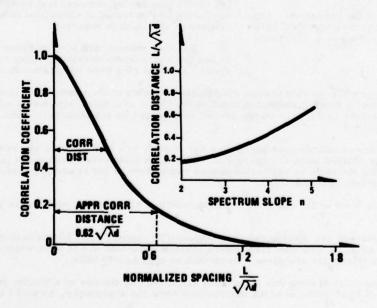


Figure 6.3 Spatial correlation of field strength (from Lee & Harp, Kjelaas)

SCATTERING FROM EARTH SURFACE IRREGULARITIES

In this section of the review we shall focus our attention on the earth's surface, this acting as a reflector of electromagnetic waves. There are several applications of such an investigation:

- The ground can be used constructively in reflecting a radio beam in a desired direction
- Ground reflection can give undesired multipath and reduced bandwidth on satellite and terrestial radio circuits
- Ground reflections can give undesirable interference between different radio systems
- Radio waves can be used as a tool in the study of the topography and of the vegetation of the earth surface

With these applications in mind, concentrating on the communication aspects, we shall perform basic calculations for the purpose of obtaining information about the interaction of electromagnetic waves with the earth surface.

In order to simplify the geometry, let us first consider the backscatter case involving a monostatic situation with both the transmitter and the receiver at the same location viewing the same geographical area.

The geometry is sketched in Figure 7.1; our aim now is to calculate the bandwidth of the reflecting surface. We have shown in chapter 3 above that this bandwidth is calculated from the delay spectrum of the reflector. Specifically, if $\sigma(z)$ be the distribution in depth of the scatterers such that the delay spectrum is $\sigma(z/c)$ where c is the wave velocity, then the following relationships hold:

TRANS-MITTER RECEIVER

Figure 7.1 The geometry of the backscatter situation. The scatterers are distributed in depth z according to a $\sigma(z)$ function

 $F(\omega) = Fourier transform of <math>\sigma(\frac{z}{c})$

Power spectrum $W(\omega) = F(\omega) F^*(\omega)$

Bandwidth of reflecting surface is half-power width of $W(\omega)$

Essentially there are two different ways of proceeding:

- A deterministic procedure in which the scattered field is derived from the geometry of the scattering object using Maxwell's equation and the appropriate boundary conditions, by calculation of the complex reflection coefficient from a finite number of discrete scattering centres
- A statistical procedure in which the statistical properties of the scattered wave are calculated on the basis of statistical information about the scattering object

The relative merits of these two procedures depend on the nature of the problem at hand. If the scattering object (scattering surface) is a complex one describable only in terms of statistical function, the statistical approach is superior.

For this reason, and also in order to be able to use the expressions developed under chapter 3 above, we shall also here apply statistical methods.

Referring again to Figure 7.1 we express the distribution in depth of the scatterers (along the direction of propagation) in terms of a depth distribution function (in terms of a delay-spectrum) $\sigma(z/c)$. Note that this depth distribution refers to the area on the ground illuminated by the transmitter and "seen" by the receiver.

Table 2 gives the results of calculations based on a set of such $\sigma(z/c)$ functions, the resulting w(f) functions are plotted in a normalized form in Figure 7.2. The depth distribution parameter z_0 is taken as 100 cm in all cases. Since the wave by reflection passes twice through the scattering medium, this implies that the scattering strata is 50 cm thick.

Note that the particular form of the depth distribution function $\sigma(z/c)$ has a pronounced influence on bandwidth.

We see that if the scatterers are distributed in an exponential manner over 50 cm in depth, the bandwidth of the reflector is 48 MHz. A gaussian distribution gives a bandwidth of 111 MHz, while a rectangular one gives 130 MHz and a triangular one gives a bandwidth as high as 200 MHz.

From a remote probing point of view this is an ideal situation; by the use of a simple experiment involving the measurement of bandwidth, detailed information about the topography, or about the vegetation, can be obtained.

DISTRIBUTION IN DEPTH OF SCATTERERS	FREQUENCY DEPENDENCE OF REFLECTING SURFACE	HALF POWER BAGOWIOTH
Za de la constitución de la cons	$W(\omega) = \frac{\sigma_{O}^{2}}{\left(\frac{c}{z_{O}}\right)^{2} + \omega^{2}}$	$\Delta F_{1/2} = 0.16 \frac{c}{z_0} \text{Hz}$
Z SAUSDAN	$W(\omega) = \frac{\pi}{4} \frac{\sigma_{O}^{2}}{\left(\frac{C}{z_{O}}\right)^{2}} e^{-\frac{\omega^{2} z_{O}^{2}}{8 c^{2}}}$	$\Delta F_{1/2} = 0.37 \frac{c}{z_0} \text{ Hz}$
Za Z	$W(\omega) = 4\sigma_O^2 \left(\frac{\sin\frac{\pi}{2c}\omega}{\omega}\right)^2$	$\Delta F_{1/2} = 0.44 \frac{c}{z_0} Hz$
TRANSULAR	$W(\omega) = \frac{64 \sigma_{O}^{2}}{\left(\frac{z_{O}}{c}\right)^{2}} \left(\frac{\sin \frac{z_{O}}{4c}\omega}{\omega}\right)^{4}$	$\Delta F_{1/2} = 0.64 \frac{c}{z_0} Hz$
	$W(\omega) = 4\sigma_0^2 (\cos \frac{x_0}{2c} \omega)^2$	$\Delta \mathbf{F}_{1/2} = 0.25 \frac{\mathbf{c}}{\mathbf{z}_0} \mathbf{Hz}$

Table 2 Bandwidth properties of some topographic surfaces

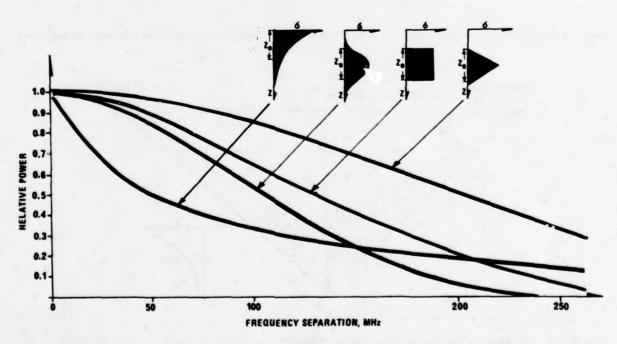


Figure 7.2 Bandwidth properties of some topographic surfaces

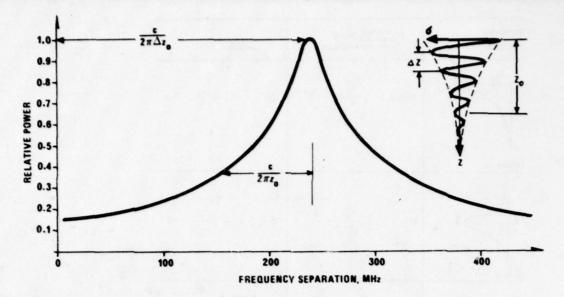


Figure 7.3 Bandwidth properties of a scattering surface in which there is a periodic structure such as evenly spaced branches of a tree

Conversely, in order to be able to calculate the effect of topographical factors on the bandwidth of a communication channel involving scattering from the ground, detailed information about the scattering surface is mandatory.

Finally, for the purpose of illustrating the influence of a periodic structure in the reflecting medium, examplified in a pine tree with equally spaced branches, Figure 7.3 is given. Here the tree is described in terms of an exponentially damped sinusoidal oscillation.

Note that the peak of the w(f) spectrum is determined by the spacing of the branches, whereas the width of the curve as before is determined by the height of the tree.

The example based on a backscatter monostatic situation is not a very realistic one from the point of view of communication.

Now let us discuss the bistatic situation in which the transmitter and the receiver are widely separated.

From simple geometrical considerations, with reference to Figure 7.4, we find that the difference in path length Δl can be expressed in terms of depth z as follows:

$$\Delta l \simeq z(\alpha + \frac{z}{d})$$

where α is half the scattering angle and d is the distance between transmitter and receiver as indicated in Figure 7.4.

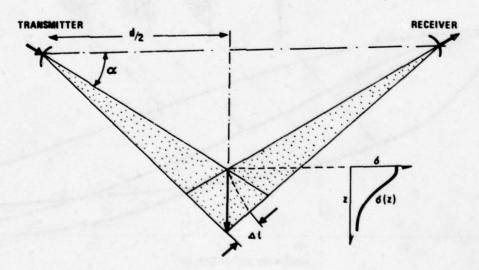


Figure 7.4 The geometry of the forward scatter situation

Thus, if the distribution in depth of the scatterers is z_0 and if the path length as an example if 50 km and the angle α is $\frac{500}{50\ 000}$ (implying that the vertical distance from the line between transmitter and receiver to the scattering area is 500 m), then the resulting delay Δl is approximately $z_0/100$.

The bandwidth of this reflector configuration is thus increased by a factor 100 relative to the pure backscatter case.

If, however, some of the transmitted power reaches the receiver directly through the line of sight path, then the spread in path length ΔI is given by

$$\Delta 1 = \frac{2H_1 H_2}{d}$$

where, as before, d is the path length. H_1 and H_2 are the height above the reflecting surface of the transmitter and receiver respectively.

In the example considered above $H_1 = H_2 = 500 \text{ m}$ and d is 50 km.

Under such multipath conditions the difference in path length is some 10 m, and the bandwidth is reduced by a factor 1000 relative to the case discussed above with forward scatter and no direct line of sight path.

Note that the locus of the reflection point for constant delay is an ellipsoidal surface with the transmitting and the receiving terminals as focal points. For the current geometry, therefore, the constant delay surfaces are horizontal and parallel near the mid-path point. As a consequence of this, it is the distribution of the scatterers (i.e. the $\sigma(z)$ function) along a vertical direction in space normal to the constant delay surface that matters.

Note also that the current treatment assumes that the scattering surface is sufficiently smooth for shadowing effects to be neglected. Focusing effects stemming from large curved surfaces are also neglected in this review. For details on this subject, the reader is referred to (21) and (22).

8 SCATTERING BY RAINFALL

A review on scattering mechanisms in relation to communication and channel characterization would be incomplete if the phenomena related to rainfall were not discussed.

In this presentation a simple qualitative discussion will be given. For details, the reader is referred to e.g. (17), (18), (19) and (20).

When studying the effect of precipitation on electromagnetic waves, several factors describing the rain structure should be considered. These are:

- Rainfall rate
- Drop-size distribution
- Shape of raindrops
- Canting angle of raindrops (orientation in space of ellipsoidal raindrops)

Rainfall rate and drop size distribution are, evidently, the most important parameters.

Consider a dielectric sphere of diameter D in an electromagnetic field where the wavelength λ is large compared with the diameter of the sphere. The sphere will give rise to an induced dipole moment as discussed in chapter 2 above, and reradiate the power which has been extracted from the incident electromagnetic field in all directions.

The region where the diameter of the sphere is very long compared with the wavelength is known as the Rayleigh region. The analysis related to this case is well known and leads to the result that the scattering cross-section of the sphere increases as the fourth power of frequency. If the sphere has a complex dielectric constant, part of the power incident on the sphere is dissipated as heat and consequently causes a reduction in the amount of reradiated power.

Increasing now the frequency of incident radiation such that its wavelength becomes comparable with the dimensions of the dielectric sphere, the problem rapidly becomes complex. One now will have to consider the field patterns within the sphere. The simplest pattern is that obtained when the circumference of the sphere is one wavelength. We then have a condition which is referred to as dipole resonance giving maximum scattering cross-section. Increasing the frequency further, a situation characterized by quadrupole resonance occurs when the circumference is two wavelengths long. Decreasing the wavelength of the field still further, hexapole resonance conditions are reached, followed by octopole, and so on until the cross-section becomes a highly complex linear superposition of these multipole radiators which finally converge to the limit known as the "geometrical" value.

Normalizing the scattering cross-section to this value, the scattering cross-section versus frequency dependence is shown in Figure 8.1.

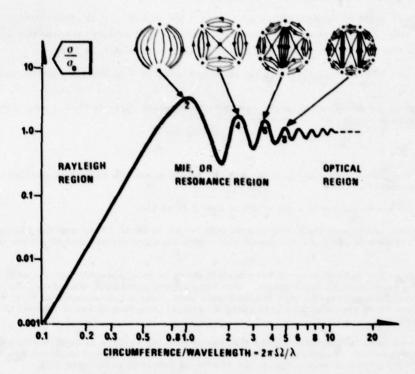


Figure 8.1 Normalized scattering cross-section of a dielectric sphere as a function of normalized wavelength

9 CONCLUSION

In the current review, consideration has been given, with varying degree of substantiation, to the scatter propagation mechanisms of importance in relation to modern communication systems.

It has been shown that phenomenologically scattering from inhomogeneities in the tropospheric refractive index structure or from topographic irregularities are very closely related. As a consequence of this, a unified theoretical approach is adopted in this review. The main results can be summarized as follows:

- On the basis of knowledge about the tropospheric structure as obtained from conventional meteorological radio soundings, all the important parameters characterising a tropospheric communication channel can be deduced.
- Channel statistics (probability distributions of important communication parameters) can be obtained by simple calculation from climatological statistics. Examples of such channel characterization parameters are bandwidth, delay spectrum width, spatial correlation of field strength, antenna-to-medium coupling loss.
- For scattering processes involving the earth surface (topography, vegetation), the communication parameters can be calculated from information about the topographic structure or from knowledge about the plants. Knowing the height distribution of the geographical area illuminated by the radio transmitter and "seen" by the receiver, as obtained from conventional topographic maps or from measurements on plants, channel parameters such as bandwidth and delay spectrum width can be calculated.

REFERENCES

- GJESSING, D. T., "Atmospheric Structure Deduced from Forward-Scatter Wave Propagation Experiments", Radio Sci 4, 12, Des 1969, pp. 1195-1210.
- 2 GJESSING, D. T. and McCORMICK, K.S., "On the Prediction of the Characteristic Parameters of Long-Distance Tropospheric Communication Links", IEEE Trans Comm 22, 9, Sep 1974.
- 3 GJESSING, D. T., "On the Use of Forward Scatter Techniques in the Study of Turbulent Stratified Layers in the Troposphere", Boundary-Layer Meteorol 4, Apr 1973, pp. 377-396.
- 4 GJESSING, D. T., "An Experimental Determination of the Spectrum of Permittivity and Air Velocity Fluctuations along a Vertical Direction in the Troposphere using Radio Propagation Methods", J. Atmosph. Terr. Phys. <u>26</u>, 2, Febr 1964.
- BULL, G. and NEISSER, J., "Untersuchungen der atmosfärischen Feinstruktur mit Hilfe von Ausbreitungsmessungen im Mikrowellenbereich", Beitr Geophys 77 (5), 1968, pp. 394-410.
- EKLUND, F. and WICKERTS, S., "Wavelength Dependence of Microwave Propagation Far Beyond the Radio Horizon", Radio Sci 3 (11), 1968, pp. 1068-1974.
- 7 FEHLABER, L., Fernmeldetechnisches Zentralamt, Deutschen Bundespost, "Diversity Abstand auf Scatter Strecken im Frequenzbereich Zwischen 1 GHz und 10 GHz", 1966, Tech Vericht 5581.
- FEHLABER, L. and GROSSKOPF, J., Fernmeldetechnisches Zentralamt, Deutsche Bundespost, "Messung der Gewinnmindering bei 1715 MHz auf einer 409 km langen Scatter-Versuchussstrecke", 1968, FTZ, A455, Tb 7.
- 9 BOLGIANO, R. Jr., Cornell University, "A Study of Wavelength Dependence of Transhorizon Radio Propagation", 1964, Res. Rep. 188.
- 10 COX, D. C. and WATERMANN, A.T. Jr., "Phase and Amplitude Measurements of Transhorizon Microwaves with a Multidata-Gathering Antenna Array", AGARD Conf. Proc. 37, 1968, 18-1 to 18-6.
- 11 GJESSING, D. T., "Scattering of Radio Waves from Regular and Irregular Time Varying Refractive-Index Structures in the Troposphere", AGARD Conf Proc 37, 1968, 15-1 to 15-17.
- 12 GJESSING, D. T., KJELAAS, A. and NORDØ, J., "Spectral Measurements and Atmospheric Stability", J. Atmosph. Sci. 26, May 1969, pp. 462-468.
- 13 GJESSING, D. T., JESKE, H. and KLINT-HANSEN, N., "An Investigation of the Tropospheric Fine Scale Properties Using Radio, Radar and Direct Methods", J. Atmosph. Terr. Phys. 31, 1969, pp. 1157-1182.
- 14 BEAN, B.R. and DUTTON, E.J., "Radio Meteorology", Washington D.C.: U.S. Government Printing Office, 1966.
- 15 GJESSING, D. T. and BØRRESEN, J. A., "The Influence of an Irregular Refractive-Index Structure on the Spatial Field-Strength Correlation of a Scattered Radio Wave", IEE (Lond.) Conf. Pub. 48, 1968, pp. 43-50.
- 16 LEE, R. W. and HARP, J. C., "Weak Scattering in Random Media", IEEE 57, 1969, p. 375.
- 17 STRATTON, J., "Electromagnetic Theory", McGraw-Hill, 1941.
- 18 KERR, D. E., "Propagation of Short Radio Waves", Dover Publication, 1965.
- McCORMICK, G. C. and IVENDRY, A., "Depolarization over a Link due to Rain, Measurement of Parameters", Radio Science 11, 1976, pp. 741-749.
- DRUFUCA, G., "Rain Attenuation Statistics for Frequencies above 10 GHz from Raingauges Observations", J. de Rech. Atm. 8, 1-2, 1974, pp. 399-411.
- 21 GJESSING, D. T., "On the Scattering of Electromagnetic Waves by a Moving Tropospheric Layer having Sinusoidal Boundaries", IEEE Trans Antennas & Propagation AG-12, 1, Jan 1964.
- 22 GJESSING, D. T. and IRGENS, F., "Scattering of Radio Waves by a Moving Supplied Layer: A Simple Model Experiment", IEEE Trans Antennas & Propagation AG-12, 6, Nov 1964.

Electro-magnetic wave propagation in an inhomogeneous medium - a laboratory study

W.G.Burrows
Formerly of Imperial College, London
now
Head of Marine Electronics Department
Brunel Technical College, Bristol.

Summary

A physical modelling technique has been used as an aid in the study of radio wave propagation in the troposphere.

The basic technique employs an optical model, scaled and constructed to represent a full size tropospheric radio system, where a coherent light beam is propagated through an inhomogeneous gaseous medium whose structures and properties might be considered to represent the real atmosphere. The model has been used, concurrently with the full scale system, to conduct a number of investigations in an attempt to establish the significance of the time varying refractive index properties of the medium in relation to changes in the structure of the propagated beam at distances from the source.

A summary of some of the many simple experimental studies that have been made is given to illustrate the value of the technique. A comparison of these results with those obtained from the full scale system gives rise to the conclusion that the primary mechanisms of trans-horizon propagation are associated with atmospheric structures in the lower region of the troposphere.

1. Introduction

Current theories on the mechanisms of radio wave propagation in the troposphere postulate trans-horizon propagation by either 'ducting' or 'scattering' processes. Whilst the 'ducting' phenomenon is attributed to atmospheric inversions the 'scattering' is generally attributed to the effects of certain types of turbulence or strata present within the confines of a 'common volume'. This 'common volume' is conveniently defined by that volume which is described at the intersection of the receiver and transmitter beams used in any given system. The principal mechanism of propagation beyond a radio horizon is therefore assumed to be one of forward scatter. In certain areas of the world 'radio-ducting' may be preferred as a possible mode of propagation.

Por many years a considerable number of research projects have been undertaken to support these hypotheses but without the measure of success that is likely to make a significant contribution to the design of radio communication systems which make use of the troposphere as a transmission medium. This work has, however, brought about the development of a large number of very elegant analytical solutions to problems of extreme complexity and which are, at least, of considerable academic interest and value. In recent years, atmospheric probe techniques involving the use of radar, lidar and acoustic sounders have been developed to display the possible boundaries of the meteorological inhomogeneities present in the lower atmosphere. Unfortunately, the value of these techniques is virtually limited to the interpretation of the results obtained from those regions scanned by the particular probes employed. Whilst these results may be of considerable value to the radio meteorologist their value to those concerned with the transmission or propagation of electro-magnetic waves at very high frequencies is somewhat limited. The practical difficulties of probing or sensing the properties of the atmospheric medium are well known and do not require further discussion. Nevertheless, the assumptions that must be applied to the results obtained from any atmospheric probe, including the radio refractometer, must be speculative if they are to be used as the basis of any subsequent description of the atmospheric region explored. The atmospheric

volume that exists between the transmitter and receiver terminals of a trans-horizon radio system is of a magnitude and complexity that defies even partial description, to say nothing of predicting future behaviour. In the British Isles, with its maritime climate, even meteorologists have some difficulty in describing the state of the atmosphere at any instant. They have even greater difficulty in predicting the weather conditions that might prevail some few hours ahead. This is in spite of an enormous store of statistical evidence and more than a modest range of instrumentation.

There is therefore, even at this present time, a not insignificant void in our knowledge of both the properties and behaviour of the troposphere as a 'region of weather' and as a propagation medium. In the final stages of the assessment of the total path loss for a proposed tropospheric radio system, theory and conjecture are forced to give way to experience, which has produced many empirical rules and laws, because of the uncertainties surrounding the actual mechanisms of propagation that might be involved. Predicting even the long term variations that these path losses may suffer is also extremely precarious, from a commercial point of view, for the same reasons. The coupling between the antennas in a system and the propagation medium is even a subject of some conjecture and which also may be directly related to the mechanisms of propagation.

In 1939 Avec (1) described a laboratory model that had been developed to demonstrate both the structures and behaviour of Benard convective cells which were produced under controlled conditions in laboratory. Since that time many meteorologists have resorted to various forms of modelling techniques in their attempts to understand the behaviour of the meteorology of the atmosphere. Indeed, there have been many areas of applied science where the physical model has proved of great value in the ultimate solution of problems by displaying features which pure theory either neglects or is unable to completely describe. In any experimental study where there is a degree of control over the significant parameters, the results obtained allow some strength to be given to any conclusions that might be subsequently made.

Some years ago the author (2) reported the development of a simple laboratory model as an aid to the study of radio wave propagation in the troposphere. At that time it was felt that whilst a number of very elegant hypotheses (3, 4, and 5.) had already suggested various mechanisms of trans-horizon propagation in the troposphere, these did not have very significant support from the practical experience being gained by those designing and operating the many successful radio systems being developed and brought into commercial service. The situation still prevails to-day in spite of the considerable research work that has been undertaken.

The model was developed by combining the type of technique used by Avsec with other modern optical techniques in order that the behaviour of a laser beam, representing a transmitter beam, may be studied when propagated through an inhomogeneous gaseous medium within the confines of a laboratory. When used in conjunction with a full scale tropospheric system, such a model provides a means of obtaining at least a greater appreciation of the physical properties of the troposphere that may be influencing the propagation of the transmitted beam on the full scale system. At best the model has the potential of almost completely representing the full scale system. A scaled model laboratory representation of the full scale system was constructed by the use of a scaling factor, derived from the ratio of the wavelengths of the model (laser) and full scale transmitters. The initial stages of construction of the model path were made relatively easy since the transmission path of the full scale link was considered 'smooth'. It was therefore, only necessary to scale such principal dimensions as path length, antenna apertures and heights etc. By protecting the 'model atmosphere' over the 'model transmission path' with

a suitable transparent enclosure a large degree of control was maintained over the various inhomogeneous conditions that could be created in the model to produce and simulate any type of fading that is experienced in a full scale system.

A summary of the simple experimental studies that have been made with this model, in conjunction with studies on a full scale system, will be given to demonstrate the facilities that the model offers. The results obtained from some of these studies suggest conclusions which may be at variance with current concepts. It should, however be appreciated that the majority of these studies have been carried out with the prime object of determining the causes of fading in transmissions through an inhomogeneous medium.

By obtaining a truly physical concept of the mechanism of fading, attention is drawn to the possibility of alternative mechanisms of propagation which are particularly applicable in the case of trans-horison propagation.

2. THE LABORATORY MODEL

2.1 The basic structure

The experimental full scale tropospheric system that was used initially as the basis of the laboratory model, operated at a frequency of 900.00 MHs (A= 30 cms.) and over a total path length of 150 km. Since the profile of this path was, for all practical purposes, considered 'smooth' the basic model path was constructed from aluminium plate whose upper surface was ground and polished. Aluminium being chosen because its conductivity and permittivity properties at optical frequencies are similar to those of 'average ground' at radio frequencies. Provision was made, on the underside of the ground plane. for heating elements to be attached for the purpose of heating and producing a temperature gradient in the gaseous medium immediately above its upper surface. The model 'transmitter' was a laser source, of 0.6328 A (632.8 n.m). The horizontally polarised beam from this source was focussed by a series of lens and spatial filters and passed through an aperture representing a scaled version of the full scale antenna aperture, to provide a conical beam having the correct beam width. This transmitter antenna aperture was sited at one end of the model path and aligned to project the beam along the centre line of the path. Since in the full scale system identical parabolic antennas were used at both the transmitter and receiver terminals, a similar aperture was used for the model 'receiver' antenna. Although basically mounted at a scaled height at the 'receiver end' of the model, the receiver aperture was mounted to allow movement, normal to the axis of the transmitter beam, in both vertical and horizontal directions. The light illuminating this aperture was transferred to a photomultiplier 'receiver' by a flexible optical fibre bundle. The Fig. 1 gives an outline of the basic layout of the essential model system. For the purpose of this report the only dimension of prime importance is that of the path length. In modelling a full scale path 150 km. for a transmission wavelength of 30 cm. the path length may be given as 150.10 /0.3 = 5. x 10. λ . For the later source, where $\lambda = 632.8$ n.m., an identical transmission path length will be 31.64 cm. For the purpose of the basic studies associated with the full scale system the path was constructed to this length. An arbitary width of 20 cms. was chosen to exceed the horisontal dimension that might be ascribed to the common volume at the intersection of the transmitter and receiver beams, which were each of 6 degrees in this case. This width was also considered to be sufficient to allow the adequate development and movement of inhomogeneous air masses due to temperature gradients etc., within the transmitter beam over the entire length of the model path. Apart from the arbitrary width of the model path, it is essential to appreciate that all the essential physical dimensions of the full

scale path are those represented through the identical dimensions of the transmission wavelength.

For most of the studies conducted on the model the gaseous medium was air, the total volume of which was basically confined to the extent of the model path by optically flat glass boundaries constructed from microscope cover glass slips. This allowed for any changes to be made in the gaseous medium to provide considerably different refractive indices if the need arose. (e.g. carbon dioxide).

In this simple form, by heating the ground plane to produce a temperature gradient which in turn gave rise to natural movement within the gaseous medium, there was the facility to study various forms of fading recorded at the model receiver.

2.2 Auxiliary equipment

Perhaps the greatest virtue of the modelling technique as a whole is that facilities for measurement are generally greater than those that might be available in the full scale situation. This is particularly true in the case of the atmosphere.

In the original development of this laboratory model, facilities were provided for the measurement of most of the parameters relevant to any particular study that might be proposed. Temperature probes, in the form of very small bead thermometers were mounted into the ground plane for the purpose of measuring surface temperature at various strategic points. In addition, similar probes could be mounted on manipulators for the purpose of the simultaneous measurement of temperatures or variations in temperatures at any array of points in the enclosed 'atmospheric volume'. This particular facility is impossible in the real atmosphere.

Similar facilities were also provided, by the use of small hot-wire anemometers mounted on probes, for the measurement of velocities or velocity changes within the gaseous medium.

The changing density gradients of the air masses moving within the 'model atmosphere' were observed, at any point on the path, by means of a simple Schlieren interferometer whose principal axis was aligned normal to the centre line of the model path. For convenience in observation and recording, the image produced by the interferometer was projected on to a television camera for subsequent display on a suitable monitor. The inclusion of diffraction gratings into the interferometer system also allowed the development of a simple method (6) of obtaining instant refractive index profiles for all points along the entire length of the model path.

The Fig. 2 shows the actual form of the laboratory model with some of the auxilliary equipment. The basic path can be seen, without its boundaries, in the centre of the picture. The remaining components may be identified in the diagram given in the Fig. 3.

Additional facilities were also provided to introduce further mechanical disturbances, in the form of controlled surface winds etc., by adding low speed wind tunnel sections. An example of such a section can be seen in the Fig. 4 when added to the model to provide surface winds in a direction normal to the propagation path. Where the effects of surface winds are to be studied when the gaseous medium is not air it is necessary that the wind tunnel additions should be of the closed circuit type.

3. PROPAGATION STUDIES

3.1 Propagation over a 'smooth earth'

3.1.1 Fading due to an inhomogeneous medium

For those who are familiar with the behaviour of tropospheric radio systems, it is well known that a very large number of investigations have been carried out over a period of many years with the object of relating the many forms of fading that can occur on a given system with the various meteorological

phenomena that are frequently assumed to be directly associated with or responsible for certain mechanisms of propagation. This is particularly applicable to the trans-horizon system which is usually characterised by the continuous fading to which it is subjected. With few exceptions, where 'ducting' is assumed, trans-horizon propagation is deemed possible as a result of a 'scatter structure' conveniently contained within a 'common volume' at the intersection of the transmitter and receiver antenna beams. In reality, and in spite of the numerous elegant hypotheses, there is very little evidence to give conclusive support to these concepts. The instrumentation that would be necessary to provide the necessary indisputable evidence is a practical impossibility. Is it therefore, correct to assume that trans-horizon propagation is only possible by a 'scatter' mechanism, or even 'ducting', in all cases?

The type of fading that is frequently experienced on a tropospheric radio link is shown in the Fig. 5. Statistically this type of fading is often described as having a 'Rayleigh' distribution. It is also subject to considerable variation in both depth and frequency depending on the state of the atmosphere along the transmission path. The particular example shown was recorded, on the full scale link operating at a frequency of 900 M.Hs, during a period when the whole tropospheric medium along the path was devoid of any significant layering, according to meteorological soundings. Only light winds and a significant array of cumulo-nimbus clouds prevailed, to suggest considerable convection or 'thermaling'.

By setting up the model with the transmitter and receiver beams adjusted as shown in the Fig. 6. and heating the ground plane to give a temperature gradient of approximately - 6°/3000 \(\lambda\) or 1 k.m. a fading record, obtained from the output of the photo-multiplier 'receiver', was produced as shown in the Fig. 7. It should be noted that the model lapse rate was constructed to identify approximately with that published for the full scale path.

Whilst the fading record was being obtained on the model, photographs or interferograms of the inhomogeneous structures within the gaseous medium were obtained from the Schlieren interferometer. The Fig. 8a is an example taken of the instantaneous structure mid-point along the centre of the path. The horizontal extent of the image is approximately 10 wavelengths. A few seconds later this image changed to that shown in the Fig. 8b. The lower edge of the image is the ground plane of the model and the 'white' region represents a positive vertical density gradient. The continuous behaviour of these structures is such that there is continual movement with considerable change in both the extent and intensity of the density distributions. This activity is to be observed over the entire path length.

With the aid of temperature probes it can be easily shown that there is a very significant correlation between this activity and the fading obtained at the receiver. Furthermore, for a given lapse rate along the path it has also been shown by experiment that there is a preferred 'angle of shoot' for both transmitter and receiver antennas to give an 'optimum signal'. This is a condition which is always encountered in setting up a tropospheric radio system and not easily explained. During the course of these simple studies there was at no time any evidence of 'scattering' from turbulence occurring at an elevated region above the regions shown.

At this stage, it is worth noting that the Schlieren interferometer is capable of adjustment to show 'density gradient' distributions in either the vertical plane, as in the examples given, or the horisontal plane. A number of studies to investigate the relationship between fading and density distributions in the horisontal plane along the path yielded no correlation whatsoever.

The effects of external mechanical forces on simple natural circulation and convection - surface winds.

For a period of some seven years, continuous studies were made of the fading characteristics of trans-horizon transmissions on the UHF band. An example of one of these studies has been reported (7) for a system operating at a frequency of 629.25 MHz. For this study the full scale system was modelled. The fading characteristics that were obtained from the full scale system were simulated for the purpose of providing some indication of the causes of the differing types of fading that occurred. In recent years a similar study was made of the fading characteristics of transmissions made on the 900 MHz system upon which the model under discussion was based. In both cases, one of the most significant results that was obtained is the high correlation between surface wind velocity and fading rate or frequency. A second result, of perhaps equal significance, is that a high correlation was found to exist between the depth of fading (Rayleigh) and surface lapse rate. The rather more detailed studies carried out on the 900 MHz system produced a particularly significant correlation between surface wind velocity and fading rate for cases where the direction of the wind was normal to the propagation path. All of these results were simulated by the model and give some confirmation to results previously reported by other workers

- (8). Examples of these results are given in the Fig. 9 to show the "smoothed" power spectra of
- (a) fading characteristics obtained from a full scale link for different surface wind velocities,
- (b) fading characteristics obtained from the model of the full scale system for different stream or 'surface wind' velocities. It will be observed that by comparing the two sets of characteristics, which were originally matched through their spectral density distribution, yield a scale factor of 72 relating the real and model surface wind velocities. These results, for both the full scale and model systems, also give good agreement with the predictions of Tatarski but only in the cases of negligible wind velocities. A justification of the wind velocity scale factor and alternative proposals to Tatarski, and which apply to all conditions, are subjects of work to be published in the near future.

In order to introduce a 'surface wind' into the model path it is only necessary to add a simple low speed wind tunnel section to the path structure. An example of a 'through flow' tunnel mounted on this model has been shown in the Fig. 4. Care must, however, be taken in the construction of such a tunnel to ensure that it is capable of maintaining a lamina flow in the air stream. It is also important to ensure that the 'ground plane' of the tunnel does not generate a significant boundary layer turbulence, even at the very low stream velocities that will be required. This can be verified usually by introducing smoke filaments, generated from good quality cigars, into the working sections. The stream velocity and turbulence at any part of the propagation path are readily measured with the aid of sensitive hot-wire anemometer probes. Observation of the interferogram displayed during the introduction of a surface wind, gives clear indications of additional movement in the density distributions shown in the Fig. 8. Indeed there are two distinct effects which can be readily observed. Depending on the sensitivity of the interferometer, the region of greatest density gradient immediately above the ground plane reduces in its vertical extent and becomes more intense with increases in stream velocity. The broken 'bubble' or 'thermal' structures, seen in the Fig. 8b, are seen to move in the direction of the stream at very low velocities. As the stream velocity is increased these structures break up into smaller components until a critical velocity is reached destroying all evidence of a cellular structure. These conditions bring about a considerable change in the shape of the cross-section of the transmitted beam, with the attendant increases in the frequency of fading. All of these features can be readily recorded on cine-film.

3.1.3. Refractive index profiles

For many years refractive index profiles measured with the aid of a radio-refractometer, have been obtained for very confined regions of propagation paths which have been the subjects of intensive study. Whilst these profiles may be of considerable interest to the radio meteorologist, their value in indicating those properties of an atmospheric medium which are relevant to propagation is somewhat limited. In a medium which is subject to fairly rapid continual changes in both structure and refractive properties, it is only those structures which predominate for extended periods that have a marked influence on the shape and character of a profile which, by the nature of the method of measurement, takes a significant period of time to complete. Even then, because of the extreme practical difficulties, it is impossible to obtain sufficient additional evidence to support the interpretation of the irregularities in a given profile to confirm the existence of structures to which they are ascribed. The statistical evidence provided by the refractometer is similarly limited in its value since it can only apply to the point or points within a very large volume, from which it has been obtained.

However, the refractive index properties of a propagation medium are clearly of prime importance to propagation whatever mechanisms are considered. It may be suggested that given structures would be characterised only by the three dimensional distribution of refracture index properties within a given medium.

The model, already described, lends itself to the development of additional techniques which allow the evaluation of these refractive index properties by virtue of its physical size and the degree of control that can be exerted on the state of the gaseous medium. The refractive index properties of such a medium is readily measured, in terms of temperature only, by the use of simple probes. In the case where the medium experiences continual change, this method will have no more value than the refractometer. However, by introducing diffraction gratings into a Schlieren interferometer system it is possible to obtain instantaneous two dimensional information, which is recorded by photographic methods for any given plane and from which refractive index profiles may be produced. The principal of the modified or Moiré -Schlieren interferometer involves the displacement of the line structure in the image of a grating. relative to a reference, due to refraction. The value of the refractive index in a particular region is calculated from an evaluation of this displacement. The resolution of the method is, of course. dependant upon the line density of the gratings used. This technique was developed (6) for use on the model by adapting the existing Schlieren interferometer. An example of the profiles obtained by this method is given in the Fig. 10. It should be noted that these profiles apply to the same region, and for the same conditions, as that shown in the Fig. 8. It should also be noted that both horizontal and vertical dimensions are given in terms of the wavelength of the model transmitter to avoid the need of unnecessary scaling factors. The method has the advantage of allowing the simultaneous recording of both the gaseous structures and their refractive index properties for the purpose of comparison.

For the example given, with air as the gaseous medium, it can be seen that the irregularities in the profiles develop and change with horizontal distance along the propagation path. In the vertical direction, the majority of these irregularities relate to the region of high density gradient and are only shown to extend some $0.1 \times 10^6 \lambda$ altitude. This upper altitude limit, would be equivalent to 3.0 km. in the full scale system.

From the array of profiles given in the Fig. 10 the horisontal refractive index gradient profiles for various altitudes may be readily obtained. Similarly the use of a simple integration programme will

yield the corresponding profiles of refractive index. From the example given, these extend over the range 248.72 to 248.974 N. units.

If any one of these profiles was obtained in practice it is unlikely that the meteorological structure implied therefrom would be that shown in the Fig. 8a.

3.1.4. Radar sounding

In addition to the use of the radio-refractometer as an atmospheric probe, radar techniques have been employed as a further aid to provide additional information on the possible presence and extensions of atmospheric structures. The boundaries of these structures being marked by those regions where permittivity values experience significant change. There are many examples of the traces from vertical radar soundings that are available to describe various structures such as layering, turbulence, Kelvin-Helmholtz waves etc. Although the technique is extremely valuable in meteorological studies it is an extremely expensive aid in general studies relating to the atmosphere as a propagation medium.

Since this model technique has been developed to allow inhomogeneous structures along a given propagation path to be both observed and defined by two dimensional distributions of refractive index, temperature and velocity, the simulation of radar sounding was considered to complete the ensemble of instrumentation.

The Schlieren interferometer provides images of structures, within a region of interest, the limits of which are defined by those regions where the density gradient changes sign (positive or negative) This feature was utilised to provide, initially, the equivalent of a vertical sounding radar facility on the model.

Each frame produced by the C.C.T.V. monitor, displaying the interferogram, was sampled with a vertical 'window' which could be displaced to any position on one horizontal line. The total video signal contained within this vertical 'window' was then differentiated with respect to the 'y' or vertical plane to give uni-directional pulses at each point where the video signal changed level from black to white and vice versa. These pulses were then applied as Z - modulation on a separate oscilloscope which was provided with a synchronised time base in the 'y' direction only, as shown in the schematic diagram given in the Fig. 11. If the image on the C.R.O. is then recorded on film which has been transported across the face of the tube at a constant velocity, then a height-time recording typical of that obtained in practice is obtained. The Fig. 12 gives typical examples of these recordings.

In the Fig.12a. is given the type of record which, if obtained by a full scale radar system, might be interpreted as indicating a 'layer' structure which is perhaps subjected to 'shear' conditions and introducing a wave motion. This record was made during the time when the record in Fig. 8a was obtained and merely displays the ceiling of convective activity. The Fig. 12b, shows a more complex situation comprising convective circulation with a secondary activity, at a higher altitude, which includes a large bubble region.

By the combined alignment of the interferometer and the C.C.T.V. camera 'soundings' may be made at all angles between the horizontal and vertical planes.

3.2. Propagation over obstacles - the effects of the atmosphere.

In the planning of modern tropospheric radio systems the essential path loss calculations that are made may, on the basis of the general path geometry have to include estimates associated with natural obstacles. In many cases the classical two dimensional 'knife-edge' or 'cylinder' is used as a suitable equivalent for the purpose of such calculations without any regard for the third dimension profile of the obstacle or, indeed, the atmospheric structures immediately above the obstacle. In the modern systems

environment, the 'shielding' effect of a natural obstacle is of similar importance to the 'obstacle gain' that it may offer. Errors arising from the use of the classical obstacle models can be extremely serious and possibly very embarrassing. Such errors can also suffer considerable variation as a result of the influences of the atmospheric medium immediately above a given obstacle.

This aspect of propagation has been the subject of a number of studies (9,10) using modelling techniques. In at least two cases the results obtained have compared favourably with the results obtained in corresponding full scale systems.

3.2.1. Diffraction due to a 'conical' mountain

Field surveys previously carried out to estimate the total path loss for a particular system, involving the use of a mountain to provide 'obstacle gain', caused some concern in respect of the predictable performance of the system. This particular mountain, being of volcanic origin and having a classical conical shape, was chosen as a subject for study in a series of experiments on obstacles.

The development of this particular study included measurements of the diffraction field in the shadow of a classical right-circular cone of vertex equal to the height of the mountain, with and without a density gradient in the gaseous medium immediately above the surface. The two simple studies demonstrated quite clearly the effects of the properties of the gaseous medium.

The cone was then remodelled to a scaled model of the actual mountain. The previous measurement procedure for the cone was repeated for the more realistic model to provide sets of measurements relative to a similar but classical shape.

Although this work has been previously reported (9) it is worth comparing the two interesting distributions given in the Fig.13. The intensity levels displayed were measured by scanning the field in directions normal to the direction of propagation, in the shadow of a model mountain at a fixed distance from the mountain and at varying angles of depression from the horizontal, with reference to its peak. The Fig. 13a. shows the distribution with a simple density gradient in the air immediately above the surface of the model and which is different from that when the air density gradient is zero. The Fig. 13b. shows the changes that occur when the air density gradient distribution is subjected to distortion by the external forces of a surface wind. The changes in the density gradient distribution can be seen in the interferograms shown in the Fig.14.

For comparison with the 'knife-edge' losses that would be used in practice, both field distributions include the 'knife-edge' losses, calculated for the centre of the propagation path. Whilst this particular study has been compared very favourably with a similar study on a full scale system, the results indicate the influence of prevailing winds on the so-called obstacles gain of a mountainous obstacle.

3.2.2. Diffraction due to a 'ridge'

The few selected studies that have so far been described have been concerned with the modelling of fairly long distance trans-horizon systems, where, in addition to diffraction effects, 'scatter' mechanisms would normally be assured. By way of some contrast with these studies, a relatively short distance path of some 9 km. which included a low smooth grass-topped ridge at a distance of 1.2 km. in front of the transmitter antenna, was modelled for study. The system was operating at a frequency of 10 GHz and the transmitter beam width was 2.3 degrees with the axis aimed at the top of the ridge obstacle some 25 m. in elevation. The height of the transmitter antenna was set at 5 m. above ground level.

This particular system was chosen because path loss data was available from field surveys that had been carried out in regions of the receiver terminal and where the differences between the values calculated from

'knife-edge' or 'smooth cylinder' models were considered significant. The short length path was also a challenge to the physical limits that the modelling technique would allow. Considerable care was required in the production of an accurately contoured model surface, in aluminium, to represent the terrain in the region considered.

an extensive study was made of the field distribution over the whole surface of the model that was subject to the transmitted field in the shadow of the ridge and with a density gradient scaled in the air above the model. The maximum error between the model and full scale path surveys at all points of measurement never exceeded † 2dB. This result includes comparisons that were made between 'shallow fading' activity that was encountered in certain regions of the terrain. Whilst a full account of this work has been published recently (10), it is worth reporting here that the surveys carried out on the model drew attention to a relative high intensity field present at some altitude, equivalent to approximately 0.9 km. above the receiver terminal. Such a field reflected from the top of the ridge, was never considered to exist in the full scale system. The possible distribution in the vertical plane above the receiver terminal, illustrating this feature, is given in the Fig. 15a. A photograph of the field distribution in the vertical plane, normal to the direction of the transmitted beam, immediately above the receiver terminal is given in the Fig. 15b. From a pure diffraction and propagation point of view this feature is of little consequence. From an interference, or 'shielding', point of view it is of considerable significance.

4. Conclusions

The selection of simple laboratory studies that have been described in this report were chosen to demonstrate that some of the principal features of tropospheric transmissions can be successfully simulated in the laboratory. By controlling the properties of a 'laboratory atmosphere' above a scaled version of the path a real system, all of the common types of fading forms, together with such features as 'drop-outs' etc., can be readily simulated. In addition, by modulating the transmitted beam, the effects of fading on various forms of 'data' transmission can be readily studied under near real conditions without the use of a full size system.

There are of course obvious physical limitations to the minimum dimensions of a full scale system that may be modelled. The shorter wavelength of the laser source operating in the visible real region of the spectrum gives rise to rather high wavelength scaling factors for modelling the majority of full scale systems operating in the U.H.F. bands. A laser source operating in the longer wavelength region (e.g. infra-red) offers considerable advantages in respect of scaling factors but there are considerable difficulties associated with low-level detectors. Perhaps the greatest disadvantage of this particular technique is that, at the present time, there is no provision for the introduction of precipitation into the scaled 'atmosphere'. However, the majority of studies conducted on the model have been concerned with the various dynamic states of the propagation medium. Any precipitate forms in the real atmosphere are usually confined to the mesocellular structures in which they are created. Similar structures in the model could therefore be assumed to possess enhanced refracture properties if precipitate was present.

Modelling the true atmosphere completely is, of course, at least as difficult as solving any problems concerning its behaviour. However, by creating an inhomogeneous gaseous medium in the laboratory, and whose total volume is described in terms of the wavelength of the electro-magnetic wave propagated through the medium, some physical appreciation is obtained of those perturbations that are relevant to fading. If in reality, fading is a function of the variations and changes that might be occurring in those structures directly associated with the mechanisms of propagation, then the model would seem to suggest that these mechanisms are associated with the lower regions of the troposphere. It will be recalled that most of the studies described, were carried out in conjunction with studies on full scale systems. Because of the phenomena suggested by the model, the results obtained on the full scale system were all related to surface data with a high degree of success. As a result, it was possible in all cases to completely simulate the behaviour of the full system on the model. The simulation includes both total path loss and fading together with a visual recording of the air mass movements taking place within the medium. In spite of the construction of 'turbulence' in the region of the so-called 'common volume', even with a carbon dioxide medium, there was no evidence of significant 'scattering' from that region.

This evidence strongly suggests that the successful operation of most, if not all tropospheric radio systems is primarily due to refractive or dispersive structures in the lower regions of the troposphere.

For a tropospheric radio system to be commercially viable, a high percentage service time is a necessary requirement. For the vast majority of regions in the world this is only likely to be achieved if the mechanisms of propagation are primarily associated with atmospheric structures which exist for considerable

proportions of the day or year (e.g. in excess of 90%). Whilst there is little or no evidence to support the existence of 'scatterers' in the form of strata, 'blobs', etc., for any significant periods of time, there is always circulation at or near the earth's surface.

Acknowledgments: -

10.

TRIVEDI A.E. :

The author would like to record his appreciation of the help and co-operation that has been given by many friends and colleagues. Particular thanks are due to the Directors of Research of the following organisations: S.R.D.E. Christchurch, Hants, B.B.C. Research Establishment, Kingswood Warren, R.R.E., Malvern, Appleton Laboratory, and Standard Telecommunications Laboratories, Harlow. Thanks are also due to the Science Research Council for providing some financial assistance with this work. The patience of my secretary, Miss D. Miller, and her ability to interpret my writing is also greatly appreciated. Reference

AVSECS, D. : 1. 'Tourbillons thermoconvectifs dan l'air application a la meteorologie'. Publications Scientifiques et Techniques du Ministère de l'Air., 1939. Report No. 155. 2. BURROWS. W.G.: Some Experimental studies of the effects of air mass movements in the troposphere on U.H.F. transmissions by the use of a laboratory model'. Proceeds of A.G.A.R.D./E.P.C. Symposium, October 1967, Ankara, Turkey. BOOKER H.G. AND 3. GORDON W.E. : A theory of radio scattering in the Troposphere. Proc. I.R.E., April 1950. FRIIS H.T., CRAWFORD A.B. AND HOGG D.C.: A reflection theory for propagation beyond the horizon. B.S.T.J., Vol. 36. May 1957. BOOKER H.G. and WALKINSHAW W .: and diffraction. Met. factors in Radio Wave propagation Phys. Soc. London. April 1946. The mode theory of tropospheric refraction and its relation to waveguides PASSIPOULARIDES D.P. : 6. D.I.C. Thesis. Imperial College 1975. 'A study of tropospheric air mass rovements on the fading characteristics 7. BURROWS W.G. : of U.H.F. transmission by the use of a laboratory model'. Proc. A.G.A.R.D./E.P.S. Symposium 1970. Dusseldorf. RIDER G.C. : 8. Some tropospheric scatter propagation measurements and test of aerial siting conditions at 858 Mc/s Proc. of the I.E.E., Vol. 105, Part B. Suppl.8, pp. 143-152 January 1958. 9. BURROWS W.G. : Radio Wave Diffraction due to a Mountain of Volcanic Origin. RIDLER J.D. : Proc. A.G.A.R.D./E.P.S. Symposium May 1973 Rome.

M. Phil. Thesis London University 1976.

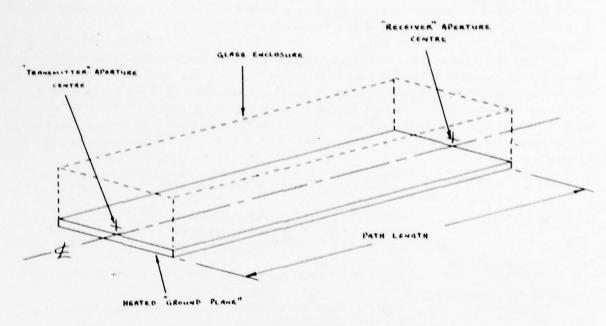


Fig. 1 Essential features of the model path.

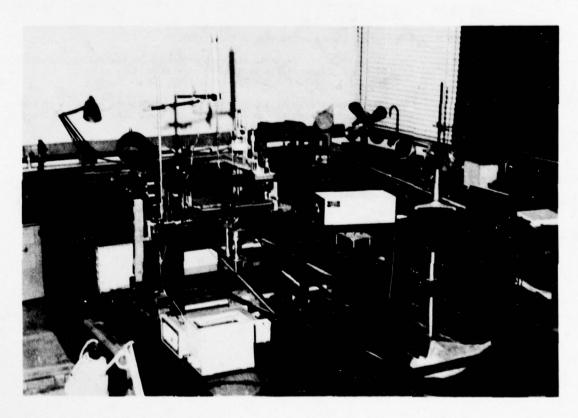


Fig. 2 Actual laboratory model (model path in centre) with auxillary equipment.

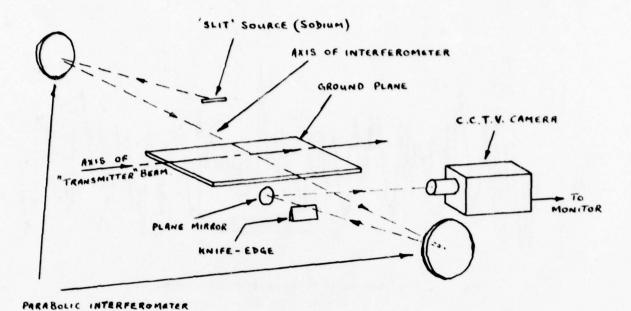


Fig. 3 Layout of interferometer relative to model path.

MIRRORS

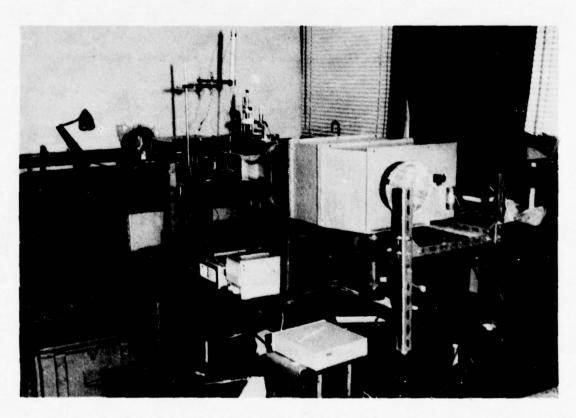


Fig. 4 Laboratory model with low speed wind tunnel section added.

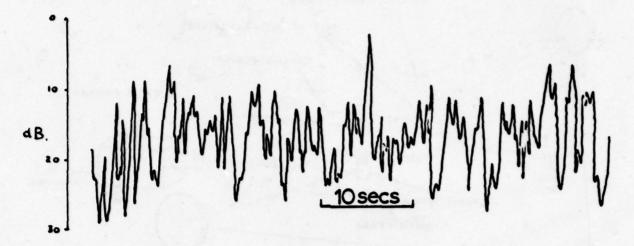


Fig. 5 Short term sample of fading on 900 M.Hz. system.

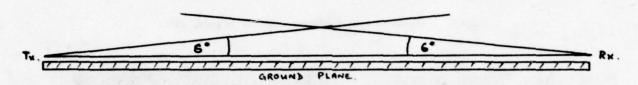


Fig. 6 "Transmitter" and "receiver" antenna attitudes above model ground plane.

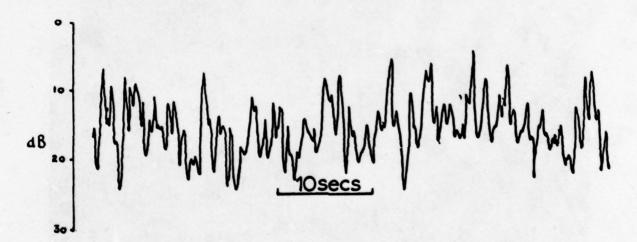


Fig. 7 Short term sample of fading on model of 900 MHs. system.

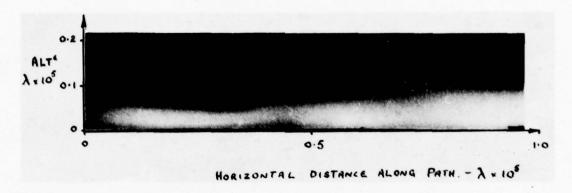


Fig. 8a. Interferogram of air density distribution above the ground plane along the centre of path and about the mid-point.

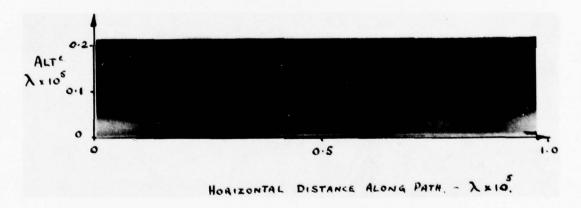


Fig. 8b. Second interferogram showing a clear 'bubble' or cell structure.

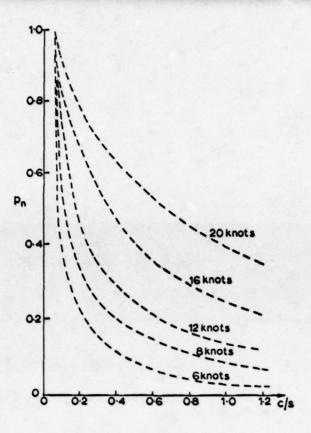


Fig. 9a. Smoothed spectral density distributors for fading samples obtained, from a full scale radio system, for different surface wind velocities.

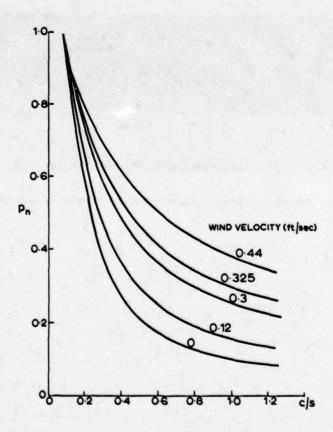
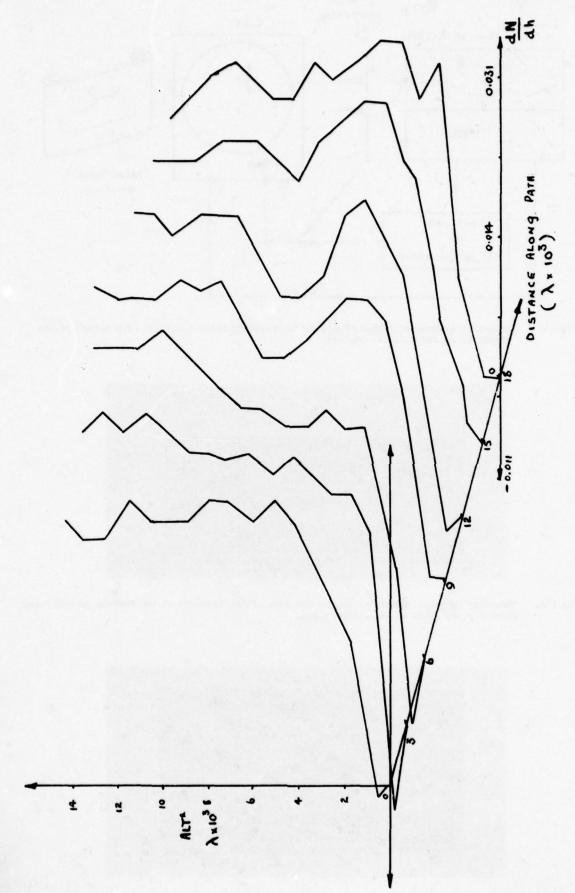


Fig. 9b. Smoothed spectral density distributions for fading samples obtained, from a scaled model of a radio system, for different surface wind velocities.



'Pamily' of instantaneous refractive index gradient profiles along the centre line of the model path. F16.10

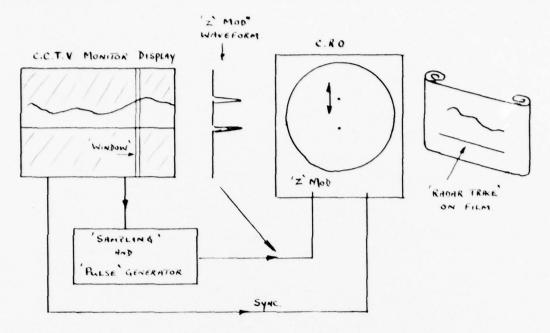


Fig.11 Schematic diagram of method of obtaining 'vertical radar sounding' from interferogram displayed on the C.C.T.V. monitor.

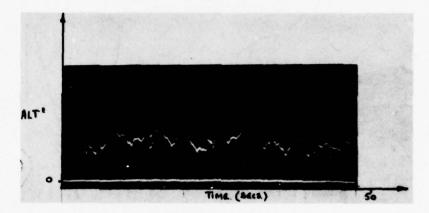


Fig. 12a. 'Sounding' showing variations in the altitude of the boundary of the surface circulation, above a given point on the ground plane.

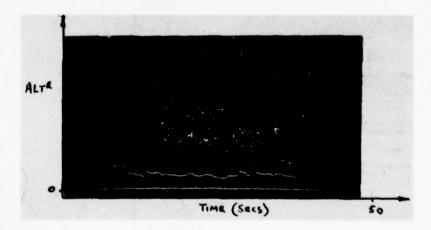


Fig. 12b. 'Sounding' showing a more complex structure, including the presence of 'bubbles' or 'plumes'.

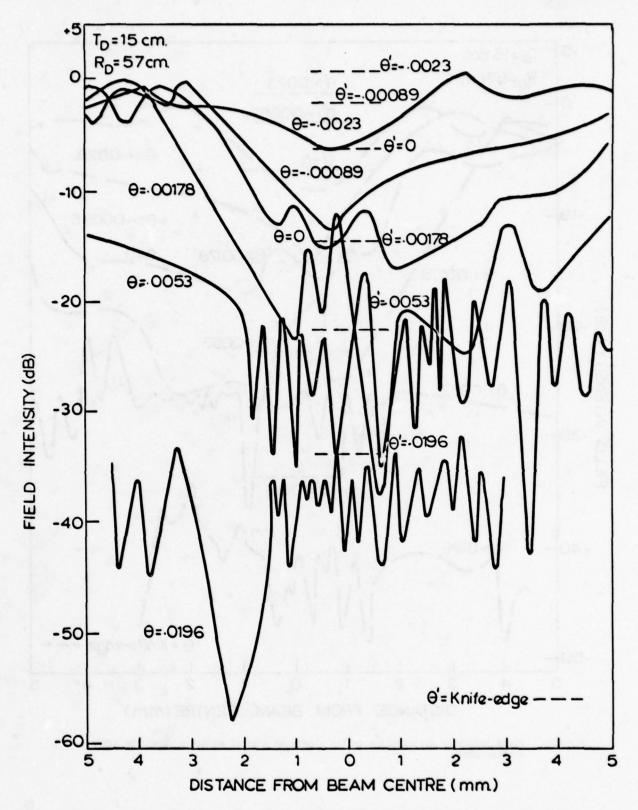
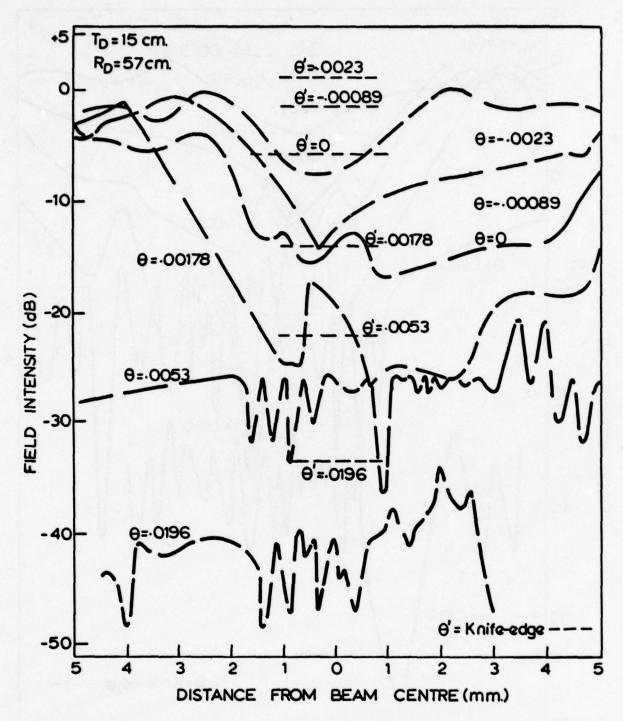


Fig.13a. Field intensity distribution in the shadow of a model mountain supporting a simple 'atmosphere'.



Pig.13b. Field intensity distribution in the shadow of a model mountain under the effects of a surface wind.

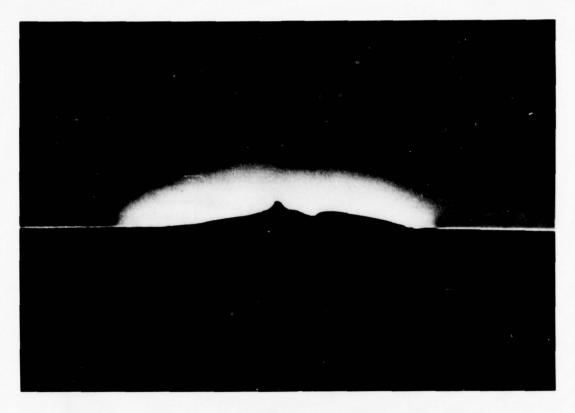


Fig. 14a. Simple atmospheric density distribution above model mountain.



Fig.14b. 'Wedge' - shaped density distribution resulting from 'surface wind'.

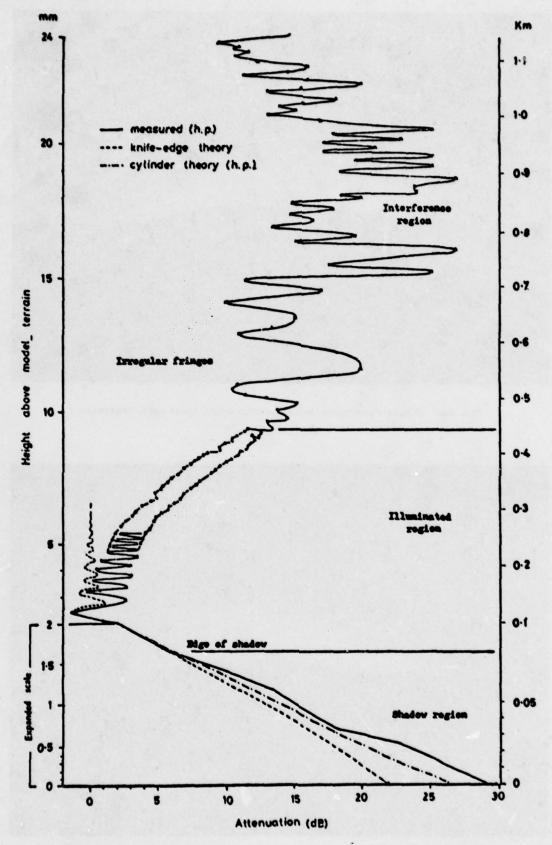


Fig. 15a. Vertical field intensity distribution at receiver terminal in the shadow of a low ridge. (ref. receiver antenna centre).



Fig.15b. Photograph of the two dimensional distribution of the field in (a).

TROPOSPHERIC REFLECTION OF DIFFERENTLY POLARIZED TRANSIENT SIGNALS

K. J. Langenberg Fachbereich 12.2 der Universität des Saarlandes Fachrichtung Elektrotechnik D-660O Saarbrücken Fed. Rep. Germany

SUMMARY

The evaporation duct model used is that of Kahan and Eckart consisting of a discontinuous drop of the otherwise constant relative permittivity at the upper duct boundary. The earth is assumed to be a perfect conductor and ideally plane. We determine the electrical field strength exactly at some fixed point within the duct layer having chosen a certain polarization of the primary source whose moment is allowed to vary arbitrarily in time. The method used for solution is essentially based on the application of two functional transforms and Cagniard's method for their inversion.

Physically, the applicability of Cagniard's idea is based on the evaluation of the field in a series of image sources of the primary source. The field strengths of the image sources combine to the total field strength with different signs for the two polarizations apart from the fact that they are of different mathematical structure. Hence we can give a physical intuitive description of the polarization dependence of the time history of the electrical field strength. Furthermore a number of numerical examples clearly show the different effect of the evaporation duct on differently polarized carrier modulated pulses. It turns out that for certain values of the carrier frequency the evaporation duct causes different arrival times for differently polarized pulses, which is explained through their different modal cut-off frequencies.

1. INTRODUCTION

Radio navigation, radar target identification and telecommunication systems are seriously affected by modification and distortion of the electromagnetic waves during their propagation. Especially, pulsed signals of nano-second durations may be strongly distorted by the evaporation duct, which is defined as a shallow simple surface duct existing over any water surface of reasonable size, in particular the sea, for a large proportion of the time (Rotheram, 1974).

A recent paper of the author (Langenberg, 1974) treated this problem in detail: a theory for the electromagnetic pulse propagation in a simple model (Kahan and Eckart, 1950) of the evaporation duct has been given for the source being a vertical magnetic dipole, hence horizontal polarization has been assumed in this paper. Yet in experiment the evaporation duct shows a polarization dependence for time harmonic signals (Jeske, personal communication, 1975); therefore the Nato Advanced Study Institute Workshop at Goslar (Fed. Rep. Germany) (Jeske, 1976) stimulated the investigation for transients. The present paper extends the above-mentioned theory to the case of a vertical electric dipole, i.e. vertical polarization. Discussion of the results occurs in comparison with those obtained for the horizontal polarization case (Finkler and Langenberg, 1975).

FORMULATION OF THE PROBLEM

Fig. 1 shows the duct model of Kahan and Eckart. A dielectric layer is assumed of relative permittivity \mathcal{E}_{\star} overlying an infinitely conducting plane earth, which is confined by the plane z=0 of a rectangular coordinate system (x,y,z). At the height h this permittivity decreases discontinuously to the value \mathcal{E}_{1} . The relative permeability μ is assumed to be constant throughout the half-space z>0. We refer to the layer as medium 1 and to the half-space z>h as medium 2. The fields which belong to the two media are marked by corresponding indices. The source of the field is assumed to be a vertical electric dipole in medium 1 at the point x=y=0, $z=\frac{c}{3}>0$ whose moment is given by $\vec{p}_{e}=\left\{0;0;F(t)\delta(x,y,z-\frac{c}{3})\right\}$, t being the time variable and δ the three-dimensional δ -distribution. Regarding F(t) we make the causality assumption $F(t)\equiv 0$ for $t\leqslant 0$. This guarantees the uniqueness of our solution. Physically, dF(t)/dt describes the time variation of the current, which flows in an equivalent short linear antenna, whose transient radiation field is not very different from the one radiated by an ideal electric dipole (Langenberg and Rech, 1976).

3. METHOD OF SOLUTION

The calculations exactly follow the flow-chart of Fig. 2.

The starting point is the wave equation for the electrical field strength $\tilde{E}(x,y,z,t)$ in the two media

$$\Delta \vec{E}^{(i)} = \frac{1}{\sqrt{i}} \frac{\partial^2 \vec{E}^{(i)}}{\partial t^2} = \begin{cases} 0 & \text{for } i=2 \\ \mu_0 \frac{d^2 F(t)}{dt^2} \delta(x, y, z-\xi) \vec{e}_z - \frac{F(t)}{\varepsilon_0 \varepsilon_A} \nabla \frac{\partial}{\partial z} \delta(x, y, z-\xi) & \text{for } i=4 \end{cases}$$
(1)

where v_i denotes the phase velocity of medium i; \dot{e}_z is a unit-vector in z-direction.

The first step is the application of a Laplace transform with respect to time, which yields a three-dimensional Helmholtz equation in the spatial coordinates for the Laplace transformed field strength $\tilde{\mathbf{e}}^{(\zeta)}$ (x,y,z,s). This step uses initial conditions: electric field strength being zero for t equal to zero. The next step is a representation of $\tilde{\mathbf{e}}^{(\zeta)}$ (x,y,z,s) as a two-dimensional inverse Fourier integral

$$\vec{e}^{(i)}(x,y,z,s) = \frac{s^2}{4\pi^2} \iint_{-\infty}^{+\infty+\infty} \underbrace{\psi^{(i)}(x,\beta,z,s)}_{=\infty} e^{is\alpha x + js\beta y} d\alpha d\beta$$
 (2)

yielding a one-dimensional Helmholtz equation in the height coordinate z for the Fourier transformed field

$$\left(\frac{\partial^{2}}{\partial z^{2}} - y_{i}^{2} s^{2}\right) \stackrel{?}{\cancel{\psi}} \stackrel{(i)}{(\alpha_{i} \beta_{i} z, s)} = \begin{cases}
0 & \text{for } i-2 \\
f(s) \left\{ -\frac{is}{\varepsilon_{i} \varepsilon_{i}} \left(\alpha \stackrel{?}{e}_{x} + \beta \stackrel{?}{e}_{y} \right) \frac{\partial}{\partial z} \delta(z-\xi) \right. \\
\left. + \left[\mu_{o} s^{2} \delta(z-\xi) - \frac{1}{\varepsilon_{o} \varepsilon_{i}} \frac{\partial^{2}}{\partial z^{2}} \delta(z-\xi) \right] \stackrel{?}{\cancel{e}_{z}} \right\} \quad \text{for } i=1$$

where $j = \sqrt{-1}$; \vec{e}_x and \vec{e}_y are unit-vectors in x- and y-direction, respectively. The function f(s) denotes the Laplace transformed excitation function F(t) and

$$\chi_{i} = \left(\alpha^{2} + \beta^{2} + v_{i}^{-2} \right)^{4/2} \tag{4}$$

with Rey; > 0; Re means real part.

The solution of the ordinary differential equation (3) can be written down immediately in terms of unknown integration constants. These constants can be determined as solution of an algebraic system of equations resulting from the boundary conditions for the electromagnetic field on the earth's surface and at the upper duct boundary. The condition of the finiteness of the field at infinity corresponds to the Laplace transformed initial conditions and is also used for the determination of the above-mentioned constants.

Thus results an integral representation of the Laplace transform of the electric field strength in terms of two-dimensional inverse Fourier integrals, i.e. for the transformed z-component:

$$e_{\frac{1}{2}}^{ch} = \frac{s^{3} \int_{S}(s)}{8\pi^{2} \epsilon_{0} \epsilon_{1}} \iint_{-\infty}^{+\infty} (\alpha^{2} + \beta^{2}) \left\{ \frac{e^{-s y_{1}(z-\xi)}}{y_{1}} + \frac{e^{-s y_{1}(\xi+z)} \left[1 + \overline{c}_{Az} e^{-2s y_{1}(k-\xi)}\right]}{y_{1} \left(1 - \overline{c}_{Az} e^{-2s y_{1}k}\right)} + \frac{\overline{c}_{Az} e^{-s y_{1}(2k-\xi-z)} \left(1 + \overline{c}_{Az} e^{-2s y_{1}k}\right)}{y_{1} \left(1 - \overline{c}_{Az} e^{-2s y_{1}k}\right)} e^{-iskx + is\beta y} d\alpha d\beta$$
(5)

with the reflection coefficient at the upper duct boundary

$$\overline{c}_{A2} = \frac{v_{A}^{2} y_{A} - v_{2}^{2} y_{2}}{v_{A}^{2} y_{A} + v_{2}^{2} y_{2}}$$
 (6)

The transformed x- and y-components of the vertical electric dipole's field are of a similar structure as $e_2^{(1)}$; they are not given here since we restrict our attention to the vertically polarized component. The same holds for all field components outside the duct layer. The difference of the field representation (5) compared with the corresponding one for the y-component in the horizontal polarization case (Finkler and Langenberg, 1975), that is to say the case of the magnetic dipole, is mainly due to the different structure of the pertinent reflection coefficients c_{42} for horizontal polarization or \bar{c}_{42} for vertical polarization, where

$$C_{42} = \frac{\chi_4 - \chi_2}{\chi_4 + \chi_2} \tag{7}$$

To come back to the original space-time-domain we use the method of Cagniard in the modification of de Hoop, which can be extended to our present problem where total reflection phenomena occur (Langenberg, 1974). This method works if we first choose $F(t) = 1/2 t^2$, yielding $f(s) = s^{-1}$, and if we secondly use a series expansion of the integrands of our integral representation (5). Physically, this series expansion yields a representation of the solution in terms of the images of the primary source, which result from the successive reflections at the earth's surface and at the upper duct boundary, the latter always yielding a multiplication with the reflection coefficient \tilde{c}_4 . Fig. 3 indicates the difference between the two polarizations. The signal from the primary source Q_p within the duct layer, that is to say the φ -component or z-component of the electric field strength is normalized to arrive with the amplitude one for both polarizations at the point of observation, which is also situated within the layer. Then the signal from its direct image at the upper duct boundary - Q_{04} - arrives with the amplitude c_{41} or \tilde{c}_{42} , respectively, since it is multiplied with the pertinent reflection coefficient at this boundary. The next part of the signal to arrive is the one from the image source Q_{04} , the image of Q_p at the perfectly conducting earth. Hence the amplitude is again of the absolute value one, but there is a change of sign for the horizontal polarization case. This change of sign is maintained if Q_{04} is reflected at the upper duct boundary resulting in Q_{02} and the amplitudes $-c_{22}$ and $+c_{32}$. On the other hand, a new change of sign occurs in the reflection of Q_{04} at the perfectly conducting earth yielding Q_{03} and again $-c_{32}$ and c_{31} . This procedure is continued resulting in image source groups of equal and opposite signs for the two polarizations. Naturally higher order groups occur with appropriate powers of the reflection coeffici

4. EXACT ANALYTICAL EXPRESSIONS FOR THE TIME DOMAIN ELECTRIC FIELD STRENGTH WITHIN THE DUCT LAYER

The result of the application of Cagniard's idea to equation (5) is the representation of $e_a^{(4)}$ (x,y,z,s) as an explicit Laplace integral. So one is able to read off the solution in the time domain for the corresponding time dependent function $E_2^{(4)}$ (x,y,z,t) as

$$E_{\frac{1}{2}}(x,y,\xi,t) = \begin{cases} 0 & \text{for } t < \tau_{min} \\ E_{\frac{1}{2}}(x,y,\xi,t) + \sum_{m=0}^{\infty} \left[u_m(x,y,\xi,t) + u_m(x,y,\xi,t) + u_m(x,y,\xi,t) + u_m(x,y,\xi,t) \right] \\ + u_m(x,y,\xi,t) + u_m(x,y,\xi,t) \right] & \text{for } t > \tau_{min} \end{cases}$$
(8)

where

with R_0 being the distance primary source - point of observation; hence $R_0 = \left[\frac{\lambda}{1+(\lambda-S)^2}\right]^{1/2}$ where r denotes the horizontal transmitter-receiver-distance; $\tau_m^{(i)}$ is given by equation (12).

 $E_2^{\text{prim}}(x,y,z,t)$ is the primary field of a vertical Hertzian dipole in free space whose moment is time dependent through $F(t) = 1/2 t^2$:

$$E_{2}^{\text{prim}} = \frac{1}{8\pi\epsilon_{0}\epsilon_{4}R_{0}v_{2}^{2}} \left[\left(2\cos^{2}\theta_{0} - \sin^{2}\theta_{0}\right) \left(\frac{t}{t_{0}}\right)^{2} - \left(2\cos^{2}\theta_{0} + \sin^{2}\theta_{0}\right) \right]$$
(10)

with the arrival time $t_0 = R_0 / v_4$ of the primary field; v_0^{ζ} is the polar angle of the direction dipole - point of observation.

The image sources may be divided into four types, the function u_n (x,y,z,t) representing that part of the field which is due to the n-th image source Q_{n_i} of the type i. It is composed of different functions whether or not the point of observation is in the region below or beyond total reflection:

$$u_{n}^{(i)}(x,y,z,t) = \begin{cases} 0 & \text{for } t < \frac{R^{(i)}}{n}/o, \\ h_{n}^{(i)}(x,y,z,t) & \text{for } t > \frac{R^{(i)}}{n}/o, \end{cases} \quad \text{for } t < \frac{S}{n}\sqrt{\frac{S}{A-S}} \\ 0 & \text{for } t < \frac{T^{(i)}}{n} \\ 1 = 0,4,2, \\ i = 4,2,3,4 \end{cases} \quad \begin{cases} f_{n}^{(i)}(x,y,z,t) & \text{for } T_{n}^{(i)} < t < \frac{R^{(i)}}{n}/o, \end{cases} \quad \text{for } \frac{S}{n}\sqrt{\frac{S}{A-S}} \leq 4 < \infty \end{cases}$$

$$\begin{cases} f_{n}^{(i)}(x,y,z,t) + g_{n}^{(i)}(x,y,z,t) & \text{for } R^{(i)}_{n}/o, < t < T^{(i)}_{n} \\ h_{n}^{(i)}(x,y,z,t) & \text{for } t > T^{(i)}_{n} \end{cases}$$

$$\begin{cases} f_{n}^{(i)}(x,y,z,t) + g_{n}^{(i)}(x,y,z,t) & \text{for } R^{(i)}_{n}/o, < t < T^{(i)}_{n} \\ h_{n}^{(i)}(x,y,z,t) & \text{for } t > T^{(i)}_{n} \end{cases}$$

where

$$\tau_{m}^{(i)} = (4-8)^{4/2} \frac{R_{n}^{(i)}}{v_{4}} \left| \cos \theta_{n}^{(i)} \right| + \frac{R_{n}^{(i)}}{v_{2}} \sin \theta_{n}^{(i)}$$
 (12)

and

$$\tau_{m}^{(G)} = \frac{R_{m}^{(G)}}{v_{4} \left(\cos \vartheta_{m}^{(G)}\right)} \left(a - \vartheta\right)^{4/2}$$
(13)

with $\delta = \frac{\epsilon_1}{\epsilon_4}$. $R_m^{(i)}$ and $\theta_m^{(i)}$ are polar coordinates with respect to the image source Q_{mi} , hence

$$R_{m}^{(i)} = (+^{2} + g_{m}^{(i)2})^{1/2}, \quad |\cos \theta_{m}^{(i)}| = S_{m}^{(i)}/R_{m}^{(i)}$$
 (14)

with

$$S_{n}^{(4)} = 2h(n+4) - S - 2$$

$$S_{n}^{(4)} = 2h(n+4) + S - 2$$

$$S_{n}^{(4)} = 2h(n+4) - S - 2$$

$$S_{n}^{(4)} = 2h + S + 2$$
(15)

The functions $h_n^{(i)}$ (x,y,z,t) denote spherical wave fronts originating from the image source Q_{n_i} , whereas $f_n^{(i)}$ (x,y,z,t) and $g_n^{(i)}$ (x,y,z,t) refer to conical wave fronts of the lateral waves, which always occur in connection with total reflection phenomena.

The theory yields in detail

$$\frac{f(i)}{f(i)} = \begin{cases}
0 & \text{for } t < R_n / v_A \\
\frac{1}{2\pi^2 \epsilon_0 \epsilon_s R_n^{(i)}} \int_{0}^{\infty} \text{Re} \left[\left[u^2(t, \psi) + q^2(t, \psi) \right] \tilde{c}_{12}(t, \psi) d\psi & \text{for } t > R_n^{(i)} / v_A \\
\frac{1}{2\pi^2 \epsilon_0 \epsilon_s R_n^{(i)}} \int_{0}^{\infty} \text{Re} \left[\left[u^2(t, \psi) + q^2(t, \psi) \right] \tilde{c}_{12}(t, \psi) d\psi & \text{for } t > R_n^{(i)} / v_A
\end{cases}$$
(16)

with

$$\overline{c}_{42} = \frac{\delta \sqrt{u^2 + q^2 + \upsilon_{4}^{-2}} - \sqrt{u^2 + q^2 + \upsilon_{4}^{-2}}}{\delta \sqrt{u^2 + q^2 + \upsilon_{4}^{-2}} + \sqrt{u^2 + q^2 + \upsilon_{4}^{-2}}}$$
(17)

and

$$q = \left(\frac{t^2}{R^{(1)2}} - \frac{4}{\sigma^2}\right)^{4/2} \sin \psi \tag{18}$$

$$u = i \frac{t \sin \theta_n^{(i)}}{R_n^{(i)}} + \left(\frac{t^2}{R_n^{(i)2}} - \frac{1}{\theta_n^2}\right)^{1/2} \cos \psi \left[\cos \theta_n^{(i)}\right]$$
(19)

Furthermore

$$\int_{0}^{(i)} \int_{0}^{\infty} \int_{0}^{\infty} \int_{0}^{\infty} \frac{\pi/2}{\left[\frac{q_{2}(t)}{2\pi^{2}} \frac{1}{66} \frac{1}{6} \frac{\pi}{6} \frac{1}{6} \frac{\pi}{6} \frac{1}{6} \frac{\pi}{6} \frac{$$

with C = 0 for n = 0 and i = 4, C = 1 for all other values of n and i, respectively. In (20) and (21) we have

$$q_{2}(t) = \left\{ \frac{1}{\sin^{2} \theta_{n}^{(i)}} \left[\frac{t}{R_{n}^{(i)}} - \left(\frac{1}{\theta_{n}^{2}} - \frac{1}{\theta_{n}^{2}} \right)^{1/2} |\cos \theta_{n}^{(i)}| \right]^{2} - \frac{1}{\theta_{n}^{2}} \right\}^{1/2}$$
(22)

$$q_{n}(t) = \left(\frac{t^{2}}{R_{n}^{(i)2}} - \frac{1}{\vartheta_{4}^{2}}\right)^{1/2}$$
(23)

$$\bar{c}_{A2}(t,\psi) = \frac{\delta \sqrt{q^2 - u^2 + v_A^{-1}} - \sqrt{\chi u^2 - q^2 - v_A^{-1}}}{\delta \sqrt{q^2 - u^2 + v_A^{-1}} + \sqrt{\chi u^2 - q^2 - v_A^{-2}}}$$
(24)

with

$$u = \frac{t \sin 9_n^{(i)}}{R_n^{(i)}} + |\cos 9_n^{(i)}| \left(q^2 + \frac{q}{9_n^2} + \frac{t^2}{R_n^{(i)2}}\right)^{1/2}$$
(25)

and

$$q = q_2(t) \sin \psi \tag{26}$$

in (20) and

$$q = \left\{ q_{n}^{2}(t) + \left[q_{n}^{2}(t) - q_{n}^{2}(t) \right] \sin^{2} \psi \right\}^{1/2}$$
 (27)

in (21) .

We can describe our present result as follows: it is the response of the communication channel "duct layer over sea surface" to the excitation function $F(t) = 1/2 t^2$ for vertical polarization at some fixed but arbitrary situation of the point of observation

in the duct layer.

An arbitrary time varying antenna current now yields the convolution of this response with the third derivative of F(t) plus certain inverse Laplace transforms (Finkler and Langenberg, 1975), which vanish if we choose F(t) = $(A - \exp(-\alpha t))^3 \hat{\Gamma}(t)$, F(t) being another arbitrary time function. The convolution integral has been numerically evaluated by means of the fast Fourier transform for the case $\hat{F}(t) = \exp(\frac{i}{3}\omega_o t)$, which corresponds to a cw antenna current with circular carrier frequency ω_o being switched on according to a rise time proportional to a^{-4} .

DISCUSSION OF THE NUMERICAL RESULTS

Fig. 4 a-f shows a series of numerical examples: the 1/2 t -responses of the electrical field strength are plotted against time for both polarizations for several transmitter-receiver-distances. The duct height has been chosen to be h = 20 m, the relative permittivities \mathcal{E}_i and \mathcal{E}_1 have the values 1.0004 and 1, respectively; transmitter and receiver height are equal to 15 m. In each case a-f the upper curve describes horizontal polarization - φ -component of the electrical field strength of a vertical magnetic dipole - and the lower curve represents vertical polarization - z-component of the electrical field strength of a vertical electric dipole.

The case r = 400 m - the lowest distance - clearly shows the arrival of the spherical wave front originating from the primary source at t-t_C = 0 and the corresponding ones of the image sources Q_{04} , Q_{04} and Q_{02} , Q_{o3} respectively, at later times, the amplitudes from higher order image sources being highly attenuated. The image source Q_{04} results from direct reflection of the primary source at the perfectly conducting earth (see Fig. 3); hence, in the case of the magnetic dipole the wave front due to this source cancels out the one from the primary source, whereas in the case of the electric dipole the two amplitudes add together. It should also be noted that Q_{02} and Q_{e3} occur with different signs for both polarizations.

The transmitter-receiver-distance of 1000 m is beyond the total reflection distance of the image source $Q_{\rm od}$ (Langenberg, 1974); hence, it shows the lateral wave front before the arrival time of the spherical wave front due to $Q_{\rm od}$. This lateral wave front travels at the upper duct boundary with the phase velocity of the half space above the layer, which is greater than the one inside the layer, resulting in very early arrival times, i.e. earlier than the primary wave fornt, as can be seen for the distance of 2600 m. This distance also shows that $Q_{\rm od}$ and $Q_{\rm od}$ have undergone total reflection. Increasing the transmitter-receiver-distance leads to very complex time histories of the field responses since more and more image sources have to be taken into account (see the cases 4000 m and 5000 m). The case of 5000 m shows another interesting detail: even the lateral fronts combine - naturally - with different signs to the total field for both polarizations, a fact which is rediscovered for the already very large distance of r = 15000 m, i.e. the modal so-called space-wave (Langenberg, 1971) is of a very different structure for either horizontal or vertical polarization. That is indeed the only essential difference for large distances: it is not very interesting to note the different signs of the peaks of the spherical wave fronts originating from a large number of image sources and arriving closely together.

Fig. 5 a-1 shows the numerical results after convolution of our 1/2 t² -field response with the third derivative of F(t), where we refer to the specially chosen F(t) = $(A-\exp(-\alpha t))^5\exp(j\omega_0 t)$ with a = $3\cdot 10^8 \, \mathrm{s}^{-4}$; hence, the curves show the time histories of the absolute value of the electrical field components for horizontal and vertical (dashed curves) polarization if a sinusoidal excitation is swithed on according to a smooth unit step function. The amplitudes for both polarizations should not be compared because they are normalized to their maximum value. Parameter of the curves is the frequency $\omega_0/2\pi$ in MHz.

For the sake of clearness, we repeat the discussion of the $\mathcal G$ -component whose characteristic behavior can be explained under modal propagation aspects (Finkler and Langenberg, 1975).

Beginning with 25 MHz, which is small compared to the cut-off frequency of the first mode, we see, that the carrier frequency is not absolutely cut off, because the received signal becomes constant for large times as well as the envelop of the input signal. Nevertheless the transmitted signal suffers great distortion for such low carrier frequencies; for example, the peaks due to the different image sources can still be distinguished. The possibility of distinguishing these sources vanishes with increasing carrier frequency (100 MHz) and the amplitude of the carrier frequency itself becomes more pronounced. The value of 180 MHz is just below the cut-off frequency of the first mode, resulting in a received signal which already is very similar to the input signal. But the distortion increases once again if the carrier frequency is again increased; if it equals 300 MHz, the maximum of the emitted signal is in the neighborhood of the first mode's frequency response maximum, so that the steep increase of this frequency response at the cut-off frequency affects the signal considerably. A small increase of the carrier frequency (320 MHz, 330 MHz) shifts the signal's spectrum into that part of the frequency response, where it is slowly varying, so that the distortion of the received signal is reduced. At 450 MHz, the distortion of the signal is nearly negligible; the only indication that it propagated through the duct is the arrival time due to the lateral waves. A further increase of the carrier frequency yields the influence of the higher order modes. The value of 500 MHz is just below the cut-off frequency of the second mode, which affects the leading tail of the received signal once again. At 1100 MHz we find ourselves in the third mode's maximum; the

result is similar to the case of 300 MHz. Finally, at 2 GHz, there is absolutely no influence of the duct on the received signal; even the arrival time coincides with the free space arrival time.

If vertical polarization is concerned, the cut-off frequencies are obviously different from the corresponding horizontal polarization ones, they are higher. Therefore the characteristic structure of the received signal in the neighborhood of cut-off frequencies occurs at other values of the circular frequency leading at certain values of ω_c to an effect, which could be interpreted as if differently polarized signals would have different travel times from the source to the point of observation (180 - 500 MHz). This effect decreases with decreasing distance, since the cut-off frequencies then loose significance (Finkler and Langenberg, 1975).

CONCLUDING REMARKS

Summarizing the results we state that the transient behavior of evaporation ducts differs in a characteristic manner concerning horizontal or vertical polarization, which can be physically explained either on the base of image sources or with the aid of modal cut-off frequencies. Furthermore distance measuring can lead to somewhat erroneous results whether the "wrong" polarization is used since it may occur that both polarizations lead to different travel times.

REFERENCES

FINKLER, H. and LANGENBERG, K.J., 1975, "Das Einschwingverhalten der elektrischen Feldstärke in einem atmosphärischen Bodenwellenleiter bei beliebiger Empfängerentfernung in Abhängigkeit von der Trägerfrequenz", AEU, vol. 29, pp. 37-46

JESKE, H.E.G. (ed.), 1976, Atmospheric Effects on Radar Target Identification and Imaging. Dordrecht: D. Reidel

KAHAN, T. and ECKART, G., 1950, "Théorie de la propagation des ondes éléctromagnétiques dans le guide d'onde atmosphérique", Ann. Physique, vol. 5, pp. 641-705

LANGENBERG, K.J., 1971, "Propagation of an electromagnetic pulse in a duct between ground and atmospheric layer", AGARD Conf. Proc. on Tropospheric Radio Wave Propagation, vol. 70, pp. 17/1-17/12

LANGENBERG, K.J., 1974, "The transient response of a dielectric layer", Appl. Phys., vol. 3, pp. 179-188

LANGENBERG, K.J. and RECH, K.D., 1976, "Transient fields of radiating structures", Proc. 6th European Microwave Conference, pp. 86-90

ROTHERAM, S., 1974, "Radiowave propagation in the evaporation duct", Marconi Review, vol. 37, pp. 18-40

ACKNOWLEDGEMENTS

The author wishes to express his very thanks to Prof. Dr. K.-D. Becker for several useful discussions and Dipl.-Phys. H. Zimmer for performing the analytical and numerical calculations.

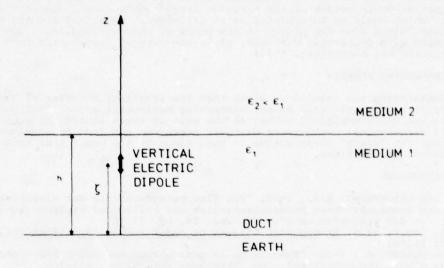


Fig.1 Geometry of the problem

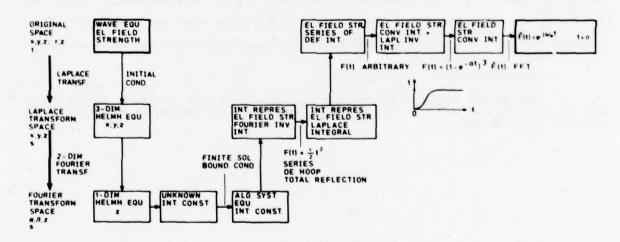


Fig.2 Flow-chart for the method of solution

	z	MAGNETIC DIPOLE (PHI-COMP)	ELECTRIC DI POLE (Z-COMP)
	022	- C ₁₂	Č12
	0 ₂₁ 0 ₁₂	C ₁₂ C ₁₂	Ē,3 Ē,3
	O ₁₁ Q ₀₂	- C ₁₂ - C ₁₂	Ē,2 Ē,2
1	Q ₀₁	C ₁₂	<u>C₁₂</u>
	Q ₀₄ Q ₀₃	- 1 - C ₁₂	1 C, ₂
	Q ₁₄ Q ₁₃	C ₁₂ C ₁₂	€,2 €,2
	0 ₂₄ 0 ₂₃	- C ₁₂ - C ₁₂	C ₁₂ C ₁₂

Fig.3 Image sources for both polarizations

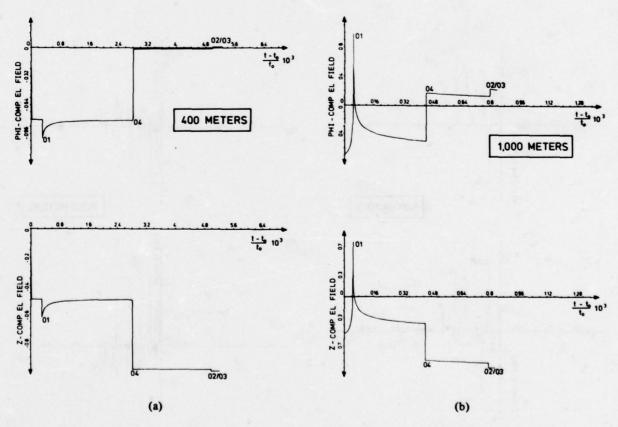


Fig.4(a)-(f) Comparison of electric field time history for both polarizations $(F(t) = 1/2 t^2)$

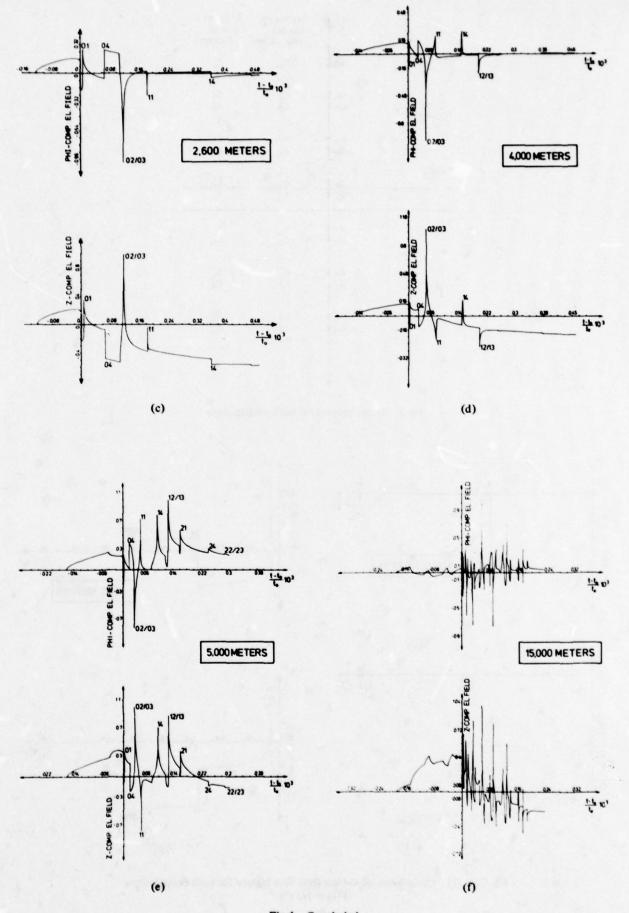


Fig.4 Concluded

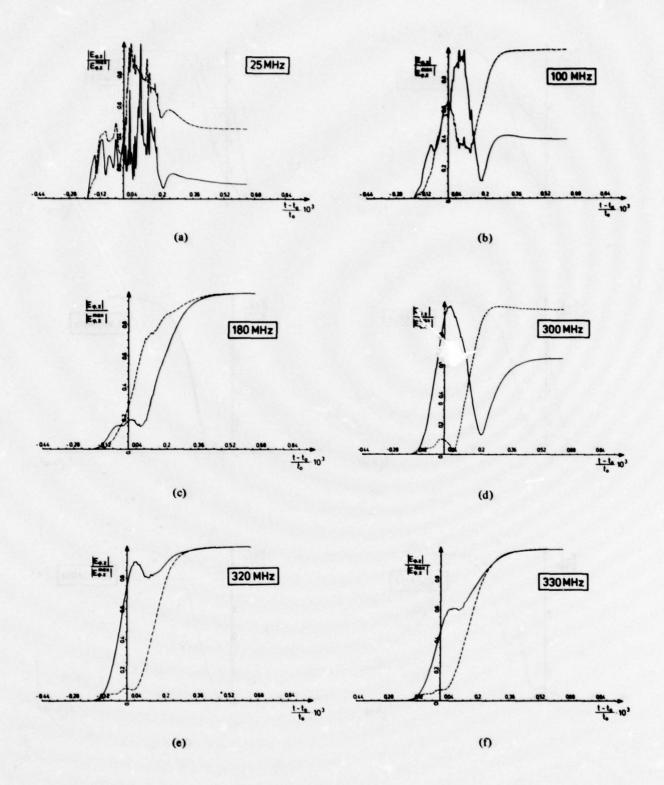


Fig. 5(a)-(l) Comparison of electric field time history for horizontal and vertical (dashed curves) polarization $(F(T)=(1-\exp(-at))^3\exp(j\omega_0t));\ r=15000\ m$

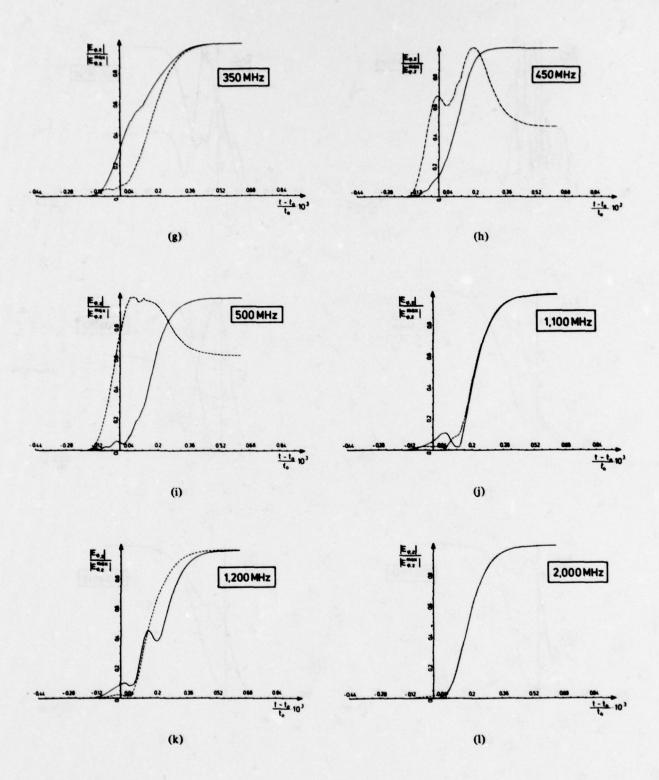


Fig.5 Concluded

L. Lewin UNIVERSITY OF COLORADO Boulder, Colorado

SUMMARY

Two basically different descriptions have been given as to the cause of aperture coupling loss in tropospheric scatter systems: non-planar wavefront due to atmospheric irregularities; and a geometric effect due to the decrease of scattering properties with height within the common volume of the beams of the transmitter and receiver antennas. The irregular wavefront explanation is examined and related to height-diversity concepts, and it is shown that the effect is determined by the angular spectrum of incoming rays; performance is related to the angle range and beam width. In the explanation via the geometric effect it is shown that increasing the antenna gain increases the on-axis power but decreases the angular range over which energy is received. The reduction in effective angular range is due to the same phenomenon as that giving rise to the loss due to the irregular phase fronts. It is concluded that the two explanations really reduce to one and the same.

A comparison is made of formulas in the literature and with available experimental results, and reasons given as to why it is difficult to validly relate the two.

The considerations of this paper indicate that narrow beams in the vertical may be more important than in the horizontal to achieve maximum gain. A suggestion is made to investigate the concepts in the laboratory with a scaled model using a laser with a variable lens, scattering the radiation from non-uniformities in a liquid suspension, and receiving the scattered radiation with a photo-detector of variable pickup angle.

1. INTRODUCTION

The coupling loss due to the nature of the scatter medium is one of the most puzzling and still unresolved features of the troposcatter process. There are two basically different descriptions given as to its cause: 1) non-planar or "crinkled" wavefront due to the irregularities in the atmosphere, 2) a geometric effect due to the decrease of scattering properties with height within the common volume of the beams of the transmitter and receiver antennas. At first sight these seem to be two quite distinct and different sources of coupling loss; and in a review paper (HARCAR, A.R. and BROWN, L. J., 1965) this is explicitly maintained, together with statements asserting that the crinkled wavefront loss could in principle be eliminated whereas the geometric effect could not, and that various authors had investigated the one cause or the other, but not both in combination. We shall attempt here a critical appraisal of some of the current theories and experimental data.

2. IRREGULAR WAVEFRONT

2.1. Height Diversity Concepts

The phenomenon of concern is intimately related to the space diversity properties of a troposcatter system. Two antennas spaced apart in height receive substantially independent signals when their spacing exceeds a certain distance, usually expressed in terms of wavelength. Since the phenomenon is phase dependent the wavelength obviously enters, and expressions like 60λ to 100λ are current. The multiplier must depend on other features of the link, such as, for example, station spacing or scatter height, but this effect is not known explicitly. When the two antennas are so large as to overlap, it is apparent that a single antenna equal in size to the diversity pair must be operating in such a way that large parts of it are fed in a mutually incoherent manner, with a consequential loss in gain. This is one way of looking at the cause of coupling loss of large antennas.

2.2. Arrival Angle Range

Another way to envisage the crinkling of the incoming wavefront at a receiver, more associated with concepts of angle diversity, is to compound many plane waves, each arriving at a slightly different angle, from the scatter volume. When the angle range is much smaller than the beam width the resultant is nearly plane, and little loss due to crinkling will result. Contrariwise, if the illuminated volume is much wider than the beam width a wide angle-range results, the wave front is very non-planar, and the antenna can only accept a part of the incoming energy. It is clear from this description that the crinkling is considered to be related to the angular range of incoming, mutually incoherent, plane waves. Their disposition is related to the argular spread of scatter sources and the importance of such spread is measured in terms of the beamwidth of the antenna. The crinkling is nothing more than a consequence of a simultaneous arrival of incoming waves from different directions. The larger the antenna the more direction-sensitive it will be, and the more it will discrimininate against energy arriving off-axis.

2.3. Uselessness of Phase Compensation

Can such a crinkled wave front be usefully compensated, at least in principle, by an adaptive phasechanging device? At first sight it might appear as if this were so. However, a completely arbitrary axial wave front, with constant amplitude and variable phase, would not satisfy Maxwell's equations at the antenna. If the phase is prescribed, it will affect the amplitude. Any real wave can be reconstructed as a sum or integral of plane waves of different arrival angles, but if the arrival angles are constrained to be within a narrow range near the axis the wave cannot be completely arbitrary. Under these conditions equalising the phase does not lead to increased pickup. To see how this comes about, consider the simplest case of two waves incident on a rectangular aperture at angles 0 and θ . The field is represented by $1 + e^{-jkx} \sin \theta$ which equals $2 \cos(\frac{1}{2}kx \sin \theta) e^{-j\frac{1}{2}kx} \sin \theta$. A phase equaliser reduces this to $2 \mid \cos(\frac{1}{2}kx \sin \theta) \mid$. The power associated with this is, of course, two units, but if θ is appreciably greater than the beam width only half will be received by a horn at the focus, the same as if no equaliser were used. An external prism which refracted the off-axis wave through an angle θ would enable it to be received, at the cost of losing the on-axis wave. If θ is of the order of the free-space beam width, then a partial refraction would help; but then the wave would have been partially received anyway!

The same limitation does not apply to a pair of diversity antennas whose outputs can be combined without loss with a suitable combining network and phase-changer. But now the individual free-space beamwidths are doubled (relative to a composite antenna of double size) so that effective pickup is over a wider angle range. All this is very close to the geometric effect which we shall now investigate.

3. THE GEOMETRIC EFFECT

3.1. Antenna Size and Scatter Volume

Suppose a receiver accepting energy from a scatter volume, and let the antenna area be doubled. One effect will be to double the received on-axis power. If the extent of the scatter volume is much less than the beam width this is about all that happens. If, on the contrary, the beam width were smaller than the extent of the scatter volume, doubling the antenna size would halve the acceptance range from which power could be received: the expected gain increase is annulled, with a consequent 3dB increase in coupling loss in this extreme case. This effect is clearly a function of the ratio of the angular extent of the scatter volume to the antenna beamwidth, though other factors might also enter. It is nothing more than the crinkled wavefront phenomenon seen from the point of view of antenna pickup! The crinkled wave front is directly related to the angular range of incoming waves, of which only part can be received by the antenna because of its beamwidth.

3.2. Phase Combination of Separate Antennas

The geometric effect <u>can</u> be overcome; by using a larger beamwidth. The antenna is, of course, smaller; but by using two separate antennas suitably combined the coupling loss is eliminated. Similarly, the crinkled wave front, as such, cannot be usefully compensated, but two smaller separate antennas can be phased to give an addition of their received powers. There is one cause, not two, of coupling loss, and it may be most easily visualised in terms of limited pickup, related to effective scatter volume and antenna beamwidth.

4. EFFECTIVE SCATTER VOLUME

4.1. Variation with Height

The scattering power of the atmosphere decreases rapidly with scatter angle, θ , and a further height factor may be involved, particularly at great heights and large distances. In a paper on troposcatter circuits (YEH, L. P., 1960), an exponential law of 10 dB decrease per degree of scatter angle is favored. Other writers have produced power laws varying from θ^{-4} to θ^{-9} . A GEC report (GEC, 1960) gives curves corresponding to a distance-dependent index varying between about 5 and 7. Although Yeh's formula gives results of the same order of magnitude near about 10 to $2^{\rm O}$ scatter angle it appears that the power law probably has a sounder basis. In either case there is no precisely delimited scatter volume. The majority of the scattered power comes from scattering at the lowest heights. A calculation, straightforward in principle, enables the transmission loss between two antennas to be assessed, and that part of it due to incomplete coupling between the antennas and the scatter medium to be extracted, and presented as the antenna-to-medium coupling loss.

The main difference between different authors stems from the different assumptions made about the scatter law and the shape of the antenna beams.

An appraisal of some of the commonly used formulas follows.

5. COUPLING LOSS FORMULAS

5.1. Formulas of Friis

In a paper dealing with reflection theory of scattering (FRIIS, H. T. et al, 1957) the authors consider a simplified model leading to a θ^{-4} scatter law and a coupling loss given by

$$\frac{\frac{8}{7}}{\frac{\alpha}{\theta}} \frac{\frac{\alpha}{\theta} f(\frac{\alpha}{\theta})}{\frac{2}{1 + \alpha/\theta}} \quad \text{where} \quad f = 1 + \frac{1}{(1 + \alpha/\theta)^4} - \frac{1}{8} \left(\frac{2 + \alpha/\theta}{1 + \alpha/\theta}\right)^4$$

where θ = scatter angle, α = 3dB antenna beamwidth.

The antenna beam takes the idealised form of a section of a wedge, and is chosen for mathematical convenience. It has the unfortunate property that the lower part of the beam is unduly narrowed, and since the lower scatter angles are the more important, it would be expected that the coupling loss effect would be exaggerated for small scatter angles. This can be seen from figures 1 and 2, which show the coupling loss between 3m dishes 5m high, as a function of distance and θ/α , for 4.7 and 8GHz respectively. The friis formula gives the largest coupling losses for formulas in this category, and the assumed shape for the antenna beam is undoubtedly mainly to blame. It seems probable that the power law is a little on the low side, and the effect would be even more severe if this change were made.

It should be stated here that the assumption is made that low gain antennas have zero coupling loss. This is, in a sense, arbitrary, since loss can be apportioned as we wish between medium scatter properties and antenna coupling. But from the point of view of a non-planar wave front which does not vary too drastically, it is apparent that small antennas should be considered to have zero loss. This enables the formulas to be compared by normalising the loss to zero for large beamwidths, and is the source of the factor 8/7 inserted into the Friis formula above.

5.2. Formulas of Staras

The GEC curve is a sort of average of several different formulas, all based on the geometric factor discussed here. It gives less coupling loss than the Friis formula, but considerably more than that of Staras (STARAS, H., 1957), who assumed a Gaussian shaped antenna beam and a scatter power law inversely as the square of the height above smooth earth. The index of this law has almost certainly been chosen too low, and Staras himself suggests it should have been somewhere between 2 and 3. The larger the index the greater the coupling loss, but it is difficult to see quantitatively from the original paper what the effect would be. Staras takes into account a turbulence anisotropy factor for horizontal as against vertical angular deviations, the effect of which is to make horizontal deviations 2 to 3 times more severe than vertical ones. Some experimental support for this is implied in the paper.

According to Staras, if α_R and α_T are the beam angles of the two antennas, then the relevant beam angle parameter α_0 for his formula is given by

$$\alpha_0^{-2} = \alpha_R^{-2} + \alpha_T^{-2}$$

Hence, if both antennas have equal beam width the effective width is 0.7 that of either. If one is much sharper than the other, it is the main determinant of the beamwidth parameter. These conclusions follow directly from the general form of his equations and his assumption of a Gaussian antenna pattern, and seem quite reasonable. They do not, however, warrant the conclusions he draws that the coupling loss is not shared equally by the transmitting and receiving antennas, even if they are identical. This seems a faulty conclusion based on the non-linearity of his curves, and ignoring the symmetry that is also there.

For small values of θ/α Staras in his fig. 4 indicates much smaller coupling losses than any other author. It is about 1.5 dB when $\theta/\alpha=1$, when Friis gives 8dB and the GEC "average" curve indicates 5dB, though several of Norton's results used in the latter give 3dB loss at this position.

5.3. Formulas of Yeh

Yeh compares various theories with what appear to be experimental points extracted from the literature. He comments that most authors are too optimistic when $\theta/\alpha < 1$ and most too pessimistic when $\theta/\alpha > 1$, though Staras, in this region, comes closest to his extrapolated experimental curve.

There are some disturbing features in Yeh's curves. Several of the theoretical curves are drawn so as to give a coupling gain at zero scatter angle. As explained earlier they should all be normalised to go through the origin. Secondly, his plot of experimental points seems doubtful. Several of them can be recognised from the list of results in table I of the GEC report, and it is clear that they refer to the change in coupling loss when one antenna size is replaced by another. In other words, the experimental points only contain partial information, and the correct results, whatever they may be, should indicate somewhat higher coupling losses, at least for large values of θ/α . This would probably bring the corrected curve close to the Staras predictions for $\theta/\alpha > 1$.

5.4. CCIR Formula

So far all these formulae have had a common basis, namely a geometric reduction factor, and have all indicated a similar trend, namely something small or zero at zero scattering angle, with an increase of loss as θ/α increases. Quite a few experimental results quoted show a similar trend. A quite different curve is presented in the CCIR Oslo 1966 Vol. II report no. 244-1, where a coupling loss independent of scatter angle is given in the form

0.7 exp
$$\left[0.055 \left(G_{T} + G_{R}\right)\right]$$
 dB

where G is the antenna gain in dB. This empirical formula gives a higher loss under most circumstances than any of the other results, except the Friis formula at large scatter angles. It is difficult to comment on this curve except to say that accurate figures for coupling loss are very difficult to come by, and that there is a region in figures 1 and 2 where all the curves give similar results within a few dB.

5.5. Formulas of Bullington

Bullington (BULLINGTON, K., 1963) goes even further. His analysis of reflection from an atmosphere with properties decreasing exponentially with height produces a coupling loss term of the form i - exp (-bh) where $b \approx 0.14/\text{km}$ and h is the difference in height between the top and bottom of the volume common to the two antenna beams. Since h = D $\alpha/2$ his coupling loss decreases with increasing distance, giving a curve of opposite slope to those derived from a geometric reduction factor. For small distances, the loss rises dramatically, as shown in the figures. Since D α Bullington's results cannot be expressed as a function of θ/α . In his paper there are quoted one or two experimental results which appear to support his formula.

6. AN APPRAISAL OF RESULTS

6.1. Comparison with Experiments

Many of the experimental results are obtained by replacing one antenna by another of different size and comparing the received powers. Some use two aerial sizes simultaneously and compare their signals. In both cases it is only the change in aperture loss of the combination that can be measured. Chisholm (CHISHOLM, J. H., et al, 1959), who used also 26° horns (scatter angle 2°), deduced a coupling loss of 3.5 dB when $\theta/\alpha = 1/3$. If the coupling loss is taken as zero for the horns, then this figure is in excess of all the geometric factor calculations except that of Friis, whose result comes out about right. Staras would indicate almost nil at this angle. On the other hand, a further loss of only 2.5 dB is incurred when going to $\theta/\alpha = 1.8$, almost exactly the excess predicted by Staras. The trend is also in the general direction of Bullington's prediction, and is way below the CCI figure.

6.2. Difficulties in Interpretation of Experiments

Many of the experimental results are hard to assess because of lack of information. It should be noted that two equal aerials spaced by the relatively small distance needed for diversity operation will give unequal instantaneous signals. It is not surprising, therefore, to find that a large antenna sometimes gives a signal not much in excess of a smaller one. It is the medians that should be compared, over similar periods.

It is a most point whether comparisons should be made for the same height of antenna centre. The effect of earth reflection will be quite different in the two cases.

The earth will also have a different effect if the polarisation is vertical, because of the small pseudo-Brewster angle. These details are not usually recorded in papers.

7. PROPOSAL FOR AN EXPERIMENTAL TEST

7.1. Geometric Scattering and Antenna Gain

The considerations in this paper suggest that tropospheric scatter is to be understood entirely in terms of scattering volumes common to the transmit and receive antennas, together with a variation in height of the strength of the scattering elements. Were it not for this height variation there would be little reason to go to high-gain antennas. What is really achieved by a higher gain is the ability to lower the effective beam angle and illuminate the stronger scatterers. To the extent that other factors, such as horizontal directivity of scatterers, do not enter, this suggests that overall gain is more fruitfully obtained by sharpening the antenna beams in the vertical. Such a possibility should be the subject of experimental verification, together with the whole concept of geometric scattering as outlined here. To do so on site, however, would be to subject a search for possibly small factors of a dB or so to the vagaries of substantial atmospheric variations outside the experimenter's control.

7.2. Scale Model Proposal

It is proposed that the essential features of troposcatter can be investigated on the laboratory bench, using a laser beam as transmitter. Available lens controls the beam angle, which can be broadened in the horizontal, the vertical, or both. The scattering could be from a suspension of particles in a suitable liquid, the settlement of the particles, which would consist of a range of sizes, giving a simulation of the atmospheric structure of actual scatterers. The receiver would be a photo-detector, again with a pickup angle that could be independently varied. Staras's somewhat questionable conclusion that coupling loss is not shared equally by identical antennas may also be capable of determination in this experimental set-up.

Even though it would be impractical to model exactly the atmospheric inhomogeneities in the scattering liquid, it is believed that useful information could well be derived from such an experiment.

8. CONCLUSIONS

A few tentative conclusions are offered.

- 1) There may be a weak distance-height effect but its effect is probably small. In particular, the Bullington prediction is not too well supported by experimental evidence, and is contrary to the majority of theories which very plausibly indicate that a function of θ/α is involved.
- The CCIR curve of constant loss irrespective of scatter angle gives rather too large figures.and is not a very plausible form.
 - 3) The Friis curve indicates too high a coupling loss.
 - 4) The Staras curve indicates too low a coupling loss.
 - 5) The Yeh assessment seems somewhat unreliable in some places.
- There seems to be some merit in the Staras formula for effective beam angle when unequal beams are involved.
- 7) The GEC empirical curve seems to be a good compromise result. It is possibly a little on the high side, and could be weighted somewhat towards the Staras curve, as indicated in figures 1 and 2.
 - 8) All the above conclusions should be taken with several grams of sodium chloride.

9. REFERENCES

BULLINGTON, K., 1963, "Reflections From an Exponential Atmosphere", B.S.T.J., pp. 2849-67.

CHISHOLM, J. H., RAINVILLE, L. P., ROCHE, J. F. and ROOT, H. G., 1959, "Angular Diversity Reception at 2290 Mc/s over a 188 Mile Path". I.R.E. Trans. C.S., p. 195.

FRIIS, H. T., CRAWFORD, A. B., and HOGG, D. C., 1957, "A Reflection theory for Propagation Beyond the Horizon", B.S.T.J., pp. 627-644.

GEC Report No. 13, 545R, February 1960, "The Application of Tropospheric Scatter Propagation to Communication Systems".

HARCAR, A. R., and BROWN, L. J., June 1965, "A Review of Unsolved Troposcatter Systems Problems", IEEE Annual Communications Convention, Conference Record, pp. 217-222.

STARAS, H., 1957, "Antenna-to-Medium Coupling Loss", I.R.E. Trans. A.P., pp. 228-231.

YEH, L. P., 1960, "Simple Methods for Designing Troposcatter Circuits", I.R.E. Trans. C.S., pp. 193-198.

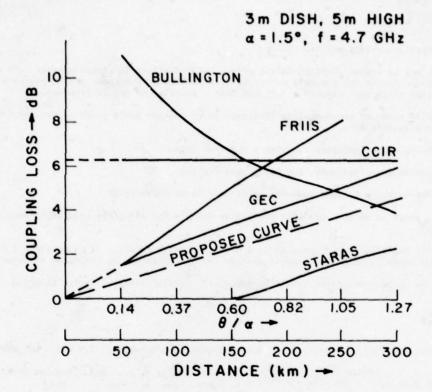


Figure 1. Coupling Loss versus Scatter Angle, f = 4.7 GHz

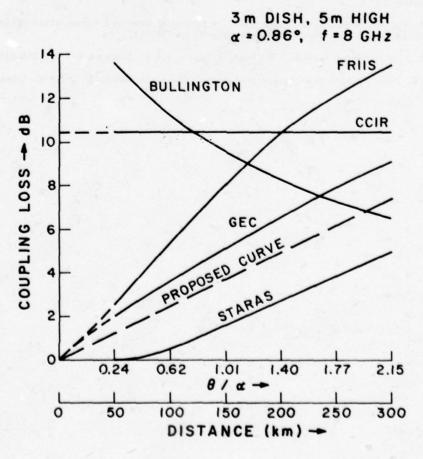


Figure 2. Coupling Loss versus Scatter Angle, f = 8 GHz

STATISTICS OF TROPOSCATTER CHANNELS WITH RESPECT TO THE APPLICATIONS

OF ADAPTIVE EQUALIZING TECHNIQUES

F. Schmitt
Forschungsinstitut für Hochfrequenzphysik
D-5307 Wachtberg-Werthhoven
FRG

ABSTRACT

Higher coherent bandwidth requirements for troposcatter communication channels may create serious problems due to the dispersion characteristics of troposcatter channels. Besides that the multipath structure of such a channel is time variant. Introduction of digital PCM-techniques, on the other side, may allow for processing schemes which result in adaptively equalizing the transmission channel. These processing schemes are based on the troposcatter channel characteristics which will be addressed in this paper.

Based on measurements on an experimental troposcatter link between Leiselheim and Werthhoven (270 km, Germany) some results will be presented and discussed concerning those link parameters that are of importance for adaptive equalizing techniques:

- a) Characteristics of the delay power spectrum (DPS) with respect to its time variability and variance.
- b) Characteristics of the instantaneous channel impulse response function (IRF) and its time dependence, which will be described by a correlation time constant. This is the time τ that passes until the impulse response function measured at time t_0 is decorrelated with that one measured at time $t_0 + \tau$ (3 dB down).
- c) Correlation analysis between delay power spectrum, received field strength, and intermodulation.
- d) Effects of airplanes inside and outside the common volume on the impulse response function.

The experiments have been made at a frequency of 0,9 GHz with a bandwidth of 10 MHz. The impulse response functions have been measured at a rate of 10 per sec for one minute, followed by intermodulation measurements for one minute and than starting the cycle again.

Although the results confirm the theory of the troposcatter channel model ("WSSUS" as developed by BELLO, in general, significant details have been discovered in terms of the statistics of the impulse response function and the time variability of the short term delay power spectrum. In view of the very low error rates $(10^{-3} - 10^{-6})$ that are required for many communication systems the tails of the DPS are of special interest. It has been found that the time spread i.e. the width of the DPS is larger than the one calculated from theory. Also the shape may be different from the theoretical one and may differ with time. Therefore, the theoretical width of the DPS is in some cases not a good basis for deciding on the length of the equalizing filter, because it gives only limited information on the actual IRF and no information on the time dependence of the IRF and of the DPS.

The paper will conclude with stressing the point that for the designer it is essential to know the statistics for the specific traposcatter link for which he is designing adaptively equalizing modems.

1. INTRODUCTION

During the first years of using the tropospheric scatter mode for transmitting communications, the experimental and theoretical work has been largely confined to measuring the field strength of monochromatic, respectively narrow-band signals and to establishing scatter models for calculating and predicting the scatter link performance.

For a long time, only a few measurements were available, which concentrated on investigating this time variable and dispersive channel with respect to broadband signal transmission. By broadband we mean using bandwidths by which the different multipath contributions can be resolved in time, thus producing severe signal distortions.

The WSSUS-model of the troposcatter channel, developed during the 60th by BELLO (1) was the first model that allowed for the calculation of the expected value of the signal distortion. Signal distortion is meant here in the sense of intermodulation or the rate of bit errors by digital modulation. One of the basic characteristics to describe the

troposcatter path is the delay power spectrum (DPS) which describes the energy distribution as a function of inherent delay times. In general, the DPS has a strong unsymmetric shape with a maximum at small time delays, showing a sharp rise and a flat fall-off.

However, the DPS describes only a stationary model of the troposcatter channel. Because it is calculated with well-known median parameters of the troposcatter mechanism, for instance the dependence of the scattering from the scatter angle and the altitude, it disregards any alterations in the scatter volume influenced by the weather.

Knowledge about the variability of the DPS cannot be obtained by theoretical methods but only by measuring the existing troposcatter paths.

This report deals with measurements of the DPS of an experimental troposcatter path operated by the Forschungsinstitut für Hochfrequenzphysik (FHP) at Werthhoven, FRG. Continuous measurement periods of three or two hours were recorded during days and nights at various times between middle of December 1976 and the end of February 1977.

The results of a total of 79 measurement hours are reported, namely: 23×3 hour- and 5×2 hour-periods. The limited number of measurement periods and the fact that all measurements were done in one section only represent an insufficient basis for general statistical applications, the results, however, give an interesting insight into the dynamic behaviour of the DPS. To my knowledge, only little description of this type of information is presently available.

Parallel to these measurements of the DPS, the intermodulation energy in a voice-channel of a FM/FDM multichannel -telephone-signal was measured. Several years ago, measurements of this type have already been made at this particular path, resulting in some conclusions on the dependence of the intermodulation from the deviation of FM-modulation and from the received power (2). At this time, its dependence from the DPS, particularly from its medium delay-width, has been examined.

Only recently, the interest in further troposcatter communication research grew when progress in adaptive filtering theory and technology improved to such an extent that implementing these techniques seems to be feasible. Furthermore, the decision to switch to DPC-modulation may result in simpler equalizing algorithms. Using equalizers, high-speed digital signals could even be transmitted if the bit length was shorter than the impulse response of the troposcatter path. Especially, the so-called decision feedback equalizer shows a high degree of equalizing capability. This is a combination of a complex linear transversal filter (FIR-filter) and a digital linear feedback filter (IIR-filter) (3).

The equalizing technique is not a new one. It has been used since many years for improving telephone channels. However, there are some basic differences between telephone channels and the troposcatter channel, which need some further investigations, part of which is the investigation of the statistic behaviour of the troposcatter channel.

Of importance is firstly the variability of the instantaneous pulse response of the channel, because the control circuits of the equalizer have to adapt to the continuously changing transfer function. Secondly, the entire length of the DPS is important because it is a significant measure for the medium length of the instantaneous impulse responses. The entire length of the equalizer is proportional to the length of the impulse response. Finally, the shape of the DPS influences the choice that has to be made with respect to the number of the taps of the FIR- and the IIR-filter. That means, for example, if the first arriving signals carry the main part of the receiving energy followed by weak signals, the signal is almost completely equalized by the digital recursive IIR-filter part. The theoretically calculated DPS shows exactly such a shape. If the later arriving signals, however, take over the maximum energy, the FIR part of the filter has to carry the burden of the equalizing work.

2. DESCRIPTION OF TROPOSCATTER PATH AND THE MEASURING METHOD

2.1 Troposcatter Path

Fig. 1 shows the profile of the scatter path ranging over a distance of 278 km, between Leiselheim near Freiburg and Werthhoven near Bonn. The 3 dB scatter volume is unsymmetric because of different elevation angles on both sides. The angle between horizontal rays amounts to 42 mrad if a 4/3 earth radius is used. This corresponds to an equivalent path length of 360 km, which would be the length of a scatter path of the same scatter angle with horizontal radiation on both sides.

Some technical details of the experimental installation:

Frequency	907,68 MHz	
Bandwidth B	10	MHz
Transmitter power	10	kW
Receiver noise figure	3	dB
Diameter of parabol antennas	8,5	m
3 dB beamwidth	2.7	0

The scatter volume ranges from 1,7 km altitude to 6,5 km above sea level. The length of the scatter volume is approximately 110 km. The difference between the lowest and the highest path of the 3 dB scatter volume is approximately 300 m corresponding to a maximum delay-time difference of 1/usec.

Fig. 2 shows the DPS of our path calculated according to BELLO for 4/3-earth radius. It has the well-known shape of a sharp rise and a flat decay. The maximum is at 0.08/usec behind the first incoming signal and the RMS delay spread is 0,12/usec. Approximately 80% of the entire received energy fall into the first 0,3 / usec of the DPS. Regarding the geometrical 3 dB scatter volume, energy portions of time-delay of 1 / usec could be expected.

2.2 Method of measuring

Fig. 3 shows the block diagram of the circuits for measuring the absolute value of impulse response and the intermodulation.

For practical reason it was decided to measure the impulse response by using a sampling technique. This means, one instantaneous impulse response is measured by using 32 consecutive code transmissions. Code length T is 0.2 msec which leads to a repetition frequency of the pictures of the impulse response of approximately 160 Hz. The relatively high number of 32 delay steps has been chosen in order to detect multipath contributions from outside the common volume (artificial scattering objects).

The control of the PN-code delay as well as the repetition frequency of the pictures is accomplished by a circuit marked: Synchronization and control. This circuit manages also the initial synchronization of the reference PN-signal.

The low-frequency output is transmitted via a twisted pair to the computer located in a laboratory at a distance of 2 km and is than digitized and stored in the magnetic disc of the HP 2100 computer for further evaluation. Storing every 16th picture will allow for recording of a continuous three-hour period. After such a procedure, the repetition rate of the picture series is 10 Hz.

Each minute, the equipment at the transmitting and receiving stations is synchroneously switched to the intermodulation measuring mode. The synchronism is controlled by the low-frequency transmitter DCF 77.

One-minute period for intermittently measuring the impulse responses and the intermodulation was chosen for the following reason: On one hand, the set of 512 single samples of impulse responses represents a true basis for a statistical description of the DPS, even though these samples sometimes are not independent. On the other hand, the period of statistical stationarity probably lasts longer due to its substantial weather dependence. Therefore, the intermittent one-minute periods of the DPS, respectively the intermodulation measurement, represent really the same statistical stationarity area.

The method of measuring the intermodulation is as follows:

At the transmitter side, one voice-channel is removed from the baseband noise signal, representing 120 voice-channels. At the receiving side, the intermodulation power in the respective voice-channel is measured. The magnitude of the intermodulation signal is transmitted via the same twisted pair to the A/D converter located in front of the computer at the laboratory.

2.3 Evaluations

The evaluation of the digitally recorded date includes the following procedures:

- a) The estimation of medium values for the one-minute periods i.e. the calculation of the one-minute short time DPS and its RMS width, respectively the calculation of the oneminute median value of the the intermodulation.
- b) The correlation between these one-minute periods of DPS and intermodulation over the entire three-hours measuring period.
- c) The short time variation of the impulse response will be described by a correlation time constant τ . This means the time τ that passes until the impulse response function at t_0 is decorrelated by a value of 0.5 with that one measured at time $t_0 + \tau$. Twenty correlation series have been averaged within the same one-minute period, because correlating signals consisting of 4-8 samples lead to a very high spread of the estimated correlation coefficient.
- d) Occasionally a correlation analysis of the time dependence of adjacent sample values of impulse response has been carried out in order to find out, whether the adjacent samples of the impulse response were correlated.

In many cases, pronounced dependence between the shape of the DPS and the weather conditions as illustrated in the weather charts have been found. Especially transient weather fronts clearly changed the DPS structure.

3.

MEASURING RESULTS

3.1 Correlation between adjacent samples of the DPS

Correlation analysis over one-minute periods of the time dependence of adjacent samples of the impulse response function yielded values between + 0,2 and - 0,2. This confirms the WSSUS-hypothesis of independent fluctuation of adjacent values which are separated due to the sampling rate by 1/B sec. This time resolution corresponds to a resolution of the layer thickness of 600 m at the lowest altitude and of 300 m at the highest altitude.

3.2 Time fluctuation of the DPS

The first figures are intented to give an impression of the variability of the observed DPSs.

Fig. 4 shows a very narrow DPS remaining almost constant over a three-hours period. The right hand curve shows the correlation time of the impulse response which amounts to several seconds, that means, the fading is very slow. (The program calculating the correlation time was, for saving computer time, limited to a correlation time maximum of 7 sec.)

The low shifting of the DPS is due to a frequency difference of the atomic frequency standards at the two stations, which is well within the limit of the specifications.

The separated signal, delayed by 0.5 msec, indicates the reflection of an airplane outside the 3 dB scatter volume. The measurement was made during night time and, therefore, almost no airplane reflection occured.

The RMS delay spread amounts to 0,11 msec, slightly below the 0,12 msec delay spread of the calculated DPS. During the measuring time and also during the previous day, high pressure weather conditions existed including high humidity within the lower altitudes.

Fig. 5 shows the DPS in the afternoon of the previous day. At one glance one immediately recognizes strong activities of airplanes. Comparing these last figures, the difference between day- and night-time measurements is clearly illustrated. In general, the airplane reflections last for short time only but their intensity can be quite high. It often exceeds the intensity of the whole remaining signal. This can be seen from the height of the reflection signals in fig. 5 which represents one-minute average values of the instantaneous power. Remarkable delay times will occure which can by far exceed the widths of the atmospherically induced DPS. Such airplane reflections represent a specific problem if one tries to compensate for the delay spread, especially because normally the circuitry is dimensioned for compensating the delay spread due to atmospherical scattering only.

It should be mentioned here that there is a danger in using equalizing techniques, because their performance can be deteriorated by intentionally placing strong scatterers like chaff outside the common volume.

In contrast, fig. 6 shows an extremely broad DPS with an average delay spread of 0,24/usec. Several airplane reflections can be recognized. The fading is extremely fast: the correlation time of the impulse response is less than 0,1 sec. The weather chart of the relevant area showed the outskirts of an extensive low pressure system with strong winds and intensive precipitation.

Comparing the narrow and broad DPSs with respect to their fading behaviour leads to the conclusion that generally a broad DPS is connected with fast fading, and narrow DPS with slow fading correspondingly. This rule is confirmed by some of the measurements that will be discussed later.

The following figures illustrate the variation not only in the width but also in the shape of the DPS. Fig. 7 also displays a flat DPS structure, the maximum of which is mainly in the right-hand side of the DPS, i.e. in the region of the higher time delays. During the first hour one even recognizes a pronounced double structure with two maxima. The decorrelation time for the impulse response sequences varies between 0.2 and 0.4 sec.

Fig. 8 indicates a highly structured broad DPS, where a double structure again can be observed for parts of the observation period. The RMS spread & is 0.23/usec. The decorrelation time of the impulse response sequences is about 0.5 sec.

The next figure has to be compared with this one because it describes a very interesting situation. The measuring periods that form the basis for the last two figures, are separated by 15 minutes only. During this time the meteorological conditions changed significantly because a high temperature weather front was moving rapidly through the scatter volume perpendicular to the line connecting both stations, thus destroying the very stable layering that existed before. Whereas fig. 8 describes the situation after the passage of the front, fig. 9 describes the condition before the event which can be deduced from the narrow shape of the DPS and the long decorrelation time of the impulse response series.

Further examples of the DPS with a characteristic variability will be shown in the next figure. These examples demonstrate within the three-hours measuring period the interrelationship between delay spread of the DPS and the fading characteristic. Fig. 10 shows a rather quick change from a narrow to a broad DPS. The decorrelation time decreases simultaneously from 3-4 sec to about 0.3 sec. A quick transfer of cold air masses in higher altitudes could have caused a change in the structure of the scatter volume.

Fig. 11 shows a steady broadening of the DPS within the course of the three-hours measurement period. Accordingly, the correlation time of the impulse response series decreases starting from values of about 2 sec for the initially very sharp shape of the DPS down to values of about 0.1 sec for the broader part of the DPS. This time dependence could probably correspond to the dissolution of the morning dust and fog. The dissolution is supported by the removal of high pressure conditions (which could be seen from the weather chart).

As far as the stationarity of the scatter process is concerned one will notice that in most of the cases there is a well pronounced similarity between the DPS-curves that have been measured (with an integration time of 1 min) in consecutive two-minutes intervals. From this it can be concluded that the scatter process is stationary at least over periods of 5 - 10 min, sometimes for much longer. It should be emphasized again that the strong fluctuations of the decorrelation times of the impulse response sequences from minute to minute is caused by the fact that the data basis for estimating these values is small as has already been mentioned above.

3.3 Correlation between intermodulation 1, time spread σ , and field strength E

In the presence of airplane reflections the above mentioned periods of stationarity are reduced to less than I minute. The method of measuring the intermodulation and the delay spread sequentially (over periods of I min each) can lead to useful correlation results only if stationarity exists over a period of succeeding measurement minutes. For this reason, the day-time recordings generally showed very weak correlation between the delay spread of the DPS and the intermodulation.

Therefore, night-time measurements, mostly undisturbed by airplane reflections, have been processed and yielded the expected good correlation between the delay spread and the intermodulation. Following below are some examples.

Fig. 12 shows a typical night measurement. Only one airplane reflection is noticeable. The DPS is changing very slowly from a flat and broad shape to a sharper one. The fading is very fast: the decorrelation time of the impulse response series is about 0.1 sec, showing a slight rise to approx. 0.2 sec versus the end of the period.

The three curves of fig. 13 show the time dependence of the minute-medium value of the intermodulation I, the delay spread σ , and the total received power E. E equals the integral taken over each 1-minute DPS. Only the variations around the respective medium values are shown. Free scaling of the Y-axis is employed in order to clearly illustrate the similarity between the I- and σ -curves. The absolute ranges of the variations of I, σ and E are in the order of 10 pW, $2\cdot 10^{-8}$ sec and 10^{-11} W respectively. Relating them to their mean values yields $\frac{\Delta I}{I} \approx 50\%$, $\frac{\Delta \sigma}{\sigma} \approx 20\%$ and $\frac{\Delta E}{E} \approx 5\%$.

One can recognize a good correlation between the above described decrease of the delay spread and the decrease of the intermodulation. The correlation coefficient is $\varrho_{\sigma,L}=0.93$. Increasing the integration time for the estimation of the intermodulation and the delay spread from I min to IO min leads to a correlation coefficient of $\varrho_{\sigma,L}=0.95$. The received power E is negatively correlated with the delay spread σ and intermodulation I. This is also typical: a broad DPS will correspond to a weak power of the received signal and vice versa. The negative correlation between the received power and the delay spread amounts to $\varrho_{E,\sigma}=-0.75$. The correlation between the received power E and the intermodulation I is $\varrho_{E,L}=-0.8$.

Following are two more examples of night-time measurements. They indicate the same dependence between the DPS delay spread, fading, intermodulation, and the total received power. Fig. 14 shows a variation not only of the delay spread but also of the shape of the DPS. At the beginning of the measurement period one recognizes a broad and flat DPS with a maximum arising at the higher delay times. In the course of the measurement period the maximum is transferred more and more towards the shorter delay times. At the same time the shape of the DPS is becoming narrower. The medium delay spread of 0.15 usec is higher than that of the previous example. (The measurement was interrupted for 20 min, approximately in the middle of the measurement period. Therefore, the movement of the maximum towards the left-hand side seems to jump.) Simultaneously with the steepening up of the DPS the fading becomes slower. The correlation time of the impulse response series rises from approx. 0.2 sec to 1 sec.

Fig. 15 shows the time dependence of the minute-medium values of intermodulation, delay spread, and total received power, corresponding to the situation in fig. 14. The same type of correlation of the intermodulation I with delay spread σ and with the received power E can be recognized in this case. The correlation coefficient between I and σ amounts to $\varrho_{\sigma,L}=0.74$. It increases to a value of 0.94 by smoothing the statistical variation of the minute-medium values over intervals of 10 min. The negative correlation between I and E respectively σ and E amounts to $\varrho_{I,E}=-0.66$ respectively $\varrho_{\sigma,E}=-0.83$. It rises by smoothing over 10 minutes to -0.85 respectively -0.94.

A third example of a night-time measurement together with the inherent correlation values between 1, σ and E is shown in the figs. 16 and 17. The delay spread (fig.16) shows a pronounced broadening in the last third of the measurement period which, however, is not so clearly reflected in the fading behaviour. Only a weak increase of the fading rate is indicated. Again a good correlation between 1, E, and σ can be seen (fig.17) although $\varrho_{\sigma,E}$ seems to be not so high as in the case mentioned before. Quantitatively: the correlation coefficient between σ and I amounts to $\varrho_{\sigma,E} = 0.65$. It increases, however, by averaging over 5 min to 0.96, by averaging over 10 min to 0.98. The correlation coefficient $\varrho_{\sigma,E}$ amounts to 0.59.

CONCLUSION

The following conclusions can be drawn from the investigations:

- The WSSUS assumption of uncorrelated behaviour of adjacent layers in the scatter volume has been confirmed for the case of a time delay resolution of 0.1 jusec, corresponding to a resolution of the layer thickness of 600 m at low altitudes and 300 m at the higher end of the scatter volume.
- 2. The delay spread of the measured DPS is in the average broader than the spread of the calculated DPS which is generally taken as a basis for comparing purposes. It is calculated with the assumption of 4/3 earth radius, \$\oint_{-5}^{-5}\$ angle dependence and a linear height dependence of the variations of the refraction index. The experienced variation of the delay spread extended from values of 0.11/usec to values of 0.26/usec, compared to a theoretical delay spread of 0.12/usec.
- 3. A higher delay spread of the DPS generally corresponds to a faster fading respectively to a faster decorrelation of the impulse response series. At the same time, the total received power decreases with the broadening of the DPS. The correlation coefficient Q_{E,F} is about -0.8.
- 4. The shape of the one-minute short-time DPS can substantially differ from the theoretical one. Often, the DPS shows its maximum value with longer delays, and often even a double structure containing two maxima arises, indicating a wide spread of the actual impulse response around the theoretical DPS structure.
- 5. Generally, adjacent one-minute DPSs show a similar structure, whereby deviations from this behaviour may be explained as a statistical spread due to the limited number of the independent samples of the impulse responses within 1 minute.

 The periods of statistical stationarity of the scattering process include time intervals of 5 10 min up to several hours.
- 6. Correlation analysis of the delay spread and the intermodulation yields correlation values $\rho_{\sigma, \tau}$ of approx. 0.95 with smoothing intervals of 5 10 min duration.
- 7. A substantial portion of the DPS, at least on our scatter link, is effected by airplane reflections. Their sporadic appearance leads to a high degree of instationarity of the scattering statistic. Due to the high scattering cross-sections of airplanes, considerable intensities may arrive from far outside the scatter volume (or arriving from sidelobes of the antenna diagram). They lead to a considerable broadening of the effective impulse response respectively of the effective DPS. Delay times up to 2/usec outside the atmospherically induced DPS were noted.

Concerning the conclusions with respect to using equalizing techniques on scatter links, particularly of the decision feedback equalizer, one can say that, according to the described measurement results, the theoretically calculated DPS is not a good basis for deciding on the length, i.e. the number of taps of the equalizer, nor, in the case of feedback systems, is it a good basis for deciding on the distribution of poles and zeroes in the transfer function. Higher efforts in terms of numbers of taps are required because of the longer duration of the impulse responses as compared to the theoretically calculated DPS.

By far, the most critical conditions for equalizing are caused by the sporadic airplane reflections. In general, relatively long delay times could be compensated by an appropriately extended recursive filter part. However, this can only be practised if the amplitudes of the reflections are less than those scattered by the atmospheric inhomogeneities.

Unfortunately, the intensities of airplane reflections often exceed the main scatter signal part. Thereby it may happen that the IIR-part cannot contribute to the equalization at all. In this case a very long FIR-filter would have to be used, thus increasing the complexity of the equalizing circuitry beyond reasonable limits. However, it exceeds the frame of this contribution to discuss these problems in detail.

References.

- [1] BELLO, P.A., 1969, "A Troposcatter Channel Model", IEEE-Trans. on Commun. Technology, Vol. COM 17, p. 130–137.
- [2] SCHMITT, F., 1967, "Intermodulationsmessungen bei troposphärischer Streuausbreitung", Kleinheubacher Berichte, Vol.12, p.139–145.
- [3] MONSEN, P., 1971, "Feedback Equalization for Fading Dispersive Channels", IEEE Trans. on Informat. Theory, Vol. IT 17, p 56-64.

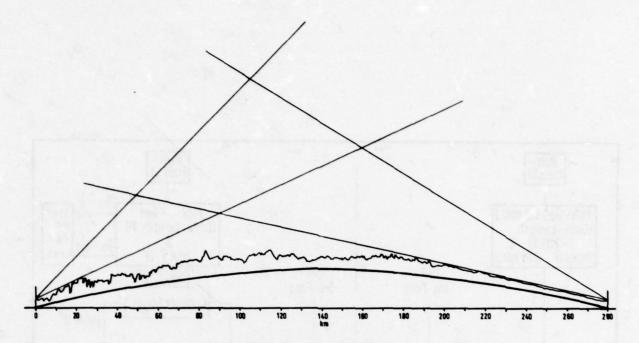


Fig.1 Troposcatter path between Leiselheim and Werthhoven

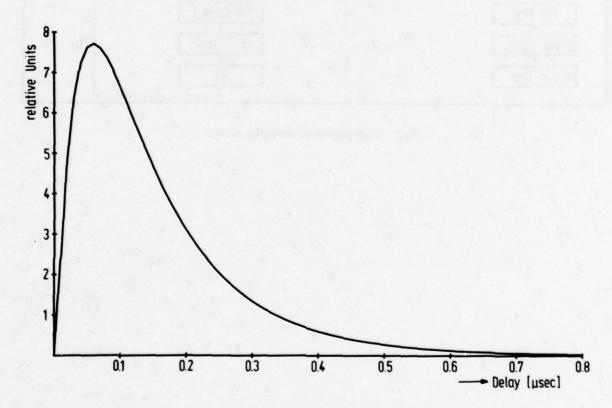


Fig. 2 Delay power spectrum of the Leiselheim-Werthhoven path

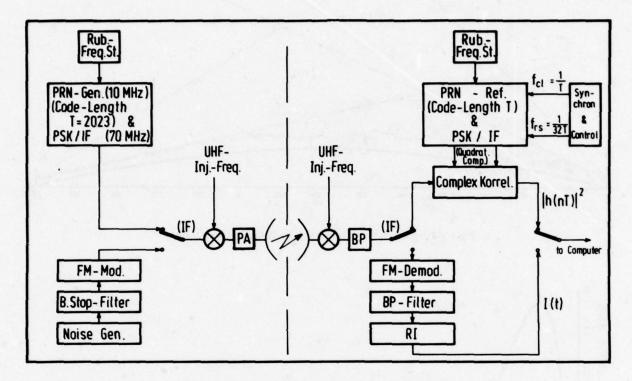
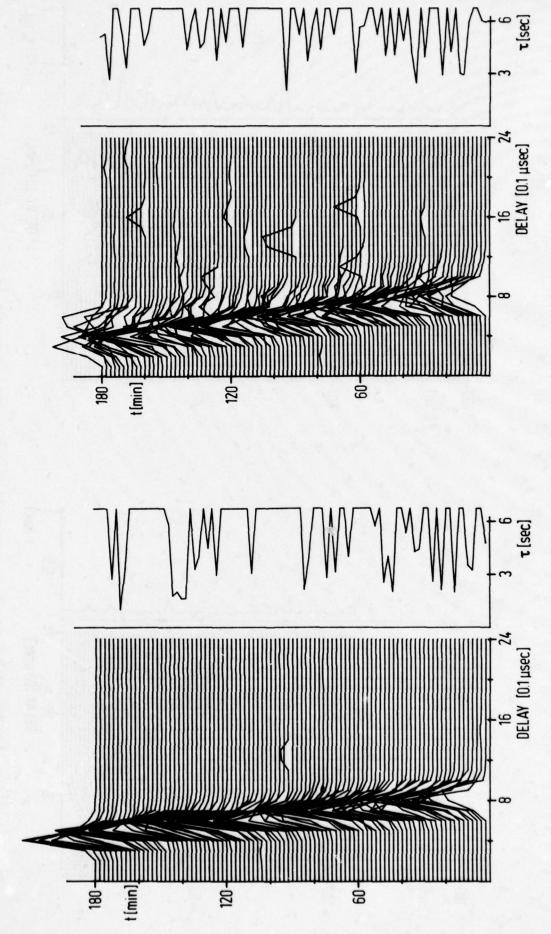
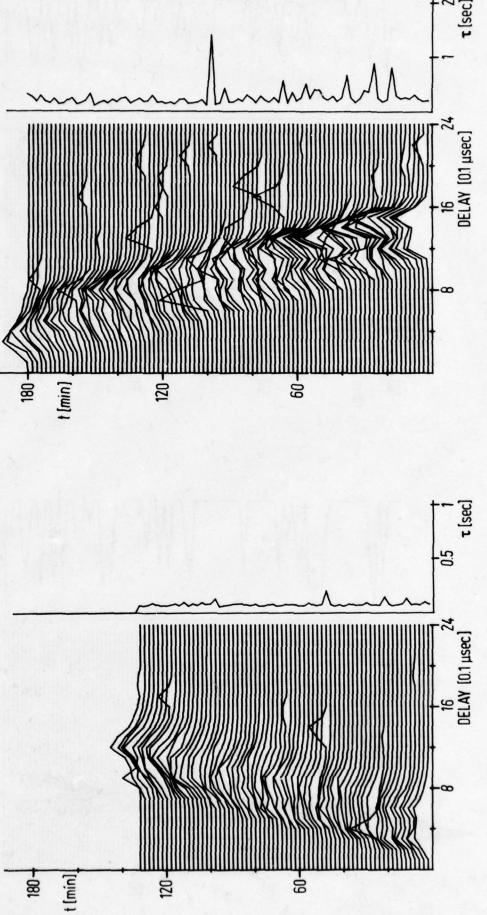


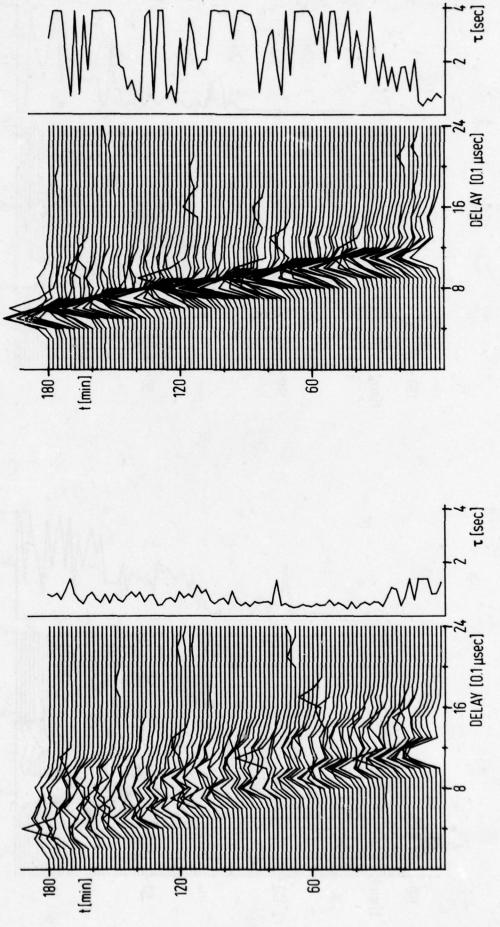
Fig.3 Block diagram of measuring circuits



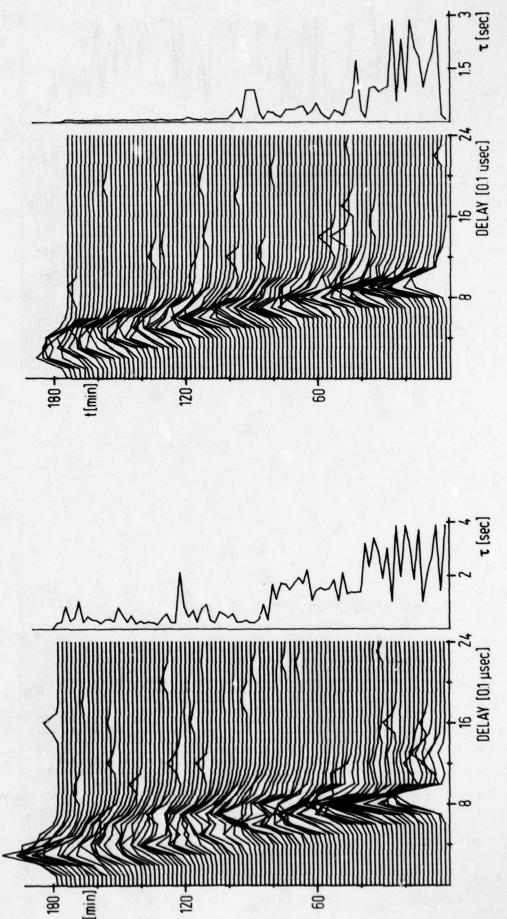
Figs 4 & 5 Examples of the time dependence of 1-min delay power spectra and decorrelation time of the impulse responsiveness



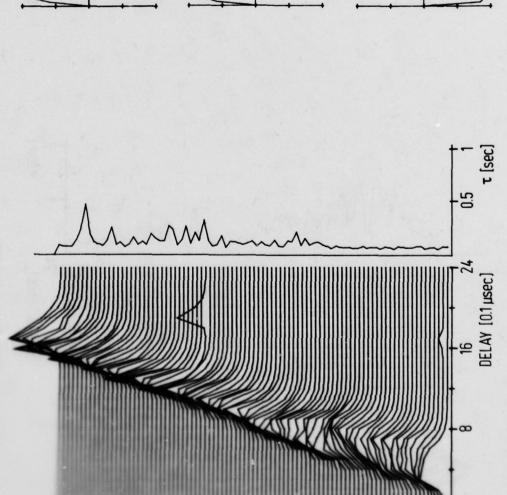
Figs 6 & 7 Examples of the time dependence of 1-min delay power spectra and decorrelation time of the impulse response series



Figs 8 & 9 Examples of the time dependence of 1-min delay power spectra and decorrelation time of the impulse response series



Figs 10 & 11 Examples of the time dependence of 1-min delay power spectra and decorrelation time of the impulse response series



Δ1(t)

Fig.12 Night-time measurements of DPS

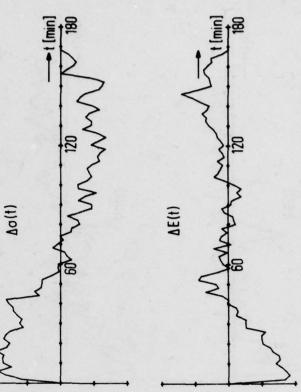


Fig.13 Time dependence of intermodulation I, delay spread of and received power E, corresponding to measurements of Figures 12, 14, 16 respectively

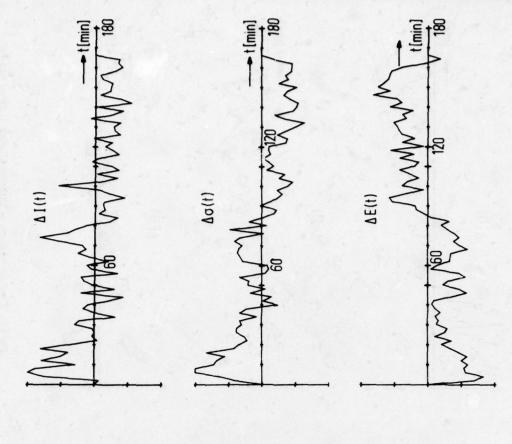


Fig.15 Time dependence of intermodulation I, delay spread σ and received power E, corresponding to measurements of Figures 12, 14, 16 respectively

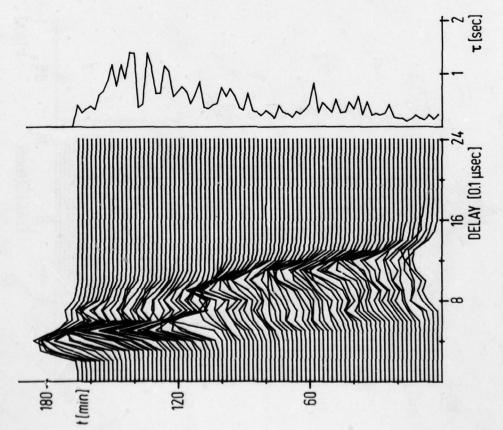
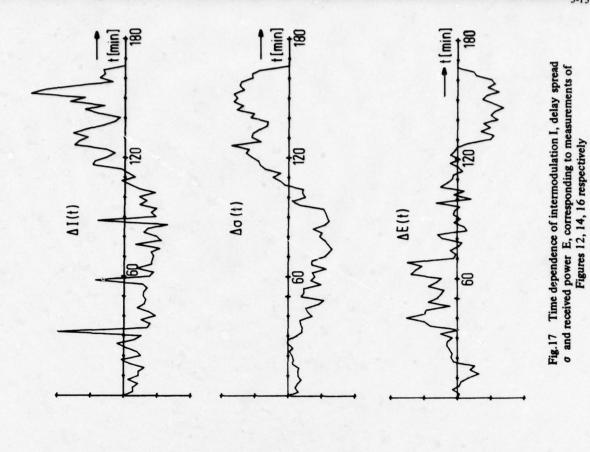


Fig.14 Night-time measurements of DPS



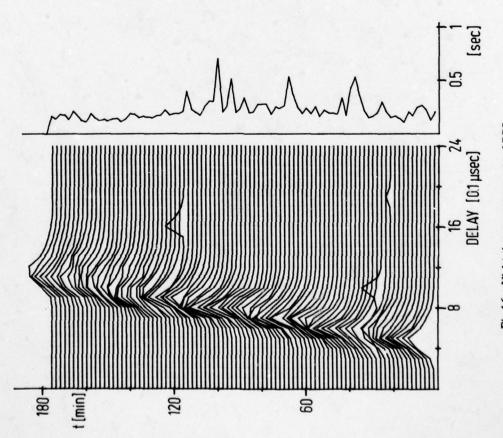


Fig.16 Night-time measurements of DPS

HF SCATTER FROM OVERDENSE METEOR TRAILS

George H. Millman General Electric Company Syracuse, New York 13201, USA

SUMMARY

The characteristics of HF radar reflections from overdense meteor ionization trails having line densities greater than 10^{14} electrons/m, are discussed. Theoretical estimates are made of the radar cross sectional area, time duration and the Doppler frequency shift of meteor echoes. Utilizing experimental meteor data recorded at 32 MHz by Greenhow and Watkins (1964), extrapolations are made of the statistical variations of the cross sectional area, the echo duration and the meteor echo rate for frequencies in the 6-MHz to 40-MHz band.

1. INTRODUCTION

Meteoric particles on entering the earth's atmosphere produce incandescence and an ionization trail extending along the path of the meteor at altitudes between approximately 80 and 120 km.

Radar echo returns from meteor trails are a source of false alarms for an HF backscatter radar designed to detect targets beyond the horizon.

In this paper, the characteristics of HF radar echoes from high density (overdense) ionization trails, i.e., line density is greater than 10^{14} electrons/m, are discussed.

Estimates are made of the radar cross section and the time duration of overdense meteor echoes utilizing the theoretical models hypothesized by Eshleman (1955, 1957). The Doppler frequency shift of meteor echoes imposed by ionospheric winds are also evaluated.

Utilizing experimental meteor data recorded at 32 MHz by Greenhow and Watkins (1964), extrapolations are made of the statistical variations of the cross sectional area, the echo time duration and the echo meteor rate for frequencies in the HF band.

2. THEORETICAL CONSIDERATIONS

2.1 Radar Cross Section

Radar pulses backscattered from meteoric ionization are aspect-sensitive in that the maximum intensities are returned when the direction of propagation is orthogonal to the trail. The reflection process is assumed to take place at the surface of the ionization trail where the condition of critical reflection is satisfied, i.e., the frequency of the incident radiation is equal to the plasma frequency of the trail.

According to Eshleman's et al. (1957) scattering theory, the maximum backscattering cross sectional area at the long wavelengths ($\lambda > 3$ m) is given by

$$\sigma_{of} \text{ (max)} = \left(\frac{\sigma_e}{4\pi}\right)^{1/4} q^{1/2} \lambda R_o \exp \left(-0.5\right) \tag{1}$$

where σ_e is the radar cross section of an electron (10⁻²⁸ m²), q is the line density (in electrons/m), λ is the wavelength (in meters) and R_0 is the perpendicular distance from the radar to the meteor trail (in meters).

Figure 1 is a plot of the radar cross section of overdense meteor trails as a function of elevation angle for frequencies in the HF band, the calculations being based on an assumed $q=10^{14}$ electrons/m and meteor altitude of 95 km. It is seen that, for propagation along the horizon, the cross section varies between approximately 2.6 x 10^6 m² and 1.7 x 10^7 m² at 40 MHz and 6 MHz, respectively, and that, the cross section decreases by an order of magnitude at an elevation angle of 70° .

2.2 Time Duration

According to Eshleman (1955), assuming that the meteor trail is an infinitely-long right circular cylinder and that the column of electrons expands by normal diffusion in a Gaussian distribution, the amplitude-time dependency of a reflected signal at the long wavelengths is of the form

$$A^{2} = A_{0}^{2} \left[t \ln \frac{\lambda^{2} q \sigma_{e}^{1/2}}{8\pi^{5/2} Dt} \right]^{1/2}$$
 (2)

where A is the maximum amplitude and D is the ambipolar diffusion coefficient (in m²/sec).

As shown in Figure 2, the radar cross section, i.e., signal amplitude, increases with time to a maximum value and then decreases to zero.

The time duration of overdense meteor trails is simply the total duration of the echo and is given by

$$\tau_{0l} = \frac{\lambda^2 q \sigma_0^{-1/2}}{8 \pi^{5/2} D} \tag{3}$$

The estimates of the time duration as a function of altitude, presented in Figure 3, are based on Greenhow's and Neufeld's (1955) model for the ambipolar diffusion coefficient which is expressed by

$$\log_{10} D = 0.0679h - 5.663$$

where h is the altitude of the meteor column (in km).

141

It is evident that the meteor echo duration increases with decreasing altitude and increasing line density. For an ionization altitude of 95 km and line density of 10^{14} electrons/m, the duration of overdense meteor echoes evaluates to 2.9 sec and 0.66 sec at 6 MHz and 40 MHz, respectively.

2.3 Doppler Frequency Shift

The Doppler frequency shift encountered by radio waves incident on meteoric ionization is mainly due to the wind motions in the ionosphere.

Assuming that, at a given altitude, the ionospheric wind speed is Rayleigh distributed and the angular orientation of the wind in a plane parallel to the tangent plane at the earth's surface is uniformly distributed, it follows that the probability density function of the Doppler frequency shift is Gaussian with a mean Doppler of zero.

It can be readily shown that the standard deviation, σ , of the Gaussian distributed Doppler frequency shift can be expressed by (Millman, 1975)

$$\sigma = 2\left(\frac{2}{\pi}\right)^{1/2} \frac{\overline{V}}{\lambda} \left(\frac{r_0}{r_0 + h}\right) \cos E \tag{5}$$

where V is the mean wind speed, r_0 is the earth's radius, h is the meteor ionization altitude, and E is the elevation angle to the meteor trail as measured from the horizon.

The estimated standard deviation and the upper decile (\approx 1.28 σ) of the Doppler frequency shifts at 6 MHz for winds at 95 km altitude are shown in Figure 4 as a function of elevation angle. The statistical distribution of the mean ionospheric wind speed was deduced from the experimental measurements summarized by Rao (1965).

According to Figure 4, at 6 MHz, the upper decile Doppler frequency shift imposed by ionospheric winds having a mean-median speed of 80 m/sec could vary between approximately 3.0 and 3.2 Hz for elevation angles less than 20°. At 40 MHz, the Doppler frequency shift, for the same conditions, varies between 20.0 and 21.3 Hz.

3. EXPERIMENTAL MEASUREMENTS

3.1 System Parameters

A study of radar reflections at 32 MHz conducted by Greenhow and Watkins (1964) in England in the fall of 1961 can be directly applied for estimating the characteristics of meteor echoes at other frequencies in the HF band. Radar meteor observations were also made at a frequency of 300 MHz, the 32-MHz data being used to assist in the interpretation of echoes occurring simultaneously at the higher frequency.

The parameters of the HF radar equipment used in the Greenhow-Watkins experiment are given in Table 1. The meteor data were collected with the antenna oriented at a fixed azimuth of 30° east of north and at an elevation angle of 10°.

TABLE 1 GREENHOW'S AND WATKINS' RADAR PARAMETERS

Frequency		32 MHz
	er Peak Power	7 kW
Pulse Len	gth	140 µ8ec
Pulse Rep	etition Frequency	50 pulses/sec
Antenna D		25 m
Antenna Be	eamwidth	25°
Antenna G	ain	16 dB
Cosmic No	oise	15,000°K
Antenna G	ain	16 dB

3.2 Experimental Results

Figure 5 is a plot of the mean heights of the 300-MHz echoes as a function of the time duration of the coincident 32-MHz echoes and the approximate values of the meteor trail line density. It is seen that the line density increases as the mean height increases which is contrary to meteor theory (Greenhow, 1963).

According to Equation (3), the line density is directly proportional to the time duration. However, as shown in Figure 6, there is a slight deviation of the line density time duration plot from a linear fit. This deviation is most likely due to the fact that the data are based on meteor echoes recorded at all altitudes and that the diffusion coefficient, which appears in Equation (3), is altitude dependent.

The meteor cross sectional area presented in Figures 7 and 8 as a function of line density and echo duration, respectively, was calculated utilizing Equation (1) with the mean altitude data of Figure 5.

A histogram of the echo duration of the 32-MHz echoes which correlated with the 300-MHz echoes is given in Figure 9.

The integration of the area under the histogram of Figure 9 results in the cumulative distribution function of echo duration shown in Figure 10. When utilizing Figure 10 in conjunction with Figures 6 and 8, it follows that the cumulative distribution function of the line density and cross sectional area can be readily derived. A summary of the statistical characteristics, i.e., lower decile, median and upper decile, of the echo duration, line density and cross sectional area, as obtained from Figures 10, 11, and 12, respectively, are summarized in Table 2.

TABLE 2 STATISTICAL CHARACTERISTICS OF GREENHOW'S AND WATKINS' METEOR DATA AT 32 MHz

	Echo Duration (sec)	Line Density (Electrons/m)	Cross Section (m ²)
Lower Decile	0.38	1.30 x 10 ¹⁴	1.38 x 10
Lower Quartile	0.48	1.75 x 10 ¹⁴	1.63 x 10
Median	0.85	4.00 x 10 ¹⁴	2.53 x 10
Upper Quartile	1.20	1.03 x 10 ¹⁵	4.70 x 10
Upper Decile	7.50	8.60 x 10 ¹⁵	1.30 x 10

Figure 13 is a plot of the diurnal variation of the meteor rate for echoes with time durations greater than one second. It is seen that the rate is a maximum of about 235 meteors/hour in the early hours of the morning and a minimum of about 40 meteors/hour in the evening.

4. EXTRAPOLATION OF EXPERIMENTAL DATA

Greenhow's and Watkins' (1964) 32-MHz meteor data can be used as a base for predicting the characteristics of meteor echoes at other frequencies in the HF band.

According to Equations (1) and (3), the meteor cross section is inversely proportional to frequency, while the time duration is inversely proportional to the square of frequency. Utilizing these relationships, it is then possible to convert the Greenhow's and Watkins' cross section and time duration results, shown in Figures 8, 10 and 12, to frequencies of interest.

Table 3 contains the statistical characteristics of meteor cross section and echo duration at 6 MHz and 40 MHz as extrapolated from Greenhow's and Watkins' (1964) data. It is seen that, at the low end of the HF band, 50 percent of the meteor echoes could persist for times greater than about 24 sec while, at the high end of the frequency band, the time durations decrease to about 0.5 sec.

An examination of the system parameters given in Table 1 reveals that the radar employed by Greenhow and Watkins (1964) observed all the overdense meteor echoes. Although the half-power beamwidth was 25°, overdense meteors could be detected as far down as 26.15° from the antenna beam axis. This value was derived by assuming the following: (1) the system sensitivity was set by the cosmic noise level; (2) a signal-to-noise ratio of 10 dB was required to detect the minimum (overdense meteor) line density of 10¹⁴ electrons/m; (3) the circular antenna was uniformly illuminated, i.e., the amplitude and phase of the radiation across the face of the antenna aperture was uniform. The normalized one-way radiation pattern of a circular antenna is given by

$$S(\gamma) = 2 \frac{J_1(\pi d \sin \gamma/\lambda)}{(\pi d \sin \gamma/\lambda)}$$
 (6)

where $J_1(\pi d \sin \gamma/\lambda)$ is the Bessel function of the first order, d is the diameter of the aperture, λ is the transmitted wavelength and γ is the angle off the beam axis.

TABLE 3
CROSS-SECTIONAL AREA AND TIME DURATION OF METEOR ECHOES
EXTRAPOLATED FROM GREENHOW'S AND WATKINS' DATA AT 32 MHz

Frequency	Statistics	Cross Section (m ²)	Echo Duration (sec)
6 MHz	Lower Decile	7. 36 x 10 ⁶	10, 81
	Lower Quartile	8.69 x 10 ⁶	16.65
	Median	1, 35 x 10 ⁷	24, 18
	Upper Quartile	2, 51 x 10 ⁷	34, 13
	Upper Decile	6, 93 x 10 ⁷	213, 33
40 MHz	Lower Decile	1. 10 x 10 ⁶	0. 24
	Lower Quartile	1, 30 x 10 ⁶	0.31
	Median	2, 02 x 10 ⁶	0.54
	Upper Quartile	3. 76 x 10 ⁶	0.77
	Upper Decile	1.04 x 10 ⁷	4.80

The area in the meteor band formed by the intersection of the antenna beam diameter of 52.3° with the 95-km altitude surface evaluates to approximately $4.20 \times 10^5 \text{ km}^2$.

In deriving the overdense meteor echo rate that could be observed with an HF backscatter radar, it is necessary to determine the area in the meteor band being illuminated by the main antenna beam and sidelobes. It is assumed that the radar has sufficient sensitivity to detect meteoric ionization in the sidelobes at all elevation angles $(E=0^{\circ}\ to\ 90^{\circ})$ and over a 180° azimuthal spread. The latter is based on the assumption that there are "holes" in the azimuth sidelobe pattern and that only one-half of the 360° azimuth angle coverage is effective in transmission and reception.

The area under illumination at an altitude of 95 km for the condition of 0° to 90° elevation angle coverage and 180° azimuth angle coverage is equal to 1.93 x 10⁶ km². It follows that an HF backscatter radar would intercept approximately 4.60 times more overdense meteors in the direct line-of-sight than detected by the Greenhow and Watkins radar.

In the operation of an HF backscatter radar, it is necessary, for the most part, to utilize the F-layer mode of propagation. Some of the overdense meteor echoes detected by reflections from the F-layer could appear in the radar range interval of the line-of-sight meteor echoes. The radar range of the F-layer reflected meteor echoes will coincide with the line-of-sight meteor range for the condition in which $R \ge R_1 + R_2$ where R is the radar-horizon range to the meteor trail and R_1 and R_2 are the ranges illustrated in Figure 14.

In estimating the magnitude of the F-layer reflection meteor echoes appearing in the line-of-sight, it is assumed that: (1) the F-layer reflections occur at an altitude of 350 km, (2) the meteor echo altitude is 95 km, and (3) the skip distance is 926.6 km (500 nmi), i.e., the minimum distance at which a ray can return to the ground after reflection from the ionosphere. It can readily be shown that, for these assumptions, the line-of-sight F-layer reflected echoes will be confined within the elevation angles of $30^{\circ}32^{\circ}$ and $34^{\circ}13^{\circ}$. The latter specifies the maximum elevation angle for the F-layer mode of propagation to exist for the above assumed conditions while the former is the elevation angle which satisfies the range condition, $R = R_1 + R_2$, shown in Figure 14.

The surface area at the meteor band encompassed by the two elevation angles having an angular difference of $3^{\circ}41'$ and the 180° azimuth spread evaluates to 2.91×10^{5} km² which is approximately 0.69 of the surface area under surveillance in the Greenhow and Watkins experiment. Thus, an HF backscatter radar would observe by F-layer reflections a factor of 0.69 the number of overdense meteor echoes reported by Greenhow and Watkins and presented in Figure 13.

Figure 15 is a plot of the estimated diurnal rate of overdense meteor echoes, as extrapolated from Figure 13, that could be detected in the line-of-sight by both direct reflections and by F-layer reflections, the average rates being 9.4 meteors/min and 1.4 meteors/min, respectively and the average total line-of-sight rate being 10.8 meteors/min. In addition to diurnal variations, the meteor rate will be modified by seasonal effects and meteor showers which are not considered in this analysis. The presence of meteor showers could increase the overdense meteor rate, depicted in Figure 15, by a factor of approximately 5 to 10.

It should be noted that, for skip distances greater than approximately 1052.6 km (568 nmi), the elevation angle defining the F-layer propagation mode for an assumed 350-km F-layer reflection altitude would be less than 30°32'. Thus, for this case, F-layer reflected meteor echoes would not be present in the range interval of the line-of-sight meteor echoes.

According to Manning and Eshleman (1959), the average meteor flux incident on the earth's atmosphere, corresponding to line densities equal to and greater than 10^{14} electrons/meter is $1.6 \times 10^{-12} \text{ m}^{-2} \text{ sec}^{-1}$. Thus, the average overdense meteor rate observed in the direct line-of-sight and by F-layer reflections should be on the order of 185.3 meteors/min and 27.9 meteors/min, respectively. It is evident that these values are about a factor of 20 times greater than the estimates obtained using the Greenhow and Watkins data. The discrepancy in the results can most likely be attributed to the fact that Manning's and Eshleman's data do not take into account aspect sensitivity effects.

The incremental meteor rate as deduced from Greenhow's and Watkins' measurements are shown in Figures 16 and 17. It is interesting to note that, for the direct line-of-sight case, an insignificant amount of overdense meteor echoes should be detected at elevation angles greater than about 20° and that the number of echoes originating from F-layer reflections should be on the same order of magnitude as the total number detected above 10° elevation angle in the direct line-of-sight.

In addition to the line-of-sight echoes, meteor returns will also appear at over-the-horizon ranges by means of F-layer reflections which, according to Figure 14, are specified by the condition $R < R_1 + R_2$. It can be shown by spherical geometry that the surface area at 95 km altitude is 1.334 x 10^7 km² for elevation angle coverage between 0° and $30^\circ32^\circ$ and 180° azimuthal coverage. This value is approximately 31.76 times greater than the area estimated to be under illumination in the meteor band by Greenhow's and Watkins' equipment. It follows that the over-the-horizon meteor rate will be about six times greater than the total line-of-sight rate, i. e., the sum of the direct and F-layer reflection line-of-sight rate. It is reiterated that this conclusion is based on the following assumptions: (1) 350-km F-layer reflection height, (2) 926.6 km (500 nautical miles) skip distance, and (3) 95-km meteor altitude.

The estimated rate of overdense meteor echoes detected at over-the-horizon ranges is presented in Figure 18 as a function of elevation angle increments.

5. CONCLUSIONS

Based on the observational data recorded by Greenhow and Watkins at 32 MHz, the median cross sectional area of overdense meteors, at 6 and 40 MHz, could be on the order of 1.35×10^7 and 2.02×10^6 m², respectively. The median time duration at the lower frequency could be as high as 24.2 sec while, at the higher frequency, it decreases to about 0.5 sec. The extrapolated cross sectional areas and time durations compare favorably with theoretical estimates.

It is estimated that, for an HF backscatter radar, the maximum number or random overdense meteors appearing in the line-of-sight could be on the order of 21 meteors/min. At over-the-horizon ranges, the maximum overdense meteor rate that could be detected could increase to about 126 meteors/min.

It is postulated from ionospheric wind measurements that, at 6 MHz, the Doppler frequency shift encountered on reflection from a meteor trail could be between 2.5 and 4.0 Hz for propagation along the horizon and decreases to zero Hz at the zenith.

The estimated characteristics of the cross sectional area, time duration and rate of overdense meteor echoes, as described in this report, are based on one set of observational data recorded by Greenhow and Watkins (1964). It would be advantageous to validate these predictions with additional experimental data.

6. REFERENCES

Abramowitz, M. and I. A. Stegun, "Handbook of Mathematical Functions with Formulas, Graphs and Mathematical Tables", National Bureau of Standards, Applied Mathematics Series 55, U.S. Government Printing Office, 1965.

Eshleman, V.R., "Meteors and Radio Propagation: Part A-Meteor Ionization Trails, Their Formation and Radio-Echoing Properties", Stanford University Technical Report No. 44, Contract No. N6onr 25132, NR 373 362, February 1955.

Eshleman, V.R., P.B. Gallagher and R.F. Mlodnosky, "Meteor Rate and Radient Studies: Theoretical and Experimental Radio Studies of Meteor Ionization Trails with Application to Radio Propagation by Meteor Reflections", Stanford University Final Report, Contract AF 19(604)-1031, February 1957.

Greenhow, J.S., "Limitations of Radar Techniques for the Study of Meteors", in Proceedings of the Symposium on the Astronomy and Physics of Meteors, Smithsonian Contributions to Astrophysics, Vol. 7, pp 5-17, 1963.

Greenhow, J.S. and E.L. Neufeld, "The Diffusion of Ionized Trails in the Upper Atmosphere", Journal of Atmospheric and Terrestrial Physics, Vol. 6, pp 133-140, March 1959.

Greenhow, J.S. and C.D. Watkins, "The Characteristics of Meteor Trails Observed at a Frequency of 300 Mc/s", Journal of Atmospheric and Terrestrial Physics, Vol. 26, pp 539-558, 1964.

Manning, L.A. and V.R. Eshleman, "Meteors in the Ionosphere", Proceedings of IRE, Vol. 47, pp 186-199, February 1959.

Millman, G.H., "Characteristics of HF Radar-Overdense Meteor Echoes", General Electric Technical Information Series Report No. R75EMH2, September 1975 (Defense Documentation Center No. AD-B016 383L).

Rao, G. L. N., "Horizontal Drifts and Anisotropy of Irregularities in the Lower Ionosphere - A Review", University of Illinois, Aeronomy Laboratory Report No. 6, June 1965.

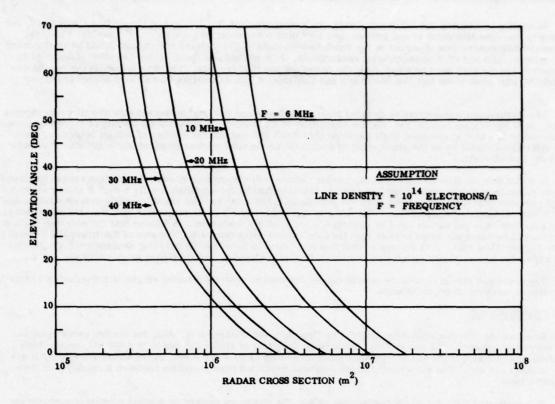


Figure 1. Overdense Meteor Cross Section at an Altitude of 95 km

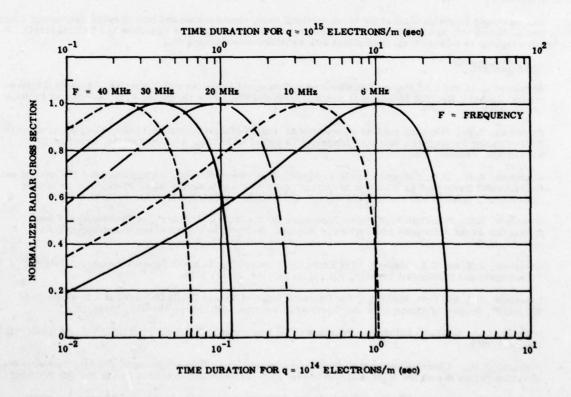


Figure 2. Normalized Radar Cross Section of Overdense Meteors as a Function of Time Duration for an Ionization Altitude of 95 km

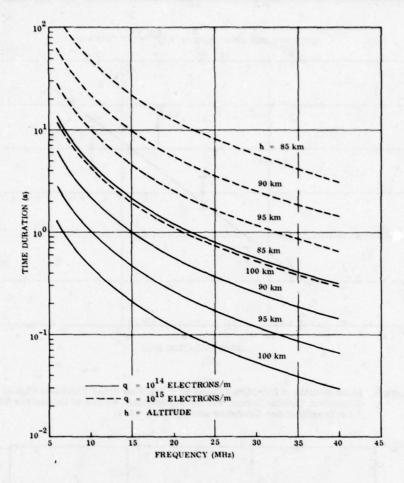


Figure 3. Time Duration of Overdense Meteor Trail Echoes at HF

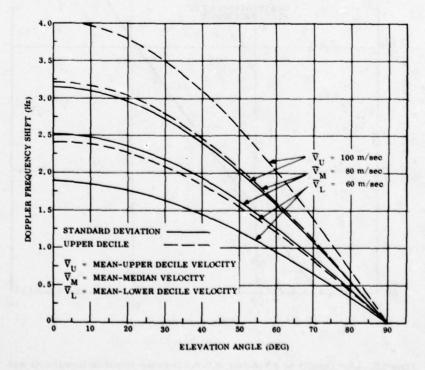


Figure 4. Distribution of Meteor Trail Doppler Frequency Shifts as a Function of Elevation Angle and Ionospheric Wind Speeds at 6 MHz

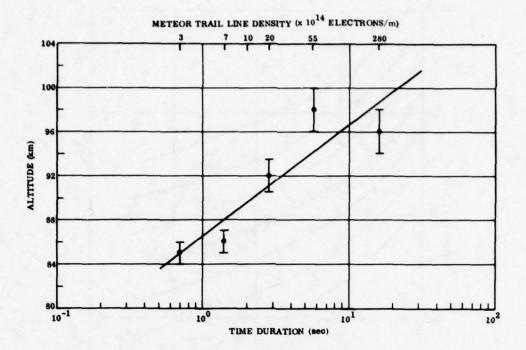


Figure 5. Mean Heights of 300-MHz Echoes as a Function of the Time Duration of the Coincident 32-MHz Echoes and the Approximate Values of the Meteor Trail Line Density (After Greenhow and Watkins, 1964)

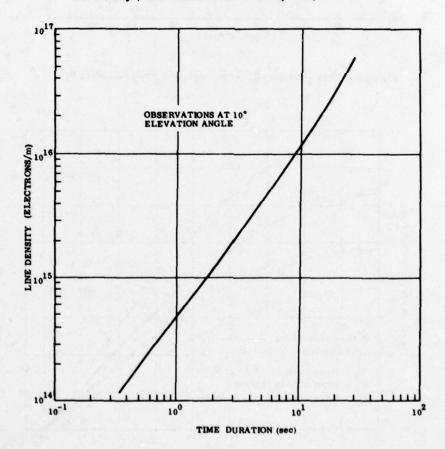


Figure 6. Line Density as a Function of Time Duration Based on Greenhow's and Watkins' Data (1964) at 32 MHz



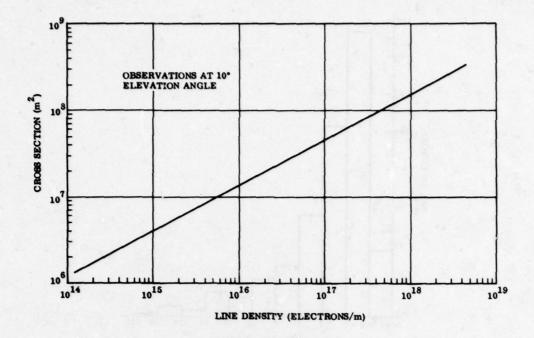


Figure 7. Cross Section as a Function of Line Density Based on Greenhow's and Watkins' Data (1964) at 32 MHz

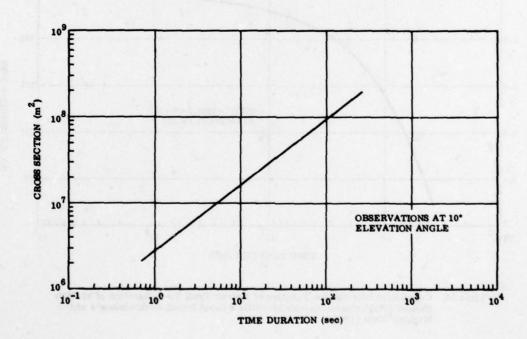


Figure 8. Radar Cross Section of Overdense Meteor Echoes as a Function of Time Duration Based on Greenhow's and Watkins' Data (1964) at 32 MHz

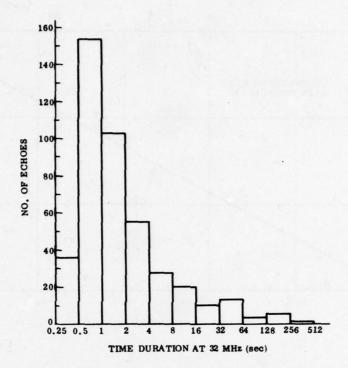


Figure 9. Time Duration Distribution of 32-MHz Echoes Which Correlate with 300-MHz Echoes (After Greenhow and Watkins, 1964)

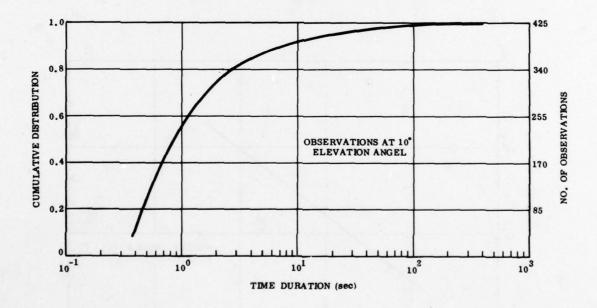


Figure 10. Cumulative Distribution Function of Meteor Trail Time Duration of 32-MHz Echoes Which Correlate with 300-MHz Echoes Based on Greenhow's and Watkins' Data (1964)

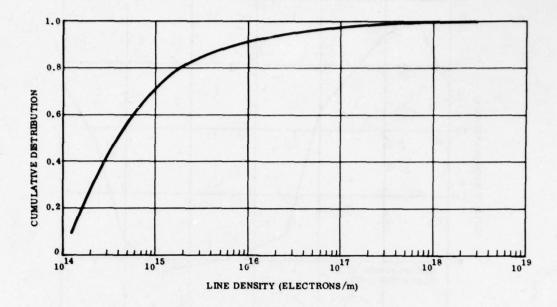


Figure 11. Cumulative Distribution Function of Meteor Line Density Based on Greenhow's and Watkins' Data (1964) at 32 MHz

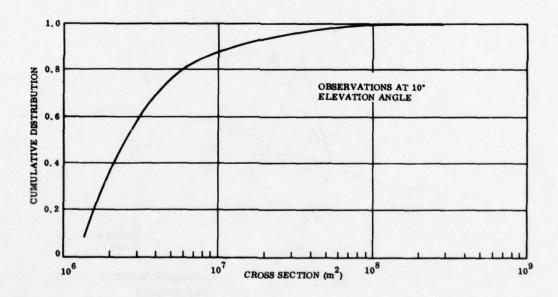
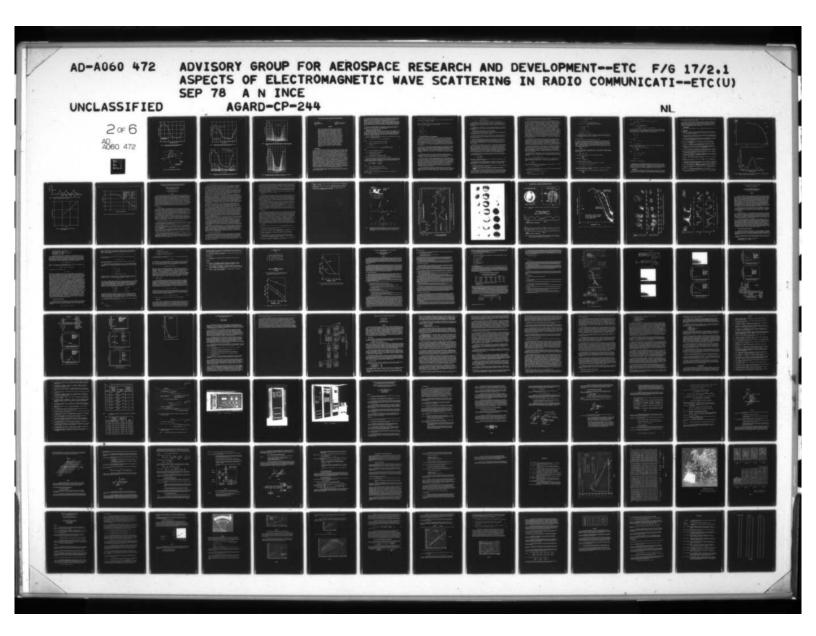
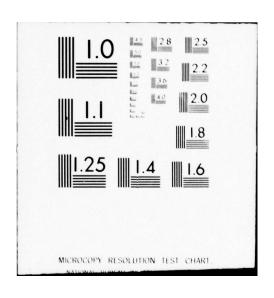


Figure 12. Cumulative Listribution Function of Meteor Cross Section of 52-MHz Echoes Which Correlate with 300-MHz Echoes Based on Greenhow's and Watkins' Data (1964)





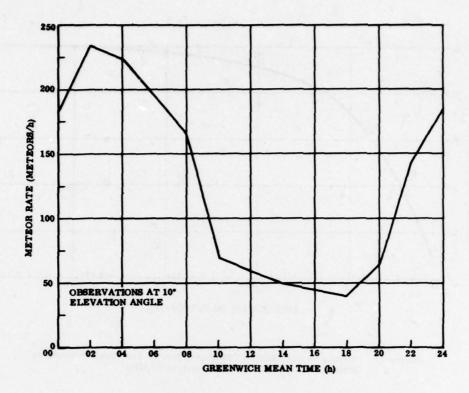


Figure 13. Rate of 32-MHz Echoes with Time Durations Greater than One Second (After Greenhow and Watkins, 1964)

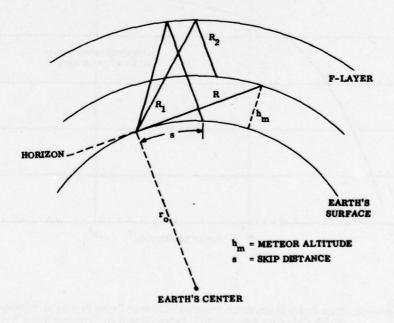


Figure 14. F-Layer Reflection Meteor Echo Geometry

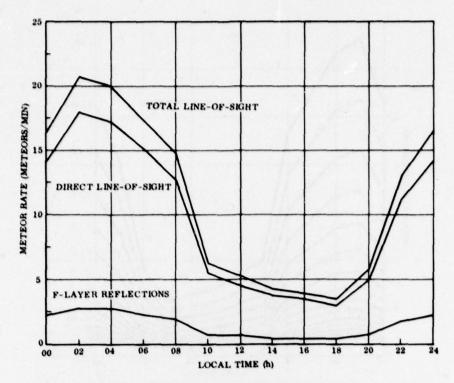


Figure 15. Estimated Rate of Overdense Meteor Echoes in Line-of-Sight at HF Band Based on Greenhow's and Watkins' Data (1964) at 32 MHz

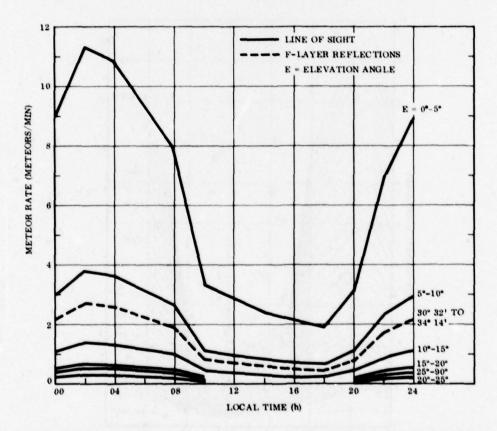


Figure 16. Estimated Incremental Rate of Overdense Meteor Echoes in Line-of-Sight at the HF Band Based on Greenhow's and Watkins' Data (1964) at 32 MHz

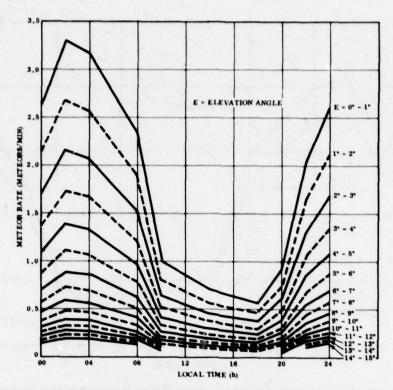


Figure 17. Estimated Rate of Overdense Meteor Echoes Between Zero and 15° Elevation Angle in the Line-of-Sight at the HF Band Based on Greenhow's and Watkins' Data (1964) at 32 MHz

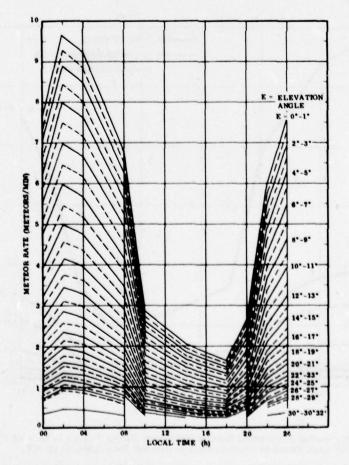


Figure 18. Estimated Incremental Rate of Overdense Meteor Echoes After F-Layer Reflection at HF Band Based on Greenhow's and Watkins' Data (1964) at 32 MHz

TIME AND FREQUENCY SPREAD IN METEOR BURST PROPAGATION PATHS

By

M. D. Grossi Raytheon Company Wayland, Mass. 01778 U.S.A. A. Javed
Bell-Northern Research Ltd.
Ottawa, Ontario Kly-4H7
Canada

ABSTRACT

Meteor burst propagation provides an intriguing medium for over-the-horizon intermittent communications at VHF, but is characterized by several undesirable properties that have severely limited, thus far, its application to links of practical relevance. In fact, this channel, in addition to being intermittent, is also characterized by time-variable multipath spread and doppler spread. Typically, in VHF links 100 to 1500 km long the gain decreases by about 10 dB after a few seconds from trail formation, the value of the multipath spread raises to a few microseconds, while doppler spread is at most a few hertz. Analog techniques did not prove fully suitable in the past for coping with this type of channel, and very few applications of meteor burst links are known to have reached practical implementation and operational use. Digital techniques, however, offer greater promise, especially is used in connection with instantaneous channel probing and with the adaptive adjustment of the data rate to the channel bandwidth. It can be shown that hourly average data rates of 20 kilobits/sec are thus reliably achievable. Basic to the design of an adaptive system is the knowledge of the channel's time spread and frequency spread. The paper reviews what is known of these channel properties.

1. INTRODUCTION

It is well known that the long electron trail produced at heights between 80 and 100 km by a meteoroid that enters the earth's upper atmosphere can be used as a highaltitude reflecting medium for burst-type communications beyond line of sight at VHF [McKinley, 1961]. In the past two decades, several communication systems, such as JANET and METEORFAX, have been actually constructed based on this principle. One of the reasons that has thus far prevented a widespread use in communications of the meteor burst channel is that this propagation path, in addition to being intermittent, is characterized by time-variable gain and by time-dependent multipath spread and doppler spread. From performing as an almost perfect rectilinear reflector at the initial instant of its formation, the trail in a fraction of a second (or at most in a few seconds) degenerates into a medium characterized by low gain and by a substantial time and frequency spread. This is due in part to the growth of the trail radius because of electron diffusion and in part to the warping of the trail into a distorted shape, caused by wind shear and turbulence. Because instances of renewed attention to meteor burst communications for special applications such as hydromet networks and blackout-free polar communications have been numerous in the recent past, it is of interest to review the subject. Nowadays in fact, due to the recent progress in digital communication techniques, it appears feasible to cope with the undesirable characteristics of this channel by implementing an adaptive scheme [Ahmad et al. 1972; Bokhari et al, 1975] that probes the channel in order to determine its instantaneous properties, processes this information to decide what is the highest usable data rate, and provides temporary storage of the information between long-lived, low data rate circuits and the short-lived, intermittent, broadband propagation path.

In order to achieve this goal, it is necessary to know in detail the time and frequency spread of this propagation path; in the following sections we review what we know of these quantities.

The time variability of the path gain and of the multipath structure were investigated, based on existing experimental data and on available analytical formulations. McKinley [1961] and the review paper by Sugar [1964] includes an analysis of the time dependence of the gain, while the recent correspondence by Akram et al [1977] illustrates an analytical formulation for the path impulse response and for its variability with time. The time dependence of the path's doppler spread was investigated based on experimental data. Later on in the paper we apply the notions acquired on the time variability of gain, of multipath structure and of doppler spread to the evaluation of the data rate and error rate that characterizes a channel that uses the above path.

The paper formulates elementary considerations on these channel quantities. No statistical analysis was performed as to the probability distribution of the time dependence of gain, multipath spread, and doppler spread.

2. VARIABILITY OF LINK'S GAIN WITH TIME

We specialize our discussion to long wavelength reflections from underdense meteor trails, the most common case. For this case, $q<10^{14}\ {\rm el/m}$. We also neglect for simplicity the typical diffraction pattern visible as a minor fluctuation of the meteor echo amplitude after the meteoroid has crossed the first Fresnel zone and continues in its path, thus creating new sections in the ionized trail that produce alternately favorable and unfavorable interference.

Under these assumptions [McKinley, 1961; Sugar, 1964], the equivalent echoing area of the trail in forward scattering is:

$$\sigma = (\sigma_e q^2 \sin^2 \gamma) \times (\text{half of first Fresnel zone})^2$$
 (1)

where

 $\sigma_{e} = 10^{-28} \text{ m}^2$ (electron scattering cross-section)

q - effective line density of the trail (el/m)

 λ = wavelength, m

(half of first Fresnel zone)² =
$$\frac{\lambda R_1 R_2}{[(R_1 + R_2)(1 - \sin^2 \phi \cos^2 \beta)]}$$
 (2)

where

R, - Distance from Transmitter to Trail

R - Distance from Trail to Receiver

- 1/2 Forward Scatter Angle

Angle between Trail and Propagation Plane

Figure 9-1 in McKinley [1961] illustrates the geometry involved.

The echoing area does not remain constant with time, because the electrons in the trail diffuse, with consequent increase of the trail's radius. Assuming that diffusion is ambipolar, the echoing area σ (equation 1) must be multiplied by a term that describes its decrease with time. This term is:

$$\exp \left[-\frac{32 \, \mu^2 \, \text{Dt}}{\lambda^2 \, \text{sec}^2 \, \phi} - \frac{8 \, \pi^2 \, \text{r}_0^2}{\lambda^2 \, \text{sec}^2 \, \phi} \right] \tag{3}$$

where

D = ambipolar diffusion coefficient, m²/sec

t - time counted from Fresnel length formation, sec

ro = initial radius of trail, m.

The value of \mathbf{r}_0 may be related to the height h of the point of tangency by the empirical formula:

$$\log_{10} r_0 = 0.075 h - 7.9$$

where h is expressed in km and r_0 in meters.

The value of the ambipolar diffusion coefficient D can be expressed (in the height range 80 km < h < 110 km) by the formula:

$$\log_{10} D = 0.0679 h - 5.663$$

where D is in m^2 /sec and h is in km. A numerical example (based on Equation 3) is worked out in Figure 1, with the following assumptions:

$$\lambda = 7.5 \text{ m} \text{ (f = 40 MHz)}$$

ø = 80°

h = 90 km

 $\log_{10} D = 0.437$

 $\log_{10} r_0 = -1.15$

D = 2.74

 $r_0 = 7 \times 10^{-2} \text{ m}$

3. MULTIPATH STRUCTURE AND ITS TIME DEPENDENCE

By following a ray tracing treatment of e.m. reflections from a single meteor trail developed by Manning [1959], Akram et al [1977] traced, for an assumed trail orientation, the ray paths that connect the transmitting with the receiving terminal. Until about 0.5 sec (or at most a few seconds) from trail generation, the trail is still rectilinear and it can be said (in the "macroscopic" sense) that there is only one path between the two terminals. After that, wind shear and turbulence warp the trail into distorted shapes. In order to find the number of paths now active, Akram et al [1977] adopted a "glint" model of the distorted trail [Manning, 1959] and specialized their analysis to a sinusoidal trail shape that provided three paths between the two terminals.

For each one of the rays that were traced, Akram et al [1977] evaluated the broadening that a 50-ns sampling pulse is expected to undergo while propagating from transmitter to receiver. This was done by using the method developed by Elliott [1957] for dispersive channels after an algebraic error which Elliott had incurred had been corrected [Knop and Cohn, 1963]. In their analysis Akram et al [1977] chose a 50-ns pulsewidth to approximate a delta function for the determination of the path's impulse response. The response of a single path to a 50-ns pulse was calculated and is given in Figure 2.

However, about 0.5 seconds (or at most a few seconds) after the formation of a trail, wind shear distorts the trail shape and gives rise to more than one path ("macroscopic" multipath structure) connecting receiver and transmitter, as a result of the appearance of additional reflecting points on the trail (glint theory).

Each one of the paths connecting transmitter and receiver is characterized by a particular group delay and the time difference between the first and last arriving path is the multipath spread. For each one of the paths the waveform broadening of Figure 2 still applies. In computing the multipath structure, Akram et al [1977] assumed again that the trail before distortion is horizontal and perpendicular to the vertical propagation plane and that after distortion the various trail portions (now no longer horizontal) that provide paths between transmitter and receiver are still perpendicular to the propagation plane, but this now is no longer a vertical one. Each trail's "reflecting" segment is tangent to a prolate spheroid that has the transmitter and receiver as focii and that is characterized by a certain group delay in the path transmitter-reflection point-receiver.

In order to establish the number of the paths that reach the receiver and to compute the group delay that characterizes each one of them, Akram et al [1977] adopted for the trail's shape, after distortion by the wind, the sinusoidal model of Manning [1959], consisting of a sinusoid on a height slope. By making the following assumptions:

 $\tan \theta = 0.03$ (θ is the slope with respect to the horizontal plane of the distorted trail)

V = 30 m/s (maximum wind velocity)

 $\lambda = 2.9 \text{ km}$ (spatial wavelength of the shear profile of the wind)

(the symbols above are the ones used by Manning [1959]), it was determined that with this model the number of paths is three and that the paths are characterized by a relative time delay of 710 ns (between the first and second arriving paths) and 940 ns (between the second and third arriving paths). Figure 3 illustrates the structure that was computed.

Concerning the time variability of the multipath spread. Figure 4 is indicative of a typical dependence. The graph was constructed combining experimental data collected by Carpenter and Ochs [1962] with other radio observations of meteor echoes available to the authors.

4. DOPPLER SPREAD IN METEOR ECHOES AND ITS TIME VARIABILITY

Still following the criterion adopted in the previous sections, we limit our considerations to the portion of the meteor echo (the so-called "body") that excludes the initial segment where the Fresnel pattern is contained.

Physically, doppler spread is due to the fact that the various reflecting portions of the trail active in a given echo produce different "body" doppler shifts because they are characterized by slightly different relative velocities with respect to the transmitter/receiver pair.

Sources of doppler spread information for meteor echoes are rather scant. One is the recording of wind-induced doppler performed by phase-coherent radars (monostatic and bistatic) that observe winds at meteor trail height [Grossi et al, 1972]. A Fourier transform of these doppler frequency versus time records makes it possible to obtain directly the desired quantity (it is the width in the frequency domain of the doppler spectrum).

Another source of information is the recording of meteor echoes amplitude versus time obtained with meteor radars [McKinley, 1961]. How these amplitude records are of use can be seen through the following argument. Let's assume that the transmitted frequency is a sine wave of frequency f_0 and that the received signal, because of the doppler spread phenomenon, is a sum of sine waves that occupy a band large B Hz (our unknown) around the doppler-shifted frequency f_1 . Kennedy and Lebow [1964] show that this received signal has a randomly varying amplitude and phase. The amplitude peaks correspond to times at which the signals received from different segments of the trail tend to reinforce, and the troughs to periods during which cancellation or fading occurs, the average duration of a reinforcement or a fade being approximately 1/B.

As pointed out by Bello [1965], Ehrman and Esposito [1968], Bello and Esposito [1970], the desired quantity B (the doppler spread) can be obtained from the amplitude data with the formula:

$$B = \frac{1}{\pi} \sqrt{\frac{2 < e^2}{\langle e^2 \rangle}} \tag{4}$$

where e(t) is the detected signal envelope, the dot indicates a time derivative, and the brackets indicate a time average.

Using Equation (4), a preliminary estimate of the doppler spread was obtained from records of VHF meteor radar echo amplitudes: it is typically ≤ 1 Hz, with minimum values of 1/10 to 1/100 Hz and maximum values of a few Hz in the life span of the trail's "body".

Considerable measurement activity must be carried out before a reliable dependence of doppler spread versus time can be established.

5. ESTIMATION OF DATA RATES AND ERROR PROBABILITY IN METEOR BURST PROPAGATION CHANNELS

As we have seen in the previous sections, the meteor burst communication channel is characterized by three time-variable parameters: gain, multipath spread and doppler spread. We compute in this section the data rate and error rate that would characterize such a channel if gain, multipath spread and doppler spread would be fixed and would acquire values typical of a meteor trail after 5 seconds from trail formation.

The adaptivity scheme proposed by Ahmad et al [1972] could be used to adjust the data rate to the instantaneous values of the channel parameters.

To calculate the data rates and error probability in the meteor channel, the formulation of Kennedy and Lebow [1964], Lebow et al [1964], and Kennedy [1969] can be used. According to this formulation, dispersion in both time and frequency domains is sufficient to characterize a dispersive channel of known gain. In dispersive channels, a transmitted signal of length T and bandwidth W is received as a signal of length T + L and bandwidth W + B, where L is the dispersion in time and B is the dispersion in frequency. If we focus our attention on any particular narrow-frequency range, its envelope will fade at an average rate of B. Portions of the transmitted spectrum within 1/L Hz of each other tend to fade coherently at a given time. These fading properties are represented pictorially in Figure 6 of Kennedy and Lebow [1964]. In that figure, the abscissa represents time and it is divided into increments of width 1/L Hz. Each rectangle in the grid system has an area of 1/BL. According to the model each rectangle represents a piece of transmitted signal with approximately constant fading properties. A transmitted pulse of width T and bandwidth W = 1/T is represented by a rectangle of length T along the time axis and length W = 1/T along the frequency axis. In part (a) of the figure mentioned previously, T = 1/2B and W = 1/T = 1/2L, so that the entire signal rectangle is contained within one grid rectangle and hence tends to fade coherently. This is described by saying that the signal has one diversity element (diversity z = 1). In part (b) of the same figure a second example is given with the signal rectangle having a time dimension 1/20 of the time unit (that is 1/B) and a frequency dimension five times the frequency unit (that is 1/L). Therefore the signal has diversity Z = 5.

The simplifying assumptions that any part of a signal within a grid rectangle fades coherently and portions within different rectangles fade independently leads one to regard the signal as the sum of the five independently fading components. This is why we say that the signal has a diversity five; in fact the term diversity Z is identified with the number of independently fading components contained in the transmitted signal. The greater the diversity of a signal, the more independent samples of fading process are observed when the signal is received. Thus, the fluctuations in the received signal energy become less pronounced as the signal diversity is increased.

By using the above definition for the diversity Z, we can formulate an estimate of the data rate and error probability that are possible over a dispersive channel for a binary modulation scheme. In this signalling scheme, a pulse of carrier frequency f_1 is used for '1' and a pulse of frequency f_0 is used for a zero. The two frequencies have to be separated by at least W + B to prevent overlap of the received signal spectra. The probability of error, P_e , depends upon both the ratio E/N_0 (where E is the received signal energy and N_0 is the receiver noise power per cycle of the bandwidth) and the diversity Z.

Kennedy and Lebow [1964] plotted in their figure 10 the probability of errors as a function of E_m/N_0 and as a function A(y), where $y=Z/(E_m/N_0)$. The function A(y) is the efficiency function. The probability of error can be approximated by the following expression:

$$P_{e} \approx 0.2 \exp \left[-\frac{1}{2} (E_{m}(N_{0}) A(y))\right]$$
 (5)

Thus, to obtain the best performance we should maximize A(y). In their figure 11, Kennedy and Lebow [1964] plotted A(y) as a function of y. The function A(y) has a fairly broad maximum centered at about y = 0.35, with a maximum value A(0.35) = 0.3. Thus,

$$\frac{1}{y} = \frac{E_{m}/N_{O}}{z} = 3 \tag{6}$$

Thus for the best performance, the $\mathrm{E/N}_0$ per diversity element should be 3. For this value of y, the error of probability is given by

$$P_{e} \approx 0.2 e^{-0.15 E_{m}/N_{O}}$$
 (7)

On the basis illustrated above, we can now evaluate the data rates obtainable with a binary meteor burst communication link.

We make the following assumptions for the link:

(a) Meteor height = 90 km

Terminal-to-terminal distance = 1000 km

$$\lambda = 7.5 \text{ m} \text{ (frequency = 40 MHz)}$$

$$q = 6.3 \times 10^{13} \text{ el/m}$$

$$P_{R} = 5 \times 10^{-32} \frac{P_{T} G_{R} G_{R}^{3} q^{2} \sin^{2} y}{R_{1} R_{2} (R_{1} + R_{2}) (1 - \sin^{2} \phi \cos^{2} \beta)}$$

$$G_{T} = G_{R} = 13 \text{ dB}$$

$$\phi \approx 80^{\circ}$$

$$\beta = 90^{\circ}$$

$$P_{R} = 2.72 \times 10^{-17} P_{T}$$
Path Loss (K) = 2.72 × 10⁻¹⁷

- (b) Galactic noise density at 40 MHz is 15 dB higher than k T_0 , where $T_0 = 300^\circ K$, and k = Boltzman's constant = 1.38 x 10^{-23} joules/°K. Therefore the equivalent noise input temperature of the receiver is $9.65 \times 10^{3\circ} K$.
- (c) $P_{T} = 100 \text{ kW}$

We aim at an error rate in data transmission that is $\leq 10^{-3}$.

Since gain, multipath spread and doppler spread are all time-variant, the signal design must be performed in such a way as to provide an error rate smaller than the specified ($\leq 10^{-3}$) for the whole duration of the propagation path. Let's see first what data rate is achievable at a time close to the trail's formation (say 0.2 second after it). Multipath spread is L \approx 0.35 µsec (see Figure 4), channel gain has not yet begun to decrease (see Figure 1), doppler spread can be assumed to be B = 1 Hz. In order to achieve an error probability $\leq 10^{-3}$ (say 2 x 10^{-4}), we must have (from figure 10 in Kennedy and Lebow, 1964)

$$\frac{E_{m} A(y)}{N_{0}} \sim 13$$

where E_m is the total energy received per "mark" or "space" (made by n chips) and N_0 is the receiver noise density. The best value of A(y) (see figure 11 of Kennedy and Lebow, 1964) is 0.3 and

$$\frac{E_m}{N_0} = \frac{13}{0.3} = 43.33$$

To achieve this (see same figure 11 of the cited paper) we must have

$$y = \frac{z \cdot n}{E_m/N_0} \sim \frac{1}{3}$$

and therefore we need

$$z \cdot n = \frac{43.33}{3} \approx 14$$

or 14 diversity elements are required.

In a 4 MHz system, with a 0.25 µsec pulsewidth (TW = 1) we have:

LW =
$$0.35 \times 10^{-6} \times 4 \times 10^{6} = 1.4$$

BT = $\frac{1}{4} \cdot 10^{-6} = 2.5 \times 10^{-7}$

and therefore the equation Z = LW applies and we have Z = 1.4 per chip. We need therefore n = 10 chips per "mark" or "space".

The achievable data rate R in a binary system can be computed as follows:

$$R = \frac{P_R/N_0}{E_m/N_0}$$

where
$$P_R = 27.20 \times 10^{-13}$$
 watts $N_0 = KT_0 = 1.38 \times 10^{-23} \times 9.65 \times 10^3 = 1.33 \times 10^{-19}$ $E_m/N_0 = 43.33$

Therefore,

$$R = \frac{27.20 \times 10^{-13}/1.33 \times 10^{-19}}{43.33}$$
$$= 10^{5} \times \frac{200}{43.33} = 4.6 \times 10^{5} = 460 \text{ kilobits/sec}$$

Let's see now what data rate is achievable near the end of the trail lifetime (say 5 seconds after formation). Multipath spread is now $L=4.5~\mu sec$ (see Figure 4), channel gain has decreased by 10 dB, doppler spread can be assumed to stay B=1~Hz. In order to achieve the same error probability as before, we must still have

$$\frac{E_{m}}{N_{0}} = 43.33$$

$$y \approx \frac{1}{3}$$

$$Z \cdot n = 14$$

Now, however:

while

BT =
$$\frac{1}{4} \times 10^{-6} \ll 1$$

Equation Z = LW still applies, but we now have Z = 18 per chip. Therefore we need only n = 1 chip per "mark" or "space".

For the achievable data rate, we now have:

$$R = \frac{P_R/N_0}{E_m/N_0}$$

where

$$P_R = 27.20 \times 10^{-14} \text{ watts}$$
 $N_0 = 1.33 \times 10^{-19}$
 $\frac{E_m}{N_0} = 43.33$

and therefore R = 46 kilobits/sec.

Figure 5 shows the instantaneous data rate affordable through the link, and its time dependence during the lifetime of the meteor trail. Based on Figure 5, we have computed the average value of the data rate during the trail lifetime by integrating the curve in the time domain between 0.2 seconds and 5 seconds. We have found for this average the value of 300 kilobits/sec. By assuming that meteor trails are available for 4 minutes every hour, the hourly average data rate is ~ 20 kilobits/sec.

6. CONCLUSIONS

By revisiting the meteor burst communication channel, one again finds this medium far from ideal, from the standpoint of the communications system engineer. However, with digital electronics techniques that have recently become available, there are now

means of coping with the problems involved in this channel, such as the time variable gain, multipath spread and doppler spread.

Basically, the approach that is potentially capable of solving the problem is the real-time probing of the medium with a waveform capable of instantaneously measuring gain (a 20 dB variability during the lifetime of the trail is typical), multipath spread (the most important quantity, with a variability approximately from 0.1 microsecond to 10 microseconds) and doppler spread (the least important parameter, with a variability from approximately 0.1 Hz to a few Hz).

7. ACKNOWLEDGMENT

This research has been supported to part by NOAA under Contract SFCP Agr. 04-4-158-16.

8. REFERENCES

- Ahmad, K.A., A. Javed and M.D. Grossi, Adaptive Communications Via Meteor Forward Scattering, Pakistan International Symposium on Electrical Engineering, November 15-17, 1972, Lahore, West Pakistan.
- Akram, F., N.M. Sheikh, A. Javed and M.D. Grossi, Impulse Response of a Meteor Burst Communications Channel Determined by Ray-Tracing Techniques, <u>IEEE Transactions on</u> Communications, April 1977, pp. 467-470.
- Bello, P.A., Some Techniques for the Instantaneous Real-Time Measurement of Multipath and Doppler Spread, <u>IEEE Transactions on Communications Technology</u>, Vol. COM-13, pp. 285-292, September 1965.
- Bello, P.A. and R. Esposito, Measurement Techniques for Time-Varying Dispersive Channels, <u>ALTA FREQUENZA</u>, No. 11, Vol. XXXIX, pp 980-310E to 996-326E, 1970.
- Bokhari, S.H., A. Javed and M.D. Grossi, Data Storage for Adaptive Meteor Scatter Communication, <u>IEEE Transactions on Communications</u>, March 1975, pp. 397-399.
- Carpenter, R.J. and G.R. Ochs, High Resolution Pulse Measurements of Meteor Burst Propagation at 41 Mc/s Over a 1295 km Path, <u>Journal of Research</u>, NBS-D. Radio Propagation Vol. 66D, No. 3, May-June 1962, pp. 249-263.
- Ehrman, L. and R. Esposito, On the Accuracy of the Envelope Method for the Measurement of Doppler Spread, Raytheon Research Div. Tech. Memo T-806, December 18, 1968.
- Elliott, R.S., Pulse Waveform Degradation Due to Dispersion in Waveguide, <u>IRE Trans.</u>
 <u>Microwave Theory Techniques</u>, pp. 254-257, October 1957.
- Grossi, M.D., R.B. Southworth and S.K. Rosenthal, Radar Observations of Meteor Winds Above Illinois, Chapter 9 of <u>Thermospheric Circulation</u> (1972), Ed. W.L. Webb, The MIT Press, Cambridge, Mass.
- Kennedy, R.S., <u>Fading Dispersive Communication Channels</u>, New York: Wiley Interscience, 1969.
- Kennedy, R.S. and I.L. Lebow, Signal Design for Dispersive Channels, <u>IEEE Spectrum</u>, March 1964, pp. 231-237.
- Knop, C.M. and G.I. Cohn, Pulse Waveform Degradation Due to Dispersion in Waveguide, IEEE Trans. Microwave Theory Techniques, Vol. MTT-11, pp. 445-447, September 1963.
- Lebow, I.L., P.R. Drouilhet, N.L. Daggett, J.N. Harris and F. Nagy, The Westford Belt as a Communications Medium, <u>Proceedings of the IEEE</u>, May 1964, pp. 543-563.
- Manning, L.A., Oblique Echoes from Overdense Meteor Trails, J. Atmospher, Terrestr. Phys., Vol. 14, 1959.
- McKinley, D.W.R., Meteor Science and Engineering, New York: McGraw-Hill, 1961.
- Sugar, G.R., Radio Propagation by Reflection from Meteor Trails, <u>Proc. of the IEEE</u>, February 1964, pp. 116-136.

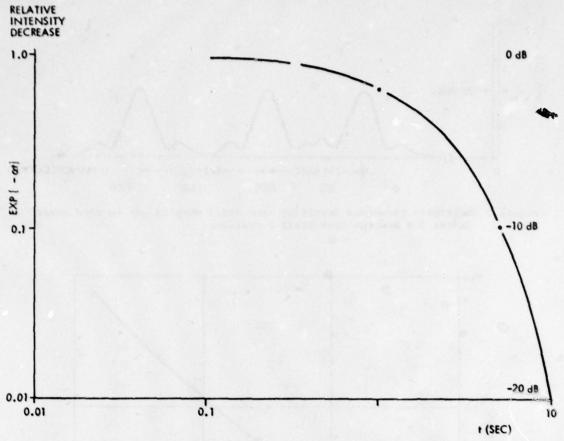


Figure 1 Decrease of Echo Intensity (Power) with Time

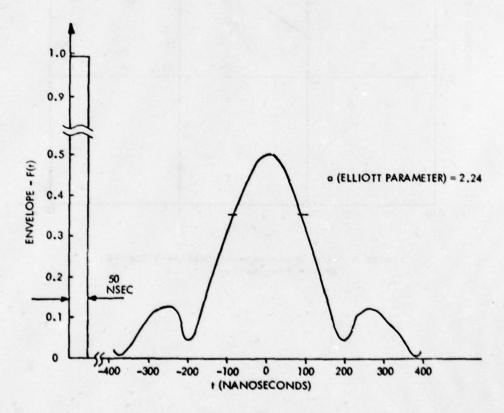


Figure 2 Envelope of the Output of a Single Path (Response to a 50 Nanosecond Pulse) Within 0.5 Seconds from Trail Formation

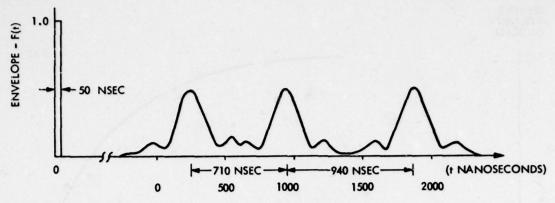


Figure 3 Multipath Structure Resulting from Trail Warping Due to Wind Shear (After 0.5 Seconds from Trail Formation)

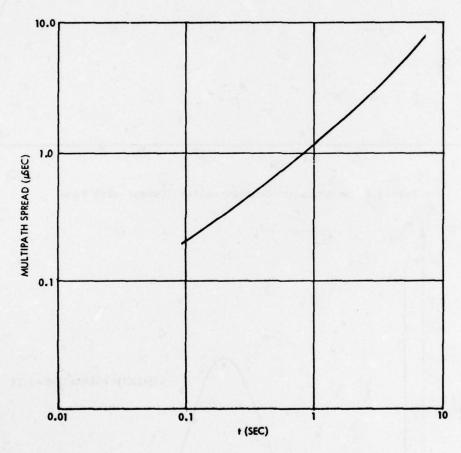


Figure 4 Time Dependence of Multipath Spread at VHF Frequencies

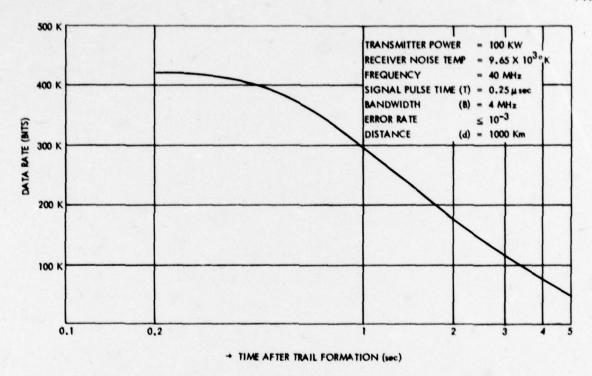


Figure 5 Instantaneous Data Rate As A Function of Time From Trail Formation

THE EVOLUTION OF SCATTERING EQUATORIAL F-REGION IRREGULARITIES AND RESULTANT EFFECTS ON TRANS-IONOSPHERIC RADIO WAVES

Herbert E. Whitney, Jules Aarons, Jurgen Buchau and Edward J. Weber Air Force Geophysics Laboratory Hanscom AFB, MA 01731

J.P. McClure University of Texas at Dallas Richardson, TX 74080

SUMMARY

Results from a series of ground and airborne experiments are presented which describe spatial and temporal characteristics of equatorial F-region irregularities and the effect of these irregularities on trans-ionospheric radio propagation. The experiments included UHF amplitude scintillation measurements from the WIDEBAND, MARISAT and LES-9 satellites, and simultaneous ionospheric measurements from the AFGL Airborne Ionospheric Observatory and the Jicamarca Radar Observatory in Peru. The results indicate a highly localized generation of the irregularities such that individual patches consist of dense irregularities of the order of 10-100% of the ambient electron density. The extent of each patch is of the order of 50-400 km East-West and at times greater than 1200 km in the North-South direction. Within these regions small scale irregularities from several kilometers to as small as 3 meters often exist. Once the patches are generated they move predominantly eastward with initial velocities of 50-150 meters per second. Aircraft measurements decrease the fading rate by flying in the direction of the ionospheric drift pattern and increase the rate by flying in the opposite Ground and airborne signal statistics, primarily frequency spectra, are direction. discussed.

INTRODUCTION

F layer irregularities, generated primarily at night, present a problem to many forms of trans-ionospheric radio propagation. Satellite communication systems have recorded fading effects at frequencies to 6 GHz (with peak to peak values of a few dB); fading of over 20 dB was noted recently at 1200 MHz, in the band used by MARISAT (Fremouw et al., 1977). A high occurrence of fading greater than 20 dB peak to peak has been

noted at 250 MHz, in the band of frequencies used by FLEETSATCOM and AFSATCOM.

Navigation systems such as GPS operating in the 1200 to 1500 MHz band are affected by scintillations, since low signal margins of some users may prevent acquisition of and locking onto the signal. Phase scintillations may also have degrading impact, since

phase coherence across the band is required.

The capability of radars operating near the geomagnetic equator (220°) at frequencies from 150 MHz to 1500 MHz to determine target signatures will deteriorate when fading of the return signal occurs. In addition, the scintillation phenomena must be evaluated in systems analysis in the case of large aperture antenna systems which might suffer loss of coherence across an aperture. The problem of coherence time for some radars is of importance since the fading limits the amount of time the system can integrate on a single target.

THE EQUATORIAL SCINTILLATION CAMPAIGNS OF OCTOBER 1976 AND MARCH 1977

The results illustrated in this paper were gathered during two periods of intensive observations, primarily in Peru (October 16-30, 1976 and March 16-30, 1977). Data were obtained from the following experimental setups.

(a) The 50 MHz backscatter radar of Jicamarca (Instituto Geofisico del Peru and

University of Texas).

(b) Two ground observatories, Ancon and Huancayo, in Peru, recording amplitude fading of the following synchronous satellites: LES-8 and LES-9 (249 MHz), GOES and ATS-3 (136 MHz), MARISAT (257 and 1541 MHz) (Instituto Geofisico del Peru and Air Force Geophysics Laboratory).

WIDEBAND satellite. SRI made observations of phase and amplitude fluctuations at Ancon in March 1977; AFGL made amplitude measurements at 137 MHz and 401 MHz at Huancayo for both periods; the AFGL aircraft made amplitude measurements at $136\,$ MHz and $378\,$ MHz during the March $1977\,$ campaign.

(d) Aircraft observations of LES-8 and 9 were made by the AFGL and by the AFAL aircraft.

(e) All-sky imaging photometer measurements from the AFGL aircraft were made of the 6300 A and 5577 A emission during the March 1977 series. The aim of this paper is to address one of the results of the campaigns, i.e., the

development and maintenance of the large scale patches of irregularities (several hundred kilometers EW and many times that NS). These patches are composed of small scale irregularities from less than 3 meters to one kilometer which produce both 50 MHz backscatter and VHF to microwave scintillation.

THE SCATTERING PHENOMENA IN THE EQUATORIAL REGION

Using the described multi-probe attack on the formation, generation, and maintenance of equatorial irregularities, a physical description of these phenomena has emerged. After sunset, for reasons still under study, a localized depletion of electron density may form in the lower F layer which then rises and moves into the middle and upper F layer. This upwelling results in "plumes" on VHF radar maps of irregularity intensity versus height and time (Woodman and La Hoz, 1976).

Another phenomenon, observed on many backscatter records and not necessarily related to the plumes, is the formation of a thin layer of irregularities of moderate intensity near the bottomside of the F-region. Scintillation activity associated with this back scatter is of the order of 5 dB on UHF records at 249 MHz whereas VHF records at 136 MHz show a sharp onset of scintillation with rapid and deep fading when the bottomside irregularities appear. The apparent difference between the behavior of the two bands is

probably due to the frequency dependence of scintillation.

The top panel of Figure 1 shows the backscatter recording of the Jicamarca Radar of October 16-17, 1976. A plume forms at 1945 LT from a thin layer of bottomside ir regularities, followed at 2045 LT by a second plume, emerging from a much wider and more disturbed layer of irregularities. The two lower panels show scintillations observed on LES-9 signals at Ancon and Huancayo. The propagation path from Ancon to LES-9 traverses the disturbed ionosphere 300 km east of Jicamarca and that from Huancayo to LES-9 475 km The time history of the formation of the plume over Jicamarca and the east of Jicamarca. onset times of scintillations at Ancon and Huancayo show a clear eastward drift of an irregularity region of well defined extent. The two plumes seen in the backscatter record result in one extended and intense scintillation event, suggesting a rather large extent in height of irregularities responsible for the scintillations. The onset times of the events yields an estimate of the eastward drift speed of the irregularity patch as ~ 100 m sec

On another day, October 18-19, the eastward drift and its magnitude were also determined by a spaced receiver technique. Using an antenna spacing of 366 m in E-W direction, cross-correlation of the observed fading patterns was made to measure the fluctuations of the E-W drift speed during the development of plumes similar to those seen in Figure 1. Rapid fluctuations of the drift speed and drift direction (E to W and

W to e) were observed (see Figure 2) during the formation of the first plume.

In the context of current measurements (McClure et al, 1977) and theories of equatorial irregularity formation as well as satellite in-situ measurements, fluctuations in vertical velocity component are expected in the initial phase. In view of our satellite observations being made at an elevation angle of about 45°, these vertical velocity fluctuations are possibly related to the rapid fluctuations in our E-W drift speed measurements. However, it was found that the maximum cross-correlation coefficient was about 0.2 during the initial phase on October 18-19, 1976. The low value of cross-correlation may signify the evolution of irregularity structures and thus seriously affect the determination of actual drift speed. Fluctuations of drift speed with more significant values of cross-correlation coefficients have been obtained with other data from this series. In these cases, the fluctuating drift speeds observed during the formation of a plume can be confidently associated with the vertical velocity fluctuations observed in satellite in-situ measurements.

Once the formation of the patch has taken place, the velocity is eastward, the autocorrelation interval ranges from 0.4 to 1.7 seconds and the cross correlation coefficient ranges from 0.3 to 0.7. The velocity in the later stages is eastward in the range of 150 meters per second for the particular example given in Figure 2.

The picture then is of vertical turbulence taking place when the depletion bubble rises; once the initial phase is completed the large scale patch and the irregularities within it display an eastward motion with a velocity of 50 to 150 meters per second.

The spacing used during the October 1976 campaign was large with the emphasis towards yielding information on space diversity. Since the diversity gain depends upon the correlation between two samples, a diversity gain can be obtained with low correlation coefficients. If the correlation coefficient is less than 0.6 the diversity gain is 8 dB or better for scintillation conditions characterized by Rayleigh fading (Schwartz

et al., 1966). From in-situ measurements (McClure et al., 1977) it appears that in the equatorial F region ambient electron density depletions over 50 km may be of one to two orders of magnitude. Small scale perturbations within these depleted bubbles produce scintillation effects. From a study of in-situ irregularity data, irregularity amplitudes ranging from 10% to 100% are found to occur in the equatorial region (Basu et al., 1976). The electron density deviation ΔN (10% of the ambient in one case cited) responsible for moderate level UHF scintillations appears typically of the order of 6 \times 10¹⁰ m⁻³ with a thickness of 200 km. Stronger electron density deviations result in S-band scintillation activity (Basu and Basu, 1976).

THE PLUME AND ITS EASTWARD MOTION

A newly developed observational technique has allowed viewing of the patches and their motion through optical imaging of associated airglow signatures. The structures typically appear as dark bands within the ambient airglow emission and are aligned in the N/S direction. The dimensions of airglow depletions are of the order of 50-400~km E-W, and greater than 1200 km N-S. Figure 3 shows the structure and eastward drift (~ 90 m/sec) of a single dark band or depletion throughout the night of March 16-17, These structures maintain their integrity over a period of several hours, although they change in form and intensity. Figure 4 shows an all-sky image as well as a schematic ground projection.

Figure 1 with data from October 16-17, 1976 showed ground observations on one night with the formation of a patch of two plumes lasting about one hour. The patch moves eastward. The total time covered from these observations is greater than 3 hours from the first onset of the plume at Jicamarca to the decrease of scintillations on the LES-9 path from Huancayo. The patch may stay together longer, probably changing in form and intensity, but observations could not cover it.

With an eastward velocity, the aircraft, which flies at roughly twice the velocity of the patches, can essentially slow down and stop the fading. The aircraft can fly in the direction of the ionospheric drift and against it. Recorded samples of the fading observed on the aircraft are shown in Figure 5. The spectra obtained from the observations are shown in Figure 6.

Engineering to mitigate the scintillation problem will utilize the spectra shown in developing methods to correct for fading.

DISCUSSION

Typical patch three dimensional structures as seen on backscatter records are shown in Figure 7. The artist's conception of the three dimensional patch with activity depending upon the stage of formation or dissolution is shown with typical local times. With the formation of a thin layer of irregularities (~ 1930 local time) UHF scintillation starts with 5 dB peak to peak values. Fading rates (on the ground) are of the order of $10/\min$. During the formation of the plume, scintillations show greater depth (5 20 dB peak to peak). Irregularity thickness and radar returns become stronger;

depth (~ 20 dB peak to peak). Irregularity thickness and radar returns become strong fading rates exceed 10/min. The occurrence of microwave scintillations most probably takes place during this time.

After formation, irregularity structures move east at speeds between 50 and 150 m \sec^{-1} . Scintillations observed during this phase are still strong. At a later stage, irregularities within a specific patch begin to decrease in intensity, resulting in lower scintillation levels. Limited observations suggest that the eastward motion of these patches slows down in the later stage, around midnight.

From the viewpoint of a single station observing on a path to a synchronous satellite, the scintillation may continue at a high level since additional plumes may con-

tinue to form in the west and drift into the ray path.

Previous work (Aarons, 1977) shows that scintillations have a strong seasonal dependence. During periods of high probability of activity, scintillations occur over many hours. One example is shown in Figure 8 where scintillation activity was noted for over four hours.

CONCLUSIONS

From the data gathered on this recent series of tests we conclude that an isolated irregularity patch may stay together for several hours, maintaining its integrity. The physics of the generating mechanism for a patch is partially understood based on experimental and theoretical studies (Woodman and La Hoz, 1976; Scannapieco and Ossakow, 1976; Kelley et al, 1976; McClure et al, 1977) but the starting conditions for the observed patches are not yet completely understood. On one night in the scintillation season, several hours of intense scintillation activity may be experienced; the following night might show none. The physics limiting the patch size in both the EW and the NS directions is not well understood. This morphology is of importance if the prediction of scintillation activity for users of transionospheric propagation information is to be attempted. The visibility of the patches on the all-sky imaging photometer holds promise for prediction. The technique is limited however to times when the F layer is below 275 km. When the layer rises above this height the emission decreases so that while a low altitude layer of great depletion of ΔN might show black areas (of low emission), the same depletion at a higher altitude will show insufficient contrast to be discriminated from the background airglow. The technique however holds great promise for the development, positioning, and size determination of the irregularity patches.

REFERENCES

- Aarons, J., 1977, Equatorial scintillations: a review, IEEE Trans. Ant. Prop., 25, 729-736.
- Basu, Sunanda, S. Basu and B.K. Khan, 1976, Model of equatorial scintillations from insitu measurements, Radio Science, 11, 821-832.
- Basu, Sunanda and S. Basu, 1976, Correlated measurements of scintillations and in-situ F-region irregularities from OGO-6, Geophys. Res. Lett., 3, 681-684.
- Fremouw, E.J., M.D. Cousins, G.K. Durfey, 1977, Wideband satellite observations, Bimonthly Progress Report 5, Contract DNA 001-75-C-0111, Stanford Research Institute, 9 March.
- Kelley, M.C., G. Haerendel, H. Kappler, A. Valenzuela, B.B. Balsley, D.A. Carter, W.L. Ecklund, C.W. Carlson, B. Hausler and R. Torbert, 1976, Evidence for a Rayleigh-Taylor type instability and upwelling of depleted density regions during equatorial spread-F, Geophys. Res. Lett., 3, 448-450.
- McClure, J.P., W.B. Hanson and J.H. Hoffman, 1977, Plasma bubbles and irregularities in the equatorial ionosphere, J. Geophys. Res., 82, 2650-2656.

- Scannapieco, A.J. and S.L. Ossakow, 1976, Non-linear equatorial spread-F, Geophys. Res. Lett., 3, 451-454.
- Schwarts, N., W.R. Bennet and S. Stein, 1966, Communication Systems and Techniques, McGraw-Hill.
- Woodman, R.F. and C. LaHoz, 1976, Radar observations of F-region equatorial irregularities, J. Geophys. Res., 81, 5447-5466.

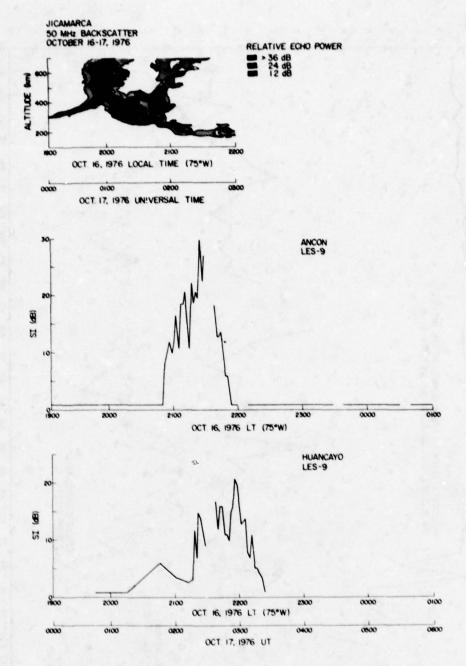
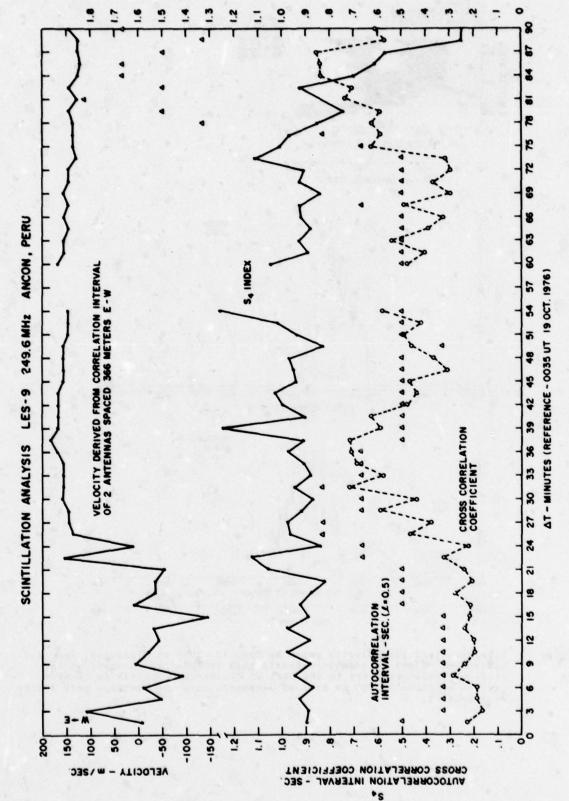
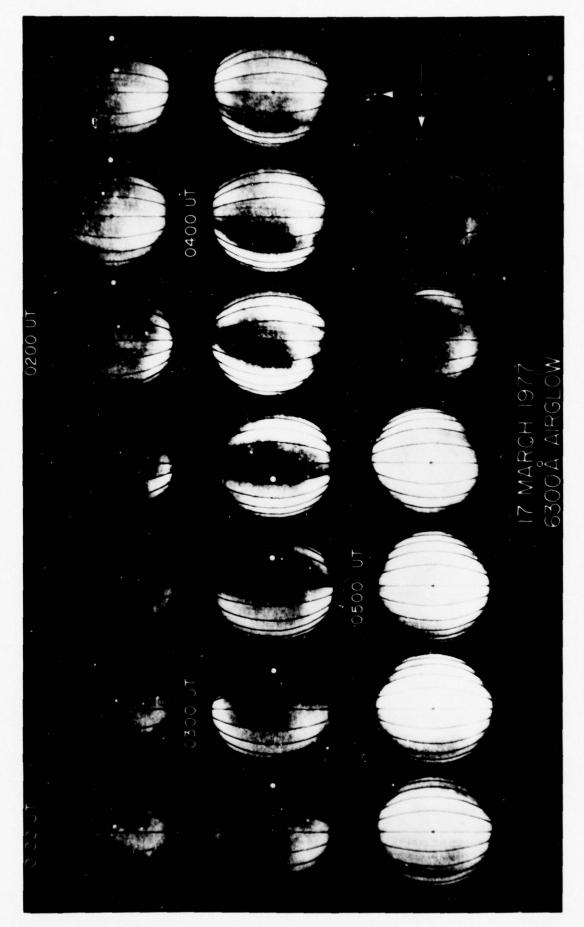


Figure 1: Development of irregularity patch on Oct. 17, 1976 at Jicamarca, Peru and subsequent effect on transionospheric path to LES-9 as observed at two stations whose paths are to the East of Jicamarca. The 350 km intersection of Ancon is 300 km East of Jicamarca with the Huancayo path 175 km east of that.



Signal analysis of scintillation observations at the beginning and developed stages of an irregularity patch on Oct. 18-19, 1976, Figure 2:



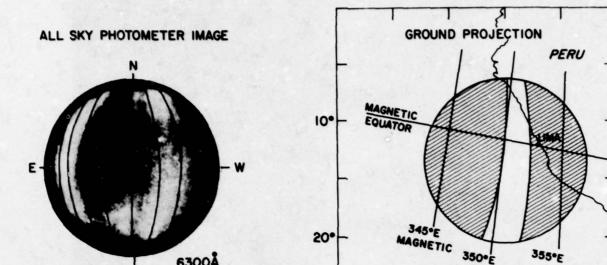
The development and motion of a patch as seen by all-sky red line observations (6300 Å) from AFGL aircraft; black patches in the central area are depletions of ionization. Figure 3:

dB

0344 UT

OVERFLIGHT HUANCAYO, HEADING 270°

EQUATORIAL AIRGLOW IRREGULARITIES



6300Å

0400 UT 17 MARCH 1977

Figure 4: Patch area as projected on a map of region studied in the March equatorial campaign.

EQUATORIAL SCINTILLATIONS

80

LES 9, 249 MHz AIRBORNE RECEPTION ON 20 OCTOBER 1976 dB 20 103 0330 UT 0329 UT OVERFLIGHT HUANCAYO, HEADING 135°

Figure 5: Slow fading of scintillation signals which takes place when the aircraft flies in the general direction of the ionospheric drift (top); rapid fading when the aircraft flies against the drift (bottom)

0343 UT

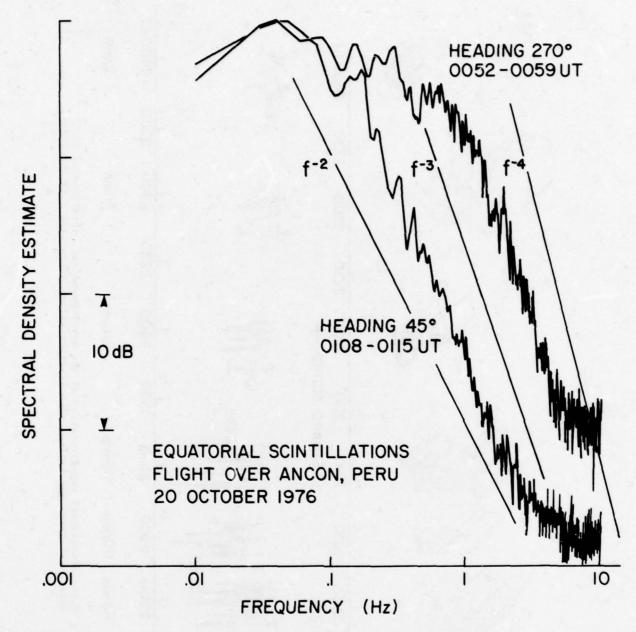


Figure 6: Spectra of the scintillations NE (with the wind) and W (against the wind)

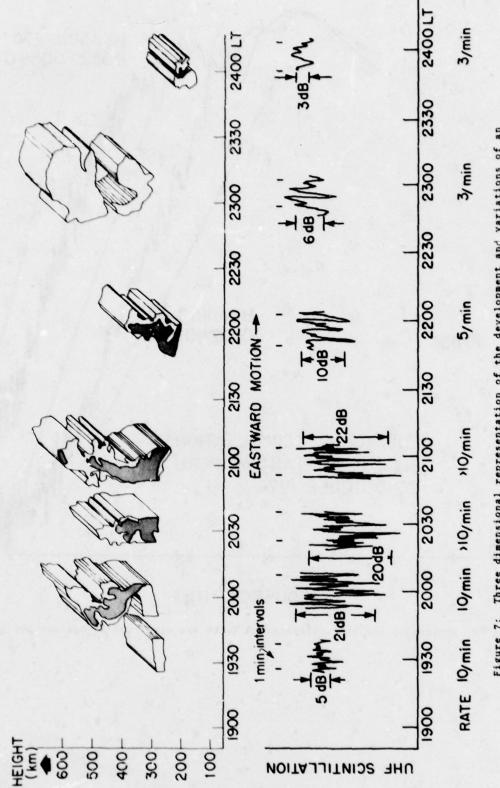


Figure 7: Three dimensional representation of the development and variations of an equatorial patch and typical scintillation values associated with the forms.

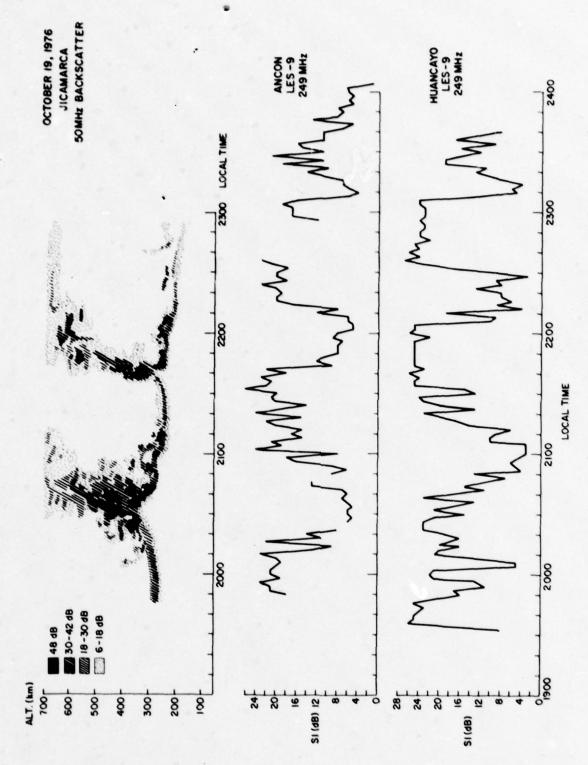


Figure 8: Backscatter observations and scintillation observations for a day with considerable scintillation activity, Oct. 19, 1977

PULSE DELAY AND PULSE DISTORTION BY RANDOM

SCATTERING IN THE IONOSPHERE

K. C. Yeh and C. H. Liu
Department of Electrical Engineering
University of Illinois at Urbana-Champaign
Urbana, Illinois 61801

SUMMARY

The dispersive effects of the ionosphere on propagating electromagnetic pulses are well known. Because of the frequency dependence of the refractive index, the speed of the propagation is given by the group velocity which is slower than the free-space velocity of light. The dispersion also affects the pulse shape by smearing and lengthening it, resulting in general degradation of the communication signal. However, the ionosphere has often been found to be permeated with random irregularities of electron density. Through scattering from these irregularities additional distortion of the signal may come about. The purpose of this paper is to investigate the effects of the random scattering on the pulse delay and the pulse width. This problem is mathematically formulated and solved. All multiple scattering effects are taken into account except the backscattering. The solutions are given in terms of many parameters which can be classified into three kinds: signal parameters, ionospheric parameters and irregularity parameters. It is found that under certain conditions effects caused by random scattering can be more important than those caused by dispersion. Various numerical examples will be given to show the importance of the effects. The implication on precise ranging systems and communication systems will be discussed.

Additional factors must be considered when the signal is weak and must therefore compete against the noise. The effect of noise on the determination of the arrival time is to introduce an error which depends on the signal-to-noise ratio. Its effect on the pulse width depends on a number of parameters. The nature of this dependence will be discussed.

1. INTRODUCTION

The dispersive effects of the ionospheric plasma on propagation of electromagnetic pulses is well known. For a narrow band pulse the transit time between two fixed points is determined by the group velocity which is slower than the free-space speed of light. That is, for a fixed distance the pulse will take longer time to arrive at the receiver than that in free-space. The excess, known as the excess time delay, is proportional to the integrated electron density along the path or electron content in the high frequency approximation. The effect of finite bandwidth has also been looked into; it contributes to pulse distortion and lengthening.

In addition to dispersion, the ionospheric plasma is often found in the turbulent state. The electrons form density irregularities. These irregularities can scatter electromagnetic energy and result in further degradation of radio signals propagating through the ionosphere. The purpose of this paper is to investigate the combined effects on electromagnetic pulses caused by dispersion and scattering. We first review the propagation geometry and the range of parameters involved in section 2. Next we introduce in section 3 the temporal moments and show how they are related to the mean arrival time and the mean pulse width. Also shown in section 3 are expressions and numerical values and curves for the mean arrival time and the mean pulse width. These expressions are derived for the ideal, noiseless communication channel. If there is present noise uncorrelated with the signal these quantities must be modified. This is discussed in section 4. The paper is concluded in section 5.

PROPAGATION GEOMETRY AND PARAMETERS

The propagation geometry is shown in Fig. 1. A plane wave signal is supposed to be impressed on top of a slab containing electron density irregularities. Scattering takes place inside the slab so that random perturbations are imparted on the wave when it leaves the base of the slab. These random perturbations are further randomized in the homogeneous region below the slab through diffractional effects before it is finally received.

In a problem such as this there are many parameters involved. In the following is a list of nine parameters and their approximate range of values pertinent to the ionosphere.

carrier frequency of the signal f: 100 - 5000 MHz signal bandwidth (∇z) $\frac{1}{2}$: less than 10 MHz plasma frequency f_p: 2 -15 MHz

propagation distance z: 100 - 1000 km rms electron density fluctuations $\sigma_N\colon \ 0$ - 0.5 slab thickness L: 10 - 500 km power law spectral exponent m: approximately 2 inner scale $r_0\colon \ 10^{-3}$ - $10^{6} m$ outer scale $\ell_0\colon \ 10^{4}$ - $10^{5} m$

In the above list the first two parameters are signal parameters, the next two are ionospheric parameters and the last five are all irregularity parameters. The carrier frequency of the signal can of course vary over a wide range. For frequencies near the lower end of VHF band the ray bending, which is ignored in this paper, may be very important. Therefore, the lower bound of carrier frequency is taken as 100 MHz. When the frequency is raised to the SHF band, the ionospheric effects are expected to become very minimal and hence an upper bound of 5 GHz is chosen. The second parameter in the above list is the signal bandwidth which is defined by the equation

$$\bar{v}^2 = (2\pi)^2 \int_{-\infty}^{\infty} |F(2\pi v)|^2 v^2 dv$$
 (1)

where F is the spectrum of the transmitted signal as a function of the modulation frequency ν . For a Gaussian signal spectrum of the form

$$F(2\pi\nu) = (2\sigma\pi^{3/2})^{-1/2} \exp(-2\pi^2\nu^2/\sigma^2)$$
 (2)

the bandwidth (1) can be computed to be

$$\overline{v^2} = \sigma^2 / 8\pi^2 \tag{3}$$

The value of the bandwidth can vary from 0, which corresponds to a pure carrier, to about 10 MHz. For most computations a value of 1 MHz is used. The third parameter $f_{\rm p}$ is an ionospheric parameter. In the actual ionosphere the plasma frequency varies with height. For theoretical convenience the model ionosphere is assumed to have a constant plasma frequency. This is partially justified because very often irregularities are observed to be confined to a slab and because even when irregularities are distributed those near the ionization peak are most effective in producing scintillation. The plasma frequency at the peak can vary from 2 to 15 MHz, a value of 10 MHz is used in computations. The parameter, propagation distance, is the distance from the top of the irregularity slab to the receiver as shown in Fig. 1. It has the minimum value of 100 km if irregularities are in the E region. Irregularities in the magnetosphere have been observed but they are not expected to affect transionospheric propagation signals because of their low density. Therefore, an approximate maximum value of 1000 km for the propagation distance is chosen. The rms electron density fluctuations had always been thought to be small, no more than 1% from the bankground, until the in situ measurements demonstrated that a surprisingly large percentage of 20 or even 50 is possible at the equator. This accounts for the rather large upper bound value of 0.5 for σ_N in the list. Based on radar data, the slab in which irregularities are confined can be as thin as 10 km and as thick as several hundred kilometers. Both scintillation measurements and in situ measurements indicate the one-dimensional power spectrum of density fluctuations has the form κ_{χ}^{-m} where κ_{χ} is the spatial wave number. The exponent m in the power-law spectrum is approximately 2. A power-law spectrum of the form κ_{χ}^{-m} has several mathematical difficulties. For example, some spectral moments will fail to exist. These difficulties can be remedied by introducing the inner scale and the outer scale. The exact values of the inner scale and the outer scale are very uncertain at present. Be on plasma physics we would expect the inner scale to be bounded below by the Debye length below which the plasma is expected to lose all its collective behavior. Therefore, the absolute lower bound is the Debye length which in the ionosphere is approximately 10^{-3} m. Based on the radar backscatter data the irregularities at 3 m length seem to belong to the same process responsible to scintillation (Morse et al., 1977). However, the more powerful Arecibo radar does not seem to have reported the spread-F type irregularities of size 0.35 m. Consequently a more reasonable value for the inner scale is probably somewhere between 0.35 m and 3 m, a value very close to the ionic gyro-radius. There is very sparse information about the outer scale, a probable range is between 10 km and 100 km as indicated in the list.

PULSE DELAY AND PULSE WIDTH

For purposes of locating the position of a pulse and determining its pulse width, it is convenient to make use of the moment concept. Let a(t,z) represent the complex amplitude of a signal and it is in general a random function of time t and position z (dependence on transverse coordinates is suppressed). Define the n th moment of the signal by

$$M^{(n)}(z) = \int_{-\infty}^{\infty} t^{n} \langle \bar{a}(t,z) | a^{*}(t,z) \rangle dt$$
 (4)

where the angular brackets are used to denote ensemble averaging. For convenience of physical interpretation the complex amplitude is assumed to be normalized so that $\mathbf{M}(0)$ (z)=1. Then, the mean time required by a pulse to propagate from z=0 to z is related to the first moment by

$$t_a(z) = M^{(1)}(z) - M^{(1)}(0)$$
 (5)

The mean square pulse width centered around the mean arrival time is related to the first two moments by

$$\tau^{2}(z) = M^{(2)}(z) - t_{a}^{2}(z)$$
 (6)

Higher order moments reveal skewness and concentration of the pulse and will not be dealt with in this paper.

Theoretical derivation of expressions for t and τ in this propagation problem can be done by solving the transport equation for the two-frequency one-position mutual coherence function. This has been done elsewhere (Yeh and Liu, 1977). Their results show that

$$t_a = t_1 + t_2 + t_3$$
 (7)

where

$$t_1 = z/c \sqrt{1 - f_p^2/f^2}$$
 (8)

$$t_2 = 3f_p^2 \overline{v}^T z/2f^* c \tag{9}$$

$$t_s = \sigma_N^2 f_p L(2z-L) \ln(t_o/r_o)/4t_o f^c$$
 (10)

The transit time t_1 is well-known since it is just the time required for a signal to propagate a distance z with the group velocity $c\sqrt{1-f_p^2/f^2}$. In the high frequency approximation (i.e. $f>>f_p$), t_1 is usually expanded and written in the form

$$t_{i} = t_{i} + \Delta t_{i} \tag{11}$$

where $t_0=z/c$ is the free space time delay and Δt is the excess time delay due to presence of electrons. The excess time delay in the high frequency approximation is proportional to the integrated electron density or electron content and has been a quantity of interest in satellite-based navigational systems (Klobuchar, 1976). The time delay t_2 given by (9) is a correction term to t_1 when the signal has a finite bandwidth $\sqrt{v^2}$ and is usually small for narrow band signals. The time delay t_3 is caused by random scattering. In order to demonstrate numerically the order of magnitude of various effects, the following model parameters are adopted.

For these parameters, the free-space time delay t_0 is 1.33426 ms which is by far the largest value. The excess time delays due to electrons, finite bandwidth and random scattering are plotted as a function of frequency in Fig. 2. In a log-log plot all three curves are straight lines. The dominant contribution to the excess delay comes from the term proportional to electron content. But, for frequencies less than 200 MHz, the scattering can increase the time delay by 1 to 10 ns.

The mean square pulse width can also be derived from the transport equation for the mutual coherence function. The result is

$$\tau^{2} = \tau_{0}^{2} + \tau_{1}^{2} + \tau_{2}^{2} + \tau_{3}^{2} + \tau_{4}^{2} + \tau_{5}^{2}$$
 (13)

where

$$\tau_{2}^{2} = f_{p}^{*} \sigma_{N}^{2} L \ell_{0} / 2 f^{*} c^{2}$$

$$\tau_{3}^{2} = f_{p}^{*} \sigma_{N}^{2} L (L^{2} - 2Lz + 3z^{2}) / 12 \pi^{2} \ell_{0} r_{0}^{2} f^{6}$$

$$\tau_{4}^{2} = f_{p}^{*} \sigma_{N}^{*} L^{2} (12z^{2} - 16zL + 6L^{2}) (\ell n \ell_{0} / r_{0})^{2} / 48 \ell_{0}^{2} f^{6} c^{2}$$
(14)

 $\tau_{5}^{2} = f_{D}^{0}\sigma_{N}^{2}zL(2z-L)\overline{v^{2}} \ln(\ell_{0}/r_{0})/2\ell_{0}f^{10}c^{2}$

Let the signal spectrum be Gaussian and be given by (2). The mean square pulse width of the impressed signal at z=0 is then

$$\tau^{2}(0) = 1/16\pi^{2} v^{2} \tag{15}$$

For a bandwidth of 1 MHz, τ^2 has the numerical value 6.3326×10^{-15} s 2 or $\tau_0=7.957\times10^{-8}$ s. It turns out that for the parameters given by (12) the dominating terms in (13) are τ^2 and τ^2_3 . That is, of the six terms in (13), τ^2_3 is most important for frequencies less than a certain value and τ^2_0 is most important for frequencies larger than the same value. Let the frequency at which $\tau^2_0=\tau^2_3$ be f_0 , then

$$f_{e}^{6} = 4\sigma_{N}^{2}L(L^{2}-2Lz+3z^{2})f_{p}^{4}\overline{v^{2}}/3\ell_{0}r_{0}^{2}$$
 (16)

When $f < f_e$, τ_0^2 has the largest value for which the original pulse width is very much lengthened, when $f > f_e$, τ_0^2 has the largest value, i.e. the original pulse width is substantially unchanged. For the parameters adopted in (12), f_e is computed to be 1.46 GHz. Hence when f < 1.46 GHz, the original pulse width of 7.9578×10^{68} s can be very much lengthened. On the other hand, when f > 1.46 GHz, the original pulse width is changed very little. It should be mentioned that τ_0 is very sensitive to the choice of an inner scale r_0 . The inner scale given in (12) is rather small. There is still question as to the validity of the forward scatter approximation in the parabolic equation method when the inner scale is so small. If, instead of 10^{-2} m, we pick $r_0 = 1$ m and leave other parameters in (12) unchanged, the dependence of pulse width on frequency is very much changed (see the second carrier in Fig. 3). Even for such a large inner scale, the pulse width at 100 MHz is lengthened by more than one order of magnitude.

4. EFFECT OF NOISE

In the above discussion the communication channel is assumed to be noiseless. In practice the communication channel is not ideal and the signal must be competing against the noise. If the random signal and the noise are statistically independent, expressions for the mean arrival time and the mean square pulse width in the noisy environment can be derived and related to the corresponding quantities in the noiseless environment. Let the detection of the signal be gated for a duration T centered at some instant t_0 which is usually close to the actual arrival time of the signal. Within the gated interval, let the signal energy be S and noise energy be N. Then the mean arrival time in the noisy environment $(t_a)_N$ is related to the mean arrival time in the ideal channel t_a by (Yeh and Liu, 1977)

$$(t_a)_N = t_a + (t_0 - t_a) N/S$$
 (17)

As can be seen in (17) the error in the arrival time is proportional to the product of two terms: t_0 - t_a and N/S. Hence the error is minimized if the initial guess is very close to the true arrival time and/or the signal-to-noise ratio S/N is very large. The mean square pulse width in the noisy environment τ^2_N can also be related to the mean square pulse width in the noiseless environment τ^2_N can also be related to the mean

$$\tau_N^2 = \tau^2 + [(t_0 - t_a)^2 + T^2/12 - \tau^2] N/S$$
 (18)

It is seen that the noise affects the pulse width in a more complicated way.

CONCLUSION

We have given analytic expressions for the mean arrival time and the mean square pulse width in (7) and (13) respectively for the propagation geometry shown in Fig. 1. Using typical ionospheric parameters, it is shown that the largest contribution to the mean arrival time is the free-space value z/c. The largest correction to the space value is probably still that proportional to the electron content. However, scattering may introduce a further delay of 1 to 10 ns for frequencies less than about 300 MHz. The pulse lengthening effect depends on the frequency $f_{\rm e}$ defined by (16). If $f > f_{\rm e}$, the original pulse width is substantially unchanged. If $f < f_{\rm e}$, the original pulse may be

very much lengthened. If is found that f is rather sensitive to the choice of the inner scale. It should be cautioned that the forward scatter theory may become invalid if the inner scale is too small.

The effects of noise on the determination of the mean arrival time and the mean square pulse width are given by (17) and (18).

ACKNOWLEDGEMENT

This research was supported by the U.S. Army Research Office under Grant DAAG 29-76-G-0286.

REFERENCES

- Klobuchar, J. A., 1976, "Review of ionospheric time delay limitations to ranging systems". In the Geophysical Use of Satellite Beacon Observations, COSPAR Satellite Beacon Symposium edited by M. Mendillo, pp. 629-633.
- Morse, F. A., B. C. Edgar, H. C. Koons, C. J. Rice, W. J. Heikkila, J. H. Hoffman, B. A. Tinsley, J. D. Winningham, A. B. Christensien, R. F. Woodman, J. Pomalaza and N. R. Teixeira, 1977, "Equion, an equatorial ionospheric irregularity experiment", J. Geophys. Res., 82, 578-592.
- Yeh, K. C. and C. H. Liu, 1977, "An investigation of temporal moments of stochastic waves". To appear in Radio Science.

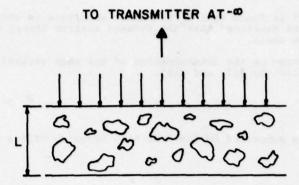




Fig. 1. The propagation geometry. The plane waves fall on top of the irregularity slab of thickness L. The randomized waves are further diffracted and received at the receiver which is a distance z from the top of the slab.

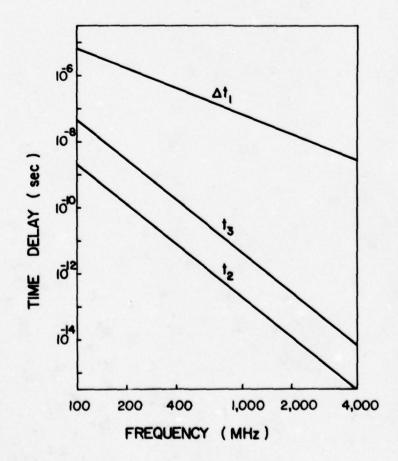


Fig. 2. Excess time delays as a function of frequency for parameters adopted in (12).

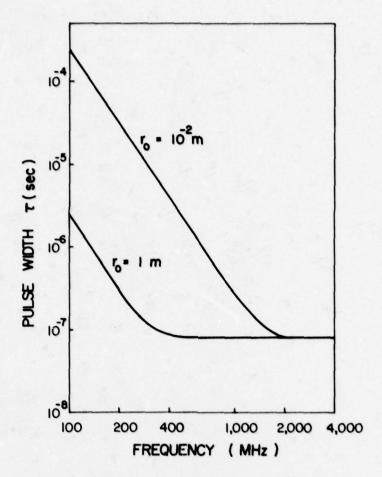


Fig. 3. Mean pulse width as a function of frequency for parameters adopted in (12) (labeled $\rm r_0$ =10⁻²m). When the inner scaled is increased by two orders of magnitude, the behavior is shown by the curve labeled $\rm r_0$ =1 m.

THE ATMOSPHERIC SCATTER CHANNEL FOR OPTICAL COMMUNICATIONS OVER-THE-HORIZON

GC Mooradian, M Geller, RA Krautwald, and D Stephens Naval Ocean Systems Center San Diego, California 92152 USA

SUMMARY

Measurements of the properties of an Over-The-Horizon optical propagation channel by scattering from normal marine atmospheric aerosols have been made. The signal loss of a 40-mile path for wavelengths in the blue-green was nominally ~100 dB when the atmospheric visibility was greater than 10 miles. This loss decreased by approximately 20 dB for the near infrared at 1.06 μ m. When atmospheric ducting occurs, the path loss for both wavelength regions decreased by 20 dB with accompanying severe scintillation. The apparent angular source size is small, less than 10 milliradians and there was no evidence of pulse dispersion for the 20-ns transmitted pulses for the 40-mile path. The scattered beam is very sharply peaked in the forward direction. A model that has been developed is in reasonable agreement with the data.

INTRODUCTION

Current Navy Operational communications system suffer from a number of problems. There is no operational communications system which is not significantly susceptible to jamming, intercept, spoofing, and direction-finding. Further, current communications systems significantly increase Fleet vulnerability to the threat of ARM (antiradiation missiles). Lastly, the existing systems suffer from limited data rates, spectrum crowding, high cost, large size, excessive weight, high power requirements, etc. Several attempts at solving these problems in the rf spectrum are being carried out. In addition, it appears that optical communications systems have great promise in solving these problems for many applications (MOORADIAN, GC, 1974). This report discusses one of the optical communications systems being-developed at NOSC: The ELOS (extended line of sight) optical communications system. This system addresses the requirement for exchange of tactical data between ships, both to the horizon and beyond. The effects of the atmosphere in the marine boundary layer represent the primary limitation to system performance and are addressed here.

ELOS OPTICAL COMMUNICATIONS

The ELOS optical communications system addresses exchange of tactical information to beyond line-of-sight ranges for the control of task force units. While the ELOS system will most likely be limited to voice bandwidths, the application of this system as an antijam, low-probability-of-intercept (AJ, LPI) augmentation of hf techniques will prove extremely valuable.

A detailed, comprehensive analysis of extended line-of-sight optical communications has been completed (MOORADIAN, GC, 1976). Links were studies utilizing both relay platforms and over-the-horizon forward scatter from aerosols (both marine aerosol haze and clouds). An in-depth review of the state of the art and near-term future advances in system component performance was included, covering lasers, filters, photodetectors, pointing and tracking systems, and platforms.

One result of this analysis was an analytical model for over-the-horizon optical scatter propagation, based upon both the single and multiple scattering approximation. The model appears to be in reasonable agreement with previously available field data for over-the-horizon propagation (CURCIO, JA, 1964).

Based on the use of systems composed of state-of-the-art (1976) components, the following conclusions were drawn (MOORAD-IAN, 1976):

- 1. The operating wavelength should be in the 1-3 μ m range for both links.
- 2. Both relay and scatter over-the-horizon data links can use the same shipboard system.
- 3. Significant performance advantages can be achieved by exploiting propagation characteristics. These include:
 - a. Use of a vertical fan beam or optimally elevated beams in a scatter link at large ranges.
 - b. Positioning the relay platform at a high altitude to take advantage of the decrease in path loss caused by the vertical falloff in aerosol concentration.
- Pulse stretching, which becomes significant at ranges beyond 100 km, limits usable data rate, reduces "peak" power of received pulses, and restructs modulation format.
- 5. Models for the optical scattering channel must include the following:
 - a. Vertical exponential decrease in aerosol concentration and attenuation coefficient.
 - b. Vertical decrease in index of refraction. The simplest approximation is to replace the radius of the earth in the model by the "4/3 radius" (modeling of temperature inversions would be desirable).
 - c. Two modes of propagation: single and multiple scattering. Contrary to intuition, the former dominates at longer ranges and the latter at shorter ranges.

The primary factor which determines the percentage of time communication over a given distance at a given bit rate can be achieved is meteorological visibility. Statistical studies of the occurrence of visibilities greater than a given value are available (McDONNEL DOUGLAS, 1968, NICODEMUS, 1972). When this information is combined with performance characteristics of a typical system, both range and link availability can be determined. Figure 1 shows the performance of a communication link based upon the results of the propagation model to fit to experimental data. For voice data rates, the transmitter is a pulsed Nd:YAG laser emitting 2.5 MW peak power pulses at 1.06 micrometres with an average power of 10 watts. Note that for a marine atmosphere and visibility as low as 5 miles, the communication range is approximately 42 miles.* For visibility of 10 miles, the range increased to 91 miles. For 20-mile visibility, the range increases to 205 miles. For teletype data rates and the same average power laser, the ranges become 51 miles, 113 miles, and 261 miles, respectively. On a worldwide basis, visibilities greater than 5 miles occur approximately 85% of the time, and visibilities greater than 10 miles approximately 70%. This link availability for a given range is not substantially different from that provided by conventional hf techniques. The communications ranges can be considerably greater at night and whenever low clouds occur to provide a scattering layer. It is important to note that areas of operation with lower average visibility (eg, the North Atlantic) also have a high occurrence of low cloud cover; and that some areas of high operational interest (eg, the Western Pacific and the Mediterranean) consistently permit greater ranges and higher availabilities. Interpretation of the visibility data on range, data rate, and availability is being continued.

EXPERIMENTAL RESULTS

To verify the propagation model developed in reference [MOORADIAN, GC, 1976], it was necessary to measure the following scatter channel characteristics during each experimental run:

- 1. The integrated path loss over the range.
- 2. The angular brightness distribution of the source as seen by the receiver
- 3. The magnitude of the pulse stretching

These propagation parameters depend critically on both the atmospheric visibility, and the elevation/azimuthal angles of the receiver. In the following section, we will describe recent experimental results derived from an over-the-horizon propagation link between San Diego and Oceanside, California. For this experiment, the integrated path loss (received power divided by transmitted power) was measured using the 514.5-nm line of a 1-watt argon laser, and the 532-nm and 1.06-\mu m lines of a Q-switched Nd:YAG laser. In the latter, both wavelengths transversed the identical propagation path.

The scattering channel selected was a 39-mile path, almost all of which is over the ocean. The transmitter was at NOSC in Point Loma. The receiver was on the beach at the Marine Base at Camp Pendleton. The geometric horizon was 25 miles from the transmitter for the CW experiments and 12 miles for the pulsed. A map presenting details of the propagation path is shown in figure 2.

A. PROPAGATION OF CW RADIATION

A synchronous transmitter was used for the cw measurements (fig 3). A cw argon ion laser emitting about 1 watt at 514.5 nm was chopped at 3 kHz and aimed very accurately in the direction of the site at Camp Pendleton. An electrical signal, synchronized with the chopping frequency, was also sent to Camp Pendleton via a standard telephone line.

The receiver at Camp Pendleton (fig 4) collected the optical chopped signal with an 8-inch-diameter telescope. The radiation was detected by an S-20 RCA 7265 photomultiplier. The synchronous signal was received from the telephone and, with the received signal, was fed into a PAR lock-in amplifier. This type of synchronous detection permitted the measurement of signals as small as 10⁻¹⁴ watt.

Figure 5 is a photograph at nighttime of the coastline from Pendleton looking southward to the source. The transmitter is pointed directly at the geometric horizon. As there was a strong temperature inversion this night (21 January 1976), the direct beam, ducted by this refractive index anomaly, is clearly visible.

Figure 6 is the same view with the transmitter elevated 0.5 degree from the horizon. Superimposed on this photograph is an angular scale to obtain an estimate of the angular size of the source.

Figure 7 is another photograph of the same view with the transmitter elevated 0.75 degree above the horizon.

Figure 8 shows the path loss as a function of transmission elevation angle. The vertical axis is the path attenuation in dB: the power received divided by the power transmitted. The path loss for the ducted beam is -83 dB. On the scale used, this data point would be outside the boundary of the graph. Part of this path loss, 51 dB, is due to the loss in beam spreading. The remaining 32 dB is from the loss of energy from the extinction coefficient integrated over this 63-kilometre path.

This enables a calculation of an integrated extinction coefficient of 0.115 km⁻¹ to be made for this very long path. This method

This enables a calculation of an integrated extinction coefficient of 0.115 km⁻¹ to be made for this very long path. This method of determining the integrated extinction coefficient is extremely valuable as visiometer and transmissometer measurements disagreed severely. This night only four data points were obtained, when the telephone failed. With sync information gone, no further data were obtained. Note on the right-hand side of the figure the pertinent data are stated: PT is the transmitted power, THETA D is the beam divergence, D REC is the receiver diameter, FOV is the field of view of the receiver, R is the propagation path, VIS is the visibility as calculated from the extinction coefficient, BETA is the extinction coefficient, H TRANS is the height of the transmitter, and H REC is the height of the receiver above sea level.

Figure 9 contains data taken on the same night of the photographs of figures 5-7. The night was remarkably clear from a strong Santa Ana condition. Note that the small value of ducting loss calculates into a visibility of 92 kilometres.

Figure 10 is another data set later in the month of January. This was a very clear night, and the ducted beam was clearly visible to the eye.

The last data set (fig 11) was taken about a month later under conditions more normal to the California coast. There was no temperature inversion, so the direct, unscattered beam was not observed. For all the four points of data, the beam was not visually seen.

The occurrence of a ducting condition is determined two ways by analyzing the data. First, a large decrease in signal level is observed when the transmitter elevation angle is increased beyond about one beam width. This change is approximately -20 dB. Second, the received ducted signal exhibits rapid large amplitude variation, characteristic of scintillation, when the transmitter is pointed at the horizon. When the transmitter beam is elevated, and a scatter condition predominates, the effective radiating volume increases by orders of magnitude (aperture averaging) and amplitude variations of the signal are very small, typically less than a few percent.

B. PROPAGATION OF PULSED RADIATION

The next set of experiments measured both the path loss and the pulse spreading in this type of scatter channel. The transmitter is a pulsed Nd(YAG) laser emitting 20-ns pulses both at the fundamental at 1.06 micrometres and the first harmonic at 532 nm (fig 12). Both wavelengths traverse the same propagation path to the receiver. The radiation is accurately pointed to Camp Pendleton with the aid of a sighting hole near the laser and a sighting mark 50 feet from the laser. The exact positions of these aiming aids were determined by a surveyor. The peak powers of the 1.06μ m and the first-harmonic beams are measured by pyroelectric pulsed energy detectors. Accurate timing of the onset of the pulse at the receiver was obtained by two rubidium clocks. These were synchronized at the start of each receiver experiment. One clock in this figure is shown sending a sync pulse to trigger the laser power supply. The other rubidium standard clock is shown in figure 13. A sync pulse from this clock, delayed for 350 μ s to account for the time of flight of the beam, initiates the Biomation digitizers. The two wavelengths, 532 nm and 1.06μ m, are collected by an 8-inch telescope receiver. The two beams are separated by a dichroic beamsplitter, detected, amplified, digitized, and recorded. Real-time displays of the pulse shapes are shown on the oscilloscopes and polaroid photographs taken.

Figures 14 and 15 show the path loss as a function of transmitter elevation and scan angle at a wavelength of 532 nm. The 1.06 μ m receiver was not operating during this test. It is important to note that the off-axis energy in azimuth is very sharply peaked in the forward direction (much more so than predicted by standard forward scattering functions). This has important implications for determining LPI and AJ levels. Figure 16 shows the path loss at the two wavelengths of 532 nm and 1.06- μ m through the identical atmosphere. As predicted by

the model, the 1.06 µm channel has approximately 20-dB less attenuation than the 532-nm channel for these atmospheric conditions and range. The electrical signal-to-noise ratio of the 1.06 µm channel was approximately 90 dB, even in daytime operation. In all these measurements there was no pulse stretching or distortion measured.

Figure 17 and 18 show further data of the path loss during conditions of patchy fog.

ANALYSIS OF PROPAGATION RESULTS

The multiple scattering model developed in reference (MOORADIAN, 1976) gave the normalized received power to be equal to

$$\frac{P_{rec}}{P_t} \approx \frac{10}{3} A_{rec} f(0) \frac{\beta \exp(-\beta R)}{R} ,$$

Prec = received optical power

Pt = transmitted peak power

A_{rec}≡ receiver area

f(0) = forward scatter function at 0°

β ≡ extinction coefficient

R = range

The parameter f(0) was assumed to be equal to 10.3; the value computed by Deirmendjian for an aerosol distribution he called "water haze "M" (DEIRMENDJIAN, 1969).

The experimental and theoretical values are compared in table 1. The column labeled EXPERIMENT is the path loss with the transmitter pointed about one beam diameter above the horizon to ensure that none of the energy is being ducted to the receiver. The next column, SGL SCATT, gives the values from the single scattering model. The column next to this one, ERROR, gives the difference between the experiment and the single scattering theory. Note that there are large differences from 16 to 30 dB. The next column, MULT SCATT, gives the results from the theory of multiple scattering. A comparison between this column and the experimental values indicates better agreement, with the differences clustered around -19 dB.

TABLE 1. COMPARISON BETWEEN EXPERIMENT AND THEORIES.

Comparison of both single scattering and multiple scattering theoretical models to experimental results over 63-km OTH range.

Date	Beta	Experiment*	SGL SCATT**	Error	MULT SCATT**	Error
1/15/76	0.115 km ⁻¹ ***	-96 dB	-117.5 dB	-21.5 dB	-118.5 dB	-22.5 dB
1/21/76	0.043 km ⁻¹ ***	-86 dB	-114.7 dB	-28.7 dB	-103 dB	-17 dB
1/28/76	0.126 km ⁻¹ ***	-102 dB	-118 dB	-16 dB	-121 dB	-19 dB
2/25/76	0.148 km ⁻¹	-108 dB	-119.4 dB	-11.4 dB	-126.5 dB	-18.5 dB

^{*}Measurement of path loss (P_{RCVR}/P_{XMTR}) at transmitter elevation angle of ~ 3 mrad.

Both models consistently underpredict the actual path loss measurement. However, the multiple scattering model seems to be in better agreement with the experimental data than the single scattering model. This was not too surprising since the optical thickness was within the multiple scattering regime. In the following, we will show that the -19-dB "error" of the multiple scattering model may be due to an <u>underestimation of the density of large particles</u> with the accompanying usage of a value of f(0) too small by a factor of 100.

Recently, it has been shown (WELLS, W, 1977) that the Deirmendjian haze M underestimates the number of large particles contained in a maritime aerosol by several orders of magnitude. Results of similar type can be obtained from Mie calculation of f(0) and β from the particle size distribution. Figure 19 is a typical particle spectrum measured with a Knollenburg spectrometer. The minimum density of particles that can be measured with this instrument is $N = 3 (10)^{-3}$ particles /cm³ μ . Table 2 shows the value of β and f(0) for the measured distribution which is extended to include particles of density equal to the sensitivity of the instrument from 18μ to 50μ , ie, $N_0 = 3 (10)^{-3}$ for $18 \mu < r < 50 \mu$. The inclusion of several large (>10 μ m) particles in the model's distribution has the effect of increasing the forward scattering function by a factor of 57, without an appreciable increase in the value of the extinction coefficient.

TABLE 2. CALCULATED VALUES OF EXTINCTION COEFFICIENT AND THE FORWARD SCATTER FUNCTION.

	β	f(0)
Measured distribution	3.1 km ⁻¹	(4.36)10
Extended distribution	3.9 km ⁻¹	(2.5)10 ³

^{**} Assuming f(0) = 10.3

^{***}Calculated from ducted beam

^{*}Knollenberg data supplied by Dr D Jensen of NOSC

The experimental results of the azimuth scan of the transmitter also lead one to suspect the forward scattering function. From figure 15 it is seen that the received power is very charply peaked in the forward direction, much more than that predicted by the phase function derived from a Deirmendjian haze M model. For this function, the scatter cross section is down by a factor of 10 approximately 12° off axis. The experimental data indicate a reduction in the received power of 10 approximately 0.17° off axis. Clearly, the scattered signal profile is not consistent with a classical Deirmendjian aerosol model. From reference (MOORADIAN, GC, 1976) it is seen that for an assumed phase function distribution of

$$f(\theta) = f(0) \left[1 - \frac{\theta}{\theta_0} \right] \quad 0 < \theta < \theta_0$$

$$= 0 \qquad \theta > \theta_0$$

ther

$$f(0) = \frac{3}{\pi \theta_0 2} .$$

While this model for the forward scattering function is obviously overly simple, the dependence of f(0) with θ_0 is important. If one relates θ_0 to the 10% points, then the measurement of 30 September 1976 indicate a θ_0 approximately 10 times smaller than from the M water haze that was assumed in the model. This again indicates an f(0) approximately 100 times that assumed in the model. If f(0) is increased by approximately 100 in the model, it is clear that good quantitative agreement is possible. While this agreement is clearly nonrigorous, the results are self-consistent.

It was fortuitous that some of the scattered beam data were obtained with a ducted beam condition. This permitted determination of the integrated value of extinction coefficient and thus a comparison between experiment and theory as shown in table 1. This favorable climatic condition did not exist on further data runs as shown in figures 17 and 18. Thus, the values of BETA and VIS were left blank. Further data are still planned for the future. But now, the values of β will be obtained by measuring the "direct beam" path loss. Another receiver, behind the scattered beam receiver and elevated in the hills will make this measurement.

FUTURE PLANS

As indicated in the above, further scattering measurements will be made. The design and construction of a one-way communication link between NOSC and San Clemente Island (a distance of 128 km over water) are in progress. Pulse interval modulation is the method to be used of transmitting higher bandwidths of information (voice) using a low-frequency pulse stream (laser pulse frequency of 200 pps).

ACKNOWLEDGMENTS

The authors are indebted to L Stotts for many technical discussions.

REFERENCES

Curcio, JA and LF Drummeter, Jr, 30 September 1964, "Experimental Observations of Forward Scattering of Light in the Lower Atmosphere", NRL Report 6152

Deirmendjian, D, 1969, "Electromagnetic Scattering On Spherical Polydispersions", New York, American Elsevier Publishing Co, Inc.

McDonnell Douglas, June 1968, "Marine Weather of the World", Report F-063

Mooradian, GC, March 1974, "Atmospheric and Space Optical Communications for Naval Applications", Proceedings of 6th DoD Conference on Laser Technology

Mooradian, GC, VJ Adrian, PH Levine, and WR Stone, June 1976, "Extended Line of Sight Optical Communications Study", NELC TR 1988

Mooradian, GC, M Geller, GJ Barstow, KE Davies, August 1976, "Over the Horizon Optical Communications Channel" Vail, Colorado, Proceedings of Workshop on Remote Sensing of the Marine Boundary Layer

Nicodemus, FE, May 1972, "Weather Effects on Infrared Systems for Point Defense", NWC, China Lake, TN 4056-16

Wells, W, Gal, G, and Munn, MW, 1977, "Aerosol Distributions in Maritime Air and Predicted Scattering Coefficients in the Infrared", Applied Optics, vol 16, no 3, p 654-9

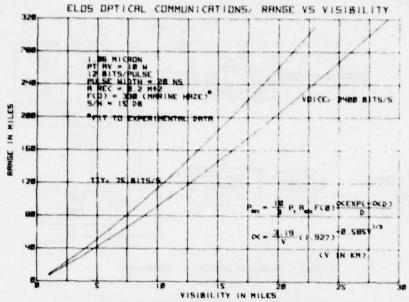


Figure 1. Performance characteristics of ELOS.

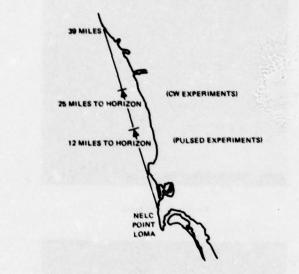


Figure 2. Propagation path for OTH scattering channel.

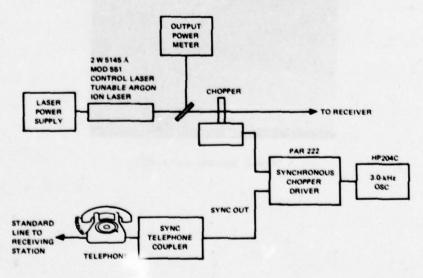


Figure 3. Synchronous transmitter for cw measurements.

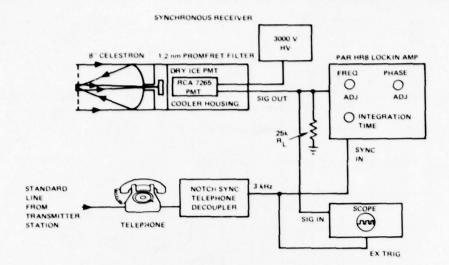


Figure 4. Synchronous detector for cw measurements.

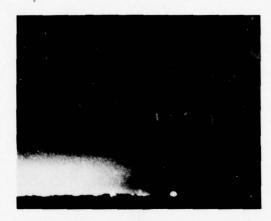


Figure 5. Ducted beam.



Figure 6. Transmitter elevated 0.5°.



Figure 7. Transmitter elevated 0.75°.

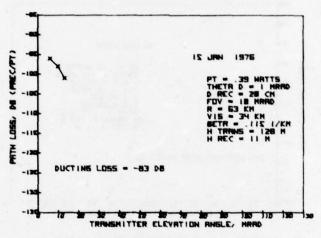


Figure 8. Path loss measurements of 15 January 1976.

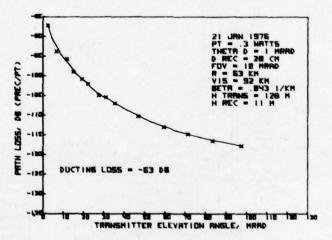


Figure 9. Path loss measurements of 21 January 1976.

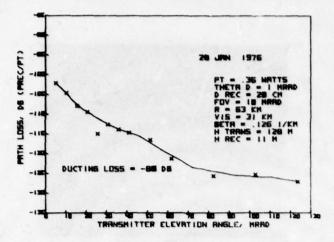


Figure 10. Path loss measurements of 28 January 1976.

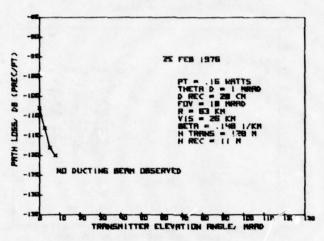


Figure 11. Path loss measurements of 25 February 1976.

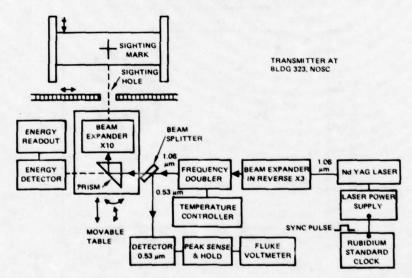


Figure 12. Schematic of dual wavelength transmitter.

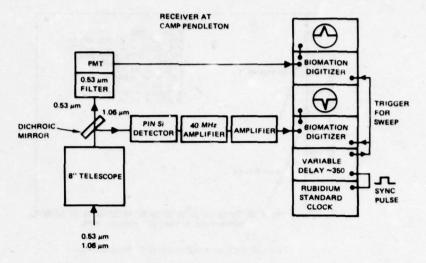


Figure 13. Schematic of dual wavelength receiver.

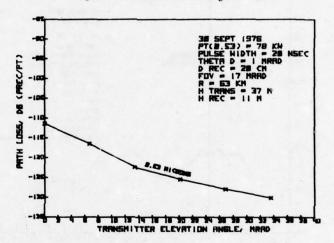


Figure 14. Path loss measurements of 30 September 1976 (elevation scan).

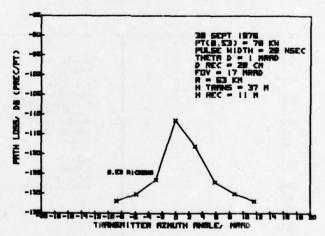


Figure 15. Path loss measurements of 30 September 1976 (azimuth scan).

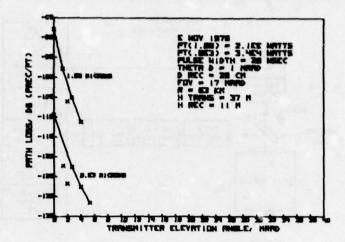


Figure 16. Path loss measurements of 5 November 1976.

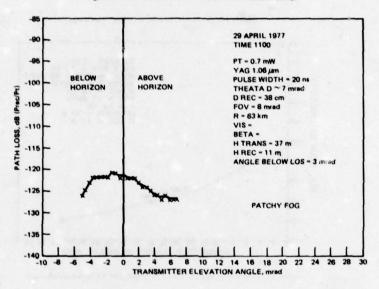


Figure 17. ELOS transmitter elevation scan.

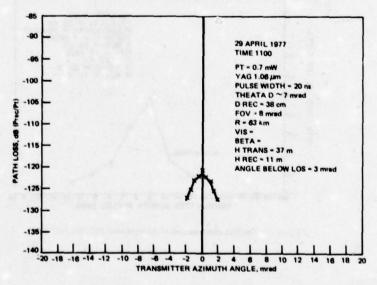


Figure 18. ELOS transmitter azimuth scan.

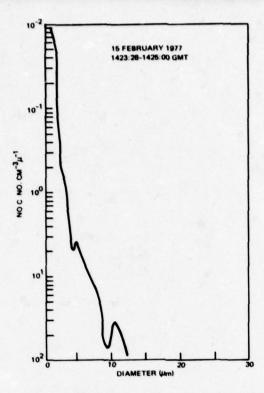


Figure 19. Particle spectrum of "clear" maritime air at NOSC.

RELATIONSHIP BETWEEN MODEM DEVELOPMENT AND CHANNEL CHARACTERIZATION

by

Phillip A. Bello CNR Inc. Needham, Mass. USA.

The most effective approach to the development of optimum modulation and demodulation techniques for a specific class of channels involves a sequence of steps as diagrammed in Fig. 1.1. These steps involve the measurement and modeling of channel characteristics to provide the basis for optimum modem design concepts and the utilization of channel simulators for the development, acceptance testing, and comparative evaluation of implemented modems prior to field testing.

As indicated in Fig. 1.1, the design of the channel measurement experiment involves an initial analytic modeling effort to determine the relationship between significant parameters in the propagation and system function models of the channel. From this modeling effort one may estimate multipath spreads, Doppler spreads, frequency correlation functions, delay power spectra, etc. as a function of propagation channel parameters such as sea state and wavelength and as a function of system parameters such as range, velocity vectors of terminals, antenna patterns, etc. The proper design of the channel probing signal, measurement equipment, and data reduction requires at least that a gross estimate of maximum multipath spread and Doppler spread be available and that the bandwidth be specified over which the channel is to be characterized.

The channel measurement experiment should involve both propagation and system function type measurements in order to validate the initially estimated relationship between the two channel models. It is important to develop such validated relationships because the time and expense associated with channel measurements prvent the collection of measurements under all physical cases of interest. Thus for example in airplane-satellite channel measurements it is desirable that sea state be measured. If, on the basis of measurements, validated relationships have been developed between, say, sea state and multipath spread, then it will be possible to estimate the effects of other sea states even though such states did not occur in the experiments.

System function channel measurements connected with the multiplicative (distoring) and additive disturbance may be taken separately because of their independence. The signal distortion properties of the channel are characterized by measurements at four levels of increasing complexity:

- (1) Measurement of gross parameters of system function (e.g., coherence bandwidth, Doppler spread, etc.).
- (2) Measurement of correlation functions of system functions (e.g., frequency correlation function, delay power spectrum, etc.).
- (3) Measurement of probability distributions of system functions (e.g., probability distributions of amplitude and phase on a received carrier).
- (4) Measurement of system functions (e.g., time-variant transfer function and impulse response).

Measurements 1 - 3 in conjunction with terminal constraints, such as bandwidth and power, are useful for bounding the distortions caused by the channel and allow a considerable narrowing of the possible modulation and demodulation techniques to be considered.

In the development of modems both software and hardware simulators are useful. Software simulations are useful during the early stages of modem development where modem concepts are checked out for inclusion in design specifications and where acceptance specifications are developed. They are also useful during the design of the modem by allowing a prediction of performance degradation that would be caused by a proposed design change. The hardware simulator comes into play when modems have been built, both for final checkout and adjustment of the modem prior to acceptance testing, and for the acceptance testing itself.

Two basic types of channel simulators may be identified, each having separate functions in modem development. These two types of simulators are called the <u>synthetic</u> channel simulator and the <u>playback</u> channel simulator. The synthetic channel simulator creates a reproducible channel which has <u>average statistical</u> properties approximating the measurements 1 - 3. Due to the validated relationships between the system function and propagation channel parameters it is then possible to create synthetic channel conditions which would have been observed if sufficient time could have been expended in the channel measurements. For example, in the case of sea states one might deduce that certain sea states not actually observed in the propagation measurements are still

reasonably likely and would produce certain multipath structure. The synthetic channel can be set to model this situation.

The playback channel is used to recreate the same instantaneous system functions that were measured in 4 above, with appropriate measured additive noise, if ordinary thermal noise is not sufficient. Whereas only the approximate statistical behaviour is reproduced by the synthetic simulation, the exact instantaneous system function (and representative noise) that existed during the measurements is "played back" by the playback simulation. While the synthetic simulator is of great help in checking out bit-sync tracking and acquisition, and further narrowing the modems of interest through comparative modem performance evaluation under identical conditions, these conditions only approximate the statistical behaviour of the actual channel. In order to achieve low error rates in digital communication it is necessary to consider the rare events on the "tails" of probability distributions which cannot be reproduced by the synthetic channel. However, all such rare events which have occurred in the system functions during channel measurements will be accurately reproduced by the playback simulator. Note, moreover, that the playback channel allows a comparative evaluation of modem performance over the same time-bandwidth portion of an actual channel, a feat which is impossible in direct field testing of modems:

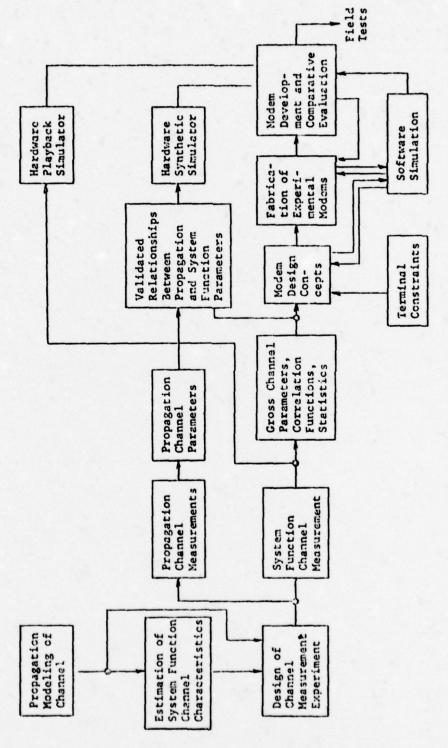


Figure 1.1: Utilisation of Channel Measurements in Modem Development

WIDEBAND LINE-OF-SIGHT CHANNEL SIMULATION SYSTEM*

Phillip A. Bello H. David Goldfein

CNR, Inc. 220 Reservoir Street Needham, Massachusetts

ABSTRACT

This paper will describe the theoretical background, methods of implementation, and utility of a multi-purpose wideband LOS (line-of-sight) channel simulation system developed by CNR, Inc., for Rome Air Development Center as a means for checking out wideband digital modems. The system provides both a channel probing/channel playback capability and a synthetic stochastic channel simulation. Propagation media effects simulated include both multipath due to refractive anomalies (refractive multipath) and scattering off the surface (surface multipath). The types of LOS channels handled by the system include airplane-airplane, ground-airplane, ground-ground, airplane-satellite. In addition, the simulator allows the introduction of controlled amounts of nonlinearity, phase jitter, and frequency offset. The simulator operates at selectable IF frequencies of 70, 300, or 700 MHz. At the two higher IF frequencies, signal bandwidths up to 100 MHz may be accommodated, while at 70 MHz, bandwidths up to 25 MHz may be handled.

1. INTRODUCTION

The development of reliable high-speed digital modems (modulators-demodulators) for use over fading dispersive radio channels can be facilitated greatly with the aid of channel simulators. Two important classes of simulators can be identified:

- · Synthetic channel simulation
- · Playback or stored channel simulation

In the case of synthetic channel simulation, deterministic or stochastic models are implemented based upon either, or both, theoretical calculations and previously measured statistics. In the case of the playback channel simulation, a long record of parameters characterizing the time-varying system function of a channel (such as tapped delay line weights) are measured with the aid of a channel prober/analyzer and recorded on magnetic tape. This tape is played back into a model of the channel which utilizes the measured parameter values in a corresponding canonic channel model (such as a tapped delay line with weights).

With the playback of a measured and stored channel, there will be identical instantaneous time- and frequency-selective channel conditions as occurred in the field. In the synthetic channel simulation, there will be only statistically similar channel conditions, but they will be adjustable to cover situations expected to occur but not measured due to the limited duration of the field tests. These simulation techniques complement each other in providing tools for modem development.

The simulator described in this paper includes both playback channel and synthetic channel simulators and probably represents the most versatile and flexible radio communications channel simulator yet developed. Some of the concepts in the present system design have been developed by Bello [1] - [7] in previous synthetic and stored-channel simulators he has designed. However, the present equipment represents an expansion of capabilities in terms of simulation bandwidth, flexibility, and operational modes.

2. APPLICABLE CHANNELS

The major cost of the simulator is associated with the measurement and simulation of propagation media fading and multipath associated with particular links, namely:

Ground-Aircraft (GA)
Aircraft-Aircraft (AA)
Aircraft-Satellite (AS)
Ground-Ground (GG)

Since propagation media are linear, their input-output behaviors are completely determined by corresponding impulse responses or transfer functions. Because radio channels are

Funds for this development were provided by the Air Force Systems Command, Rome Air Development Center, Griffiss Air Force Base, Rome, New York, under Contract No. F30602-75-C-0242.

time-variant, both the impulse response and transfer function must be regarded as time-variant. It may be shown that the complexity of equipment required to measure, record, and reproduce the characteristics of the propagation channel over a finite bandwidth depends directly upon two gross channel parameters, the <u>multipath spread</u> and the <u>Doppler spread</u>. The multipath spread is a measure of the duration of the impulse response of the channel while the Doppler spread is a measure of the width of the spectrum of a received carrier.

In discussing the values of Doppler spread and multipath spread of a channel and their impact on channel simulator design, it is necessary to distinguish various propagation modes. For the four canonic LOS channels of interest here (GA, AA, AS, GG), the following three propagation modes are of interest:

- · Refractive multipath
- Surface multipath
- Ionospheric scintillation (AS only)

An elevated tropospheric layer with a scale much larger than the wavelength of the carrier can act as a lens which, under proper conditions, focuses the transmitted signal into the receiver over multiple paths. The frequency and intensity of the meteorological conditions which result in such multipath-producing propagation have been studied experimentally [8] - [21]. The resulting multipath structure has been examined at CNR under three contracts with RADC [22] - [24], and the numerical results [25] agree quite favorably with the experimental data [8] - [21].

Refractive multipath is a term used to describe the channel characteristics caused by these steep negative gradients in refractive index. The net effect of this gradient is to produce discrete multipath, i.e., a finite set of paths in addition to the direct path between transmitter and receiver. An analysis of the impulse response structure by CNR indicates a maximum of seven paths for a path length of 200 miles. Calculations of multipath are not made beyond 200 miles because the theory assumes a continuous layer and it does not seem likely that layers will extend so long. However, there is a lack of experimental knowledge on layer lengths, so the assumption is purely arbitrary at this point.

Refractive multipath will only occur on LOS paths having an elevation angle of less than 2°-3°, and is not normally experienced on channels employing a satellite relay which usually do not attempt to communicate at such low elevation angles. On the other hand, the AA, GA, and GG channel perforce operate at low elevation angles of the line-of-sight and thus experience refractive multipath whenever the corresponding propagation conditions exist. On the basis of the propagation model used by CNR, it is found that over most of the world, the worst-case multipath spread is within 65 nanoseconds. The worst Doppler spreads are found to be less than .5 Hz/Mach No./GHz of carrier frequency. Channel measurement would probably be undertaken at speeds of less than Mach .7. For the typical military operating frequency of 8 GHz, we find an expected worst-case Doppler spread of 5.6 Hz.

We consider now the multipath and Doppler spread associated with <u>surface multipath</u>. CNR has carried out considerable study on modeling surface multipath. Although the underlying scattering process which causes this multipath is the same for AS/GS and AA/GA links, operational as well as numerical considerations make the models somewhat different. The AS/GS model was developed at CNR under contract to the Department of Transportation [26],[27] while the AA/GA model was developed at CNR under contract to RADC [29].

The earliest arriving component of the surface multipath is from the "specular" point, i.e., the point of mirror reflection from the surface. Later multipath components come from annular rings at successively larger distance from the specular point. There are two sharp contrasts between surface multipath and refractive multipath. First we note the gap in delay between the direct path and the specular delay within which no surface multipath may occur. Refractive multipath is generally clustered soon after the direct path and will frequently be so close as to be unresolvable from the direct path. Second, we note that except for reflections from large objects like mountains or buildings or a "specular" reflection emanating from the average surface around the specular point, the surface multipath consists of a very large number of very small components distributed in delay. Thus it is of a "continuous" nature as opposed to the discrete nature of refractive multipath.

Two other contrasts we wish to make are the behavior of these modes of propagation as a function of antenna size and operating frequency. Refractive multipath is virtually unaffected by antenna size because the discrete paths are clustered very close to the direct path, deviating only tenths of a degree. Surface multipath is strongly affected by the antenna pattern which can, in principle, be focused to eliminate reflections and scattering from the surface. In practice, antenna sizes are sharply limited for airplane use and surface multipath cannot always be eliminated.

Consider now the effect of changing the operating frequency. In the case of refractive multipath, the relative path delays are to first order, not a function of operating

frequency. However, as the operating frequency is lowered sufficiently, the multipath spread will become less than a period of the carrier frequency, and the channel will behave like a single fading path for information transmission. As the frequency is lowered such that the multipath spread is a small fraction of a carrier frequency period, the fading will disappear because the multipath components will add in-phase.

In the case of surface multipath, the frequency and angle of incidence to the specular point can have a pronounced effect on multipath characteristics. The signal scattered from the surface of the earth (land, water, ice, etc.) has a discrete or specular and a diffuse component. The specular component characterizes the mean signal scattered from the surface, while the diffuse component characterizes the random return due to the roughness of the surface and produces the "continuous" multipath. It may be shown that, for a fixed grazing angle and surface roughness, the multipath will tend to be continuous at the higher (microwave) frequencies and specular or discrete at the lower (UHF) frequencies. For the military links being considered here, there are many naturally-occurring surfaces (e.g., the ocean, hilly terrain, desert, snow drifts, etc.) which will cause diffuse scatter to exist.

The delay difference between the specular and direct signal paths can amount to tens of microseconds for an AS link, while the Doppler difference would be at most 7 Hz/Mach No./GHz of carrier flight for level flight.

We consider now the amount of multipath spread produced by the surface multipath. It has been shown by CNR [26] - [28] that for sufficiently wide beam antennas and low elevation angles to the satellite, up to 10 μ s of multipath spread exist. Since military operational antennas are directive to provide for increased gain, multipath rejection, secure communication, etc. (see [30]), multipath spread calculations should be made for typical military situations. It is assumed that the satellite antenna provides broad coverage in a sector which contains the military aircraft, and therefore provides for little or no multipath discrimination. However, the aircraft antennas used to communicate with satellites can range from upper hemispherical coverage at UHF to a few degrees beamwidth at the higher microwave frequencies.* The coverage provided by these antennas is shown diagrammatically in Figure 1. Since the antennas are designed for satellite communications, the usual case is for the multipath to occur in a sidelobe, as shown in Figures 1(a) and 1(b). However, when the satellite is at a very low elevation angle, the multipath may occur in the main beam of the antenna, as shown in Figure 1(c).

Approximate calculations of multipath spread due to sidelobe illumination have been carried out by CNR for various grazing angles γ and beamwidths θ for diffuse scatter at microwave frequencies. For antenna beamwidths less than about 3° , the maximum (sidelobe) delay spread has been found to be about 200 nanoseconds at an aircraft altitude of 30 thousand feet.

If the main beam illuminates the earth's surface as it may when the satellite is near the horizon, the scattered power can be calculated from the scattering cross-section, the surface roughness, and the $1/R^2$ losses. In calculating the multipath power, we have assumed worst-case rms surface slope α , i.e.,

$$\alpha = \alpha_{\text{max}} = \tan \gamma \tag{1}$$

where γ is the grazing angle to the specular set. (The rougher the surface, the larger the surface area over which scattering takes place and the larger the multipath spread.) When $\alpha > \tan \gamma$, a significant part of the surface becomes shadowed by the surface irregularities, and the multipath power is typically reduced by an order of magnitude [31, p. 116]. The results of such an approximate calculation show that, for grazing angles less than about 3° , the multipath spread (defined here as the delay beyond the specular delay at which the multipath power drops to 1/e of its maximum value) is less than 200 ns.

Similarly, one may calculate the Doppler spreads for the cases of sidelobe illumination and main beam illumination of the surface at low grazing angles. One may show that, for an 8-GHz carrier frequency and Mach .7, Doppler spreads of less than 10 Hz are predicted for a beamwidth of 3° in the case of sidelobe illumination and for any beamwidth in the case of mainlobe illumination of the surface. Note that the Doppler spread decreases with decreasing grazing angle.

In the case of the AA and GA links, surface multipath will occur in addition to refractive multipath. The AA/GA links differ from the AS link, however, in that the multipath is always generated at low grazing angles and within the radio horizon. As a result

^{*}In three years of airborne testing [31], blade, dipole, and crossed slot UHF antennas were used to provide upper hemispherical coverage; at S-band, a $\pm 2^{\circ}$ beamwidth antenna was used. In [30], a 32-inch Cassegrain with a 3° beamwidth at SHF was mounted on a KC-135.

of these differences, the surface scatter multipath on AA/GA has a specular component which is delayed only a few hundred nanoseconds from the direct path and shifted by at most 10 or 20 Hz. The multipath spread is worst for AA links. For AA links, one may calculate that aircraft at 30 thousand feet with antenna beamwidths less than $3^{\rm O}$ experience diffuse multipath with delay spreads of less than about 150 nanoseconds for grazing angles above $1^{\rm O}$. At angles below $1^{\rm O}$, the diffuse multipath power decreases due to shadowing and due to the tendency of the multipath to be specular near grazing incidence.

Calculations of Doppler spreads indicate small values of the order of these found in the other cases, e.g., $10~\rm{Hz}$ or less for $8~\rm{GHz}$, Mach .7, and $3^{\rm{O}}$ beamwidths.

In the case of GG links with parameters representative of those used in conventional microwave relay communications, multipath spreads and Doppler spreads will be much smaller than those quoted for the other links. Calculations are available in a report by CNR [22].

As a final channel characteristic, we consider ionospheric scintillation. This phenomenon is of relevance only for AS links in which the LOS pierces regions of the ionosphere which are perturbed anomalously in the vicinity of the equator. From an input-output point of view, the effect is one of causing amplitude and phase fluctuations, i.e., Doppler spread with negligible multipath spread. The effect is quite important at UHF but will be negligible at the higher microwave frequencies, e.g., 8 GHz. The Doppler spread, in any case, is quite low — a few Hz at most.

The simulation system described in this paper is designed to measure and playback or synthesize the fading dispersive characteristics of GA, AA, AS, and GG links for various combinations of refractive multipath, surface multipath, and ionospheric scintillation.

3. MEASUREMENT AND SIMULATION APPROACH

The problem of channel measurements on fading dispersive channels has been studied extensively by Bello [34] - [39].

The channel measurement approach used here involves transmission of a pseudo-random binary PSK (0,180°) with the (0,180°) states controlled by the (0,1) states of a maximal length shift register sequence. The received process is (complex) correlated with delayed replicas of the pseudo-random probing signal to produce lowpass in-phase and quadrature estimates of the channel* time-variant impulse response at a set of equally-spaced delay samples. This set of time-varying samples is digitized and recorded on magnetic tape. In playback, the reverse operation takes place - the tape is played back into a unit that unpacks the samples, filters them, and D/A converts the tape information into the lowpass in-phase and quadrature information needed to drive the analog complex modulators of an analog tapped delay line model of the channel.

To keep the system complexity reasonable, provision is made for separately and simultaneously measuring the surface multipath starting at the earliest arriving specular component and ignoring the "empty" region between the direct/refractive multipath and the surface multipath. By using this procedure, maximum utilization is made of the hardware in measuring and reproducing multipath.

The preceding discussion introduced some of the basic signal processing elements in the channel playback simulation system. However, practical utilization of this system requires the incorporation of additional features for the LOS channels which have moving terminals (GA, AA, AS). The changing path length causes both a time variation in path loss and a time variation in mean path delay for the direct path, refractive multipath, and surface multipath. To handle the time-variant delays, two tracking loops are used which adjust the timing of two separate PN sequence generators. The early tracker removes the time-variant group delay of direct/refractive multipath group while the late tracker separately removes the time-variant group delay of the surface multipath. Frequently, refractive multipath will be absent and the direct path alone will be tracked in the early group. The changing path delays also produce Doppler shifts. A Doppler tracking loop is provided to track out the Doppler shift of the direct/refractive multipath group. wise, the output lowpass filters would have to be made very wide in bandwidth to accommodate this Doppler shift. The Doppler shift of the surface multipath group will differ from that of the direct/refractive multipath group, but for channel measurement with airplanes flying at level height, the differential Doppler will be at most 10 - 20 Hz, and this shift is small enough to be absorbed by the analyzer lowpass filter bandwidth ranges.

^{*}The channel impulse response includes all terminal equipment filters.

Actually, different frequency and time error discriminators are provided for tracking refractive multipath as opposed to tracking a resolvable direct path in order to optimize tracking performance under the fading dispersive conditions of refractive multipath.

Therefore, in the interest of cost savings, no separate Doppler tracker is provided for the surface multipath.

In channel playback, ideally, the variable delays and Doppler shifts should be reinserted. It has been found prohibitively expensive to provide time-variable delays covering the range of delays required. Moreover, there appears no need to have this feature, from a modem evaluation point of view. Differential and direct path Doppler may be set manually at measured values recorded in the log of the flight test. Differential delay will be fixed but manually-selectable from a range of values. Again, information from the log of the experiment would provide suitable values for this delay. Direct path delay would not be reproduced since it is irrelevant for modem testing. Note that simply setting the bit sync clocks at different rates for the digital modulator and demodulator simulates changing relative path delay.

Path loss variation will be significant only for the AA and GA links where variations of path length greater than 10:1 may occur during a channel measurement period, causing in excess of a 20-dB variation in average SNR during a measurement interval. To make maximum utilization of the dynamic range of the analog correlators employed in the analyzer, an AGC is provided. Since the path loss variation will be slow, a long-time constant is provided in the AGC. Cases may exist where the fading multipath could have low enough frequency components to be affected by the AGC, and provision is made for recording the gain variations and reproducing them in the channel playback by means of a variable attenuator.

We consider now the synthetic simulation of the propagation channel. The same tapped delay line is used as in playback simulation, but now the complex tap gains must be generated synthetically.

The two major harmful propagation effects that require some complexity in implementation are refractive and surface multipath. From a mathematical-statistical point of view, these two propagation effects present a study of contrasts. The refractive multipath consists of a small number of individual paths while the surface multipath (aside from a possible specular component) consists of a very large number of small diffuse scattered components and has a continuous type of representation.

From a statistical point of view, the refractive multipath is far more nonstationary than the surface scatter. Consider an AG link. As the airplane passes near the layer of steep negative gradient in refractive index which causes the refractive multipath, multiple ray paths appear, move in delay relative to one another, coalesce, disappear, and new paths appear. As discussed in [23], the amplitudes and delays change much slower than the relative phases. Compare this behavior with the surface scatter in an AS link. The airplane antenna is illuminating (through a main or sidelobe) a large portion of the surface of the earth. Many small reflections occur from the surface, and the law of large numbers gives some statistical regularity to the continuum of multipath components. No abrupt changes will be noticed unless the terrain or airplane antenna orientation changes abruptly. Over the ocean, statistical regularity will be the rule rather than the exception.

It may be shown [33] that, as the reciprocal channel bandwidth to be characterized becomes small compared to the multipath spread in surface or volume scatter, the tapped delay line model of the channel approaches the case in which the tap gains are complex Gaussian and independent. This is the basic model employed for synthetic simulation of surface multipath. The complex Gaussian weights are obtained by filtering pseudo-random sequences.

Since the tapped delay line model, with taps spaced 1/W seconds apart and complex weights, provides a perfectly general representation for a linear operation over a bandwidth W, it is possible to find a mathematical relationship between the delay and amplitude of a discrete set of paths and the complex weights in a tapped delay line model. This relationship is implemented with the aid of a small computer whose input is a tape providing the time-varying path delays and amplitudes associated with the refractive multipath of a given AA/AG/GG scenario. The calculated tap weights are continually generated by the computer and fed as control inputs to the tapped delay line complex modulators. Continuous movement of up to seven discrete paths is provided with the software.

The computer also generates the ionospheric scintillation modulation. The model used involves independent Gaussian noises of different strengths on the in-phase and quadrature inputs of the complex modulator together with a specified nonfading component on the in-phase part.

4. PROBER/ANALYZER/SIMULATOR SYSTEM FEATURES

This section summarizes the basic features of the Prober/Analyzer/Simulator system. We consider the prober/analyzer first.

The prober/analyzer has several classes of operating modes:

- · Characterization Bandwidth Modes
- IF Frequency Modes
- · Integration Time Modes
- · Correlator Grouping Modes
- Tracking Modes
- · Gain Control Modes

Characterization bandwidths of 25 and 100 MHz may be selected. In the 25-MHz case, an IF frequency of 70 MHz only can be selected, while in the 100-MHz case either 300 MHz or 700 MHz can be selected. It is important to note that the quoted bandwidth characterization, e.g., 100 MHz, is not a nominal characterization but a precise characterization in the sense that the system provides essentially transparent performance over this bandwidth as far as modem error rate reproducibility is concerned in channel playback. (Of course, this statement is subject to the requirement that sufficient SNR is available during measurement and that the Doppler and multipath spread do not exceed the design values.) Separate IF channelizing filters must be switched in for the 25- and 100-MHz bandwidths to limit alias crosstalk due to the sampling of the impulse response and also separate equalizing filters must be switched into the simulator in the playback mode to counteract the coloring of the prober spectrum. The probing signal in the case of 100-MHz characterization consists of a pseudo-random $(0,180^{\circ})$ sequence with chip period Δ_0 of 10 ns, i.e., a 100M chips/second rate, while in the 25-MHz characterization, Δ =40 ns and the chip rate is 25M chips/second. A sequence length of 2047 is used in the 100-MHz mode providing a PN sequence period of 20.47 µs, while in the 25-MHz mode, a sequence length of 511 is used providing a PN sequence period of 20.44 µs.

Analog integrate-and-dump takes place over exactly one PN sequence period at the correlator output. Further integration is done digitally by summing successive analog I&D outputs. It is convenient in discussing system performance to define six modes of operation I - VI, as indicated on Table 1, for the various values of total integration time T possible for the system, where T = I T_0 , I = 1,2,4,8,16,32.

Table 2 presents the recording time and tape speed for a roll of instrumentation tape for each mode I-VI listed in Table 1. Note that because of the approximately 20- μ s period of the PN sequence, an ambiguity in multipath delay will occur for paths delayed from the direct path more than 20 μ s. This 20- μ s ambiguity does not constitute a real limitation to collection of data by the system because long differential delays occur only in the AS channel for which the multipath spread is predicted to be much less than 20 μ s. The differential delay can be computed fairly accurately for the radio link geometry so that one may avoid foldover effects for multipath near the 20- μ s boundary. In addition, it is only at low grazing angles that any multipath is predicted, and for these grazing angles the differential delay will be smaller than 20 μ s.

As discussed above, the channel multipath structure will consist of either a single group of paths or two groups, depending on the simultaneous existence of refractive and surface multipath. Flexibility exists within the analyzer to apportion one subset of the correlators to the early multipath group and one subset to the late multipath group. However, for playback, the early group must consist of no more than eight taps in the 100-MHz mode (and two taps in the 25-MHz mode*) because of the physical construction of the simulator. In this split mode of operation, 52.5 ns of refractive multipath (including the equipment channel) can be measured. A direct path is separately measurable when there is no refractive multipath, leaving 31 samples to characterize the surface multipath.

The direct path and surface multipath are separately tracked in delay while only the Doppler shift of the direct path is tracked. Calculations of differential Doppler for collection of data in level flight show that it is small enough to be handled by the bandwidths used in measuring the tap gains. When refractive multipath is present, the fading distortion can affect operation of the coherent direct path tracking. Consequently, alternate delay and Doppler error discriminators more tolerant to multipath and fading are provided and may be selected when refractive multipath is being tracked.

Due to the fact that the path length can change significantly during a collection interval of 30 minutes for AA and AG links, the received signal strength can vary significantly during a run, say, 20 dB. Two modes of gain control are provided, manual and automatic, both over a range of 60 dB. In the AGC mode, a long time constant is used to attempt tracking only the slow path loss variations. However, refractive multipath can vary slowly and, to avoid any possible distortion caused by tracking out refractive multipath

^{*}Because of equipment impulse response spreading, the use of two taps to represent a multipath group appears risky. Thus it may be preferable not to use the 25-MHz mode when both refractive and surface multipath occur.

fluctuations, the automatic gain fluctuations are recorded on tape and reproduced by a variable attenuator in the channel playback process.

Additional features in the analyzer include a received signal level (RSL) indicator with a LED numeric display, a multipath signal display showing the correlator I&D outputs on an oscilloscope, and a differential path delay indicator with a LED numeric display. Direct-path Doppler may be estimated from the vernier on the Doppler tracking VCXO. There is also an indication for overflow of the A/D converters and under-driving of the correlators.

The simulator has several modes of operation. As far as control of the complex modulators is concerned, there are five basic modes of operation, each one of which may be independently selected for each complex modulator input:

- Playback
- Computer Control
- Synthetic Complex Gaussian
- · Calibrate Check
- External Modulation

The playback mode derives its complex modulator input from playback of the recorded multipath analyzer outputs. When this mode is used, an analog equalizer must be switched in to compensate for the non-white prober spectrum. In addition, as pointed out above, if the AGC mode is used in the analyzer, then a gain voltage will be played back to control an output attenuator.

Any set of complex modulator inputs may be controlled by the PDP-11/04 minicomputer provided with the simulator. This computer can provide simulations of refractive multipath, ionospheric scintillation, specular components, arbitrary complex fixed filters, and special programs for checking out the tap modulators and D/A converters. The simulation of refractive multipath utilizes the minicomputer to prepare digital tapes of relative amplitudes and delays of discrete multipath components vs. time, corresponding to a particular scenario of interest. This tape is played back by the minicomputer so that it may generate the complex modulator time-variant gains corresponding to that scenario. Ionospheric scintillation is modeled by use of programs to generate pseudo-random Gaussian modulations.

Special hardware generates the pseudo-random complex Gaussian noise tap modulation used to model surface multipath. The rms Doppler spread of this noise is selected at the front panel in the range 0.1 Hz to 1 kHz. This noise can be reset to the same starting point. A very long PN sequence (shift register length 52) is used to provide an accurate Gaussian probability density, and the period of the PN sequence is very much longer than any measurement interval of interest.

In the calibrate mode, each tap may be set to one of four phases, 0, 180° , 90° , -90° , or OFF manually. By sending a test signal into the simulator and examining the system output for each separate modulator, it is possible to check directly on the complex modulator performance. This check, in conjunction with similar tests directed from the minicomputer, can be used to isolate and verify performance.

Finally, there is an external modulation mode where the in-phase and quadrature components of any tap complex modulator may be controlled by an external modulation source.

There are two basic differential delay options: a short differential delay for AA and AG links, and a long differential delay for AS links. The value of the short differential delay may be selected from the values 100, 200, 300, and 400 ns, while the long differential delay may be selected from the values 4.1, 8.1, 12.1, and 16.1 μ s.

Figures 2, 3, and 4 show photographs of the fabricated system. Figure 2 shows the prober, Figure 3 the multipath analyzer, and Figure 4 the simulator. The analog and RF signal processing elements are in a double-bay rack cabinet along with the digital signal sources for synthetic surface scatter multipath generation and test modes. The computer and playback tape signal sources are in a second cabinet.

ACKNOWLEDGEMENT

The design and fabrication of this wideband LOS simulator represents a two-year intensive effort by several members of the CNR staff. The dedicated efforts of Paul Jauniskis, who was responsible for the analog portions, and Tony Lavely, who was responsible for the digital portions of the system, require particular acknowledgement. Finally, we wish to acknowledge the interest and encouragement of the RADC project Engineer, John Evanowsky.

REFERENCES

- [1] "Forward Scatter Measurements," Final Report on Contract F19628-71-C-0082 for Rome Air Development Center.
- [2] "VHF Tactical Channel Simulator," Final Report on Contract DAABO7-71-C-0019 for U. S. Army, Ft. Monmouth, NJ.
- [3] "Urban Channel Simulator," Final Report on Contract DOT-TSC-84 for Transportation Systems Center, Department of Transportation, Cambridge, MA.
- [4] P. A. Bello, C. J. Boardman, D. Chase, and J. K. DeRosa, "Impact of Satellite Aeronautical Channel on Modem Specifications," Report No. FAA-RD-74-54, Final Report by CNR, Inc., on Contract DOT-TSC-516-1, March 1974.
- [5] P. A. Bello, et al., "Underwater Communications," Contract No. N00140-68-C-0051, and "Generalized Channel Measurement Software," Contract No. N00600-71-C-0100, Final Reports for Naval Research Labs.
- [6] P. A. Bello and L. Ehrman, "Troposcatter Modem Performance Prediction with a Complex Gaussian Troposcatter Channel Simulator," <u>Record of the IEEE 1969 International</u> <u>Conference on Communication</u>, pp. 48-11 - 48-16.
- [7] P. A. Bello and R. W. Pinto, "HF Stored Channel Simulation," Final Report by CNR, Inc., on Contract N00014-74-C-0048 for NRL.
- [8] F. Ikegami, "Influence of an Atmospheric Duct on Microwave Fading," <u>IRE Trans. on</u> Antennas and Propagation, July 1959, pp. 252-257.
- [9] M. S. Wong, "Refraction Anomalies in Airborne Propagation," <u>Proceedings of the IEEE</u>, Vol. 46, September 1958, pp. 1628-1638.
- [10] N. W. Guinard, et al., "Propagation Through an Elevated Duct: Tradewinds III," IEEE PGAP, July 1964, pp. 479-490.
- [11] B. R. Bean and E. J. Dutton, <u>Radio Meteorology</u>, National Bureau of Standards Monograph 92, 1 March 1966.
- [12] B. R. Bean, et al., "A World Atlas of Atmospheric Radio Refractivity," Essa Mono-graph No. 1, U. S. Government Printing Office, Washington, DC, 1966.
- [13] H. T. Dougherty, "A Survey of Microwave Fading Mechanisms, Remedies, and Applications," <u>Essa Technical Report ERL 69-WPL4</u>, U. S. Government Printing Office, Washington, DC, March 1968.
- [14] E. E. Gossard, "The Reflection of Microwaves by a Refractive Layer Perturbed by Waves," IEEE Trans. on Antennas and Propagation, May 1962, pp. 317-325.
- [15] C. C. Watterson, J. R. Juroshek, and J. L. Demmer, "SHF Bandwidth Study, Phase III," NBS Report 8842, U. S. Department of Commerce, NBS, Boulder, Colorado.
- [16] M. C. Thompson, Jr., H. B. Jánes, L. E. Wood, and D. Smith, "Phase and Amplitude Scintillation of Microwave Signals Over an Elevated Atmospheric Path," Report of NASA Contract Order No. L-31028, ITS, Boulder, Colorado, 10 May 1971.
- [17] O. E. DeLange, "Propagation Studies at Microwave Frequencies by Means of Very Short Pulses," <u>BSTJ</u>, January 1952, pp. 91-103.
- [18] A. B. Crawford and W. C. Jakes, Jr., "Selective Fading of Microwaves," <u>BSTJ</u>, January 1952, pp. 68-90.
- [19] G. M. Babler, "A Study of Frequency-Selective Fading for a Microwave Line-of-Sight Narrowband Radio Channel," <u>BSTJ</u>, Vol. 51, No. 3, March 1972.
- [20] G. M. Babler, "Selectivity Fading Non-Diversity and Space Diversity Narrowband Microwave Radio Channels," <u>BSTJ</u>, Vol. 52, No. 2, February 1973.
- [21] K. Bullington, "Phase and Amplitude Variations in Multipath Fading of Microwave Signals," BSTJ, Vol. 50, No. 6, July-August 1971, pp. 2039-2053.

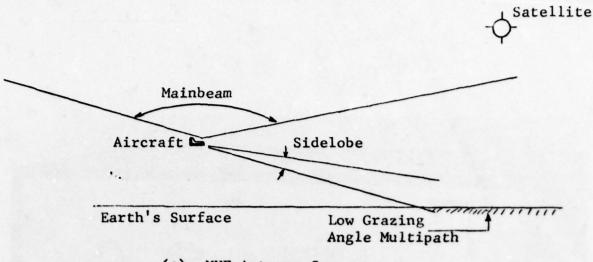
- [22] P. A. Bello, J. K. DeRosa, and C. J. Boardman, "Line-of-Sight Wideband Propagation," Final Report by CNR, Inc., on Contract No. F30602-73-C-0013 for Rome Air Development Center, May 1973.
- [23] P. A. Bello, C. J. Boardman, D. Chase, and J. K. DeRosa, "Line-of-Sight Technical Investigations," Final Report by CNR, Inc., on Contract No. F30602-73-C-0244 for Rome Air Development Center, June 1974.
- [24] P. A. Bello, L. W. Pickering, and C. J. Boardman, "Multipath Over LOS Channel Study," Final Report by CNR, Inc., on Contract No. F30602-76-C-0419 for Rome Air Development Center.
- [25] J. K. DeRosa, "Tropospheric Refractive Multipath on LOS Links," CNR Executive Software Package No. 9-24.
- [26] P. A. Bello, C. J. Boardman, D. Chase, and J. K. DeRosa, "Impact of Satellite Aero-nautical Channel on Modem Specification," Finel Report by CNR, Inc., on Contract No. FAA-RD-74-54 for DOT/FAA, March 1974.
- [27] P. A. Bello, "Aeronautical Channel Characterization," IEEE Trans. on Communications, May 1973, pp. 548-563.
- [28] P. A. Bello, D. Chase, J. K. DeRosa, L. J. Weng, and M. G. Bello, "Impact of Satellite Aeronautical Channel on Modem Specification, Phase II: Oceanic Multipath and Modem Concepts," Final Report by CNR, Inc., on Contract No. DOT-TSC-516-2 for DOT/FAA, March 1974.
- [29] P. A. Bello, J. K. DeRosa, and C. J. Boardman, "Line-of-Sight Wideband Propagation," Final Report by CNR, Inc., on Contract No. F30602-73-C-0013 for Rome Air Development Center, May 1973.
- [30] NATO/AGARD, "Antennas for Avionics," <u>Conference Proceedings</u>, No. 139, AD-782-310, November 1973.
- [31] A. L. Johnson and M. A. Miller, "Three Years of Airborne Communication Testing Via Satellite Relay," AFAL Report TR-70-156, November 1970.
- [32] T. P. McGarty, "Models of Multipath Propagation Effects in a Ground-to-Air Surveillance System," Lincoln Lab., Tech. Note 1974-7.
- [33] P. A. Bello, "Characterization of Randomly Time-Variant Linear Channels," <u>IEEE Trans.</u> on Comm. Systems, Vol. CS-11, No. 4, December 1963, pp. 360-393.
- [34] P. A. Beilo and R. Esposito, "Measurement Techniques for Time-Varying Dispersive Channels," <u>Alta Frequenza</u>, N. 11, Vol. XXXIX, 1970, pp. 980-996.
- [35] P. A. Bello, "The Effects of Oscillator Instability, Time Jitter, and Time-Scale Change Upon Four Channel Probing Techniques," <u>Aspects of Network and System Theory</u>, Holt, Rinehart and Winston, Inc., 1970.
- [36] P. A. Bello, "Measurement of Random Time-Variant Linear Channels," <u>IEEE Trans. on Information Theory</u>, Vol. IT-15, No. 4, July 1969, pp. 469-475.
- [37] P. A. Bello, "Some Techniques for the Instantaneous Real-Time Measurement of Multipath and Doppler Spread," <u>IEEE Trans. on Comm. Technology</u>, Vol. COM-13, No. 3, September 1965, pp. 285-292.
- [38] P. A. Bello, "On the Measurement of a Channel Correlation Function," <u>IEEE Trans. on Information Theory</u>, Vol. IT-10, No. 4, October 1964, pp. 382-383.
- [39] P. A. Bello, "Measurement of the Complex Time-Frequency Channel Correlation Function," <u>Radio Science J. of Research</u>, NBS/USNC-URSI, Vol. 68D, No. 10, October 1964, pp. 1161-1165.

Table 1 Definition of Some Modes of Operation of Prober/Analyzer

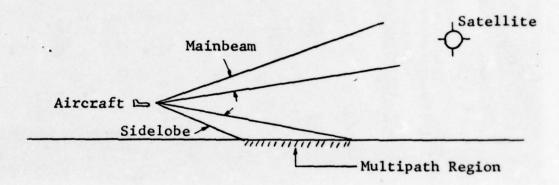
Mode	Characteri- zation Bandwidth (MHz)		PN Sequence Length		Samples Integrated Prior to Recording
I	100	25	2047	511	1
11	100	25	2047	511	2
111	100	25	2047	511	4
IV	100	25	2047	511	8
v	100	25	2047	511	16
VI	100	25	2047	511	32

Table 2 Differential Delay Ambiguity, Recording Capability, and Tape Speed for Each Mode

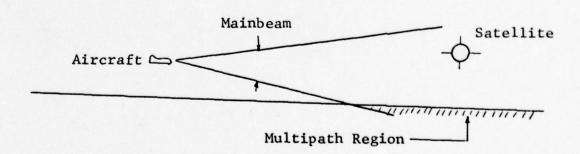
Mode	Unambiguous Delay Resolution (Nearest µs)	Recording Duration of One Roll of Tape	Tape Speed	
I	20 μs	15 mins	120 ips	
II	20 μs	30 mins	60 ips	
III	20 μs	60 mins	30 ips	
IV	20 μs	2 hrs	15 ips	
V	20 μs	4 hrs	7½ ips	
VI	20 μs	8 hrs	3% ips	



(a) UHF Antenna Coverage



(b) Higher Frequency Microwave Antenna Coverage at High Elevation Angle



(c) Higher Frequency Microwave Antenna Coverage at Low Elevation Angle

Figure 1 Antenna Coverage on Military Aircraft-Satellite Links

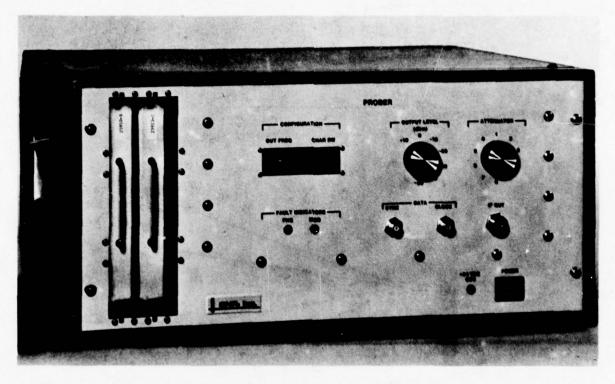


Figure 2 LOS Channel Prober

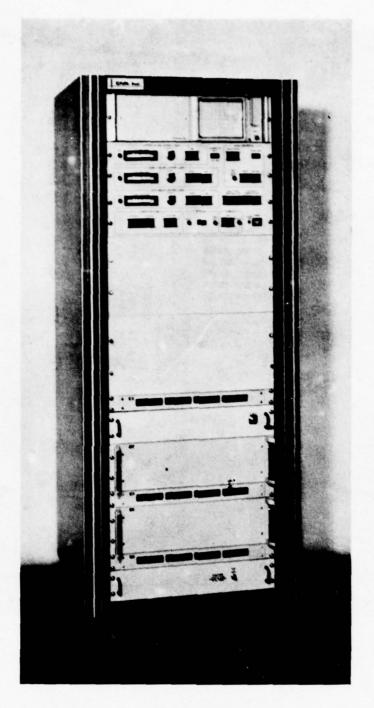


Figure 3 Analyzer

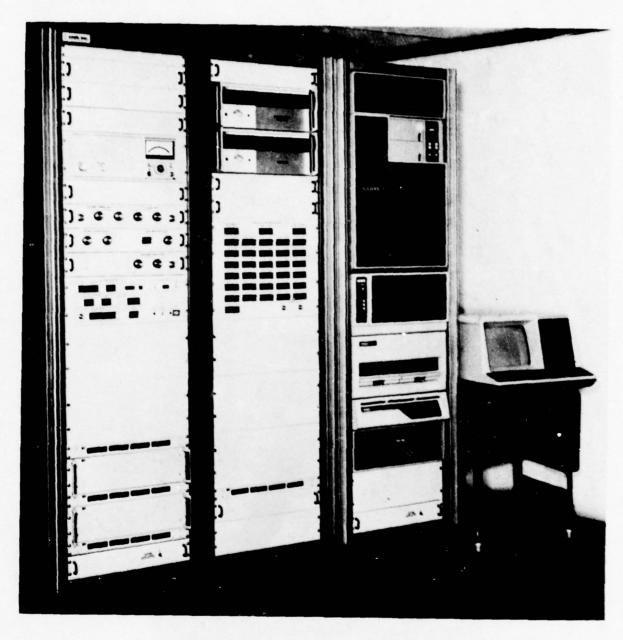


Figure 4 LOS Simulator

TECHNIQUE DE SONDAGE ELECTROMAGNETIQUE PAR ECHANTILLONNAGE SPATIO – FREQUENCIEL DES SIGNAUX DE RECEPTION, APPLICATION A L'ETUDE DES INHOMOGENEITES DU PLASMA IONOSPHERIQUE

ELECTROMAGNETIC SOUNDING TECHNIQUE USING SPATIAL AND SPECTRAL SAMPLING OF THE RECEPTION SIGNALS, APPLICATION TO THE STUDY OF INHOMOGENEITIES IN IONOSPHERIC PLASMA

par

C.Goutelard, J.Caratori et A.Joisel
Laboratoire d'Etude des Transmissions Ionosphériques
Université Paris-Sud
9 avenue de la Division Leclerc
94230 Cachan, France

RESUME

L'étude des propriétés de diffusion du plasma ionosphérique est liée, notamment, aux inhomogénéités de la densité d'électrons libres.

L'étude de ces inhomogénéités peut se faire par différentes méthodes, mais il est toujours nécessaire de disposer de systèmes de mesure très sensibles.

La méthode de sondage par rétrodiffusion est une technique utilisable qui nécessite des installations importantes. Elle peut devenir extrèmement intéressante si on lui adjoint un principe de double échantillonnage temps fréquence portant à la fois sur le signal d'émission et sur le signal de réception.

Un ensemble utilisant ce principe a été réalisé et permet d'effectuer simplement des mesures d'une grande sensibilité et d'une grande précision. Des résolutions fréquentielles pouvant dépasser 0,01 Hz sont couramment atteintes, bien que les points de mesure soient effectués toutes les 0,05 secondes. Les résolutions temporelles ne sont limitées que par des aspects technologiques.

Cette technique est utilisée dans les sondages ionosphériques par rétrodiffusion et permet de mettre en évidence des inhomogénéités de faibles valeurs du plasma ionosphérique ainsi que certaines modifications locales de courte durée telles que les trainées ionisées crées par les météorites.

Cette méthode, utilisable également pour l'étude des milieux diffusants autres que l'ionosphére, présente surtout l'avantage d'assurer une très grande protection vis -à-vis des brouillages. On atteint couramment 70 dB de réjectionet d'offrir des mesures très précises avec des points de mesure fréquents.

SUMMARY

The study of diffusion properties of ionospheric plasma is connected in particular to inhomogéneities of the density of free electrons.

The study of these inhomogeneities may be carried out by different methods, but it is always necessary to use very sensitive measuring systems.

The backscatter sounding method necessitates important installations. This technique may become very interesting if used in conjonction with a time and frequency sampling principe bearing on both the emission and reception signals.

A sounding station, using this principle, has been constructed. Very accurate and precise measurements may be readely obtained. Frequency resolutions better than 0,01 Hz are usualy reached although measurements points are separated by only 0,05 s. Spatial resolutions are only limited by technological aspects.

This technique is used in backscatter ionosphéric soundings and allows low value inhomogeneities in ionospheric plasma to be revealed, as well as certain brief local changes such as ionized meteor trails.

The main advantage of this method, wich may also be used for the study of other diffusing medium than the ionosphere, is to assure great protection against jamming - a 70 dB rejection is commonly obtained - and to permit great precision even for measurements at very short intervals.

1 - INTRODUCTION

Les canaux de transmission à caractéristiques aléatoires non stationnaires sont souvent caractérisés par leur réponse impulsionnelle. Les milieux de transmission sièges de phénomènes de diffusion se classent dans cette catégorie. La caractérisation de ces milieux peut se faire de façon expérimentale par l'émission d'ondes modulées en impulsions et par la réception de ce signal après son transfert à travers le canal. On obtient alors directement la réponse impulsionnelle du milieu mais cette méthode classique impose souvent des puissances d'émission importantes et ne fournit qu'un échantillonnage des variations de la réponse impulsionnelle. D'autres méthodes peuvent être utilisées pour pallier ces inconvénients. Elles se rattachent à des techniques de compression d'impulsion (1) (2) qui permettent de diminuer la puissance, ou à des techniques de codage d'émission continue (3) qui se trouvent limitées par la stationnarité du milieu et demandent des antennes d'émission et de réception découplées.

La méthode proposée dans cet exposé repose sur le principe d'émission d'impulsions longues codées en phase, mais elle est associée à une technique de double échantillonnage qui permet de se libérer de la condition de stationnarité nécessaire dans les autres méthodes.

Cetteméthode a été appliquée dans le cadre du sondage de l'ionosphère et est exposée dans ce sens. Elle est applicable directement à tout autre milieu à caractéristiques aléatoires non stationnaires.

L'étude des inhomogéneités du plasma ionosphérique, présente un grand interêt, non seulement au point de vue géophysique, mais aussi pour les télécommunications.

L'investigation systématique de l'ionosphère s'effectue, encore de nos jours, principalement par l'intermédiaire de stations de sondage terrestres. Le principe utilisé consiste à observer les facteurs affectant une onde de caractéristiques connues, contrôlée par un ensemble d'émetteur récepteur étalonné (ou sondeur). L'ionosphère modifie: l'amplitude, la phase et la polarisation de l'onde de test, mais elle affecte aussi sa trajectoire, donc son temps de propagation et son angle d'arrivée.

Le type de sondeur le plus répandu est le sondeur à impulsions dont on peut distinguer deux classes,

- a Les sondeurs monostatiques ; l'émetteur et le récepteur sont réunis en un même lieu. L'ensemble fonctionne comme un radar dont la cible peut être :
 - l'ionosphère, c'est le cas des sondeurs zénithaux qui sont les plus répandus car les plus simples à mettre en oeuvre
 - le sol, c'est le cas des sondeurs à retrodiffusion.
- b Les sondeurs bistatiques : l'emetteur et le récepteur sont éloignés l'un de l'autre, ce qui nécessite des dispositifs complexes de synchronisation. L'émission peut être:
 - soit impulsionnelle, en utilisant éventuellement la compression d'impulsions (4). Cette technique permet la mesure : des modes de propagation, du temps de propagation, de l'amplitude, de l'angle d'arrivée de la polarisation, du fading et du doppler.
 - soit selon la technique "chirp sounding "(3) qui permet la mesure des mêmes paramètres que précédemment à l'exception de la polarisation du fading et de l'effet doppler. De plus, la dispersivité du milieu introduit des erreurs de mesure systématiques.

Des méthodes existent qui, à partir de sondages à fréquence variable, permettent de remonter au profil d'ionisation moyen de l'ionosphère, ou à l'indice de réfraction; c'est en particulier le cas pour les sondages zénithaux qui, grâce au nombre de stations installées à travers le monde permettent l'élaboration des prévisions à long terme.

L'étude des perturbations ionosphériques peut se faire par ces méthodes de sondage, mais le sondeur par rétrodiffusion est particulièrement bien adapté à ce genre d'études s'il possède une antenne à lobe étroit et orientable (5). On peut alors localiser les phénomènes et en mesurer les dimensions et la vitesse d'évolution.

Cependant, la mise en oeuvre du sondeur à rétrodiffusion à impulsion nécessite des puissances d'émission considérables (supérieures ou égales à 100 kW) compte tenu de l'affaiblissement important subi par l'onde à la rétrodiffusion (de l'ordre de 100 dB) (6), et du rapport signal à bruit nécessaire pour une réception convenable. On peut diminuer la puissance crête d'émission par des techniques de compression d'impulsion (1) ou par l' utilisation de la technique "chirp" qui cependant interdit la mesure de certains paramètres et introduit des erreurs de mesure systématiques.

Il est possible par l'utilisation d'impulsions longues codées de réaliser un système qui associe les qualités des techniques de compression d'impulsions et de chirp sans en avoir les inconvénients. Cette méthode repose sur le choix d'un signal d'émission, ou signal test adapté au canal ionosphérique et sur la possibilité d'un double échantillonnage du signal de réception, dans les domaines temporel et fréquentiel. Son interêt vient du fait que la réponse impulsionnelle est déduite de la mesure directe de la fonction de répartition. En effet, dans les systèmes de mesure directe de la réponse termorelle, la durée de la mesure est limitée par la stationnarité d'ordre 1 du canal alors que re la mesure de la fonction de répartition, cette durée n'est limitée que par la stationnarite d'ordre 2.

2 - CHOIX D'UN SIGNAL DE TEST ADAPTE AU CANAL IONOSPHERIQUE

2. I Caractéristiques du canal ionosphérique

Les caractéristiques radio électriques de l'ionosphère sont liées à son indice de réfraction complexe "n" donné par la formule d'APPLETON et HARTREE (7). L'indice est une fonction du lieu, du temps et de la fréquence que l'on peut noter :

$$n = n (x, y, z, t, f,)$$
 (1)

Comme l'indice dépend aussi d'un double signe, il apparait que le plasma magnétisé qu'est l'ionosphère est à la fois : absorbant, dispersif, biréfringent, hétérogène et non stationnaire. D'autre part, dans la mesure où les puissances mises en jeu, ne dépassent pas une centaine de kilowatts, on peut admettre que le milieu est linéaire. Enfin, compte tenu de la densité d'occupation du spectre HF, le niveau d'interférence est très important et généralement bien supérieur au niveau du bruit atmosphérique ou industriel.

Pour le sondeur qui émet le signal de test x (t) et perçoit le signal reçu y (t) le canal ionosphérique est équivalent à un quadripôle linéaire, dispersif, non stationnaire et trés bruité.

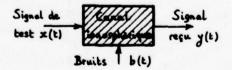


Figure 1

Lorsque x (t) est une impulsion de Dimc, le sondeur mesure la réponse impulsionnelle du canal. L'ionosphère étant non stationnaire, cette réponse dépend non seulement du temps t, mais aussi de l'instant d'émission 6 de x (t) (8), c'est à dire que si :

$$x (t - \theta) = x (t)$$
alors:
$$y (t - \theta) \neq y (t)$$
 (2)

Comme le canal est linéaire, on peut décomposer le signal reçu en un signal utile yu et un signal parasite b, et écrire :

$$y(t, \theta) = yu(t, \theta) + b(t, \theta)$$
 (3)

Il est important de noter que ce signal dépend aussi du matériel utilisé : récepteur, antennes, et que ce qui est effectivement mesuré par le sondeur c'est la réponse impulsionnelle du système "ionosphère-sondeur". Dans la pretique, l'impulsion de Dirac est remplacée par une impulsion HF de fréquence Fe et de carte durée.

Lors de son transit dans l'ionosphère, l'impulsion de test subit à la fois :

- une dispersion spatiale due à l'inhomogéneité et à la dispersivité du milieu
- une dispersion fréquentielle due à sa non stationnarité.

Cet effet dispersif est décrit par la "fonction de répartition" (aussi appelée "fonction de diffusion" ou "scattering") (9): D (fd, \mathcal{T}), qui représente l'amplitude complexe \mathcal{L} de la réponse impulsionnelle en fonction du temps de propagation \mathcal{T} et de la fréquence doppler fd = Fr - Fe, où Fr est la fréquence instantanée du signal reçu (Figure 2).

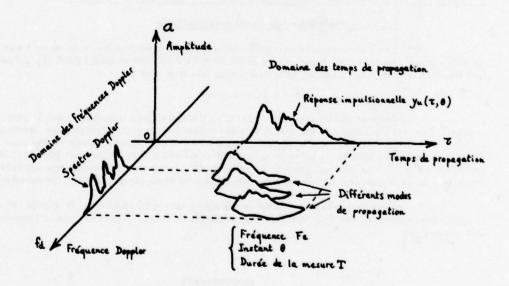


Figure 2

La fonction de répartition caractérise le canal à un instant donné et pour une fréquence donnée. Sa projection sur l'axe des temps donne la réponse impulsionnelle du canal, tandis que sa projection sur l'axe des fréquences donne le spectre doppler de ce signal. Sa mesure est donc bien plus riche en informations que la simple mesure de la réponse impulsionnelle.

2.2 - Mesure des caractéristiques du canal ionosphérique

Les caractéristiques du canal ionosphérique sont entièrement contenues dans la fonction de répartition, c'est donc cette grandeur qu'il faut mesurer. Pour obtenir un point de la fonction de répartition, il est nécessaire de mesurer trois paramètres:

- T temps de propagation
- fd fréquence doppler
- A amplitude (ou energie) de l'échantillon de coordonnées (T, fd)

En pratique, la mesure de ces paramètres est entachée d'incertitude. Nous noterons : $\Delta \tau$, Δ fd et ΔA les résolutions en temps, fréquence et amplitude du système de mesure.

Dans la suite, ces paramètres seront appelés "paramètres "d'analyse", tandis que $\mathcal C$, fd et A seront appelés "paramètres principaux "

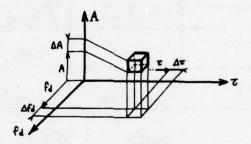


Figure 3

Le canal ionosphérique fixe les limites des paramètres d'analyse qui sont liés au signal de test et détermine ses caractéristiques :

- a une bonne résolution temporelle nécessite l'utilisation de signaux à spectres étendus. La limitation est introduite par la dispersivité du canal ionosphérique qui fixe la bande utilisable à environ 50kHz. Nous avons adopté cette valeur comme une limite qui fixe la résolution temporelle maximale théorique $\Delta T = 20 \mu S$ soit une résolution spatiale égale à 6 km.
- b dans les systèmes classiques, la stationnarité d'ordre l limite la durée de la mesure, donc la résolution fréquentielle. La durée de la mesure est alors, en rétrodiffusion, limitée à l seconde. Au contraire, dans la mesure directe de la fonction de répartition, la durée de la mesure est limitée par la stationnarité d'ordre 2. La durée du signal de test peut, dans ce cas, être portée à plusieurs minutes. La résolution en fréquence maximale peut donc être de l'ordre de quelques millièmes de Hertz.

c - La résolution en amplitude est liée au rapport signal / bruit du signal détecté et à la dynamique propre du récepteur. Le rapport signal / bruit étant une fonction directe de l'énergie émise pour une mesure. La possibilité d'accroître la durée du signal test permet d'atteindre avec de faibles puissances d'émission de trés bons rapports signal/bruit. Dans les applications courantes une dynamique de 40 dB, soit $\frac{\Delta A}{A}$ = 1% est jugée

Il apparait que les paramètres d'analyse, donc la résolution du système, dépendent presque exclusivement des propriétés du canal ionosphérique. Au contraire, la gamme de variation des paramètres principaux ne dépend que du type de sondage envisage. Le tableau ci-dessous indique dans chaque cas la gamme nécessaire:

convenable.

Type de sondage Paramètres Principaux	Zénithal	Bistatique	Rétrodiffusion
Temps de propagation	0 à 10 ms (1500 km)	0 à 20 ms (6000 km)	0 à 100 ms (15000 km)
Fréquence doppler fd	† 99 . Hz	± 99, Hz	± 99. Hz
Amplitude A (ou dynamique)	dyn. 20 dB	dyn. 20à40dB	dyn. min. 40dE

Figure 4

Certaines perturbations passagères, commes les météorites, peuvent provoquer un doppler très important, dont l'observation et la mesure nécessitent une gamme de fréquence d'analyse de plusieurs dizaines de Hertz.

Pour couvrir l'ensemble des cas possibles il faut donc disposer d'un système possédant les caractéristiques suivantes :

- gamme de temps de propagation : 0 à 100 ms, résolution : 20 \square
- gamme de fréquence doppler : 30 à + 30 Hz, résolution qq. 10 Hz
- dynamique AA/A: 40 dB minimum

2,3 Choix du signal de test

Le canal ionosphérique impose pour le signal test un spectre dont l'étendue n'excède pas 50 kHz et une durée comprise entre plusieurs secondes et plusieurs minutes.

Il s'ensuit que la réception d'un tel signal ne peut être effectuée que par un récepteur du type à corrélation, qui élabore la fonction :

$$C_{xy}(\tau, Fdo) = \frac{\Lambda}{\tau} \int_{0}^{\tau} x(t-\tau_{0}, Fdo) \cdot y(t) \cdot dt$$
 (4)

où

- fde représente la translation dans le domaine fréquentiel du signal de référence

To représente la translation temporelle du signal de référence

- T représente la durée du signal de test

Le signal reçu est défini à partir de la fonction de répartition par la relation :

X (f) est la transformée de Fourier du signal de test x (t), et et l'expression (4) peut se mettre sous la forme :

avec

$$C_{xy_i}(\varepsilon_o, f_{do}) = \frac{1}{T} \int_0^T x(t-\varepsilon_o, f_{do}). y_i(t, \varepsilon, f_d). dt$$

En remplaçant dans cette expression yi (t, \$\mathcal{t}\$, fd) par sa valeur et en inversant les ordres d' intégration, il vient finalement :

$$C_{xy_{i}}(r_{o},fd_{o}) = \frac{D(r,fd)}{T} \int_{-\infty}^{+\infty} X(f). X^{*}(f+F).e^{-2\pi j(f+F)\theta} e^{2\pi jFr} df$$

La fonction Cxy (To, fdo)vaut alors

$$C_{xy}(\tau_0, fd_0) = \frac{1}{T} \int_{fd} \int_{\tau} D(\tau, fd) \cdot B(\tau, fd) \cdot d\tau \cdot dfd$$

où

$$B(\tau, f_d) = e^{2\pi i f \tau} \int_{-\infty}^{+\infty} \chi(f) \cdot \chi^*(f+F) \cdot e^{-2\pi i f(f+F)\theta} df$$

Cette fonction qui ne dépend que du signal peut se mettre sous la forme : $B(\tau, f_d) = A(\theta + \tau_0, F + f_{d_0}). e^{2\pi i f_0}$ où

 $A(\theta,F) = \int_{-\infty}^{+\infty} \times (t) \hat{x}(t-\theta,F) dt = \int_{-\infty}^{+\infty} X(f) X^*(f-F) e^{2\pi i (f-F)\theta} df$

est appelée fonction d'ambiguité du signal.

La mesure de l'échantillonnée de D (fd, %) pourrait se faire avec un signal dont la fonction d'ambiguité serait Ao (0, F) telle que :

$$A_{\circ}(\theta,F) = \delta(\theta).\delta(F)$$

Il n'est possible, en fait, que de trouver des signaux dont la fonction d'ambiguité s'approche de cette loi.

On dit que pour ces signaux, la fonction d'ambiguité est du type à'pointe unique " (10)

La valeur d'un échantillon de la fonction de répartition mesurée est alors obtenue par l'intégrale du produit de la fonction de répartition théorique par la fonction d'ambiguité décalée de To, fdo (Fig. 5)

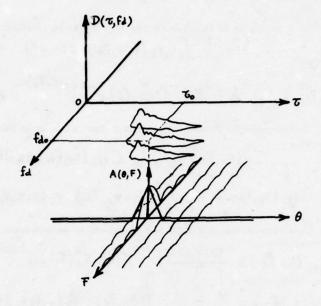


Figure 5

Deux types de signaux caractéristiques possédant cette propriété peuvent être utilisés pour moduler l'onde émise :

- un signal aléatoire constitué par un bruit blanc
- un signal binaire pseudo-aléatoire dont la forme de la fonction d'ambiguité est donnée figure 6.

Pour des raisons pratiques, nous avons choisi le deuxième type de signal dont la production et le traitement sont plus simples. Il est alors défini par :

- la durée d'un élément du code Ta : elle est choisie en fonction de la résolution temporelle souhaitée, donc Ta min = 20 \(\mu \)s.
- le nombre d'éléments du code N: il est choisi en fonction de la résolution fréquentielle désirée, donc (NT ϱ) max = 2/fd min ce qui conduit en général à des valeurs de N très élevées.

Outre les avantages déjà cités, l'utilisation d'un signal de test codé par un code pseudo aléatoire confère au système une trés bonne protection vis à vis des brouilleurs cohérents; qui sont plus gênants que le bruit atmosphérique dans la gamme des ondes courtes. Le même procédé qui, à la réception, permet de reconstituer un signal cohérent à partir du signal utile, transforme le brouilleur cohérent en signal pseudo aléatoire. Par suite de l'intégration, le signal

parasite est fortement atténué, alors que le signal utile est amplifié. Le rapport signal à bruit est augmenté dans le rapport de N. Ainsi pour N = 10000 (valeur courante, on va jusqu'à 10⁶), le gain est d'environ 40 dB par rapport au système à impulsion classique.

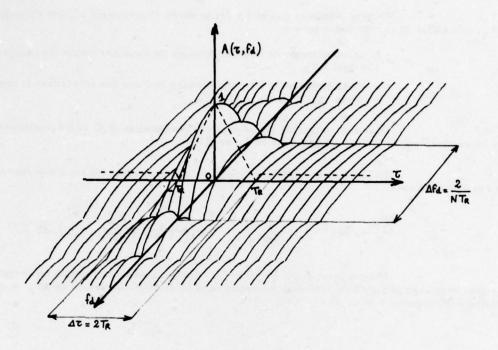


Figure 6

De plus, l'émission pouvant être continue, ou quasi continue, la puissance crête peut être notablement réduite pour une puissance moyenne donnée, ce qui permet de faire fonctionner l'émetteur dans des conditions optimales. La réduction de puissance, par rapport aux systèmes impulsionnels classiques, peut atteindre plusieurs centaines

3 - SYSTEME D'ANALYSE SPATIO-FREQUENTIELLE

3.1 - Contraintes générales

La réalisation du système de mesure directe de la fonction de répartition décrite dans cet exposé a été faite en vue de son utilisation dans un sondeur ionosphérique par rétrodifission.

La mesure de $D(\mathcal{T}, fd)$ ne peut être envisagée sans réaliser au moins un échantillonnage de l'un ou l'autre des axes temps-fréquence. En réalité, la complexité du signal impose un double échantillonnage de la fonction de répartition, car la réception ne peut se faire

par l'utilisation de filtres adaptés mais par l'utilisation de corrélateurs qui ne peuvent fournir qu'un point de D (, fd).

Le choix des pas d'échantillonnage doit se faire de façon optimale, de sorte que l'échantillonnée calculée D (v. fd) de D (v. fd) permette la restitution exacte de la fonction de répartition.

On peut montrer, que si T_R est la durée d'un élément binaire du code de durée N. T_R , aux effets du second ordre près :

- le choix optimum de l'échantillonnage de l'axe des temps correspond à un pas égal à T_R
- le choix optimum de l'échantillonnage de l'axe des fréquences correspond à un pas égal à Δ F_R = 1/N, T_R

Dans ces conditions les résolutions temporelles Δ ∇ et fréquentielles Δ fd, sont respectivement de l'ordre de grandeur de T_R et ΔF_R

La fonction de répartition mesurée par la relation (4) est alors représentée par son échantillonnée.

$$\widetilde{D}(t_0, \tau_0, f_{do}) = \frac{1}{T} \int_{t_0}^{t_0+T} x(t-pT_R, q\Delta F_R).y(t).dt$$

Chaque point de l'échantillonnée apparait comme la fonction de corrélation du signal reçu avec le signal de référence translaté dans le domaine des temps de pT_R et dans le domaine des fréquences de q. Δ F_R (Fig. 7)

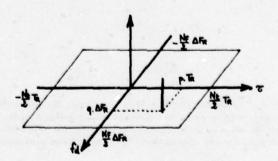


Figure 7

Pour l'exploration d'une sone définie par une longueur temporelle Nt T_R et par une largeur fréquentielle Nf, Δ F_R le nombre de corrélateurs nécessaire est égal λ Nc = Nt. Nf.

Dans cette configuration le temps de calcul de la fonction de répartition est égal à N. T_R . Dans une version simple qui consisterait à calculer de façon sequentielle cette fonction, on aboutirait à un échantillonnage temporel de la fonction de répartition au pas de N. T_R . Chaque point de l'échantillonnée D (τ , fd) calculé par la relation 5 se trouve donc, en se limitant un lobe principal du filtre équivalant) à l'opération d'intégration, filtré avec une bande passante égale à

1/N, T_R (figure 6). La restitution exacte de la fonction de répartition peut donc se faire si l'échantillonnage respecte le théorème de SHANNON, c'est à dire si le calcul de la fonction de répartition se fait avec une cadence inférieure à N. T_R /2. C'est la raison qui nous a conduit à élaborer un système effectuant un échantillonnage au pas de N. T_R /8 par le processus suivant :

si on pose:
$$p = x(t-pT_R, q. \Delta F_R). y(t)$$

la relation 5 peut se mettre sous la forme

$$\widetilde{D}(t_0, \tau_0, f_{do}) = \frac{1}{T} \left\{ \int_{t_0}^{t_0 + \frac{T}{8}} p \, dt + \int_{t_0 + \frac{T}{8}}^{t_0 + \frac{2T}{8}} p \, dt + \dots + \int_{t_0 + \frac{T}{8}}^{t_0 + T} p \, dt \right\}$$

qui fait apparaître les intégrations partielles.

$$P(t_1) = \int_{t_0}^{t_0 + \frac{T}{8}} p. dt$$

Si on range les intégrations partielles successives dans des mémoires, que nous appellerons "memoires partielles" dans la suite de cet exposé, l'échantillonnée D (to, To, fdo) s'exprime par

$$\widetilde{D}(t_0, \tau_0, f_{d_0}) = \sum_{n=0}^{n+7} P(t_0 + n \frac{T}{8})$$

De même on obtient: $\widetilde{D}(t_0+n_g^T, t_0, f_{00}) = \sum_{n=0}^{n=7} P(t_0+\frac{T}{8}+n_g^T)$

Dans ce dernier cas l'intégration partielle P (to) a été remplacée par P (to + T/8). Il est donc possible avec un ensemble de 8 mémoires partielles de réaliser un échantillonnage temporel de la fonction de répartition avec un pas de quantification égal à T/8.

Si l'ensemble des contraintes qui ont été examinées sont respectées, nous verrons qu'il est alors possible de reconstituer intégralement la fonction de répartition et, par conséquent, les grandeurs qui s'en déduisent.

3,2 - Elaboration d'un système (12)

La réalisation d'un système permettant la mesure directe de D (T, fd) peut se faire par l'utilisation d'un corrélateur parallèle ou d'un correlateur à structure mixte.

L'utilisation d'un corrélateur série étant à exclure, compte tenu de sa lenteur, deux systèmes ont été étudiés.

- le premier, à structure mixte est composé de 100 corrélateurs montés en parallèle et permettant de réaliser des explorations de la fonction de répartition par des coupes successives à fd constant (ou à C constant) selon un mode série.
- le second, à structure parallèle, est constitué de 4096 corrélateurs permettant une exploration instantanée de la fonction de répartition.

Ces réalisations ont été faites en technique numérique avec des technologies TTL et MOS. Elles différent uniquement par le système d'élaboration de la fonction de répartition qui a été appelé unité de traitement et sont connectables l'une et l'autre à un même sondeur.

3, 2, 1 - Schéma général du sondeur

Le schéma général du sondeur utilisé par le LETTI est représenté sur la

figure 8.

Il est constitué par une partie analogique comprenant une antenne à lobe orientable A, un commutateur d'antenne TR, un émetteur large bande 1-30 MHz fournissant une puissance maximale crête de 2kW et une puissance moyenne maximale de 1 kW, un récepteur

.../...

aménage R, et un pilote à quartz fournissant les différentes fréquences utiles.

Une partie numérique réalise le traitement du signal. Elle comprend, outre l'unité de traitement BC citée précedemment. :

- un générateur de signaux de référence REF chargé d'élaborer le signal test x (t) et les signaux de référence des Nt Nf voies d'analyse qui s'en déduisent par les translations suivant les axes ct et fd.
- une mémoire de lecture L, interface de sortie, autorisant l'accés séquentiel aux résultats acquis en fin de cycle par l'unité de traitement.
- des convertisseurs numérique-analogique N/A et analogique/numérique A/N
 permettant au système d'échanger les informations x(t) et y(t) avec l'
 émetteur et le récepteur.
- un ensemble d'horloges H fixant le rythme d'exécution de l'ensemble des opérations.

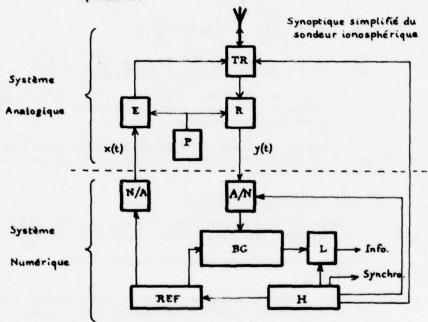


Figure 8

3, 2, 2. Unité de traitement à structure série parallèle 100 points

L'unité de traitement 100 points a été réalisée avec les caractéristiques

suivantes

- calcul d'un point de la fonction de répartition sur 24 bits longueur des codes pseudo aléatoires utilisés : de N = 2^5 1 à 2 15 1
- résolution spatiale maximale : 7,5 km
- résolution fréquentielle maximale : 0,01 Hz

L'exploration de la fonction de répartition peut se faire par des coupes à fd constante, ou à 6 constant, et des translations temporelles ou fréquentielles du signal de réception permettent de réaliser des explorations multiples de la fonction de répartition. Ces deux types d'exploration sont équivalents.

3.2.3. - Unité de traitement parallèle 4096 points

L'unité de traitement 4096 points a été réalisée avec les caractéristiques

suivantes :

- calcul d'un point de la fonction de répartition sur 24 bits longueur des codes pseudo aléatoires utilisés : de N = 2^8 1 à 2^{20} 1
- résolution spatiale max = 30 km
- résolution fréquentielle maximale 0,001 Hz

L'exploration de la fonction de répartition se fait en choisissant N, = 2ⁿet Nf = 2^m tel que m + n = 12, n et m pouvant varier de 0 à 12. Cette possibilité offre une grande souplesse d'exploration de la fonction de répartition. Comme dans le cas de l'unité de traitement 100 points, des translations d'ensemble de la zone d'exploration peuvent être effectuées dans le domaine des fréquences fel et des temps 7 l permettant de la centrer au gré de l'utilisateur. Le système a été réalisé en technologie TTL et MOS selon le schéma bloc de la figure 10.

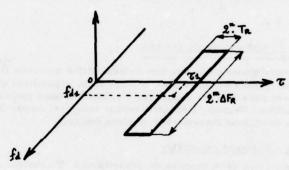


Fig. 9

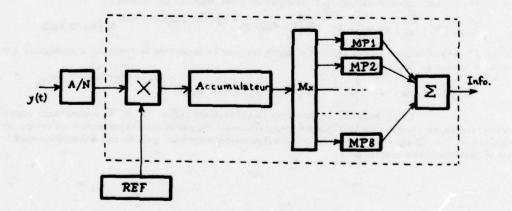


Figure 10

3. 2. 4. - Exemple de calcul des paramètres dans le cas d'un sondage par rétrodiffusion

Pour un sondage par rétrodiffusion il est usuel d'utiliser les paramètres d'

analyse suivants :

- résolution spatiale 60 km

Fr = 0,02 Hz - résolution fréquentielle :

L'étendue spectrale de la fonction de répartition étant limitée à 1Hz, on en déduit les paramètres suivants :

- Valeur de Nt > 100. On est donc conduit à choisir Nt = 2 7 = 128 soit

- Valeur de T_R : 0,4 ms pour conserver la résolution de 60 km

- Long ueur du code : imposée par TR et la résolution fréquentielle:

$$N = \frac{1}{F_R} T_R = 125000.$$

On est donc conduit à choisir un code de longueur N = 2 17 - 1 qui assure une protection de 51 dB vis-à-vis des brouilleurs cohérents et des echos parasites.

- La zone explorée est alors fixée par m = 5 et n = 7 ce qui assureNt . TR =

51,2 8.

3.3 - Performances du système

L'échantillonnée de la fonction de répartition mesurée D (7, fd) permet de retrouver toutes les informations contenues dans la fonction de répartition qui peut être reconstituée - aux effets du second ordre près - si les conditions d'échantillonnage spatio-fréquentiel citées au paragraphe 31 sont respectées. De plus, l'échantillonnage temporel au pas T/8 des résultats permet de reconstituer toutes les évolutions instantanées de cette fonction.

3.3.1 - Analyses spectrales

L'exploration de la fonction de répartition à T constant donne les spectres de la réponse impulsionnelle. En effet, d'après la relation (4), si on note :

$$x(t) = A(t).e^{2\pi i f_0 t}$$

où A (t) représente la modulation de l'onde par le code utilisé, on obtient :
$$C_{xy}(\tau_0, f_{do}) = \frac{1}{T} \int_0^T A(t - \tau_0) e^{2\pi i j(f_0 - f_{do})(t - \tau_0)} y(t, \tau) dt$$

où y (t, T) représente le signal reçu et compte tenu de la forme de la fonction d'ambiguité aux

ont petits du ler ordre près:
$$C_{xy}(\tau_0, f_{do}) = \frac{1}{T} \int_0^T A(t-\tau_0).y(t,\tau_0).e^{-2\pi j(f_{do}-f_0)(t-\tau_0)}.dt$$

Cette relation montre que l'exploration selon T = To = constante représente la transformée de Fourier de la réponse impulsionnelle du canal correspondant à un temps de propagation To. Il est donc possible de déterminer notamment, grâce aux échantillonnages utilisés, les spectres instantanés.

3.3.2 - Restitution de la réponse impulsionnelle

La restitution de la réponse impulsionnelle peut être faite très simplement puisque l'exploration de D (τ , fd) à τ = pT_R, représente l'échantillonnée de la réponse impulsionnelle du canal. Pour chaque valeur de pT_R, la réponse impulsionnelle s'en déduit donc par le simple calcul de la transformée de Fourier discrète inverse. On obtient alors la réponse impulsionnelle du signal pour toute valeur du temps de propagation τ , grâce à l'échantillonnage spatial T_R adopté et pour toute valeur du temps grâce à l'échantillonnage temporel T/8 adopté. Les interpolations peuvent être faites par un procédé numérique ou analogique.

3.3.3 - Détection optimale

Les signaux recueillis dans les sondages ionosphériques sont affectés d'un effet de fading souvent important dû aux interférences entre les signaux reçus par les trajectoires multiples causées par les inhomogeneités et l'anisotropie de l'ionosphére. L'amplitude est maximale lorsque les signaux sont en phase, minimale lorsqu'ils sont en opposition de phase.

La séparation de ces différents signaux est naturellement obtenue dans le système d'analyse proposé. On a vu comment, par la prise en compte de leurs amplitudes complexes, il était possible de déterminer la réponse impulsionnelle du canal et d'en faire son analyse spectrale.

La détection peut être considérée comme optimale dans le cas où l'amplitude du signal détecté peut être rendue maximale sans augmentation du bruit. Cette opération peut être faite par la sommation pour chaque valeur de τ = p. τ des modules des amplitudes complexes du signal détecté. Cette opération est faite simplement par une technique numérique.

4 - RESULTATS EXPERIMENTAUX OBTENUS

Les résultats présentés dans ce paragraphe ont été obtenus avec l'unité de traitement série parallèle 100 points.

4.I. - Spectres des signaux de rétrodiffusion dans le cas d'une ionosphère calme

Le système expérimental utilisé pour effectuer les sondages est équipé d'une antenne orientable à périodicité logarithmique opérant dans la bande 6, 4 - 30 MHz et dont le lobe principal ne présente pas une directivité importante en élévation tandis que son ouverture azimutale est de l'ordre de 35°.

On peut montrer (6) que, les mouvements de l'ionosphère introduisent un effet doppler caractérisé par un spectre constitué de 3 triplets principaux. Ces triplets sont la conséquence de l'effet de diffusion du sol, de l'anisotropie de l'ionosphère crée par le champ magnétique terrestre et de l'existence des rayons haut et bas. Selon qu'à l'aller ou au retour la trajectoire utilise le rayon haut ou bas, on distingue trois modes : haut si le rayon haut est emprunté à l'aller et au retour, bas s'il s'agit du rayon bas et mixte dans le cas où le trajet emprunté à l'aller n'est pas le même qu'au retour. Les amplitudes de ces différentes raies spectrales sont représentées sur la figure l1 dans le cas d'un modèle d'ionosphère parabolique. On constate qu'au voisinage de la focalisation les trois modes ont des amplitudes comparables mais qu'au delà le mode bas a une amplitude prédominante et que le mode haut s'atténue le plus vite. Les fréquences doppler qui affectent chaque raie peuvent être calculées à partir de ce modèle (11) et la vérification expérimentale qui a été faite consolide les résultats théoriques.

Les résultats représentés sur la figure 12 montrent un échantillonnage des mesures réalisées à partir de la station de sondage du LETTI installée à BRUZ aux environs de RENNES (FRANCE). L'enregistrement a été le 06/07/77 à 8h36 T.U. au moment où l'ionisation des couches ionosphèriques augmente et où la hauteur du maximum d'ionisation diminue.

La direction du lobe d'émission est située dans le SUD et la fréquence d' d'émission est Fe = 20 MHz. Dans ces conditions (fig. 13) la rétrodiffusion se produit sur le désert du Sahara et l'effet doppler ne peut donc être attribué qu'à l'ionosphère.

Les paramètres d'analyse sont :

- Longueur du code N = 32767

- Résolution temporelle : T_R = 1ms - Résolution fréquentielle : F_R = 0,03 Hz

La puissance d'émission est de 600 W,

On constate la présence des trois raies spectrales au voisinage de la zone de focalisation et la disparition progressive des modes haut et mixte.

La cohérence des spectres observés en fonction du temps montre une évolution régulière de l'ionosphère et une absence de perturbation.

4.2 - Influence des inhomogeneités sur les spectres

La figure 14 représente une série de mesures effectuées le 8.7.1977 entre 10H20 et 13h10 T. U dans le cap 200° avec une puissance d'émission de 800 W.

Les paramètres d'analyse choisi sont :

- Longueur du code 32767

- Résolution temporelle : $T_R = 1 \text{ ms}$ - Résolution fréquentielle : $F_R = 0,06 \text{ Hz}$

La série de clichés montre l'évolution de la fonction de répartition du signal en fonction de l'heure de la journée. Sur le premier cliché - 10h20 TU - on observe la présence des trois modes au voisinage de la zone de focalisation et l'existence du seul mode bas loin de la zone.

Le cliché 2 - 10h5O TU - montre l'évolution normale du diagramme de diffusion en fonction du temps : l'augmentation de l'ionisation crée une diminution de la distance de bond, mais les trois modes sont toujours apparents. Le cliché 3 - 1h30 - montre l' apparition d'un spectre sur les premières voies d'analyse et son déplacement vers les prises éloignées sur le cliché 4 - 12h10 - où on constate un élargissement important de ce spectre qui traduit la présence d'une diffusion importante.

Le cliché 5 fait apparaitre un spectre doppler dont la valeur importante a fait que l'opérateur a interrompu l'analyse pour changer la résolution fréquentielle. Sur les clichés suivants, on peut voir l'évolution de ce spectre qui traduit le déplacement d'une perturbation vers le sud puisque ce spectre détecté sur la prise 2 apparait successivement sur les prises 3 puis 4, en même temps que la fréquence doppler prend les valeurs successives -3Hz, -4Hz, - 6Hz qui peuvent s'interpréter par le fait que la vitesse radiale tend par valeur inférieure vers la vitesse réelle à cause de la géométrie des rayons.

Le cliché 8 montre le retour vers une ionosphère normale.

5 - CONCLUSION

La méthode d'analyse par échantillonnage spatio-fréquentiel qui a été étudiée offre des avantages que l'on peut résumer en la comparant à deux méthodes existantes. Par rapport à la méthode impulsionnelle elle présente le premier avantage de réduire la puissance crête d'émission dans un rapport de plusieurs centaines. De plus, elle offre une importante protection contre les brouilleurs et fournit directement la fonction de répartition.

Par rapport à la technique "chirp sounding "elle présente les mêmes avantages de réduction de puissance et de protection contre les brouilleurs, mais par contre elle permet d'effectuer des mesures à fréquence d'émission constante, caractéristique importante dans un milieu dispersif. L'inconvénient majeur de la technique chirp vient cependant de son impossibilité de reconstitution de la fonction de répartition.

Présentée dans le cadre des sondages ionosphèriques, cette méthode est cependant applicable à tout milieu caractérisable par sa fonction de répartition (ou de diffusion) notamment à tous les canaux à caractéristiques aléatoires stationnaires ou non stationnaires.

BIBLIOGRAPHIE

- (1) R.H. BARKER Group synchronizing of binary digital systems in communication theory -London Butterworth -p. 273-287
- (2) M. J. E. GOLAY Complementary series -IRE Trans. on Inf. The. Vol. IT -7- p. 82,87.
- (3) G. BARRY, R.B. FENWICK Extra terrestrial and ionospheric sounding with synthesized frequency sweeps - H ewlett -Packard Journal - Vol. 16 (11), p. 8 -12
- (4) D. C. COLL, J. R. STOREY Ionospheric sounding using coded pulse signals Radio Science J. on Reasearch - Vol. 68 D (10) -p. 1155 - 1159
- (4bis) D.C. COLL, J.R. STOREY A note on the application of pulse compression techniques to ionospheric sounding - Radio Science Journal of Research NBS - Vol. 69 D - n°8 August 1965 - p. 119I -1193
- (5) J. C. BLAIR, R. D. HUNSUCKER, L. H. TVETEN Ionospheric mapping by backscatter AGARD Conference Proceedings n° 49 - 1969
- (6) C. GOUTELARD Analyse de la structure fine des échos de sol obtenus par rétrodiffusion des ondes décamètriques. Application à l'étude des perturbations ionosphèriques - Thèse d'Etat - 1968
- (7) K. DAVIES Ionospheric Radio Propagation US Départment of Commerce NBS Monograph 80 -1965 -
- (8) AL. SPATARU Théorie de la transmission de l'information Masson et Cie -1970 -
- (9). DARNELL Channel estimation techniques for HF communications -AGARD Conference Proceedings n° 173 -Radio systems and the ionosphere Athènes - Mai 1975
- (10) M. CARPENTIER Radar concepts nouveaux Dunod 1966 -
- (11) C. GOUTELARD, J. L. COATANHAY Conséquences de la diffusion et de la dépolarisation des ondes électromagnétiques par le sol dans les problèmes de rétrodiffusion - AGARD Symposium on E. M. propagation characteristics of surface materials and interface aspects - Istambul - October 1976 -
- (12) Brevet d'invention n° 7325351

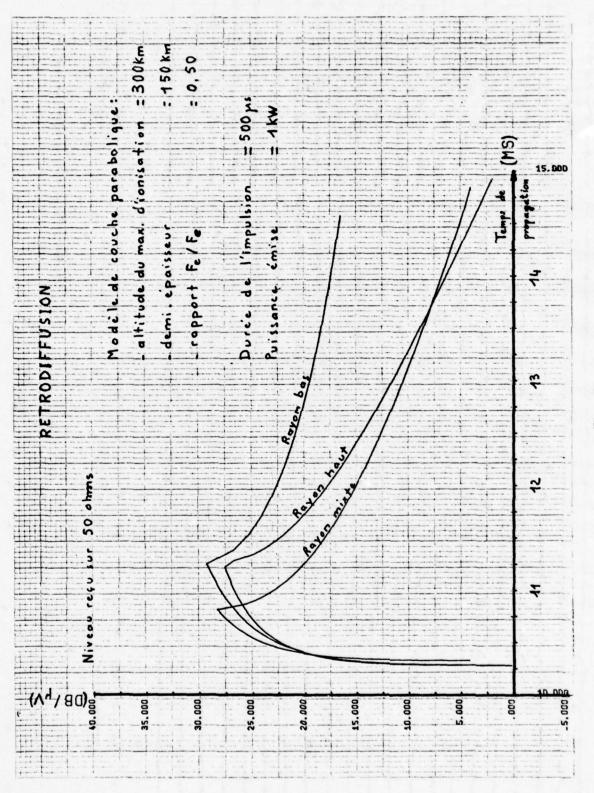
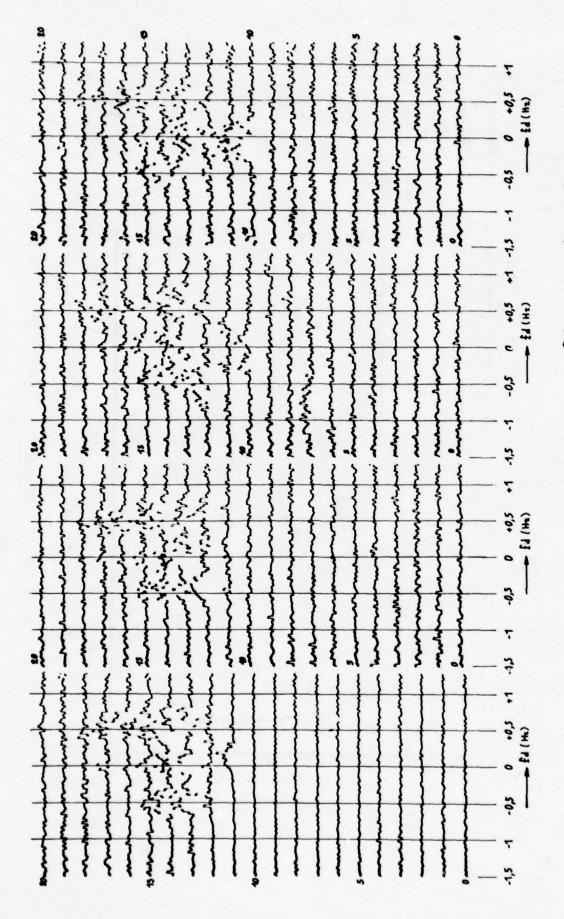
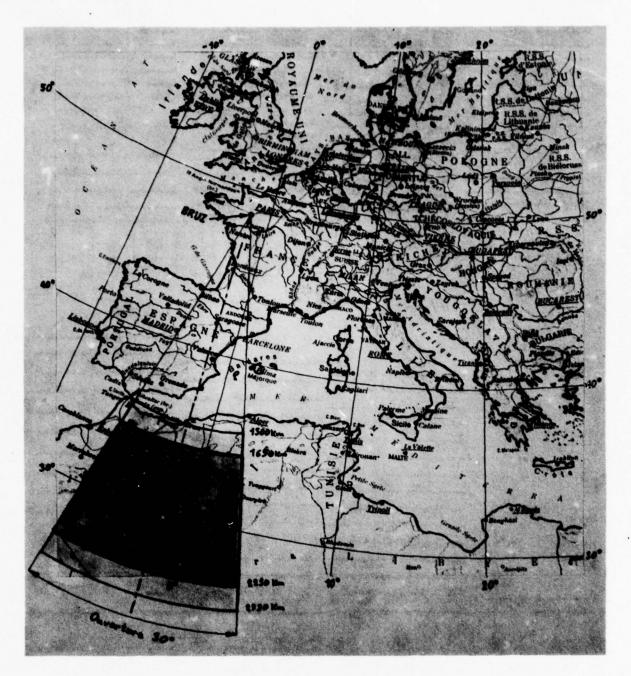


Figure 11



Ordonnée : tempe de propugation en ms

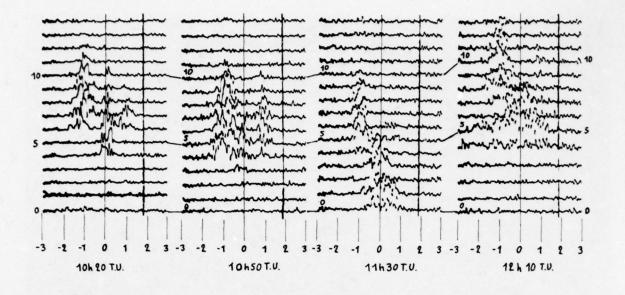
Figure 12

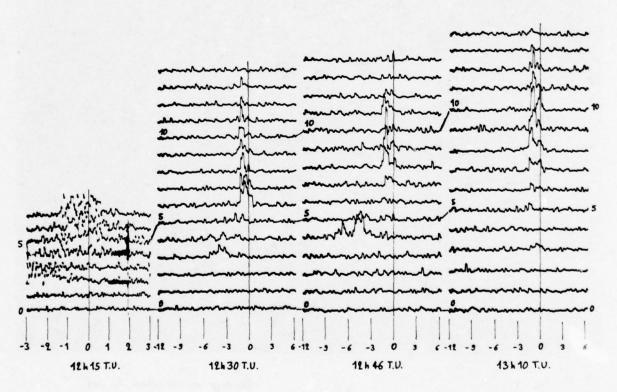


Sondage en direction du sud

frontières du domaine illumine'
limites extrêmes du domaine illumine'

Figure 13





Abscisse : frequence doppler en Hz Ordonne'e : temps de propagation en ms

Figure 14

APPLICATION DE LA TECHNIQUE BACKSCATTER AUX PREVISIONS DE TRANSMISSION IONOSPHERIQUES A TRES COURT TERME

APPLICATION OF BACKSCATTER TECHNIQUE TO IONOSPHERIC SHORT TERM PREDICTIONS

par

C.Goutelard, J.Caratori, J.L.Coatanhay et R.Rolland Laboratoire d'Etudes des Transmissions Ionosphériques Université de Paris Sud 9 avenue de la Division Leclerc 94230 Cachan, France

SUMMARY

Short term and long term predictions are based upon well experimented technique. Very short term forecasts for transmissions can be made from oblique sounder networks and by the use of the backscatter technique.

This paper describes a forecasting method based upon the use of the spectrals analysis of backscatter echoes and on the "inversion" of backscatter ionograms.

The inversion program, which makes use of regression curves can easily be processed using a small computer.

The exploitation of the spectrals analysis of backscatter echoes allows instantaneous measurement of dynamic parameters of the ionized Layers and brings about a considerable increase in the probabity of a link being well established.

Experimental results carried out on real cases show the validity of the method

An operational station can be planned needing only a minimum of equipments.

The backscatter ionograms can be sampled and reduced to a very small number of points. The real time spectral analysis of echoes can be achieved in a simple manner and with an accuracy of about 0,05 Hz, which is sufficient for thier practical use. The bulk and the duration of computations are then considerably reduced.

RESUME

Les prévisions de transmissions ionosphèriques à long et court terme reposent sur des techniques très éprouvées. Les prévisions de transmission à très court terme peuvent être effectuées à partir des réseaux de sondeurs obliques et par la technique de sondage backscatter.

Le présent article expose une méthode de prévisions basée sur l'utilisation des analyses spectrales des échos de rétrodiffusion et sur l'inversion des ionogrammes de rétrodiffusion.

Le programme d'inversion, basé sur l'utilisation de courbes de regréssion peut être traité sans difficultés par un petit calculateur. L'exploitation des analyses spectrales des échos de rétrodiffusion permet la mesure instantanée des paramètres dynamiques des couches ionosphèriques et apporte une importante amélioration de la probabilitée bon établissement d'une liaison.

Les résultats expérimentaux obtenus dans des cas réels montrent la validité de la méthode.

Une station opérationnelle peut être envisagée avec un minimum de matériel installé. Les ionogrammes de rétrodiffusion peuvent être échantillonnés et réduits à un nombre très limité de points. Les analyses spectrales des échos peuvent être effectués de façon simple en temps réel avec des résolutions de l'ordre de 0,05 Hz suffisantes pour leur exploitation.

Un exemple de réalisation est proposé.

An exemple of such a plan is provided.

1 - INTRODUCTION

L'ionosphère et le sol jouent le rôle de réflecteurs pour les ondes décamétriques et permettent l'établissement des liaisons à très grande distance avec de faibles puissances. Comme le bruit atmosphérique et l'absorption dans la basse ionosphère (couche D) décroissent lorsque la fréquence augmente, il est intéressant de travailler avec des fréquences aussi élevées que possible. Cependant, pour une liaison donnée, il existe une limite supérieure aux fréquences susceptibles d'être réfractées par l'ionosphère. Cette limite, appelée MUF (Maximum Usuable Frequency), est contrôlée directement par l'ionisation des couches supérieures (principalement F2) et, comme elle, dépend d'un grand nombre de paramètres (1) (2) (3), dont il est actuellement impossible de rendre compte par une expression analytique, on a alors recours à des procédés statistiques.

Grâce aux observations régulières effectuées dans le monde entier, un certain nombre d'organismes spécialisés peuvent fournir aux utilisateurs des prévisions de la MUF avec des préavis variables de six mois (prévisions à long terme) à une semaine (prévisions à court terme) Or, les prévisions à court terme qui sont un ajustement des prévisions à long terme, ne permettent de prévoir que la valeur médiane de la MUF. L'utilisateur emploie couramment une fréquence inférieure, la FOT, Fréquence Optimale de trafic, égale à 0,85. MUF, assurant une probabilité de liaison de 90%. Cette pratique est restrictive pour deux raisons.

- la MUF réelle est souvent très supérieure à la MUF médiane et l'emploi de la FOT ne permet pas d'utiliser au mieux le réflecteur ionosphèrique

- une probabilité de liaison de 90% est insuffisante pour certains types de communications et l'utilisation de la FOT s'avère alors hasardeuse.

La probabilité de liaison peut être considérablement accrue, notamment au niveau de l'exploitation des réseaux fixes. Dans ce cas, la méthode employée consiste à effectuer périodiquement des sondages obliques entre les différents points du réseau à l'aide de sondeurs automatiques. L'information issue des récepteurs est traitée par un ordinateur qui contient les programmes des prévisions, basés sur l'étude de l'autocorrélation des paramètres de chaque liaison (4) (5) et qui fournit les fréquences à utiliser avec une probabilité de 99%.

Cependant, on peut reprocher à un tel dispositif, en plus de son coût élevé et de la difficulté de synchroniser des stations éloignées, le fait qu'il ne puisse s'adapter rapidement à une nouvelle liaison. En effet, compte tenu de la variabilité des conditions de propagation, dés que l'angle des trajectoires dépasse 5 à 10°, il nécessite l'installation d'un nouveau sondeur et la mise au point d'un nouveau programme de prévisions. (5)

L'utilisation d'une station de sondage par rétrodiffusion, équipée d'une antenne rotative résoud théoriquement l'ensemble de ces problèmes. Cependant, une difficulté apparait, liée à la méthode de sondage elle même. En effet, l'ionogramme de rétrodiffusion ne donne pas la distance de bond, contrairement à l'ionogramme oblique ce qui permettrait de lire directement la MUF, mais le temps de propagation, qui n'est pas relié de façon simple à la distance atteinte (6).

En adoptant pour base de départ l'ionogramme de rétrodiffusion, nous nous sommes proposés de rechercher une méthode simple et rapide de détermination du profil moyen de l'ionosphère, car il est facile de calculer la MUF à partir de ce dernier. L'opération qui consiste à remonter de l'ionogramme au profil d'ionisation a été baptisée "inversion de l'ionogramme"

L'étude du cas général est très complexe car il n'existe pas de relation analytique entre le profil vertical des couches et l'ionogramme de rétrodiffusion, ce qui nous a conduit à procéder par simulation.

Le modèle utilisé pour cette étude est un modèle simple - modèle parabolique - qui offre une précision suffisante pour l'établissement de prévisions de transmission.

Les prévisions à très court terme sont établies de l'observation périodique d'ionogrammes. Une meilleure prévision doit pouvoir être obtenue si on est en état de pouvoir mesurer la vitesse de variation des paramètres du modèle. Une approche de ce problème a été faite par l'utilisation des spectres doppler des échos obtenus en rétrodiffusion.

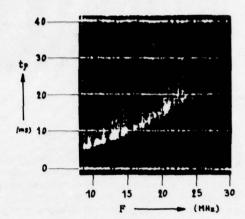
.../...

Les paramètress servant à définir le profil d'ionisation ont été appelés paramètres principaux et ceux utilisés pour définir leurs variations ont été appelés paramètres dynamiques.

2 - EXPLOITATION DES IONOGRAMMES DE RETRODIFFUSION DETERMINATION DES PARAMETRES PRINCIPAUX

2. I - Modélisation de l'ionosphère

Rappelons qu'on appelle ionogramme l'enregistrement du temps de propagation de groupe de l'écho rétrodiffusé en fonction de la fréquence d'émission. La figure l'montre que la structure de l'ionogramme est très complexe et que si l'on ne veut pas compliquer exagérément l'étude il est nécessaire de dégager une grandeur caractéristique contenant l'essentiel de l'information présente dans l'enregistrement. Nous avons retenu la trace frontale de l'ionogramme qui est assez bien définie et représente le temps minimal de propagation, ou temps de focalisation, en fonction de la fréquence.



BRUZ le 19/09/1975

à 15h55mn

Azimut 180°

Figure 1

Pour simuler cette trace frontale, nous nous sommes placés dans l'hypothèse terre sphérique - ionosphère concentrique, et nous avons assimilé l'ionosphère à une couche unique à profil vertical parabolique. Le profil (fig. 2) est donc caractérisé par trois paramètres

- Fc : fréquence critique de la couche
- Hm altitude du maximum d'ionisation
- Ym: demi épaisseur de la couche

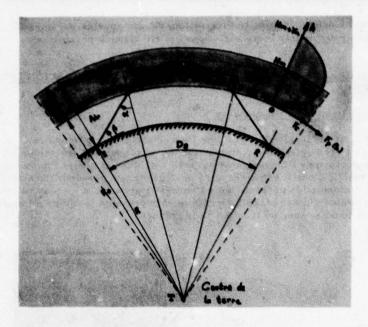


Figure 2

Compte tenu des fréquences d'émissionven rétrodiffusion, l'influence des collisions est négligeable dans la détermination des rayons et, celle du champ magnétique faible et susceptible d'être prise en compte d'une manière simple (6). Le calcul du rayon peut alors s'effectuer à l'aide des lois de l'optique géométrique. La figure 2 rappelle les notations employées. Le temps de propagation est donné par la formule classique (7).

Tp est minimum pour un angle β Foc tel que $\frac{dTp}{d\beta} = 0$. Cette équation étant transcendante, ni β Foc ni $T_F = Tp$ (β Foc), qui représente l'ionogramme simulé, ne possèdent d'expressions analytiques.

La figure 3 représente la simulation de la trace frontale d'un ionogramme Elle est à rapprocher de l'enregistrement réel de la figure 1 et permet de constater que l' allure générale est la même dans les deux cas.

Une étude qualitative de l'influence des paramètres du profil sur la forme de l'ionogramme simulé, montre que Fc et Hm ont un effet important tandis que Ym a toujours une influence mineure (8). D'autre part, la formule 1 montre que Tp, donc T_F ne dépend pas directement de F ou de Fc mais de leur rapport. Cette remarque permet de simplifier l'étude de l'ionogramme en ramenant de 3 à 2 le nombre de paramètres dont il dépend.

.../...

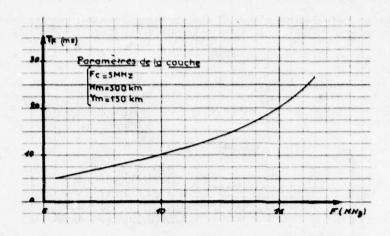


Figure 3

2, 2 - Recherche d'un modèle simple pour l'ionogramme simulé

Plusieurs solutions ont été envisagées pour inverser l'ionogramme. Elles ont été abandonnées, soit pour leur complexité, soit parcequ'elles conduisaient à des temps d'inversion excessifs. L'idée que nous avons retenue consiste à rechercher un modèle analytique de l'ionogramme suffisamment simple, même au prix de quelques concessions, sous réserve que ces dernières n'introduisent pas d'erreurs supérieures à celles dûes aux erreurs de mesure.

Différents modèles ont été essayés : polynôme, fonction puissance, fonction exponentielle. C'est ce dernier modèle que nous avons retenu. En effet, si on trace l'ionogramme dans un plan aux échelles semi-logarithmiques, la courbe obtenue présente un point d'inflexion (voir figure 4) donc une partie quasi-rectiligne.

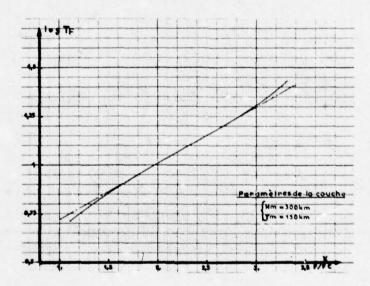


Figure 4

Au niveau de l'exploitation, cette rectitude apparait clairement et donne une mesure simple. L'ajustement de l'ionogramme modifié par la méthode des moindres carrés conduit à la relation:

$$\log T_F = Ao, x + Bo = A, F + Bo$$
 (2)

Dans cette formule. Ao et Bo ne dépendent que de Hm et Ym, tandis que A = Ao/Fc dépend des 3 paramètres. La généralité de ce modèle a été vérifiée en traçant les ionogrammes modifiés correspondant à 44 couples (Hm, Ym) (figure5) couvrant tous les cas usuellement rencontrés (8);

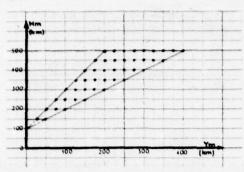


Figure 5

La figure 6 montre clairement la vadilité du modèle exponentiel.

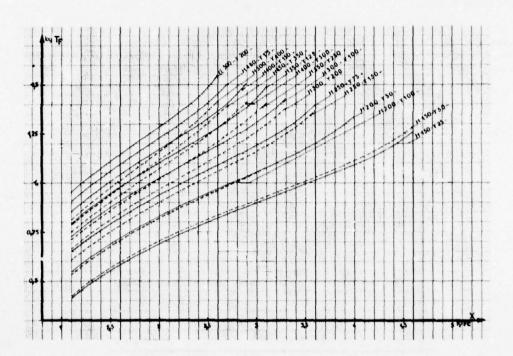


Figure 6

Cependant, il convient de remarquer dès à présent que, puisque le profil comporte 3 paramètres, le modèle d'ionogramme devrait aussi en comporter 3 pour permettre l'inversion, alors qu'il n'en comporte que 2. Compte tenu de la précision d'obtention des ionogrammes expérimentaux, il s'avère que le choix d'un modèle plus complexe conduit à une incertitude importante sur la détermination des valeurs des paramètres du modèle. C'est pourquoi nous avons conservé le modèle exponentiel, en sachant bien qu'il serait nécessaire de trouver une relation supplèmentaire entre Fc, Hm et Ym indépendante de l'ionogramme.

L'ionogramme modifié peut donc être caractérisé par deux paramètres Ao et Bo fonctions de Hm et Ym uniquement. Afin de découvrir les relations qui existent entre ces 4 grandeurs, nous avons procédé à une étude graphique et numérique (consistant en une succession d'ajustements par la méthode des moindres carrés), en prenant comme base les 44 couples (Ao, Bo) déduits par ajustements des ionogrammes modifiés. Nous avons abouti aux équations suivantes :

A o = 1, 1.
$$10^{-4}$$
 Ym + 1, 892, 10^{-2} Hm^{0, 46} = A, Fc

Bo = 0, 519. \log_{10} Hm - 0, 6223 ($\frac{\text{Ym}}{\text{Hm}}$) + O, 3558 ($\frac{\text{Ym}}{\text{Hm}}$) - 0, 8544

(4)

(Hm et Ym en Km)

Pour contrôler la validité de ces relations, nous avons regroupé dans le tableau l: les 44 couples (Hm, Ym), les couples (Ao, Bo) obtenus par ajustement des ionogrammes modifiés, les couples (Ao, Bo) calculés à l'aide des formules 3 et 4, ainsi que les écarts relatifs exprimés en pourcentage. Nous voyons que l'erreur commise en utilisant les expressions analytiques est en moyenne de 0,68% pour Ao avec un maximum de 1,76%, tandis que pour Bo elle est en moyenne de 1,2% avec un maximum de 3,2%. Il apparait d'autre part, que les écarts les plus importants sont observés pour les valeurs extrêmes de Hm et Ym, donc dans des cas peu fréquemment rencontrés en pratique. Ces remarques jointes au fait que les précisions d'obtention des relevés expérimentaux sont de l'ordre de 2 à 3% nous amènent à penser que les erreurs commises en utilisant les formules (3) et (4) sont tout à fait acceptables.

2.3. - Inversion de l'ionogramme de retrodiffusion

Comme nous l'avons remarqué précédemment, il est nécessaire d'introduire une relation indépendante de l'ionogramme qui, jointe aux équations 3 et 4 formera un système complet permettant l'inversion. Nous avons adopté la formule de Schimazaki (9):

Hm F2 =
$$\frac{1490}{M(3000) F2}$$
 - 176 où M(3000)F2 = $\frac{MUF(3000)F2}{FoF2}$ (5)

Cette relation est toujours en très bon accord avec les observations lorsque l'ionosphère peut être assimilée à une couche unique (ionosphère nocturne). De jour, la présence de la couche E entraine une diminution de M (3000)F2 qui se traduit par un accroissement apparent de HmF2. Il est alors préférable d'utiliser une formule corrigée, telle la formule de BRADLEY-DUDENEY (10):

Hm F2 =
$$\frac{1490}{M(3000)F2 + \Delta M}$$
 - 176 où $\Delta M = \frac{0.18}{\frac{\text{FoF2}}{\text{FoF}} - 1.4}$ (6)

Néanmoins l'utilisation de cette relation introduirait la variable supplèmentaire FoE, ce qui compliquerait encore le problème. C'est la raison pour laquelle nous avons conservé dans un premier temps, la formule SC HIMAZAKI, tout en sachant bien que les résultats que nous en déduisons ne sont rigoureusement valables que pour l'ionosphère nocturne et, dans une certaine mesure, pour l'ionosphère d'hiver (FoF 2 >> FoE).

La possibilité de tenir compte de la couche E demeure cependant totale si on remarque qu'elle est d'une part connue avec une grande précision et mesurable directement par un sondage en rétrodiffusion.

L'équation 5 n'est pas directement utilisable sous la forme indiquée, car M (3000) ne peut être déduit de l'ionogramme de rétrodiffusion. Cependant, si on porte sur un même graphique les valeurs de 1/M(3000) déduites des ionogrammes simulés et la droite d'équation :

$$\frac{Hm + 176}{1490} = \frac{1}{M(3000)} \tag{7}$$

qui représente la relation de SCHIMAZAKI, il apparait que le rapport YM/HM n'est pas constant,

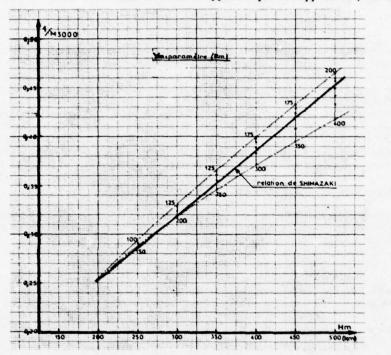


Figure 7

mais varie légèrement le long de cette droite. (fig. 7)

L'ajustement de la fonction Ym/Hm par la méthode des moindres carrés nous a conduit à l'expression suivante : $\underline{Ym} = -1,709.10^{-6} \text{ Hm}^2 + 1,227.10^{-3} \text{ Hm} + 0,4351$

$$\frac{\text{Ym}}{\text{Hm}} = -1,709.10^{-6} \text{ Hm}^2 + 1,227.10^{-3} \text{ Hm} + 0,4351$$
 (8)

Les équations 3,4 et 8 forment un système de 3 équations à 3inconnues qu'il est possible de résoudre numériquement, ou bien encore graphiquement à l'aide d'abaques(8). Cependant, le rapprochement des équations 4 et 8 montre que Hm et Ym ne dépendent que de

Bo, d'où il résulte d'aprés 3 que Ao ne dépend lui aussi que de Bo. Cette remarque permet d'envisager une forme analytique simple pour les solutions; nous avons opté pour un ajustement par des polynômes des moindres carrés. La nécessité de conserver une précision relative supérieure à 1% nous a imposé des polynômes du neuvième degré;

Hm =
$$2.7089 + 6.6953.10^2$$
 Bo - $1.0688.10^3$ Bo² - $1.1995.10^3$ Bo³ + $5.2813.10^3$ Bo⁴ + $5.6189.10^4$ Bo⁵ - $9.3653.10^4$ Bo⁶ - $1.3303.10^5$ Bo⁷ + $3.0769.10^5$ Bo⁸ - $1.2668.10^5$ Bo⁹ (9)

$$Ym = -43,627 + 9,4968.10^{2}Bo - 3,0246.10^{3}Bo^{2} + 1,0769.10^{3}Bo^{3} + 1,0431.10^{4}Bo^{4} + 3,8805.10^{4}Bo^{5} - 9,0788.10^{4}Bo^{6} - 9,6061.10^{4}Bo^{7} + 2,5072.10^{5}Bo^{8} - 9,8179.10^{4}Bo^{9}$$
(10)

Ao =
$$0.084326 + 0.51416 \text{ Bo} - 0.76094 \text{ Bo}^2 + 0.33042 \text{ Bo}^3 - 1.5479 \text{ Bo}^4 + 50.280 \text{ Bo}^5 - 105.43 \text{ Bo}^6 - 50.319 \text{ Bo}^7 + 268.82 \text{ Bo}^8 - 167.44 \text{ Bo}^9$$
 (11)

En pratique, la connaissance de Bo permet de calculer Hm, Ym, puis Ao qui associé à A donne Fc = Ao/A. L'erreur commise en utilisant les formules 9 à 11 est en moyenne de 1% quand Hm et Ym vérifient la relation de Schimazaki. Dans le cas contraire, la précision reste bonne comme va le montrer un exemple numérique. A partir du triplet Fc = 5 MHz, Hm = 500 km, Ym = 325 km, nous avons simulé l'ionogramme, puis, par ajustement, déterminé les paramètres A et Bo que nous avons introduits dans les formules d'inversion. Le nouveau triplet obtenu : Fc = 5,052 MHz, Hm = 500,95 km, Ym = 311 km, montre que l'écart le plus important est enregistré sur Ym. Ce paramètre ayant une influence mineure dans les prévisions de transmission, l'erreur qui en résulte est négligeable ainsi que le prouvent les ionogrammes simulés dans les deux cas et représentés à la figure 8

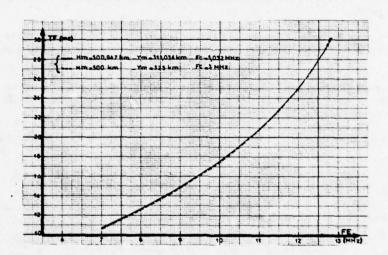


Figure 8

Afin de procéder à une vérification expérimentale, nous avons comparé les paramètres ionosphèriques déduits d'ionogrammes de rétrodiffusion par la méthode proposée à ceux mesurés en sondage zénithal dans la zone où les rayons émis de BRUZ (01° 44' 10" W, 47°59'36"N) atteignent leur apogée. La station choisie, TORTOSA en Espagne (00°35'E, 40° 56'N), distante de 806 km de BRUZ se situe à la limite inférieure de la zone de réflexion. Les résultats sont regroupés dans le tableau II, qui comporte en outre les valeurs des paramètres mesurés en sondage zénithal à LANNION (03°27'W, 48°45'N), celà afin de permettre l'évaluation des gradients horizontaux et la localisation approximative de la zone de réflexion.

Malgré le petit nombre d'ionogrammes traités (dû à la difficulté d'obtenir les mesures des stations de sondage zénithal), il apparait que les paramètres déduits par inversion sont en bon accord avec les résultats déduits des mesures de Lannion et Tortosa, bien que les conditions d'expérience ne soient pas optimales. En effet, tous nos ionogrammes ont été relevés de jour en présence de la couche E et de gradients horizontaux.

Cette première étude est actuellement complétée par extension de la méthode à une ionosphère à 2 ou 3 couches avec gradients horizontaux, et par une vérification expérimentale sur un grand nombre de données.

3 - UTILISATION DE LA FONCTION DE REPARTITION - PARAMETRES DYNAMIQUES-

Les spectres des signaux reçus dans les sondages par rétrodiffusion traduisent les mouvements de l'ionosphère et, dans certains cas, ceux de la surface de diffusion, notamment de la mer (11)(12).

Dans le cas où le modèle ionosphèrique est celui décrit au paragraphe 21, il est possible de calculer les fréquences doppler qui affectent les trois raies principales du spectre. L'existence de ces raies a été expliquée (13), et les fréquences doppler qui les caractérisent ont été calculées. En résumé:

- pour le mode bas caractérisé par le fait que la trajectoire utilise le rayon bas à l'aller comme au retour, les variations de la fréquence critique des couches ont une influence assez faible.

- pour le mode haut caractérisé par le fait que la trajectoire utilise le rayon haut à l'aller comme au retour, les variations de la fréquence critique de couche ont un rôle important.

- pour le mode mixte caractérisé par le fait que la trajectoire utilise le rayon bas (haut) à l'aller et le rayon haut (bas) au retour, la fréquence doppler dont il est affecté est égale à la moyenne arithmétique des deux précédents.

La fréquence doppler Fd de chacun des modes peut être exprimée par la relation :

$$\mathrm{Fd} = -\mathrm{F}\left[\frac{3\cancel{p}}{3\mathrm{Hm}}\left(Y_{m,x}\right)\frac{3\mathrm{Hm}}{3\mathrm{t}} + \frac{3\cancel{p}}{3Y_{m}}\left(\mathrm{Hm},x\right)\frac{3Y_{m}}{3\mathrm{t}} + \frac{3\cancel{p}}{3x^{1}}\left(\mathrm{Hm},Y_{m}\right)\frac{3x^{1}}{3\mathrm{t}}\right]$$

où Ø est le chemin de phase de l'onde, et où les coefficients :

$$\frac{\partial h}{\partial h}(Y_m,x)$$
, $\frac{\partial \phi}{\partial Y_m}(H_m,x)$, $\frac{\partial \phi}{\partial x^{-1}}(H_m,Y_m)$

ont été calculés pour les couples (Hm, Ym) cités au paragraphe 2 et pour différentes valeurs deFc. Ils varient entre les valeurs extrêmes données sur le tableau suivant :

Mode	Bas	Mixte	Haut	Unité	
34m	3,4/6,8	4,2/9,1	5/9.4	(MHz, Km) ⁻¹	
3¢ -3/-6		-3/-5,3	-3/-6	(MHz, km)	
34	-0,1/-0,5	-0,9/-4,2	-2,5/-7,5	MHz-1	

Tableau III

Le rayon mixte n'apporte en fait aucune information mais peut servir à vérifier la position des raies dans la mesure de la fonction de répartition (14) représentant l'amplitude complexe $\mathcal Q$ du signal reçu en fonction de la fréquence doppler Fd et du temps de propagation $\mathcal T$, et dont un exemple d'enregistrement est donné figure 9.

La mesure des fréquences doppler fournit donc deux équations qui associées à la relation de Schimazaki - ou de Bradley -Dudeney - utilisée précédemment permettent de déduire les valeurs des paramètres dynamiques.

Les mouvements du sol peuvent modifier le spectre dans le cas notamment de la diffusion sur la mer. Dans ce cas, le spectre des échos de rétrodiffusion peut présenter des dédoublements des raies dus aux effets du premier ordre de la diffraction de Bragg par la houle. Ces dédoublements, de l'ordre de quelques dixièmes de Hertz apparaissent lorsque la longueur d'onde de l'onde émise est voisine de deux fois la longueur d'onde de la houle.

L'effet doppler introduit par la mer est en général faible devant celui dû à l'ionosphère et s'il se produit, il peut être détecté par l'analyse de la fonction de répartition, qui fait apparaître ces dédoublements.

Une vérification expérimentale statistique de ces résultats théoriques a été faite (13) et a montré leur bonne concordance sur une période d'enregistrement de 1 mois.

La figure 10 montre la confrontation entre une série de mesures effectuées le 18 septembre 1975 à partir de la station de sondage de BRUZ et les résultats théoriques déduits des mesures du sondage zénithal de LANNION. On peut noter la bonne concordance de ces résultats bien que la station de LANNION soit située à environ 800 km au nord du point de réflexion des ondes dans l'ionosphère.

4 - ELABORATION D'UN SYSTEME DE PREVISION A TRES COURT TERME

A partir d'une station de sondage ionosphèrique par rétrodiffusion il apparait possible de déduire dans la cas d'un modèle parabolique :

- les valeurs des paramètres principaux Fc, Hm, Ym à partir du relevé de l'ionogramme de rétrodiffusion. La variation monotone de la trace frontale en fonction de la fréquence d'émission permet de réaliser un échantillonnage de l'ionogramme avec un maximum d'une dizaine de points de mesure, rendant ainsi le relévé extrèmement rapide.

- les valeurs des paramètres $\frac{\partial F_c}{\partial t}$, $\frac{\partial H_m}{\partial t}$, $\frac{\partial Y_m}{\partial t}$, à partir du relevé

d'une fonction de répartition (14). Un seul relevé suffit pour la mesure des paramètres dynamiques.

La durée de ces mesures demeure de l'ordre de l minute avec l'utilisation d'un système d'analyse spatio-fréquentiel (14). Leur traitement peut se faire à l'aide d'un petit calculateur grâce aux formes analytiques des relations permettant de calculer les paramètres ionosphèriques.

L'association d'une antenne orientable permet de dresser une cartographie de l'ionosphère autour de la station pour la prévision des liaisons situées dans une zone de 6000 km de diamètre centrée sur la station.

La précision des prévisions peut être accrue en adjoignant un sondeur zénithal à la station et en tenant compte dans le programme d'exploitation de paramètres connus comme les paramètres de la couche E, la corrélation des variations géographiques du paramètre Fc......

5 - CONCLUSION

Le problème des prévisions ionosphèriques à très court terme a été abordé sous différents aspects.

L'utilisation d'une station de sondage par rétrodiffusion pose le problème général de l'inversion de l'ionogramme.

La solution proposée ici consiste, à partir d'un modèle de couche simple, mais suffisant pour l'établissement de paramètres de transmission, à utiliser des relations analytiques qui permettent un calcul rapide des paramètres du profil.

La centralisation du système de sondage permet une mesure économique des spectres des échos de rétrodiffusion. Leur exploitation conduit à la connaissance instantanée des vitesses de variation des paramètres du profil, qui sont des éléments importants dans le calcul prévisionnel à très court terme.

En vue d'une application, deux points doivent cependant être developpés.

Tout d'abord, le modèle de l'ionosphère doit être affiné pour tenir compte des gradients d'ionisation horizontaux et de la présence de plusieurs couches.

Ensuite, il y a lieu de procéder à l'exploitation des spectres des échos en vue de la détermination de l'effet doppler et du fading dans les transmissions point à point. En effet, la détermination de ces effets se déduit théoriquement du spectre des échos mais une vérification expérimentale statistique demeure à faire.

Ces deux points sont actuellement en cours d'étude.

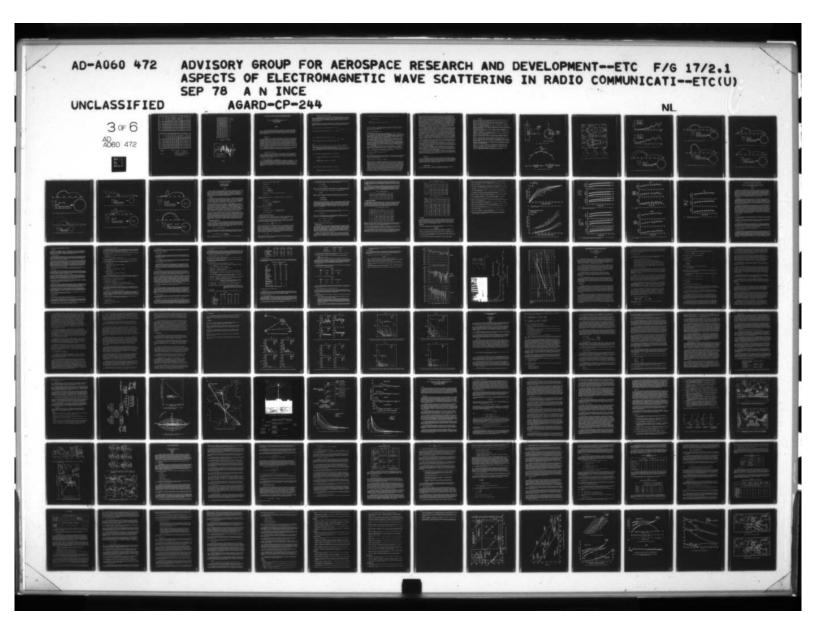
BIBLIOGRAPHIE

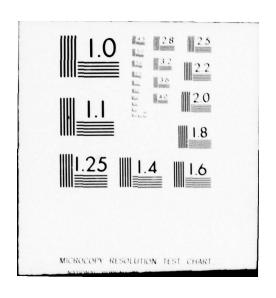
- (1) K. DAVIES Ionospheric Radio Propagation United States Department of commerce NBS Monograph 80 -1965
- (2) AGARD Lecture series XXIX Radio Wave Propagation -July 1968
- (3) CNET DPI Propagation des ondes radio électriques dans l'environnement terrestre 2 tomes 1970
- (4) J. W. AMES, R. D. EGAN Digital recording and short-term prediction of oblique ionospheric propagation -IEEE Antennas and propagation - Vol AP 15 - n°3-May 1967
- (5) The use of ionosphere sounders to improve h-f communications Granger associates technical bulletin n°3 March 1966
- (6) C. GOUTELARD Analyse de la structure fine des échos de sol obtenus par rétrodiffusion des ondes décamètriques. Application à l'étude des perturbations ionosphériques - Thèse d'état - 1968 -
- (7) E. V. APPLETON and J. W BEYNON The application of ionospheric data to radio communications problems -Part I - Proceedings Phys. Soc. London -1940- Vol. 52 n°202 - p. 518 -533
- (8) R. ROLLAND Contribution à l'étude des prévisions ionosphériques à très court terme.

 Transformation rapide: Ionogramme de rétrodiffusion Profils verticaux d'ionisation Mémoire CNAM -1975 -
- (9) T. SCHIMAZAKI World Wide daily variations in the height of the maximum electron density in the ionospheric F2 layer - J. Radio Research Laboratories (Japan), 2 (1), 85 - 97 (1955)
- (10) P.A. BRADLEY and J.R. DUDENEY A simple model of the vertical distribution of electron concentration in the ionosphere -Journal of Atmospheric and Terrestrial Physics -1973 -Vol. 35 -p. 2131 à 2146.
- (11) D. E. BARRICK, J. M. HEADRICK, R. W. BOGLE, D. D. CROMBIE Sea backscatter at HF: interpretation and utilization of the écho - Proceedings of IEEE -Vol. 62 nº 6 - June 1974 -
- (12) J. L. AHEARN, S.R. CURLEY, J. M. HEADRICK, D. B. TRIZNA Tests of remote skywave measurement of ocean surface conditions - Proceedings of IEEE Vol. 62 - n°6 - june 1974
- (13) C. GOUTELARD, J. L. COATANHAY Conséquences de la diffusion et de la dépolarisation des ondes electromagnétiques par le sol dans les problèmes de rétrodiffusion AGARD Symposium on E. M. propagation characteristics of surface materials and interface aspects. -Istambul - October 1976 -
- (14) C. GOUTELARD, J. CARATORI, A. JOISEL Technique de sondage electromagnétique par échantillonnage spatio-fréquentiel des signaux de réception. Application à l'étude des inhomogenéités du plasma ionosphérique -23ème Symposium AGARD - Boston - October 1977 -

PARAMETRES DES COUCHES		PAR	AMETRE AC		PARAMETRE BO			
ни	YM	AO DON.	AO CAL.	ER REL	BO DON.	BO CAL.	ER REL	
150.	25.	.193	.193	217				
150.	50.	.197	.195	851	.319	.313	-1.763	
200.	50.	.223	.222	364	.323	.324	191	
200.	15.	.227	.225	911	.389	.388		
200.	100.	.231	.228	-1.443			.835	
250.	15.	.250	.248	656	.361	.360	171	
250.	100.	.253	.251	748	.429		.432	
250.	125.	.255	.254	446	.415	.432	.750	
250.	150.	.260	.257	-1.311		.411	-1.058	
300.	100.	.272	.212	.044	.480	.480	-1.821	
300.	125.	.275	.275	047	.471	.471	012	
300.	150.	.279	.278	495			074	
300.	175.	.282	.280	579	.455	.452	731	
300.	200.	.284	.283	310	.397	.385	-1.629	
350.	125.	.294	.294	.020			-3.136	
350.	150.	.296	.297	.273	.513	.513	003	
350.	175.	.249	.300	.187	.504	.503	150	
350.	200.	.303	.302		.490	.486	738	
350.	225.	.305	.305	228	.469	.462	-1.407	
				.019	.442	.431	-2.430	
350.	250.	.307	.308	.263	.406	. 393	-3.198	
400.	150.	.313	.315	.499	.541	.541	.053	
400.	175.	.316	.317	.416	.532	.532	076	
400.	200.	.319	.320	.334	,519	.516	489	
400.	225.	.321	.353	.564	.503	.496	-1.422	
400.	250.	.325	.326	.174	.479	.470	-1.921	
400.	275.	.327	.358	.402	.451	.438	-2.825	
400.	300.	.331	.331	.020	.409	.402	-1.840	
450.	175.	.332	.334	.574	.565	.566	.199	
450.	200.	.334	.337	.794	.557	.557	052	
450.	225.	.337	.339	.713	.545	.543	369	
450.	250.	.340	.342	.634	.530	.525	953	
450.	275.	.341	.345	1.141	.514	.503	-5.531	
450.	300.	.343	.348	1.350	.490	.476	-2.889	
450.	325.	.347	.350	.978	.457	.445	-2.631	
450.	350.	.350	.353	.899	.416	.410	-1.472	
500.	200.	.350	.352	.651	.584	.588	.736	
500.	225.	.352	.355	.859	.577	.579	.390	
500.	250.	.355	.358	.782	.567	.567	050	
500.	275.	.355	.361	1.548	.558	.551	-1.318	
500.	300.	.357	.363	1.746	.543	.531	-2.198	
500.	325.	.361	.366	1.386	.520	.508	-2.294	
500.	350.	.363	.369	1.582	.496	.482	-2.917	
500.	375.	.367	.372	1.229	.460	.452	-1.801	
500.	400.	.369	.374	1.423	.420	.418	391	

Tableau I





Date	Heure T.U.	Mesures							Estimations		
		Rétrodiffusion BRUZ			Zénithal LANNION		Zénithal TORTOSA		Dr	Fc(MHz)	
		Fc	Hm	Ym	Fc	Hm	Fc	Hm	(km)	L/T	PAL
05/09/74	15h20	6, 73	270	170	6,0	237	6,3	305	1520	6,53	6,68
	16h00	7,26	267	170	6,0	241	6,7	290	1130	6,95	6,57
06/09/74	16h00	6,46	230	145	5,6	262	6,4	269	650	6,16	5,35
	18h00	6, 62	250	160	6,2	302	6, 35	305	1750	6,50	7,41
31/10/74	10h20	9,15	290	187	/	/	9,4	238	760	/	/
	13h00	7,05	250	157	/	/	7,3	256	650	/	/

Date	Heure	Prévisions à long terme					Gradients				
		Nord à 1000 km		Sud à 1000 km		Sud à 2000 km		LANNION TORTOSA		Normaux Prévisions	
		Fc	Hm	Fc	Hm	Fc	Hm	ar/ad	9H-/9D	2 Fz/20	2H-/2D
05/09/74	15h20	4,89	279	5, 72	278	7,21	269	0,480	108,8	0,830	-1
	16h00	4,88	277	5,79	274	7,28	264	1,120	78,4	0,910	1-
06/09/74	16h00	4,88	277	5, 79	274	7,28	264	2,240	11,2	0,910	-3
	18h00	4,99	247	6,29	216	7,35	194	0,240	4,8	1,30	-31
31/10/74	10h20	5,90	246	6,95	231	7,51	228	/	/	1,050	-15
	13h00	6,10	247	6,81	251	7,99	250	/	/	0,710	+4

TABLEAU II

Légende :

Fc en MHz

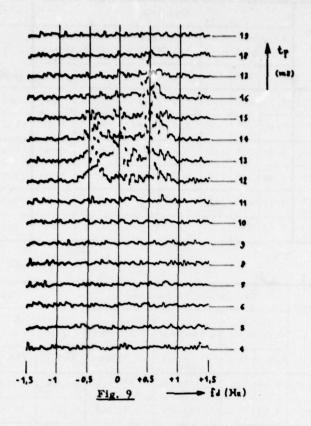
Hm, Ym en km

ər en MHz/ Mm

2Hm en km/Mm

Azimut 180°

Dr distance du point de réflexion estimé L/T Lannion-Tortosa PAL prévisions à long terme



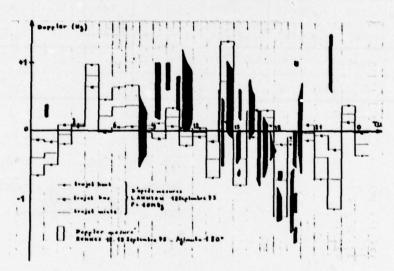


Fig. 10

CALCULATION OF THE SCATTERING CROSS-SECTION OF PERFECTLY CONDUCTING OR DIELECTRIC BODIES BY NUMERICAL OR PERTURBATIONAL METHODS

K.-D. Becker
Fachbereich 12.2 der Universität des Saarlandes
Fachrichtung Elektrotechnik
D-6600 Saarbrücken
Fed. Rep. Germany

SUMMARY

For the calculation of the scattering cross-section of perfectly conducting or dielectric cylinders of rough surfaces two methods are used: A numerical method, based on integral equation formalism, and a perturbational method. The validity of the results based on these methods is examined in their dependence on selected characteristic parameters. Also, the influence of these characteristic parameters on the far-field cross-section is studied.

1. INTRODUCTION

The properties of a scattered electromagnetic field depend on the geometry of the scattering object. In cases, where the shape of the scatterer is not a simple geometry for example propagation over irregular terrain (Beckmann, P. and Spizzichino, A.,1963) or scattering by rain (Morrison, J.A. and Cross, M.-J.,1974), hail (Bringi, V.N. and Seliga, T.A.,1977), trees or buildings (Giloi, H.-G.,1974) - no analytical solutions can be found and approximate analytical or numerical methods are the only alternative. Concerning approximate analytical methods, a perturbational approach has been suggested and applied to perfectly conducting or dielectric cylindrical or spherical scatterers (Clemmow, P.C. and Weston, V.H.,1961; Yeh, C.,1964; Erma, V.A.,1968a, 1968b, 1969; Becker, K.-D.,1968) as well as to plane structures (Becker, K.-D., Dobmann, G. and Langenberg, K.J.,1975). On the other hand, a number of numerical means have been developed (Mittra, R.,1973) and serve as a tool to treat scattering by "perturbed" scatterers, the most famous beeing the method of moments (Harrington, R.F.,1968).

a tool to treat scattering by "perturbed" scatterers, the most famous beeing the method of moments (Harrington, R.F., 1968).

The purpose of the present contribution is two-fold; how does a perturbed scattering surface affect the far-field scattering cross-section and how about the validity of the results, which are based either on a perturbational or numerical method.

FORMULATION OF THE PROBLEM

As shown by Fig. 1, the scatterer has been modeled as a periodically deformed perfectly conducting or dielectric cylinder of infinite length, which has already been considered by Bolomey and Wirgin (Bolomey, J.C. and Wirgin, A.,1974) for comparison of different numerical approaches. The incident field is either a TM- or TE-polarized plane wave of wave number k; its angle of incidence is $\mathcal{J}_{\mathbf{c}}$. The surface perturbation \mathcal{S} (\mathcal{S}) of the cylinder of radius a is given by

 Δ a being its amplitude and V its frequency.

As already suggested by Clemmow and Weston (Clemmow, P.C. and Weston, V.H.,1961), but to the author's knowledge never performed, we treat the problem systematically in terms of the three parameters ka (dimension of the scatterer relative to wavelength), k Δ a (dimension of the perturbation amplitude relative to wavelength) and V (frequency of the "ripples"). Apractical application of such problems has been recently given by Bringi and Seliga (Bringi, V.N. and Seliga, T.A.,1977) during the U.R.S.I.-Commission F Symposium in France, who considered scattering from naturally occurring hailstones with such surface perturbations.

3.

A common approach to the solution of the problems mentioned above is the formulation of integral equations for the induced electric and magnetic surface current densities \vec{J} and \vec{K} and solving them numerically (Mittra, R.,1973). If the scattering object is perfectly conducting, we have two independent equivalent Fredholm equations of the first and second kind, respectively, for \vec{J} . We assume transverse magnetic or transverse electric polarization and the form

for the z-dependence of the incident plane wave \vec{E}_1 , \vec{H}_1 . Taking into account the cylindrical structure of the scattering object, the integral equations decouple into two sets of equations for each current density component $\vec{J} = \vec{t} J_{t} + \vec{e}_{z} J_{z}$ and arbitrary \vec{v}_{z} (Bollig, G. 1976):

$$\frac{1}{4} \omega_{jk} \oint_{C} J_{e}(\vec{s}') H_{o}^{(i)}(k_{i} m_{i} l_{i} | \vec{s} - \vec{s}'|) \vec{\pi}(\vec{s}') d\vec{c}' = E_{ie}(\vec{s})$$

$$\frac{1}{4} J_{e}(\vec{s}) - \frac{1}{4} \oint_{C} J_{e}(\vec{s}') \frac{1}{2\pi} H_{o}^{(i)}(k_{i} m_{i} l_{i} | \vec{s} - \vec{s}'|) d\vec{c}' = -H_{ie}(\vec{s})$$

$$TE-case$$

$$\frac{1}{4} \lim_{n \to \infty} \sin^{2} \frac{1}{2} \left(\vec{g}' \right) H_{0}^{(1)} \left(k \sin \theta_{0} | \vec{g} - \vec{g}' | \right) d\vec{\zeta}' = E_{1,2} \left(\vec{g} \right)$$

$$\frac{1}{4} \lim_{n \to \infty} \sin^{2} \theta_{0} = \frac{1}{4} \left(\vec{g}' \right) + \frac{1}{4} \left(\vec{g}' \right) \frac{1}{2} \left(\vec{g}' \right) \frac{1}{2}$$

with

 $\vec{e}_z \cdot \vec{H}_i = H_{iz}$, $\vec{e}_z \cdot \vec{E}_i = E_{iz}$, $\vec{t} \cdot \vec{H}_i = H_{it}$, $\vec{t} \cdot \vec{E}_i = E_{it}$, \vec{e}_z unit vector in z-direction, \vec{t}

tangential unit vector t.e = 0, H Hankel-function of zero order and first kind. In each case only one integral equation has to be solved.

For dielectric scatterers, there exist two coupled integral equations for the electric and magnetic surface current densities, which remain a coupled system in the four current density components J_t , J_z , K_t , K_z for both polarizations (Bollig, G.,1976):

$$\begin{split} E_{(x)}(\vec{g}) &= \frac{1}{2E} \left\{ K_{\xi}(\vec{g}') + \frac{1}{4E} \oint_{\vec{g}} K_{\xi}(\vec{g}') \frac{3}{3\pi} \left[E H_{0}^{(t)}(v) - E H_{0}^{(t)}(u) \right] d\zeta' \right. \\ &+ \frac{1}{4\omega E} \oint_{\vec{g}} \left\{ J_{x}(\vec{g}') \left[K^{t} \sin^{2}\theta_{s} H_{0}^{(t)}(v) - \left(K^{t}_{s} - K^{t} \cos^{2}\theta_{s} \right) H_{0}^{(t)}(u) \right] \right\} d\zeta' \\ &+ \frac{1}{4\omega E} \oint_{\vec{g}} \left[\frac{3}{3E} , J_{\xi}(\vec{g}') \right] \left[H_{0}^{(t)}(v) - H_{0}^{(t)}(u) \right] d\zeta' \end{split}$$

To get the associated two dual equations, one has to replace $E_i \to \vec{H}_i$, $\vec{J} \to -\vec{K}$, $\vec{K} \to -\vec{J}$, $\xi \to -/$, $M \to -E$. The index i denotes the interior $0 < g < a + \Delta a = g$ of the scatterer; we used the appreviations

For perpendicular incidence only we get two independent systems; hence, in general, depolarization occurs in the scattering by dielectric bodies.

We solve these integral equations by the method of moments with subdomain base functions defined in the interval ΔC (Fig.2). As proposed by Daniel (Daniel. S.M., 1971), we approximate the current density J at k discrete points according to a parabola of second order, which takes into account the current density in the midpoints of the neighbouring intervals. Testing occurs with δ -distributions.

For the Fredholm equation of the first kind, we found best results, if two testpoints are situated 1/3 ΔC from the ends of the interval, whereas for the second kind equations one does best to let the current density and test-points coincide. The latter method has been chosen to yield the following results:

latter method has been chosen to yield the following results:

Fig. 3 shows the differential scattering cross-section for perpendicular incidence for ka = 5 on perfectly conducting cylinders with increasing surface roughness. In the transverse-magnetic and transverse-electric case, we see that especially the backscattering increases with the roughness. Furthermore we see, that sidelobes appear, whose direction is independent from the roughness amplitude. Naturally, transverse electric polarized waves are much more sensitive to surface perturbations, but in principal, they show the same behaviour.

Fig. 4 shows the pertinent surface currents as function of ${\bf y}$. These well known curves correspond to the circular cylinder. It is interesting to note, that in the case of a surface perturbation - at least in the TM-case - the current density amplitude follows closely the surface structure; its amplitude increases with increasing

Another method to treat scatterers of irregular shape is a perturbational approach. At first, we write the surface equation in the form

introducing a perturbation parameter & with

Now the field strength perturbations are assumed to be of the same order as the perturbations of the surface of the scatterer. That means, the electromagnetic field strengths are expanded in a perturbation series according to powers of δ : (We only give the equation for the electric field strength.)

$$\vec{E}_{t}^{(1)}(\vec{r}) = \vec{E}_{u}^{(1)}(\vec{r}) + \delta \vec{E}_{s}^{(1)}(\vec{r}) + \delta^{t} \vec{E}_{s}^{(1)}(\vec{r}) + \dots ,$$

 $\vec{E}_{i}^{(i)}(\vec{r})$ being the n-th perturbed field in medium i. $\vec{E}_{i}^{(i)}(\vec{r})$ stands for the unperturbed scattered or diffracted field of a circular cylinder. In a next step, the transition conditions for the total fields $\vec{E}_{i}^{(i)}(\vec{r})$, $\vec{H}_{i}^{(i)}(\vec{r})$ are expanded into Taylor series around the unperturbed surface $|\vec{r}| = a$. Since on this surface, the unperturbed fields fullfill homogeneous transition conditions, the result of this procedure are separate inhomogeneous transition conditions for perturbed fields along for every order n. As formulated by suppose the second conditions for perturbed fields along for every order n. As formulated by suppose the second conditions for perturbed fields along for every order n. As formulated by suppose the second conditions for perturbed fields along for every order n. transition conditions for perturbed fields alone for every order n. As formulated by Erma (Erma, V.A., 1968), this step is tantamount to replacing the single "necessary" boundary condition by an infinite set of "sufficient" boundary conditions. By means of the eigenfunction expansion for the unperturbed field and similar series expansion with unknown coefficients for the n-th order perturbed fields, these coefficients can be determined from this set of sufficient boundary conditions. Provided, that this series converges, the resulting solution is exact; it is thus equally valid in the near and far zones as well as over all ranges of the physical parameters of interest. But it is already a very tedious task to develop only the second order solution explicitly. Hence, in most

applications one dealt with the first order terms, hoping they would approximate the exact solution pretty well. In fact, the question turns on the accuracy of this linearization, when k Δa and the other parameters of the problem are prescribed. Hence, we compared the accuracy of the first and second order perturbation approximation with our results derived by the numerical method. Fig. 5 shows the differential scattering cross section of a perfectly conducting cylinder, whose surface is given by the unbroken curve; the arrow indicates the perpendicularly incident wave (ka = 5). The unbroken curve corresponds to the exact series solution, the dashed curve represents the first order perturbation approximation if this circular cylinder is assumed to be a perturbation of this dashed circular cylinder (k Δa = 0,5; ripple parameter v = 0). The pointed curve is the second order perturbation solution. Hence, one can really state convergence, at least as far as the first two terms of the series are taken into account. This result is not observed for higher values of the wavenumber as we shall see later on. Now, we increase the ripple period v as shown in Fig. 6. Here v = 2 is resulting an elliptic perturbation of the circular cylinder; the unbroken curve is found numerically. In principle, the same behaviour is observed as for v = 0, yet the first order perturbation is already more exact, a fact, which is redicovered for v = 4 in Fig. 7.

A further increase of v up to 10 (Fig. 8) shows a very good agreement of the first order perturbation solution, whereas the second one is worse again. Here, the per-

A further increase of v up to 10 (Fig. 8) shows a very good agreement of the first order perturbation solution, whereas the second one is worse again. Here, the perturbation series does not converge as far as its first two terms are considered. Yet we state, that these are intermediate values of V, for instance v=6 or so, where the perturbation approximation yields excellent results. These results can be interpreted as if a slowly rippled cylinder represents a better linear perturbation of a circular cylinder than a very rough or elliptic one. But if we reduce the perturbation amplitude of this rough cylinder to only 4% (Fig. 9), we have absolute agreement of numerical and perturbational values. Hence, convergence of the perturbation series depends on the relation between v and Δ a, and this relation is again dependent on the wave number. If we choose, for example, ka=2.5, returning to the 10% value of Δ a (Fig. 10), we have even for v=0 a complete agreement of the second order perturbation with the numerical values. On the other side, sonsidering the same case for ka=10 (Fig. 11), we see that there is no convergence in the above mentioned sense. The results become again somewhat better, if the ripple frequency v is increased (Fig. 12). But again, we cannot speak of a uniform convergence. Reducing the perturbation amplitude yields once again better agreement.

In general one could say, that especially in the foreward scattering direction, first order perturbation solutions are a good tool for treating irregularly shaped perfectly conducting scatterers. Backscattering and sidelobes should be investigated more carefully, especially at higher values of ka.

Now, turning to the results for a perturbed dielectric cylinder with relative permittivity equal to 4. They are very similar to the previous ones, except for two special features: the effect of different ripple amplitudes on dielectric cylinders does not influence the differential cross section much, at least as far as ka values up to 2 are considered, whereas increasing of the ripple frequency increases both backscattering and foreward scattering amplitudes.

Concerning the convergence of the perturbation series, the frequency of the incident field must be considerably reduced in comparison with the perfectly conducting case. As an example Fig. 13 shows, with ka = 2,5 and a lot perturbation, a very bad result, at least for Y = 0. But here, we observe a strong tendency towards better results if the ripple frequency is increased, as we can see in Fig. 14. This effect is more pronounced than in the perfectly conducting case.

All these results hold for perpendicular incidence. But if the angle of incidence is reduced from its 90 value, the quality of the perturbation results decreases

All these results hold for perpendicular incidence. But if the angle of incidence is reduced from its 90° value, the quality of the perturbation results decreases very quickly. For instance, for ka = 1.5 and \sqrt{s} = 30°, the second order perturbational approach to the scattering from a rough dielectric cylinder is absolutely wrong for large ripple periods and perturbations about 10% (Fig. 15).

4. CONCLUSION

By comparison of the numerical method, based on integral equation formalism, and the perturbational method, one could say, that epecially in the foreward scattering direction, first order perturbation solutions are a good tool for treating rough perfectly conducting and dielectric scatterers. Concerning backscattscattering and sidelobes calculations by the perturbational approach, especially at higher values of ka, should be interpreted carefully. Also, if the angle of incidence is reduced from its 90°, the perturbational results become more and more unrealistic.

ACKNOWLEDGEMENT

The autor wishes to thank Dr. K.J. Langenberg for many useful hints and discussions and Dipl.-Phys. G. Bollig for performing the calculations.

REFERENCES

Becker, K.-D., 1968 "Die Störung des elektromagnetischen Feldes einer Antenne durch ein sie umgebendes Dielektrikum", A.E.U. $\underline{22}$, 548 - 553.

Becker, K.-D., Dobmann, G. and Langenberg, K.J., 1975 "Space wave field produced by a vertical electric dipole above a rough surface", Appl. Phys. $\underline{6}$, 35 - 42.

Beckmann, P. and Spizzichino, A., 1963 "The scattering of electromagnetic waves from rough surfaces", Pergamon Press Oxford.

Bollig, G., 1975 "Numerische Lösung zweidimensionaler Beugungsprobleme", Diplomarbeit Universität des Saarlandes, Saarbrücken.

Bolomey, I.C. and Wirgin, A., 1974 "Numerical comparison of the Green's function and the Waterman and Rayleigh theories of scattering from a cylinder with arbitrary cross-section", Proc. IEEE $\underline{121}$, 794 - 804.

Bringi, V.N. and Selige, T.A., 1977 "Scattering from non-spherical hydrometeors", Proceedings of the open symposium of U.R.S.I. commission F La Baule (France) 28. Avril - 6. Mai 1977, 199 - 204.

Clemmow, P.C. and Weston, V.H., 1961 "Diffraction of a plane wave by an almost circular cylinder", Proc. Roy. Soc. (London) A 264, 246 - 268.

Daniel, S.M., 1971 "Optimal solution to the two-dimensional scattering problem", Ph. D. Thesis, University of Illinois, Urbana.

Erma, V.A., 1968 "An exact solution for the scattering of electromagnetic waves from conductors of arbitrary shape.I. Case of cylindrical symmetry", Phys. Rev. 173, 1243 - 1257.

Erma, V.A., 1968 "Exact solution for the scattering of electromagnetic waves from conductors of arbitrary shape.II. General case", Phys. Rev. 176, 1544 - 1553.

Erma, V.A., 1969 "Exact solution for the scattering of electromagnetic waves from bodies of arbitrary shape.III. Obstacles with arbitrary electromagnetic properties" Phys. Rev. 179, 1238 - 1246.

Giloi, H.-G., 1974 "Messung der auf Richtfunkverbindungen auftretenden Echos von festen Objekten", Kleinheubacher Berichte Bd. 17 (1974), 545 - 552, herausgegeben vom Fernmeldetechnischen Zentralamt Darmstadt.

Harrington, R.F., 1968 "Field computation by moment methods", Mac Millan New York.

Mittra, R., 1973 "Computer techniques for electromagnetics", Pergamon Press Oxford.

Morrison, J.A. and Cross, M.-J., 1974 "Scattering of a plane electromagnetic wave by axisymmetric raindrops", Bell Syst. Techn. J. $\underline{53}$, 955

Yeh, C., 1964 "Perturbation approach to the diffraction of electromagnetic waves by arbitrarily shaped dielectric obstacles", Phys. Rev. 135, 1193 - 1201.

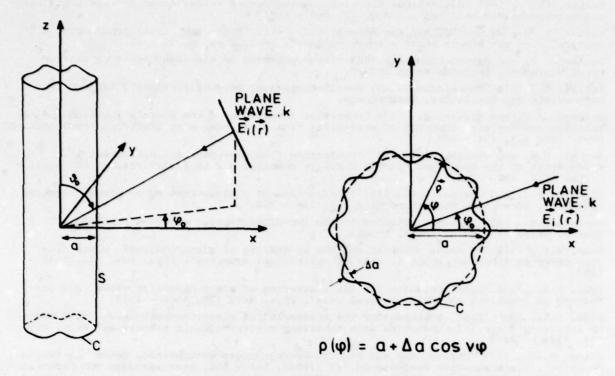
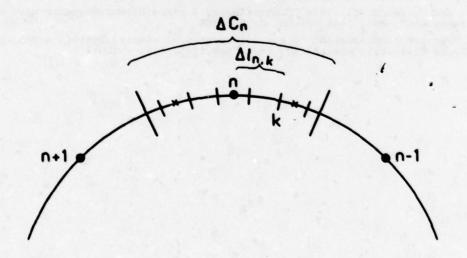


Fig. 1 Geometry of the problem



$$J_{n,k} = J_n + \frac{J_{n+1} - J_{n-1}}{2\Delta C_n} \Delta l_{n,k} + \frac{J_{n+1} - 2J_n + J_{n-1}}{2(\Delta C_n)^2} (\Delta l_{n,k})^2$$

Fig. 2 Numerical method used by Daniel

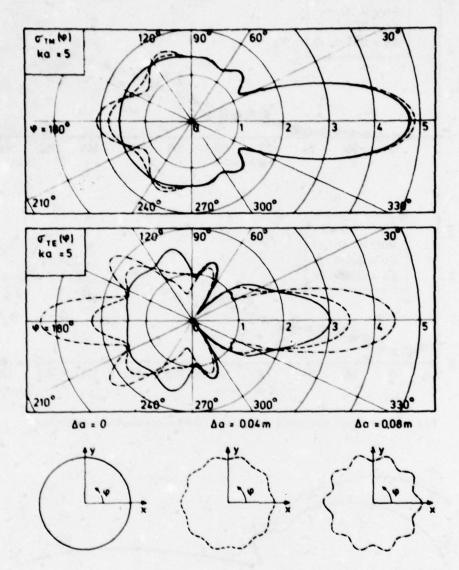


Fig. 3 Scattering cross-section of a perfectly conducting cylinder

..

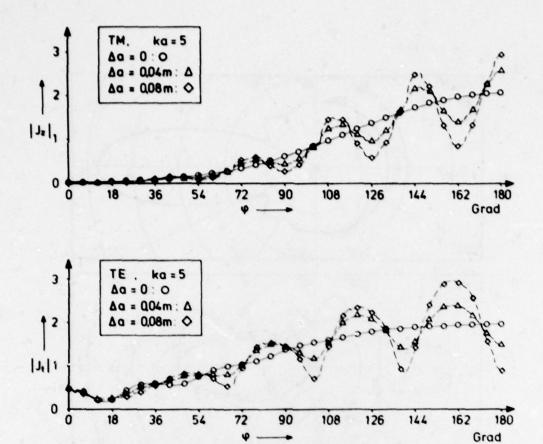


Fig. 4 Surface currents for a perfectly conducting cylinder

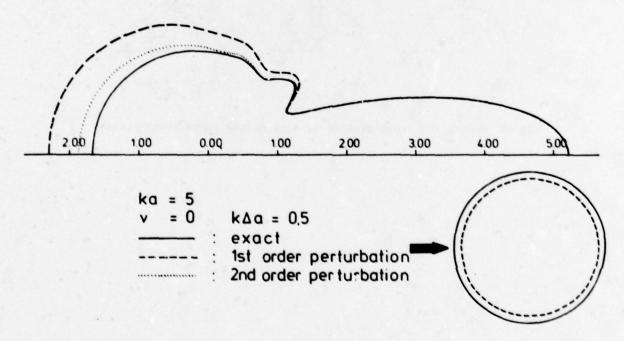


Fig. 5 Differential scattering cross-section; ka = 5; V = 0; Δa = 10%; & = ∞

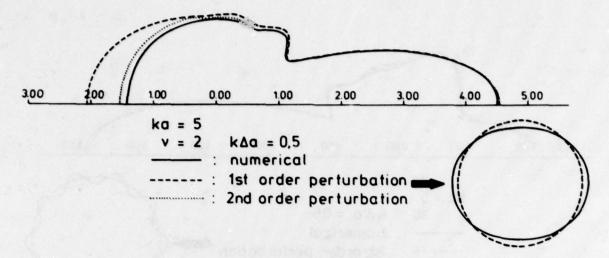


Fig. 6 Differential scattering cross-section; ka = 5; V = 2; Δa = 10%; 6 = **

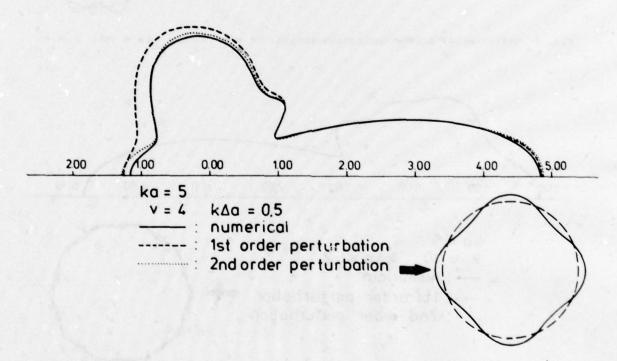


Fig. 7 Differential scattering cross-section; ka = 5; v = 4; $\Delta a = 108$; $\sigma' = \infty$

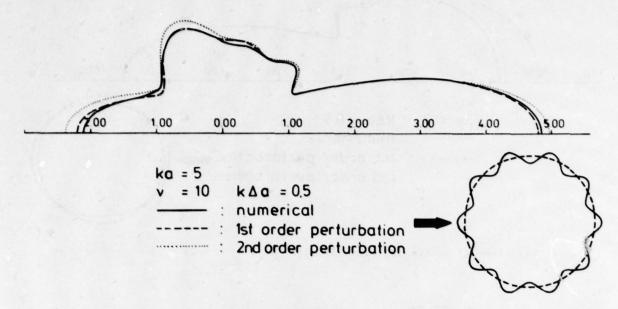


Fig. 8 Differential scattering cross-section; ka = 5; v = 10; $\Delta a = 108$; $c = \infty$

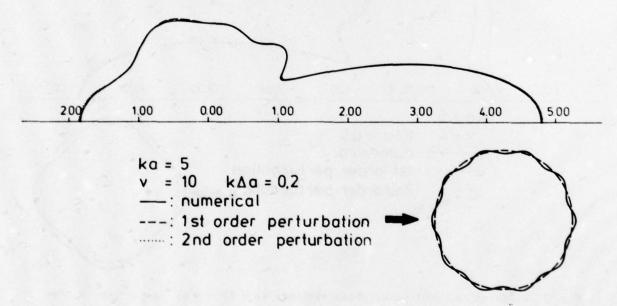


Fig. 9 Differential scattering cross-section; ka = 5; v=10; $\Delta a = 48$; $d = \infty$

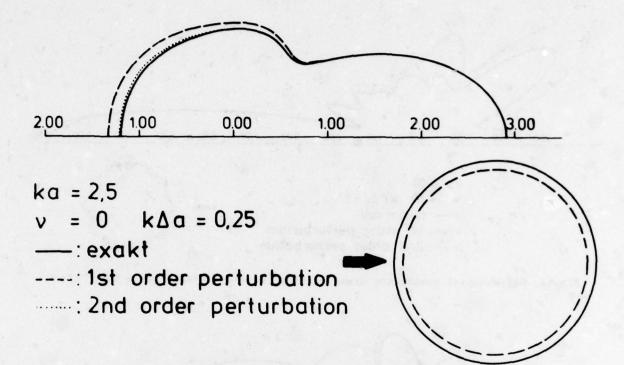


Fig. 10 Differential scattering cross-section; ka =2,5; v=0; $\Delta a = 108$; $\sigma = \infty$

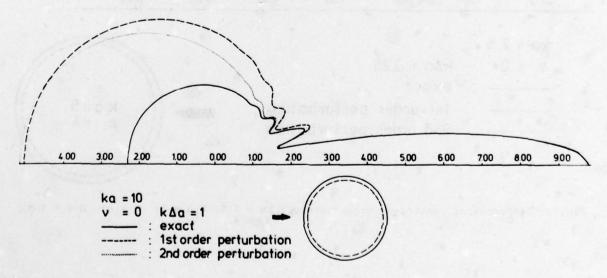


Fig. 11 Differential scattering cross-section; ka =10; v = 0; \(\Delta = 10\); d = **

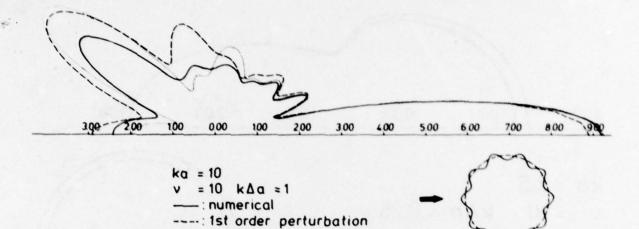


Fig. 12 Differential scattering cross-section; ka =10; V=10; Δa = 10%; d = ...

: 2nd order perturbation

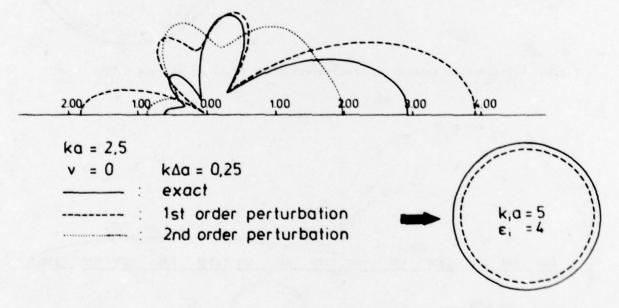


Fig.13 Differential scattering cross-section; ka = 2.5; $k_1a = 5$; v = 0; $\Delta a = 108$; $\epsilon_1 = 4$

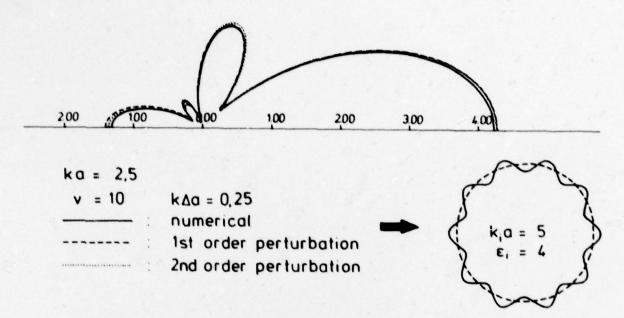


Fig.14 Differential scattering cross-section; ka = 2.5; $k_1a = 5$; v = 10; $\Delta a = 108$; $\frac{\epsilon_1}{\epsilon_2} = 4$

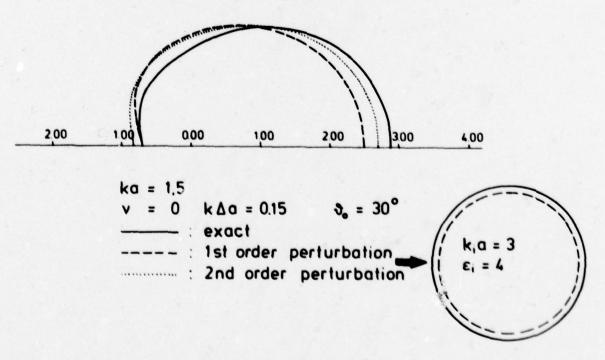


Fig. 15 Differential scattering cross-section; $k_a = 1.5$; $k_{ia} = 3$; v = 0; $\Delta a = 100$; $\xi = 4$

A SCATTER MODEL FOR LEAFY VEGETATION

A. K. Fung and F. T. Ulaby Remote Sensing Laboratory University of Kansas Lawrence, Kansas 66045

ABSTRACT

A model for vegetation scatter is developed using the first-order renormalization method. The vegetated medium is taken to be an inhomogeneous medium characterized by a random permittivity function with a cylindrically symmetric, fast-decaying correlation function. The permittivity of the vegetation (taken to be a combination of water and some solid material) is estimated by mixing formula after de Loor (1968) and the permittivity of the vegetated medium (taken to be a combination of vegetation and air) is estimated using a formula by Pierce (1955). The backscattering coefficient from such a model is computed as a function of the incidence angle, frequency and the moisture content of the vegetation. Comparisons are made with measured data from soybeans, alfalfa and corn.

1. INTRODUCTION

It appears natural to model a vegetated medium as a collection of randomly located discrete scatterers and to expect some of the existing multiple scattering theories to be applicable. Indeed, multiple scattering theories for random distributions (Twersky, V., 1962) or for arbitrary configurations (Twersky, V., 1967) are available. However, such theories are so complicated that when it comes to computation it is impractical to consider more than three scatterers (Wilton, D. R. and R. Mittra, 1972; Howarth, B. A. And T. J. F. Pavlasek, 1973). In the interest of arriving at a practical model, only single-scattering approach has been applied to discrete models (Du, L. J. and W. H. Peake, 1969).

When a vegetated medium can be modeled as a continuous inhomogeneous medium with strong permittivity fluctuations, theories on wave scattering and propagation in such media become applicable (Frisch, V., 1968). Attempts have been made to convert such theories for an unbounded inhomogeneous medium (Frisch, V., 1968; Tatarskii, V. I., 1964) to those (Rosenbaum, S., 1969; Bassanini, P., C. Cercignani, F. Sernagiotto, and G. Tironi, 1967; Stogryn, A, 1974; Kupiec, I., L. B. Felsen, S. Rosenbaum, J. B. Keller, and P. Chow, 1969) suitable for a half-space inhomogeneous medium. When a three-dimensional randomly inhomogeneous half-space is considered, Stogryn (1974) showed that the resulting complications demanded numerical analysis. More recently fung and Fung (1977) applied the first-order renormalization method to a half-space characterized by a random permittivity function with a large variance and a cylindrically symmetric, fast-decaying correlation function. They were able to obtain an approximate close form solution to the bistatic scattering coefficient using a technique after Kupiec, et al. (1969).

A scatter model for an inhomogeneous medium cannot, in general, be viewed as a scatter model for vegetation. It is necessary that both the geometric parameters and the physical parameters of the medium resemble those of the vegetated medium. In particular, the behaviors of the average permittivity of the medium and the variances of the fluctuating part of the permittivity function must be known as a function of frequency, moisture content, and the volume fraction of vegetation in the medium. In this paper the scatter model for an inhomogeneous half-space developed by Fung and Fung (1977) is extended to a scatter model for leafy vegetations by developing a permittivity model first for a single leaf and then for a vegetation canopy. The choice of some of the relevant parameters in the permittivity model is based upon existing permittivity measurements. The vegetation scatter model resulting from the use of such a permittivity model is then tested against scatterometer data acquired from soybeans, alfalfa and corn canopies.

2. THE BACKSCATTERING COEFFICIENT

When the inhomogeneous half-space is characterized by a relative random permittivity function of the form $\varepsilon(r) = \varepsilon_0 + \varepsilon_S(r)$ where ε_a is the mean (or average) permittivity and $\varepsilon_S(r)$ is the fluctuating part of the permittivity function, it is intuitively clear that for a vegetated medium modeled by a collection of leaves, $\varepsilon_S(r)$ must have a fast-decaying correlation coefficient. This follows from the fact that leaves have very small thickness. It is also intuitively clear that most leaves do not stand straight up. Hence, if symmetry property is assumed it must be cylindrical instead of spherical in nature. When the correlation coefficient is taken to have cylindrical symmetry, i.e.

$$\rho(\xi_n, \zeta) = \exp\left[-\frac{(\xi^2 + \eta^2)^{1/2}}{\xi} - \frac{|\zeta|}{\xi_-}\right]$$

where ℓ is the correlation length in the horizontal plane and ℓ_z is the correlation length in the vertical direction, the backscattering coefficient from such an inhomogeneous half-space due to an impinging plane wave at an incident angle, θ , has been shown to be given approximately by (Fung, A. K. and H. S. Fung, 1977)

$$\sigma_{pp}^{*}(\theta) = 2k^{6}\sigma_{s}^{2}\epsilon^{2}\cos^{2}\theta |\alpha_{pp}|^{2} \frac{1(k\sin\theta)}{[1 + (2k\epsilon\sin\theta)^{2}]^{3/2}}$$
 (1)

where k is the wave number in air, σ^2 is the sum of the variances of the real and the imaginary parts of $\epsilon_{\rm s}(r)$ (i.e., $\sigma_{\rm s}^2 = \sigma_{\rm cr}^2 + \sigma_{\rm cl}^2$), and

$$\begin{split} &l \left(k \sin \theta \right) = \pm_{z} (1 - D_{r} \pm_{z}) \left[D_{r} (1 - 2D_{r} \pm_{z} + |D|^{2} \pm_{z}^{2}) \right]^{-1} \\ &D_{r} = \text{Real part of } D \\ &D = j \left(k_{e1} + k_{a}^{1} \right) \\ &k_{a}^{1} = \left(k_{a}^{2} - k^{2} \sin^{2} \theta \right)^{1/2} \\ &k_{e1}^{2} = k_{a}^{1} - j \frac{k^{4} \pm^{2} \pm_{z} \sigma_{d}^{2} l_{O}}{2\pi k_{a}^{1} \left(\left(k_{a}^{1} \pm_{z} \right)^{2} + 1 \right]} \\ &l_{O} = \int_{-\infty}^{\infty} \left(k_{a}^{2} - u^{2} - v^{2} \right)^{-1/2} \left[1 + \pm^{2} \left(\left(u + k \sin \theta \right)^{2} + v^{2} \right) \right]^{-3/2} du dv \\ &\sigma_{d}^{2} = \sigma_{er}^{2} - \sigma_{el}^{2} \end{split}$$

In the above k_a is the average wave number in the inhomogeneous random medium. For horizontal polarizations $\alpha_{pp} = \alpha_{hh}$ and

$$A_{h} = A_{h}/(k\cos\theta + k_{e}^{1})$$

$$A_{h} = 2\cos\theta [k\cos\theta + k_{e}^{1} - \frac{(1 - jk_{e}^{2}t_{z}^{2})(k\cos\theta + k_{e}^{2})}{(1 - jk_{e}^{1}t_{z}^{2})}]^{-1}$$

$$k_{e2} = -j\frac{1}{t_{z}} - \frac{k^{4}\epsilon^{2}\epsilon_{z}^{2}\sigma_{d}^{2}t_{o}^{2}}{2\pi[(k_{e}^{1}t_{z}^{2})^{2} + 1]}$$

For vertical polarization $\alpha_{pp} = \alpha_{vv}$ and

$$\alpha_{VV} = A_{V}/(k\epsilon_{a}\cos\theta + k_{a}^{1})$$

$$A_{V} = 2k\cos\theta [k\cos\theta + (k_{e1}/\epsilon_{e1}) - \frac{(1 - jk_{e2}t_{z})(k\cos\theta + k_{e2}/\epsilon_{e2})}{(1 - jk_{e1}t_{z})}]^{-\frac{1}{2}}$$

$$\epsilon_{e1,2} = \sin^{2}\theta + k_{e1,2}^{2}/k^{2}$$

3. A PERMITTIVITY MODEL FOR LEAFY VEGETATION

The scattering coefficient given in the previous section is defined in terms of the permittivity of the vegetated medium. Until an estimate of this parameter for a given type of vegetation is known, the scattering coefficient formula cannot be viewed as a scatter model for vegetation.

To arrive at an estimate for the average value and the variance of the permittivity of the medium it is necessary first to obtain an estimate of the permittivity of a single leaf. When a leaf is taken to be a mixture of some solid material with water granules embedded, the relative static permittivity of the mixture can be expressed in the form (de Loor, G. P., 1968)

$$\epsilon_{m} = \epsilon_{s} + (V_{w}/3)(\epsilon_{w} - \epsilon_{s}) \sum_{i=1}^{3} 1/\{1 + ((\epsilon_{w}/\epsilon^{\pm}) - 1)A_{j}\}$$
(2)

where V_w is the volume filling factor of the dispersed granules; ε_w , ε_s are the permittivities of water and the solid material respectively; ε^* is the effective 'internal' dielectric constant which is really not known but can be taken to be ε_s in this case; and A_j 's are the depolarization factors along the main axes of the ellipsoidal granules. In general, the permittivity of a mixture is not estimated directly but rather the upper and lower bounds are estimated by interchanging the roles of water and the solid material, i.e., by considering granules of water dispersed in a continuum of the solid material in one case and the dispersing of granules of solid material in water in the other case. For the purpose of this paper we shall model the leaf as a mixture of water granules dispersed in a continuum of some solid material. According to de Loor (1968) for disc-shaped granules, $A_j = 0$; 0; 1. Under this assumption, the relative macroscopic static permittivity of a leaf is given by

$$\epsilon_{m} = 5 + 51.568_{w}$$
 (3)

where ϵ_s is taken to be 5 and ϵ_w to be 80. The above formula is expected to be valid when V_w lies between 0.1 and 0.6 For materials with very high water contents ($V_w > 75\%$), other estimating formulae were recommended by de Loor and Meijboom (1966).

To find the complex permittivity of a leaf at microwave frequencies, the following formulae (given by de Loor and Meijboom, 1966) for the real and the imaginary parts may be used

$$\varepsilon_r = 5.5 + \frac{\varepsilon_m - 5.5}{1 + f^2 \tau^2} \tag{4a}$$

$$\epsilon_{\parallel} = (\epsilon_{\rm m} - 5.5) \frac{f_{\tau}}{1 + f^2 \tau^2} \tag{4b}$$

where τ is the relaxation time of water which depends on temperature, f is the frequency under consideration. At 20°C, f τ is approximately equal to (1.85/ λ), where λ is the electromagnetic wavelength in cm.

For a single leaf the moisture content is usually measured on a wet weight basis, i.e.

$$M = \frac{M_t - M_d}{M_t}$$

where W_t is the total wet weight of the leaf and W_d is the weight after drying. To find the relation between M and V_w let d_s be the density of the solid material and d_w be the density of water. Then

$$M = \frac{V_{w}d_{w}}{V_{w}d_{w} + (1 - V_{w})d_{s}}$$
$$= \frac{V_{w}}{V_{w} + (1 - V_{w})(d_{s}/d_{w})}$$

A plot of M versus V_W using the ratio, d_W/d_S , as a parameter is shown in Figure 1. When d_W/d_S is chosen in the range 3 and 5, the computed values of ε_Γ and ε_1 at 8.5 GHz compare reasonably well with Carlson's (1967) permittivity data for leaves as shown in Figure 2. In view of the scatter in the data, there are clearly other possible choices in the parameters of the permittivity model for a single leaf. However, until more permittivity measurements are available the above choice will serve well as an illustration. Thus, when the moisture content is given either in terms of V_W or M, ε_m can be computed using (3) and then ε_Γ and ε_1 can be obtained for a given frequency and temperature via (4). The permittivity of a single leaf, ε_ϱ , is then given by

With the permittivity for a single leaf known the average permittivity of the medium consisting of leaves and air may be estimated by a simple mixing formula (Pierce, C., 1955):

$$\epsilon_a = (\epsilon_t V_t + V_a)/V$$
 (5)

where V is the total volume of the medium; V_{ℓ} is the volume occupied by leaves and V_{a} is the volume occupied by air. The variances of the real and the imagingery parts of the fluctuating relative permittivity, $\varepsilon_{s}(r)$ of the vegetated medium can be estimated by

$$\sigma_{\epsilon r}^{2} = (\epsilon_{r} - \epsilon_{ar})^{2} V_{g} / V + (1 - \epsilon_{ar})^{2} V_{a} / V$$
 (6a)

$$\sigma_{e_i}^2 = (\varepsilon_i - \varepsilon_{a_i})^2 V_e / V + \varepsilon_{a_i}^2 V_a / V \tag{6b}$$

where ϵ_{ar} , ϵ_{ai} are the real and the imaginary parts of ϵ_{a} .

4. THEORETICAL RESULTS

With the scatter model defined by (1) and the parameters associated with the permittivity function of the medium given by (5) and (6), theoretical curves of $\sigma_{pp}^{\circ}(\theta)$ as a function of frequency, incident angle, and moisture are shown in Figures 3 and 4. The geometric parameter ℓ_z is a quantity proportional to the thickness of the leaf and the parameter ℓ is the horizontal correlation length of the fluctuating permittivity. The normalized quantity ki is an effective quantity since the exploring wavelength is known to have a filtering characteristic. The values of $k\ell_z$ and $k\ell$ used for computation of curves in Figures 3 and 4 are tabulated in Table 1. In general, a large $k\ell$ values causes the $\sigma_{pp}^{\circ}(\theta)$ curve to drop off faster with the incident angle and a larger $k\ell_z$ value simply raises the level of the $\sigma_{pp}^{\circ}(\theta)$ curve. The value of ℓ_z , however, must be a fraction of a millimeter.

In Figure 2 it was shown that the ratio of the densities of $d_{\rm w}/d_{\rm s}$ is around 3 to 5 for reasonable fit of Carlson's data. The effect due to the choice of this ratio on $\sigma_{\rm pp}^{\rm p}(\theta)$ is shown in Figure 3. It is seen that in general there is an increase in the level of $\sigma_{\rm pp}^{\rm o}(\theta)$ over all frequencies and incident angles as this ratio is decreased from 5 to 3. The amount of change is around 1 dB indicating that an error in the choice of this parameter within the indicated range does not lead to significant differences in $\sigma_{\rm pp}^{\rm o}(\theta)$.

Figure 4 shows the effect of the percent volume of vegetation on the computed $\sigma_{pp}^{\bullet}(\theta)$ curves. As this parameter increases, the level of $\sigma_{pp}^{\bullet}(\theta)$ decreases. The effect may not be real since the model for the vegetated medium assumes a plane air-vegetation boundary. The most significant effect in changing this parameter is that smaller percent volume of vegetation causes $\sigma_{pp}^{\bullet}(\theta)$ curve to drop off slower with the incident angle.

From the above study it is seen that with the percent volume restricted to be less than 1% (Attema, ir E. P. W. and F. T. Ulaby, 1976) and the ratio of densities lying in the range 3 to 5, the dielectric model for the vegetated medium is completely specified. Of the two geometric parameters, \mathbf{L}_z must be a fraction of a millimeter (since it represents the effective thickness of the leaf) and \mathbf{L}_z , the correlation length of the fluctuating permittivity, is the only parameter whose value is uncertain. For a given vegetation at a given point in time, kt can only be determined at a given frequency by fitting the measured $\sigma_{\rm pp}^{\rm e}(\theta)$.

Table 1. Theoretical Parameters

		For Figure	es 3 and 4		
Frequency	8.6 GHz	11 GHz	13 GHz	15 GHz	17 GHz
ktz	. 108	.138	.174	. 193	.213
kt	.30	.35	. 36	. 365	.37

5. COMPARI SONS WITH MEASUREMENTS

Measured $\sigma_{\rm pp}^{\bullet}(\theta)$ values for alfalfa, soybeans, and corn have been reported by Bush and Ulaby (1975), Bush, Ulaby, and Metzler (1975), and Ulaby and Bush (1975). It is noted in these references that after accounting for possible difference due to calibration the level of $\sigma_{\rm VV}^{0}(\theta)$ for vertical polarization is only slightly higher (less than 1/2 dB) than the corresponding $\sigma_{\rm HV}^{0}(\theta)$. Hence, only $\sigma_{\rm HV}^{0}(\theta)$ is shown for comparison in Figures 5 through 7. The moisture content of alfalfa when fully grown in height stays essentially constant around 0.805 which is the value used for the theoretical curves shown in Figure 5. Other parameters used in the theory are tabulated in Table 2.

Table 2. Parameter Values for Alfalfa

V£/V	0.5%					
Frequency	8.6 GHz	11 GHz	13 GHz	15 GHz	17 GHz	
klz Lz = 0.4mm	.072	. 092	.109	.126	.142	
kt	.24	.29	. 295	.31	.315	
۲.	1.1420 -j.0608	1.1279 -j.0682	1.1167 -j.0716	1.1065 -j.0732	1.0974 -j.0733	
o _{er} 2	3.716	2.993	2.474	2.040	1.688	
o ₆₁ 2	0.7319	0.9216	1.0167	1.0605	1.0643	

Note that in Table 2 the three parameters associated with the permittivity are obtained from the permittivity model and are not subject to choice. The value of ℓ_z once chosen determines the values of $k\ell_z$ at all frequencies. As seen in Figure 5, satisfactory agreements in absolute level and trends are obtained at different incident angles over the entire frequency range considered.

The moisture content of soybeans after reaching maturity is always over 0.80. The theoretical value used in Figure 6 is 0.816. Other parameters used in the theory are tabulated in Table 3. As seen from Figure 6, very good agreements between theory and measured values of $\sigma_{\text{HH}}^{\circ}(\theta)$ are obtained.

In Figure 7, comparisons are made with data taken from corn. The data shown vary in moisture content from approximately 0.73 to 0.84. As a result two theoretical curves are computed at 0.73 and 0.84 moisture values. The upper curve at each incident angle corresponds to the higher moisture value. Other parameters used in the theory are shown in Table 4. Here again very good agreements are obtained in both the absolute level and the trends in incidence angle, frequency and moisture content.

Table 3. Parameter Values for Soybeans

VE/V		0.3	*		
Frequency	8.6 HHz	11 GHz	13 GHz	15 GHz	17 GHz
klz lz = 0.458 mm	. 0825	.106	. 125	.138	. 165
kt	. 246	.315	. 346	. 355	. 360
٠.	1.0873 -j.0376	1.0786 -j.0422	1.0717	1.0654 -j.0453	1.0597 -j.0453
o _{er} 2	2.355	1.894	1.564	1.288	1.065
σ _{ε i}	. 4682	. 5896	. 6504	.6784	. 6808

Table 4. Parameter Values for Corn

Vt/V		0.35			
Frequency	8.6 GHz	11 GHz	13.8 GHz	15.4 GHz	17 GHz
ktz tz = 0.48 mm	. 0865	.1110	.1400	.1540	.1710
kt	. 28	. 35	. 38	. 39	.40
M = 0.84	1.0951 -j.0417	1.0854 -j.0468	1.0748 -j.0497	1.0694 -j.0502	1.0644 -j.0503
oer 2	2.8078	2.2506	1.7104	1.4605	1.2498
σ _ε i	. 5763	.7258	.8188	.8379	.8381
H = 8.73	1.7025 -J.0297	1.0657 -j.0334	1.0581 -j.0355	1.0542 -j.0359	1.0507 -j.03587
o _{er} 2	1.6014	1.3005	1.0064	. 8692	. 7530
σ _{ε1}	. 2931	. 3692	.4165	. 4262	. 4263

6. CONCLUSIONS

For the leafy type vegetation, a permittivity model has been found which when used with a first-order renormalization theory (Fung, A. K. and H. S. Fung, 1977) provides satisfactory predictions of $\sigma_{pp}^{\infty}(\theta)$ values over incident angles from 30° to 70° and over a frequency range from 8.6 GHz to 17 GHz. Note that smaller incident angles are not chosen to avoid possible ground effects. The theory used does not account for the irregular air vegetation boundary and is restricted to densely populated vegetations. It is expected that in order to predict the height of the vegetations over their growth period further refinement of the theory or other type of modeling is necessary.

ACKNOWLE DGMENT

This work was supported in part by the National Science Foundation under grant ENG 75-03220 and in part by the U.S. Army Research Office under grant DAAG29-77-G-0075.

REFERENCES

- Attema, ir E. P. W. and F. T. Ulaby, 1976, "Modeling a Vegetation Canopy at Microwave Frequencies as a Water Cloud," RSL TR 330-2, University of Kansas, Center for Research, Inc., September.
- Bassanini, P., C. Cercignani, F. Sernagiotto, and G. Tironi, 1967, "Scattering of Waves by a Medium with Strong Fluctuations of Refractive Index," Radio Science, vol. 2, no. 1, pp. 1-18, January.
- Bush, T. F. and F. T. Ulaby, 1975, "Radar Return from a Continuous Vegetation Canopy, IEEE Trans. Ant. and Prop., vol. 24, no. 3, pp. 269-276, May '76, RSL TR 177-56, University of Kansas, Center for Research, Inc., Lawrence, Kansas, August, 1975.
- Bush, T. F., F. T. Ulaby, and T. Metzler, 1975, "Radar Backscatter Properties of Milo and Soybeans," RSL TR 177-59, University of Kansas, Center for Research, Inc., Lawrence, Kansas, October.

- Carlson, N. L., 1967, "Dielectric Constant of Vegetation at 8.5 GHz," Technical Report 1903-5, Electro-Science Laboratory, Ohio State University, Columbus, Ohio, March.
- de Loor, G. P., 1968, "Dielectric Properties of Heterogeneous Mixtures Containing Water," J. Microwave Power, vol. 3, pp. 67-73.
- de Loor, G. P. and F. W. Meijboom, 1966, "The Dielectric Constant of Foods and Other Materials with High Water Contents at Microwave Frequencies," J. Fd Technol., vol. 1, pp. 313-322.
- Du, L. J. and W. H. Peake, 1969, "Rayleigh Scattering from Leaves," Proc. IEEE, vol. 57, no. 6, pp. 1227-1229, June.
- Frisch, V., 1968, "Wave Propagation in Random Media," Probablistic Methods in Applied Mathematics, vol. 1, pp. 75-198, Academic Press.
- Fung, A. K. and H. S. Fung, 1977, "Application of First-Order Renormalization Method to Scattering from a Vegetation Like Half-Space," IEEE Trans. Geoscience Electronics, October.
- Howarth, B. A. and T. J. F. Pavlesek, 1973, "Multiple Induction A Novel Formulation of Multiple Scattering of Scalar Waves," J. Appl. Phys., vol. 44, pp. 1162, May.
- Kupiec, I., L. B. Felsen, S. Rosenbaum, J. B. Keller and P. Chow, 1969, "Reflection and Transmission by a Random Medium," Radio Science, vol. 4, no. 11, pp. 1067-1077, November.
- Pierce, C., 1955, "The Permittivity of Two Phase Mixtures," Brit. J. A. Phys., vol. 6, October.
- Rosenbaum, S., 1969, "On the Coherent Wave Motion in Bounded, Randomly Fluctuating Regions," Radio Science, vol. 4, no. 2, pp. 709-719, August.
- Stogryn, A., 1974, "Electromagnetic Scattering by Random Dielectric Constant Fluctuations in a Bounded Medium," Radio Science, vol. 9, pp. 509-518, May.
- Tatarskii, V. I., 1964, "Propagation of Electromagnetic Waves in a Medium with Strong Dielectric Constant Fluctuations," Soviet Physics, JETP, vol. 19, no. 4, pp. 946-953, October.
- Twersky, V., 1967, "Multiple Scattering of Electromagnetic Waves by Arbitrary Configurations," J. Math. Phys., vol. 8, no. 3, pp. 489-610, March.
- Twersky, V., 1962, "On Scattering of Waves by Random Distributions," J. Math. Phys, vol. 3, no. 4, pp. 700-715, July-August.
- Ulaby, F. T. and T. F. Bush, 1975, "Corn Growth as Monitored by Radar," RSL TR 177-57, University of Kansas, Center for Research, Inc., Lawrence, Kansas, November.
- Wilton, D. R. and R. Mittra, 1972, "A New Numerical Approach to the Calculation of Electromagnetic Scattering Properties of Two Dimensional Bodies of Arbitrary Cross-Section," IEEE Trans. on Ant. and Prop., AP-20, no. 2, pp. 310-317.

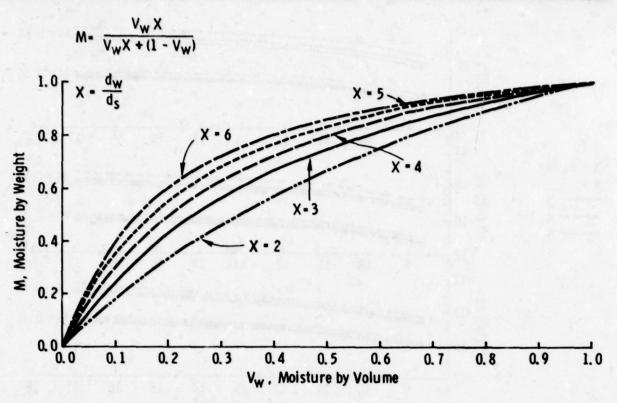


Figure 1. Relation Between the Volume Fraction of Water, V_N, in a Leaf and the Fraction of Water by Weight, M, in a Leaf

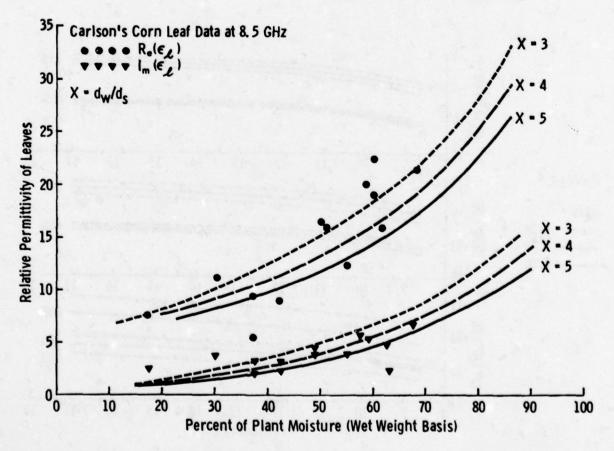


Figure 2. Comparison Between the Theoretical Permittivity Model and Measured Data

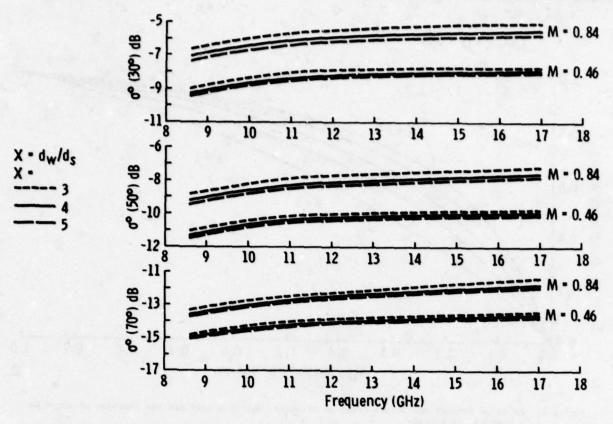


Figure 3. Theoretical Backscattering Coefficient Versus Frequency Curves for Different Incident Angles and Values of the Density Radio d_w/d_s

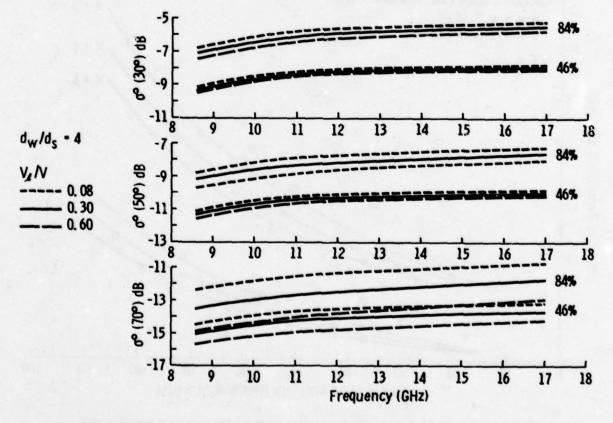


Figure 4. Theoretical Backscattering Coefficients Versus Frequency Curves for Different Incident Angles and Per Cent Volume of Vegetation in a Vegetated Medium

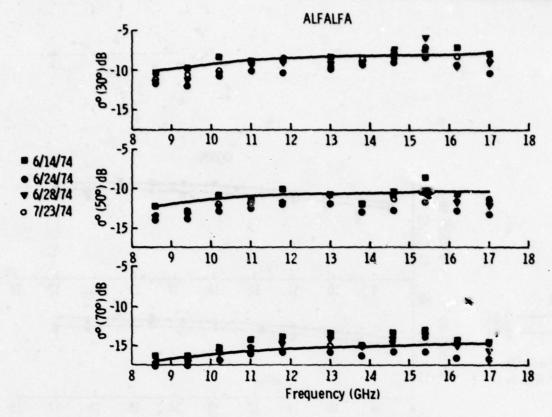


Figure 5. Comparison Between $\sigma^{\bullet}(\theta)$ and Measured Data from Alfalfa at Various Frequencies and Incident Angles

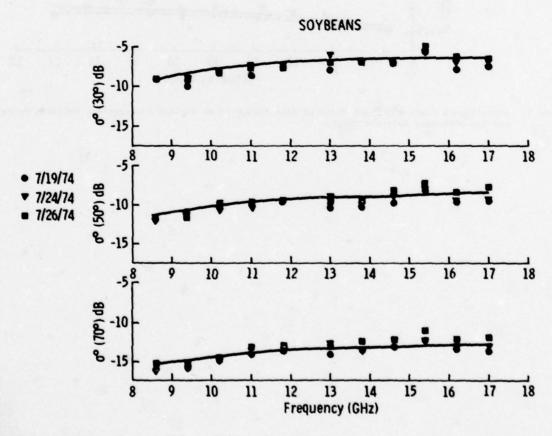


Figure 6. Comparison Between $\sigma^{\bullet}(\theta)$ and Measured Data from Soybeans at Various Frequencies and Incident Angles

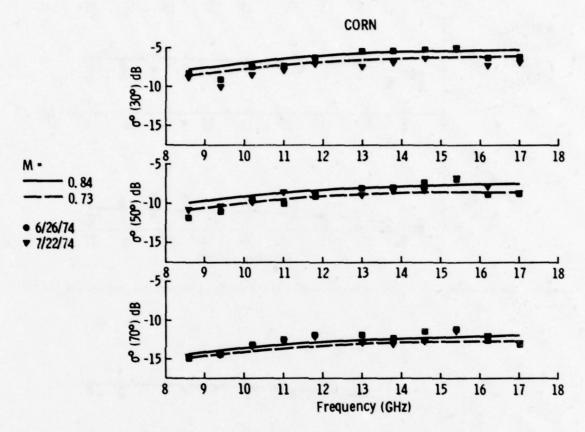


Figure 7. Comparison Between $\sigma^{\bullet}(\theta)$ and Measured Data from Corn at Various Frequencies, Incident Angles, and Two Different Moisture Values

VHF PROPAGATION PREDICTION WITH PATH PROFILE METHODS

B.K. LEE

British Aircraft Corporation Limited - A British Aerospace Company Electronic & Space Systems Group, Guided Weapons Division Filton, Bristol BS99 7AR England.

SUMMARY

Propagation prediction models applicable to VHF military type links in W. Germany have been derived. These relate to a static base station located to give good area coverage operating to various vehicular outstation sites. The initial stages of the work involved the measurement of propagation losses (and local signal variations) for 830 paths at 3 frequencies, and also the construction of a digitised topographic data base for the area considered. The latter enabled two dimensional path profiles with associated surface features (such as trees and buildings) to be rapidly produced between any two points within the data base area. The measured data were analysed in conjunction with the associated path profiles to produce prediction models for both the median propagation loss and the local signal variations as functions of the path profile. The standard deviation of prediction error for the former was 7.3 dB, whilst the average standard deviation for the signal distributions for the latter was 2.5 dB.

1. INTRODUCTION

The requirement for a VHF prediction method originated with the need to simulate the performance of proposed VHF communications systems for the British Army. In such simulations of communicability and electromagnetic compatibility the transmission loss is usually the least well defined parameter. In order to provide realistic predictions for deployments of equipments in W. Germany, it was necessary to obtain trials data in that area. Further, for optimum realism, it was decided to develop a path profile related method and this in turn required the production of a computerised topographic data base. Although path profile methods are in existence for certain situations, no validated approach applicable to military VHF links in W. Germany has been available.

The decision to develop a path profile method was taken because of the technical drawbacks of the simpler statistical terrain equations for the applications proposed. The latter approach (as demonstrated, for example, by Egli, ref.1) gives the mean value and standard deviation of path loss as a function of range, frequency and antenna heights for a given terrain type, site selection method and polarisation. This type of equation is of value in assessing and comparing the performances of systems in the conceptual stage. However, problems arise when considering specific deployments; for example, given terminal equipments at specified locations A and B, it is not always sufficient to use a statistical terrain equation to say that for such terminals at the range AB in this general type of terrain there is a 10% chance of successful communication. The link AB might be perfectly usable and may indeed fulfil an important operational role. It may well be carefully selected with regard to the path profile or known to be workable from prior experience. In order to reflect this dependence it is necessary to devise a prediction method based on a consideration of individual path profiles.

2. TERRAIN DATA BASE

2.1 General

A data base is required to produce terrain heights and associated surface features (such as trees) for paths within the area considered. A computerised digital data base is clearly desirable to enable profiles to be rapidly produced.

The accuracy of a path profile is determined by the basic accuracy of the data set, together with any interpolation errors. In the context of propagation loss prediction, the greatest precision is usually required near the terminals, particularly for a low or vehicle mounted antenna.

2.2 German Data Base

BAC have produced a computerised terrain data base covering a 200 x 85 km area within Germany. The terrain heights and surface features were extracted from points on 1: 50,000 maps using a variable grid size. In generally flat areas a 500 m square grid was used, in undulating terrain a 250 m grid and in hilly areas a 125 m grid. In the extraction of the terrain heights, the grid points were often situated between two contour lines and the heights were estimated by interpolation.

The surface features associated with each grid point were classified with one of 7 categories indicating such details as buildings, woods, open water and open ground.

2.3 Usage of the Data Base

With respect to the application to VHF propagation prediction, two simplifying assumptions were made. Firstly it was assumed that the two dimensional path profile sufficiently defined the propagation features. This disregard of the terrain bordering the path is probably justified for the area of Germany considered. In more mountainous areas, three dimensional effects such as reflections from mountain sides may be significant. It was further assumed that the effects of ray bending in the atmosphere due to the variation in refractive index with height could be included by the use of an effective earth radius of 4/3 true earth radius. This is referred to as a standard atmosphere (ref. 2). In order to represent rays on a profile as straight lines, the terrain elevations on each path profile were medified in accordance with the 4/3 earth radius.

3. DESCRIPTION OF THE VHF PROPAGATION TRIALS IN GERMANY

3.1 Introduction

The purpose of the propagation trial was to collect measured data for use with the EMC analysis of deployments of military equipments in Germany. Following a study of the terrain of West Germany and that of the UK, it was decided that to obtain representative measurements the trial would have to be held in West Germany. This was because the topography in W. Germany was characterised by distinctive heavily wooded high ground; in the UK most of the high ground is not covered by trees.

3.2 Measurement Equipment

The trials frequencies allocated were 41.9, 74.5 and 107.5 MHz. The base station radiated all three frequencies simultaneously from independent crystal controlled transmitters which supplied approximately 15 w of cw RF power at each antenna. A separate vertically polarised unipole antenna mounted on a Clark mast was used for each frequency with the antenna feed point 13 m above ground level. The masts were separated from each other by at least 3 wavelengths.

The vehicular receiver was designed to receive on only one of the three frequencies at any one time. This obviated the need for more than one antenna on the vehicle (a Landrover) with the attendant potential problems of distortion of antenna radiation patterns. The antenna used was a vertically polarised centre fed whip with a feed point about 2.7 m above ground level. The output from this antenna was connected through an antenna tuning unit and an adjustable attenuator to a frequency converter, which in turn fed a narrowband receiver set to 24 MHz. The IF bandwidth of this system was 400 Hz which gave the equipment the capability of measuring path losses of up to 164 dB. The minimum measurable path loss with the RF attenuators used was 72 dB. The received signal level was recorded both on magnetic tape and a pen recorder for each frequency and receiver location.

The standard deviation of path loss measurement error was experimentally found to be 2 dB, and this was largely due to the variations in the vehicular antenna radiation pattern with orientation.

3.3 Site Selection

The transmitter and receiver sites were selected taking into account the main purpose of the trial, namely the production of a set of measured propagation losses between base stations located on high ground and a number of randomly located mobile outstation sites. In conjunction with this was the need to have an accurate knowledge of the location of both the base station and the outstation as the measurements were to be used to develop a path profile related prediction technique.

One of the technical requirements of the sitings was to provide as complete a cross section as possible of the profile types within the trials area. The receiver site was further required to permit measurements to be taken by the mobile receiving vehicle over a distance of not less than 100 metres, and this implied that the receiver sites generally had to be on sections of road. As the measurements were to be repeated for each of the three frequencies, and the location had to be easily found on a map and recognised on arrival, road junctions were usually selected as receiver locations.

Seven transmitter sites and 830 receiver sites were used during the trial, although due to equipment malfunction not all three frequencies were measured at some of these receiver locations. The final data set comprised 2323 measurements with link ranges from 1.7 to 61 km.

3.4 Measurement Procedure

At each receiver location, a recording of the signal strength was made for each frequency in turn over a 100 metre range. This provided information on both the path loss and local signal fluctuations. A sketch map of the site was drawn and a photograph taken showing the terrain in the direction of the transmitter. These provided guidance on the local clutter around the receiver antenna. A sample of all the data taken at a receiver site is shown in Fig.1, together with a computer generated path profile.

Throughout the duration of the trial, both the transmitter and receiver equipment were regularly checked to ensure the accuracy of the measured path losses. On most days, one site would be repeated at the end of the day; this would either be a site used previously that day or a standard repeat site for the appropriate transmitter. Little variation of median path loss was found and usually measurements were within 1 dB of each other.

Since a common vehicular orientation would have been used, the spread implied by the 2 dB standard deviation of path loss measurement accuracy does not apply.

4. ANALYSIS OF RESULTS

4.1 Introduction

Each of the 2323 trials measurements was processed to produce the median path loss, the standard deviation of the signal variations and the upper and lower decile points.

Prediction models for the median signal level were produced using a data set comprising the median path losses and the associated path profiles. The statistical terrain approach, which permits comparison with the Egli model (ref. 1) is given in Section 4.2. A semi-theoretical and a statistical path profile related prediction method are described in Sections 4.3 and 4.4 respectively.

The statistics of the local signal variations were analysed in conjunction with the path profiles to produce a prediction model for the small sector signal distribution, Section 4.5.

4.2 Statistical Terrain Prediction Method

Although the propagation trials were not specifically designed to produce statistical terrain equations, a comparison with the Egli method (ref. 1) is appropriate since this relates to fixed to vehicular links at VRF. It was estimated that the population of results was sufficient to compare with Egli over the range interval 3 to 28 km and the frequencies covered by the trials.

An equation was derived by linearly regressing the trials data against log (Range) and log (Frequency) the results being as follows:-

Median Path Loss = 70.1 + 36.9 log10R + 9.9 log10F, dB ("all paths" equation)

Standard Deviation - 13.3 dB

where R is the link range in km and F the frequency in MHz.

In order to indicate statistically the effect of obstacles, subsets of the results were taken and statistical equations derived.

In the classification of path types, a line of sight path was defined as one where a line drawn between the two antennas cleared the terrain. Fresnel zones were ignored.

(a) Line of Sight Paths.

Median Path Loss = 72.0 + 27.8 log₁₀R + 7.8 log₁₀F, dB Standard Deviation = 8.7 dB.

(b) One Obstacle.

Median Path Loss = $75.5 + 28.3 \log_{10} R + 12.7 \log_{10} F$, dB Standard Deviation = 10.0 dB.

(c) Multiple Obstacles.

Median Path Loss = $93.1 + 19.3 \log_{10} R + 14.4 \log_{10} F$, dB Standard Deviation = 9.9 dB.

All the above equations are shown in Fig.2 for a frequency of 75 MHz, together with the Egli equation. The latter, for one antenna height greater than 30' and the other less than 30' may be expressed as follows:

Median Path Loss = 76.3 + 40 log10R + 20 log10F - Hg, dB

where H_C = 20 log₁₀ h_r + 10 log₁₀ h_R for h_r > 30', h_R < 30'

Standard Deviation = 5 log10F - 2 dB

where the range R is in km, the frequency F in MRs and the heights have in metres.

For the 13 m and 2.7 m antenna heights used in the German trials, the equation becomes:-

Median Path Loss = 49.7 + 40 log10R + 20 log10F, dB.

It is apparent from Fig.2 that the median loss predicted by the "all paths" equation is in close agreement with that of the Egli equation. However, the standard deviation of prediction error for the latter is much lower, probably due to the use of 1-2 mile sampling intervals for Egli's measured data (rather than 100 m).

4.3 Semi-Theoretical Path Profile Related Prediction Method

For this approach, it was assumed that the basic path loss was comprised of the free space loss plus additional losses introduced by the presence of the earth. The propagation features considered were diffractions over hills, reflections from the ground and scattering and absorption from clutter in the vicinity of the terminals. This afforded an opportunity to correlate the trials results with basic propagation theory. The procedure adopted was to start with the measured losses and subtract the losses due to each propagation mechanism.

Initially, the free space losses were subtracted from the measured losses and subsequently the diffraction, reflection and clutter mechanisms were considered in turn.

4.3.1. Free Space Loss

This was the standard formula:-

Path Loss - 32.4 + 20 log10R + 20 log10F, dB

for R in km and F in MHz.

4.3.2. Diffraction Loss

It was assumed that all obstacles could be considered as perfectly absorbing knife edges. Although obviously untrue for some situations, it was considered that for the terrain in the trials area it was a reasonable assumption for VHF frequencies.

Paths were categorised as follows.

(a) Line of Sight

On the basis of initial tests, the effect of below line of sight diffraction was ignored. For most paths this was a small loss; the maximum value would be 6 dB. The residual loss for each of these paths was calculated as the measured loss less the free space loss. The mean was 26.5 dB and the standard deviation 9.1 dB.

(b) Single Obstacle

For a single obstacle, the diffraction loss was calculated from the standard Fresnel integral (ref. 2). The residual losses, i.e. the measured losses less free space and diffraction losses, had a mean of 24.9 dB and a standard deviation of 10.4 dB.

(c) Multiple Obstacles

The extension of the single knife edge diffraction theory to two or more obstacles involves considerable mathematical complexity. Various approximations have been published, for example, Bullington, ref. 3, Epstein Peterson, ref. 4, Japanese atlas, ref. 5 and Deygout, ref. 6. In the analysis of the trials data, all four methods were tested. The Epstein Peterson method was finally chosen as this gave the best fit to the trials data. The mean residuals for 2, 3 and 4 edges were 25.6, 24.0 and 20.1 dB respectively, while the standard deviations of the residuals were 9.4, 9.7 and 9.7 dB.

4.3.3. Reflection Loss

The calculation of the loss caused by reflections from the earth's surface is more difficult to define than the diffraction loss, particularly for a computerised prediction model. This is mainly due to the difficulty of identifying significant reflecting planes using a computer. Given a profile, it is relatively easy for a trained observer to recognise by eye the position of the reflecting plane or planes. Further, the size of the reflecting plane may be considered and compared with the area cut by the first Fresnel zone associated with the ray, to indicate the significance of the reflection.

In practice, some assumptions were made to simplify the computation of the reflection plane location. In particular, for obstructed paths, it was assumed that the only significant reflection occurred on ground between the 2.7 m high receiver and nearest obstacle. Having defined a reflection plane, the reflection loss may be calculated from the effective antenna heights and reflection coefficient. The latter was theoretically computed from a knowledge of the signal polarization, frequency, reflection angle, permittivity and conductivity of the ground. This coefficient was modified using an empirical correction (ref. 2) related to the terrain roughness within the first Fresnel zone and the reflection angle. However, for the small reflection angles encountered, this factor was usually nearly unity. Following the procedure of producing the best fit of the residual losses, the transmitter effective height was referred to the reflection plane, but the receiver height was set to the actual antenna height. This clearly only involves a physical propagation mechanism when the receiver is located on the reflecting plane.

At this stage, the average value for the residual loss (that is the average of the measured losses less the free space, reflection and diffraction losses) was about 10 dB.

4.3.4. Clutter Loss

This is the loss attributable to local terminal conditions, such as trees and buildings. In order to calculate such a loss, a higher degree of detail of the terrain data base would have been required, for example, including such parameters as foliage/building heights and thicknesses. In the absence of such data on the profiles, the clutter loss was determined empirically against the trials data to produce an overall zero mean error. Profile features such as the data base definition of trees within 500 metres of the receiver and the angle between the ray and the ground in the vicinity of the transmitter were considered. In order to improve prediction accuracy, the data were subdivided into 5 different clutter categories for each path type (line of sight, single and multiple obstructions) and a total of 15 equations produced.

4.3.5. Prediction Equation

The equation produced was designed for use on the computer in conjunction with the terrain data base and since the details were complex, the full equation is not reproduced here. As described above, the equation has the form:-

Median Path Loss = Free Space Loss + Diffraction Loss + Reflection Loss + Clutter Loss.

When applied to the trials data, the overall average standard deviation of prediction accuracy for the 15 equations was 7.4 dB. The predicted loss relates to links from a 13 m high antenna to a 2.7 m high antenna. Although trials data were not obtained for other heights, the correlation of the results with Egli for 13 m/2.7 m antenna heights (Section 4.2) suggests that the Egli height gain factors would be appropriate. With these factors, the median propagation loss falls as the antenna height (h) is increased at a rate given by 10 log₁₀h for h less than 30 feet and at a rate of 20 log₁₀h for h above 30 feet.

4.4 Statistical Path Profile Related Prediction Method

4.4.1. Introduction

This prediction method was based on a statistical analysis of the measured median propagation losses and the associated path profiles. The analysis initially involved the establishment of a file of the path profile for each of the trials paths, from which a number of factors related to the prediction of propagation loss were evaluated. The mathematical technique of ridge regression was employed to determine the most suitable subset of these factors and multiple linear regression was used to give the coefficients.

The equation for propagation loss was set to the following form:-

where the x_i are the factors related to the path profile and the a_i are the coefficients. The factors (x_i) need not be linear, for example, log range was used.

The advantage of using this approach is that a lower standard deviation of prediction error can be obtained compared to the semi-theoretical approach above.

4.4.2. Factors Selected

The significant factors selected using ridge regression were as follows:-

- Log (R): This is Log₁₀ of the horizontal range in km between the transmitter and the receiver location.
- 2. Log (F): This is Log10 of the frequency in megahertz.
- 3. Diffraction Loss) The values in dB are calculated using the
- 4. Reflection Loss) approach given in Section 4.3.
- 5. Obstacle Width. This is the distance between the transmitter and receiver horizons in km.
- PR/MN This is the ratio of the distance of the obstacle nearest the receiver to the total
 path length.
- 7. Height PR-MN This is the height of the obstacle nearest the receiver (or the transmitter for line of sight paths) less the receiver height, in metres.
- 8. Height Trees. This factor is the average height of the trees (in metres) at the transmitter site.
- Number TX Trees. This factor is the number of 100 metre segments within 500 metres of the transmitter which are obstructed by trees.
- 10. Transmitter Clearance Angle. This is the angle in radians between the direct ray from the transmitter to first obstacle and the straight line fitted to the ground in front of the transmitter site.
- 11. Transmitter Gradient) This is the gradient of the ray from the antenna considered to the
- 12. Receiver Gradient) nearest obstacle in the path with respect to the horizontal.
- 13. Negative Weighted Receiver Clearance. This is produced by determining the ray clearance at 100 metre intervals within 500 metres of the receiver, and multiplying by a weighting factor which is 1 at the point nearest the receiver and 6 at the point furthest from the receiver.

4.4.3. Data Spreads

The data spreads of the above coefficients with respect to the trials results were as follows.

			PATH TY	PE			
	FACTOR	LINE	OF SIGHT	SINGL	E OBS.	MULTI	PLE OBS.
		MEAN	STD.DEV.	MEAN	STD.DEV.	MEAN	STD.DEV.
1.	LOG (R)	1.2	0.34	1.1	0.27	1.2	0.16
2.	LOG (F)	1.9	0.16	1.8	0.17	1.8	0.17
3.	DIFFRACTION LOSS	-	-	13.1	4.2	23.8	5.7
4.	REFLECTION LOSS	16.3	6.7	12.4	5.6	11.8	5.4
5.	OBSTACLE WIDTH		-	0.080	0.087	7.4	5.6
6.	PR/MN			0.70	0.29	0.87	0.15
7.	HEIGHT PR-MN	271	122	144	106	101	83
8.	HEIGHT TREES	11.0	6.7	12.8	7.5	13.8	8.6

FACTOR	LINE	OF SIGHT	SINGI	E OBS.	MULTIP	LE OBS.
	MEAN	STD.DEV.	MEAN	STD.DEV.	MEAN	STD.DEV.
9. NUMBER TX TREES	2.8	2.0	2.9	2.3	4.1	2.1
10. TX CLEARANCE ANGLE	0.068	0.06	0.074	0.07	0.035	0.057
11. TX GRADIENT	-0.021	0.016	-0.006	0.016	-0.0007	0.01
12. RX GRADIENT	0.021	0.016	0.054	0.041	0.066	0.038
13WT RX CLEARANCE	189	186	216	203	186	186
MEASURED PATH LOSS, dB	118.9	12.9	130.8	12.8	143.5	10.4

4.4.4. Prediction Equation

The coefficients of the regression equation are given below. As with the semi-theoretical approach, the regression equation was designed for use in conjunction with the terrain data base and the Egli height gain factor may be used.

COEFFICIENTS OF THE REGRESSION EQUATION

		PATH TYPE	
FACTOR	LINE OF SIGHT	SINGLE OBS.	MULTIPLE OBS
CONSTANT	78.9	42.7	58.8
LOG (R)	20.6	26.6	27.5
LOG (F)	6.9	16.2	9.7
DIFFRACTION LOSS	0.0	0.0	0.54
REFLECTION LOSS	0.27	0.22	0.14
OBSTACLE WIDTH	0.0	3.1	-0.07
PR/MN	0.0	14.8	23.1
HEIGHT PR-MN	0.0017	0.043	0.032
HEIGHT TREES	0.26	0.46	0.53
NUMBER TX TREES	0.77	1.05	-0.67
TX CLEARANCE ANGLE	-28.1	-25.1	-71.6
TX GRADIENT	76.1	39.3	274.6
RX GRADIENT	0.0	45.2	0.38
-WT RX CLEARANCE	-0.017	-0.013	-0.008
STANDARD DEVIATION OF PREDICTION ERROR, dB	6.8	7.7	7.0
MULTIPLE CORRELATION COEFFICIENT	0.85	0.80	0.74
NUMBER OF OBSERVATIONS	707	1017	599

OVERALL STANDARD DEVIATION OF PREDICTION ERROR: 7.3 dB.

4.5 Prediction of Small Sector Signal Variations

4.5.1. Introduction

This relates to the variation of the received signal strength when the receiving terminal is moved over a relatively short distance. The main cause of such variations is usually attributed to local clutter to the receiver, such as trees and buildings. Under severely cluttered conditions, for example an urban environment, the signal distribution would be expected to approximate to Rayleigh.

4.5.2. Analysis of Measured Data

The trials measurements provided data on the signal level variations over a 100 m range. The standard deviation of the signal distributions about the median and the upper and lower decile points were calculated for each measurement. The results showed that generally the upper and lower decile points were not symmetric about the median. It was found that a reasonable fit could be obtained to the trials data using two log normal distributions. Each of these distributions would have a zero mean and a standard deviation such as to fit either the upper or lower decile of the skewed distribution as appropriate.

In the first stage of the analysis of the results, the population was split into line of sight, single obstruction and multiple obstruction paths, with the following result.

PATH TYPE	UPPER	DECILE	LOWER	DECILE
Line of Sight	2.8	dB	2.7	dB
1 obstruction	3.4	dB	3.3	dB
multiple obstructions	3.6	dB	3.5	dB

This showed that diffraction along the path contributed to location variability. The data were further analysed with respect to a number of path profile features.

The regression analysis performed indicated high correlation with the following parameters.

- . Frequency
- . Number of obstacles on a path
- . Receiver clutter, i.e. the data base definition of trees/buildings close to an antenna.

Although receiver clutter was highly correlated for line of sight links, it was virtually uncorrelated for obstructed paths and this feature was not incorporated into the prediction model since the upper and lower deciles were relatively small for line of sight paths. It should be noted that this result was obtained from the data set of receiver locations measured and had these included a large proportion of urban situations, the small sector signal distribution would have been significant.

4.5.3. Prediction Model

The prediction model produced for the upper and lower deciles of the small sector signal distribution was as follows (log normal distributions were assumed).

(a) Upper Decile (i.e. higher propagation loss)

		PATH TYPE	
FREQUENCY (MHz)	Line of Sight	1 Obstacle	Multiple Obstacles
41.9	2.5 dB	3.0 dB	2.9 dB
74.5	3.0 dB	3.5 dB	3.8 dB
107.5	3.0 dB	3.7 dB	4.3 dB

(b) Lower Decile (i.e. lower propagation loss)

PATH	TVDE
PAIR	LIFE

FREQUENCY (MHz)	Line of Sight	1 Obstacle	Multiple Obstacles
41.9	2.3	2.8	2.8
74.5	2.9	3.5	3.5
107.5	2.9	3.7	4.1

Since log normal distributions were assumed, the deciles are equivalent to 1.3 x (standard deviation). Therefore, the corresponding standard deviations ranged from 1.8 to 3.3 dB and the average standard deviation was 2.5 dB.

These results apply to the low (2.7 m) vehicular receiver only.

The small sector prediction model performs two functions. First, it allows the selection of a representative additional loss or gain value to account for the uncertainty in the location of a halted vehicle. Secondly, the statistical description of the small sector signal variations allows a prediction of the type of fading that would be experienced by a moving terminal.

5. CONCLUSIONS

The analysis of propagation trials in Germany in conjunction with a computerised terrain data base indicated the following.

- The median propagation losses were similar to those reported by Egli, although the spreads were greater because of the shorter sampling distance.
- 2. A purely theoretical approach was found to be inadequate for the path profile analysis of the data and empirical methods were employed. Of the two prediction equations developed, the statistical path profile related method was more accurate than the semi-theoretical approach when applied to the measured data. Standard deviations of prediction error of 6.8 dB (line of sight paths), 7.7 dB (one obstacle paths) and 7.0 dB (multiple obstructions) were obtained for the statistical method.
- 3. The small sector signal variations were dependent most on the operating frequency and number of obstacles on a path, for the receiver sites measured. The distribution of signal levels was

slightly skew with respect to a simple log normal fit and the average standard deviation for the distribution was 2.5 dB.

6. ACKNOWLEDGEMENTS

The author wishes to thank colleagues who contributed to the work on which this paper is based. In particular, acknowledgement is due to Mr. C. Felix for his work on the propagation trials and the data analysis and Messrs. R.J. Morrow and R.G. Bryant for their work on the initial development of the prediction model.

The work was carried out as part of a Ministry of Defence Contract.

REFERENCES

- 1. Egli, J.J. "Radio Propagation above 40 Mc over Irregular Terrain". Proc. IRE. Oct. 57.
- Rice, P.L., Longley A.G., Norton K.A. and Barsis A.P. "Transmission Loss Predictions for Tropospheric Communication Circuits". National Bureau of Standards, Tech.Note 101, 1967.
- 3. Bullington, K. "Radio Propagation at Frequencies above 30 Mc." Proc. IRE. 1947. 35, pp 1122-1136.
- Epstein, J. and Peterson D. "An Experimental Study of Wave Propagation at 850 Mc/s." IRE. Trans. 1955 pp 595-611.
- 5. The Radio Research Laboratory. "Atlas of Radio Wave Propagation Curves for Frequencies between 30 and 10,000 Mc/s." Ministry of Postal Services, Tokyo, Japan.
- 6. Deygout, J. "Multiple Knife Edge Diffraction of Microwaves". IEEE Trans. 1966. AP.14, pp 480-489.

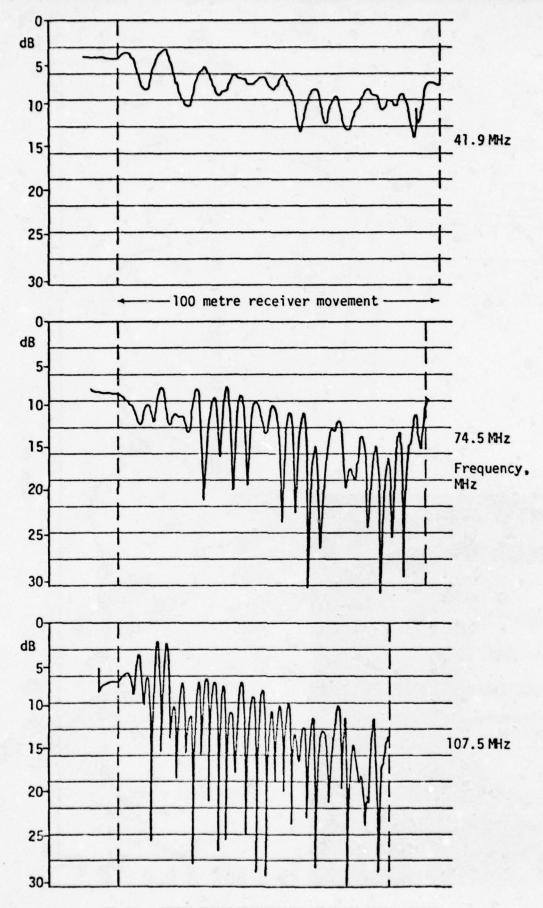


Fig.1a SAMPLE TRIALS MEASUREMENTS; MEASURED SIGNAL LEVELS

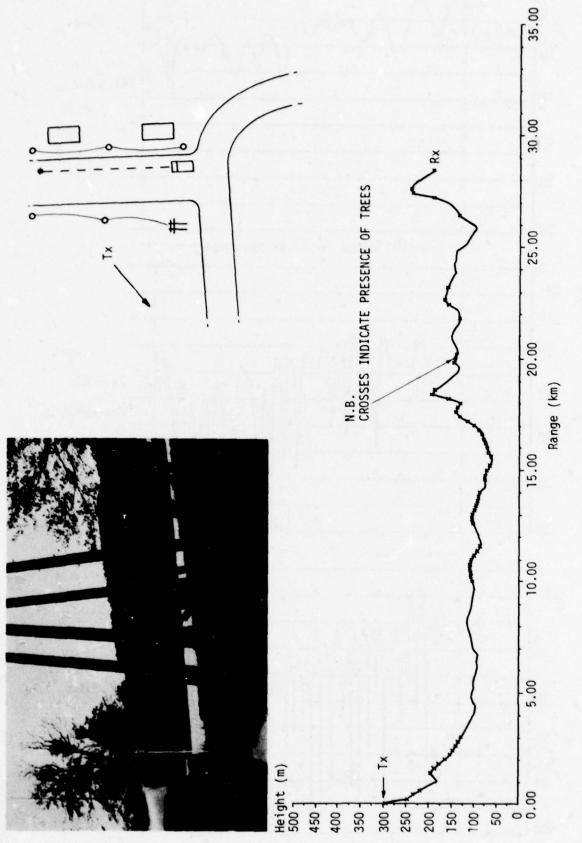


Fig.1b SAMPLE TRIALS MEASUREMENTS; PATH PROFILE INFORMATION

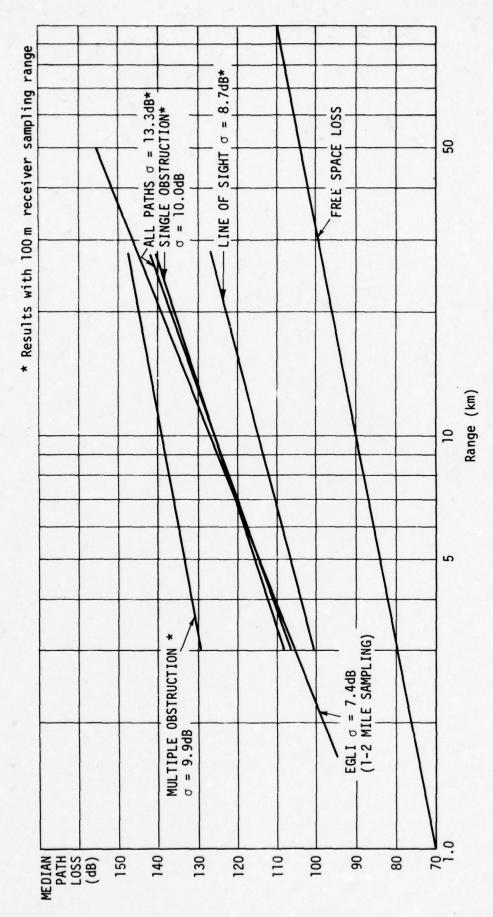


Fig.2 PROPAGATION LOSSES AT 75 MHz FOR A WELL SITED 13 m TRANSMITTER MAST OPERATING TO A RANDOMLY SITED 3 m RECEIVER MAST

Lars Ladell

National Defence Research Institute S-104 50 Stockholm Sweden

SUMMARY

Quite extensive measurements have been carried out in order to get a better knowledge concerning multipath characteristics in rural irregular terrain. These measurements have then been used in a comparison with two different theoretical models, which have been developed to more generally find out the behaviour of multipath propagation in different kinds of terrain. The aim of our investigation is also to present a kind of risk model for future digital UHF radio link systems.

In a deterministic theoretical model, the field strength of a delayed wave component is calculated assuming a given vertical reflection obstacle oriented for optimum reflection. From this model, the effects on multipath propagation by changing polarization, frequency or antenna height, may be assessed. By means of a Monte Carlo technique this deterministic model together with a statistical description of terrain characteristics have been utilized to create a stochastic model. It has been used for risk analysis of multipath propagation effects in different kinds of irregular terrain.

A measuring equipment has been developed, allowing a direct analysis of multipath propagation effects in irregular terrain. Measurements have been obtained from different rural paths at 445 as well as 900 MHz using vertical and horizontal polarization with two different antenna heights.

After a brief introduction the deterministic as well as the stochastic propagation model will be presented. Observed delay profiles from some different paths may exemplify the experimental results. A preliminary statistical analysis of multipath characteristics in rural irregular terrain will be given. These experimental results are then compared with corresponding theoretical results showing a comparatively good agreement.

1. INTRODUCTION

Wave reflections from obstacles in rural irregular terrain may possibly limit the maximum usable bit rate in digital radio communication systems. Most investigations so far have been dealing with urban paths and particularly from very large U.S. cities (Turin et al., 1972, Cox, 1972). In this paper we will only deal with rural irregular terrain with hills, mountains and valleys, sometimes covered with vegetation, but with no or unimportant housing. The present investigation has been limited to the UHF region, and to 445 and 900 MHz in particular, where bit rates of the order of 1 Mbit/s are of practical interest for radio links.

In the UHF band there are of course many different phenomena which yield wave components with different time delays. If these multipath components are strong enough and the time delays relative to the wanted wave are of the order of one data element or more, there is a risk for severe disturbance on that path. The most significant phenomenon seems to be wave reflection from near vertical terrain obstacles such as large blocks of stones, mountain sides, etc. Other phenomena, more or less insignificant, are wave diffraction around large terrain obstacles, wave scattering form small-scaled obstacles in the rural terrain, and wave reflection from aircraft, tropospheric layers and possibly ionospheric layers comprising auroras and meteor trails. In this paper we will only treate the main disturbing phenomenon which thus is terrain reflection.

Multipath characteristics can be given in at least two ways. Either as a deterministic description of wave amplitude vs. time delay corresponding to a given set of obstacles in the surrounding terrain, or as a statistical description giving the probability that multipath components of a given strength and time delay will occur on a random path.

2. WAVE PROPAGATION - MODELS

A deterministic description of reflection from obstacles in irregular terrain requires some assumptions and simplifications (Ladell, 1976 and 1977 a). Let us consequently assume:

- 1. The obstacle is surrounded by a smooth flat earth.
- 2. Only one reflection obstacle at a given position is taken into account.
- 3. The reflection obstacle is replaced by a vertical rectangular rough flat surface with height A and width B. The center of the surface is situated at a height H above ground.
- 4. The obstacle surface, which has a relative dielectric constant ϵ_{r} , is oriented for optimal reflection (specular reflection). It has a roughness parameter Δh (10 % to 90 % level).
- 5. Geometrical opcics may be applied.

The main calculation parameters and the geometry can be seen in figure 1. Wave components reflected from obstacles situated on the same ellipse with transmitter (T) and receiver (R) in foci have the same time delay relative to the direct path transmitter to receiver. This will be denoted the relative time delay At in the following, With a bit rate of the order of 1 Mbit/s, we are interested in time delays from around 1 us and more.

Transmitter as well as receiver are assumed to be equipped with arbitrary directional antennas directed against each other. The obstacle (0) is seen under an angle $\phi_{\rm T}$ from the transmitter (R-T-O) and ϕ_R from the receiver (T-R-O) giving corresponding antenna pattern factors $g_{\eta}(\phi_R)$ and $g_{R}(\phi_R)$. Easy geometrical calculations together with our assumption No. 4 give the grazing angle ψ at the reflection surface. Let us assume that the obstacle reflection can be described by the usual Fresnel reflection coefficient Ro with a correction factor p taking the surface roughness into account.

One of the most important parameters regarding multipath propagation is the signal strength of the delayed component measured relative to the wanted direct wave. Let us consequently define the relative field strength AE as this ratio. The purpose with this deterministic model is to calculate the relative field strength for a given set of parameters, as given in figure 1, as a function of obstacle position. This position, given by two co-ordinates, is also equivalent to a specific time delay.

To calculate the propagation factor F on the path T-O-R, see figure 1, it is suitable to mirror the transmitter T in the surface 0 to its image T'. The new path T'-O-R then lies in a plane and is easier to handle. In this configuration transmitter T' illuminates receiver R through an aperture 0 with height A and width Bsin ψ reducing the field by the factor ρ . R_0 . The propagation factor F_{TOR} is now evaluated by means of a four-ray-approximation. Ground reflection has been comprised as well as diffraction through the reduced aperture. Diffraction loss is calculated using the well-known Fresnel and Kirchhoff theory.

The relative field strength can be written
$$\Delta E = \begin{bmatrix} g_{T}(\phi_{T}) & g_{R}(\phi_{R}) \\ g_{T}(0) & g_{R}(0) \end{bmatrix} & \frac{d}{r_{T} + r_{R}} \cdot \begin{vmatrix} F_{TOR} \\ F_{TR} \end{vmatrix}$$
(1)

where the propagation factor FTR on the direct path T-R in most cases can be approximated by (cf. assumptions Nos. 1 and 5).

$$F_{TR} = 2 \cdot \sin \frac{2\pi h_T h_R}{\lambda d} \tag{2}$$

where as usual & denotes the wave-length.

By means of the four-ray-approximation the delayed wave component can be written

$$\mathbf{F}_{\text{TOR}} = \rho \cdot \mathbf{R}_0 \cdot \mathbf{F}(\frac{\mathbf{v} \cdot \mathbf{Bsin}^{\psi}}{2}) \cdot \left[\mathbf{F}_1 + \mathbf{F}_4 - (\mathbf{F}_2 + \mathbf{F}_3) e^{\mathbf{j}\phi} \right]$$
 (3)

where the symbol F (without index) is the Fresnel integral

$$F(x) = \int_{0}^{x} \exp \left(j \frac{\pi}{2} v^{2}\right) dv \tag{4}$$

Furthermore we have

$$\mathbf{v} = \left[\frac{2}{\lambda} \left(\frac{1}{r_{\rm T}} + \frac{1}{r_{\rm R}}\right)\right]^{1/2} \tag{5}$$

$$\phi = \frac{4\pi h_T h_R}{\lambda (r_m + r_R)} \tag{6}$$

The roughness correction factor may in the most simple case be written

$$\rho = \exp\left[-8\pi^2(\frac{\Delta h \cdot \sin\psi}{\lambda})^2\right] \tag{7}$$

This factor seems to reduce the wave component too much for large values on the parameter $\Delta h \cdot \sin \psi / \lambda$ which in some cases may require a modification.

The four different rays which determine the delayed field component can be described by means of the following factors

$$F_{1,2} = F[v(H - \kappa_{1,2} + A/2)] - F[v(H - \kappa_{1,2} - A/2)]$$
 (8)

and

$$F_{3,4} = F[v(H + \kappa_{2,1} + A/2)] - F[v(H + \kappa_{2,1} - A/2)]$$
 (9)

where

$$\kappa_1 = \frac{r_{\rm T}h_{\rm R} + r_{\rm R}h_{\rm T}}{r_{\rm T} + r_{\rm R}} \tag{10}$$

Most geometrical parameters are explained in figure 1.

It has been shown (Ladell, 1976) that, in practice, the limitations caused by the assumptions do not affect the relative field strength very much. The model has been generalized to a smooth spherical earth as well as comprising the surface wave (cf. assumptions Nos. 1 and 5).

This deterministic model is based on very simple theoretical considerations. Nevertheless, it has much to tell about the influence on digital systems when changing the frequency, polarization, antenna heights, etc. (Ladell, 1976 and 1977 b).

The deterministic model does not give any information at all regarding the risk level when multipath propagation effects limits the bit rate. That is the reason why it is essential to have a pure stochastic model based on wave propagation theory and a suitable terrain description. This stochastic model, which is presented below, is based on simulation technique including the complete deterministic model (Ladell, 1977 a).

The terrain description given below is an attempt and may be adjusted in the future by means of experimental experiences. The terrain region is primarily characterized by the obstacle density, which is the number of reflection surfaces per km² exceeding a certain level (for instance 1 m²). The obstacle co-ordinates are assumed to be uniformly distributed within the actual terrain region.

In the deterministic model all surfaces were assumed to be oriented for specular reflection but in the stochastic model the angle of orientation, which is the direction of a normal vector relative to north, is assumed to be uniformly distributed between 0 and 2m radians. The reflection condition is now altered from a fix orientation to a certain interval depending on the nominal grazing angle. This is due to the real wave structure instead of ray optics.

The size of the obstable surface was given by A and B in the previous. We have tried to estimate the cumulative distributions for these parameters in some "typical" terrain region. Numerically we have put a median value of 5 and 10 m for A and B, respectively, with an upper limit of 100 m for both. Also the height H from ground to the center of the surface is given a stochastic description with a median value such that the lower boundary of the surface is at ground level (lowest possible!) The height of this lower boundary does not exceed 80 m in the assumed terrain model.

The roughness parameter Δh is assumed to be uniformly distributed between 0 and a specified maximum value. The correction to the reflection coefficient by equation (7) is intended to take the real surface structure into account.

Using a suitable random number generator in the computer, it would now be possible to calculate the relative field strength ΔE vs. relative time delay $\Delta \tau$, which means a calculated delay profile. This is done by means of the deterministic model. However, one stochastic parameter remains before the stochastic model is complete. It is the field strength variability, which is well-known from analogous technique. The cumulative distributions of the signals F_{TOR} and F_{TR} in equation (1) are assumed to be log-normal (Ladell, 1977 a). The random number generator then gives the final relative field strength in the different cases.

This Monte Carlo technique makes it possible to simulate a large number of multipath propagation "measurements" by computer. Every single synthetical measurement creat s its own needful parameters by means of the random number generator and the specified cumulative distributions.

This stochastic model is based on a relative large number of terrain parameters which are poorly known. They may be adjusted either by means of a better knowledge of terrain structure, or by results from measurements. Then the model acts as a cheap instrument for testing the influence on different system parameters.

3. MEASUREMENTS

In order to produce a good validity for the models it is necessary to perform measurements for verifications and modifications. This is done with a wideband system using the correlation properties of pseudorandom shift register sequences in a manner essentially equivalent to channel probing with a short RF pulse. The measuring equipment has been described in detail by others, e.g. for multipath propagation studies in urban areas (Cox, 1972).

The just finished measurements have been obtained on 52 different paths. Of these are 10 paths analysed only with the frequency 445 MHz and 16 paths with 445 as well as 900 MHz at the same sites. These 26 paths are all rural from the south-east part of Sweden where the terrain may be characterized as hilly. Furthermore, 20 rural paths are from the north part of Sweden with hilly of mountainous terrain analysed with 445 as well as 900 MHz. The remaining 6 paths are from Stockholm City and thus typical urban paths analysed with 445 and 900 MHz. In this paper the discussion will be restricted only to the 16 paths analysed with two frequencies from the south-east area.

Both transmitter and receiver are mobile and equipped with a 17 element Yagi antenna at the top of a mobile telescopic tower which can be elevated between 10 and 20 m. The radiated power from the transmitter has been chosen to about 80 W. On-line processing by means of a computer at the receiver makes it possible to control the experiment in real time. The 16 paths in the actual study are representing distances between 8.5 and 47.1 km with a median distance of 19.5 km.

Before presenting statistics from the whole material it may be instructive to study some individual delay profiles, which are defined as the relative field strength vs. relative time delay. Figure 2 shows the measured delay profiles obtained on a relatively short path, only 8.5 km, with the two frequencies 445 and 900 MHz and for different antenna polarizations. The antenna heights were just above 20 m each. In all four different propagation cases the pulse far to the left with a relative field strength ΔΕ = 0 dB and a relative time delay Δτ = 0 us indicating the direct wave. It has been propagated along the shortest path between transmitter and receiver. Multipath components are observed with various amplitudes and delays. Components which are 40 dB less than the direct wave can be observed with relative time delays less than 9 μs. Let us define the mostrisky multipath component as the one which has the greatest amplitude for a relative time delay greater than 1 μs (cf. 1 Mbit/s). From figure 2 these risky components have the following amplitudes: -23 dB at 445 MHz using vertical polarization (hereafter denoted 445 VP, etc.), -35 dB at 445 HP -24 dB at 900 VP, and -38 dB at 900 HP. These values seem satisfactory and the risk for disturbing multipath propagation is negliable.

The next example of the measurements is illustrated in figure 3 with four propagation cases equivalent to the previous example. The transmission loss on this 19.5 km path is rather large and this has somewhat reduced the possibility to observe very small multipath components. This new observation limit is in this case -28 dB at 445 MHz and -20 dB at 900 MHz. The risky components in figure 3 have the following amplitudes: -12 dB at 445 VP, -22 dB at 445 HP, -7 dB at 900 VP, and less than -20 dB at 900 HP. Digital transmissions using vertical polarization at both 445 and 900 MHz will consequently be more or less severe affected by multipath propagation on this path. By using only horizontal polarization the risk for multipath disturbances is negliable.

Both examples studied so far are not typical for the whole measurements. In fact they are the two worst examples out of the 16 in the present study, Figure 4 shows some more typical results taken on a 37.0 km path. This time the multipath components are very small and may not affect a digital transmission system at all. The risky components are in this case: -36 dB at 445 VP, -39 dB at 445 HP, -31 dB at 900 VP, and less than -40 dB at 900 MHz using horizontal polarization.

The measurements were performed with two different combinations of antenna heights. Besides an antenna height of 20 m, which is the actual value in this study, also 10 m was analysed. At this early stage in the analysis it may be noted that 10 m antenna heights cause considerably stronger multipath components than 20 m. This observation and the fact that vertical antenna polarization is more risky than horizontal, illustrated by the figures 2, 3 and 4, confirm results obtained from the deterministic model (Ladell, 1976 and 1977 b).

4. COMPARISON BETWEEN MODELS AND MEASUREMENTS

It is possible to collect the results from the measurements in different ways. In the present study it is made by presenting the probability contours $p(>\Delta E,>\Delta \tau)$. That means the probability for multipath components with a relative field strength exceeding a fixed level ΔE and with a relative time delay exceeding another fixed level $\Delta \tau$.

Figure 5 shows a comparison between the measurements and results from the stochastic model for the case with 445 MHz, vertical antenna polarization and using directional antennas situated 20 m above ground. A probability of 1/16, for instance, means that in one case out of the 16 the values on ΔK and Δτ, given by the solid line, was exceeded. A statistical result based on only 16 individual measurements is very weak, indeed, but nevertheless since experimental activity of this kind is very expensive it has been necessary to accept this limitation. May be these paths are representative for the whole terrain region. The most uncertain statistics are the low probability values, e.g. 1/16 and 2/16. Keeping this weak statistical base in mind figure 5 gives a probability for disturbing multipath propagation of the order of 6 \$ (~ 1/16) if the transmission system can accept ΔE < -10 dB for Δτ > 1 μs. This probability value may also be denoted as the actual risk level.

In figure 5 the results obtained from the stochastic model has also been given by dashed lines. Only one single set of terrain parameters has been tried so far why a better agreement may be possible. In the calculations it was assumed that the obstacle density was 50 surfaces per km^2 , where each surface had a maximum surface roughness of $\Delta h = 0.2$ m. That means on the average one surface on each square with a side equals 141 m and where the surface is rough with a deviation from the mean of about \pm 0.1 m or less. Furthermore, each individual calculation is repeated 500 times which means that 500 different measurements are simulated compared with the actual 16 in this study.

In spite of the large number of terrain parameters which are poorly known it seems to be quite a good correspondence between the results from the stochastic model and the actual measurements. The risk level, defined earlier, may be extrapolated to about 2 % for this propagation case given by the model.

The next case under consideration is 445 MHz, horizontal polarization, and using directional antennas at a height of 20 m. In comparison with the previous case the antenna polarization has been changed. Figure 6 shows the result from the measurements and model. This time it seems to be a discrepancy between the two sets of curves especially for low probabilities. This may be explained primarily as a result of the weak statistically base. One single path with strong multipath components are probably not representative for the whole terrain region. The probability contours, except p = 1/16, seem to coincide quite well. From the figure it is possible to obtain a value on the risk level. The experimental results give a rather overestimated value of about 6 % why the stochastic model gives a value of only about 0.5 %.

Changing the frequency from 445 to 900 MHz would produce a 12.2 dB increase for the multipath components assuming they were smooth (Ladell, 1976 and 1977 b). For rough surfaces, as assumed in this paper, this strong increase will be reduced and even changed to a decrease depending on the roughness parameter and the grazing angle. Figure 7 shows the statistics from the measurements at 900 MHz using vertical polarization together with the results from the simulation. Only results from 15 paths are used at 900 MHz because too large transmission loss eliminated one path. A comparison between the two frequency cases using vertical polarization, figures 5 and 7, shows a very close correspondence, which may surprise.

The contours at 900 MHz are steeper than those at 445 MHz which means that the probability to find multipath components with a given strength with large relative time delays are less at 900 than at 445 MHz. The simulation does not show this steep tendency. From figure 7 the risk level may be obtained, resulting in about 10 % for the experimental results and 3 % approximately for the stochastic model. Thus, on the average, a doubling in frequency from 445 to 900 MHz does not result in any remarkable change in probability levels in this kind of terrain.

The last example showing probability contours is figure 8 for a frequency of 900 MHz, horizontal antenna polarization and an antenna height of 20 m using 17 element Yagi antennas directed against each other. As in the previous case the curves at 900 MHz are steeper than those at 445 MHz and possibly also reduced in strength somewhat. From figure 8 the risk level is obtained to about 5 % from the measurements and to 0.3 % approximately from the stochastic model. This deviation may also be explained by a too disturbed path which is not representative for the whole region.

The measurements from the south-east part of Sweden presented here were performed in June 1977 while the measurements from the north part of Sweden were performed in September 1977. The time for data reduction has thus been too short for a more complete comparison of the statistically properties of multipath propagation in rural irregular terrain. The results obtained seem to confirm the validity of the presented models although the analysis of the measurements is not complete.

With the assumed definition of a risk criterion it is observed that the risk level for 445 as well as 900 MHz at vertical antenna polarization using directional antennas at a height of 20 m is

of the order of 3 % neglecting the influence of a single strong disturbed path. With the same argument the risk level using horizontal antenna polarization is only of the order of 0.5 %. It seems to be no preference of using one of the two frequencies before the other, while using horizontal antenna polarization is much less risky than using vertical, regarding the influence of multipath propagation. As mentioned before it is also less risky to use high elevated antennas than low.

One observation obtained from the statistical properties of multipath characteristics is that the probability contours from measurements are more steeper than those from the stochastic model, particularly at 900 MHz.One possible explanation of this discrepancy may be that wave propagation on the three paths T-R, T-O and O-R, see figure 1, are not of the simple flat earth case. The signal attenuation on the two distant paths T-R and T-O, assuming the obstacle 0 is situated in the neighbourhood of the receiver R, are generally correlated (Ladell, 1977 a). Therefore the multipath signal strength is most sensitive to the attenuation on the short path O-R. The shielding effect caused by the irregular terrain will consequently reduce the relative field strength. Modifying the stochastic model with such increased attenuation on the short path O-R would thus result in steeper contours, more at 900 MHz and less at 445 MHz, just as observed from measurements.

5. CONCLUDING REMARKS

Two theoretical models have been developed using rather simple assumptions, one deterministic and the other stochastic. It has been possible to analyse the influence of different system parameters on multipath propagation. Preliminary results from quite extensive measurements in rural irregular terrain seem to confirm the confidence of the presented models.

Measurements at 445 as well as 900 MHz from the same sites have been analysed path by path in order to give a deterministic explanation of the multipath components observed. Furthermore, results from the measurements have been collected in a way such that multipath propagation can be described statistically. This statistics has been compared with results from the stochastic model.

It is obvious from the deterministic model that a higher frequency gives stronger multipath components if the obstacle surface is assumed to be smooth. So is seldom the case in real terrain. Assuming that the surface is rough has thus shown much better agreement with measurements. In reality a higher frequency gives stronger or weaker multipath components depending upon the surface roughness parameter and the grazing angle. It seems therefore in general to be no real advantage in choosing one of the frequencies before the other in order to reduce multipath disturbances.

Measurements as well as models have shown that a less elevated antenna is more risky than a more elevated and that using vertical antenna polarization is more risky than using horizontal, regarding the presence of strong multipath components causing disturbances.

One system parameter we have not discussed so far is the antenna and its influence on multipath propagation. As seen from equation (1) it is obvious that the antenna pattern has a discriminating effect on multipath components provided that the antennas are directional and directed towards each other. From the actual measurements it is known that an omnidirectional antenna produces much stronger multipath components. In order to reduce multipath propagation effects it is consequently necessary to choose as directional antennas as possible.

Using 17 element Yagi antennas the risk probability obtained in the present study in hilly terrain is of the order of 3 % at 445 as well as 900 MHz using vertical antenna polarization and 20 m antenna heights. Changing the antenna polarization to horizontal gives approximately only 0.5 % risk probability. That means 6 and 1 severe disturbed paths out of 200, respectively.

6. ACKNOWLEDGEMENTS

The author wishes to thank Messrs. Nils Berggren, Björn Fredriksson, Krister Gunmar and Folke Land at the National Defence Research Institute and Klas-Rune Larsson formerly at the NDRI for the development of the measuring equipment and for the stimulating co-operation during the measurements.

7. REFERENCES

COX, D.C. (1972), Delay doppler characteristics of multipath propagation at 910 MHz in a suburban mobile radio environment, IEEE Trans Antennas Propagat, AP-20, 625-635.

LADELL, L. (1976), Multipath propagation in irregular terrain at VHF and UHF: General considerations and recommendations, National Defence Research Institute, Stockholm, Report A 30007-E2 (In Swedish).

LADELL, L.(1977 a), Multipath propagation in irregular terrain at UHF: Risk analysis by means of simulation techniques, National Defence Research Institute, Stockholm, Report C 30089-E2 (In Swedish).

LADELL, L.(1977 b), Multipath propagation over irregular terrain at UHF, Proc URSI Commission F, La Baule 1977, 469-474.

TURIN, G.L., et al. (1972), A statistical model of urban multipath propagation, IEEE Trans Vehicul Technol, VT-21, 1-9.

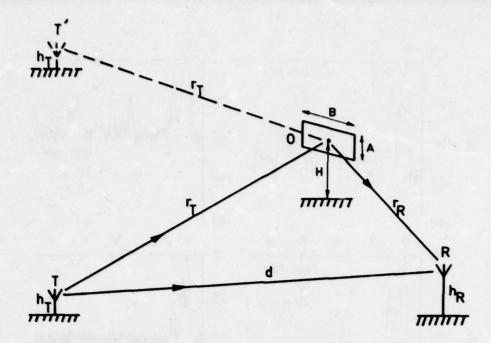


Fig. 1 Three-dimensional geometry for the propagation paths.

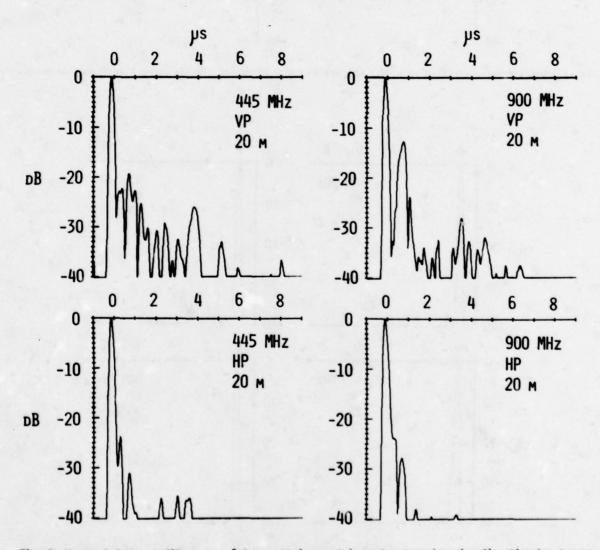


Fig. 2 Observed delay profiles on an 8.5 km path in rural irregular terrain using directional antennas.

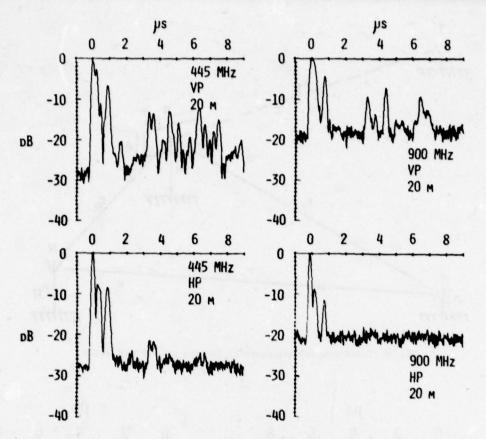


Fig. 3 Observed delay profiles on a 19.5 km path in rural irregular terrain using directional antennas.

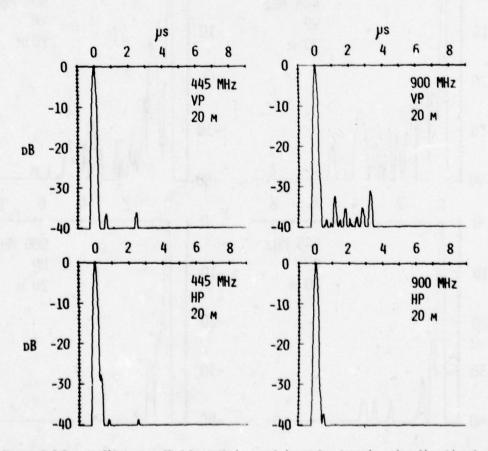


Fig. 4 Observed delay profiles on a 37.0 km path in rural irregular terrain using directional antennas.

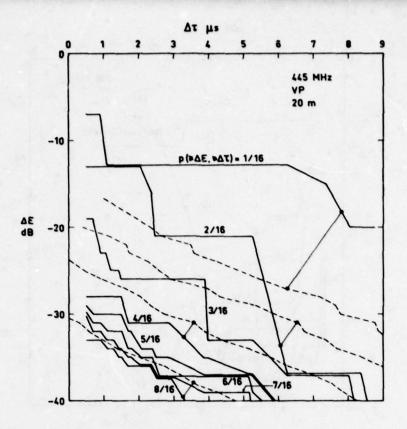


Fig. 5 Probability contours p(\$ΔΕ,\$Δτ) at 445 MHz in rural irregular terrain using vertical polarized directional antennas. Solid lines are measured data and dashed lines calculated data by simulation.

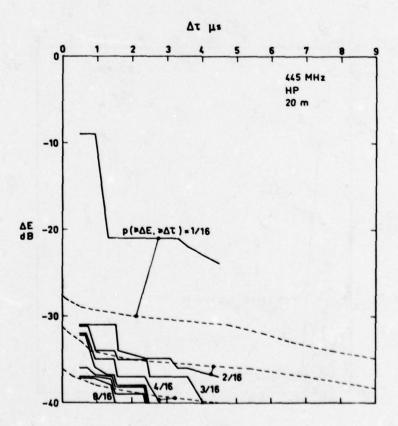


Fig. 6 Probability contours p(>ΔΕ,>Δτ) at 445 MHz in rural irregular terrain using horizontal polarized directional antennas. Solid lines are measured data and dashed lines calculated data by simulation.

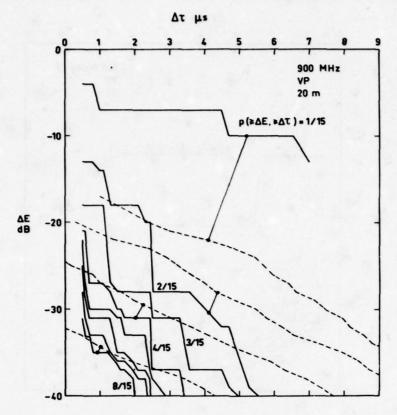


Fig. 7 Probability contours p(>ΔE,>Δτ) at 900 MHz in rural irregular terrain using vertical polarized directional antennas. Solid lines are measured data and dashed lines calculated data by simulation.

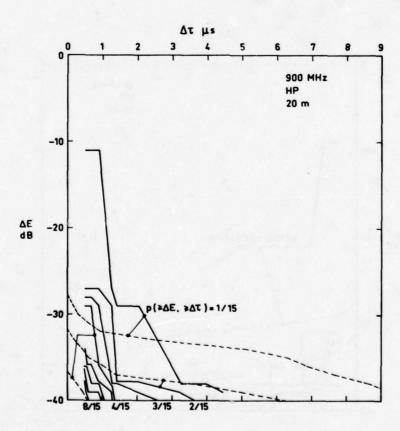


Fig. 8 Probability contours p(→ΔE,→Δτ) at 900 MHz in rural irregular terrain using horizontal polarized directional antennas. Solid lines are measured data and dashed lines calculated data by simulation.

INTERCEPTION OF SIGNALS TRANSMITTED VIA METEOR TRAILS

by

A.N. Ince SHAPE Technical Centre P.O. Box 174 The Hague Netherlands

SUMMA RY

In order to test the vulnerability of meteor-burst signals to interception and jamming, a 1000 -km circuit between La Crau, near Toulon, France, and Staalduinen near The Hague, Netherlands, was monitored at five different locations. These were Harrogate in the UK, Saclay near Paris, Breisach near Freiburg, Santa Marinella near Rome, and Noordwijk, some 35 km from the terminal at Staalduinen.

It was found that at Noordwijk the same signal bursts were received as at the northern terminal some 35 km away, and interception was practically total. At the other four locations, interception was mainly due to the simultaneous occurrence of two meteor trails reflecting waves in different directions. The amount of information intercepted was on the average between 3% and 16%, but could occasionally be 100% due to sporadic-E layer reflections. However, the experiments used a frequency of 36 MHz; by operating at 70 MHz or higher interception due to abnormal ionospheric propagation conditions could be virtually eliminated.

It is estimated that jamming a meteor-burst link from beyond the horizon would be very inefficient unless considerable power were used, since the power ratio is about 25 to 1 in favour of the link at 40 MHz. At higher frequencies the advantage for the link would be much greater.

The results of the interception tests show that meteor-burst systems can be used for broadcasting provided that three separate antenna systems are employed to cover ranges up to 2000 km and to repeat the message continuously from one to several minutes to achieve a high probability of reception. Frequency sharing between several meteorburst links operating in the same area also appears to be feasible with frequencies high enough to eliminate ionospheric scatter and sporadic-E layer reflections.

INTRODUCTION

Meteor reflections and their application to communication have been investigated at SHAPE
Technical Centre (STC) over a period of several years. These studies led to the development of a system
named COMET [1] (Communications by Meteor Trails) which makes use of a combination of space and frequency
diversity reception and the technique of automatic request for repetition (ARQ). This system has the
advantage over the earlier Janet-type systems [2] of making efficient use of the available duty cycle while
at the same time keeping the error rate under control. A block diagram of COMET is shown in Fig.1. The
system was tested for several years on a 1000-km path between the Netherlands and Southern France at
frequencies in the 40 and 100 MHz bands. Transmitting and receiving antennas were five element Yagi arrays
with a free-space gain of 10 dB relative to isotropic, and having a beamwidth in the horizontal plane of
50° between 3-dB points. Instantaneous transmission speed was 2000 bands and frequency-shift keying (FSK)
with + 3 kHz deviation was used. The performance obtainable at different frequencies is shown in Fig. 2.
The relationships found between the duty cycle, D, the wavelength, \(\lambda\), and the transmitter power, P, are

$$D \sim \lambda^4$$
 (1)

and

$$p \sim p^{0.6}$$
 (2)

It is to be noted that the simple theory, ignoring ceiling effects and the loss of efficiency due to short bursts, would predict a frequency dependence of the form

$$D \sim \lambda^{2.5}$$

At 40 MHz, and with a transmitter power of 200 watts, the COMET system maintained, over the test circuit, a 24-hour average capacity roughly equivalent to three 50-baud telegraph channels (duty cycle of 7.5%) and an error rate better than 1 in 3000 for 90% of the time. High reliability communications are therefore possible with meteor-burst systems. This feature, coupled with the simplicity of fixed-frequency operation at frequencies which are not very much affected by ionospheric disturbances, makes the meteor-burst system potentially suitable for military applications.

The purpose of the present paper is to report on a series of experiments which were carried out in parallel with the communications tests conducted on the circuit itself to find out principally the extent to which the transmission is immune from interception and interference. These are features of great interest, particularly for the military. Using the results obtained from the interception tests the paper also discusses the possibility of operating several meteor-burst links at the same frequencies in the same geographical area (frequency sharing), and the suitability of meteor-burst propagation for broadcasting or for communicating simultaneously between a central station and a limited number of peripheral stations.

2. THEORETICAL CONSIDERATIONS

The need to investigate the various aspects of meteor-burst communications mentioned in the previous section arises from the fact that meteor trails are known to reflect radio signals in certain

privileged directions. The full transmission equations for underdense (equation (3)) and overdense (equation (4)) meteor trails are given below:

$$\frac{P_{R}(t)}{P_{T}} = \frac{G_{T}G_{R}^{3} \frac{3^{2} r_{R}^{2} sos}{sos^{2} \mu}}{16\pi^{2} R_{T}R_{R}(R_{T}^{2} + R_{R}^{2})(1 - \cos^{2}\beta sin^{2}\psi)} = \exp\left(\frac{8\pi^{2} r_{O}^{2}}{\lambda^{2} sec^{2}\psi}\right) \exp\left(\frac{32\pi^{2} dt}{\lambda^{2} sec^{2}\psi}\right)$$
(3)

$$\frac{P_{R}(t)}{P_{T}} = \frac{G_{T}G_{R}^{\lambda^{2}\cos^{2}\mu}}{32\pi^{2}R_{T}R_{R}(R_{T}+R_{R})(1-\cos^{2}\beta\sin^{2}\psi)} \left| \frac{4dt+r_{o}^{2}}{\sec^{2}\psi} \log_{e}(\frac{r_{e}q^{\lambda^{2}}\sec^{2}\psi}{\pi^{2}(4dt+r_{o}^{2})}) \right|^{\frac{1}{2}}$$
(4)

where $P_{_{\mathbf{R}}}$ ans $P_{_{\mathbf{T}}}$ are the received and transmitted powers

 G_{p} and G_{p} are the transmitting and receiving antenna gains

 R_{p} and R_{p} are the distances from the transmitter and the receiver to the target point on the trail

 λ is the wavelength

ß is the angle between the trail and the projection of the transmission plane via the tangent plane

 ψ is half the included angle between $R_{\mbox{\scriptsize T}}$ and $R_{\mbox{\scriptsize R}}$

 μ is the angle between the incident vector and the electric vector accepted by the receiving antenna

r is the classical radius of the electron

q is the electron line density in the trail

r is the initial radius of the trail

d is the diffusion constant at the centre of the principal Fresnel zone

Signals from overdense trails last much longer than do underdense signals and have very different shapes. Despite this, the peak heights of both types of signal vary as λ^2 and in both cases the duration varies as λ^2 .

Some interesting spatial properties of meteor-burst propagation can be deduced from equations (3) and (4) above if we assume the meteors to be randomly distributed with respect to the earth. The attenuation occurring with $R_{\rm m}$ and $R_{\rm m}$ makes the neighbourhood of the two antennas the region in which the largest number of suitably-oriented trails will be found. The dependence of signal duration on $\sec^2\psi$ is the reason why, from a communications point of view, the centre of the path is the most important area. However, because meteors tangent to an ellipsoid at the path's mid-point must be travelling parallel to the ground, signals from this region are relatively rare. Instead, the areas that contributed most to the duty cycle of a meteor-burst link are two large regions just off the great circle path on either side of the mid-point, i.e., the so-called "hot spots". Figure 3, taken from Ref [3], shows the relative cumulative signal durations for contributions from various parts of the meteor region. The data were computed for a 1000 km transmitter-receiver separation, a meteor trail height of 100 km, and an isotropic distribution of incident meteors. In practice the actual distribution will differ from this, with the result that there will only be one hot-spot on one side of the great circle path, the actual location and size of which will depend on the geographical location and orientation of the circuit (Ref [4]).

As can be seen from Fig 3, the most effective trails are to be expected 5 to 10° off the great circle path. It therefore follows that two stations laterally separated from each other by more than about 200 km would, in general, receive signals reflected by meteor trails found in different regions of the space between the stations. It must also be expected that the probability of the two stations receiving the same signal burst would decrease more slowly along the axis of propagation than in the direction perpendicular to it $\begin{bmatrix} 5 \end{bmatrix}$.

Under the above conditions the possibility will also exist for the signal from the transmitter to reach the two receivers simultaneously by reflection from two trails which occur at the same time in two different regions. The probability of such coincidences which makes "interception" possible is not directly related to the distance separating the two receivers but is determined mainly by the positions of the receiving stations relative to the transmitter.

The test setup used in the interception trials described below was arranged to verify some of the theoretical predictions mentioned above.

DESCRIPTION OF THE TESTS

3.1 General

Four monitoring stations, the locations of which are shown in Fig 4, were installed in different countries in Europe as follows:

Saclay near Paris, Breisach near Freiburg, Germany Forest Moor near Harrogate, UK Sta Marinella near Rome, Italy A fifth station was operated in Noordwijk, the Netherlands, some 35 km to the northeast of Staalduinen, the northern terminal of the link. The monitoring stations were all tuned to receive the signal emitted by the southern terminal of the link, installed at La Crau near Toulon, France.

The equipment was essentially the same in all five stations. The antenna was a four-element Yagi (see photograph in Fig 5). The lobe was directed towards the ionosphere (80-100 km height) so as to intersect with the antenna lobes of the link terminals in the manner depicted in Fig 4. The receiving equipment consisted of a super-heterodyne receiver with crystal-controlled local and calibration oscillators. A paper recorder was used for continuous monitoring of the propagation conditions, and a magnetic-tape recorder for collecting samples of the signal received, for subsequent playback and analysis.

Tests were conducted for a period of one year at the rate of one week in every other month. The data collected were thus statistically representative of the various phases of an annual cycle, which included the winter season, characterized by a low meteor rate, and the summer season, during which reflections from sporadic-E layers are relatively frequent. During each test period, the receivers were calibrated every half hour by injecting a standard signal which varied in discrete steps over the range from -173 to -113 dBW, i.e., between 30 dB below and 30 dB above one microvolt from a 50 -ohm open source. The transmitter at La Crau was switched on and off at regular intervals so as to be on the air for 7½ minutes and off for 2½ minutes. The tape recorders were switched on at intervals of 3 hours for 35 minutes, so that each recording included three signal periods of 7½ minutes and two calibration scales, one at the beginning and one at the end. The operation was fully automatic and followed a programme set by an electric clock.

The power level and the modulation characteristics (FSK) of the carrier emitted always remain the same whether the link was closed or interrupted, but no significant amount of message information was actually released by either transmitter unless contact was established in both directions by a suitable reflection. Only by analysis of the information contained in the modulation could it be ascertained whether traffic had passed over the circuit at any particular time. To facilitate the analysis of the signal received at the monitoring stations, the La Crau transmitter emitted a second carrier on either of two frequencies according to the state of the link, closed or interrupted. The exact values of the frequencies of the two carriers were as follows:

Main carrier "Mark" 36.584 MHz
"Space" 36.590 MHz
Auxiliary carrier "Circuit closed" 36.5985 MHz

"Circuit interrupted" 36,5995 MHz

3.2 The Receiving Equipment

A block diagram of the receiving equipment is shown in Fig 6. The "space" component of the main carrier was converted down to 13.5 KHz in the receiver, passed through a narrow-band filter to eliminate the modulation, and detected to obtain a voltage representing the envelope of the signal bursts. This voltage was then converted into a frequency-modulated tone for recording on magnetic tape. At the same time the same carrier was passed through a wider filter and detected to recover the modulation.

The auxiliary carrier was also converted down to the audio frequency range. It was then applied at the input of two filters tuned to frequencies of 4 and 5 kHz, corresponding to the conditions "circuit closed" and "circuit interrupted" respectively.

All four signals were recorded on magnetic tapes for analysis in the STC laboratories.

3.3 The Analysis Equipment

The analysis equipment was shown schematically in Fig 7. The voltage derived from the envelope of the main carrier was first restored to its original form by an FM/DC converter, and then fed into a level distribution recorder. This included a group of 14 biased gates (numbered 1, 3 27) which delivered pulses when the instantaneous value of the voltage applied at the input exceeded a preset value. The output of each gate was registered by a counter (numbered 1, 3 27) whose total represented the portion of time spent by the signal above the threshold for which the gate was set.

The voltage derived from the auxiliary carrier was detected either by a positive-polarity or negative-polarity detector, depending on its frequency at any particular time. The detected voltage drove a trigger circuit (bistable) which opened gates 2 to 28 (even numbers) whenever the frequency received corresponded to the circuit closed condition. The output of each of gates 1 to 27 passed through one of gates 2 to 28 and was registered by a counter (even numbers 2 to 28) whose reading represented the portion of time during which the information passed over the circuit was intercepted with an amplitude exceeding the preset value.

The analysis equipment was programmed to operate in synchronism with the periods of signal recorded on tape. The data collected by the level distribution recorder were printed out at the end of each 74-minute signal period to give the amplitude distributions of the level received and, at the end of each noise interruption, to give the noise level. Calibration of the biased gates was carried out by playing back the calibration scales at the beginning and end of each recording.

4. RESULTS

4.1 Propagation Data

The statistical distribution of the signals received at the monitoring stations was derived from

the totals recorded by counters 1 to 27 for each period of 75 minutes. As explained in the previous section, the counters operated on the signal level, regardless of the information content. Their data could thus be used to compare the propagation performance over the different paths between La Crau on the one hand, and Staalduinen and the various monitoring on the other.

From each statistical distribution, the percentage of time "P" during which the signal-to-noise ratio (SNR) exceeded 10 dB was determined. The threshold of 10 dB was chosen because it had been found experimentally to be the average value of the minimum SNR required for error-free reception.

A cummulative distribution of the values of P for Staalduinen and the monitoring stations is given in Fig 8. It shows how the propagation conditions differed over the six paths, the best being the paths to Staalduinen and Noordwijk and the worst to Sta Marinella. The fact that the poorest reception was observed in Italy was not unexpected since the Italian station is very unfavourably situated with respect to the La Crau transmitter. These results show, however, that backward propagation by meteor reflections is not negligible, since the value of P exceeded 5% in about 20% of periods. The relatively good reception conditions observed at Forest Moor, which was 900 km away from the circuit midpoint and therefore almost at the extreme distance for meteor-burst propagation, may be predicted from equations (3) and (4).

In order to compare more closely the propagation conditions over the different paths, the values of P for the five monitoring stations were normalized, i.e., they were divided by the value of P measured at Staalduinen over the same period. The statistical distributions of the ratios obtained are given in Fig 9, except for Noordwijk, which indicated no difference compared with Staalduinen. It is obvious from this figure that there is no close correlation between the signals received at the various locations. If signal bursts had come from the same trails the distribution for the monitoring stations would have tended to peak around values of P of less than 1.0. At Porest Moor, for instance, the value of the time percentage was on the average 0.7 times the value measured at Staalduinen, but the ratio actually varied between 0.1 and 1.5. A similar spread of the data is seen on all four diagrams. The samples at the tails of the distributions correspond to periods during which relatively long reflections occurred on one path and not on the other.

In interpreting these results, it must be borne in mind that the transmitting antenna was pointed in the direction of Staalduinen with a 3 dB horizontal beamwidth of 50°, and that the beam elevation was optimum for the length of the link, namely 1000 km. It must also be noted that the antennas used at the monitoring stations were designed and orientated for maximum overlap with the common volume of the correlation link rather than for optimum reception of the La Crau signal. Forest Moor was within the beam of the transmitter (see Fig 4), but the distance from La Crau was 400 km longer than optimum. Moreover, the angle of interception, i.e., the angle between the axis of the transmitting beam and that of the receiving beam, was 23°. Saclay and Breisach were also within the transmitting beam, but the distances were 700 km for the first and 500 km for the second, and the angles of interception were 34° and 47° respectively. In the case of Sta Marinella, which is 470 km from La Crau, the propagation path followed a broken line, the total length of which was of the order of 1000 km, and the interception angle was 140°.

From these results, it is apparent that it is possible to communicate by meteor bursts between a point such as La Crau and a number of others as far apart as Breisach and Forest Moor, without necessarily changing the transmitter power and the antenna system. It is, however, certain that reception conditions could be improved, especially at the shorter distances, if the antenna patterns were designed specifically for this purpose. Reception at a point such as Sta Marinella by reflections in a backward direction appears possible though the signals received would probably be weak.

4.2 Interception Data

Statistical distributions of intercepted signals were derived from the data registered by counters 2 to 28 of the level distribution recorder. Here again the time percentage "P" corresponding to an SNR of 10 dB was determined for each period of 7^h minutes. This percentage P, which represents the fraction of time during which traffic passed over the link was intercepted, was divided by the duty cycle D of the circuit for the same period. The ratio I = P cmlled the interception ratio, represents the proportion of intercepted information.

Figure 10 depicts the distribution of the values of I measured at Forest Moor, Saclay, Breisach and Sta Marinella.

It can be seen that interception was more frequent where reception was better, the average value of the interception ratio, being:

Forest Moor : 0.16
Saclay : 0.08
Breisach : 0.06
Sta Marinella : 0.03

In fact, all four distributions have asymptotic tails reaching I = 1. Indeed, on a few rare occasions, cases of total interception were observed at each site due to propagation by sporadic-E layer reflection, or by intense ionospheric scatter lasting from a few minutes to half an hour.

At Noordwijk, the values of I were always between 0.9 and 1.0, the message being intercepted practically all the time.

Except at Noordwijk, where the recordings of the signal received showed a great similarity in the details with those made at Staalduinen, there was often no visable correlation between the signal bursts received at the other stations. If signal bursts occurring on the circuit path and on the interception

path are not supported by the same meteor trails, they should be statistically independent. In that case, the probability that they overlap in time is equal to the product P.D. and the interception ratio I, as defined above, is on average, equal to P.

This was found to be the case in Saclay, Breisach and Sta Marinella. At Forest Moor the values of I were usually somewhat higher than those of P, showing that some meteor trails reflected signals both to Staalduinen and Forest Moor.

If Noordwijk is excepted, it can be concluded from the above results that the propagation over the various paths was largely due to reflections from different meteor trails, and that simultaneous reception of signals at two different points was mainly coincidental. Such coincidences are, of course, more likely to happen when the burst rate of occurrence is higher. It should be noted that for maximum interception the antennas of the intercepting stations should be arranged to maximize the duty cycle with the transmitting station rather transpectation or orientated necessarily towards the mid-point of the communication link.

An important parameter in meteor-burst propagation is the forward scatter angle made by the paths joining the transmitter and the receiver to the point of reflection on the trail. As can be seen from equations (3) and (4), both the amplitude and the duration of signal bursts are increasing functions of this angle. Typical values of the forward-scatter angle are 155° for a 1500-km hop, 153° for a 1000-km hop, and 100° for a 200-km hop. For the La Crau-Sta Marinella path, which follows a broken line, the angle is of the order of 40° only, as compared, for instance, with 140° for the La Crau-Breisach path. Since propagation was still possible in such conditions, it can be concluded that the range of distances that can be spanned by meteor-trail reflections extends from the limit of the optical or refraction range to the maximum of about 2000-km set by the curvature of the earth's surface. It is clear, however, that the same antenna system could not cover this whole range of distances and give equal performance on all paths. Different vertical radiation patterns would be required for hops of,say, up to 500 km, between 500 and 1000 km, and between 1000 and 2000 km. The propagation time percentages obtained in Breisach can be considered as the minimum performance expected on any hop lengths within the limits mentioned above, with 200 watts of transmitter power and with properly designed antennas.

In the case of a broadcasting application, the problem would be to ascertain that the signal emitted by the broadcasting station was received all over the area of interest for a minimum percentage of time. The results of the propagation show that it is possible to obtain a signal duty cycle of 1% with a reliability of at least 80% to 90%, at all stations located within the beam of the transmitting antenna. As pointed out earlier, better results could certainly be obtained if antennas were specifically designed for the purpose. It must be noted, however, that the Yagi antennas used for the tests had a horizontal beamwidth of 50° and that any extension of the azimuthal coverage would have been at the expense of antenna gain. This factor would have had to be compensated for by an increase in transmitter power. Further consideration to the use of meteor-trail reflections for broadcasting is given in the following section in which special transmission techniques are discussed.

5. INTERCEPTION AND JAMMING VULNERABILITY

For an assessment of the vulnerability of the system to interception, reference is made to Fig 10, which indicates that the probability of intercepting a certain proportion of the traffic is given by functions which are approximately exponential. For stations located within the beam of the transmitting antenna and at several hundred kilometres from the receiving terminal, the average percentage of traffic intercepted varies between 5 and 16%. For stations outside the transmitting beam, the percentages are lower though not zero. Since the interception ratio is of the same order as the percentage duty cycle on the path to the interception path, the risks of interception can be reduced to a minimum by transmitting at high speed in short bursts, and by keeping the transmitter power to the lowest level required to obtain the duty cycle needed at any given time. Total interception, of course, always has a low but finite probability.

The problems of vulnerability to jamming and to interception are similar as far as propagation is concerned. There are, however, some fundamental differences between them. Whereas there is little an interceptor can do to increase its efficiency once its location is defined, the jammer disposes of one degree of freedom, namely the transmitter power, which has a direct influence on its efficiency. On the other hand, a given percentage success value has a different meaning for an interceptor and for a jammer. For instance, intercepting 10% of the traffic passed over a link may be of considerable interest; whereas jamming this link for 10% of the time means slowing down the traffic by the same amount, which is of no real consequence. Unless the power of the jammer is sufficiently high to propagate signals continuously by ionospheric scatter the chances of successfully jamming a meteor-burst link from long distance appear problematic. Taking Forest Moor as an example, it is estimated that a 5-kW jammer would be needed to interfere with the 200-watt STC link for 90% of the time Ref [6]. This advantage of 25 to 1 in power ratio is inherent in the propagation mechanism and is preserved at all power levels. If resistance to jamming is essential, the transmitter power used on the link could be raised to 5 or 10 kW, the transmission rate being increased in proportion, so that jamming efficiently from long distances could be practically impossible. Here again, however, the choice of frequencies substantially higher than 40 MHz might be a preferable solution.

The 200-watt STC link had a duty ratio of 7.5% and, with a transmission speed of 2000 baud, it had an average capacity of 150 baud. If the frequency were raised to 80 MHz and the power to 2 kW, from equations (1) and (2), the duty cycle would be about 2%. If the transmission speed is now raised to 48000 bits the duty cycle would be reduced to 0.3%, but the circuit capacity would increase to about 150 baud, ie., to the value it had at 40 MHz with 200 watts. To jam this link at 80 MHz for 90% of time would now require a jammer power in excess of 150 kW (assuming λ^{-5} relationship for the SNR in ionoscatter propagation). It should be observed that a high signalling rate implies a low duty-cycle, which in turn implies the possibility of long message delays. The average rate of transfer of information would be higher, but the delays to short messages might be longer. Long messages would pass at the average rate and would therefore be presented with shorter delays at a higher signalling speed.

FREQUENCY SHARING

To be able to use meteor-burst propagation for communicating at the same frequencies and in both directions between a central post and a number of peripheral stations, interference between signals converging towards the common receiver would have to be avoided, i.e. the probability of a burst occurring on more than one path at a time would have to be low. For this to be possible, two conditions would have to be met. Firstly, the stations should be sufficiently dispersed. Typical minimum requirements for their dispersion would be an angle of 15° between path bearings, or a separation of 400 km between stations. Secondly, the duty cycle of each link should be limited to a few percent, say, less than five. However, at frequencies as low as 40 MHz the duty cycle is sometimes much higher due to the occurrence of ionospheric scatter or of reflections from sporadic-E layers. As seen from Fig 2 the situation would be much more favourable in the frequency range above 70 MHz where propagation modes other than meteor scatter become very exceptional.

Frequency sharing between several meteor-burst links operating in the same area poses a problem which is very similar to that of the star-shaped network discussed above. There again, one situation must be avoided in which wanted and unwanted signals often reached a given receiver at the same instant. Strictly speaking, such coincidences cannot be excluded completely since they have been observed even in Sta Marinella; however, if their average probability is a few percent only, the risks of mutual interference would not be very serious. As already mentioned, reflections from sporadic-E layers are still relatively frequent in summer at 40 MHz and are sufficiently strong to cause interference through back or sidelobes of antennas at distances of up to 2000 km. The possibilities of frequency sharing therefore appear very remote except at higher frequencies.

7. CONSIDERATIONS ON THE USE OF METEOR SCATTER FOR BROADCASTING APPLICATIONS

The broadcasting of information by meteor-trail reflections requires techniques which necessarily differ from those used on two-way communication links. Since no feedback is possible from the receiver to the transmitter, ARQ systems are not applicable. The information must be repeated by the transmitting terminal until the probability of reception is deemed to have reached the required level. Meteor reflections occur at random and their duration varies unpredictably between a fraction of a second and several seconds. Nevertheless, their statistical characteristics are sufficiently well known to determine how long a message should be repeated before it reaches its destination.

Different approaches can be followed in devising a broadcasting system based on meteor-burst propagation. The simplest one is briefly discussed below. Each message is handled as one indivisible block of information, the transmission of which relies on the occurrence of one single burst of sufficient duration. The block is emitted at high speed and repeated for a period of time which depends on its length. Since the receiver is not in permanent contact with the transmitter, synchronization must be established. This can be realized by inserting a special signal between two successive emissions of a block, in much the same way as the ARQ signal is inserted between two repetition cycles in the STC system. The synchronization signal therefore marks both the beginning and the end of the message.

As for the choice of a code, it is clear that some protected code is necessary to discriminate between signal and noise or interference at the output of the receiver. Unless a very long code is used, however, many errors would be made by the receiver during the intervals between bursts, when only noise is present. A more efficient solution would be to use a simple error-detecting code, for instance, the ARQ code, and to set the condition that no apparently correct character can be accepted unless the following "n" characters also appear to be correct. With the ARQ code and at 2000 baud for instance, the value n=11 leads to a probability of one error in 16 hours.

If dual diversity reception is available, the technique used in the STC system can be applied with a view to reducing n. Before the receiver outputs can be processed and the message read out, it is required that the synchronization signal be identified simultaneously in the two diversity branches. This indicates almost with certainty that a meteor burst is present, so that the checking procedure need not be so severe afterwards. With n=5, the probability of error would be about one in 4000 bursts, which should be quite acceptable.

With a transmission rate of 2000 band, a message of 150 characters (25 words) requires a burst of half a second at least. Measurements on the La Crau-Staalduinen circuit have shown that the average rate of occurrence of such bursts is one every 15 or 20 seconds when the duty cycle is 12.5% (early morning) and one per minute when the duty cycle is 2.5% (late afternoon). Practically, to take into account deviations from the statistical average and to obtain a probability of reception of 99%,it would be necessary to repeat the message during a period of time equal to four or five times the average interval between bursts.

Shorter messages require bursts of shorter duration, which are of course more frequent, as shown by the comparative figures contained in the table below:

No of characters per message	15	150
Average time interval between suitable bursts early morning	5-10 seconds	15~20 seconds
late afternoon	20 seconds	1 minute
Duration of repetition period		
early morning late afternoon	5 to 1 minute 15 minutes	15 minutes 4-5 minutes

It must be noted that it is possible to increase the rate of signalling much beyond 2000 baud, thereby reducing the delays in the transmission of messages. At 20,000 baud for instance, and with 2 kW

of power, messages of 150 characters would not have to be repeated longer than 15 minutes on a path where the duty cycle is not lower than 2.5%.

8. CONCLUSIONS

While the STC meteor-burst system was tested on the link La Crau-Staalduinen, measurements were made at five monitoring stations which were all tuned to receive the signal emitted by the La Crau transmitter. One of these stations, Noordwijk, was only 35 km away from the Staalduinen terminal. The other four were several hundreds of kilometres away from either terminal.

The results of these tests showed that the signal from La Crau, which was emitted continuously but carried traffic only by intermittence, could be received by bursts for a certain percentage of time in all stations. Reception at Noordwijk was practically as good as at Staillduinen. Next came Forest Moor, Saclay, Breisach, and finally Sta Marinella which was in the least favourable position and received the signal about ten times less frequently than Staalduinen. These results demonstrate the potential capability of meteorburst systems to operate over ranges from 200 to 2000 km.

A second result was to show that the correlation between signal bursts received at Staalduinen on the one hand and at the monitoring stations on the other was nil or low, except at Noordwijk where the correlation was almost total. Interception of the traffic passed over the link was generally due to the simultaneous occurrence of two meteor trails which reflected the signal in two different directions. When the duty cycle was low, say less than 5%, such coincidences were rare and the proportion of intercepted information was not more than a few percent. In summer, however, the occurrence of sporadic-E layers in the ionosphere made interception possible quasi-continuously for periods of a few minutes to half an hour.

From the results of the interception tests, it is concluded that jamming from long distances would be inefficient, and that relatively high power would be needed to interrupt a meteor-burst link completely.

The possibility of sharing frequencies between several links was studied, both in the case of a network having a star configuration and in the case of independent circuits. Although it appears that this possibility wists in principle with meteor-burst systems, it is considered that the risks of mutual interference are too high at 40 MHz due to the occurrence of competing modes of propagation, such as ionospheric reflection and scattering. The risks would be considerably reduced at higher frequencies.

From the propagation data collected, it can be concluded that meteor-burst propagation can be used for broadcasting applications. To obtain, however, a nearly equal time percentage of reception at all distances from 200 to 2000 km, three antenna systems having different vertical radiation patterns would be needed. With transmitter powers in the kilowatt range, a message of 25 words would have to be repeated during one to five minutes to achieve a probability of reception in excess of 90%.

9. ACKNOWLEDGEMENT

This paper is based upon the work of many individuals presently and formerly with the Communications Division, SHAPE Technical Centre. Acknowledgement is particularly due to Mr P J Bartholomé,now withthe European Space Research and Technology Centre at Noordwidjk, Netherlands, who carried out most of the work reported in this paper.

REFERENCES

- BARTHOLOME, P.J. and VOGT, I.M., April 1968, "COMET A New Meteor-Burst System incorporating ARQ and Diversity Reception". IEEE Trans. Com. Technology, Vol COM-16, p. 268.
- 2. DAVIES, G.W.L., et al, Dec 1957, "The Canadian Janet System", Proc. IRE, p. 1666.
- HINES, C.O. and PUGH, R.E., 1956, "The Spacial distribution of signal sources in meteoric forward forward scattering". Can J Physics 34, p. 1005.
- VILLARD, O.G., et al, Oct 1955, "The role of Meteors in Extended-range VHF Propagation". Proc. IRE, p. 1473.
- VILLARD, O.G., et al, May 1955, "Some Properties of Oblique Radio Reflections from Meteor Ionization Trails". Standford University, Radio Propagation Laboratory, Technical Report 85, Unclassified.
- INCE, A.N., et al, 3-7 Oct 1977, "A Review of Scatter Communication Systems". AGARD Symposium
 "Aspects of Electro-magnetic Scattering in Radio Communications", Cambridge, Mass.

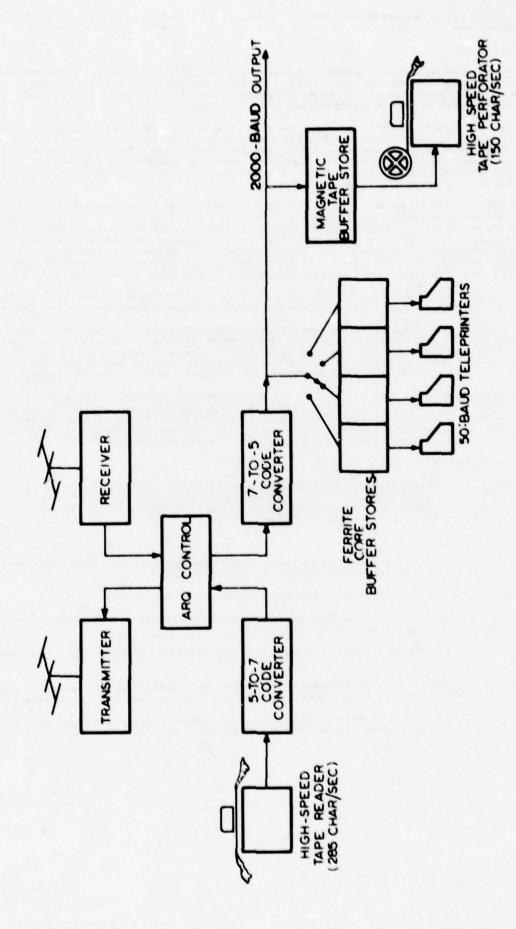


Fig. 1: Block diagram of STC meteor-burst system (COMET)

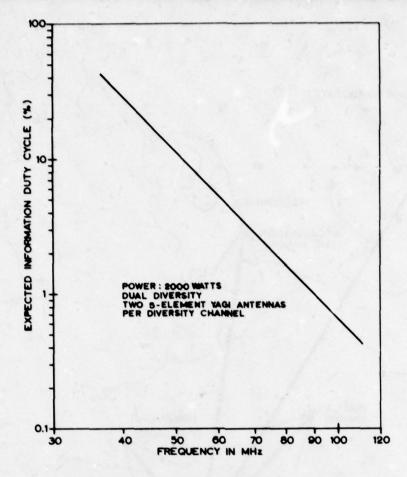


Fig. 2: Long-term average information duty cycle for the COMET system, as a function of frequency.

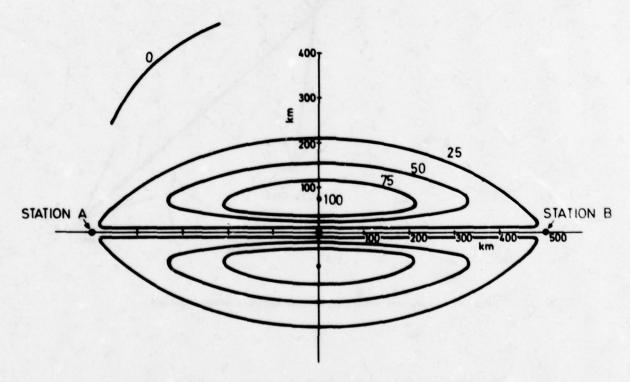


Fig. 3: Relative signal contributions form various parts of the meteor region computer for a 1000 km path

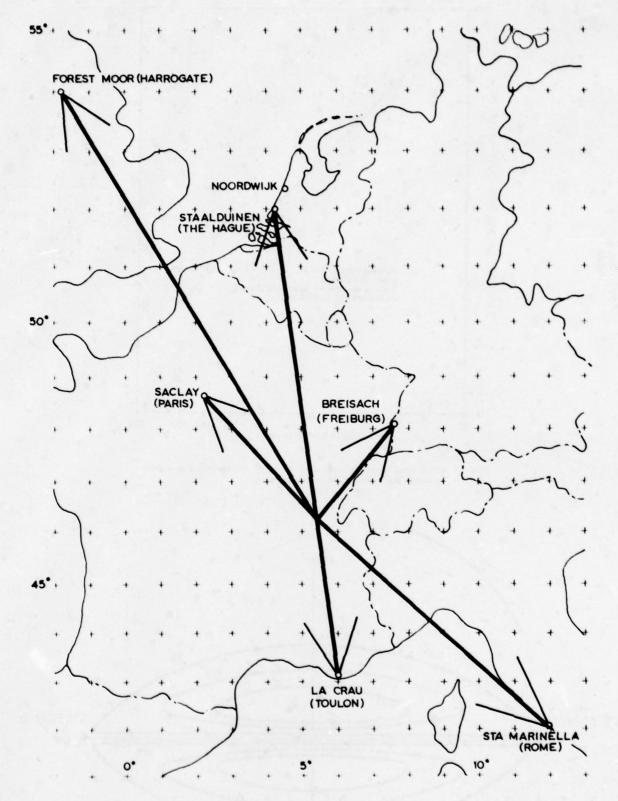


Fig. 4: Map showing meteor-burst link and monitoring stations

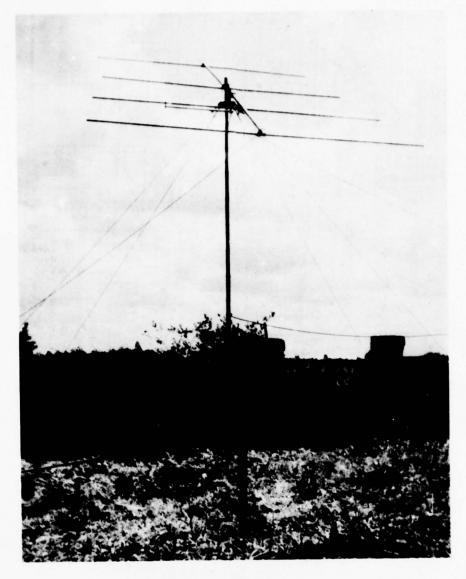


Fig. 5: Photograph of the receiving antenna used at Saclay

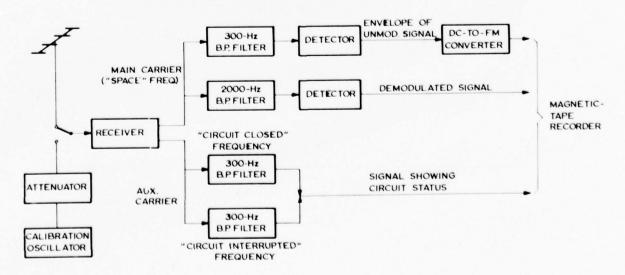


Fig. 6: Block diagram of receiving equipment

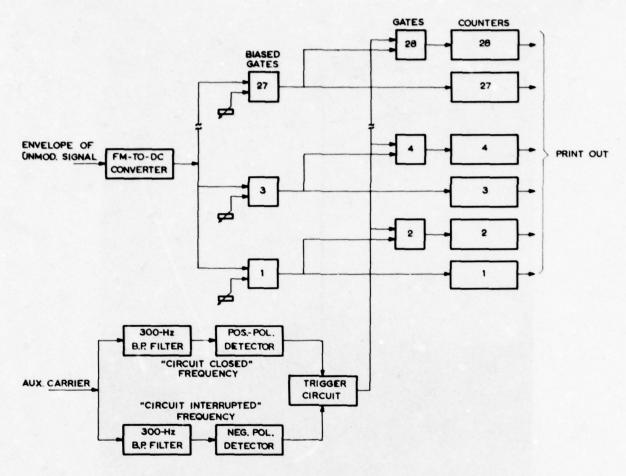


Fig. 7: Block diagram of analysis aquipment

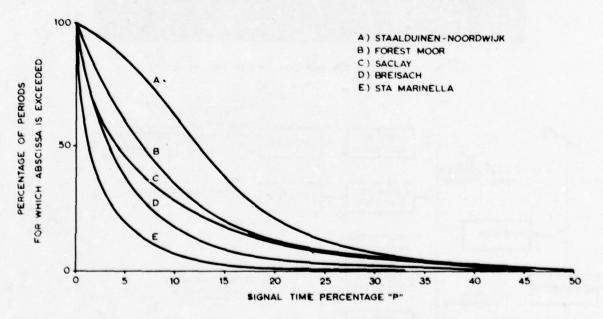


Fig. 8: Cumulative distribution of propagation time percentage (Feb - Dec 1966)

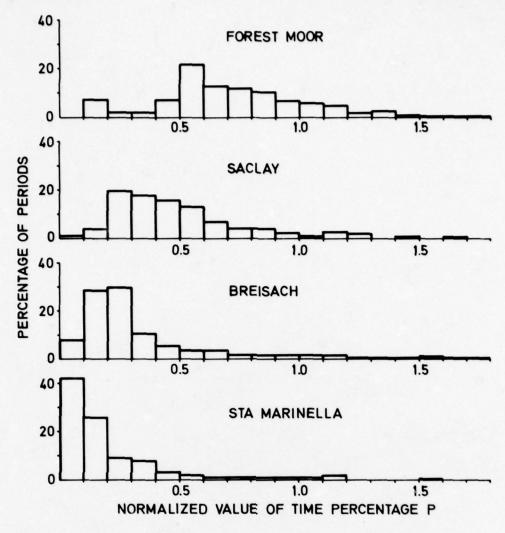


Fig. 9. Statistical distribution of normalized values of time percentage p (Feb - Dec)

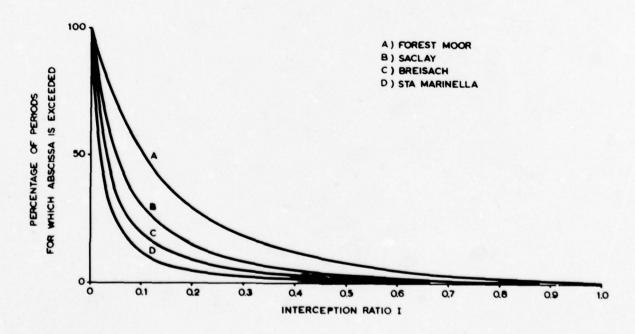


Fig. 10: Cumulative distribution of interception ratios (Feb - Dec)

TROPOSPHERIC STRATIFICATION AND ANOMALOUS PROPAGATION

hv

Harold T. Dougherty, Institute for Telecommunication Sciences
Burgette A. Hart, Policy Research Division
Office of Telecommunications
U. S. Department of Commerce
Boulder, Colorado 80302

SUMMARY

This paper summarizes the progress to date in predicting the enhanced fields that are encountered in the presence of a stratified atmosphere. Of particular interest are the ducting conditions associated with supercritical refractivity gradients both aloft and at or near the surface. As a basis for estimating the likelihood of these supportive conditions, the available information is surveyed. It is suggested that the access to computers and the availability of historical radiosonde data be exploited to map the pertinent characteristics of tropospheric layers on a worldwide basis to meet the interference prediction requirements of the telecommunications regulatory agencies.

I INTRODUCTION

The ducting or guiding of radio waves by the stratified troposphere, i.e. by strong refractivity gradients at and near the surface or aloft, has been the subject of recurring experimental and theoretical investigations since World War II [1, 2, 3]. However, recent significant theoretical advances have been sparked by a renewed interest. One source of this interest has been the preparation for the 1979 General World Administrative Radio Conference (GWARC-79) of the International Telecommunications Union (ITU). This interest results from the fact that the enhanced fields associated with tropospheric layering contribute to the potential co-channel interference problems that are of concern to the radio regulators [4].

At frequencies below about 30 MHz, the non-ionized atmosphere and its temporal or spatial variation are readily accommodated by either the effective-earth-radius factor or the exponential atmospheric model, and their effects upon radio propagation are readily approximated by minor modifications of the standard prediction methods. However as VHF and higher frequencies are considered, the effects of the non-standard conditions (i.e., the stratified troposphere) become increasingly significant. The resulting propagation modes become anomalous (i.e., non-standard); the received radio signals are then either markedly weaker or stronger (degraded or enhanced) than would be expected with a standard atmosphere.

The anomalous degradation of the received signal (fading) has been the subject of many theoretical and experimental investigations of line-of-sight propagation paths. These are well documented; the results have been surveyed and catagorized [5]. This signal degradation impairs system performance. It is an intra-system problem for which remedies are available; they may be applied in anticipation or after-the-fact.

On the other hand, the anomalous improvement of the received signal (an enhanced field) is of interest primarily because the more volatile problem of inter-system interference can result, particularly for beyond-line-of-sight (transhorizon) systems. Since these enhanced fields pose the threat of interference to and from other systems, they play a large role in the determination of the co-ordination distances required by the national and international regulatory agencies. These enhanced fields and their supportive conditions have not been studied as extensively as have the degraded (fading) fields, nor have they been as well understood in a quantitative sense until recently.

For short transhorizon paths (for which the standard mode of propagation is diffraction), the enhanced fields are on the order of the free-space field. Their occurrence, ducting, is almost always associated with the presence of superrefractive gradients at or near the surface. These are more common and extensive on maritime or over-water paths than on overland paths [6].

For the longer transhorizon paths (for which the standard mode of propagation is troposcatter), the enhanced fields can be most dramatic. In the presence of super-refractive elevated layers, the standard (attenuated, rapidly fluctuating) troposcatter signal may be replaced by a very strong (up to 45 dB stronger), very slowly varying signal [6].

Despite the significant advances in theoretical treatment summarized in the following section, the description of the supportive atmospheric conditions (tropospheric layering) has not kept pace. The purpose of this summary paper is to document the presently available data on the refractivity gradients encountered in tropospheric layers aloft and at or near the surface.

II DUCT PROPAGATION RELATIONSHIPS

A milestone in the study of wave propagation via tropospheric layers and ducts was achieved in 1962, when Wait reviewed the then-available duct propagation theories, placing them into a common context [7]. The wide variety of theoretical solutions were primarily extensions of two basic formulations, the Booker and Walkinshaw mode theory [2] and the Furry asymptotic theory [3]. The extensions all assumed a simple duct (cylindrically uniform above a concentric cylindrical earth); their variety lay in the mathematical representation of the vertical (radial) refractivity profile within the duct. Since 1962, there has been progress at an increasing pace; computer programming of the full-wave solution for tropospheric ducts has provided quantitative results for the (piecewise) linear variation of refractivity within, and in the vicinity of, the duct. The most recent advance has been the extension of the full-wave solution (and its computer programming) to the non-uniform duct, wherein the vertical refractivity profile varies along the duct [8].

A Propagation Within the Duct

As the use of these computer programs becomes more widespread and familiar, it is expected that their results will be reduced to the engineering-type formulas and curves that are required for the prediction of these anomalous fields on an operational basis. From the point of view of radio regulation and estimating interference potential, however, the observational data and theory already permit lower-bound estimates of system transmission loss [6].

When both the signal source and the observer are well-immersed within the duct, the signal is propagated with very low losses [9]. For frequencies greater than a critical value [10]

$$f_{c} = \frac{1572}{D^{1.8}} \quad GHz \tag{1}$$

(where D is the duct thickness in meters), the full wave solution will determine a first-mode attenuation coefficient as $\alpha \le 0.03$ dR/km. The duct transmission loss within the duct will then equal or exceed the value [6]

$$L_b = 92.45 + 20 \log f + 10 \log d + 0.03d + A$$
 (2)

(in decibels), where f is the transmission frequency in gigahertz, d is the nominal path length in kilometers, and A is the aperture-to-medium coupling loss. The coupling loss results when the antenna (half-power) beamwidth Ω is so large that not all of the main-lobe radiation is trapped and propagated along the duct. An estimate of this coupling loss is given per terminal antenna by [6]

$$A = -10 \log |2\theta_{c}/\Omega| \quad \text{for } 2|\theta_{c}|<\Omega ,$$

$$= 0 \quad \text{for } 2|\theta_{c}|\geq\Omega ,$$
(3)

where

$$|\theta_{c}| = \sqrt{2|\Delta M|} \sqrt{1-y/\Delta h} \quad \text{for } 0 \le y \le \Delta h \qquad ,$$

$$= \sqrt{2|\Delta M|} \sqrt{1+y/(D-\Delta h)} \quad \text{for } \Delta h - D \le y \le 0 \qquad .$$
(4)

Here, $\theta_{\rm C}$ is in milliradians when the modified refractivity lapse ΔM within the duct is in M units, and y is the vertical displacement of the terminal from the base of the superrefractive layer (i.e. y=0 for z=h in Fig. 1). There is a very similar per terminal coupling loss when one or both terminals are within the elevation range of the duct but beyond the duct's horizontal extent. This "end-fire" coupling loss would be given by (3) if the $2|\theta_{\rm C}|$ were replaced by $D/d_{\rm L}$. Here, D is the duct thickness, and $d_{\rm L}$ is the distance from the end of the duct to the terminal beyond (exterior to) the duct [11].

Note that (2) can be considerably less than the free-space loss

$$L_{bo} = 92.45 + 20 \log f + 20 \log d dB$$
, (5)

since one effect of the trapped propagation is to constrain the spread of energy in the vertical direction.

B Propagation Near The Duct

When one or both terminals are exterior to (and above) the duct, observational and theoretical data suggest that the free-space loss of (5) may be a reasonable lower bound. When both terminals are exterior to (and below) the duct, an estimated lower bound may be free-space plus 20 to 24 dB (i.e. (5) plus 20 or 24 dB)---about 10 to 12 dB per terminal exterior to the duct. These appear consistent with limited operational data [6] and early theoretical results for the non-uniform duct [8].

III PREDICTION OF SURFACE DUCTS

The occurrence and characteristics (refractivity gradients, thickness, etc.) of surface ducts (illustrations (a) and (b) of Fig. 1) have been described and mapped by Bean and his associates [12]. Although the coverage therein is nominally worldwide, it is based primarily on land stations and is primarily descriptive of overland ducts. Therefore, in the following material, we shall concentrate on the more prevalent and extensive sea-surface ducts.

From Fig. 1 and the previous section, we see that the duct propagation depends upon the superrefractive gradient (its strength, vertical extent, and horizontal continuity) which can vary with time of day and year or the distribution of weather elements. One useful categorization of superrefractive layers would be in terms of their vertical extent. Deep layers (extending 25 m or more above the surface) would be relevant to ocean-vessel communication; communication antennas have been at about 24 m above the sea on most naval vessels, and search radars on capital ships have been at about 30 m above the sea. On the other hand, shallow layers (extending to 15 m or less) would have significance for propagation between terminals (communication terminals or low-sited radars) on smaller craft. For the prediction of sea-surface layers, a preferable classification may be that of the meteorologists, who categorize atmospheric layers in terms of their dominant causative mechanism. Fortunately, this latter classification approximates the former; advection-type layers tend to be deep, and evaporation-type layers tend to be shallow.

A Superrefractive Advection Layers

The deep, superrefractive advection layers result from the movement of warm, dry air over the sea [12]. For example, during the late summer and early fall, the prevailing winds move continentally modified (warm, dry) air masses offshore over cooler maritime air. As a result, favorable locations for the occurrence of these advection layers border certain east coasts of continents or large islands [6].

Similarly, the circulation patterns of air and ocean combine to produce advection layers near the sea surface. For example, large oceanic semi-permanent highs are characterized at lower elevations by a large mass of air which has warmed and dried adiabatically during its descent. Therefore, superrefractive advection layers also occur near the west edge of continents, at latitudes of approximately 15° to 35° N or S, where the eastern section of a semi-permanent high tilts down toward the sea surface in the vicinity of a cold ocean current [6].

B Superrefractive Fvaporation Layers

Shallow superrefractive evaporation layers are found over extensive areas of the ocean, whenever conditions are conducive to rapid evaporation rates. These layers result primarily from the humidity-temperature contrasts between air and sea in a shallow transition layer adjacent to the surface. In addition, the evaporation rate per unit area and, consequently, the occurrence and strength of these layers is strongly influenced by the speed and steadiness of the local wind.

The strongest evaporation rates are found north of 35°N (or south of 35°S) in winter over warm ocean currents such as the Kuroshio (Japan), the North Atlantic Drift, the Alaskan Current and the Fast Australian Current [13]. In middle latitudes the amount of evaporation per unit area varies with the seasons, reaching a minimum in summer (June and July in the Northern Hemisphere) and a maximum in the fall and early winter (September, October, and November in the Northern Hemisphere) when, although the air is cold, the water is still relatively warm [13].

In the tropics, evaporation takes place all of the time, since the sea-surface temperature is normally higher than that of the air above it. However, because this difference in temperature (and in the corresponding absolute humidity) is small, the actual rate of evaporation per unit area is not as great as in the middle latitudes, but the resulting shallow superrefractive layer can be very intense. These strong evaporation layers are reported as a semi-permanent feature in the Caribbean, disrupted by, and reforming immediately after, the passage of squall lines [14]. Other tradewind areas, where evaporation exceeds precipitation (see figure 2), are also likely regions for strong evaporation layers [15].

All oceans experience fluctuations in the evaporation at certain periods and in certain regions; these appear to be related to the persistence of anomalies in the monthly and yearly sea-surface temperatures. Anomalies also occur in the humidity or water vapor structure, but conclusive determination of humidity fluxes over the sea is still lacking [6]. Superrefractive layers are sometimes associated with steam fog or "Arctic smoke," although this is usually an indication of the onset of the layer's disintegration.

C Overwater Prediction Charts

The foregoing demonstrates how an understanding of the causative physical processes permits an identification of the ocean areas favorable for the occurrence of super-refractive layers. This is essential if the meteorological data obtained from the very limited number of marine observational stations are to be extrapolated over the oceans of the world [16]. In addition, quantitative estimates of certain layer characteristics

are necessary, for radio propagation prediction purposes. Although these characteristics of interest (the strength of the gradient, its vertical and horizontal extents, and its occurrence) are not adequately measured at present, some estimates are available.

Figure 3 indicates those world oceanic areas for which estimates are available of the characteristics of subrefractive and superrefractive layers. These represent a substantial beginning but further estimates are necessary; estimates of the diurnal variation of the layer characteristics are particularly limited. The ocean areas of figure 3 with the diagonal shading //// are those for which charts, primarily of advection layers, are available. The ocean areas with the reverse diagonal shading are those for which charts, primarily of evaporation layers, are available.

A particularly useful type of prediction chart, illustrated in figure 4, gives the percent expectancy of extended ranges (50% or greater increase in range) for L, S, and X-Band Radar for superrefractive layers [17]. These and the many others available [6] are actually charts determined from the potential refractive index observed at shipbridge heights and under various wind conditions. For an assumed height distribution of refractive index, these variables permit an estimate of the sea-surface-layer refractivity gradient and its vertical extent. Those variables associated with super-critical gradients are then combined into one convenient parameter, the "maximum-trapped-wavelength", that results from Schelkunoff's solution [18] of the simplest guided-wave propagation problem. Although this maximum trapped wavelength is only an approximation and is generally less than the critical frequency of (1), it has served as a convenient parameter for charting the multiplicity of surface-layer characteristics pertinent to propagation via the sea-surface duct.

IV PREDICTION OF ELEVATED LAYERS

When one summarizes the characteristics of enhanced fields, it is clear that their occurrence at VHF and lower frequencies for transhorizon paths of 500 to 700 km may be caused either by tropospheric or by ionospheric layering [6]. However, here our interest is in those enhanced fields associated with tropospheric layering, elevated refractivity layers.

A Occurrence of Flevated Layers

Enhanced fields have been observed in the presence of atmospheric subsidence that produced elevated layers generally consisting of dry warm air overlying cool moist air. One would therefore expect that these tropospheric layers that are conducive to high fields will occur over large land masses generally because of subsidence effects. Advection can also produce these same conditions, particularly in coastal regions, although more frequently over water than over land. Subsidence is also the mechanism that produces the semi-permanent trade wind elevated layers, roughly 5°N to 30°N and 5°S to 30°S, over the oceans. An example of these elevated layers is illustrated by figure 5 [6, 19].

Published information also suggests similar (though less common) elevated layers over ocean regions north of the trade wind region; see figures 6 and 7. Such layering was sufficient on one occasion to support the transmission of an excellent TV picture and sound that persisted over a 1200 mile overwater path (during broadcast hours) for more than two days.

For elevated layers and ducts formed by advection or subsidence, the foregoing indicates that such layers range from semi-permanent conditions (in the tradewind and some coastal regions) to increasingly rare phenomena as we move poleward. Although there are considerable radiosonde data available as historical records and on a world-wide basis, only a very limited amount have been processed into the refractivity-height profiles from which layer characteristics can be determined. Mappings of some characteristics have been long available: very sketchily on a worldwide basis [21,22], in more detail for localized areas [23], and in appreciable detail for the Atlantic tradewind region. For example, the Atlantic tradewind system is well behaved and adequately described in terms of temporal distributions of gradients, heights, thickness, etc. as the high-pressure cells follow a well-defined pattern of shifting with the season (between the West Indies and the Madeira Islands in the North Atlantic and near Ascension Island in the South Atlantic). Of course trapping requires gradients less than -157 N units/km, which are not always achieved by the tradewind inversion layer; the occurrence of tradewind trapping layers (ducts) in the Atlantic tradewind regions varies with the season, from about 30% to 55% of the time. Similarly, these elevated ducts increase in height from east to west and range with the season from about 1.2 to 3.0 km above the sea surface [19].

On most overland troposcatter paths in the temperate zones, the horizontal extent of strong surface refractivity gradients is often limited by the large-scale terrain irregularities. The effect of these gradients, then, is primarily that of improving the coupling efficiency for the elevated layer mode (by reducing the angle of incidence at the elevated layer) rather than providing a surface ducting mode of propagation. These strong, surface, over-land gradients occur more often in the tropics than in the temperate or polar zones [6, 20].

On the other hand, overwater troposcatter paths encounter sea-surface refractivity gradients that are more common, generally stronger, and of greater horizontal extent so that trapping can occur and be effective for greater distances. In this situation, the contribution to the coupling of an elevated-layer mode depends upon leakage from the strong surface layer. The energy that strikes the elevated layer may, therefore, be dispersed over a larger horizontal extent of the elevated layer, and in general, a less marked field enhancement can then be expected. Of course, the signal trapped by the sea-surface refractivity gradient can also contribute to the received field on transhorizon paths, but non-uniformity of the surface layer characteristics (refractivity gradient, layer thickness) can also provide a strong attenuation with distance. Marked field enhancement (via elevated layers) would therefore appear more likely in the VHF and lower SHF frequency range for the long overwater troposcatter paths.

V CONCLUSION

Since 1944, some prediction charts have been available for estimating the occurrence and characteristics of the superrefractive elevated layers or surface layers that constitute surface ducts. The world's land surface and most of the waters bordering the Asian continent have been so charted for both advection and evaporation layers. Most of the world's oceans have been so charted for the occurrence of surface advection layers and also for a few of their characteristics pertinent to anomalous propagation. These charts have limitations due to the available marine meteorological data. The data are particularly inadequate in spatial and temporal coverage. For example, much more data would be useful for the temporal and spatial variation of the layer (or duct) vertical thickness and horizontal extent. Programs such as the BOMEX Sea-Air Interaction Study and the U.S. Coast Guard National Data Buoy Project could lead to a substantially improved data base for the prediction of sea-surface duct characteristics.

Since 1958, estimates have become increasingly available for the occurrence of elevated layers that are sufficiently superrefractive to serve as the upper portion of elevated atmospheric ducts. Summary data on the characteristics of these elevated layers are most sparse overland; the tradewind regions of the world appear to yield the most systematic characteristics, although there is presently much less data available for the Pacific than for the Atlantic tradewind regions. The available meteorological (radiosonde) data have yet to be adequately exploited and processed; one could then determine elevated layer characteristics on a more satisfactory worldwide basis.

From the point of view of operational system design (for communications or long-distance monitoring via ducts), there is a further limitation. This results primarily from the fact that the available solutions have not been reduced as yet to the engineering-type formulas or curves required for the prediction of these anomalous fields on an operational basis.

From the point of view of radio regulation and estimating interference, the observational data and the theory already permit lower-bound predictions of transmission loss. However, prediction of the associated percent occurrence is presently hampered by inadequate summaries of elevated and surface duct characteristics.

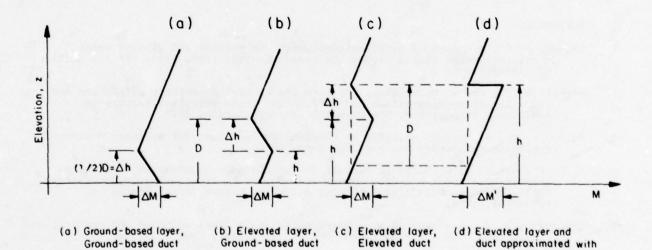
VI REFERENCES

- Booker, H. G., Elements of radio meteorology: How weather and climate cause unorthodox radar vision beyond the geometrical horizon, Proc. IEE Pt. 3A(1) 93, 69-78, 1946.
- Booker, H. G., and W. Walkinshaw, The mode theory of tropospheric refraction and its relation to wave-guides and diffraction, Meteorological Factors In Radio-Wave Propagation, The Physical Society, London, 1946.
- Furry, W. H., Methods of calculating characteristic values for bilinear M-curves, Radiation Lab Report No. 795, February, 1946.
- CCIR, Evaluation of propagation factors in interference problems at frequencies greater than about 0.6 GHz, Report 569, Volume V, Propagation In Non-Ionized Media, 258-287, CCIR XIIIth Plenary Assembly, Geneva (NTIS* Access No. PB244005), 1974.
- Dougherty, H. T., A survey of microwave fading mechanisms, remedies and applications, ESSA Tech. Rep., (NTIS* Access No. COM-71-50288), March, 1968.
- Dougherty, H. T., and B. A. Hart, Anomalous Propagation And Interference Fields, OT Report (NTIS* Access No. PB262477), December, 1976.
- Wait, J. R., Electromagnetic Waves in Stratified Media, Chaps. XI and XII, Pergamon Press, New York, 1962. There is also a Second Edition, 1970.
- Cho, S. H., and J. R. Wait, EM Wave Propagation In A Laterally Non-Uniform Troposphere, FM Report 1, Cooperative Institute for Research In Environmental Sciences (CIRES), University of Colorado, Boulder, CO, June, 1977.

- Wait, J. R., and K. P. Spies, Internal guiding of microwaves by an elevated tropospheric layer, Radio Science 4, No. 4, April, 319-326, 1969.
 Ratner, A. S., Propagation of Flectromagnetic waves in elevated tropospheric 9.
- ducts, limited distribution, 1976.

 Misme, P., Affaiblissement de transmission en propagation guide par conduit 11. atmospherique, Ann. des Telecomm. 29, No. 3-4, March-April, 1/10-10/10, 1974.
- Bean, B. R., B. A. Cahoon, C. A. Samson, and G. D. Thayer, A World Atlas of Atmospheric Radio Refractivity, FSSA Monograph No. 1 (NTIS Access No. 12. AD648-805), 1966.
- 13.
- Sverdrup, H. U., Oceanography for Meteorologists, Prentice-Hall, Inc., New York, 1943.
 Katzin, M., R. W. Buchanan, and W. Binnian, 3 and 9 centimeter propagation in low ocean ducts, Proc. IRE 35, No. 9, September, 891-905, 1947.
 Gentilli, J., A Geography of Climate, The University of Western Australia Press, 14.
- 15.
- Perth, Australia, 1958.
 Richter, J. H., and H. V. Hitney, IREPS: A refractive effects assessment system, 16. Seventh Technical Fxchange Conference, Fl Paso, Texas, 30 Nov. to 3 Dec., 1976.
- 17. Gossard, E. F., and L. J. Anderson, Near Fast and Southeast Asia radio-radar propagation conditions for fleet units, Navy Flectronics Laboratory Report 683, San Diego, California, 1956.
- Schelkunoff, S. A., Microwave transmission in a non-homogeneous atmosphere, 18.
- Bell Tel. Lab. Rep. MM-44-110-53, 1944.

 Dougherty, H. T., L. P. Piggs, W. B. Sweezy, Characteristics of The Atlantic 19. trade wind system significant for radio propagation ESSA Tech. Report (NTIS Access No. AD 651541), April, 1967.
 Hart, B. A., G. D. Thayer, and H. T. Dougherty, Local and Diurnal Variations in
- 20. Ground-Based Radio Refractivity Gradients at Tropical Locations, Office of Telecommunications Rept. OT/TRER 23 (NTIS Access No. COM-75-10831/AS), November, 1971.
- 21. Randall, D. L., A summary of tropospheric duct meteorology at VHF and UHF as observed on a trip around the world, World Conference On Radio Meteorology, Boulder, CO (American Met. Soc. Boston, MA), Spring, 1964.
- 22. Cahoon, B. A., and L. P. Riggs, Climatology of elevated superrefractive layers arising from atmospheric subsidence, World Conference on Radio Meteorology, Boulder, CO (American Met. Soc., Boston, MA), Spring, 1964.
- Hall, M. P. M., Statistics of tropospheric radio-refractive-index soundings 23. taken over a 3-year period in the United Kingdom, Proc. IEE 116, No. 5, May, 685-690, 1969.



an M-discontinuity.

Figure 1. Elevated-layer and surface layer parameters for ducting conditions.

National Technical Information Service, 5285 Port Royal Rd., Springfield, VA 22161 U.S.A.

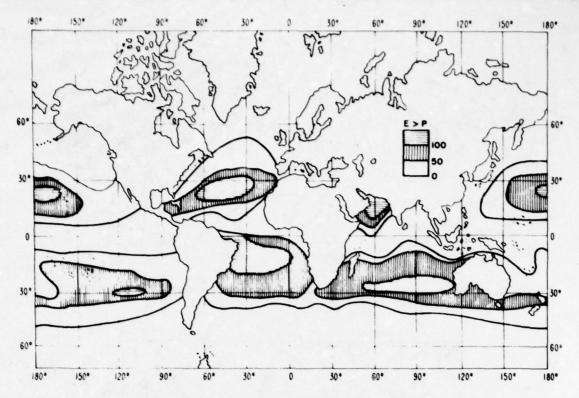
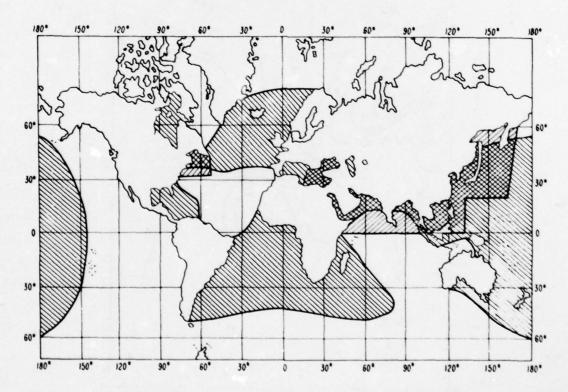


Figure 2. Areas of the world where evaporation exceeds precipitation. The estimated difference is given in centimeters per year [15].



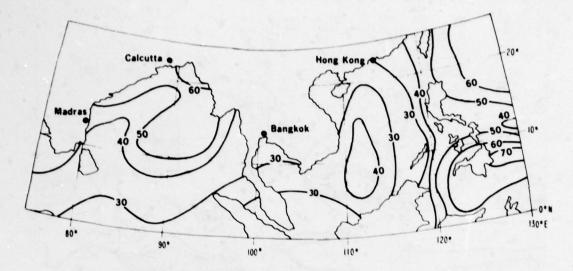


Figure 4. Percent expectancy of extended coverage, S-band radar, Southeast Asia, January [17].

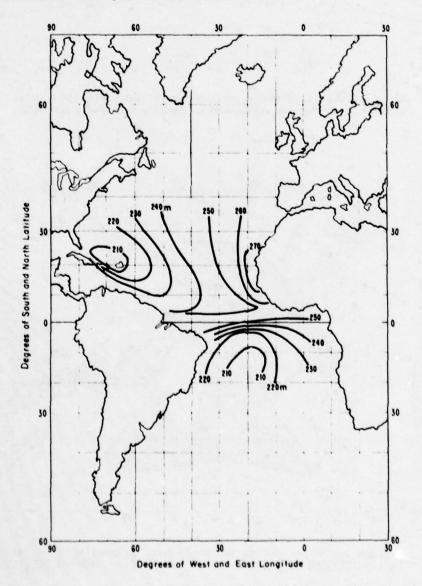


Figure 5. Contours of the mean layer thickness (in meters) for the trade wind inversion in February [19].

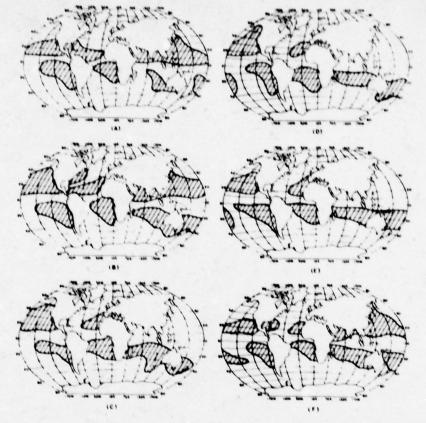


Figure 6. Areas of the world oceans where conditions are favorable for the formation of elevated layers. The charts A through F are for, respectively, January, March, May, July, September, and November [21].

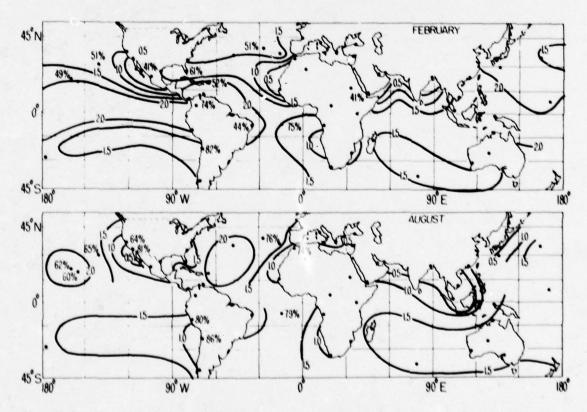


Figure 7. Mean heights (in meters) and percent occurrences (>40%) for elevated layers with gradients <-157 N units/km [22].

A REVIEW OF SCATTER COMMUNICATIONS

by

A.N. Ince, I.M. Vogt and H.P. Williams
SHAPE Technical Centre
P.O. Box 174
The Hague
Netherlands

SUMMARY

Six distinct forms of scatter communication are reviewed, namely ionoscatter, meteorscatter, field aligned scatter, troposcatter, chaff or needles and a novel short range from using ultra-violet radiation. A summary is provided in the form of a figure giving typical values of the frequencies and distances involved; together with the multipath and frequency spreads and typical scatter losses. Each type of scatter communication is then discussed briefly, though because of the greater importance of troposcatter systems this form is dealt with at some length. It is pointed out that troposcatter predictions are still subject to errors in the path loss of 10 dB or more, and that a better knowledge is required of the effect of climatic conditions. A neglected type of scatter communication is meteor burst which offers a simple solution to the transmission of a few telegraph channels for distances of up to 2000 km.

The review concludes with an outline of future prospects and of the problems which require further investigation.

INTRODUCTION

1.1 Scope of Review

Investigations into the scattering of electromagnetic waves from irregularities and inhomogenities tend to fall into three different categories. These are the study and elucidation of geophysical phenomena, the alleviation of interference between radio systems and thirdly the gathering of information for the design of reliable and economic communication systems. These fields are, of course, all inter-related: indeed, in practically all the forms of scatter communication discussed in this review, it was the unexpected discovery of scatter propagated signals which led to the recognition and subsequent investigation of the geophysical phenomena. Conversely studies of the phenomena as such have greatly helped to provide a quantitive information for communication purposes.

This review concentrates on the communication aspects of scatter phenomena and the various forms under discussion are as follows:

- 1. Ionoscatter
- 2. Meteor Bursts
- 3. Field Aligned Scatter
- 4. Troposcatter
- 5. Chaff and Needles
- 6. Optical Scattering by Aerosols

Of the above, by far the most important in practice is troposcatter and therefore this form of scatter communication will be dealt with at greater length than the others.

1.2 A Summary of Basic System Parameters

The various forms of scatter communications under review are shown by the rectangular blocks in Fig 1. These blocks have been drawn indicating the typical frequency ranges involved and the typical distances covered by each type of scatter node. Also indicated are some typical values of the scatter losses incurred and also of time and frequency spreads. The losses quoted are those due solely to the scattering effect and are therefore additional to free space losses. The magnitude of the free space transmission losses can be judged by the sloping dotted lines which are shown for basic transmission losses of 80 to 160 dB in steps of 20 dB. At the microwave end of the spectrum the increase in antenna gains which are possible will more than compensate for the increase in transmission loss except for gains above say 50 dB.

To complete the picture some typical parameters of non-scatter method of communication have also been included in Fig 1, such systems are indicated between arrows to avoid confusion with the blocked in scatter systems.

As is to be expected, scatter systems only come into question at higher radio frequencies, where the wavelengths are small enough to be comparable to the size of irregularities in the propagation medium. Thus the lowest frequencies involved in scatter modes of propagation are those at the upper end of the HF band. For most purposes it can be said that for both ionoscatter and meteorscatter systems the lower frequency limit is about 30 MHz. Also both modes involve scattering from approximately the same altitudes namely 80 to 100 km, with the ionoscatter mode favouring the lower end of this range.

However, there is a marked difference in the rate at which the signal-to-noise deteriorates in the two cases as the frequency of operation is increased. In the case of ionoscatter, the received signal-

to-noise ratio falls off approximately as the fifth power of the frequency, i.e. as f^{-5} , whereas for meteorscatter systems the decrease is approximately proportional to $f^{-2.5}$. This difference is reflected in Fig 1 by drawing the upper frequency limits at 50 MHz and 100 MHz respectively.

The maximum range is about 2000 km for both modes of propagation on account of the more or less equal heights at which scattering takes place. Minimum ranges are determined essentially by the increase in scattering angle in the case of ionoscatter, and by the reduction of the effective length of an ionized trail where meteorscatter is concerned. In practice both modes and also sporadic-E reflections can occur on the same circuit, and this leads to difficulties in the interpretation of ionoscatter statistics since they would be contaminated by the stronger, though intermittent, signals from meteorscatter as well as by sporadic-E reflections of various intensities.

A problem which exists with the longer ranges is to obtain antenna systems with an appropriate low angle of fire. For a circuit length of 1200 km this angle is about 5°, but for a 2000 km circuit the optimum angle is less than 1°, so that the use of an elevated site or very high antennas becomes imperative.

Although the possible range covered by field-aligned scatter is from zero to well over 2000 km, the actual possible dispositions of the terminals is very limited. For these reasons the block is shown with dashed lines and the qualifer "zone restrictions" added in Fig 1.

Turning now to troposcatter one finds a very wide choice of frequencies available. Theory indicates that the signal power should decrease inversely with frequency, but in practice the decrease is usually less than this and may only be inversely proportional to the square root of the frequency.

The maximum distance for a troposcatter system is limited by the increase in scattering angle and to some extent by the gradual reduction in scattering efficiency for common volumes above the height of 2 km. Minimum ranges are simply those for which the scattering angle becomes zero at which point line-of-sight conditions prevail. Before the condition of zero scattering angle is reached, quasi-line-of-sight conditions may occur if there is appreciable diffraction due to knife-edge like contours along the transmission path.

A narrow column on the right-hand side of Fig 1 shows the region around 8 GHz which was used for the "Needles" scatter experiment. This system, which was later named "West Ford", used the scatter from a belt of needle-like copper dipoles placed in a polar orbit at a height of about 4000 km. Although not an unqualified success the system parameters are of interest since extreme multipath and Doppler spreads were involved. Indeed it was this sytem which encouraged further research into the optimum processing of such highly scattered signals.

Needles can be regarded as a special case of chaff. While chaff is normally used to deceive enemy radars, it can also be used to provide a temporary scatter system of communication. Experiments on these lines have shown the feasibility of such a technique and have provided the necessary design data. These experiments are described in one of the following sections.

Finally, mention might be made of recent investigations having been made into an entirely new mode of electro-magnetic scatter propagation namely that of ultra-violet light by aerosols. Such systems are essentially very short range, less than about 2 km, but offer communication possibilities around obstacles which actually improve in the presence of rain. The frequencies to choose for this type of communication are in the range 1.1 to 1.3 x 10^6 GHz, i.e. in the wavelength range 2300 to 2800 Angstroms. This represents the range for which the absorption due to ozone is very great so that all extra-terrestrial sources of noise are obliterated.

With the exception of the ultra-violet system, Fig 1 provides a convenient overall insight into scatter systems as far as propagation characterisites are concerned. However, one should also bear in mind the noise levels which may be encountered and this can be done by reference to Fig 2 which shows noise levels over the same frequency range as used in Fig 1. The need for low noise level locations is clearly high-lighted by Fig 2.

Granted a low ambient noise level, it is apparent that for troposcatter systems (whose frequencies are usually in the range 800 to 5000 MHz) neither the receiver noise figure nor the sky temperature increases much with frequency. Hence the resultant signal-to-noise ratios are not a marked function of frequencies available for this type of communication. The worst situation which can arise is if the sun is in the receiving beam and there is considerable solar activity. This situation is illustrated in Fig 2 for an antenna gain of 23 dB which corresponds to a beam width of about 16°. Taken together Figs 1 and 2 provide a good insight into the possibilities offered by the various scatter systems. However the channel capacities are not necessarily approximately equal to the inverse of the time spread. This is because the system might be intermittent in operation, as is the case in meteorscatter, or because the system may be using adaptive modems.

1.3 Signal Characteristics

Apart from the attenuation due to distance and to scatter losses, signals suffer distortion due to spreading in time and frequency. Some typical time and frequency spreads for the various forms of scatter mechanism are indicated on Fig 1. These spreads are normally measured between the two sigma limits. In practice the tails of the spreads may be quite appreciable as can be seen from the scatter diagram for a troposcatter link as shown in Fig 3. This particular diagram is based on an example given by Barrow (Ref. 1) who describes the results achieved using a RAKE type receiver (Ref. 2)

A number of adaptive techniques are possible, one being the use of adaptive matched filtering based on the correlation of the received signal with a stored reference continuously updated in a

recycling delay line. This offers reasonable performance for only moderately dispersive channels. For strongly dispersive channels the more complicated but efficient method of adaptive weighting of each tap can be used. This leads to a set of waveforms the processing of which has some common features with diversity systems.

Whether the waveforms concerned are derived from separate antennas (space diversity), or resolvable multipaths (time diversity), or from non-overlapping frequency bands (frequency diversity), the analysis follows a similar procedure. The various members of the set can be represented by elements of a column matrix Z, in which each element expresses a sum of the signal and noise voltages, i.e. Z = S + N.

The signal plus noise is put through a weighting filter represented by the column matrix W. The expected value of the output is the scalar W_t Z_1 where the suffix t denotes the transpose. It can readily be shown that the expected value of the noise power is the variance

$$\delta = W_t E (N N_t) W \tag{1.1}$$

The middle term is the covariance noise matrix which is denoted by M where

$$M = E (N N_t)$$
 (1.2)

The leading diagonal gives the aupcorrelation terms whilst the remaining terms are the cross modulation products. Since $M_t \approx M$ the covariance matrix can be diagonalized, the diagonal terms being the eigenvalues and the column vectors of the unitary transform the eigenvectors. This has as its physical equivalent the insertion of a matrix between the channel sources and the weighting filters which transforms the problem into one in which all channels have equal uncorrelated noise power components. Optimum combining then consists of a maximal-ratio combiner as discussed by Brennan (Ref. 3). Brennan's proof involves the use of the Schwartz inequality which enables one to replace the square of the sum of the cross products by the more simply evaluated product of the sum of the squares.

This optimum signal-to-noise ratio is given by

$$(S_N)_{\text{opt}} = S_t h^{-1} S^{\mathbf{g}}$$
 (1.3)

This is given by making the weighting matrix

$$W = K M^{-1} S^{2}$$
 (1.4)

where K is a non-zero complex number and the asterisk denotes the complex conjugate.

The probability of error is determined by the optimum Bayes test for detection. This test expresses the a posteriori probability of the true message occurring conditional upon the received signal having occurred.

Since M is liable to vary considerably an explicit matrix inversion of M in real time is often not practical. The alternative is a recursive relaxation algorithm which simultaneously estimates M and recursively computes W.

The above outline sketches the essential steps taken in any form of adaptive combining of diversity channels. Practical versions can vary in detail and are classified according to the algorithm used. Among the best known are maximum signal-to-noise (MSN) algorithm (Refs. 4, 5) and the least mean square (LMS) algorithm (Refs. 6, 7).

2. IONOSCATTER COMMUNICATION SYSTEMS

2.1 Scatter From The Lower Ionosphere

The possibility that radio waves might be transmitted via irregularities in the ionosphere was considered as long ago as 1913 in an article by Kennelly (Ref. 8). Later Eckersley observed the scattering of echoes from the lower regions in the ionosphere, i.e. at heights of 80 to 90 km, and developed a quantitative theory of such scattering (Ref. 9). Twenty years later Bailey et al (Ref. 10) reported on the results of experiments at 50 MHz over a 1250 km circuit. The reason for the use of the relatively high frequency was to minimize the usual ionospheric absorptions, especially those occurring during SIDs. These experiments demonstrate the potential value of ionoscatter to communications. In later years the interest in ionoscatter systems diminished on account of its inefficiency, i.e. high powers and large antennas were needed if a multichannel system was required. Furthermore the performance in Arctic regions was somewhat disappointing for the reduction in blackouts was not as great as had been hoped.

The design of ionoscatter communication systems cannot be based on any well established formula, for considerable disagreement arises in the basic equations, as derived by different authors. In all cases the formula for the ratio of the received power P_R to the transmitted power P_T takes the form

$$-\frac{P_R}{P_T} \propto \frac{(f_N)^4}{(f)^m} \cdot \frac{1}{r^2 \left(\sin \frac{\theta}{2}\right)^n}$$
 (2.1)

f, = plasma frequency

r = distance from common volume to receiver (or transmitter)

0 = scatter angle

m and n = exponents whose values depend on the author.

In the Booker-Gordon theory (Ref. 11) m = 4 and n = 5, according to Eckersley (Ref. 9) m = 8 and n = 9, while Villers and Weisskoff (Ref. 12) give values of m = 13/3 and n = 16/3 or of m = 11 and n = 12 depending on certain conditions.

Experimentally one finds that n usually lies betwen 6 and 8 but extremes of 4 and 12 can occur. Marked variations in the value of n occur not only between different circuits but for different seasons and time of day, even when the probable effect of meteors has been allowed for. Whatever the exact relationship may be, the fact remains that the scatter losses are appreciable so that high gain antennas and powers in the range of tens of kilowatts are indicated.

2.2 A Transportable Ionoscatter System

In order to reduce the power and antenna requirements SHAPE Technical Centre experimented with a system restricted to only four 50-baud telegraphy channels (Ref. 13). To reduce the error rate the system employed ARQ (automatic request for repetition), a method which had previously been confined to HF systems. ARQ will reduce errors at the expense of intermittent operation, ie. the effective data rate will be reduced. However, the use of diversity considerably diminishes this loss as can be seen from Fig. 4.

In the no-diversity case (curve I) the distribution function is of the Rayleigh type in the lower part of the amplitude range where the signal is essentially due to ionoscatter. In the upper part, the signal is constituted by meteor reflections and the curve bends upwards as shown. In a conventional system where transmission is continuous, the signal is required to be received all the time, or in practice say 99.9% of the time corresponding to an error-rate of 1:10³. A fading margin of about 28 dB between the median level and the minimum acceptable level must therefore be added to the transmission loss when calculating the system parameters.

The use of ARQ introduces the possibility of reducing the fading margin. A reduction of the fading margin from 28 to 8 dB brings the signal duty cycle down from 99.9% to 90% ie. by a relatively small amount because the fades are of short duration.

If the average capacity of traffic is to be kept constant, the transmission rate must be increased by a factor equal to the inverse of the circuit duty cycle. This however, requires widening the channel bandwidth and the resulting increase in receiver noise level offsets part of the saving made on the fading margin. Since there is no correlation between the signal fluctuations on the two opposite paths of an ionoscatter link because of the difference in frequency, the circuit duty cycle can be taken to be the square of the signal duty cycle D and the speed-up factor is equal to $1/D^2$. For a signal duty cycle of 50% for instance, the circuit duty cycle is 25% and the speed-up factor is 4. Curve IV in Fig 4 shows how the transmission rate must be raised in order to keep the traffic capacity constant when the duty cycle decreases.

It can be seen that, as one begins to reduce the fading margin and to transmit faster, the saving increases more steeply than the loss until a maximum is reached for a signal duty cycle of about 50%. As one carries on beyond that point, one gradually enters the region where meteor bursts predominate over the ionoscatter signal and the distribution deviates from the Rayleigh curve. This part of the curve will be considered in the next section.

Distribution functions for dual and quadruple diversity are also given in Fig 4 (Curve II and III). When diversity is applied at the reception, one starts with a substantial advantage over the no-diversity case and the signal distribution follows a less steep curve.

Fig 5 illustrates the power saving as a function of duty cycle. The curves shown have been derived from the previous figure by determining the difference in dB between curves I, II and III on the one hand and curve IV on the other. Starting from the left end of the diagram (continuous transmission), a first maximum is found for a circuit duty cycle of about 40% in the no-diversity case. It corresponds to a power saving of 22 dB. When diversity is used, this maximum occurs earlier and is not so pronounced. Continuing towards lower duty cycle values, the curve bends upwards and rises steadily in the region applicable to meteor burst propagation.

The STC ionoscatter system has a speed-up factor of about 1.1 and therefore needs a circuit duty cycle of 90%. It uses eight-fold diversity and the conditions in which it works are approximately those of the first maximum of Fig 5.

2.3 Two Examples: A Transportable and a Fixed System

The following Table gives the main parameters of the STC system and the corresponding parameters of a more conventional ionoscatter system.

Table 1
Two Examples of Ionoscatter Systems

Circuit	Toulon - The Hague	Naples - Izmir		
Length (km)	1000	1170		
Frequencies (MHz)	40	33 and 48		
Transmitter (kW) power	5	60		
Antennas	Double 5-element Yagis	Corner reflectors with 6 full-wave elements		
Antenna gains (db) Transmitting Receiving	13 13	23 23		
Diversity	Height Space In-band Frequency	Space Frequency		
No of channels Telegraphy Voice	4	16 1		
Reliability at Error Rate of	99.9 1 in 3000	94 - 97 1 in 3000		
Other features	Uses ARQ	Reliability = 99.9% with 4 telegraphy channels only		

The difference in equipment is considerable both as regards transmitter powers and antenna sizes. However where reliabilities of 99.9% are concerned exact comparisons cannot readily be made on account of the statistical rareness of events leading to loss or severe degradation of signals. As an example of the variability of such statistics in one direction the Naples-Izmir circuit gave a 99.9% reliability with as many as 16 channels.

3. METEOR BURST SYSTEMS

3.1 Reflections from Meteor Trails

Recordings of the received signal on ionoscatter links show irregularly spaced bursts of augmented signal strength whose durations are of the order of 1 sec. These are due to reflections from the ionized trails left by meteors as they pass through the atmosphere in the region 80 to 120 km high. Because of the intermittent and peaky nature of these signals, it is usual to refer to "meteor bursts" and to systems using this phenomenon as "meteor burst systems" - it is not implied that the meteor itself is bursting though it most undoubtedly is being worn away.

As would be expected, the variability of the signal powers reflected from the ionized trails caused by meteors is much greater than the variability arising in ionoscatter systems. However, the stronger signals, though few in number, are appreciably stronger than the corresponding ionoscatter signals and this fact is indicated in Fig 1 by attributing a typical scatter loss for the meteor case which is lower by 20 dB. Therefore systems using such ionized trails can operate at lower power levels and lower antenna 4 gains than an ionoscatter system over the same route. The penalty that has to be paid is that reception is intermittent with duty cycles which could be as low as one percent. This point was illustrated in the curves of Fig 4 where it can be seen that if a duty cycle of only is can be tolerated then a gain of some 20 dB results with respect to the median value of the equivalent ionoscatter case.

Explicit expressions can be obtained for the reflected power from meteor trails. These divide into two groups according to whether or not the reradiated energy is from electrons which are close enough for secondary scattering to be appreciable. For trails of small radius the dividing line occurs for an electron line density of about 2 x 10^{14} electrons per metre. Below this density the trails are classified as "underdense" and the effect is a pure scattering phenomena, while higher densities are termed "overdense" and the operative behaviour corresponds to reflection at the surface of the trail.

Underdense trails cause a sharp rise in signal strength followed by an exponential decay, whilst the overdense condition leads to slower rises and a temporary persistence of the signal before rapid decay sets in. Because of the distinct nature of each burst of signal it has been argued that neither space nor frequency diversity are of value in meteorscatter communication. However this ignores the fine structure of the tails of the signals. By making use of the diversity which exists in the tails it is actually possible to double the duty cycle. An example of the diversity obtained in the tails of a meteor burst system is given in Fig 6. For an underdense trail the transmission equation can be expressed as:

$$\frac{P_{R}(t)}{P_{T}} = \frac{G_{T}G_{R}^{\lambda^{2}}}{64\pi^{3}R_{T}^{2}R_{R}^{2}} \cdot \sigma \cdot A_{1} \cdot A_{2}(t)$$
(3.1)

Except for the two terms A_1 and A_2 (t) the equation resembles the well-known radar equation when the distances to the transmitter and receiver are equal.

 A_1 and $A_2(t)$ are two attentuation factors which are equal to unity for zero trail radius and zero time respectively. Both vary exponentially according to the factor, $\exp\left(-\lambda^2\sec^2\phi\right)^{-1}$ where \flat is the angle of of incidence at the trail. Fig 7 shows the transmission loss as given by equation (3.1) for three different frequencies assuming unity antenna gains. Since in practice it is easier to obtain gain at the higher frequencies – especially where low angles of fire are concerned – the favoured frequency range for meteorscatter is 30 to 40 MHz. However, as one of the companion papers will show both higher and lower frequencies have their applications. Experimental circuits have typically used frequencies between 30 to 40 MHz and circuits about 1000 to 1500 km long.

A good example was a system cailed COMET which was operated by STC over a 1000-km path between La Crau in Southern France and Staalduinen in Holland. This is described in Ref. 14. COMET was also tested operationally over an 850 km path between Oslo and Bodø in Northern Norway. This path was a difficult one being largely in the auroral zone. An average capacity of two 50-baud encrypted telegraph circuits was obtained with character error rates generally below 10^{-4} . COMET incorporated two features which were new to meteor burst systems, namely the use of diversity and of ARQ.

Meteor burst trails carried out in Canada showed that even at 100 MHz blackouts could occur (Ref. 15) though at this frequency the number of blackouts in 18 months was only 3 and the total time involved being 7 hours. It is worth noting that experience at HF has shown that, for a given geomagnetic latitude, the blackouts experienced in Canada exceed those in Norway. One would, therefore, expect a better performance in Norway on meteor burst links at the same geomagnetic latitude.

On the experimental side, much remains to be done to determine the frequency and direction of suitable meteors at different latitudes over different distances. No worldwide data on the distribution of meteors are available although some data exists over parts of Canada, the United States, Germany, Italy the United Kingdom, Australia and New Zealand. It is estimated that the data available may be adequate for the prediction of the performance of meteor burst systems to within 10 dB, but this has not yet been demonstrated.

From an applications point-of-view, the following possibilities exist for meteor burst communication:

- (i) Telegraphy communications over medium distances of say 500 to 2000 km using powers of a few kilowatts. The operating frequency could be in the range 30 to 40 MHz, though for military purposes 70 MHz would be better, while for Arctic conditions 100 MHz should be given consideration.
- (ii) The relaying of information from sensors where the information rate is low. Very simple systems would then suffice.
- (iii) Order wire circuits in conjunction with HF systems. For this purpose frequencies in the top half of the HF range would be appropriate. In most cases no extra antenna system would be required.
- (iv) Ground-to-air communication over large stretches of the ocean when delays are not so important. Frequencies in the region of 70 MHz suggest themselves for this purpose.

As far as equipment is concerned, the progress which has been made in storage and processing techniques is so great that a modern version of systems like the COMET would be far smaller and more reliable. Only the antenna systems would remain unchanged though even here an improved knowledge of the hot-spots might lead to better designs.

4. FIELD ALIGNED SCATTER SYSTEMS

Some fifty years' ago it was suggested that the ionosphere could be heated by the use of a powerful transmitter operating at a frequency close to the gyro-frequency. However the required frequency is so low that the antenna systems needed would be prohibitively large and expensive. By making use of deviation absorption to cause heating, a much higher frequency can be used to modify the electron temperature, for the plasma frequency of the F layer can be as high as 10 MHz. It was found that significant changes are caused with transmitter powers of only 160 kW and an antenna consisting of crossed dipoles i.e. a power aperture product of about 100 MW m². However, most of the experimental work done so far used the full output of 1.9 MW of the transmitter at Platteville, Colorado, with the associated antenna giving gains of 19 dB in the HF band (Ref. 16)

From a communications point-of-view the most significant of these changes is the formation of field aligned irregularities which consist of filaments of increased ionization (the increase is of the order of 1%) aligned with the earth's magnetic field. These striations in the electron density pattern owe their existence to the fact that in a collisional plasma, parametric instabilities occur at levels which are many orders of magnitude below those in a collisionless plasma. Non-linear coupling between the electromagnetic heating frequency and the electrostatic plasma frequency produces density fluctuations by ohmic heating.

The irregularities are capable of scattering incident electro-magnetic radiation at frequencies ranging from HF to UHF. Although such field aligned scattering (FAS) can provide communications over ranges

from zero to well over 2000 km, it is highly aspect sensitive, so that communications via FAS is limited to certain zones. This feature has both advantages and disadvantages depending on the application.

From the above it is evident that the communications utilizing the field-aligned scatterers would depend on:

- (1) direction and magnitude of the magnetic field in the disturbed ionospheric region.
- (2) transmitter and receiver locations.
- (3) size of the modified ionospheric volume
- (4) altitude of the modified ionospheric volume,
- (5) ionospheric electron density profiles in the path between the transmitter, the modified inonospheric volume and the receiver.

All these factors are involved in the limitations imposed by the aspect sensitivity. A global map showing the areas which cannot be covered is given in Ref. 17. The map assumes the heater induced irregularities are at a typical height for the F layer. In the North Hemisphere the areas over which reception is not possible include the whole of Canada and Europe north of the Alps. Figs. 8 (a) and (b) show two examples of the type of coverage offered in the Mediterranean at two different cloud heights each for four different positions of heating transmitter in the Adriatic region and a communications transmitter in Spain. The four loci of reception shown in each case represent perfect mirror reflection. In practice reception is possible over a region corresponding to deviations from mirror reflection of up to a degree or two. Even allowing for this spread it is clear that if the cloud height were to increase by natural causes from 240 to 260 km a given region may no longer be covered. Even bigger differences can arise if the frequency is changed since the effects of refraction must be taken into account. Thus a change of frequency to 30 MHz would result in a substantially different coverage at the extremes of the zones.

A practical communications system would therefore have to use a judicious mixture of ionospheric predictions plus real time computer control,

As far as the actual received signal strength is concerned extensive measurements have shown that typical signals have a strength corresponding to scattering cross sections of some 40 to 80 dB above 1 sq. metre. Fig 9 is from Ref. 18 and shows the variation of the minimum echoing area with frequency for experimental circuits of about 2000 km length from Texas to California using the heating transmitter at Plattville, Colorado. The values indicated were for a power of 1.7 MW from the Plattville transmitter and an antenna gain in the vertical direction of 19 dB. If the heater power is decreased the echoing area tends to decrease in roughly the same proportion.

The diurnal variation of the echoing area is shown in Fig. 10 for a frequency of 35 MHz. At higher frequencies the diurnal variations of both the peak and median values are reduced and become more nearly equal.

Knowing the effective echoing area it is a simple matter to calculate the received signal using the radar equation. As an illustration we may take the not untypical case in which the distance, R, between transmitter and receiver is approximately equal to $R_1 + R_2$ where R_1 and R_2 are the paths to and from the cloud, and there R_1 and R_2 are roughly equal. The transmission loss is then given by:

$$\frac{P_{R}}{P_{T}} = \frac{G_{T}G_{R}\lambda^{2}}{4\pi^{3}R^{4}} \cdot \sigma$$

$$= G_{T}G_{R} \left(\frac{\lambda}{4\pi R}\right)^{2} \cdot \frac{4}{\pi R^{2}} \cdot \sigma$$
(4.1)

Where $G_{T,R}$ = transmitting and receiving antenna gains respectively σ = echoing area

The bracketed term in equation (4.1) represents the free space loss and the following two terms the extra loss due to scattering. Let us assume:

$$R = 2 \times 10^{6} \text{m}$$

 $f = 60 \text{ MHz}$
 $G_T G_R = 18 \text{ dB}$
 $P_T = 1.5 \text{ kW}$

Then in terms of decibels equation (4.1) gives:

$$\frac{P_R}{P_T}$$
 = 18 - 134 - 125 + 60 = 181 dB and P_R = - 149 dBW

Assuming the dominant noise is of comsic origin then Fig 2 gives a noise figure of 10 dB re T at 60 MHz. Thus the signal-to-noise ratio in a 3 kHz bandwidth would be 10 dB.

It is of interest to note that over a path of this length, having the same transmitter power, receiver bandwidth and antenna gains as stipulated above, signal-to-noise ratios of 10 to 15 dB were obtained using a heater power at Plattville of only 160 kW and a pair of crossed dipoles for the antenna (Ref. 19). These experiments were performed at frequencies of 30 and 50 MHz, the inferred echoing cross section being of the order of 65 dB sqm.

From the measured results of radar cross-section as a function of frequency Rao and Thome (Ref. 20) have calculated the density of the field aligned striations using a weak scattering model developed by Booker (Ref. 21) for auroral zone propagation from the field aligned irregularities which can occur naturally in such regions. The results indicated that the striations consisted of patches whose electron density had been augmented by some 1% above the ambient value when using the full heater power of 1.9 MW. The region over which such striations occurred was about 100 km in diameter horizontally for the antenna system in question and had an estimated depth of 15 km. The authors concluded that the width of the reception zones would be more a matter of the dimensions of the cloud of irregularities than of the sensitivity to aspect.

As would be expected, the short term signal fluctuations follow a Rayleigh distribution. In order to combat the fading antenna spacings of at least 5 wavelengths are required. Polarization diversity can be obtained since the amplitude correlation coefficients of signals from collocated cross-polarized antennas are in the range 0.3 to 0.5. Frequency diversity requires only a modest spacing in frequency, since correlation bandwidths in the range 30 to 60 MHz are about 3 KHz in the day and only about 1 KHz at night (Ref. 18). Doppler shifts at 50 MHz are about 1 to 2 Hz in the daytime and two to three times as great at night when the shifts are more nearly proportional to frequency.

Although the foregoing resume refers only to FAS, two other forms of scatter phenomena also occur when the ionosphere is irradiated with a powerful transmitter. These are plasma-line scatter (PLS) and ion-acoustic scatter (IAS). However, in both these cases the return frequency is no longer the same as the incident frequency. In the case of PLS the scattered signals appear as a pair of sidebands to the transmitted frequency displaced by an amount equal to the heater frequency. For IAS, unlike FAS and PLS, the relevant irregularities are aligned more or less perpendicular to the geomagnetic field. The response is only to a selected frequency and results in two widebands displaced by a few hundred hertz from the carrier frequency, each sideband having a Doppler spread of about 40 Hz. At present there would appear to be no communications application of either PLS or IAS. In the case of IAS the extreme weakness of the signals received would seem to rule out all practical applications.

The future of FAS as far as communications are concerned is difficult to assess, but it might well have special military applications since the heater could be switched on and off at will. In this respect it may be noted that a period of a few seconds is required for the build-up of FAS and a similar time is taken for its decay. Both build-up and decay are shorter for higher frequencies, which is presumably due to the more rapid initiation and decay of the smaller sized scatterers. A point which could be of practical importance, is the fact that peak heater power rather than average power is the more significant variable (Ref. 18). Using a repetition frequency of 33 pps and duty cycles of either 50% or 25%, much the same result was obtained as with continuous radiation of the same peak power.

5. TROPOSCATTER SYSTEMS

5.1 General

During the early days of Radar there were many incidences of radar signals being occasionally reflected from objects well beyond the radio horizon. These cases could be explained by super-refraction producing radio ducts in the atmosphere. Experiments made after the war showed that beyond the horizon signal levels existed which, though not as powerful as ducted signals, were well in excess of the levels that could be accounted for by diffraction. These signals were explained by scattering from the irregularities which exist in the troposphere, and their average intensity is sufficiently high to provide communication links. Present troposcatter systems provide a capacity of up to say 120 voice channels which compares favourably with the capacity of the other modes of scatter propagation. Indeed, judged solely by the number of circuits in operation troposcatter is by far the most important form of scatter communication.

The wide range of frequencies and the useful distances covered by troposcatter links is apparent in Fig 1. The shorter ranges, i.e. distances in the region of 50 km and just above, fall in an intermediate region where, depending on the details of the path profile, links might make use of diffraction to compensate for non-line-of-sight conditions.

A good insight into the merging of LOS conditions into troposcatter is afforded by the curves shown in Fig 11. Most of the points shown in this figure come from Ref. 22, but some have also been deduced from Ref. 23. It will be seen that the fading range settles down to a Rayleigh distribution as the scatter angle exceeds about 0.7 degrees. Over a smooth earth and for low antenna heights this would correspond to a distance of about 100 km. The losses at the optical horizon of 25 to 30 dB agree with calculations based on the method of Domb and Pryce (Ref. 24).

Due to the high scatter loss, troposcatter links require large antennas, high transmitter powers and frequency coordination areas which are considerably greater than those for line-of-sight radio relay systems. An example is shown in Fig. 12 for a 330 km tropospheric scatter link and an equivalent chain of six LOS links. Although there is not much difference between the two systems, as far as the efficiency of frequency usage (coordination area times the number of frequencies used) is concerned, the larger area for the troposcatter system would complicate the frequency coordination procedures, particularly in Europe where, several countries may be affected.

Although the channel capacity of troposcatter systems is large compared with other scatter systems,

in many cases it is not sufficent for civil transmission links. Because of this and for the reasons given in the previous paragraph the use of troposcatter systems is limited to military applications and to cases where suitably spaced relay stations cannot be provided, e.g. if communications are requird to be over water or over territory which for political reasons is inaccessible. A recent example of the former is the provision of troposcatter communications to British oilrigs in the North Sea.

While most existing troposcatter links employ FDM/FM modulation, the development of high speed digital transmission techniques for LOS and satellite communications has recently led to an interest in considering simi'ar techniques for troposcatter channels. This interest is heightened by the need for encryption and the desire to intergrate troposcatter systems into largers digital nets. Due to the fading and dispersive nature of the troposcatter channel, however, igh speed digital transmission over such channels is more difficult than for LOS or satellite and generally requires the use of adaptive receiver techniques.

5.2 Path Loss Calculations

Several methods have been devised for calculating the path loss from data such as path profile, climatical information and surface refractive index. A comparison of the accuracy of five such methods was made by Larsen (Ref. 25) using experimental data from fifteen different links. Surprisingly enough the method showing the least r.m.s. errors was a graphical one which did not include any climatic factors. However the most widely used methods are those by NBS (Ref. 26) and CCIR (Ref. 27). The CCIR method is in fact based on the NBS method but is easier to use.

The CCIR formula for the long-term median transmission loss is as follows:

$$L(50) = 30 \log f - 20 \log d - F(\theta d) - V(d_e) - G_p dB$$
 (5.1)

where

f = carrier frequency in MHz

d = distance in km

 $F(\theta d)$ = the tropospheric attenuation function

 θ = scatter angle in radians

 $V(d_e)$ = a climatic factor which is a function of the effective distance d_e

GD = the realized combined gain of the antennas

The function $F(\theta d)$ is based on the NBS report and is given in a graphical form parametric in R_S , the surface refractivity. For example for N_S = 301 the values of $F(\theta d)$ are 140, 173 and 224 for θd products of 1, 10 and 100 respectively. These high attenuation values allow for distance as well as scatter angle so that the purely distance term in equation (11) is actually negative. A formula by Yeh (Ref. 28) - which came second best in the comparisons made by Larsen (Ref. 25) - keeps the θ and d functions separate and therefore his 20 log d term is positive.

The climatic factor $V(d_e)$ is also expressed graphically; in this case for nine different types of climate. For values of d_e below 100 km the climatic factor is zero, but for appreciably longer distances this factor can have values of up to \pm 8 dB depending on the climate. The "effective distance" in this context is a function of both the actual distance and of the antenna heights with respect to their foregrounds.

Clearly a good deal of adjustment has gone into the derivation of equation (5.1) which has a distinctly contrived look.

The realized gain of the antennas is given by the sum of the transmitter and receiver antenna gains minus the so-called "antenna-to-medium coupling loss". No exact expression for this coupling loss exists; the CCIR formula for Gp is semi-empirical and is given by

$$G_p = G_T + G_R - 0.07 \exp \left[0.055 \left(G_T + G_R\right)\right] dB$$
 (5.2)

The coupling loss amounts to about 10 dB for antennas whose gain is 45 dB (i.e. if $G_T = G_R = 45$ dB). So unless the antenna gains are exceptionally large, errors in the prediction of the antenna-to-medium coupling loss will not affect the prediction of the transmission loss to any marked extent.

Statistical variations in the transmission loss are taken into account in the CCIR method by the following expression

$$L(p) = L(50) - Y(p) dB$$
 (5.3)

where

L(p) = transmission loss for a given percentage of time, p

Y(p) = function of distance and climate obtainable from graphs

CCIR also given an estimate of the standard error of prediciton, σ_{Δ} , for any percentage, p, of the time. The formula is

$$\sigma_{\Delta}$$
 (p) = $\sqrt{13 + 0.12 \text{ y}^2(\text{p})}$ dB (5.4)

According to this formula the standard error of prediction amounts to 3.6 dB for the long-term median path loss, but can be as high as 14 dB if p is given the high value of 99.99%.

An extensive comparison between measured path loss and path loss calculated using the NBS method has been reported by Longley et al (Ref. 29). On the 279 scatter paths evaluated by these authors the measured tong-term median path loss was on the average 4 dB higher than predicted, i.e. the mean prediction error, $\bar{\Delta}$, of the median path loss was 4 dB. The standard deviation, σ_{Δ} , of the prediction error was 6.5 dB; this relatively large value of the standard deviation was attributed to the short period of measurement on some of the links.

However, similarly high values for the standard deviation have been obtained by Larsen (Ref. 25) from a comparison on 15 links and by STC from measurements on seven links which form part of the so-called ACE-HIGH system in Europe (see Fig. 13). In the latter case, signal recordings were made continuously for more than a year and surface refractive index was measured at all stations. The details of these measurements are given in a companion paper (Ref. 30). A comparison of calculated and measured values of the median transmission loss is shown in Table 2 below.

Table 2

Calculated and Measured Values of the Median

Transmission Loss

OL IL ISSUED BUILD THE TOTAL	CALCULATED		MEASURED	Life time that on the factor	
	LNBS	LCCIR	L _m	L _{NBS} -L _m	L _{CCIR} -L _m
l. Shetland-Sola	130	125	130	0	-5
2. Emden-M.Gladbach	125	125.5	126	-1	-0.5
3. Paris N M.Gladbach	127	126.5	125	+2	+1.5
4. Athens-Izmir	125	126.5	115	+10	+11.5
5. Eskisehir-Izmir	133	123.5	117.5	+15.5	+6
6. Athens-Kefallinia	125	118	117	+8	+1
7. Catanzaro-Kefallinia	121	117	108	+13	+9

In most cases the measured transmission loss was lower than that calculated by either the NBS or CCIR methods. The greater differences between measured and calculated results occurred on links 4 to 7, all of which are located in the Mediterranean area. For these climate type 5, i.e. Mediterranean, of Ref. 27 should have been used. Unfortunately no curves are available for this climate and the predictions had to be based on the curves given for "Maritime Temperate" climate. This may account for some of the discrepancies.

The mean and the standard deviation of the prediction error for the median path losses and for the 99.9% values are shown in Table 3 together with results given in Refs. 25 and 29.

<u>Table 3</u>

Median and Standard Deviation of Prediction Error

		Median path loss		Path loss not exceeded for 99.9%	
		Δ (Calcmeas.) (dB)	σ _Δ (dB)	Δ (Calcmeas.) (dB)	σ _Δ (dB)
Longley (Ref. 29)	NBS	-4.0	6.5		-
Larsen (Ref. 25)	NBS CCIR	-4.0 -4.5	7.2	- 1	-
STC (ACE HIGH)	NBS CCIR	6.8 3.4	6.5 5.8	6.3	8.9

It is interesting to note that there is little difference in the standard deviations of the prediction error for the median path loss. This value ranges from 5.8 to 7.2 dB which is distinctly higher than the predicted values of 3.6 dB. As expected, the standard deviation of the prdiction error for the 99.9% value is higher than that for the median value, for the STC measurements the difference is about 2 dB.

None of the results presented above is very encouraging to an engineer who is faced with the

task of designing a particular troposcatter link. Assuming that a service probability of 90% is desired, the uncertainties involved amount to some 10 dB (1.3 σ - see Table 3). In some cases additional uncertainties may arise because of path profiles which might or might not support propagation by knife-edge diffraction, or for paths along coastal areas where different types of climate could be assumed in the calculations. For example, in 1971 it was planned to install a troposcatter link between Lisbon and Gibralter (440 km). There were two types of climate (Ref. 27) which could be applied with almost equal justifications:

Type 6 : Continental temperate

Type 7a: Maritime temperate, overland

The difference in predicted path loss for the applicable percentage of time was about 10 dB, resulting in estimates for the required transmitter power of 25 kw for climate type 7a but only of 3 kW for climate type 6! A third possibility, namely the assumption of a "Mediterranean" type climate, was not evaluated due to lack of information.

The question arises whether the predictions of the path loss statistics can be improved by taking into account more details of the meteorological conditions. For instance, a high correlation between surface refractive index and montly median transmission loss was observed during the STC measurements (Ref. 30) on those links where sufficient meteorological data were available. However, a large spread in the slopes of the regression lines was also found, so that in fact reliable predictions of the monthly median transmission loss from the surface refractivity would not be possible. Larsen's (Ref. 25) analysis even shows that a better prediction of the path loss can be obtained by removing the terms dependent on Ns from the formulas given by NBS and CCIR.

Thus it would appear that some additional meteorological parameters will have to be used if the accuracy of the predictions is to be improved. In 1968 Battesti et al (Ref. 31) proposed a prediction method based on two meteorological factors. They introduced a parameter T which is given by

$$\mathbf{T} = -\frac{3}{8} \, G_{\rm e} - \frac{5}{4} \, G_{\rm c} \tag{5.5}$$

where

G = the "equivalent gradient" between the ground and the common volume

 G_{C} = the difference between the value of N at a point one kilometre above the base of the common volume and the value at that base

For uniform atmospheric conditions the equivalent gradient is equal to $-\Delta N$, the difference between the surface refractive index and the refractive index measured 1 km above the surface. The T parameter is used with a different expression for path loss to that given by equation (5.1). Comments given in CCIR Report 238-2 state that while good checks with experimental values have been obtained, it is considered that further improvements are possible. Unfortunately details are not given, so it is not possible to judge how successful this method is in allowing for meteorological conditions.

A somewhat different approach is taken by Gjessing (Ref. 32). He determines the slope of the refractive index spectrum from meteorological measurements and uses this to predict the statistical distribution of certain parameters of the link, such as time delay spectrum and effective antenna gain. In addition he calculates the statistical distribution of the effective radius of the earth. No attempt is made in Ref. 32 to use these parameters for the prediction of path loss statistics.

- 5.3 Channel Characterization
- (a) The Channel Model

A typical scatter diagram for the signals received over a troposcatter circuit is shown in Fig. 3. In this example the time spread is about 1 $\,\mu s$ while the frequency spread is about 1 Hz. It is reasonable to assume that the signals can be represented by a continuum of statistically fading paths. This leads to the view that the channel can be modelled as a time varying linear filter whose general form consists of a tapped delay line filter as shown in Fig 14.

By making the two further assumptions that on a short-term basis:

- a received carrier can be characterised as a stationary narrow-band Gaussian process, and
- for narrow-band signals, scatter contributions with different delays exhibit uncorrelated fading

one is led to the generally accepted so-called Wide Sense Stationary Uncorrelated Scattering (WSSUS) model, in which all tap gains are independent, stationary, gaussian processes. This model is described by Bello in Ref. 33.

Using this model it is often convenient to consider the delay power spectrum or multipath profile, which can be pictured with the aid of Fig. 14 as the variance of the complex tap gains as a function of delay. It can be shown that the delay power spectrum is related to the more generally known frequency correlation function by the Fourier transform. In the literature the two-sigma value of the delay power spectrum is usually referred to as multipath delay spread (MDS).

It is important to emphasise the limitation of the WSSUS model for practical troposcatter applications. First of all, it is a stationary model which does not account for long-term variations caused by changing refractivity and meteorological conditions. Moreover, it does not in its basic form account for special propagation effects such as diffraction, ducting or aircraft reflections. To the

extent that such effects can be adequately modelled by the presence of a constant signal in addition to the fading troposcatter signal, it is possible to generalize the tapped delay line model to include them.

It was noted above that the WSSUS is a "short-term" model only. However, it is important to acquire a quantitive feeling for what short-term really means.

Apart from aircraft fading, typical fade rates for troposcatter channels range from 0.1 Hz to 10 Hz. This means that for periods not exceeding, say 0.1s, the channel could be modelled as a time-invariant linear channel (this period is still very long compared with the symbol duration). The term "frozen channel" representation has been coined for this situation. For longer periods, perhaps up to about a quarter of an hour, the stationary WSSUS model applies. Any description to be valid over periods exceeding 4 hour must necessarily be non-stationary in nature. These observations are summarized in Table 4 below.

<u>Table 4</u>

<u>Approximate periods of validity for troposcatter</u>

channel models

Term	Statistical Description	Period of Validity
Frozen channel	Time-invariant	0.1 sec
Short-term Rayleigh	Time-varying stationary	15 min
Long-term	Time-varying non-stationary	-

(b) Analogue Systems

The performance quality of troposcatter radio links utilising frequency modulation (FM) is normally limited by basic thermal noise at low RF signal levels and at high levels by intermodulation noise generated by non-linearities in the equipment or by multipath propagation. For the prediction of the performance of a proposed troposcatter link it is therefore necessary to predict multipath characteristics as well as the path loss statistics. Multipath intermodulation noise may be a limiting factor when the number of voice channels is large. It will also affect the selection of an optimum frequency deviation (Ref. 34).

A comparison between calculated and measured values of multipath intermodulation noise was carried out by STC for five ACE-High links (Ref. 30). The calculations were based on the method presented by C.D. Beach and J.M. Trecker (Ref. 35). Care was taken in the measurements to separate the two sources of intermodulation noise, namely equipment intermodulation and multipath intermodulation. The results of the measurements are summarized in Table 5 below.

Summary of Calculated and Measured Data on 5 ACE-High Links

LINK:	1 SHETLANDS- SOLA	2 EMDEN- M. GLADBACH	PARIS N M. GLADBACH	4 ATHENS- IZMIR	5 ESKISEHIR- IZMIR			
	CALCULATED	CALCULATED AVERAGE MULTIPATH INTERMODULATION(S/I)						
	dВ	dB	đВ	dB	dB			
36 CHANNELS:FM 152kHz CHANNEL 70kHz DEVIATION	45	50	49	63	50			
60 CHANNELS:FM 290kHz CHANNEL 63kHz DEVIATION	39	46.5	44	57.5	43.5			
60 CHANNELS:PRE- EMPHASIS 290kHz CHANNEL 40kHz AV. DEVIATION	51.5	58	56.5	70	56			

	Tibho	SURED MULTIPATH INTE	SAMODOLATION (S)		
290kHz CHANNEL	34	-	48	MULTIPATH INTERMOD. NOT DISTINGUISHABLE FROM BN AND IM.	-
152kHz CHANNEL	39	51.5	54		46
105kHz CHANNEL	41	54	-		49.5
MEASUREMENT IS x.dB BETTER/ WORSE THAN CALCULATION	COMPARIS 5db Worse	ON OF VALUES REFERE	AING TO THE TOP (CHANNEL _	4db Worse

On Link 1, which is an oversea path, and on Link 5 themeasured values of intermodualtion noise are higher than those calculated by 5 dB and 4 dB respectively, whereas on Links 2 and 4 the measured values are better by 1.5 and 4 dB.

Considering the simplifying assumptions made in the method of predicting multipath intermodulation noise, it can be said that the measured and the calculated values are in good agreement.

(c) Digital Systems

If an attempt were made to transmit digital data at a megabit rate over a troposcatter channel, using a standard high-speed quaternary phase shift keyed (QSPK) modem designed for satellite or LOS communication, the resulting error rate would probably render the link useless, even for larger carrier to noise density ratios. This is because the performance would be limited by intersymbol interference resulting from multipath propagation rather than by thermal noise. The error rate resulting from intersymbol interference is often referred to as the irreducible error rate since it cannot be reduced by an increase in the transmit power; it can only be counteracted by the employment of more sophisticated modem designs involving advanced signal processing techniques. A short summary of the techniques which can be used to combat intersymbol interference is given in the Appendix.

Digital modems tend to exhibit very rapid performance degradation as the signal-to-noise ratio decreases below a certain, critical value. This threshold effect combined with the large amount of fading experienced on troposcatter channels tends to make a specification of long-term average performance less useful than for an analogue system. It is therefore almost certain that a digital system would be specified in terms of certain performance limits and the percentages of time during which these limits may be violated (see Ref. 36). The detailed method of specification, however, would depend on user requirements and network structure. Specifications may for example be in terms of:

- (a) rate and duration of outages, an outage being defined as an interval exceeding, say, 0.1 s or 1.0 s, during which the error rate remains above a certain threshold, for example, 10^{-4} .
- (b) average bit error rate (BER), as measured over, say a 15-min interval, not to be exceeded for more than a certain percentage of time.

A user requirement would often be stated in a fashion similar to (a), while a specification such as (b) has the advantage of lending itself more readily to measurement.

In addition there is an important performance measure for digital communications systems which counterpart in the analogue field, namely statistics for loss of bit count integrity (BCI). Loss of any occur in the timing recovery circuits within the modem, but it may also result from excessive error loss of frame synchronisation in an associated TDM equipment, in which latter case the loss closely related to the outage statistics (a) described above.

prediction of link performance the joint statistics of the multipath delay spread (MDS) mould be available. These statistics can be used in conjunction with a short-term the wasts model to derive predicted sample statistics (i.e. frozen channel statistics).

The problem as illustrated in Fig 15. If outage statistics are desired (see statistics) are used with the frozen to obtain average BER statistics, the predicted short-term average modem performance on a WSSUS channel, see

There are the statistics referred to above in sufficient detail. There are the statistics referred to above in sufficient detail. There are the statistics referred to above in sufficient detail. There are the statistics referred to above in sufficient detail. There are the statistics referred to above in sufficient detail. There are the statistics referred to above in sufficient detail.

The experimental results of Ehrman and Graham (Ref. 38) show good correlation between path loss and MDS. However, the experimental data obtained by Sherwood and Fantera (Ref. 39) exhibit a considerable amount of scatter. A low value of correlation can be explained if it is assumed that variations in the path loss occur largely on account of changes in the scatter mechanism within the common volume, e.g. if in the formula for path loss the exponent of the scatter angle were to vary significantly. In this connection it is worth noting that equation (5.5) attaches more significance to G, the parameter accounting for changes in the scatter mechanism, than to G, the parameter determining changes in the effective radius of the earth. In any case there is no doubt that further measurements are needed to determine the long-term statistics of the MDS and the correlation between MDS and path loss.

5.4 Surveys and Economic Factors

Because of the uncertainties which still exist with the setting up of a troposcatter system, in most cases it is worth making a preliminary survey over the intended path. Some of the costs involved in such a survey can be recovered in the cost of the final design since the information acquired on seasonal and diurnal variations as well as on special characteristics of the link such as the presence of knife-edge diffraction can then be put to good use. The final design can then be tackled with greater confidence and with less risk of failing to meet the requirements.

For many surveys the full antenna gains need not be used so that dishes of around 20 ft in diameter are adequate provided they are mounted at the heights of the proposed design. An allowance must, of course, be made for differences in antenna-to-medium coupling losses.

In the case of digital systems the proper measurement of MDS statistics requires that the antenna sizes should be the same as those intended for the final implementation of the link since the delay spread depends on the antenna beamwidths. However, should the maximum expected multipath spread be well within the MDS handling capability of the adaptive modem to be used, then the system can be designed by considering the predicted path loss statistics only.

The period of survey should cover the worst months of the year. These are normally from December to April. The high correlation between the surface refractive index and the montly median signal level can be put to good use in preliminary surveys (Ref. 30). Meteorological records of past years may be used to determine the month wich has a high probability of being the worst month. Comparison of the surface refractive index measured during the survey with records can help to predict the monthly median signal levels for other months of the year and to verify whether the worst case was indeed included in the measurements.

The possibility of effecting economics by a careful assessment of the required relaibilities should not be overlooked, particularly where links in tandem are concerned. If the CCIR recommendations (Ref. 40) are taken as the basis of planning, then the performance requirements are referred to a hypothetical reference circuit (HRC) for e.g. 99.9% of any month. The percentage, p, of any month for which the performance requirement is to be met on the actual circuit of length, L, is then determined by

$$p = 100 - 0.1 - \frac{L}{2500}$$
 (5.6)

where

L = circuit length in km

The method assumes that the periods of degradation occur independently on the different sections of the circuit. This assumption was substantiated by STC measurements taken on two adjacent links of the ACE-High system. These showed that the short-term median signal levels received on the two links are practically uncorrelated (except for high signal levels - see Ref. 30).

Assuming that there is only one worst month in the year, a troposcatter link of 250 km (ie one tenth of the HRC) would then have to be planned on the basis that the stated requirements are met for about 99.99% of the year. A probability as high as this is hardly meaningful in practical terms.

A relaxation of these requirements may be possible when the troposcatter link is to form part of a switched network where alternate routes exist. In this case, performance criteria could be provided to the switching centres to prevent them from selecting temporarily bad circuits. For example, if alternate routes of equal reliability were provided, the applicable CCIR performance criteria would have to be met for 99.7 instead of 99.999% of the year. For a path of 250 km this results in a saving of transmitter power of some 6 to 8 dB, depending on the type of climate.

In systems where a chain of troposcatter links is to be installed it is often found that there is only one link for which it is most difficult to meet the performance criteria. It may then be advantageous to relax the requirements on that link and to tighten them on the other links.

A reduction of transmitter power may also be possible, particularly on diffraction links, by providing steerable feeds (Ref. 41) so that the beam can always be pointed in the optimum direction.

Finally a saving in running cost can be achieved by adjusting the transmit power to match the propagation conditions, e.g. by controlling the beam voltage of the power amplifier klystron as a function of the median signal level received at the other station.

5.5 Frequency Considerations

At present there are no specific frequency bands allocated by the ITU for exclusive use by troposcatter systems. Consequently these systems must share the bands allocated to other terrestrial services, such as multi-channel LOS and TV broadcasts. For example in the frequency band 790 to 960 MHz (in which

most of the ACE-High stations operate) troposcatter systems may operate only on a secondary basis to TV broadcasting. Information from Western European Nations indicates that the number of TV emissions on this band (TB-band V) will continue to increase.

A move will be made at the 1979 WARC Meeting to recommend preferred frequency bands for troposcatter communications, but it is not expected that adequate frequency space will become available.

Digital troposcatter systems employing PCM as analogue to digital conversion techniques require more than twice the bandwidth of analogue systems. The introduction of such systems will further aggravate the situation, so there are good reasons for investigations on how to reduce the bandwidth occupancy.

By abandoning frequency diversity the bandwidth occupancy can be halved. Alternative methods of diversity could be used instead. These are:

(a) Angle diversity, (Ref. 42)

Vertically displaced feed horns are used at the receiving antennas to produce two or more beams with a vertical separation of about one to two beamwidths. The signal levels received on the higher beams are lower than the level received on the low beam, but they are still sufficient to provide diversity gains. It has been found that 3 vertically displaced beams would effectively provide dual diversity (Ref. 42).

(b) Space-polarization diversity (Ref. 43)

Orthogonally polarized signals are transmitted by two antennas. Each receiving antenna receives both transmitted signals, resulting in four received signals. Here the two orthogonal polarisations are used to provide additional space diversity. Since the signals on the crosspaths are highly correlated an effective three-fold diversity can be obtained. However, there are considerations which indicate that the high correlation on the cross-path could be alleviated by using different antenna spacings at the two sites, the distance between antennas at one site being about twice the distance between antennas at the other site.

Yet another way of preserving bandwidth on digital systems is to use modems employing multi-level signalling. However, to achieve the same performance as with say QPSK modems an increase in transmitter power is required.

6. NEEDLES AND CHAFF

In the Second World War considerable use was made of clouds of small metal strips to deceive enemy radars. Such clouds were given various names but are now generally known as "chaff". While the purpose of chaff was originally to create a strong backscatter signal, it can equally well be used bi-statically and therefore lend itself to providing a communications link.

In the summer of 1958 a very special version of chaff was conceived in which extremely thin dipoles were to be spread in a belt around the globe at a height of some 4000 km. Because of the nature of the dipoles the project was at first called "Needles" but later was given the name "West Ford" (Ref. 50). The second launch, which was in May 1963, put a pay load of 20 kg into a nearly circular polar orbit with a mean altitude of 3700 km. The load consisted of 5 X 10^8 copper dipoles each 1.78 cm in length.

On the chart in Fig 1 the original name "Needles" has been used on account of being more descriptive of the system. The figure shows the frequencies involved as around 8 GHz, with a range of operation from close by to in excess of the 2000 km to which the graph goes. The scatter loss is shown as being as high as 153 dB. This is not surprising considering that within a month of being launched the needles had dispersed to such an extent that they were now about 400 metres apart on the average. Thus the common volume to 60 dB ground antennas contained only about 600 dipoles. The resulting echoing area would be of the order of a tenth of a square meter. At this stage the system was only capable of sustaining a single telegraphy channel even with the use of powers in the region of 100 kW.

A system on the lines of the needles experiment has considerable advantages from a military point of view since it would be immune to physical attack and direct jamming. Continuous world-wide coverage could be obtained with only two 8000 km altitude belts, one polar and one equatorial. However, there was considerable opposition to the scheme from astronomers and other bodies, not so much on account of the West Ford experiment itself (which was deliberately designed to limit the existence of the belt to a few years) as on the grounds that it would lead to the establishing of further belts of greater density.

Because of the considerable multipath spread involved in the West Ford experiment, the study of suitable techniques to combat such multipath effects was greatly stimulated. This was one of the bye-products of the experiment which, in its technical details, may be said to have been in good quantative agreement with predictions (Ref. 51).

If circumstances are such that even only a short period of communication is of value, then chaff could be dropped in a common volume using either an aeroplane or dispersal from a rocket. A requirement of this nature could arise if the middle terminal of two tropospheric links in tandem were out of action and the signals were required to overpass this terminal to span a total distance of, say, 600 km. Another application would be to mobile communications between terminals which were not in line-of-sight yet not separated by a distance of more than, say, 250 km.

Both cases have been considered in detail by Ince et al (Ref. 52) in an article which includes experimental evidence obtained by dropped chaff from an aircraft. The aircraft experiments were performed at a frequency in the region of 900 MHz. The dispensing of some 2.5 kg of chaff at an altitude of about

20,000 ft took about 4 seconds and resulted in useful signals for a period of 10 to 30 minutes between terminals 600 km apart. In order to ensure that cross-polarization signals could be received it was necessary to prevent the chaff falling too much horizontally and so the aluminium strips were made twisted. The resultant rotation in the air was probably the cause of the fairly rapid Rayleigh fading experienced (4 to 5 fades per second). The time the chaff is in the common volume is much affected by the wind conditions. Since the wind velocity tends to increase markedly above about 25,000 ft it is best to carry out the dispensing at below this height.

For use between mobile terminals, a possible system is one using 1 kw of power at 3 GHz and 1 meter dishes. Then it is estimated that a rocket with a payload of 4 kg of chaff released at 30,000 ft could provide a single FM voice channel for about one hour. This assumes that the terminals track the cloud of chaff until it has fallen to about 7,000 ft.

OPTICAL SCATTERING BY AEROLS

The word "optical" is used in its broadest sense here to distinguish the part of the spectrum used here from the radio spectrum. A practical system employing scatter in the visual range is at present out of the question on account of the competing radiations (Refs. 53 and 54). However, by going to the far ultra-violet region, the natural radiation from the sun is very greatly attenuated - indeed it is impossible to measure the radiation level in this region at ground level. At the same time there are no interfering sources.

The extremely high attenuation to ultra-violet radiation from the sun afforded by the ozone in the atmosphere is illustrated by Fig 16 which is based on attenuation figures given by Wulf and Deming (Refs. 55 and 56). The maximum attenuation is at a wavelength of 2600 % and is as high as 400 dB, a remarkable figure when one considers that the total ozone content of the atmosphere is equivalent to a layer of only 2.5 millimetres thickness at ground level. Fig. 16 has also on it the attenuation due to the other constituents of the atmosphere calculated via measured values at ground level (Ref. 57) where the contribution to the attenuation by ozone is relatively small. To convert the latter curve to values at ground level one can use the fact that the height of the homogeneous atmosphere is about 6 km.

A system using scattering in the region 2300 to 2800 $\overset{\land}{A}$ is described in Ref. 58. The transmitter consisted of a high power flashlamp with a maximum output of 1000 joules per flash, when operated at about 1000 V. Flashes were of about 1 msec duration.

For the receiver multilayer filters were used to pass only the required part of the spectrum. Experiments were performed with different blocking angles, i.e. for different scattering angles at a distance around 1 km. Greatly enhanced signals were obtained at high angles of elevation when there was an appreciable rainfall.

All this work is still in the preliminary experimental stage and some of it is classified. It is therefore too early to give a more detailed account.

8. CONCLUDING REMARKS

Of the five distinct radiowave scatter systems considered in this review, three rely on quite small perturbations on the ambient conditions. The other two, namely meteor burst and chaff, depend on scattering from greatly augmented ionisation and from highly conducting strips respectively. However, from a systems point of view these distinctions are academic. A more practical grouping is into systems involving man-made scatter conditions, i.e. field aligned scatter and chaff or naturally occurring scatter phenomena.

Both the man-made scattering phenomena would seem to have their major applications in military systems, where they would have the advantage of being capable of being switched on at will - in the case of field aligned scatter the system can also be switched off at will. The very special nature of both of these two artificially generating scatter systems makes it difficult to forecast the applications to which they may be put in the future. It is worth noting that field aligned scatter also occurs naturally in the auroral zone and communication has often been achieved using frequencies in the VHF band, but the results achieved so far are too variable to be of practical use.

The scatter mode with the most obvious wide application is troposcatter. In the fairly extensive review of troposcatter systems made in this paper it is clear that performance tredictions still leave something to be desired. Estimates which can be 10 dB or more out are not a cheerful prospect for the designer. The problem is aggravated by the fact that our knowledge of climatic effects is still limited to certain regions of the world.

Less obvious, but surely with a certain future in special applications, is the use of meteor burst communications. The neglect of this form of communication can be attributed to a number of factors, but the vast improvements made in the last two decades in circuitry will act very much to the advantage of meteor burst systems. Here again there is a need for a more world-wide knowledge of scatter mechanism-in this case of the distribution of the radiants of meteors.

APPENDIX

Principles of Modulation and Signal-Processing Techniques for Troposcatter Channels

During the past few years, several study programmes have been directed towards the problem of choosing an efficient modem design for megabit-per-second digital transmission over troposcatter links. The findings of these studies have been extensively reported in the literature (Ref. 44 to 49).

The adoption of a suitable digital baseband modulation technique (Ref. 48) would enable digital traffic to be passed over existing FDM/FM troposcatter links. For a link carrying 72 voice channels, the maximum achievable data rate is about 0.5 Mbit/s, which is entirely inadequate to carry an amount of

traffic equivalent to 72 voice channels in digital form. Other modulation methods must therefore be sought which utilize bandwidth more efficiently.

Assuming that QPSK is a suitable modulation technique, the question remains of how the technique may be modified to provide adequate multipath protection features. At least five basic approaches to this problem are known to exist.

- (a) Parallel processing
- (b) Transmitter time gating
- (c) Receiver time gating
- (d) Adaptive diversity equalization
- (e) Viterbi decoding algorithm

Of these, (b), and (c) are applicable only to situations where the multipath spread is not large compared to the bit duration, while (a), (d) and (e), at least in principle, will work on any time-variant linear channel. A typical value of the multipath spread for a long troposcatter hop is about 250 ns.

The idea behind parallel processing is to split the high-speed data stream into a number of low-speed signals which can be transmitted in parallel over the channel by the use of some kind of frequency division multiplexing. In this way the symbol rate on each subsignal becomes low enough to make multipath effects unimportant. However, the equipment complexity grows almost linearly with the number of sub-signals, and intermodulation distortion is a potential problem when the number of subsignals is large.

With transmitter time gating a guard interval is established between adjacent symbols. If the guard time can be made to exceed the multipath spread, intersymbol interference becomes negligible. Transmission rates up to about 4 Mbit/s can be achieved for channels having a multipath spread of 250 ns, but the bandwidth requirements increase with increasing multipath spread.

Receiver time gating implies that the receiver disregards that part of a received symbol which is known to be most heavily corrupted by interference from adjacent symbols. The method is inefficient in terms of received power utilization and is limited to data rates not exceeding 3 Mbit/s for a multipath spread of 250 ns (Ref. 47).

Adaptive diversity equalization is a technique by which the received signal is processed in a time-varying linear transversal filter to remove intersymbol interference. The filter tap gains are continuously adjusted to match the channel characteristics at any instant in time.

The number of taps required depends on the multipath spread and the transmission rate. A limit to the number of taps, and therefore to the attainable transmission rate, will ultimately be imposed by a degradation in signal-to-noise ratio and by equipment hardware constraints. However, data rates in excess of 10 Mb/s should be achievable.

The Viterbi decoding algorithm can be employed for the maximum likelihood detection of a digital signal which has been corrupted by intersymbol interference (Ref. 49). With this approach, the troposcatter channel is viewed as a natural convolutional coder for which the code is both unknown and time-varying, so that the receiver has the dual task of estimating the code and of performing the decoding. For transmission at megabit data rates, the processing speed required for the digital circuitry is extremely high, but the Viterbi decoder is potentially capable of handling data rates in excess of 10 Mbit/s.

Obviously, these five basic methods can be combined in several ways to meet a given set of requirements in a more efficient and/or economical fashion. For instance, transmitter time gating can be combined with a simple equalizer to remove residual intersymbol interference.

It is essential to realize that multipath propagation is not necessarily an entirely undesirable feature of the troposcatter medium. In fact, a properly designed modem is capable of exploiting the time dispersion of the channel as a sort of implicit diversity. When viewed in the frequency domain, the diversity effect arises whenever the spectrum of the digital signal is much wider than the correlation bandwidth of the channel, with the result that fading is very unlikely to affect the whole spectrum at the same time.

To summarize briefly, multipath effects associated with the troposcatter channel significantly complicate the modem design, but with a proper modem the presence of multipath has a beneficial effect in that it tends to reduce the impairments caused by fading.

REFERENCES

INTRODUCTION:

- BARROW, Bruce B., Sept/Oct 1968, "Tropospheric-scatter measurements using a RAKE receiver". IFE Conf. Publication No. 48., pp. 125-137.
- PRICE, R., and GREEN, P.E. jr., March 1958, "A communication technique for multipath channels". Proc. IRE, Vol. 46, pp. 555-570.
- BRENNAN, D.G., October 1955, "On the maximum signal-to-noise ratio realizable from several noisy signals". Proc. IRE Vol. 43, p. 1530 (letter).
- 4. APPLEBAUM, S.P., September 1976, "Adaptive arrays". IEEE Trans., Vol. AP-24, po. 585-598.

- BRENNAN, L.E. and REED, L.S., March 1973, "Theory of adpative radar" IEEE Trans., Vol. AES-9, pp. 237-252.
- WIDROW, B., MANTLEY, P.E., GRIFFITHS, L.J. and GOODE, B.B., December 1967, "Adaptive antenna arrays". Proc. IEEE, Vol. 55, pp. 2143-2159.
- GRIFFITH, L.J., October 1969, "A simple adaptive algorithm for real-time processing in antenna arrays".
 Proc. IEEE, Vol. 57, pp. 1696 1704.

IONOSCATTER:

- 8. KENNELLY, A.E., July 1913, "The daylight effect in radio telegraph". Proc. IRE, Vol. 1, pp. 39-62.
- 9. ECKERSLEY, T.L., September 1932, "Studies in radio transmission". Jour. IEE, Vol. 71, pp. 405-454.
- BAILEY, D.K., BATEMAN, R. and KIRBY, R.C., October 1955, "Radio transmission at VHF by scattering and other processes in the lower ionosphere". Proc. IRE, Vol. 43, pp. 1181-1230.
- 11. BOOKER, H.G. and GORDON, W.E., September 1957, "The role of stratospheric scattering in radio communication". Proc. IRE, Vol. 45, pp. 1223-1227.
- VILLARS, F. and WEISSKOPF, October 1955, "On the scattering of radio waves by turbulent fluctuations of the atmosphere". Proc. IRE, Vol. 43, pp. 1232-1239.
- BARTHOLOME, P.J., 1968, "Survey of ionospheric and meteor scatter communications". "Ionospheric Radio Communications" ed. K. Folkestad, Plenum Press, pp. 143-154.

METEOR BURST:

- BARTHOLOME, P.J. and VOGT, I., April 1968, "COMET A new meteor-burst system incorporating ARQ and diversity reception". IEEE Trans, Vol. COM-16, pp. 268-278.
- MAYNARD, L.A., 1968, "Meteor burst communications in the Arctic". "Ionospheric Radio Communication", ed. K. Folkestad, Plenum Press, New York, pp. 165-173.

FIELD ALIGNED SCATTER:

- CARROLL, J.C., VIOLETTE, E.J., and UTLAUT, W.F., November 1974, "The Platteville high power facility" Radio Sci., Vol. 9, pp. 889-894.
- STATHACOPOULOS, A.D. and BARRY, G.H., November 1974, "Geometric considerations in the design of communications circuits using field-aligned ionospheric scatter". Radio Sci., Vol. 9, pp. 1021-1024.
- BARRY, G.H., November 1974, "HF-VHF communications experiment using man-made field-aligned ionospheric scatterers". Radio Sci., Vol. 9, pp. 1025-1032.
- ULTAUT, W.F., VIOLETTE, E.J., and MELANSON, L.L., November 1974, "Radar cross section measurements and vertical incidence effects observed with Platteville at reduced power". Radio Sci. Vol. 9, pp. 1033-1040.
- RAO, P.B., and THOME, G.D., November 1974, "A model for RF scattering from field-aligned heater-induced irregularities". Radio Sci., Vol. 9, pp 987 996.
- BOOKER, H.G., 1956, "A theory of scattering by non-isotropic irregularities with application to radar reflections from the aurora". J. Atmos. Terr. Phys., Vol. 8, pp. 204 - 221.

TROPOSCATTER:

- 22. JANES, H.B., April 1955, "An analysis of within-the-hour fading in 100- to 1000 Mc transmissions". J. of Res. NBS Vol. 54, pp. 231-250.
- MELLEN, G.L., MORROW, W.E. Jnr., POTÉ, A; J., RADFORD, W.H. and WIESNER, J.B., October 1955, "UHF long-range communication systems". Proc. IRE Vol. 43, pp. 1269-1281.
- DOMB, C. and PRYCE, M.H.L., September 1947, "The calculation of field strengths over a spherical earth".
 Jour. IEE Vol. 94, Pt. III, pp. 325-336.
- 25. LARSEN, R., 30 September 2 October 1968, "A comparison of some troposcatter prediction methods". "Tropospheric Wave Propagation". IEE Conference Publication No. 48, pp. 110-117, Inst. of Elect. Eng., London.
- RICE, P.L., LONGLEY, A.G., NORTON, K.A., BARSIS, A.P., "Transmission Loss Predictions for Tropospheric Communication Circuits". NBS Tech. Note 101.
- CCIR Report 238-2(1974), "Propagation data required for trans-horizon radio-relay systems". XIIIth Plenary Assembly, Vol. V, pp. 209-229, Geneva 1974.
- YEH, Leang P., September 1960, "Simple methods for designing troposcatter circuits". IRB Trans. Vol. CS-8, pp. 193-198.
- 29. LONGLEY, A.G., July 1971, "Measured and predicted long-term distributions of tropospheric transmission

- loss". Rep. No. OT/TRER 16, US Dept. of Commerce, Office of Telecommunications.
- INCE, A.N. and WOGT, I.M., October 1977, "Propagation measurements on the ACE-High troposcatter systems, AGARD Symposium on "Aspects of Electro-magnetic scattering in radio communications". Cambridge, Mass.
- BATTESTI, J., BOTHIAS, L. and MISME, P., Mai-Juin 1968, "Calcul des affaiblissements en propagation transhorizon à partir des paramètres radiométeorologiques". Ann. des télécomm. Tome 23 pp. 129-140.
- GJESSING, D.T. and McCORMICK, K.S., September 1974, "On the prediction of the characteristic parameters of long-distance tropospheric communication links". IEEE Trans. Vol. COM-22 pp. 1325-1331.
- 33. BELLO, Phillip A., April 1969, "A troposcatter channel model". IEEE Trans. Vol. COM-17 pp. 130-137.
- CCIR Report 446 (1974), "Trans-horizon radio-relay systems" XIIIth Plenary Assembly, Vol. IX, pp. 228-231.
- 35. BEACH, C.D. and TRECKER, J.M., January 1963, "A method for predicting interchannel modulation due to multipath propagation in FM and PM tropospheric radio systems". BSTJ pp. 1-36.
- CCIR Report 378-2, "Digital radio-relay systems" XIII Plenary Assembly, Vol. IX, pp. 212-218, Geneva 1974.
- 37. BELLO, P.A., EHRMAN, L and ALEXANDER, P, February 1971, "Signal distortion and intermodulation with tropospheric scatter". AGARD Conf. Proc. No. 70 "Tropospheric Radiowave Propagation", Pt. II pp. 36-17.
- 38. EHRMAN, L and GRAHAM, J.W., January 1973, "Digital troposcatter experiments" RADC Rep. RADC-TR-72-350 from Signatron Inc. Rep. SIG-A-125.
- 39. SHERWOOD, A.R. and FANTERA, December 1975, "Multipath measurements over troposcatter paths with application to digital transmissions". Nat. Tele. Conf., Conf. Ref., Vol. 2, pp. 28-1 tp 28.5 IEEE Cat. No. 75CH 1015-7 CSCB.
- CCIR Recommendation 397-2, 1974, "Trans-horizon radio relay systems". XIIIth Plenary Assembly, Vol. IX, pp. 47-48.
- MONSEN, P, PARL, S.and PIENNE, J.N., "Adpative antenna control". Interim Tech. Rep., Signatron 0AAB07-76-C8085.
- MONSEN, P., April 1972, "Performance of an experimental angle-diversity troposcatter system". IEEE Trans. Vol. COM-20 pp. 242-247.
- FLORMAN, E.F., April 1968, "Comparison of space-polarization and space-frequency diversity". IEEE Trans. Vol. COM-16 pp. 283-288.
- 44. BOXALL, F.S., March 1975, "Time shared codecs for multichannel delta modulation and differential PCM", IEEE Transactions on Communications, Vol. COM-23, No. 3, pp. 367-378.
- 45. MONSEN, P. and RICHMAN, S.H., August 1973, "Adaptive Data Transmission Study", RADC-TR-73-268.
- 46. CREPEAU, P.J., June 1973, "Digital Troposcatter: State-of-the-Art Modulation Techniques", Technical Report ECCM-4132, US Army Electronics Command, Fort Monmouth, New Jersey.
- 47. BELLO, P.A. et al., May 1967, "Troposcatter Multichannel Digital Systems Study", RADC-TR-67-218.
- 48. BELLO, P.A., April 1969, "Selection of Multichannel Digital Data Systems for Troposcatter Channels". IEEE Trans. Comm. Techn. Vol. COM-17, No. 2, pp. 138-161.
- 49. FORNEY, G.D. Jr., May 1972, "Maximum-Likelihood Sequence Estimation of Digital Sequences in the Presence of Intersymbol Interference", IEEE Trans. Inf. Th., Vol. IT-18, No. 3, pp. 363-378.

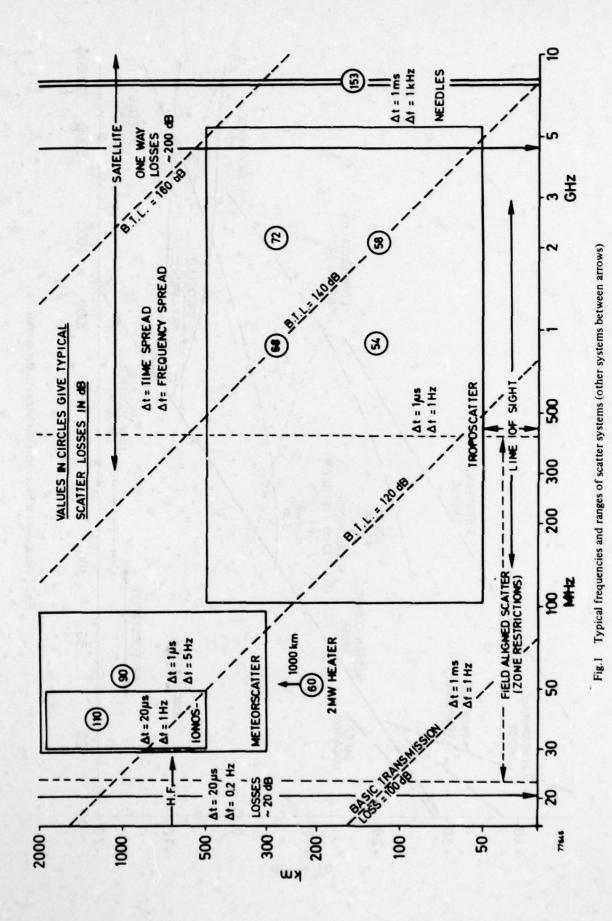
NEEDLES AND CHAFF:

- MORROW, W.E. Jr., and ROGERS, T.F., May 1964, "The West Ford experiment and introduction to this issue" Proc. IEEE, Vol 52, pp. 461-468.
- LEBOW, I.L., DROUILLET, P.R. Jr., DAGGETT, N.L., HARRIS, J.N. and NAGY, F. Jr., May 1964, "The West Ford belt as a communications medium". Proc. IEEE, Vol. 52, pp. 543-563, May 1964.
- 52. INCE, A.N. VOGT, I.M. and GÖSSL, H., August 1976, "Design of chaff and chaff-supported communication systems". IEEE Trans., Vol. COM-24, pp. 785-803.

OPTICAL SCATTERING:

- LENNER, Robert M. and HOLLAND, Alfred E., October 1970, "The optical scatter channel" Proc. IEEE, Vol. 58., pp. 1547.
- KENNEDY, Robert S., October 1970, "Communication through optical scattering channels: an introduction". Proc. IEEE, Vol. 58, pp. 1651.

- 55. WULF, O.R. and DENING, L.S., 1936, "The theoretical calculation of the distribution of photochemically formed ozone in the atmosphere". J. of Terr. Magn. Atmos. Elect., Vol. 41, pp. 299-310.
- 56. WULF, O.R. and DEMING, L.S., 1937, "The distribution of atmospheric ozone in equilibrium with solar radiation and the rate of maintenance of the distribution". J. of Terr. Magn. Atmos. Elect., Vol. 42., pp. 195-202.
- 57. DAWSON, L.H., GRANATH, L.P. and HULBURT, E.O., 1 July 1929, "The attenuation of ultra-violet light by the lower atmosphere". Phys. Rev., Vol. 34, pp. 136-139.
- STOKES, FISHBURNE, E., NEEK, Michael E and SANDRI, Guido, February 1976, "Voice communication via scattered ultravoilet radiation". ARAP Rep. No. 274, Vol. 1. US Army Elect. Command, Fort Monmouth, NJ.



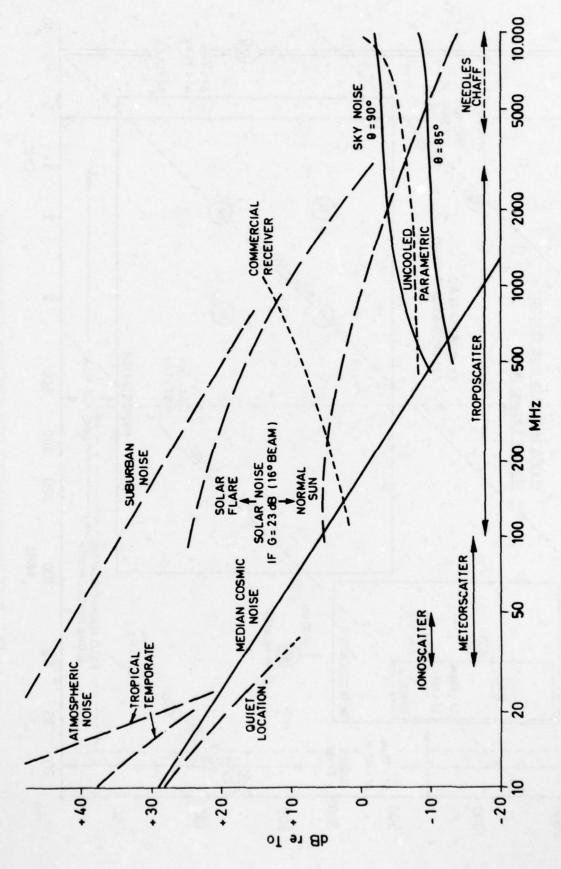


Fig. 2 Noise levels at frequencies involved in scatter systems

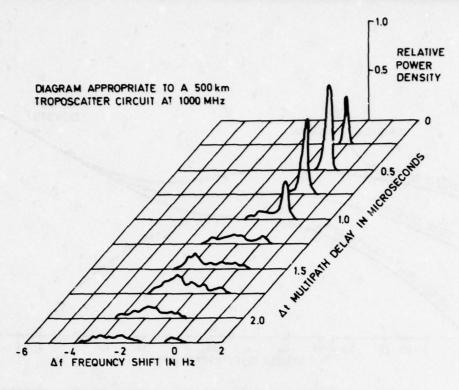


Fig.3 Typical scatter function diagram

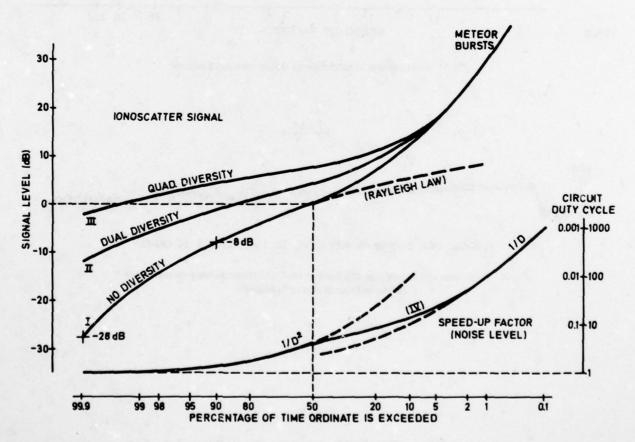


Fig.4 Statistical distribution of signal levels at 40 MHz on a 1000 km circuit

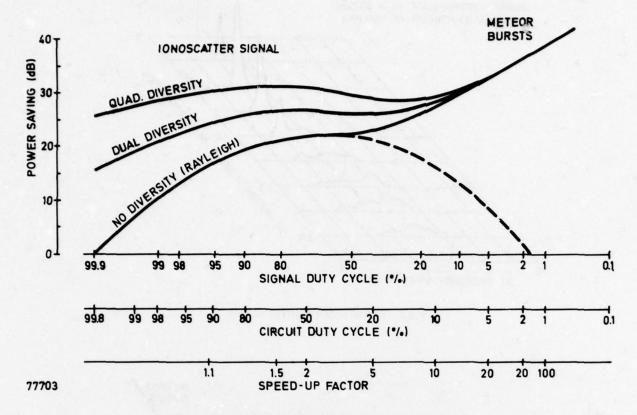


Fig.5 Power saving in intermittent scatter communications

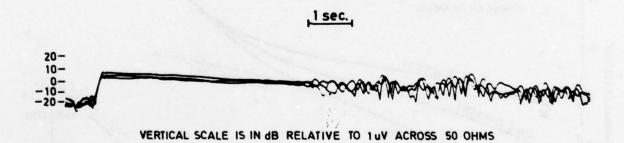


Fig.6 Superimposed recordings of a meteor trail reflection showing uncorrelated fading in three diversity branches

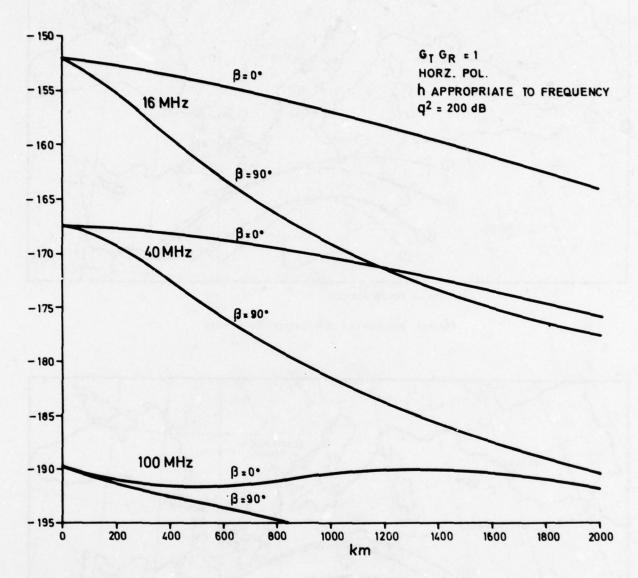


Fig.7 Transmission loss for underdense meteor trails

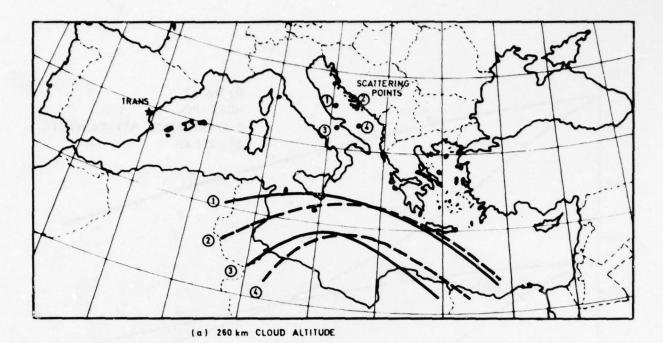


Fig.8(a) Example of F.A.S. coverage f = 50 MHz

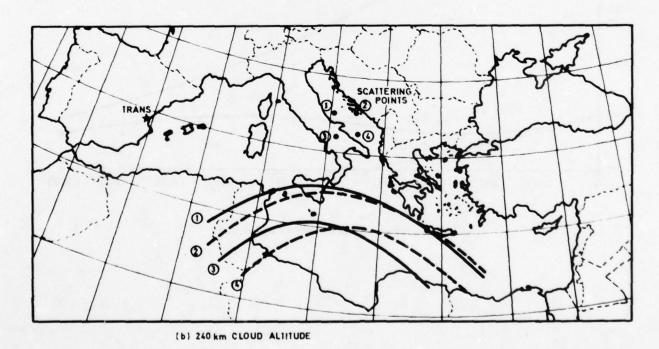
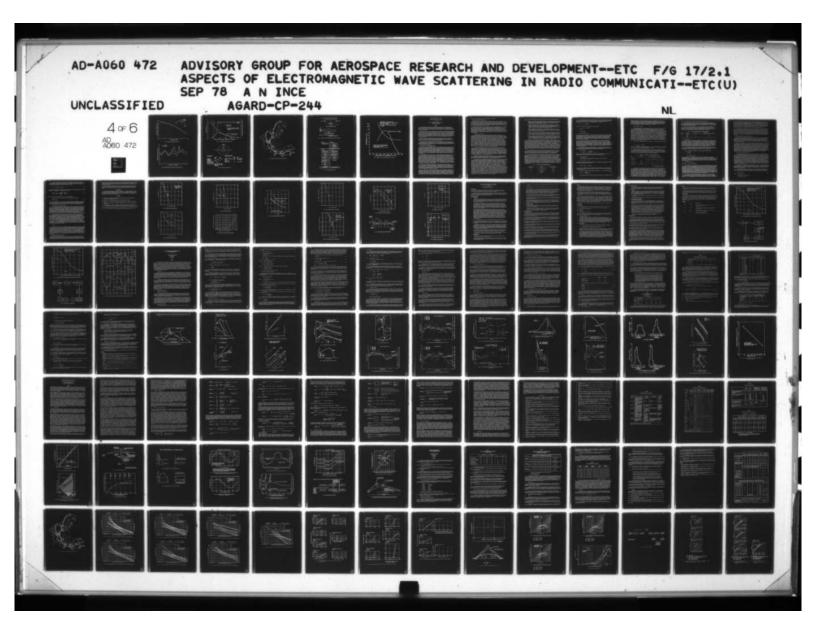
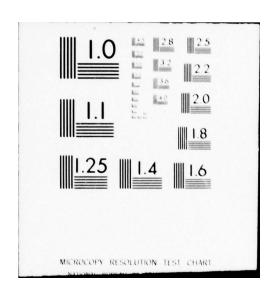


Fig.8(b) Example of F.A.S. coverage f = 50 MHz





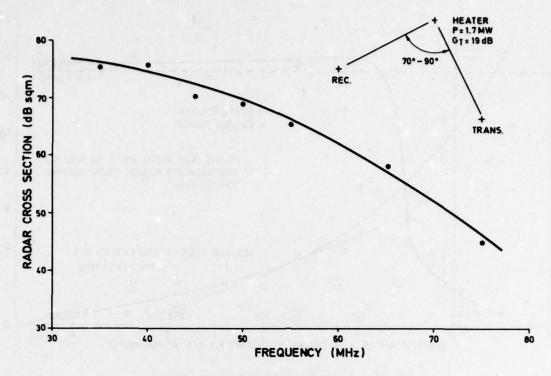


Fig.9 Maximum observed radar cross section

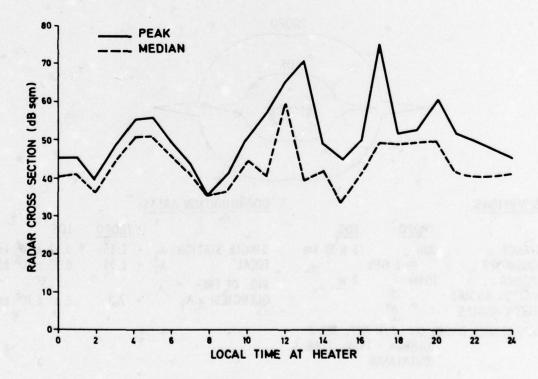


Fig.10 Diurnal variation of radar cross section of field aligned cloud

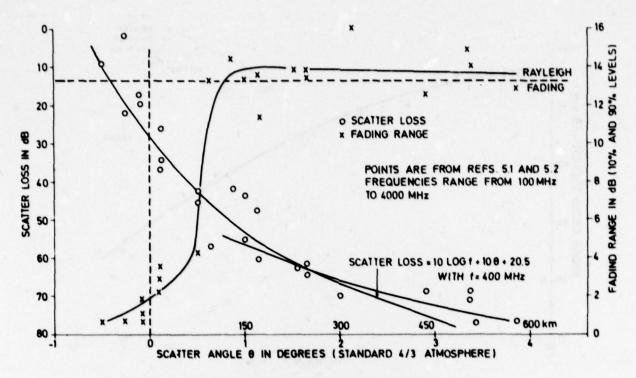
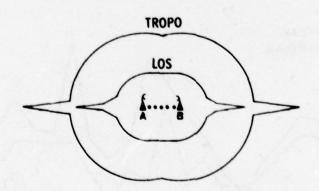


Fig.11 Attenuation and fading in troposcatter



ASSUMPTIONS:

TROPO LOS DISTANCE 330 6 x 55 km FREQUENCIES ≈ 1 GHz TX-POWER 10 kw 2 w ELEVATION ANGLES 0° HORIZON ANGLES 0° CALCULATIONS BASED ON CCIR REP. 382-2 (GENEVA - 1974), ZONE A

(OVERLAND)

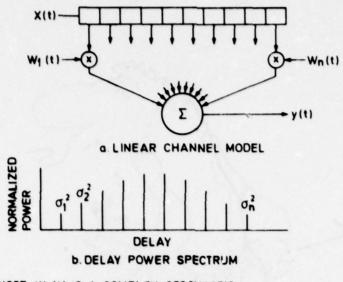
COORDINATION AREAS:

		TROPO	LOS			
SINGLE STATION, A1	•	1.15	0, 22 0, 32	X	106	km ²
TOTAL AT	•	1, 55	0, 32	X	106	km ²
(NO. OF FRE- QUENCIES) x A1		2.3	2,6			

Fig.12 Comparison of coordination areas



Fig.13 Outline of the NATO ACE-high troposcatter system



NOTE: W; (t) IS A COMPLEX STOCHASTIC
PROCESS OF VARIANCE O; 2

Fig. 14 Troposcatter channel model and associated delay power spectrum

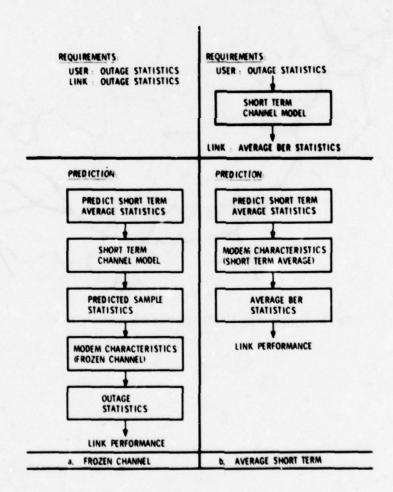


Fig.15 Link prediction approaches

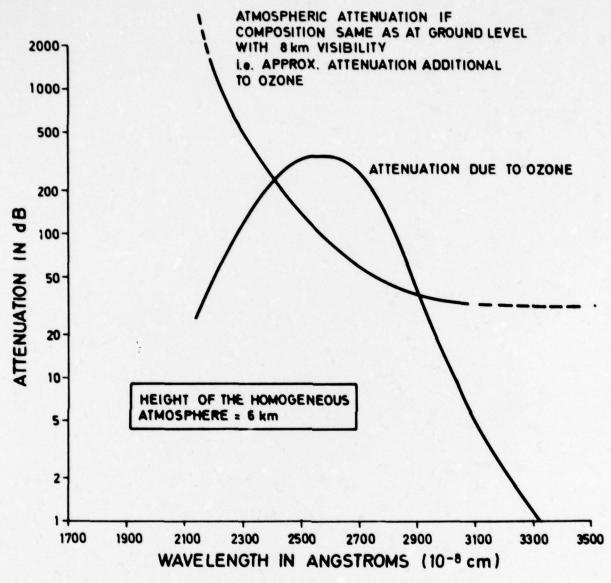


Fig.16 Attenuation of solar ultra-violet radiation by the atmosphere

DESIGN CONSIDERATIONS FOR DIGITAL

TROPOSCATTER COMMUNICATIONS SYSTEMS

J. L. Osterholz

Defense Communications Engineering Center 1860 Wiehle Avenue Reston, Virginia 22090

SUMMARY

The recent development of adaptive signal processing techniques such as the Adaptive Decision Feedback Equalizer (ADFE) and the Distortion Adaptive Receiver (DAR) has enabled the reliable transmission of digital data over the troposcatter channel at multimegabit rates. Implementation of these techniques has progressed to the point where the development of user oriented system design and performance criteria can proceed.

The performance of digitized voice channels under fading conditions is measurably different than the performance of conventional analog voice channels under the same conditions. Therefore the applicability of existing analog transmission link and system design criteria to the design of a digital transmission system is negligable. This paper proposes performance criteria for digitized voice channels which more accurately reflect the expected temporal distribution of channel outages given the fading statistics of the troposcatter channel. Measured data is presented along with a digital troposcatter channel model which effectively bounds voice channel outage statistics on digital troposcatter links and relates these statistics to link design parameters such as link signal to noise ratio, multipath dispersion and diversity configuration.

Performance criteria are also proposed for digital data users in terms of error free block probability. The effect of error free block probability requirements on the design of digital troposcatter links is shown along with an assessment of the relative difficulty of meeting digitized voice and data channel quality requirements in a hypothetical system design.

The dynamic effects of the fading dispersive troposcatter channel are also felt in the design of link and system synchronization strategies. For digital transmission systems, the maintenance of symbol and frame synchronization is of major importance. This paper compares the predicted timing stability of a digital troposcatter link with measured data taken at the symbol and frame synchronization levels (i.e., at the modem, TDM and PCM/TDM levels).

1. FOUNDATIONS OF DIGITAL FADING CHANNEL QUALITY

The recent successful implementation of channel adaptive digital signal processing techniques such as Adaptive Decision Feedback Equalization (ADFE) [1] and the Distortion Adaptive Receiver (DAR) [2] has made possible the transmission of digital data over the troposcatter channel at multimegabit rates. The transmission system designer who plans to use these techniques can now proceed with the development of user oriented digital transmission system design and performance criteria. At first glance, one would expect that the development of digital transmission performance criteria should evolve directly from existing analog transmission performance standards. However, the digitization of voice circuits which are the basic quanta of any multichannel transmission system results in voice channel performance which is related to system and link design parameters in a notably different manner than that evidenced in analog systems.

In analog (FDM) channels, the major sources of noise are media noise and intermodulation noise which tend to accumulate more or less on a mileage basis. In digital (PCM) channels, the major source of channel noise, except during deep fading, is analog to digital conversion or quantizing noise which accumulates only when the basic PCM multiplexer is traversed. During periods of deep fading, the analog and digital voice channels also behave differently. With analog channels, the voice user is nearly always aware of background channel noise which increases in intensity as the channel fades. With digital channels, the voice user is unaware of any substantial background noise until the PCM outage threshold is traversed. At that time, the noise environment of the channel becomes quite intensive -- resulting in a period of unusability which will last as long as the channel is below threshold. The duration and frequency of these disturbances or "channel outages" is then closely related to the quality of the voice channel itself. Thus for the digital voice channel, if the frequency and duration of channel outages can be controlled by proper link design then specification of voice channel performance can be formulated in terms that are more relevant to the voice user.

The digital data user requires a different type of channel specification for which there is no current parallel in analog transmission system design. The specification of error free block probability fulfills this requirement. The overall efficiency of data system can be effectively related to its error free probability. Therefore, specification of an acceptable error free block probability on a transmission link is tantamount to specifying a lower bound on the efficiency of the data system itself since most data users employ some form of error coding (error detection or ARQ or error correction or FEC) to further improve the efficiency of these systems.

Finally, reliable digital transmission requires that a state of synchronism be reliably maintained between data source and sink. This means that all intervening digital equipments (multiplexers and modems) must also be synchronized. In a digital transmission system, synchronization can be maintained by pulse stuffing, master-slave or plesiochronous techniques. The dynamics of a fading channel such as troposcatter can deliteriously affect the timing stability of the transmission system, no matter what the synchronization method, by depriving the digital equipments of reliable symbol, bit or frame clock during fading events. Thus the design of synchronization acquisition and maintenance algorithms also

represents a very important aspect of digital transmission system design.

2. CHANNEL QUALITY MEASURES AND LINK DESIGN

The primary measure of transmission quality for a digital system is its error performance. Transmission errors will occur in the digital transmission system in two distinctly different modes. One mode is a relatively constant, long-term error rate which will occur due to equipment degradation (as opposed to failure), due to interference and due to long-term power fading such as seen on satellite links. This error rate should be specified to be at least one order of magnitude more stringent than the level at which significant user disturbance occurs. For 64 kb/s PCM, a channel is generally considered unavailable when its steady-state error rate is greater than 10^{-6} .

The other system error mode results from fading on line-of-sight and troposcatter links. To describe these instances, dynamic measures of error performance are needed. Multipath fading occurs with such rapid variation that the error performance changes too quickly to be characterized by a "rate". In addition, isolated single bit errors are of little importance since, in the transmission of digitized voice via PCM, the occurrence of a single isolated bit error will hardly be noticed by the user. It is the temporal relationship between errors, i.e., whether they are grouped together in time so that they reinforce each other's disturbing effect that is the important measure of voice channel quality. Similarly, for most modern data transmission systems which use coding for error control, single bit errors are of little consequence.

2.1 The Digitized Voice Channel

For properly designed line-of-sight and troposcatter links, the error performance of a traversing digital channel will be characterized by relatively long periods with very few or no errors interspersed with considerably shorter periods of deep fade in which errors are grouped closely enough together to consitute an essentially continuous interruption to the usability of the channel. Transition of the channel from the error-free state to the severely disturbed state is quite rapid. User perception of 64 kb/s PCM channel quality changes dramatically with a two order-of-magnitude change in error probability from around 3·10-6 (on the order of one error every 5 seconds) to 3·10-4 (20 errors per second). In this vicinity of error probability, a two order-of-magnitude change results from about a 2 dB change in received signal to noise ratio. During deep multipath fades, the received signal to noise ratio may be expected to change by tens of dB per second. Thus if the channel, as perceived by the user, transitions from good to bad in a 2 dB range of signal level, this transition will generally occur in less than a few hundred milliseconds. The mean fade duration on quad diversity troposcatter links will generally be on the order of one second or less. Since the transition period from a good channel to a severely disturbed one is so short relative to the actual fade duration, such fades can be described by only their duration, assuming essentially complete unacceptability from the onset of the fade to its end. It remains necessary only to choose an appropriate threshold at which to measure the beginning and ending of a fade outage to complete the outage characterization.

If a 64 kb/s PCM channel is observed during a multipath fade, the fade will generally have reached a considerable depth before the first bit error occurs on the channel. Due to the rapid subsequent onset of errors in a fading channel, the signal to noise ratio at which the first bit error is expected to occur is a reasonable threshold for determining the duration of the fade. This level will not be the same for each fade since error occurrences are a probabilistic phenomenon. However, a signal to noise ratio can be defined which represents the mean value of the signal to noise ratio at which the onset of errors is expected. This mean value is a function of fade rate. The more rapidly the signal level fades, the lower will be the point at which the onset of errors occur. For a typical fade rate of 10 dB/second, the mean signal to noise ratio of error onset is approximately the magnitude corresponding to a 10-4 bit error probability. This is an appropriate signal to noise ratio threshold for the range of fade rates expected to occur on digital troposcatter links.

Having defined a threshold above which the channel is considered to be unperturbed, and below which the channel is considered to be unacceptable, a fade outage is defined as the event that begins when the diversity branch signal to noise ratio of a link falls below the specified threshold and ends when the diversity signal to noise ratio has again risen through the threshold value.

The characteristics of fade outages have been examined for a typical digital troposcatter channel. It has been found that a channel which traverses a number of troposcatter links will experience three distinctly different categories of fade outage with markedly different user interference potential. The first broad category occurs when a voice user is subjected to an isolated fade outage of very short duration, e.g., less than 200 milliseconds. His reaction will be to barely notice the disturbance. This will be true even for repeated but suitably infrequent outages of such short duration. The second broad category occurs over some range of longer fade duration, e.g., 1/5 second to 5 seconds. The user will experience significant annoyance but will continue to communicate when the outage is over. Similarly, for some recurrent rate of short duration outages, e.g., 2 to 4 outages per minute, none of which is greater than 200 milliseconds in duration, annoyance rather than total disruption will occur. This type of recurrent disturbance is typical of a troposcatter channel during long-term fading and thus will afflict the user with a relatively long period of disturbed performance whereas the 1/2 to 5 second fade will normally be an isolated event. Finally, the third broad category occurs when the outage exceeds some duration such that calls are abandoned due to lack of patience. Outages of any noticeable duration will be disturbing to the user and their probability of occurrence should be controlled. Outages which are long enough to cause call abandonment are a much more severe disturbance than outages for which calls are not abandoned. Thus, the probability of occurrence of these longer outages should be made substantially less than the probability of occurrence of these longer outages should be made substantially less than the probability of occurrence of these longer outages should be made substantially less than the probability of occurrence of these longer outages should be made substantially less than the prob

In view of these considerations, five specific ranges of voice channel outage are defined as follows:

- Range I. Outages under 200 milliseconds duration which are significantly separated in time from any other outage. Such outages will normally occur on a troposcatter link operating with adequate margin. The allowable probability of occurrence of these outages need not be specified since their effect on the user is trivial.
- Range II. Outages with durations in the range from 200 milliseconds to five seconds which
 are significantly separated in time from any other outage. Such outages will occur on a
 troposcatter link operating with adequate margin (or less than adequate margin if the
 frequency of occurrence is high). The allowable probability of occurrence of such an outage
 should be specified with a value based on its annoyance to the user.
- Range III. Outages with durations greater than 5 seconds but less than 2 minutes. The
 allowable probability of occurrences of such outages should be specified with a requirement
 more stringent than that for Range II since such an outage is considered to be a disruption
 to the user which would cause call termination.
- Range IV. A recurrent set of outages of average duration under 200 milliseconds which occurs
 at an average rate of from 2 to 5 per minute. This condition will normally occur on a troposcatter link operating with barely adequate margin. The allowable probability of existence
 of such a condition should be specified with a value based on its annoyance to the user.
- Range V. Outages with duration greater than 2 minutes or recurrent outages of any duration which occur more frequently than 5 per minute. The duration of any such outages or period of recurrent outages should be included in the total unavailability specification since the channel is considered essentially unusable. The outages described by this range will normally occur on a troposcatter link with long-term fading in excess of the fade margin.

In summary, it is proposed that the basic performance parameter of digital voice channels in the digital transmission system be described by the probability of occurrence of temporally grouped errors where such an error grouping is called a 'fade outage'. A fade outage is defined in terms of a diversity signal to noise ratio threshold corresponding to a 10-4 bit error probability. Five ranges of fade outage conditions are defined, one of which is considered to be negligible (Range I), one of which is of sufficient duration to be included in the unavailability specification (Range V) and three (Ranges II, III and IV) which are proposed to be controlled by separate probability of occurrence specifications which consider the disturbing effect of the specific outage ranges addressed. These measures of channel quality have the considerable advantage over either average bit error rate of availability in that they actually reflect the types of fading phenomena which occur. As an example, outage probabilities for each of the relevant outage ranges have been established for Defense Communications System (DCS) digital troposcatter links. These probabilities are listed in Table I and will be used to illustrate the proposed digital troposcatter link design procedure. Other outage probabilities are possible based on different system designs.

The troposcatter channel is generally viewed as having a compound fading characteristic with short term Rayleigh fading impressed on a longer diurnal and annual fading distribution. Historically, the performance of analog troposcatter links was related to the percentage of time that a particular short term average Signal-to-Noise Ratio (SNR) could be maintained out of the longer term fading ensemble (i.e., time availability). The essence of this convention will be continued here.

Since methods for the prediction of the long-term distribution of short term $\overline{\rm SNR}$ are extensively covered in existing literature [3], [4], it is unnecessary to further explore this area. The following paragraphs will instead concentrate on the characterization and specification of short term digital performance (e.g., on a per call basis) as a function of the short term $\overline{\rm SNR}$. This parameter, short term $\overline{\rm SNR}$, will be deonted by the symbol γ_0 . The γ_0 necessary to obtain a specified short term performance (here described on the basis of outage rates and duration) will then be described in unavailability fashion (i.e., to be maintained for all but a certain percentage of time) for various digital troposcatter transmission configurations. The link performance criteria to be used to illustrate this characterization are given in Table 1 and are based on the mix of transmission media utilized in the DCS. A quad diversity troposcatter system is modeled against these criteria with the most demanding criteria (in the long-term sense) determining the link design requirements. Since outage statistics are dependent on the fade rate of the transmission channel, link performance will be characterized to mean fade rates of .1 and 5 Hz. This range of mean fade rates is inclusive of the fading characteristics observed on most L, S and C-Band troposcatter links.

TABLE 1. DCS PCM VOICE PERFORMANCE CHARACTERISTICS

A OUTAGE RANGE	B CRITERIA	C OUTAGE PROBABILITY	
11	.2 sec ≤ outage < 5 sec.	7.5.10-4	
III	5 sec < outage < 1 min.	7.5.10-5	
IV	2 < outages/min. < 5	2.5.10-3	
V	5 < outages/min.	1.10-4	

Under the assumptions of Rayleigh law fading, maximal ratio diversity combining and a neglibable intersymbol interference penalty, the conditional probability that a digital channel traversing a digital troposcatter link will fall below the 10-4 bit error probability threshold can be determined via the expression previously derived in [5]. This probability, $(P_0|\gamma_0)$, is given by

$$(P_0|_{Y_0}) = 1 - b \sum_{R=1}^{m} \frac{R^{-1}}{(R-1)!}$$
 (1)

.

where $(P_0|_{Y_0})$ = probability of an outage given a short-term \overline{SNR} , Y_0

$$b = (2P_e)^n i/\gamma_o = (2 \times 10^{-4})^n i/\gamma_o$$

£ = - In b

y = short term SNR

m = total diversity = n. n.

The above value for m is the product of the ratio of the transmitted bandwidth to the channel frequency correlation bandwidth and the order of explicited diversity of the link. The value of m thus accounts for the presence of an "implicit diversity" advantage. Digital troposcatter modems take advantage of decorrelated fading between various portions of the transmitted spectrum to gain this additional diversity advantage. At multimegabit rates, most medium length quad diversity troposcatter paths are expected to provide an effective implicit diversity gain (n_1) on the order of two resulting in a total equivalent diversity of eighth order.

Expression (1) is based on the relationship between bit-error-rate and mean SNR for DPSK modulation. This allows the statement of outage probability in terms of γ_0 which is the parameter normally used in troposcatter link design. A conversion factor is provided later to allow conversion of the finally derived link design requirements to any other type of modulation. Figure 1 is a plot of (1) illustrating $(P_0|\gamma_0)$ for quad diversity operation. Also shown in Figure 1 are measured data points taken during 9.4 Mb/s link tests of the Megabit Digital Troposcatter Subsystem (MDTS). The MDTS employs Adaptive Decision Feedback Equalization (ADFE) to mitigate the effects of intersymbol interference and provide an implicit diversity gain. The tests were conducted on a 168 mile troposcatter link in the 4.4-5.0 GHz military band.

Having characterized cumulative outage probability, it is now appropriate to examine the temporal distribution of outages. Again using the expressions developed in [5], conditional outage rate and duration statistics can be expressed for diversity troposcatter transmission.

Mean Outage Rate

$$\eta_0 = 2.4 \text{ mNs}^{1/2} \text{d} \quad 1 - b \frac{R=2}{1-b} \frac{(R-1)!}{(R-1)!} \quad (\text{sec}^{-1})$$
(2)

where ϵ , b and m are as defined previously and N is defined as the mean channel fade rate in Hz. The Mean-Time-Between-Fade Outage (MTBFO) for troposcatter can then be expressed as $\frac{1}{n}$.

· Mean Outage Duration

Knowing MTBFO and P_0 , the mean duration of an outage, t_0 , can be expressed as

$$t_0 = P_0 \cdot MTBO \quad (sec) \tag{3}$$

The distribution of fade durations relative to the mean can be determined from assumptions of a narrow-band process and expressed as derived in [6] by

$$p(t) = \frac{2}{u} I_1 \left(\frac{2}{\pi u^2} \right) \cdot \exp \left[-\frac{2}{\pi u^2} \right]$$
 (4)

where $u=t/t_0$, I_1 is the modified Bessel function of the first order and P(t) is the probability that an outage will have a duration of t seconds or less. Figures 2, 3 and 4 illustrate the relationship of n_0 , t_0 , and P(t) to γ_0 .

The Mean-Time-Between-Fade Outages (MTBFO) with duration $t_1 \le t \le t_2$ can then be calculated by

MTBFO
$$(t_1, t_2) = \frac{MTBFO}{P(t_2) - P(T_1)}$$
 (5)

The above discussion led to expressions for the relationship between γ_0 and probability of fade

outage per call-minute. This expression determines the short term $\overline{\text{SNR}}$ needed to meet the first two performance requirements of Table 1. Under certain conditions of γ_0 and mean channel fade rate, the troposcatter channel will fade rapidly enough to cause several short fade outages per minute, hence the third and fourth requirements in Table 1. The probability that between two and five fade outages will occur during a minute and the probability that greater than five fade outages will occur during a minute can be obtained from (2) be determining the values of γ_0 for which

$$\frac{2}{60} \le {}^{n}_{o} \le \frac{5}{60} \text{ and } {}^{n}_{o} > \frac{5}{60}.$$
 (6)

The preceding paragraphs have described expressions relating the occurrence probability of the various outage ranges tabulated in Table 1 conditioned on a particular value of γ_0 . Since γ_0 is in itself a time varying parameter, it is characterized by a probability distribution and is normally expressed in the form of a time availability. The total probability of occurrence of a particular outage range from Table 1 is estimated by the probability of attaining a partcular γ_0 or worse multiplied by the probability of outage occurrence given γ_0 . Since the latter probability is a steep function of γ_0 (see Figure 1), the probability of outage occurrence during a typical call holding time goes rapidly from a very low value to a value near unity over a small range of γ_0 . Thus, it is assumed that the most likely occurrence of an outage during a call results from the channel γ_0 falling to the level where the probability of outage occurrence given that level of γ_0 is very nearly unity. Based on this assumption, values of γ_0 have been chosen, for each of the outage ranges of Table 1, which result in a near-unity probability of occurrence for that outage range during a nominal call holding time (5 minutes). These values of γ_0 are listed in Table 2. The corresponding unavailability requirements (1 minus time availability) are then simply the outage probability requirements of Table 1. Table 2 thus represents a set of candidate combinations of γ_0 and unavailability, R, where each combination satisfies one of the requirements statements of Table 1. The dominant requirements for each digital troposcatter transmission configuration can then be determined by using the long-term distribution of γ_0 to find which of the candidate requirements of Table 2 requires the most system gain.

The distribution describing the long-term variation of $\gamma_{_{\rm O}}$ is generally assumed to be log normal. I.e.,

$$P(\gamma_0) = \frac{1}{\sigma \sqrt{2\pi}} \exp{-\frac{(\gamma_0 - \gamma)^2}{2\sigma^2}}$$
 (7)

where $P(\gamma)$ is the <u>probability</u> distribution function of γ_0 , γ_0 is as previously defined, γ is the long-term (i.e°, yearly) \overline{SNR} and σ is the standard deviation of γ_0 about γ . As seen in Figure 5, most troposcatter paths will exhibit standard deviations between 4 and 8 dB.

Based on observations of the slope of the long term γ_o distribution as evidenced in this figure, and the candidate γ_o values tabulated in Table 2, it is obvious that the most stringest long-term requirements are represented by the Range V outage requirement in C-Band and either the Range II or Range III requirement in L or S Band, depending on the value of σ for a particular L or S Band path. The σ of each L or S Band troposcatter path to be digitized should be calculated to determine whether that particular path should be designed to Range III requirements.

TABLE 2. CANDIDATE Y * REQUIREMENTS FOR DIGITAL TROPOSCATTER LINKS

BAND	DIVERSITY	Yo (DB) EXCEEDED ALL BUT R PCT OF TIME				
L (790-960 MHZ)			R _{III} = .0075			
S (1.7-2.4 GHZ)	QUAD	10	5	4	N/A	
C (4.4-5.0 GHZ)	QUAD	5	N/A	9	8	

* (WITHOUT IMPLEMENTATION MARGIN)

As a general rule, for values of σ less than 6 dB, the most stringest design requirement is given by the Range II γ_0 and associated time unavailability requirement. For most L and S Band links, it is expected that the long-term $\overline{\text{SNR}}$ requirements for Range II will dominate and therefore it is expected that most L and S Band digital troposcatter links will be designed to satisfy Range II requirements. The resultant values of γ_0 and their associated time unavailabilities, selected from Table 2 in accordance with this rationale, are presented in Table 3. Design of digital troposcatter links to the requirements tabulated in Table 3 should insure meeting the dominant outage probabilities and exceeding all others. It should be emphasized that the link design requirements indicated in Table 3 were derived directly from the choice of link performance criteria listed earlier in Table 1 and reflect end to end performance objectives and mix of transmission media appropriate to the DCS. Transmission media utilizations peculiar to other system designs may differ from that considered for the DCS. A difference in the percentage of total channel miles attributed to troposcatter transmission will be reflected in the choice of different link outage probabilities from that listed in Table 1. This, in turn, may

result in a slight change in the link design requirements summarized in Table 3.

The derivation of the troposcatter link design criteria related above was based on the assumption that DPSK modulation is used. To effect a translation to other digital modulation techniques, a factor which represents the ratio in dB between the non-fading $\overline{\rm SNR}$ of DPSK at a bit error probability of 10^{-4} and the non-fading $\overline{\rm SNR}$ corresponding to a 10^{-4} bit error probability for the alternate technique must be added to the values shown in Table 3.

On links with little dispersion (e.g., short diffraction paths) where the maintenance of at least dual implicit diversity during periods of high long-term path loss is doubtful, alternate performance criteria are required. This links should be implemented in quad diversity and will require a value of $\gamma_{\rm Q}$ that is approximately 5 dB greater than that specified in Table 3 since no implicit diversity gain will be achieved and there will be no inband diversity power sharing.

TABLE 3. γ_o DCS DIGITAL TROPOSCATTER LINK DESIGN REQUIREMENTS

BAND	DIVERSITY	Yo (dB)	EXCEEDED ALL BUT RO PCT OF TIME		
L.S	QUAD	10	.075		
C	QUAD	8	.01		

2.2 The Data Channel

Most modern data transmission system separate the data to be transmitted into blocks for error control purposes. A parameter of interest to the data user is the percentage of such blocks which are transmitted with no errors. In a system using ARQ error control techniques, all blocks which are not error-free must be retransmitted. In a system using error correction coding, a small number of errors can be corrected, but blocks with a large number of errors must be retransmitted. The performance of data transmission channels can be usefully described by the probability of fade outage requirements described in the preceding section, supplemented by an error-free block requirement. The composite specification then describes the incidence of outages where a number of adjacent blocks are affected by errors as well as the total percentage of data blocks which are expected contain errors.

Due to the steepness of the expression for bit error probability as a function of SNR, the probability of receiving a data block of n bits duration with at least one error is very nearly given by the probability that the bit error probability is 1/n or worse. Thus, from equation (1)

P(BE|
$$\gamma_o$$
) = Probability of receiving a block in error given a short term \overline{SNR} , γ_o

$$b_g = (\frac{2}{n})^{2/\gamma_o}$$

$$a_g = -\ln b_g$$

$$m = 8$$
, for quad diversity

The total probability of occurrence of a non error free block is determined by the probability of attaining a particular γ_0 or worse multiplied by the probability of block error occurrence given γ_0 . Since, for high orders of diversity, the latter probability is a steep function of γ_0 (see Figure 6), the probability of a block error goes rapidly from a very low value to a value near unity over a small range of γ_0 . Thus, it is assumed that the most likely occurrence of a block error results when the channel γ_0 is very nearly unity.

where $P(BE|_{Y}) = 1$ and $P(_{Y})$ is given by (7)

For a typical data block of 10^3 bits, Figure 6a illustrates the expected distribution of block error probability given γ_0 . An interesting conclusion resulting from (9) is that for most system designs, digital channel voice quality requirements appear to require more system gain than data channel quality requirements. This conclusion stems from the observation that the link design requirements listed in Table 3 (which were derived based on PCM voice considerations) will result in an overall block error probability on the order of 10^{-7} as expected over an operating year on a single link. Thus an extremely large number of troposcatter links can be tandemed while still perserving an excellent block error probability on an end to end basis. Most transmission systems can afford to have relatively relaxed data performance requirements since the performance of most record and data systems is more strongly affected by message preparation and delivery times and only weekly affected by data block retransmissions. Thus a reduction in the effective bit rate of a data system due to excessive data block retransmissions, when they occur, will not in most cases notably affect its overall performance.

The formulation of block error probability given in (8) does not consider the effects of correlated bit errors due to the slow fading experienced on troposcatter links. One would expect significant correlation between bit errors in troposcatter communication, particularly at moderate to low values of γ_o . Thus it was appropriate to obtain experimental data to estimate the error suffered by

using (8) in the design of digital troposcatter links. Figure 6b represents the results of 7.0 Mb/s tests conducted using the Distortion Adaptive Receiver (DAR). The blocks were of 100 msec in duration an thus contained $7 \cdot 10^5$ bits. Although this length is larger than that normally found on terrestrial systems, it was experimentally convenient to generate it. What is interesting about Figure 6b is that (8) bounds the conditional block error probability relatively well even with extreme block length used. It is expected that the order of implicit diversity actually achieved during these tests was sufficient high so as to significantly reduce the correlation between bit errors. For data block lengths of the more normal variety, (8) is thus expected to provide an even closer bound. Thus, (8) has been provisionally accepted for use in the engineering of DCS digital troposcatter links.

The capability to utilize implicit diversity provides a significant performance enhancement without necessitating additional system gain in the form of higher transmitter powers or more diversity receivers. An interesting facet of this concept is that for a given order of explicit diversity (e.g., number of diversity receivers), the digital troposcatter link performance actually improves as the bit rate increases as long as the design limits of the technique are not exceeded. Figure 7, taken during tests of the DAR modem, illustrate the performance improvement attributable to the implicit diversity. In Figure 7, 3.5 and 7.0 Mb/s error free block performance is shown as a function of mean bit error rate. At a mean bit error rate of 10^{-5} approximately 94 percent of all data blocks transmitted were received as error free at 710 Mb/s while at 3.5 Mb/s only about 76 percent of all transmitted data blocks were error free.

3. SYSTEM SYNCHRONIZATION FOR DIGITAL TROPOSCATTER LINKS

The design of digital troposcatter links must account for the effects of fading on the performance of the TDM equipment used to develop the multimegabit trunk transmission rates. Figure 8 illustrates a hypothetical digital troposcatter synchronization section composed of a digital troposcatter link and representative Pulse Code Modulation (PCM) channel banks and a Level 2 Asynchronous Time Division Multiplexer (TDM). Because of the inherent network flexabilities afforded by the Asynchronous TDM, the hypothetical synchronization section of Figure 8 will postulate this equipment for use in developing the final transmission trunk rates.

If a loss of synchronization occurs at any of the interfaces illustrated in Figure 1, the traversing digital channels will experience a period of unavailability lasting until synchronization is reestablished. Moderu TDM digital equipments will reestablish synchronization in less than 50 msec [6] once the traversing channels are above the outage threshold. Further, the mean outage duration for well designed digital troposcatter links will be on the order of a few hundred milliseconds. Thus isolated synchronization losses will represent a negligable incremental unavailability penalty to the design of digital troposcatter links. Of more importance is the frequency at which synchronization can be expected to be lost since repeated synchronization losses which are not isolated can result in a significant system availability penalty. This section will review a method for predicting the mean time between loss of synchronization or Bit Count Integrity (BCI) for the digital equipments used on digital troposcatter links. Reference will be made to actual link synchronization performance data which was obtained during digital troposcatter system tests accomplished between January - February 1976 using digital equipments functionally similar to those which will be applied to the DCS.

3.1 Synchronization of the Level 2 TDM

The interface between the Level 2 TDM and the radio is synchronous since both data and timing transit this interface and the bit rate of the TDM is known to the accuracy of the timing signal. Loss of BCI can occur in the second level TDM due to a loss of BCI in the digital troposcatter radio facility or a loss of BCI occuring in the TDM itself. Loss of synchronization or BCI in the radio facility has been demonstrated to be extremely rare and therefore loss of BCI in the level two TDM will be assumed to originate exclusively in the TDM. The major cause of potential BCI loss in the second level TDM results from a lack of correlation between the received TDM frame pattern and the locally stored replica. This lack of correlation can occur because transmission errors alter the received frame pattern to give the impression that an actual loss of BCI has occured. Recognizing this, most TDM equipments maintain synchronization by permitting a certain degree of frame decorrelation to exist as long as a prescribed correlation threshold is not exceeded. Correlation is typically determined by identifying the number of frame bits which are received in error and relating this number to the permitted number of frame errors. If the received frame error count is greater than the threshold count, loss of BCI is declared. Certain TDM designs will further delay a loss of BCI declaration by additional accumulation and processing of individual frame decorrelation events.

Unfortunately most TDM equipments have been designed on the basis of a nonfading channel model and therefore their ability to maintain BCI can be degraded by the higher bit error densities associated with fading channels. The effect of this degradation will be quantified by a parameter called Mean Time Between Loss of BCI (MTLBCI) and will be related to link design through a review of previous work at DCEC [7] including measured data.

Utilizing an expression previously derived in [5] it is possible to develop estimates of the MTLBCI for any TDM design. In general, the probability that a loss of frame will be declared at the synchronous Level 2 TDM/Digital Troposcatter interface can be expressed for small frame lengths as

$$q = {n \choose x} p^X (1-p)^{n-X}$$
 (10)

where n = frame length in bits

x = frame correlation threshold in bits

p = probability of bit error

In order to estimate the BCI performance of TDM equipments in troposcatter applications, the fading statistics of the channel must be considered. A mean probability of frame loss, q, can be calculated given a suitable density function for the bit error probability. Such a function was derived in [5] and was utilized earlier in this paper to obtain (1). Thus

$$\overline{q} = \int_{0}^{.5} {n \choose x} p^{x} (1-p)^{n-x} p(p) dp$$
 (11)

where p(p) is the density function derived in [5] which describes the occurrence probability of a particular range of bit error probability. For quad diversity, p(p) is

$$p(p) dp = \frac{1}{(4n_i - 1)!} \frac{(-1n2P)^{4n_i - 1}}{(\frac{\gamma_o}{n_i})^{4n_i}} \frac{2^{n_i/\gamma_o}}{p^{1 - n_i/\gamma_o}} dp$$
 (12)

where p is the bit error probability and n_i and γ_o are as defined in (1).

The Mean Time to Loss of BCI, MTLBCI, can then be conservatively estimated as

$$MTLBCI \leq \frac{1}{N_{\phi}\overline{q}}$$
 (13)

where N $_{\rm f}$ is the frame rate in b/s. Figure 9 shows MTLBCI calcualted for the AN/GSC-24 as a function of $\gamma_{\rm O}$. Also shown in Figure 9 are MTLBCI data points measured with the AN/GSC-24 TDM operating at 6.3 Mb/s over a 168 mile quad diversity digital troposcatter link. Note that at the values of $\gamma_{\rm O}$ specified in Table 3, the predicted MTLBCI will be of little concern in the design of digital troposcatter links.

3.2 Synchronization of the PCM Channel Bank

The interface between the Level 2 TDM and the PCM channel bank will likely be synchronous for at least an initial set of DCS applications. Since this interface will be asynchronous, loss of BCI can result in the PCM channel bank from two distinct phenomena. The first phenomena is seen to result from the identical situation previously discussed with respect to the Level 2 TDM, viz insufficient frame correlation. Thus the determination of MTLBCI induced due to frame word decorrelation for an arbitrary PCM channel bank design can be accomplished in the manner similar to that outlined for the Level 2 TDM. Such a determination was made for the TD-968, PCM Channel Bank and is shown in Figure 10. The TD-968 differs slightly from normal PCM/TDM designs in that it accumulates individual instances of frame decorrelation prior to a loss of BCI during fading. Expression II was adapted to include this capability by replacing the expression for q with an expression which considered frame error accumulation.

Of greater importance is the possibility that loss of BCI could occur in the PCM bank due to errors in decoding asynchronous port stuff control words by the Level 2 TDM. To enable the efficient multiplexing of asynchronous (or time varying) source bit rates, the pulse stuffing asynchronous multiplexing technique is generally used. This technique is implemented by buffering each source and sampling the buffers at a synchronous rate which is greater than the maximum expected input rate. Stuff bits are added at specified opportunities, when the sampling rate overtakes the input rate. The receive side of the Level 2 TDM must properly decode each stuff bit to derive the correct asynchronous source rate. Incorrect decoding of these stuff commands because of fading induced errors will cause loss of BCI. In order to protect against potential losses of BCI, each stuff bit is normally signalled by an n bit (n = 3, 5, 7, 9,...) code where the correct polarity of the stuff control bit (l = stuff bit transmitted, 0 = no stuff bit transmitted) results from a majority logic decision rule. As an example, the standard CCITT Level 2 TDM design employs a 3 bit stuff code. MTLBCI due to stuff word error can be calculated by using (11) with only a slight modification. Specifically, the effect of the majority logic decision rule can be considered by letting

$$x = \frac{n+1}{2} \tag{13}$$

MTLBCI due to incorrect stuff command decoding has been calculated as a function of γ_0 for the AN/GSC-24 TDM and is shown in Figure 10. It should be remembered that although the stuff command decoding error occurs in the Level 2 TDM loss of BCI results only in the PCM channel bank. Figure 10 shows that at the AN/GSC-24 TDM and the TD-968 PCM channel bank interface the overall MTLBCI is dominated by the probability that loss of BCI will occur due to stuff command error. This will be generally true for most asynchronous interface designs since the probability of BCI loss due to frame decorrelation can be minimized by externally inhibiting frame loss declaration via the use of inservice performance monitoring techniques. Also shown in Figure 10 is the result of 6.3 Mb/s system tests which were accomplished on a 168 mile digital troposcatter link. Note that for the link design criteria stated in Table 1, loss of BCI in the PCM channel bank will not noticably contribute to the unavailability of a traversing communications channel.

4. CONCLUSIONS AND AREAS FOR FURTHER STUDY

The system engineering presented herein represents an initial but nevertheless unique attempt to quantitatively describe digital troposcatter transmission performance in user relevant terms. This treatment differs conceptually from currently used analog transmission practices which relate performance only in cummulative terms without specific regard to the temporal distribution of outages. The lack of

a closed form for the probability of error density function for the ADFE and DAR techniques necessitated formulations which tend to bound rather than truely characterize outage statistics. However, it is felt that these formulations are sufficiently conservative so that initial systems can be installed with a high degree of confidence.

Multilink digital troposcatter operational test bed systems should be installed utilizing the link design criteria summarized in Table 3. A serious effort should then be expended to reexamine these criteria with the aim of possibly reducing the system gain requirements below the levels implied by Table 3.

ACKNOWLEDGEMENT

The authors wish to acknowledge Dr. M. Unkauf of Raytheon, Inc. for making the necessary bit error distribution instrumentation available and again to Dr. Unkauf, Dr. P. Monsen of Signatron Inc. and Mr. W. Cybrowski of USAECOM for their cooperation in collecting the experimental data. Acknowledgement is also given to Mr. K. Kirk of DCEC for his contribution to the development of the basic digital transmission performance concepts described herein.

REFERENCES

- [1] GTE Sylvania, Inc., "Megabit Digital Troposcatter Subsystem (MDTS) Research and Development Technical Report," ECOM-0040-F, July 1976.
- [2] Raytheon, Inc., "Hybrid Tropo Transmission System," RADC-TD-76-250, August 1976.
- [3] CCIR Report 244-1, "Estimation of Tropospheric-Wave Transmission Loss," Volume II, Gctober 1966.
- [4] "Transmission Loss Predictions for Tropospheric Communications Circuits," NBS Technical Note 101, January 1967.
- [5] J. L. Osterholz and D. R. Smith, "The Effects of Digital Tropo Error Statistics on Asynchronous Digital System Design," 1975 Nation Telecommunications Conference Proceedings, Volume II, pp 28-24 ff.
- [6] U.S. Army Electronics Command, Specification for TD-968 PCM Multiplexer, EL-CP0047-001A, April 1969.
- [7] J. L. Osterholz, "Application of Digital Troposcatter Transmission to the DCS," DCEC TR 17-76.

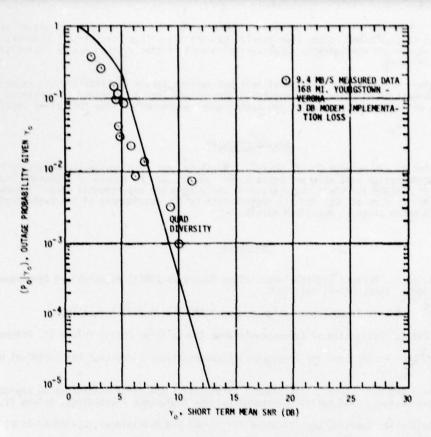


Fig.1 Troposcatter RF link outage probability

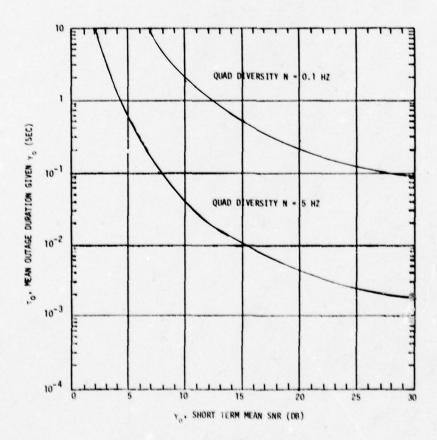


Fig.2 Troposcatter link outage duration

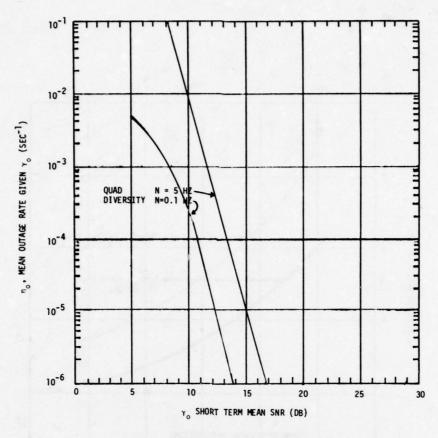


Fig.3 Troposcatter link outage rate

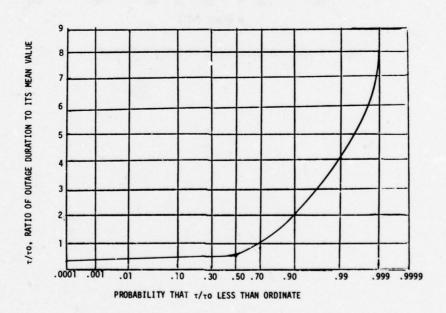


Fig.4 Distribution of troposcatter link outage duration

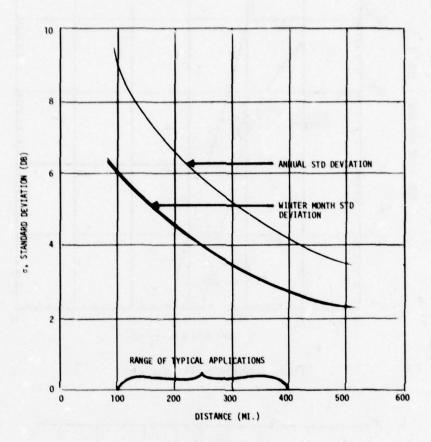


Fig. 5 Tropo path loss standard deviation vs distance

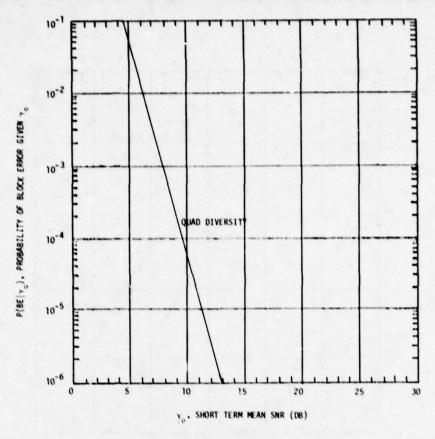


Fig.6(a) Troposcatter link block error probability

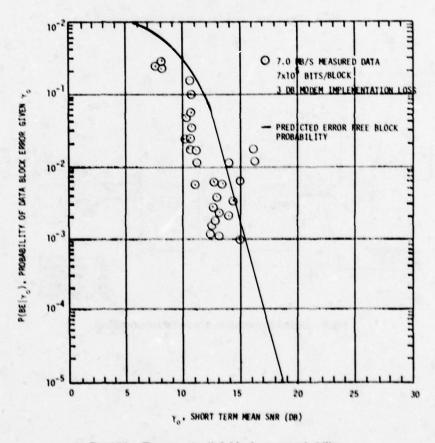


Fig.6(b) Troposcatter link block error probability

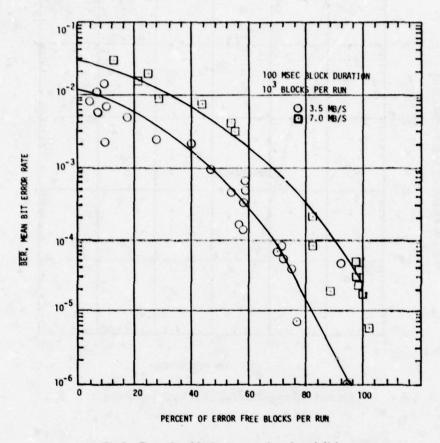


Fig.7 Error free blocks vs mean ber (quad div)

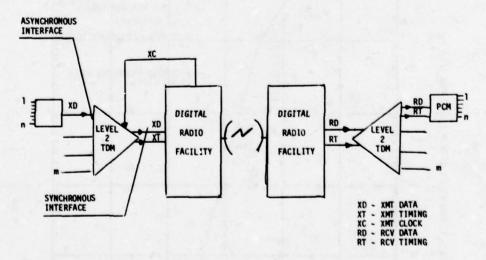


Fig.8 Digital transmission synchronization section

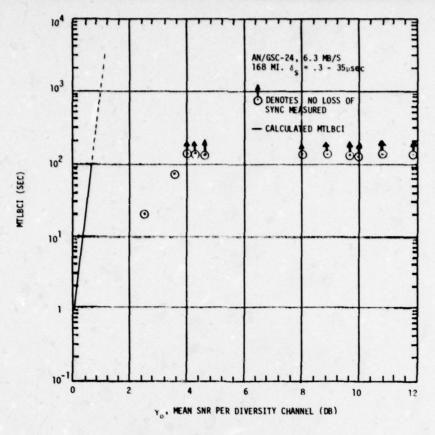


Fig.9 MTLBCI - level 2 TDM

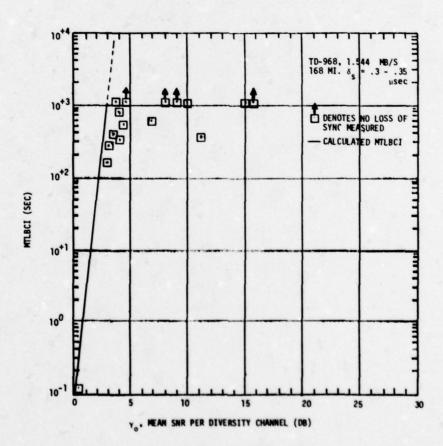


Fig.10 MTLBCI - PCM channel bank

LEVEL CONTROL IN TROPOSPHERIC SCATTER SYSTEMS

B. S. SKINGLEY

Marconi Communication Systems Limited Chelmsford, Essex. England.

INTRODUCTION

A simple automatic level control technique is described, which, when applied to receivers in a tropospheric scatter system, is able to improve the ability of the system designer and frequency planner to co-site tropospheric scatter systems closely spaced in frequency.

The paper also shows how tropospheric scatter transmitters can be adapted to minimise interference to other users during periods of enhanced propagation conditions, and goes on to describe how both techniques may be accommodated within a given transmission path to provide the maximum possible protection, both to other systems and to the link or network in question.

RECEIVE LEVEL CONTROL

a) The Problem

Conventional FM/FDM LOS Microwave Systems, with their limited dynamic range requirements, rely primarily upon I.F. selectivity to limit interference noise from adjacent channels. Whilst the R.F. filter can give additional protection at channels further removed, its principle function is to limit interference from Transmitter to Receiver, and from image components for which no I.F. protection can be afforded.

Tropospheric scatter systems have to cope with a much larger dynamic range of input signal levels, particularly in some climatic regions, and especially in the up-fade regions. (1) Fig.1 illustrates the signal level variations expected in the North Sea (4). The high level signals encountered for short time periods will saturate the input circuits and, for closely spaced multiple input signals, as are encountered on densely packed systems, interference related inter-modulation (IM) products are created, some of which will lie within the pass-band of the I.F. filter. These products cannot be removed by Intermediate frequency filtering alone, and an alternative solution is required.

This problem was examined in some detail to enable an optimum solution to be determined. Initial thoughts hinged around providing much more selectivity at the Radio frequency and the possibility of providing a radio frequency filter with the required characteristics was examined. System considerations involving trade-offs between degradations due to interference noise, intermodulation noise and additional loss of the narrow bandwidth filter were examined with a frequency plan using 3 MHz carrier spacing. The interference characteristic yielded a requirement to attenuate adjacent, unwanted carriers by more than 10dB, without increasing the insertion loss by more than 2dB, or adding more than 100 pWp to the worst slot of a 72 channel system. A closer examination of the problem revealed that a practical filter using direct coupled W/G technique could be made to meet the specification providing that the adjacent carriers were unmodulated. Modulating the adjacent carriers reduced the protection until at full system deviation spectral overlap occurred and the protection became virtually non-existant; although protection was still provided for carriers further removed. This effect was traced to the following mechanisms:

- (i) Reduced protection from convolution of interference spectrum with filter response curve.
- (ii) Direct Adjacent Channel Interference (D.A.C.I.) due to the angle modulation on the interfering carrier being converted to amplitude modulation products by the steep skirts of the filter, which are re-converted to phase modulation on the wanted carrier by any AM/PM conversion mechanism in the receiver.

An improved solution is thus required which can provide the required protection in a high level closely spaced carrier environment. Since an R.F. filter cannot provide all of the necessary protection, the I.F. filter must, as in LOS systems, provide the greater part of the rejection characteristic. In order for this to be a practical proposition, the intermodulation effects have to be prevented from occurring in the receiver front end. This can, with the dynamic range considered, only be achieved by preventing the input signal rising above critical levels by the use of an automatic level control system.

The Intermediate Frequency filter can provide greater protection to adjacent carriers than an R.F. filter as the insertion loss criterion is no longer a limiting factor, and the improved protection is obtained by increasing the number of sections, and hence the skirt rejection.

On economic grounds the above technical argument is vindicated by an examination of the costs of manufacturing R.F. filters to the accuracy and temperature stability required.

b) <u>Implementation</u>

The level control system is implemented by providing an electrically controlled variable attenuator in the aerial input to each receiver.

The minimum loss of the attenuator is obviously critical, as it directly affects the system performance during periods of low signal level, whilst the range must be sufficient to cope with the largest expected up-fade.

Consideration of system performance requirements yields a minimum insertion loss of 1dB with a 40dB range.

The attenuation is controlled by a signal derived from a detector operating at intermediate frequency. Figure 2.

A critical question to be answered is whether to position the detector before or after the I.F. filter. If the detector is positioned after the filter, then it only monitors the carrier level and ignores the possibility of the interfering signal(s) being higher than the wanted carrier and causing intermodulation products on carrier due to their higher level. On the other hand, positioning the detector before the filter measures total power passing through the R.F. filter. Whilst this gives more protection from interfering carriers, it can produce poor performance during periods when the wanted signal is fading down relative to the interferers.

A more sophisticated solution would detect the signal power at both the input and output of the I.F. filter and use the information so obtained to maximise the availability of the wanted signal whilst minimising the level of the unwanted carriers and the total receive power.

The level control loop acts in a similar fashion to an A.G.C. loop, and, when incorporated with a complete receiver, compatibility of time constants has to be considered between the level control systems, and the conventional A.G.C.

Serious consideration of this problem suggests that the level control time constants should be at least an order of magnitude greater than the conventional A.G.C. In practice the receiver A.G.C. is dictated by the maximum fade rate expected, and is typically a few milliseconds to cope with aircraft fading. The Level Control System (RLC) has only to cope with the long term fading structure and a time constant around 1 second is considered adequate.

c) Improvement Obtained.

Studies so far completed suggest that the use of RLC with improved I.F. filtering will cope with all interference situations envisaged in the North Sea where Rx signal levels up to +15dBm can be expected for short periods.

Assuming a uniform closely spaced frequency plan, with frequency spacing f_a of the same order as the I.F. filter f_B , then sufficient attenuation will be produced by the I.F. filter to enable high negative C/I ratios to be handled, provided that Receive Level Control is employed to maintain the front end of the Receiver in the linear region.

TRANSMIT LEVEL CONTROL

Tropospheric scatter systems have to be engineered to meet exacting availability targets, frequently as high as 99.99%. High circuit availability, usually defined in terms of an acceptable signal-noise ratio (S.N.R.), or channel data bit error rate (B.E.R.), implies the use of the highest practical level of transmitter power consistent with system economics, whilst consideration of inverference into other systems requires the opposite approach.

The efficiency of the scattering mechanism in the troposphere varies widely during the course of the year and, for the frequency ranges in question, (700 MHz - 5.0 GHz) the long term fading characteristic can give up to 120dB between the 99.9% and the 0.1% levels (Fig.1). Thus the transmitted signal is, for considerable periods of the year, higher than required, substantially increasing the probability that it will interfere with other communication systems.

Whilst this also applies to L.O.S. and broadcast transmission at ranges in excess of 180 km, we are here concerned with tropospheric scatter systems with high radiated power which operate in frequency bands where the largest variations occur.

These facts have contributed to a reluctance on the part of some regulatory authorities, particularly those with an already crowded electro-magnetic spectrum, to allow tropospheric scatter systems to operate within their sphere of influence.

A level control system has been devised to minimise these effects by reducing the transmitted power during periods of low path loss when an unacceptably high signal would have been received both by the receiver and, as an interfering signal, by other systems.

The effect of this system is to modify the received signal distribution to attenuate the higher levels as shown in Fig. 3, which also gives a considerable reduction in interference to other systems since there is generally a high correlation between periods of high signal strength along any given path.

This reduction of interference, by employing a Transmit Level Control System, can be used to minimise interference between existing systems or it can be used from the planning stage to reduce the co-ordination distance between systems.

The first of these systems is currently operating on all 3 hops of the tropospheric scatter system between Ekofisk Oil and Gas Production Centre in the North Sea, and Emden in Northern Germany. The use of a correctly designed level control system was instrumental in obtaining the permission of the regulatory authority to implement a tropospheric scatter system in the congested ether of the Northern European sub continent.

Operation

Operation of the level control system is controlled by detecting the received signal immediately after the intermediate frequency filter; the d.c. signals so obtained being fed to comparator circuits, which establish upper and lower trigger levels for the power control operation. A 'window' is thus established in terms of received carrier levels. For carrier levels below the window an 'increase power' command is sent to the transmitter; as the received carrier rises through the 'window' the command is first changed to 'hold power' and finally to decrease power as the carrier level passes out of the window above the second trigger point.

These commands can be passed to the transmitter by any convenient means, but an especially convenient system is to use a VFT channel in the sub baseband of the reverse link, the increase power, hold, and decrease power commands being transmitted by CONTINUOUS MARK, MARK-SPACE reversal at band rate and CONTINUOUS SPACE indications respectively. Figure 4 shows a simplified version of the system block diagram.

Upon receipt of a decrease power command the attenuator, which is usually placed between the drive and the P.A. is increased by 5dB and then holds. If, after an interval allowing the complete loop to operate, a decrease power command is still received, a further 5dB attenuation is inserted. A severe up-fade will see this repeated until the attenuator is at maximum attenuation. If, however, after any particular step, a hold command is received, then the attenuator will remain at the position previously set and a static situation will exist, until a further change occurs in the propagation conditions. A down-fade now will cause the received signal to fall below the window, and an increase power command will be sent to the transmitter. Again, this will be repeated, until either a hold command is sent from the receiver, or the attenuator reaches the minimum attenuation position.

Reference (2) gives a detailed description of the hardware used in implementing a Transmitter Control System.

Design Criteria

The basic requirements of the level control system which are established in the design above are:

- (i) The 'trigger' levels referred to the receiver input at which the commands change.
- (ii) The level control range required.
- (iii) Operate time.
- (iv) Redundancy.
- (v) Type and position of attenuator.

The fundamental design aim is to ensure that the parameters adopted for a particular system are such that the incidence of interference into other systems is reduced to a minimum consistent with the creation of no significant degradation in the main circuit performance.

(i) Choice of Trigger Levels.

Examination of fading structures both in depth and time from many parts of the world (5) has revealed that short down-fades from a ducting situation of up to 25dB can occur. In order that these down-fades cannot destroy the system, the lower trigger level is positioned at least 30dB above f.m. threshold. The upper trigger level is positioned 5dB above this value. Since the system will spend the majority of the time at or below the window, careful consideration has to be given to the mean SNR produced by these levels, and if necessary raised to ensure a satisfactory mean or median SNR performance. Raising the window levels will obviously increase the interference level to other systems so a careful trade off is required.

(ii) Time to Operate

A survey of available propogation information from many different climates revealed that:

- a) Large level changes (>20dB) can occur at rates up to 16dB/minute.
- b) Sharp transition of up to 10dB can occur in 7 seconds.

Ideally the loop operate time should be of the order of 4 seconds per 5dB step. In the present implementation this has been achieved except over the first 5dB where approximately 15 seconds are required due to the non-linear nature of the motorised attenuator chosen for that system.

Fig. 5 shows the effects on both the wanted scatter link and a remote LOS system (on the line of shoot and with adjacent channel spacing) of a particular fading scenario on a specific link. This scenario, deliberately chosen to fully explore any weaknesses in the system, is highly artificial and is considerably worse than anything likely to be encountered in practice. The upper half of the diagram reveals that the loop cannot respond to all the fast transitions. Examination of the effect on interference into a remote LOS system reveals that considerable protection is provided for large percentages of the time, breakdown only occurring at (f + 120) seconds after 3 successive fast transitions at the maximum fade rate. With more practical fading scenarios the protection indicated in the left hand side of the diagram is maintained throughout.

(iii) Range of Control

In the ideal case some 75dB of level control range is desirable, but practical considerations (time to remove all attenuation in 5dB steps, noise contribution from the P.A., practical attenuators available) restrict the available control range to around 45dB in nine steps of 5dB.

(iv) Redundancy

Redundancy is largely dictated by the inherent redundancy of the tropospheric scatter equipment employed. Generally for a quadruple diversity system two drives, two P.A's and four receivers are used, indicating that two control attenuators, two sets of control logic, two VFT transmission paths and four detectors are required. Two comparators are used with the lower signal from each pair of receivers controlling the loop.

This maintains the design philosophy of the equipment where any one part can fail without loss of communication.

As far as is possible the level control equipment is built on a fail safe basis which removes all attenuation for any fault.

(v) Type and Position of Attemuator

A motorised passive component is used to satisfy the requirement of a continuously variable component to avoid transient levels, whilst active components are avoided to prevent the creation of unwanted Intermodulation products. Although stepping motors could be used, conventional motors are used in the present design to simplify the circuitry for fail-safe and manual over-ride considerations.

The position of the level control attenuator is dependent upon the type of final amplifier used in the system. For medium power, Class C solid state amplifiers, the attenuator is positioned between the amplifier and the antenna - which imposes an additional power dissipation constraint on the attenuator specification: whilst the minimum loss specification is all-important if the worst month performance is not to be significantly degraded. For 1 and 10Kwatt Klystron Amplifiers an output attenuator becomes impractical and it becomes necessary to vary the drive to the amplifier. Whilst this eases the specification of the attenuator in terms of power dissipation and minimum loss, care has to be taken to avoid degrading the system, either by driving the amplifier into saturation, or at the other extreme by reducing the drive level to the point where the KTRF noise of the amplifier becomes significant. For 1kwatt Klystron Amplifiers the high power performance has been found to be critically dependent on tube type, whilst tubes so far tested have not exhibited significant KTRF noise for level variations in excess of 40dB.

The effects of, and the improvements obtained by the use of Transmit Level Control in particular situations have been investigated and described in Reference (3).

COMBINED SYSTEMS

The use of Transmit Level Control on a particular link confers a considerable measure of protection to other systems, whilst Receive Level Control provides interference protection from other systems.

In the paper we have examined the benefits and implementation of both Transmit and Receive Level Control when realized individually. Maximum benefit would accrue to a complex communication system if the individual links used both Transmit and Receive Level Control, enabling the most efficient use of the spectrum by allowing closer frequency spacing and re-use of frequencies at smaller co-ordination distances.

The implementation of a combined system needs careful thought since it contains three control loops, and overall stability becomes an important criterion.

Stability is ensured by arranging for the AGC loop to have a short time constant of about imsec., the Receive Level Control Loop to be substantially longer at just under a second while the outer, Transmit Level Control Loop, requires 4-5 seconds to implement each 5dB step of control.

The step control for the outer loop is a further aid to stability, whilst a further measure is to use the position of the Receive Level Control attenuator as part of the control information for the transmit loop, rather than the actual signal levels.

In this way an increase in signal level is first dealt with by the AGC, the Receiver Control Loop starting to react after 1 second and inserting attenuation before the receiver. The AGC reacts quickly to the revised situation and restores the correct overall receiver gain. The position of the receiver attenuator is now used to establish a 'decrease power' command to the transmitter, the receiver control loop restoring after the transmit power is reduced. The 'hold' command is now transmitted, a 'decrease power' command is not transmitted unless or until the resultant signal falls outside the window, below the second trigger level. If the path loss continues to fall, the Transmit attenuator continues to rise until its maximum level is reached. At this point the Receive attenuator should still be at zero (assuming a slow fall of path loss) and will now increase as the path loss decreases to minimise the signal applied to the I.F. filter. A similar inverse procedure is used as the path loss falls.

The above procedure makes no provision for dealing with interfering signals into the receiver; this in a practical system could be implemented by inhibiting the Transmit Loop when the Receive Loop is controlled by total input signal (pre I.F.filter) rather than the wanted signal (post I.F.filter). The approach used would have to be dictated by the need to maintain satisfactory C/I ratios at the receiver input.

SUMMARY

The paper has outlined the methods used to implement the various level control techniques and described the design criteria used in setting various critical parameters and in establishing specific approaches.

It is noted that Receive Level Control alone is sufficient to enable the filters to be effective in minimising interference into any given link from other systems, whilst Transmitter Control is required to minimise interference to, and hence reduce the co-ordination distance with, other systems. Finally a method is described whereby both systems can be implemented to gain the advantages of both.

ACKNOWLEDGEMENTS

The author wishes to thank the British Post Office, The Management of the Philips Petroleum Company (Norway) and the Director of Engineering, Marconi Communication Systems Limited, for permission to publish this article. He would also express his appreciation of the keen interest shown in, and support of, this work by Mr. J. Cooling, of the British Post Office and Mr. T. Estes of Philips Petroleum (Europe and Africa). The author would like to take this opportunity to acknowledge the outstanding contribution, in both theoretical and practical work, made by Mr. J.K.Johnson, of Marconi Communication Systems Limited. Finally the patient assistance of Mrs. D. McNicol in typing the transcript is gratefully acknowledged.

REFERENCES

Ref. 1	C.C.I.R.	Report 238 - 2 Vol.V Geneva, 1974
Ref. 2	A.R.Kennedy	'Tropospheric Scatter - Automatic Power Level Control' Communication and Broadcasting Summer, 1976.
Ref. 3	J.K.Johnson	'Interference Estimates Relating to the use of an Automatic Power Level Control in a Tropospheric Scatter System'. To be published.
Ref. 4	Home Office	Unpublished Technical Memoranda. Private Communication from the Directorate of Radio Technology.
Ref. 5	Various	Unpublished Technical Memoranda. Marconi Research Propogation Group.

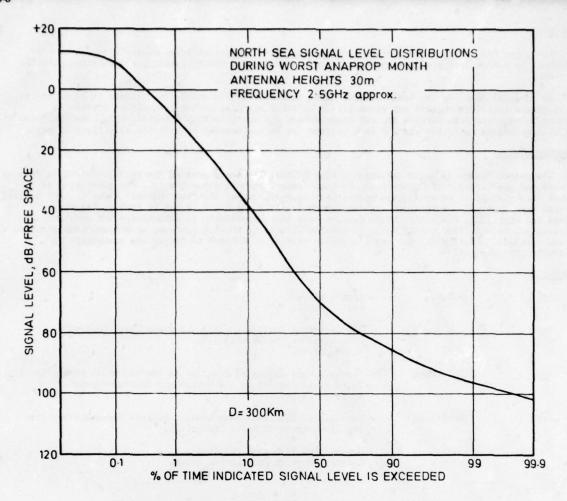


Fig.1 Cumulative distribution. Received signal levels. North Sea

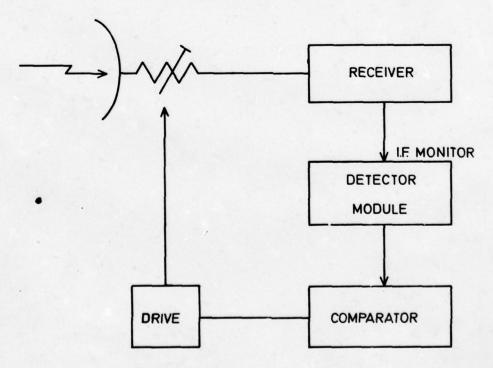


Fig.2 Receive level control. Block diagram

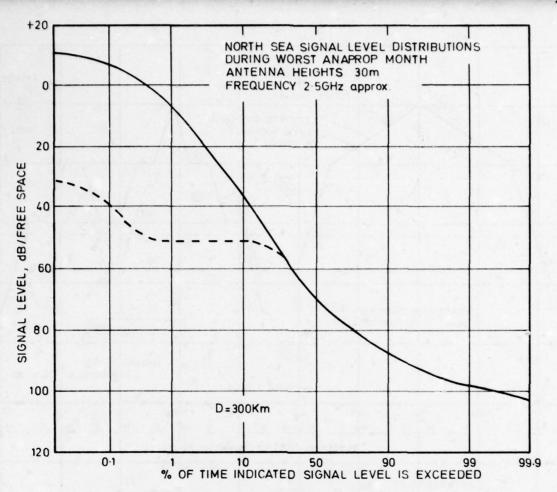


Fig.3 Cumulative distribution. Received signal level. Modified by transmit level control

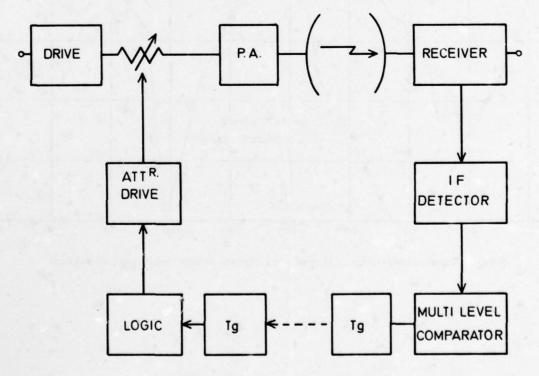


Fig.4 Transmit level control. Block diagram

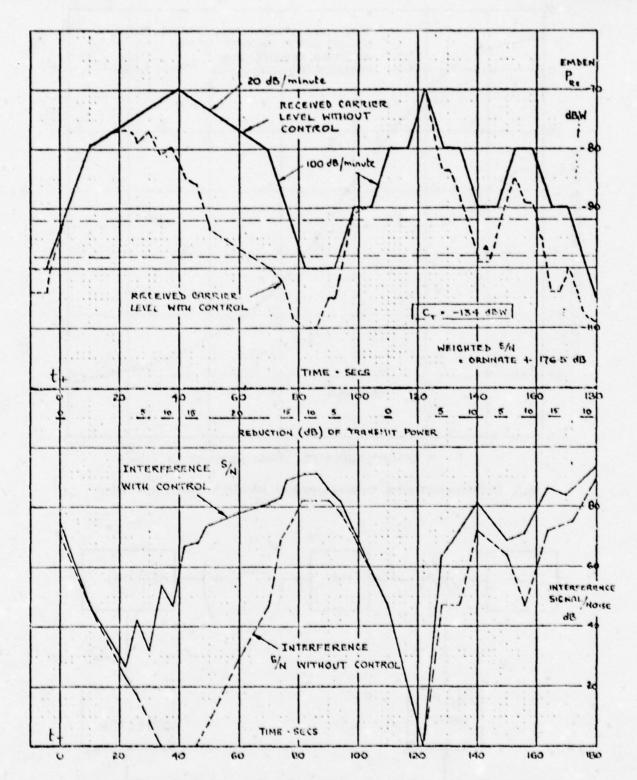


Fig.5 Transmit level control. Effect of control system on interference to another system

THE PERFORMANCE OF METEOR-BURST COMMUNICATIONS AT DIFFERENT FREQUENCIES

by

D.W. Brown and H.P. Williams SHAPE Technical Centre P.O. Box 174 The Hague Netherlands

SUMMARY

The paper reviews the phenomenon of propagation via meteor trails and briefly describes the STC meteor burst communication system. COMET, which used ARQ and diversity reception to provide several telegraph channels on a 1000 km path. The results of extensive testing of COMET at frequencies near 40 and 100 MHz are presented. Signal level statistics as well as burst length and interval statistics are presented for both frequencies. The traffic capacity of the COMET system at the two frequencies is compared on the basis of extensive trials using simple yagi antennas and transmitter powers of 200 W and 2000 W at 40 and 100 MHz respectively. The experimental results suggest a χ^4 dependance for traffic capacity in contrast to the χ^2 dependance predicted upon the basis of simple theory. The reasons for the observed dependance are developed and it is due primarily to the physics of meteor propagation rather than to inefficiencies in the COMET system. Two possible applications of a COMET system which were of particular interest to SHAPE Technical Centre (STC), a low capacity jamming resistant circuit and a reliable orderwire for an HF system, are briefly discussed and suggested circuit parameters set out.

1 INTRODUCTION

Twenty years ago the work on meteorscatter propagation and communication was declassified in the United States and a special issue on this subject appeared in the Proceedings of the I.R.E. in December 1957. In the following ten years SHAPE Technical Centre (STC), took a major part in the work in this field developing an improved 40 MHz communications system called COMET, conducting interception tests, and investigating the performance of COMET at 100 MHz. Consideration was also given to the use of meteor-burst signals in the HF band. This work was mainly described in internal literature, but two papers were published in the open literature: these are given in Refs. 1 and 2. We are now witnessing a revival of interest in meteor-burst systems and this paper will consider the frequency aspect of such systems and discuss the practical implications raised.

The frequencies most commonly used for meteor-burst systems were those in the range 30 to 40 MHz. At these frequencies the duty cycle generally proved to be a few percent. While a higher duty cycle is possible at lower frequencies, this would encroach on the HF band and also make the signals more susceptible to D-layer attenuation. Going to higher frequencies reduces the duty cycle but offers greater immunity to jamming and interception because of the lower duty cycle and on account of the reduced likelihood of sporadic-E reflections.

Depending on the requirements of a system, a frequency either higher or lower than those commonly used may prove to have an overall advantage. In addition to studies using frequencies in the band 30-40 MHz STC were interested in two departures from the normal range. One was the use of a higher frequency to avoid jamming and interception: the other was the deliberate use of a frequency in the HF band to provide an engineering circuit, or back-up circuit, without the need of extra transmitters or antennas. On the first problem tests were carried out at nominal frequencies of 40 MHz and 100 MHz which represent the extreme frequencies of interest. On the second problem no tests have yet been conducted and only theoretical estimates will be given.

2. THEORETICAL CONSIDERATIONS

2.1 Classification of Meteor Trails

Meteor trails can be divided into two categories on the basis of the line density of the free electrons. If the line density is less than about 2×10^{-4} electrons per metre, the trail is termed "underdense". Underdense trails have such low densities that each electron acts individually in scattering radio waves, whereas overdense trails contain such a high density of electrons that a radio wave, after slight initial penetration, is completely reflected.

The dividing line of about $_3^2$ x 10^{14} electrons per metre corresponds to the ionization produced by meteors whose weight is about $_{10}^{-3}$ grams. Meteors which are heavier than this will produce overdense trails while lighter meteors result in underdense trails. When averaged over 24 hours the number of meteors is almost inversely proportional to the weight. One would therefore expect that the number of underdense trails would greatly exceed the number of overdense. However, the signals reflected from underdense trails fall off roughly in proportion to the square of the weight (signals from overdense trails increase only a little with weight) so that in practice it is found that perhaps only 70% of the signals received have been transmitted via underdense trails. This still means that such trails predominate and are therefore the mainstay of any meteorburst system.

2.2 Geometry of Meteor Trails

For an appreciable amount of energy to be transmitted the ionized trail must be tangent to a

prolate spheroid whose foci are at the transmitter and receiver locations. The total path length between transmitter and receiver via a point on the trail is a minimum for reflections from the tangent points. This point is shown as P in Fig. 1 while the distances to the transmitter T and receiverR are shown as R and R, respectively. At some point P^1 along the meteor trail the distance $(R^1_1+R^1_2)$ exceeds $(R^1_1+R^1_2)$ by $\lambda/4$. Therefore P^1 marks the beginning of a further Fresnel zone from which reflections will be in antiphase to those along P^1 .

All contributions from within the principal Fresnel zone, when added vectorially at the receiver, increase the signal strength. Other more remote Fresnel zones produce signal increases and decreases which more or less cancel each other out. Thus the signal strength received from that portion of the trail which lies in the principal Fresnel zone gives a close approximation to the total signal taking all zones into account. The total length of the trail in the first Fresnel zone is 2L since P¹ represents only half the portion within the principal zone.

The trail is in the tangent plane and makes an angle β with the intersection of this plane with the plane of propagation (i.e. the plane containing T, P and R). R_1 and R_2 subtend equal angles, \emptyset , to the normal to the tangent plane. Provided R_1 and $R_2 >> L$ we have

$$L = \left[\frac{\lambda R_1 R_2}{(R_1 + R_2) (1 - \sin^2 \theta \cos^2 \beta)} \right]^{\frac{1}{2}}$$
 (1)

In the radar case (back scattering) R, - R, and Ø - 0 so that

$$L = \left(\frac{\Lambda R}{2}\right)^{k_1} \tag{2}$$

When T and R are separated there is a maximum value for L when the trail is in the plane of propagation ($\beta=0^{\circ}$) and a minimum when at right angles to this plane ($\beta=90^{\circ}$). For example if TR = 1000 km and $\lambda=7.5$ m then, assuming a trail at 100 km altitude, the maximum and minimum values are 5.9 km and 1.4 km.

The cross section of the trail must also be taken into consideration. The model most commonly used is to assume that ambipolar diffusion causes the radial density of electrons to have a Gaussian distribution and that the volume density is reduced while the line density remains constant. These assumptions lead to an equation for the volume density as a function of radius, r and time, t which is:

$$N(r, t) = \frac{q}{\pi (4Dt + r_0^2)} = \exp \left[\frac{-r^2}{(4Dt + r_0^2)} \right]$$
(3)

where q - line density in electrons per metre

D = diffusion constant in metres 2/ sec

t = time in seconds

ro= initial radius of trail

Both D and roare marked functions of height so that some estimate of the heights involved is important. For this purpose, the results of measurements by Greenhow and Hall (Ref. 3) will be used. Fig. 2 shows a plot of the average heights and the maximum heights these authors measured. In all three cases the distribution of number of echoes versus height was approximately Gaussian. A suitable equation relating average height to frequency is as follows:

$$h = -17 \log f + 124$$
where h = average height of trail in km
$$f = frequency in MHz$$
(4)

Figure 3 shows the value of the initial radius r as a function of height. McKinley (Ref. 4) states that the formula due to Manning (Ref. 5) fits experimental evidence better than that given by Optik (Ref. 6). However, the subsequent publication by Greenhow and Hall (Ref. 3) indicated that the radius at the lower heights was by no means as small as would be inferred by the Manning relationship. This difference is almost certainly due to the presence of meteors of the dustball variety. These presumably disintegrate into a cloud of particles with a resultant broadening of the trail. For the calculations in this paper, the dotted line shown in Fig. 3 has been assumed. This is a compromise curve heavily biased in favour of the Greenhow and Hall values. The equation for this line is as follows:

$$log r_o = 0.035 h - 3.45$$

where $r_o = initial radius$ of trail in meters (5)

Although the diffusion constant varies greatly with height, there is more general agreement here as can be seen from the curves in Fig. 4. Also shown in Fig. 4 is a curve of typical meteor velocities as a function of height. In the expression for the signal strength from underdense trails it is the ratio V to D which counts, and for the purposes of this paper a convenient expression of this ratio has been derived which is as follows:

$$\frac{D}{V} = (0.0015 \text{ h} + 0.035 + 0.0013 \text{ (h} - 90)^2) \times 10^{-3}$$
 (6)

Time constants are a function of D and not D/V in which case the following formula for D is used in this paper

$$\log_{10} D = 0.067 h - 5.6$$
 (7)

2.3 Reflections from Meteor Trails

(a) Underdense Trails

The transmission loss of reflections from underdense trails can be expressed as follows (Ref. 4):

$$\frac{P_R(t)}{P_T} = \frac{G_T G_R}{64 \pi^3 R_1^2 R_2^2} \cdot \sigma \cdot A_1 \cdot A_2(t)$$
 (8)

Where $P_R(t)$ = received signal power at time t

P_m = transmitted signal power

G_m = gain of transmitting antenna

Gp = gain of receiving antenna

R, & R, = distances to reflection point from transmitter and receiver respectively

 λ = wavelength in metres

σ = echoing area of the trail

A, = loss factor due to finite initial radius

A2(t) = loss factor due to diffusion

The first two terms are the same as the normal radar equation if $R_1 = R_2$. The condition $R_1 = R_2$ is a convenient assumption to make when calculating the magnitude of the power one would expect to receive over a given circuit.

The echoing area is given by:

$$\sigma = 4 \pi r_0^2 q^2 L^2 \cos^2 \mu \tag{9}$$

where r = effective radius of electron

$$= 2.8 \times 10^{-15} \text{ m}$$

 μ = angle between incident electric vector and electric vector accepted by the receiving antenna

If horizontal polaristion is used at both terminals, the cos μ term is unity. In typical cases the value of σ will be in the region of 10 km^2 .

The first of the loss factors is given by:

$$A_1 = \exp \left[\frac{-8 \pi^2 r_o^2}{\lambda^2 \sec^2 \emptyset} \right]$$
 (10)

The loss is due to interference between the reradiation from the electrons wherever the thickness of the trail is comparable with the wavelength.

The second loss factor is due to the increase in the radius of the trail on account of diffusion. It can be expressed as:

$$A_2(t) = \exp\left[\frac{-32 \pi^2 Dt}{\lambda^2 \sec^2 \emptyset}\right]$$
 (11)

Equation (11) is the only time dependant factor and gives the decay time of the reflected signal power. Defining the time constant as the time for the power to decay by a factor of e^{-2} (i.e. 8.7 dB) we have:

$$T_{\rm un} = \frac{\lambda^2 \sec^2 \delta}{16\pi^2 p} \tag{12}$$

With grazing reflections the value of $\sec^2 \emptyset$ will be large and give a substantial increase in the duration of the echo. For short distances the time constant decreases greatly except for the lowest frequencies. However the time constant is only an indirect measure of the duration of the received echo, since the latter depends on the noise threshold. Generally the duration of the received signal is several times greater than the time constant.

The increase in radius due to diffusion can be appreciable even for as short a period as is required for the formation of the trail. The extent to which the radius has grown will, of course, depend on the portion of the trail under consideration. It can be shown (Ref. 4) that the overall effect with regard to the reflected power is the same as would be obtained if the trail within the first Fresnel zone had expanded to the same extent as the midpoint of this trail. Since this portion is of length 2L the radius at this midpoint is that arising after a time lapse of L/V seconds, i.e. the time taken for the meteor to transverse the second half of the first Fresnel zone. Calling this time interval t we have:

(a) For the radar case and trails at right angles to the plane of propagation ($\beta = 90^{\circ}$)

$$t_0 = (\frac{\lambda R}{2})^{\frac{1}{2}} \cdot \frac{1}{V} \tag{13a}$$

(b) For trails in the plane of propagation $(\beta = 0^{\circ})$

$$t_{Q} = \left(\frac{\lambda R}{2}\right)^{\frac{1}{2}} \cdot \frac{\sec \beta}{V} \tag{13b}$$

Inserting the value of t given by (13a) in equation (11) gives:

$$A_2(t_0) = \exp\left[-\frac{32}{\sec^2\theta} \left(\frac{R}{2}\right)^{\frac{1}{2}} \frac{D}{V}\right]$$
 (14)

For the $\beta = 0^{\circ}$ case the exponential term is sec \emptyset times greater.

Because of the increase in initial radius and diffusion at greater heights, the two loss factors increase with height. This is illustrated in Fig. 5 in which the full lines are for a fixed distance of 1000 km while the dotted lines give the monostatic case. The increase of attenuation gives a ceiling to the height of reflection for any particular frequency. This ceiling will, of course, depend on the system margin available.

In Fig. 2 the ceilings for 17.6, 36 and 70 MHz are about 112, 104 and 98 km respectively. These values would fit in accurately with Fig. 5 if the system margin is put at 20 dB. A more likely value for the system margin is 40 dB, in which case the fit is only fair. However, in view of the uncertainties involved, it may be said that there is a quite reasonable agreement between the theoretical values in Fig. 5 and the experimental values of Fig. 2.

Fig. 5 indicates that, for a distance of 1000 km, the ceiling for a given frequency could be some 10 to 15 km higher than for the zero distance (monostatic radar) case. This means that for long distances a greater depth of meteor trails will be effective in the transmission of signals than at zero distance. However the signals via the higher trails will be relatively weaker on account of greater diffusion. It is questionable whether the gain in overall performance is appreciably enhanced by these signals from higher regions. Much depends on the sensitivity of the communication system. Ideally an integration should be performed which also takes into account the height distribution of the trails. However in view of the uncertainties involved, it was considered that a fair indication of the typical transmission losses involved would be given by taking the average heights for the monostatic case as shown in Fig. 2.

Assuming an electron density of 10^{14} per metre, we can arrive at a set of transmission loss curves as shown in Fig. 6. Because the angles of the meteor trails with respect to the plane of propagation will be randomly distributed and only the two extreme cases are shown, namely those for $\beta=0^\circ$ and $\beta=90^\circ$. The big advantage enjoyed by the lower frequencies is clearly shown. Also shown in Fig. 6 are dotted curves applicable to the case where the heights of the trails are 12 km higher than for the solid curves. The loss in signal strength is very apparent especially at the shorter distances and for the higher frequencies (the corresponding 100 MHz curves are off the scale).

All the curves in Fig. 6 are standardized to unity gain for both transmitting and receiving antennas. For a circuit length of 1000 km possible values for the combined gain $G_{\mathbf{p}}G_{\mathbf{R}^{\mathbf{q}}}$ are:

- (i) for 16 MHz about 12 dB (horizontal dipoles)
- (ii) for 40 MHz about 25 dB (5 element Yagis)
- (iii) for 100 MHz about 25 dB (5 element Yagis)

Since the angle of fire for this distance is in the region of 7 to 8° , the antennas would have to be elevated some two wave-lengths. This would mean 40 m high masts in the case of 16 MHz. Decreasing the antenna height to 20 m would involve an overall loss of 6 dB. For 40 MHz a mast height of 15 m is sufficient (in the STC experiments at 36 MHz a mast some 20 m high was used supporting a vertical stack of two 5-element Yagis for reception to give a further 3 dB gain).

The same antenna gain is quoted above for the 100 MHz case as for 40 MHz. This is because the polar diagram cannot be sharpended any further to advantage since the geographical areas from which the most useful reflections take place are relatively broad. For this reason the STC experiments at 40 MHz and 100 MHz used the same radiation patterns for the two cases.

(b) Overdense Trails

In the transmission equation for the overdense trail the concept of an expanding metallic cylinder replaces the summation over individual scattering electrons. The trail is assumed to have been formed with an initial radius, r, and a Gaussian distribution of electron density about the trail axis. The Gaussian distribution is maintained as the trail dissipates by ambipolar diffusion but, of course, the parameters change with time. Because of the skin depth effects, the core must have sufficent size as well as sufficient

electron density.

The development of a rigorous transmission equation for forward scatter from an overdense trail presents difficulties. These are discussed by von Eshleman (Ref. 7) who developed approximate formulae. A heuristic approach based on analogy with the underdense case, gives the following expression for the transmission loss when the received signal has reached its maximum value:

$$\frac{P_{R}(t)}{P_{T}} = \frac{G_{T}G_{R}}{64 \pi^{3} R_{1}^{2} R_{2}^{2}} \cdot 2 L^{2} \left(\frac{qr_{e}}{e}\right)^{\frac{1}{2}}$$
(15)

Where e = the exponential, i.e. 2.718

Thus the effective echoing area is given by

$$\sigma_{\text{ov}} = 2L^2 \left(\frac{qr_e}{e}\right)^{\frac{1}{2}}$$
 (16)

The application of equation (1) for L² shows that σ_{OV} varies as λ if β = 90° and λ sec Ø if β = 0°. Therefore, the transmission equation gives a received power which varies as λ^3 . This is the same as in the case of an underdense trail.

It should be particularly noted that the received signal power is now only proportional to q¹. Thus increases in signal power with increasing size of meteor are relatively modest for overdense trails. Since the incidence of the larger meteors is low, it follows that the incidence of really strong meteor signals is quite low.

The duration of the overdense signals is given by (Ref. 4).

$$T_{OV} = \frac{q}{4 \pi N_{C}D} - \frac{r_{O}^{2}}{4D}$$

$$= \frac{q}{4 \pi N_{C}D} = \frac{q \lambda^{2} \sec^{2} \beta r_{e}}{4\pi^{2}D}$$

$$= 7 \times 10^{-17} \quad \frac{\lambda^{2}q}{D} \quad \text{if } \beta = 0^{\circ}$$
(17)

Where N = critical value of ionization density

$$=\frac{\pi}{\lambda^2 r_e}$$

The time at which the maximum signal occurs is equal to T /e. The value of this maximum is given by equation (15). An example of the signals from a typical overdense trail is given in Fig. 7 together with an underdense echo.

In marginal cases, it is possible for T of be less than the time taken to establish an adequate radius (i.e. at least one skin depth) throughout the trail. In such cases an overdense echo will not be obtained, even if the volume density on the axis was at first great enough for such reflections. Thus the incidence of overdense trails is less than would otherwise be expected.

(c) Transition Frequencies

The formulas given so far in this paper assume that the time taken for the meteor to traverse the first Fresnel zone is short compared with the duration of the burst of signal, i.e. t << T or T. This ceases to be true as the frequency is increased and eventually, when t >> T or t

$$\lambda_{\rm T} = \left[\frac{128 \, \pi^4 \, {\rm p}^2 \, {\rm R}}{{\rm v}^2} \right]^{\frac{1}{2}} \tag{18}$$

where λ_m = transition wavelength

For the forward scatter case the value of the transition frequency f_m is multiplied by (sec \emptyset) $^{2/3}$ and (sec \emptyset) $^{4/3}$ for the case of $\beta = 90^{\circ}$ and $\beta = 0^{\circ}$ respectively. Values of f_m appropriate to zero distance and to a distance of 1000 km are shown by the dotted lines in Fig. 2. In the case of zero distance, the transition frequencies are low enough to invalidate the application of the equations given above at frequencies above about 50 MHz. Thus the experimental point for 70 MHz shown in Fig. 2 falls in the range where the equations no longer apply. This point was considered by the authors concerned (Ref. 3) who attributed their anomalous measured height-velocity relationship at 70 MHz to the effects of rapid diffusion invalidating the usual equations.

The STC circuit was 1000 km long and for this distance the transition frequency for a given height is distinctly higher than in the monstatic case. Nevertheless the upper frequency used, namely 106.5 MHz, is very close to the transition frequency for transverse trails ($\beta = 90^{\circ}$) at the probable average height of

about 85 km. One would expect therefore that our results would be influenced by this fact. From the formulas given below, one can readily see that a greater variation of duty cycle with frequency than would otherwise be predicted should result and this indeed was the case.

Sugar (Ref. 8) gives the following relationships for both underdense and overdense trails for signals above the transition frequency:

$${}^{P}_{R_{/P_{T}}} = \frac{\lambda^{6} v^{2}}{D^{2}}$$
 (19)

$$T = \frac{D}{v^2 \lambda}$$
 (20)

Equation (19) shows that the transmission loss increases dramatically as the wavelength decreases. On the other hand the time constant actually increases: however the losses involved become so great with decreasing wavelength that meteor-burst echoes are unknown in the UHF band.

A further point is that the time constant given by equation (20) is proportional to D instead of D as in equations (12) and (17). This feature forms the basis of an argument used in Section 4.2.2 to explain the experimental result that at 106.5 MHz the early morning bursts had longer durations on the average than those in the early evening whereas the reverse would be expected from the normal equations.

Equations (19) and (20) apply to both backscatter and forward scatter where bursts from underdense trails are concerned. For overdense trails, however, their validity has so far only been established for the backscatter case. However, it is unlikely that the factors expressing the basic proportionalities are any different in the forward scatter mode.

EXPERIMENTAL PROGRAMME

3.1 General Features

The experimental programme described below came at the end of STC's work on meteor burst communications and followed extensive trials at frequencies near 40 MHz. The object of the tests reported here was to compare the performance of a meteor-burst system at two well spaced frequencies. For this purpose the COMET system (Ref. 1) had a 100 MHz facility added to it in addition to the normal operating frequency of around 40 MHz. The same circuit as before was used, namely the 1000 km circuit between La Crau and Staalduinen. These two terminals are situated as shown in Fig. 8. Although we shall refer to the two cases as the 40 MHz and 100 MHz cases, the actual carrier frequencies used were 36.59 MHz and 106.47 MHz at La Crau and 39.25 MHz and 104.85 MHz at Staalduinen.

Substantially the same equipment was used for both 40 and 100 MHz. Only the antennas and the receiver front-ends were different. Similar radiation patterns were used for 40 MHz and 100 MHz. In each case the antenna system for each diversity branch consisted of a pair of 5-element Yagi antennas. These antenna systems were mounted at heights of 1.2λ and 2.6λ above ground level on each of two masts, placed about 50 metres apart at right-angles to the path. Signals from a given pair of antennas were amplified and then converted to the frequencies used in the 40 MHz tests. The signals were then fed to the old receivers and control equipment.

Information was transmitted by FSK using a total deviation of 6 KHz at a signalling rate of 2000 baud. ARQ was used and for this purpose the five-element characters were converted to seven-element characters which could be checked for a 3 to 4 ratio of marks to spaces. When correct, the information was reconverted to the five-element code.

The first tests began in March 1967 and were designed to compare 40 and 100 MHz in terms of traffic capacity and the statistics of signal strengths. These tests used simultaneous transmissions, on 40 and 100 MHz, and continued until mid-November. In June, a second series began, using 100 MHz transmissions only, for an investigation of traffic capacity, burst length and burst interval statistics at this frequency and to compare space and height diversity. These tests continued until the end of December 1967.

3.2 100 MHz-Only Tests

These tests were carried out using a series of test periods consisting of five days and four nights in order to obtain adequate data on the burst lengths and burst intervals. The statistics measured were those of "information bursts", so that not all bursts which occurred were included. For a burst to be an "information burst" not only must synchronization between the two terminals be achieved, but more than 10 characters must be sent thus ensuring, by the very nature of the COMET system (Ref. 1) that a two-way path exists.

During the tests the transmitters at both ends were repeatedly turned on automatically for 75 minutes and off for 25 minutes. The receivers were calibrated twice perhour by means of an injected standard signal, which varied in steps of 10 dB from 30 dB below, to 30 dB above one micro-volt from a 50-ohm open source. Detected signals from both space-diversity branches were recorded on a chart recorder, so that signals could be distinguished from interference, for duty-cycle as opposed to signal-level measurements.

Traffic capacity was measured by sending a message from both ends. The entire message consisted of a single character, namely "idle-time β ". The number of correctly-received characters, the number of transpositions (undetected errors) and the number of detected errors were recorded automatically by a digital recorder at the Staalduinen end for 7 minutes of each 75-minute transmission period.

Other data collected during these periods were the percentage of time during which the signal amplitude exceeded 10 preset levels for both of the diversity branches, the number of transmission bursts (and intervals) of various durations and also the number of characters received each minute or 7 minutes. Noise measurements were made during the breaks in transmission.

The frequencies assigned for the tests were 104.847 and 104.853 MHz for mark and space frequencies at Staalduinen and 106.457 and 106.473 at La Crau. The mark and space frequencies from each antenna system were precombined and the combined outputs were then added in the diversity combiner. This was done so that the output from both antenna systems and the output of the combiner could all be used for the decision process in the "multidetector". Decisions are taken in the "multidetector" for each character on a code conformity basis. Those branches which do not contain a character consisting of 3 marks and 4 spaces are eliminated from further consideration. There must be an agreement between two remaining branches before a character is accepted. If two branches containing the same code-conforming character cannot be found, a request for a repetition of the character is initiated. The transmitter power for all the 100-MHz-only tests was 2000 watts. Some tests employed horizontal space diversity and others height diversity. As was expected, at 100 MHz no great diversity effects were noted. The diversity gain at 40 MHz comes from the uncorrelated fading of the tails of the bursts which is caused by distortion of the meteor trail by turbulent winds and is almost absent at 100 MHz, because at that frequency the majority of signals do not last long enough to be affected by winds.

3.3 The 40 and 100-MHz Comparative Tests

The comparative tests were designed to compare the two frequencies with regard to traffic capacity and the relation between duty cycle and signal strength using data measured simultaneously. Since dual sets of COMET control circuitry (one for each frequency) did not exist, a scheme was devised whereby two 40-MHz and two 100-MHz receiver outputs could be fed simultaneously to the COMET equipment.

In the direction, Staalduinen - La Crau, the traffic was carried basically on 40 MHz. The power used was 2000 watts, in order to ensure that a North-South path existed whenever the lower-power South-North path was present. In the North-South direction, a 100-MHz path was also used in case a burst at 100 MHz should be present when there was no 40-MHz path. The 100-MHz transmitter power was 4000 watts. At the La Crau terminal all signals were combined and the character decisions were taken in a 5-branch multidetector.

From La Crau, 40-MHz signals were transmitted at 200 watts and in the early tests 100-MHz signals at 4000 watts. Later, the La Crau 190-MHz power was lowered to 2000 watts. All the 100 MHz results presented in this paper have been normalized to 2000 watts. In Staalduinen, all signals were used by the COMET system in a 5-branch multidetector. With the help of this combined frequency system it was possible to communicate via a trail at 100 MHz or 40 MHz, or even one way with one frequency and back with the other. It was only necessary to ensure that the 40 MHz and 100 MHz transmitter keyers were fed in phase.

At the Staalduinen terminal, the number of characters correctly received during communications was recorded for both frequencies. An extensive switched test was performed to determine what relation the traffic capacity figure measured in the above way bore to the traffic capacity measurements for each frequency alone and using equal transmitter powers at the two ends of the circuit. During this calibration test which lasted 6 days, the system was switched from the above configuration to purely 40 MHz or purely 100 MHz after each 7½ minute transmission period. In each hour, therefore, there were comparative periods and three single-frequency periods. In this way, the normalisation factors of 0 dB for 40 MHz and -2.5 dB for 100 MHz were obtained. All the results have been normalized and represent true comparisons between COMET systems operating at 200 watts, 36.59 MHz and 2000 watts, 106.47 MHz.

Duty-cycle vs signal-level data were also gathered at Staalduinen. Signals from one 40-MHz antenna system at a height of 2.6 λ and one 100-MHz antenna system at a height of 2.6 λ were fed to the digital recorder. The percentage of time during which each signal exceeded its 10 preset levels was recorded for each 7-minute period. Here again, the relevant frequencies constituting the basis for the comparison are 36.59 and 106.47 MHz at transmitter powers of 200 and 2000 watts, respectively.

4. EXPERIMENTAL RESULTS

4.1 Traffic Capacity

4.1.1 The Hourly Average Capacity

A large number of results were obtained of the average hourly capacity of the circuit at both 40 and 100 MHz. Examples are given here in Figs. 9 to 11. The first two are for 40 MHz and 100 MHz over the same time period, namely 13-17 Nov, 1967. Both show a sinusoidal variation of duty cycles over the day. However, at 40 MHz this sinusoidal variation was always quite distinct, whereas at 100 MHz this was often obscured by the presence of meteor showers. This effect is illustrated in Fig. 11 where the diurnal variation is far from being sinusoidal.

This difference in diurnal patterns between 40 MHz and 100 MHz transmissions comes about because the distribution of different sizes of meteors in meteoric showers is different from that for the background of sporadically-appearing meteors, which carry the bulk of traffic at low VHF frequencies. At high frequencies, the signal from a given meteor trail tends to last a much shorter time than at low frequencies. In fact, the many small meteors which carry so much of the traffic at 40 MHz do not last long enough at 100 MHz to allow the COMET system to attain synchronization. Meteor showers, however, tend to contain a higher proportion of large meteors than is usually the case for the sporadic variety, and so, whereas a shower may only cause a small increase in the background at 40 MHz, it can cause large increases at 100 MHz. Another reason for the departure from sinusoidal shape is the lower sensitivity of 100-MHz traffic capacity to cosmic noise. At 100 MHz the noise level is determined for the greater part of the day by receiver noise. Only for a few hours a day, when cosmic noise is at its peak, does it limit reception at 100 MHz. In contrast to this, the 40-MHz noise level is always determined by

cosmic noise and, as a result, may vary as much as 10 dB in the course of a day. The effects of this can be seen clearly during the 13-17 November comparative test. The 40-MHz traffic capacity, Fig. 9., has a deep depression around 15:00, the time of the noise maximum at Staalduinen for that time of year. The 100-MHz results (Fig. 10) lack this feature and have, instead, a smaller minimum at 17:00 - 18:00, when the number of meteors is at a minimum.

4.1.2 Comparison of Capacity at 40 and 100 MHz

Fig. 12 gives a summary of the measured duty cycles, Ic, for both 40 MHz and 100 MHz showing average values for each of the 4 or 5 day test periods, together with the maximum and minimum values during each period. For convenience, smooth dotted lines have been drawn through the average values.

Six plots were made of the ratio of the duty cycles involved as a function of the time of day and Fig. 13 gives one of these. The difference in noise dependance at 40 and 100 MHz is very noticeable in ratio plots such as Fig. 13. In such figures there was nearly always a dip, representing better relative 100-MHz performance at high cosmic noise levels. The position of the Staalduinen noise maximum is marked on Fig. 13 with an arrow, since it is the noise at this terminal which determines traffic capacity - the noise at La Crau varied but little during the day.

Another clearly evident tendency in Fig. 13 is a peak around noon. This feature is nearly always present and is presumably due to the prevalence at that time of propagation modes other than meteor burst on 40 MHz. Peak ionoscatter occurs at maximum sun elevation and the phenonmenon is still important at 40 MHz, whereas at 100 MHz it is totally absent.

The ratio of the average daily traffic capacities is 17.6 in Fig. 13. Except for the two tests in June, all the ratios obtained were in the range 19 ± 1.5 . The June values are such lower, indicating that 100-MHz propagation was relatively better during that month. This is in line with the fact that the whole month of June is characterized by important day-time meteor showers. The Arietids and Zeta Perseids reached a broad peak of activity around 8 June. Just as these two large showers were fading in mid-June, the Beta Taurids were beginning to build up towards a maximum on 30 June. As previously explained, meteor showers tend to favour 100-MHz propagation.

4.1.3 The Influence of Shower Meteors on Traffic Capacity

For communication purposes, shower meteors are generally considered to be of little importance compared with sporadic meteors. However, it has been shown that this is untrue at the higher frequencies while even at 40 MHz, showers play an important role in meteor burst communication as evidenced by our records in June. The 13-17 November comparative test ended just too soon to record the full potential of the 1967 display of the Leonid periodic shower but much increased capacity can be seen between 0600 and 0900 on 17 November as the shower started (Figs. 9 and 10). In general though, it is only showers which recur every year that have an important effect on meteor communication.

Owing to the fact that shower meteors move in defined orbits around the sun, all the meteors of a given shower enter the earth's atmosphere from a common direction i.e. from the same radiant. For showers which have radiants near the ecliptic plane, the radiant point rises, traverses the sky from east to west like the sun and then sets. For a north-south communications circuit, this produces a typical two-humped increase in traffic capacity as the radiant is suitably oriented for the two "hot-spots" on either side of the path. This sort of behaviour is typical of the Arietids, Perseids and Taurids of June. Fig. 11 clearly shows the two peaks, at 0700 and 1400 hours, respectively. If a shower has a radiant point near the pole star, as is the case with the Ursid shower of late December, it can affect propagation for 24 hours a day over the entire duration of the shower. An east-west path, for instance, could expect enhanced traffic capacity 24 hours a day for nearly 1 week from the Ursids. A north-south link, however, has only the two-humped response even to this shower. This was borne out by two peaks at 0300-0400 and 1300-1500 on the records for 21 and 22 December.

4.1.4 Statistical Variation of Traffic Capacities at 100 MHz

Fig. 14 shows the variation for the 7-minute traffic capacity as normalized to the pertinent hourly value. In the same way that the hourly 100-MHz values are more variable than are their 40 MHz counterparts the 7-minute values are likewise more variable than is the case at 40 MHz. It was found that the short-term 40 MHz traffic capacity over 7-minute periods was bounded by 0.5 and 2.0 times the hourly value in 90% of cases. This compares with 90% boundaries at 0.25 and 5.0 times the hourly capacity for 100 MHz.

4.2 Burst Statistics

4.2.1 The Definition of a Burst

The statistics presented here concern "information bursts", during which information is passed both ways on the circuit. In keeping with this definition and the ARQ techniques used in COMET, all bursts where less than 10 characters were received at the Staalduinen terminal have been disregarded. In the same way, short interruptions in the middle of bursts where a repetition was requested, have been disregarded. They were not counted as part of the burst because no information was passed, but neither, on the other hand, were they regarded as marking the end of one burst and the beginning of the next. This overcomes the problem that previous workers have experienced in distinguishing between new bursts and fades in an old one. The distinction is drawn automatically in COMET circuitry, on the basis of the length of the "fade" and whether the "new burst" has a different path length after the "fade".

4.2.2 Burst Length Statistics

The data used to calculate burst-length and interval statistics were collected during five tests covering the period 15 September to 22 December 1967. This extensive testing was necessary to obtain a

large sample of information bursts which are considerably rarer at 100 MHz than at 40 MHz.

Fig. 15 shows the probability distribution of burst-lengths at 40 MHz (based on former terts) and 100 MHz. It can be seen that neither 40 nor 100-MHz burst-lengths fit an exponential probability distribution, except for short bursts of less than 0.5 seconds. From equation (10) one would expect that the probability distribution of burst-lengths for "underdense" bursts should follow an exponential law. This would seem to hold true in the underdense region, up to about 0.5 seconds duration. Bursts longer than about this value are probably overdense and should not be expected to fit an exponental distribution. In fact, the statistics for such long-duration bursts could be better characterized by a power law as can be seen from Fig. 16 where the probability distribution is shown plotted in log-log coordinates.

Because evening meteors have lower velocities than morning meteors and therefore produce their ionization lower down in the earth's atmosphere, it might be expected that long-duration meteor-bursts would be more prevalent in the evening hours. This is because the duration of bursts, is inversely proportional to the diffusion constant and this decreases rapidly with decreasing height. As can be seen from Fig. 15, at 40 MHz the experiments showed only a slight increase in burst length for the afternoon period. On the other hand at 100 MHz the reverse effect is shown, namely the longer bursts occur in the morning. This "reverse effect" is characteristic of the long duration echoes and would therefore appear to be associated mainly with overdense echoes. An explanation for the reverse effect can be found in the fact that the frequency concerned is close to the transition frequency discussed in section 2.3(c).

Ignoring the wavelength terms in the time constants, we have the following proportionalities for the time constants at frequencies below or above the transition frequency $f_{_{\rm T}}$

$$T_1 = \frac{\sec^2 \theta}{D}$$
 $f < f_T$ (21)

$$T_2 = \frac{D}{V^2 \sec^2 \theta} \qquad f > f_T \qquad (22)$$

These equations apply to both the underdense and overdense trails though in the case of T_2 the extension of equation (22) to the forward scatter overdense case has yet to be confirmed (Ref. 8).

Possible values for morning and evening parameters for frequencies in the region of 100 MHz are as follows:

	Morning	Evening
Velocity in km/sec	35	15
Height in km	100	90
Diffusion constant	12	2.7
Sec # for 1000 km	4.30	4.67

Inserting these values in equations (21) and (22) gives the following ratios:

$$\frac{\text{Evening T}_1}{\text{Morning T}_1} = 5.25 \tag{23}$$

Evening
$$T_2 = 1.04$$
 (24)
Morning T_2

Now the actual durations depend also on the sensitivity of the system. A suitable simple criterion is to take the product of the echo amplitude and the time constant. Then from Fig. 5 it can be seen that for $f < f_{_T}$ the result is roughly independent of the time of day, while for $f > f_{_T}$ afternoon echoes would be favoured, though not so strongly as the ratio of (23) to (24). Thus we should expect the durations for $f < f_{_T}$ to show only slight variations with time of day, whereas for $f > f_{_T}$ the morning echoes would be favoured.

Because of the difference in the decay of the underdense and overdense echoes, the durations of the latter amemuch less influenced by the sensitivity of the system. Therefore in comparison with underdense echoes, the overdense echoes should conform more to equations (23) and (24) and less to the product criterion.

Thus we can explain in qualitive terms both features shown in the experimental results of Fig. 15, namely that at 100 MHz it is the morning echoes which have the longer duration, and also that this effect occurs essentially for reflections from overdense trails.

4.2.3 Burst-Interval Statistics

The distributions of burst-intervals shown in Fig. 17 all fit exponential curves, as is to be expected when one considers that meteors occur at random. The difference between 40 MHz and 100 MHz is marked, 100-MHz bursts bein such less frequent. This can also be seen in Fig. 18, where the statistics for the number of bursts per minute period for 40 and 100 MHz are compared.

4.3 Signal Level Statistics

4.3.1 Diurnal Variation of Signal Statistics

There has been some attention given in the past to determining whether the slope of the signal level distribution varies with the time of day. The 40-100 MHz comparative data were examined for this effect. The results from the tests of 19-22 September and 10-13 October were averaged out and plotted in two-hour intervals. Each curve was an average of about 10-12 hours of data as taken from the relevant time interval on the days when the two tests were held. The results may be summarized by saying that the 100-MHz curves showed no consistent variations in slope. The 40-MHz curves showed a tendency for a high duty-cycle intercept to be associated with a lower slope value. The tendency was not pronounced and may have owed something to the tendency of the curves to bunch as noise level is approached. At that time of the year the noise level at Staalduinen reaches its daily maximum at about 1700 hours and would have a value near -10 dB. Values for 0 dB and above can certainly be assumed to be free of noise influence. Thus if there is a slope dependence on the time of day, the effect is not pronounced.

4.3.2 Results from the Comparative Tests

For the comparative tests, one signal from a 40-MHz and one signal from a 100-MHz receiver, were selected for signal-level recording. The signals chosen came from antennas with the same radiation pattern, i.e, the signal from a 40-MHz antenna at a height of 2.6λ was compared with the signal from a 100-MHz antenna at the same relative height. However, very little difference in the duty cycle for high and low antennas was observed.

The results are shown in Fig. 19 and represent the signal distribution, averaged out for each frequency and test. Assuming a matched load, and a receiving antenna gain of 10 dB, the 0 dB point on the abscissa corresponds to -143 dBW. The averages were carefully taken over three or four whole 24-hour periods for each test, in order to avoid bias with regard to any particular time of day. It an be seen that all the curves are approximately parallel and in fact the values of the intercepts at a given signal level follow about the same increasing order as do the 24-hour average traffic capacities. Any small difference can be attributed to one of two factors:

- (a) The traffic capacity results are influenced by noise level and by the time of the daily noise level maximum, whereas the signal statistics are independent of noise.
- (b) The traffic capacity and signal statistics results may have been based on slightly different samples of data. In deriving the traffic-capacity results almost all the different types of data were used. Only those 75-minute periods in which severe and lengthy interference was present were excluded from the averages. Short bursts of interference were considered to have no effect on traffic capacity, especially at 100 MHz, where interference bursts may occur between meteor-bursts without any adverse result. However, any interference can upset the signal-level results and lead to over-optimistic curves. All periods containing interference were excluded from the averaging process which produced the duty-cycle vs signal-level curves. (Periods of sporadic-E reflections, observed on the lower frequency only, have been excluded from all the results).

Fig. 20 represents an average of signal-level statistics drawn from all the tests and is therefore useful for predicting the yearly average duty cycle for any system proposed. It can be seen that the slopes of the two curves in Fig. 20 are equal in the expected operating regions, namely 2000-Hz bandwidth, cosmic noise, 10-15 dB SNR. In fact, the curves are very closely parallel and have uniform slopes except at very high thresholds so that the curves can be approximated by the relation D $^{\alpha}$ V $^{-R}$, where D is the duty cycle at a given input voltage, V is the voltage level of the received signal, and K is a constant with value 1.2. The value of the slope K, indicates that it is very advantageous, in terms of information capacity to increase the signalling rate and bandwidth.

In terms of received power we have D \propto P $_R^{-0.6}$ and this relationship can be used for adjusting for the difference in transmitted powers when comparing the results obtained at the two frequencies. Using equation (8) we obtain the theoretical values for the transmission losses at the two frequencies, given in Table I.

Table I
Theoretical Transmission Losses

1000 km Circuit q = 10¹⁴ electrons/m

Frequency in MHz Angle, β, of Meteor Trail	36.6		106.5	
	00	90°	00	90°
Losses in dB				
(a) $h = -17 \log f + 124$	169.0	180.5	186.1	195.4
(b) h = -17 log f + 136	174.9	183.1	197.6	200.6

For case (a) the heights used are the average values as shown in Fig. 2. However the much higher ceilings which apply in the case of oblique transmissions (see Fig. 5) suggest that the contributions of reflections from greater heights may be significant. So for case (b) an increase in height of 12 km has been assumed. In view of the uncertaintities involved, compromise values have been adopted for the

difference between the losses at 36.6 MHz and 106.5 MHz. These compromise values are shown in Table II.

TABLE II

Relative Values of Transmission Losses

Frequency in MHz	36.6	106.5
Transwerse trail (3 = 90°)	0 dB	16 dB
Longitudinal trail (8 = 0°)	0 dB	20 dB

In the present case the powers used differed by 10 dB. Thus we would expect the curve for 106.5 MHz to be displaced horizontally by 6 dB and 10 dB relative to the 36.6 MHz curve for the transverse and iongitudinal cases respectively. Now the experiments would have involved a whole range of differently angled trails, so that each experimental curve represents an averaging of all usable radiants. In the absence of more exact knowledge, the dotted theoretical curves for 106.5 MHz in Fig. 20 are drawn using horizontal displacements of 6 dB and 10 dB from the measured curve for 36.6 MHz.

The predicted vertical displacement would depend on the relative time constants (or, more accurately, on the relative durations) and on the relative number of meteor trails involved in each case. If we had only a λ^2 relationship to deal with the vertical displacement would be a factor of 8.5. However, as shown by equation (11) the time constant is also a function of 1/D where D is the diffusion constant which in turn is a marked function of height. A further complication is that the upper frequency of 106.5 MHz is approaching the transition frequency. There is therefore no valid simple theoretical relationship for assessing the relative durations. Experimentally a ratio of about 2.3 is given from an examination of the higher probability levels in Fig. 15.

The number of meteors involved can be estimated from the burst interval distribution. Reading from Fig. 17 suggests a ratio of about 3.5: 1 for the two frequencies concerned. The product of this with the ratio for the durations is close to 8: 1 and this is the value used in Fig. 20. A vertical displacement of this value leads to the two dotted lines shown. Since the radiants must be fairly evenly distributed, the curve predicted in this way would lie somewhere in the middle of the two dotted lines.

The experimental results however show a ratio of the duty cycles closer to 17:1 than 8:1 and the fact that the upper test frequency is approaching the transition frequency must be primarily responsible for this.

The experimental results may be summarized as follows:

(a) the variation of duty cycle at a given received power with power is given by

$$p_{c} \propto p_{R}^{-0.6} \tag{17}$$

(b) the variation of information duty cycle for constant signal-to-noise ratio could be expressed as:

$$r_c \propto \lambda^4$$
 (18)

Equation (17) holds for a fairly wide range of signal levels as witnessed by Fig. 19. Equation (18) is a combination of the experimental value of 17: 1 duty cycle difference referred to above, plus the fact that cosmic noise varies as $\lambda^{2.3}$. The latter relationship gives an 11.6: 1 ratio in the noise levels, at 36.6 and 106.5 MHz, and by equation (17) this translates to an equivalent power ratio of 0.23: 1.

Using the fourth power relationship in equation (18) gives a I ratio of 70.73. Multiplying this by 0.23 gives 16.3, which is a good approximation to the value of 17 as deduced previously.

- 4.4 Comparison of Performance at 40 and 100 MHz
- 4.4.1 Information Duty Cycles

A summary of the measured average information duty cycles is given below.

	Information Duty Cycle, I _C (percentage)		
Dates (all 1967)	36.6 MHz	106.5 MHz	
26 - 28 April	5.94	0.336	
8 - 12 May	8.17	0.435	
6 - 9 June	13.5	0.94	
13 - 16 June	-	0.903	
20 - 23 June	12.9	1.05	
28 - 30 June	-	0.691	
12 - 15 September		0.353	
19 - 22 September	9.14	0.474	
10 - 13 October		0.55	
6 - 10 November	-	0.373	
13 - 17 November	14.0	0.725	
20 - 24 November	- 100 m	0.352	
27 Nov - 1 Dec	-	0.807	
18 - 22 December	7 1 · 1	0.606	
verage value	10.618	0.614%	

The ratio of the two average values is 17.3:1. This is only in fair agreement with the ratio of 12:1 as derived from Fig. 20 at the 12 dB SNR levels. However, it should be noted that extremes of only plus and minus 2 dB in the required signal to noise ratio could change the ratio to one of 24:1.

The abscissa values shown for 12 dB SNR in Fig. 20 are based on the following formula for the cosmic noise power per unit bandwidth.

$$P_N = -152 -23 \log_{10} f_{MHz} dBW$$
 (19)

If we equate the radiated powers so that both are for a radiated power of 2000 watts then according to equation (17) the duty cycle of the 36.6 MHz case should be increased by a factor of 4. The ratio of the information duty cycles then becomes 42.44 to 0.614 i.e. 69.1:1. This ratio is almost exactly the value given by a λ^4 law. Fig. 21 shows a plot on log-log paper of the measured average values of I_{C} , the information duty cycle as a function of frequency using a straight line to join the two extreme points at 36.6 and 106.5 MHz.

The λ^4 law represented by this line is a considerable departure from the often quoted simple theoretical law of $\lambda^{2.7}$ as given by the combination of a cube law for the peak power, a square law for the duration and a 2.3 power law for cosmic noise. However this theoretical law assumes that the same meteor trails are involved at all wavelengths.

A more appropriate relationship is obtained if the change in the number of effective trails is allowed for, and if an allowance is made for changes in the average height of the reflection (i.e. for changes in the diffusion constant). The parameters involved are then as given in the table below.

Index Parameter		Value of Index	
	Symbol	Underdense	Overdense
Peak receiver power Time constant	n p n _t	3 2 th	3 2 th
Cosmic noise level Distribution	n _n	2.3	2.3

The information duty cycle ratio is given by

$$I_{c} \propto \lambda(n_{p} - n_{n}) n_{d} + n_{t}$$
 (20)

 $[\]mathbf{\hat{x}}$ The time constant varies as D^{-1} (where D is the diffusion constant) and since D varies approximately as λ on account of the increase in height with λ , a more accurate value for n_t would be unity. This might be called the "ceiling effect" value.

For underdense trails and no ceiling effect we have from the table above,

$$I_c \propto \lambda^{2.35}$$

Allowing for ceiling effect gives

For overdense trails, the corresponding relationships are:

$$I_{\alpha} \propto \lambda^{3.4}$$
 for no ceiling effect

$$I_{\alpha} \propto \lambda^{2.4}$$
 with ceiling effect

Whatever mixture of underdense and overdense trails one assumes, these relationships fall far short of the experimental fourth power law. One can only suppose that the proximity of the upper frequency used to the transition frequency has played a big part. If so, a reduced power law would apply to frequencies below 106.5 MHz. Put in another way, one may be confident that for frequencies of, say, 70 MHz the loss in duty cycle in comparison with 36.6 MHz will certainly not exceed that indicated by Fig. 21.

The values for n_d arise out of the fact that P_R is proportional to q^2 for underdense trails and to q^2 for overdense trails. Thus if only underdense trails were involved one would expect the duty cycle to vary as $P_R^{-0.5}$. Our experimental value of 0.6 for n_d suggests that reflections from underdense trails dominated in our system. A similar result was obtained by Montgomery and Sugar (Ref. 9).

It is apparent that the results shown in Fig. 21 cannot be extrapolated to lower frequencies. In this respect it is important to remember that below about 50 MHz the statistics will be contaminated by the presence of ionoscatter signals. Fig. 21 will, however, give a convenient picture of the probable behaviour of frequencies between 40 and 100 MHz. For example, using a frequency of 70 MHz (when the intrusion of sporadic-E-reflections can virtually be forgotten) the information duty cycle will be about 2.5%. This would give one 50 baud circuit if a transmission rate of 2000 baud is used.

4.4.2 Effect of Bandwidth on Performance

Using the fact that the noise power is proportional to the bandwidth, one can derive the variation of the information duty cycle with bandwidth from Fig. 20. The result is

$$I_{c} \propto B^{-0.6}$$
 (21)

Where B = bandwidth in Hz

The information transferred, I, is proportional to the signalling rate times the duty cycle, and the former may be assumed to be proportional to the bandwidth. We therefore have

Equation (22) is independent of frequency and indicates that, for maximum information transfer, the bandwidth and signalling rate should be as high as possible. The only limitations are those imposed by bandwidth availability and by the maximum acceptable delay in transmitting a message. The latter limitation arises because a high signalling rate implies a low duty cycle which in turn implies the possibility of longer message delays.

No limitation is likely to be set by the coherency bandwidth since this bandwidth is of the order of several MHz for the main part of the burst. Even for the tails of the burst (when fading takes place due to wind shears) the coherency bandwidth is some hundreds of KHz. Calculations on this point, together with some experimental verification may be found in Ref. 10.

CONCLUSIONS

5.1 Experimental Results

From the experimental results described in this paper for a 1000 km circuit between Southern France and Holland the following conclusions can be drawn:

(a) The long term average of the duty cycle (the fraction of the time that the received signal level exceeds the system threshold) is related to the transmitted power as follows:

$$D_{c} \propto p^{0.6}$$
 (23)

where D = duty cycle

P = radiated power

Equation (23) is valid over a wide dynamic range and for frequencies in the range 40 to 100 MHz. The exponent is not markedly dependent on the time of day.

(b) The measured information duty cycle (the fraction of time that information is transmitted over the circuit) varied as follows:

$$I_{c} \propto \lambda^{4}$$
 (24)

where I - information duty cycle

λ = wavelength

Actual values of I for a 2000 watt transmitter are 42% and 0.6% for 36.6 MHz and 106.5 MHz respectively. This assumes the relationship given in equation (23) for converting the 10.6% value at 36.6 MHz for 200 W to the corresponding percentage for 2000 W.

A fourth power law differs considerably from that predicted by even the most refined theory. Since the theory concerns D it might be thought that the difference arises out of the time delays inherent in the equipment if I is being measured. However an examination of the signal level curves in Fig. 20 shows that this is not so. If we take the vertical distance between the 12 dB SNR operating point on the curve for 106.5 MHz and the operating point on a curve for 36.6 MHz obtained by displacing the curve shown by 10 dB (to allow for the power difference) then the D ratio obtained is about 60:1. This corresponds to a 3.8 power law and is therefore much nearer the fourth power law measured for $I_{\rm C}$ than the theoretical 2.7 power law for $D_{\rm C}$.

- (c) The slight differences in the diurnal variations of the traffic capacities at 40 and 100 MHz can be explained by the prevalence of meteor showers at certain times, and of other modes of propagation at 40 MHz, particularly around mid-day.
- 5.2 Parameters for a Jam-Resistant Circuit

If a jamming resistant circuit were required, the results would indicate the use of a frequency in the region of 70 MHz. With 2 Kw of transmitter power, antenna gains of about 13 dB, and a transmission rate of 20,000 baud, a minimum signalling rate of one 50 baud channel and an average rate of 2.5 channels could be expected with an errorrate of better than 1 in 10⁴ in the absence of jamming.

A distant jammer could not hope to reduce the throughput of a COMET system by more than a few percent by jamming via meteorburst propagation. A study of the available information on sporadic E reflections indicates that the jammer might expect such a propagation mode for less than 's percent of the time at 70 MHz but of course he could then disrupt all communication on the circuit.

5.3 Parameters for an Order Wire Circuit

In HF systems the problem often arises as to how to re-establish contact when the operating frequency has faded out. This could be done by using transmissions in the meteor-burst mode, for which purpose the highest allocated frequency is themost suitable. Assuming this to be about 16 MHz, one could switch over to meteorburst modems and, with antenna gains of 6 to 8 dB, achieve approximately the same performance as obtained on the STC experimental link at 40 MHz using antenna gains of 13 dB.

Because of band-width limitations at HF via which the circuit would work for some fraction of the time, the transmission rate could not be increased above the value used in COMET, i.e. 2000 band. But even this would give the equivalent of several 50 band channels on the average, and at least one such channel at any time, with transmitter powers of 1 kW.

Antenna patterns which favoured propagation by meteorburst modes would automatically also enable full use to be made of sporadic-E reflections.

REFERENCES

- BARTHOLOME, P.J., and VOGT, I., April 1968, "COMET A new meteorburst system incorporating ARQ and diversity reception", IEEE Trans. Vol. COM-16, pp 268 - 278.
- BARTHOLOME, P.J., 1968, "Survey of ionospheric and meteor scatter communications", "Ionospheric Radio Communications", ed. K. Folkestad, Plenum Press, New York, pp 143 -154.
- GREENHOW, J.S., and HALL, J.E., 1960, "The importance of initial trail radius on the apparent height and number distributions of meteor echoes", Monthly Notices Royal Astron. Soc., Vol. 121, pp 183 - 196.
- 4. McKINLEY, D.W.R., 1961, "Meteor Science and Engineering", McGraw-Hill Book Co., Inc., New York.
- 5. MANNING, L.A., 1958, "The initial radius of meteoric ionization", J. of Geo. Res., Vol. 63, pp 181 196.
- 6. OPIK, E., 1955, "Meteors and the upper atmosphere" Irish Astron. J. Vol. 3, pp 165 181.
- ESHLEMAN von, R., January 1955, "Theory of radio reflections from electron-ion clouds", IRE Trans. Vol. AP-3, pp 32 - 39.
- SUGAR, George R., February 1964, "Radio propagation by reflection from meteor trails", Proc. IEEE, Vol. 52, pp 116 - 136.
- MONTGOMERY, G.F., and SUGAR, G.R., December 1957, "The utility of meteor bursts for intermittent radio communication", Proc. IRE, Vol. 45, pp 1684 - 1693.

 FAHREM, Akram, SHEIKH, Noor M., JAVED, A and GROSSI, M.D., April 1977, "Impulse response of a meteor burst communications channel determined by ray-tracing techniques", IEEE Trans. Vol. COM-25 pp 467 -470 (corres).

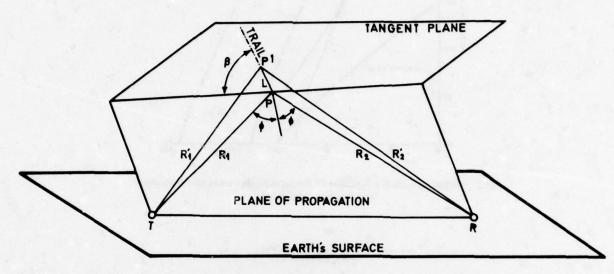


Fig.1 Ray geometry for a meteor-burst propagation path

EXPERIMENTAL POINTS FROM REF. 3
MARKED BY O AND X (MONOSTATIC CASE)
DOTTED LINES SHOW TRANSITION FREQUENCIES
(FOR MONOSTATIC CASE R1 - 0 150 km)

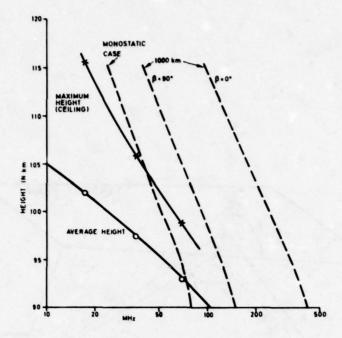


Fig. 2 Height of trail as a function of frequency (also transition frequency as a function of height)

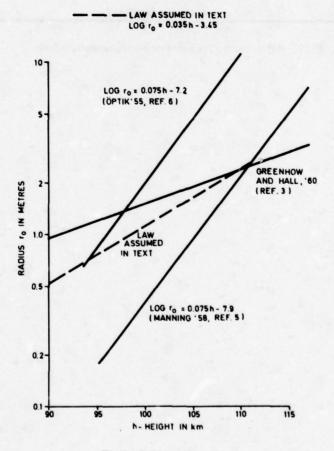


Fig.3 Initial radius of trail

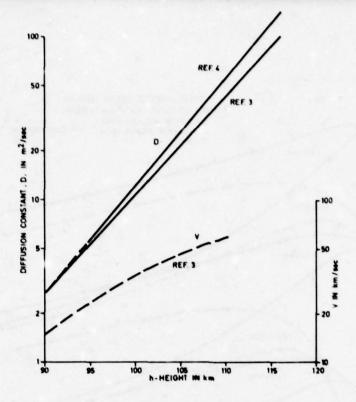


Fig.4 Diffusion constant and velocity of meteors as a function of height

O - EXPERIMENTAL CEILING HEIGHTS FROM REF.3 ASSUMING a 20 dB SYSTEM MARGIN AND MONOSTATIC CONDITIONS i.e. d = 0 km

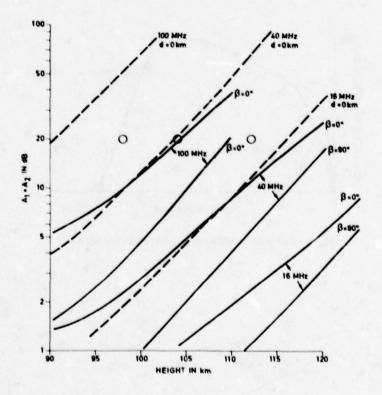


Fig.5 Initial attenuation A1 + A2 (d = 1000 km)

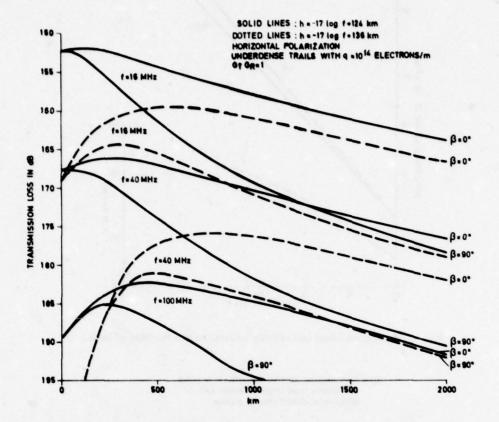


Fig.6 Transmission loss as a function of distance

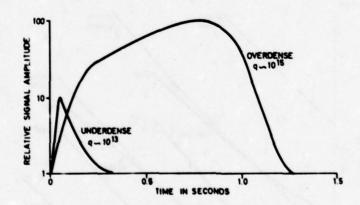


Fig.7 Examples of underdense and overdense signals

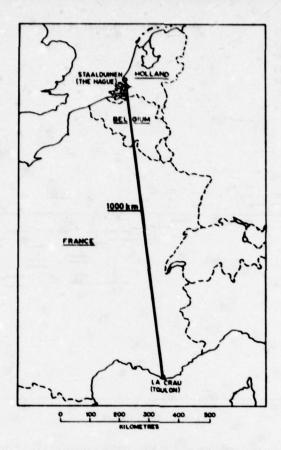


Fig.8 The STC meteor burst circuit

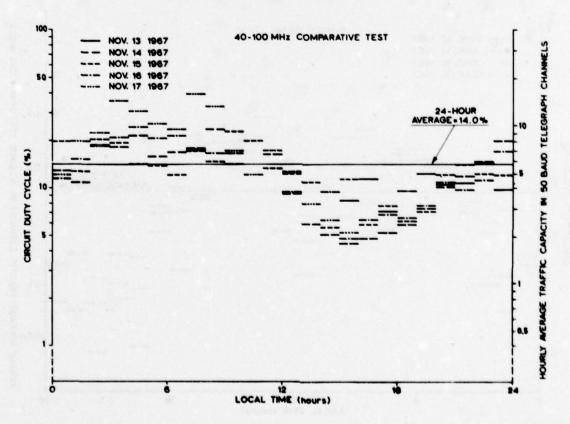


Fig.9 Diurnal variation of 40 MHz traffic capacity (13-17 Nov. 67)

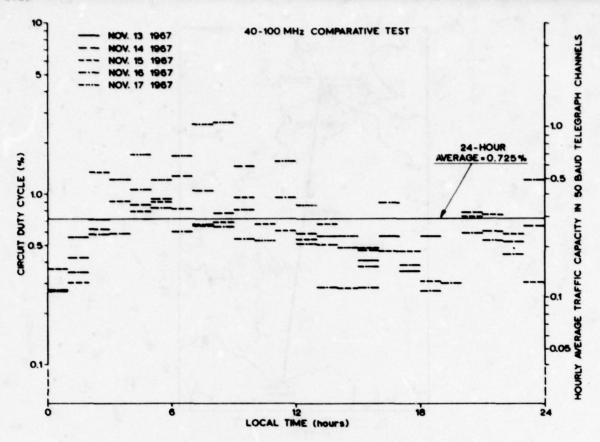


Fig.10 Diurnal variation of 100 MHz traffic capacity (13-17 Nov. 67)

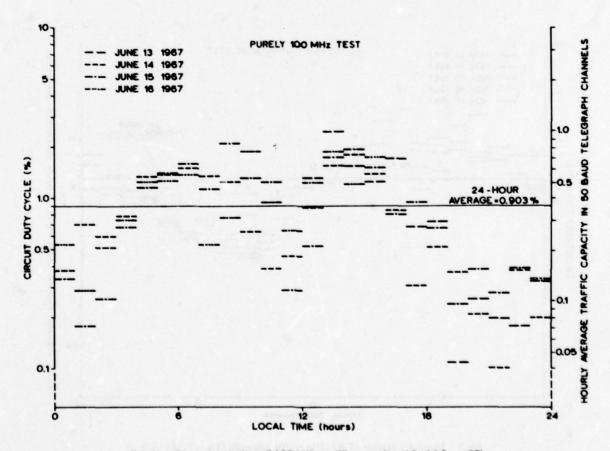


Fig.11 Diurnal variation of 100 MHz traffic capacity (13-16 June 67)

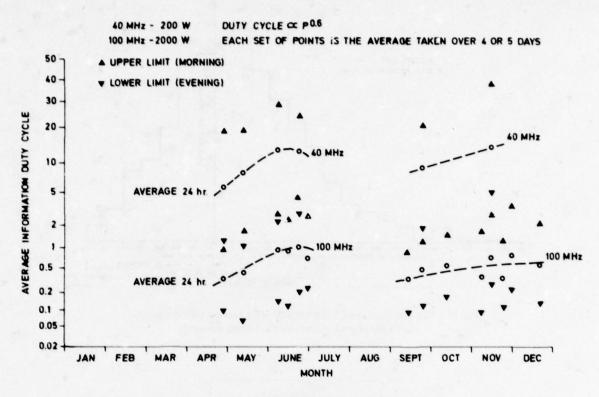


Fig. 12 Circuit duty cycles for 40 MHz and 100 MHz (1000 km circuit year 1967)

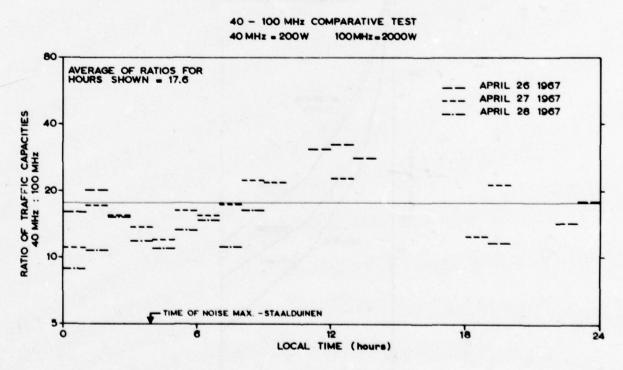


Fig.13 Diurnal variation of the ratio of 40 MHz to 100 MHz traffic capacities (26-28 April 67)

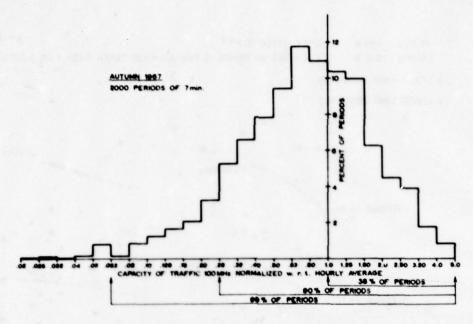


Fig. 14 The distribution of 7 minute 100 MHz average traffic capacities (normalized with respect to the hourly average)

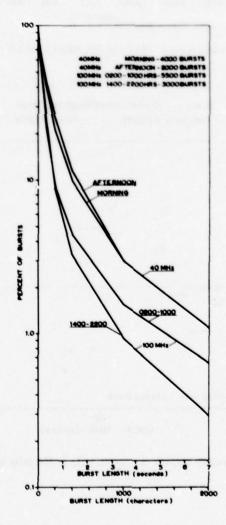


Fig.15 Probability distribution of burst lengths

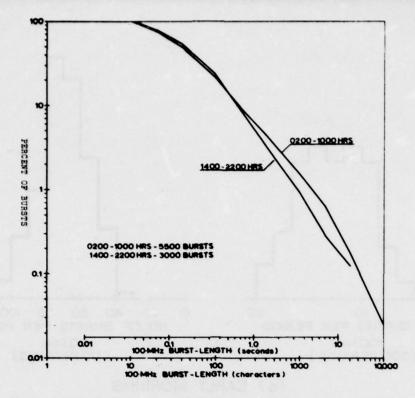


Fig.16 Probability distribution of 100 MHz burst-lengths on log-log coordinates

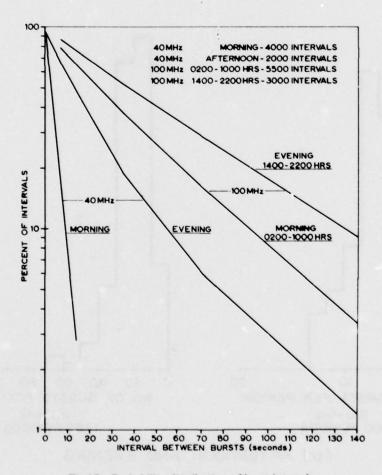
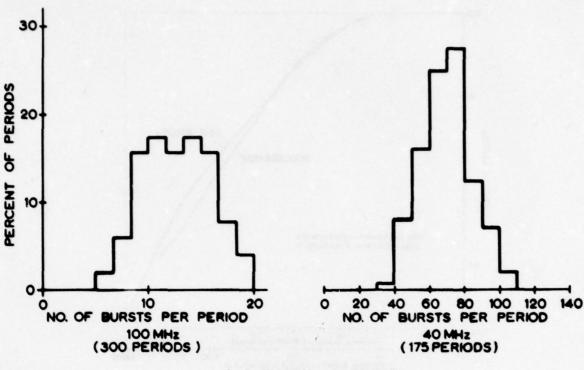
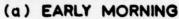


Fig.17 Probability distribution of burst-intervals





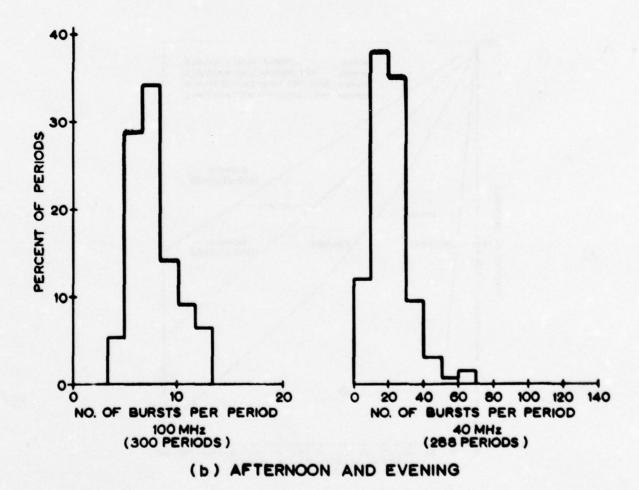


Fig.18 Number of transmission bursts per 7 minute period

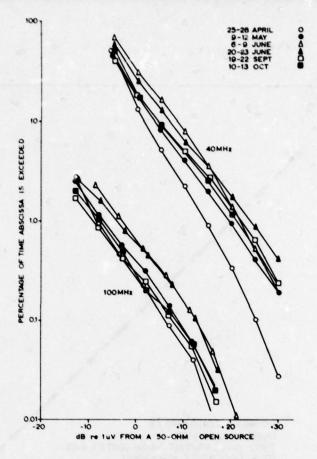


Fig.19 Distribution of signal levels (average for each comparative test)

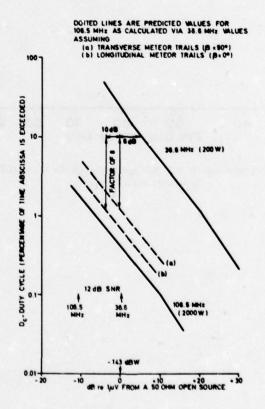


Fig. 20 Yearly distribution of signal levels (Southern France - Holland)

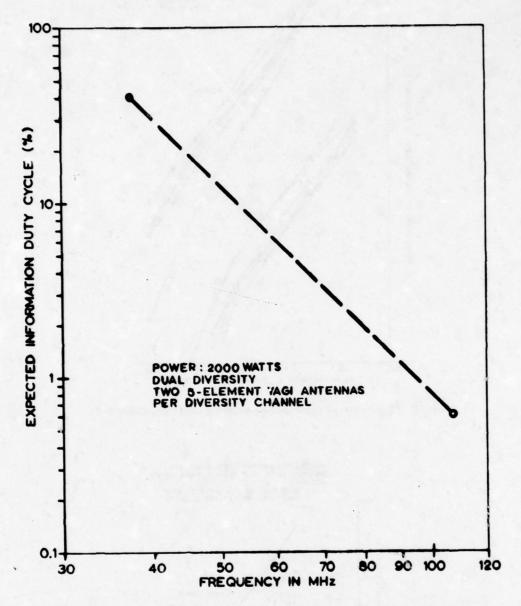


Fig.21 Long term average information duty cycle for the COMET system as a function of frequency

COMMUNICATIONS VIA METEOR TRAILS

Frank J. Sites
Consultant--California Microwave
2117 Loma Alta Drive
Fullerton, California 92633

SUMMARY

Unique methods of communications and control at very high frequencies (VHF) are shown to be possible with these techniques to automatically collect small amounts of data as often as every minute from a multitude of mobile, unattended remote and/or portable stations which may be located up to 2000 kilometers from any one of the several control centers. Work over the last several years (1) supports this conviction, (2) has developed theoretical and empirical data into useful analytical expressions, and (3) has produced novel relationships.

This paper addresses the current state-of-the-art of meteoric communications, basic meteoric conditions, system engineering implications, and why these developments constitute a departure from, or provide unique applications of, current technology. Accordingly, a brief historical development is provided and followed by an explanation of the nature, availability, and radio characteristics of meteor trails. Such material includes justified propagation-availability models, availability improvement techniques, optimization of radio system provisions, and other new information. It is shown that a departure from conventional bistatic paths, point-to-point practices, and brute force techniques promotes a host of unique and intriguing system possibilities.

Meteor trails support essentially a satellite-type system where Nature continuously provides a multitude of short-lived, low-altitude (passive) satellites for all areas of the world. Thus, most of the advantageous features of low-altitude communications satellites, some features not possible with communications satellites, and a no-cost system of satellites for any area apply. Interesting system information, such as exceptional frequency and bandwidth conservation, excellent availability, optimum data rates, unusual intercept immunity, modulation considerations, resistance to interference from others, low transmitter powers, adaptive network capabilities, related system applications, and automatic system potentials, is also referenced. Provisions to satisfy many applications that can probably be handled by these techniques have not heretofore been economically and technically practical.

INTRODUCTION

In addition to the major bodies of the solar system--nine major planets, a number of minor planets or asteroids, and a multitude of comets--an astronomical number of minor or meteoric bodies are scattered throughout solar space. These minor bodies range in size from the finest grains* of material or dust to the dimensions of the lesser asteroids. The orgin of such potential meteors and meteorites remains a matter of conjecture, although plausible theories have been advanced by Whipple (Whipple, F.L., 1951), Oort, and others.

Though most meteors are completely consumed during the firey plunge through the earth's atmosphere, occasionally the mass of the particle is sufficient to survive the fireball state and the residue falls to earth as a solid body or meteorite. Such survival presumes that the weight of the particle before capture by the earth is at least 5 kilograms (Baldet, M.F., 1964). Meteoric events from the capture of the finest grains of material, which produce trails that can only be detected by radio means, to the visually observed shooting stars and infrequent fireballs represents a wide range of dissimilar occurences. Figure 1 illustrates these effects and the related observations of several early investigators. Because of the magnitude and nature of these variations, all meteors cannot be described as originating from the same source. Present data supports an intrasolar system origin for meteoric material and produces firm evidence that the space position of meteor showers and the orbits of comets are interrelated. This confirmed source of material for meteor showers may also apply for the more predominate sporadic meteors, but the limited mass of cometary debris suggests that other origins, at least for the large meteorites, must exist. Table I shows some of the near-earth relationships that apply for meteors and meteorites.

Observations have confirmed a strong correlation between the orbits of material that produce meteor showers and the paths of probable parent comets. This relationship was first suggested by Kirkwood in 1861 and confirmed by Schiaparelli in 1886 from evidence that the Perseids shower had the same orbit as the comet Swift-Tuttle, 1862 III (Baldet, M.F., 1964). The most dramatic substantiation of this generic postulate is the unquestionable association of the comparatively new Giacobinid shower with the comet Giacobini-Zinner, 1946 V. Table II identifies and includes data concerning the more prominent meteor streams. The developments that follow are solely concerned with sporadic meteors and the occurence of meteor streams represents an enhancement over these representations for the more prolific sporadic meteors.

*Particles smaller than about one micron in diameter are repelled by the sun since solar radiation pressure on such microparticles is greater than gravitational attraction.

The motion of the earth around the sun produces a diurnal variation in the rate of arrival of meteor radiants for positions on earth. Meteors along the apex of the earth's way are swept by the earth, while radiants at the antapex are produced by meteors which overtake the earth. An observer's meridan is at the apex at 0600 am local time, thus a relative abundance of meteor trails can be expected at this time. Conversely, observers along the meridan for the antapex, or equivalently at 6 pm local time, can expect a minimum in the daily incident rate. These relationships produce a sine-like diurnal variation with a minimum at 6 pm and a maximum around 6 am local time for a uniform distribution of meteors. The region of appearance of a radiant is a function of velocity and elongation.

The velocity relationships are depicted by Figure 2 and involve both retrograde and direct orbits for the space debris. Since the escape velocity from the solar system is about 42 km/sec at one au. from the sun and the velocity of the earth is 30 km/sec, the maximum geocentric velocity for a head-on collision would be 72 km/sec. In comparison, such a collision with a particle from interstellar space would represent a velocity of about 76.5 km/sec. Maximum velocities appear to not exceed 72 km/sec, confirming that such space debris is not from interstellar space.

This introductory information is consistent with observed relationships. Accordingly, it explains the data to be introduced. First however, a review of past activities in meteor-burst communications seems necessary to establish the state of the art of and to complete the introduction to this technology.

1.1 Background

The influence of meteoric ionization on radio propagation was not fully appreciated until after 1940 and the potential of meteoric events to support a unique mode of propagation was not acknowledged until 1951. Though numerous radio investigators reported unusual bursts of high frequency and very high frequency activity within the E region of the ionosphere, the first reference to meteors as the cause appears to have been made by Nagaoka of Japan in 1929 (Skellet, A.M., 1935). He failed to recognize the contribution as an enhancement. The work of Skellet (Skellet, A.M., 1931 and 1935) is generally recognized as the first acceptable description of meteoric ionization as the cause of these radio anomalies. This meteoric ionization is always present at a height of about 93 km, regardless of day or night or time of the year. The radio observations of meteorionization prior to 1950 were primarily the by-product of other research and development, but such observations, particularly with radar, were given strong impetus by the technological advances of World War II.

Two events heralded developments in meteoric communications—(1) the intense interest of radio scientists in and the resultant data from the dramatic Giacobinid shower of October 9-10, 1946, as a consequence of emerging radar technology, and (2) the historical experiment of 1951 to prove the validity of ionospheric scatter theory (Bailey, D.K. et al, 1952). This latter test proved that the lower E region could support a weak but continuous signal at frequencies in the lower VHF band over distances far beyond line-of-sight ranges. A transmitter power output of 25 kilowatts at 49.8 MHz was used by NBS in these tests to communicate from Cedar Rapids, Iowa, to a receiver 1245 miles away at Sterling, Virginia. Sporadic enhancements in signal level were superimposed over the expected weak but continuous signal of ionospheric scatter. Many of these strong bursts were definitely associated with the occurrence of meteor trails. Numerous investigators undertook analyses of the cause and effect of this experiment. Pineo of NBS is credited by Montgomery and Sugar (Montgomery, G.F. and Sugar, G.R., 1957) with suggesting in 1951 the use of meteor trails to support intermittent communications over long distances. It appears that other individuals, including McKinley, Eshleman, and Forsyth, could also have suggested these techniques.

The Stanford Electronic Laboratories (SEL) initiated meteor studies (Manning, L.A., 1948; Eshleman, V.R. and Manning, L.A., ;954; Manning L.A. and Eshleman, V.R., 1959; Eshleman, V.R., 1958; Mlodnosky, R.F. and Eshleman V.R., 1952; Mlodnosky, R.F., 1960; etc.) prior to the NBS ionospheric scatter tests. SEL remained active in radiant investigations and related radar detection analyses up to the late 1960s. Forsyth and his co-workers for the National Research Council, Ottawa, Canada, demonstrated a practical closed-loop communications system, as part of the JANET effort, in 1954 (Forsyth, P.A. et al, 1957; Davis, G.W.L. et al, 1957). Australians at the University of Adelaide, including Weiss and Huxley, began meteor studies in 1952 and New Zealand (Ellyett, C.D., 1955) followed this lead in 1953. Lovell of Jodrell Bank fame pursued radio astronomy studies at the University of Manchester during the late 1940's. Many others, including USSR scientists, were purported to be involved in these early meteoric studies.

The only known operational systems that were designed for the meteor trail mode of communications were the JANET and the COMET systems. JANET was the product of the Defense Research Board of Canada as the result of numerous experiments from 1954 to 1957, while COMET became a NATO system in 1968 after earlier experiments and studies by the Shape Technical Center (Bartholome, P.J. and Vogt, I.M., 1968, Bartholome, P.J., 1967). Though several experimental links of JANET were in operation earlier, the permanent link between Edmonton and Yellow Knife (Crysdale, J.H., 1960) became fully operational in 1958. Stanford University facilities included links from Palo Alto to Bozeman, Montana and Phoenix, Arizona. Transmitter power was about 2 kilowatts. Hughes Aircraft also operated a satellite station near Los Angeles, which worked with the Stanford complex. NBS (Montgomery, G.F. and Sugar, G.R., 1957; Sugar, G.R., 1964) likewise sponsored num-

erous tests during the period. RCA (Bliss, W.H. et al, 1957) and Hughes performed investigations for the U.S. Air Force and Meeks et al of the Georgia Institute of Technology (Meeks, M.L. and James, J.C., 1957; Meeks, M.L., 1961) conducted experiments for both the U.S. Navy and Air Force. Hughes Aircraft, in conjunction with the Wright Air Development Center, developed and demonstrated an air-to-ground meteor-burst system (Hannum, A.J. et al, 1960). Melpar was active in the multimode communications effort of the U.S. Army (Richter, W.J., 1967). None of these early U.S. investigations produced an operational system. Activity in England, Holland, Russia, Oceania, and other areas may have led to more permanent capabilities, but the COMET and the discontinued JANET systems are the only efforts known that resulted in operational systems. The U.S. Department of Agriculture is currently procuring a meteor-burst system for the Soil Conservation Service. It will be tested from July 1977 through February of 1978. This system, JANET, and COMET were designed to use midpath illumination techniques and transmitter powers of 300 to 1000 watts.

GENERAL INFORMATION

Meteor trails, or equivalent phenomena, effect specular reflection which enhances propagation efficiency over scattering mechanisms and creates discrete patterns or footprints as a function of the relative trail geometries. The path loss over free space for an 800 km path for an improved type of meteor-burst system is 40 to 60 dB. Losses over free space for this same distance would be about 90 dB for the ionospheric-scatter mode and about 120 dB for the tropospheric-scatter mode. Random orientation of trails results in a random pattern of footprints as implied by Figure 3. Figure 4 shows the expected minimum widths of such footprints. Accordingly, each remote station in a large network of distributed stations could essentially be randomly and separately illuminated, resulting in a form of random assignment, time division multiplex (TDM). This random form of time division multiplex or switching by Nature not only permits large numbers of stations to share the same frequency but also facilitates adaptive adjustment by data collection centers to changing network configurations and conditions. Such system potentials and other unique relationships are developed in this section after the availability and basic propagation models are introduced.

Geometric and electromagnetic influences, in association with the implications of trail availability and factors related to trail formation and composition, determine the applicability of these phenomena for feasible radio communications. To avoid the complicated interrelationships between radio characteristics and trail statistics, separate radio and availability models are used. Table III provides information of interest for both models.

2.1 Radio or Propagation Model

This basic propagation or radio model is justified by a wealth of empirical data and uses essentially the expressions derived by Dr. Eshleman of Stanford University (Eshleman, V. R., 1958; Forsyth, P.A. et al, 1957).

A particle in transiting the magnetosphere and entering the ionosphere does not experience significant interaction with atmospheric molecules until the relatively dense region in the vicinity of 120 km is reached. During ablation at lower heights, atoms are vaporized from the parent meteor and these atoms are capable of producing free charges through multiple collisions before being deaccelerated to thermal velocities. The number of ions forming the trail or the trail density is thus representative of the mass of the material dissipated from the meteor. Table III shows that the line density is directly representative of the initial mass of meteors that are completely consumed upon entry. Up to a line density of about 10¹⁴ electrons per meter, the trail acts as a line array of independent scatterers and, for lengths greater than the diameter of the first Fresnel zone, an incident radio wave is specularly reflected. These are the characteristics of an underdense trail. At higher densities, the trail is not transparent to long wavelengths and radio energy is reflected by the trail in a manner analogous to ionosheric reflection. At wavelengths of 5 to 10 meters, trail duration is long compared to the time of formation of the trail. Such trails are considered to be overdense and degenerate with time, generally erratically, into an underdense trail or trails. Figures 5 and 6 show the typical waveforms of signals from underdense and overdense trails, respectively.

The processes of recombination and attachment can generally be ignored for meteor trails, particularly for the less dense trails and early history of the very dense but infrequent trails of meteorites, and when trail durations of less than 0.5 seconds are of interest. These observations are supported by the derivations of Booker (Booker, H.G. and Cohn, R., 1956). The diffusion process is significant. The diffusion coefficient increases from about 0.5 m^2/sec at a height of 80 km to 140 m^2/sec at 115 km.

The definition of terms and the expressions that follow represent a sequential development of relationships. The source or use to define symbols is shown above the reference line and the input equations by number or applicable equalities are shown below the reference line for each expression.

See Ref (2)
$$\log_{10} D=0.067h-5.6$$
 (Greenhow, J.S. et al, 1959)

Sym def (3) $\binom{r_0}{r(t)} = \frac{radius}{trail}$ (at formation at time t Initial after formation)

See Ref (4) $r(t) = \left[4Dt + r_0^2\right]^{1/2}$ (Eshleman, V.R., 1958)

1,3

Radar Eq (5) $P_R = \frac{P_T G_R G_T^{\lambda^2}}{(4\pi)^2 R^4} \sigma$ (Sugar, G.R., 1964, p. 22, etc.)

Sym def (6) $P_T = \left[\frac{r_0}{r_0}\right] = \left[\frac{r_0}{r_0}\right] \left[\frac{r_0}{r_0}\right] \left[\frac{r_0}{r_0}\right] \left[\frac{r_0}{r_0}\right] = \left[\frac{r_0}{r_0}\right] \left[\frac{r_0}{r$

Since the electrons in an underdense trail appear as a line array to incident radio signals, the resultant cross-sectional area for the applicable direction can be determined by summing the contributions from each electron in amplitude and phase. These conditions for specular reflections and the critical role of the first Fresnel zone in such determinations were emphasized by Eshleman. His expression for the cross-sectional area of an underdense trail, where remains is the classical radius of an electron and q is the line density, follows:

See Ref (11)
$$\sigma_b = (r_e q)^2$$
 (RA/2) (Eshelman, V.R., 1958)

Sym def (12) $\binom{N_o}{N(t)} = \text{Volumetric electron density}$ Initial At time t

See Ref (13) $N(t) = \binom{N_o \exp\left[-(r(t)/r_b)^2\right]}{(q_o/\pi r_b^2) \exp\left[-(r(t)/r_b)^2\right]}$ (Booker, H.G. and Cohn, R., 1956, p. 710)

$$\frac{13}{r_b = \lambda/2\pi}$$
 (14) $N(t) = N_o \exp\left[-(2\pi r(t)/\lambda)^2\right]$

$$\frac{14}{4, r_0 = 0} \quad \text{(15)} \quad \text{N(t)} = \text{N}_0 \exp \left[-16\pi^2 \text{ Dt/}\lambda^2\right]$$

Therefore,

$$\frac{9,14}{11} \qquad (16) \quad \sigma_{b}(t) = (r_{e}q)^{2} \quad (R\lambda/2) \exp \left[-32\pi^{2} \text{ Dt/}\lambda^{2}\right]$$

The effect for a finite initial radius for the trail may be handled by defining a shift in the time scale,

$$\frac{4}{t=t_{i}} \qquad (17) \quad r(t_{i})^{2} = 4Dt_{i} + r_{o}^{2} = r_{i}^{2}$$

$$\frac{16}{t^{2}} \qquad (18) \quad \sigma_{b}(t) = \sigma_{b}(t_{i}) \exp\left[-8\pi^{2}(r_{i}^{2}/\lambda)^{2}\right] \exp\left[-32\pi^{2}D(t-t_{i})/\lambda^{2}\right]$$

Backscatter-Underdense

$$\frac{5}{18, 11} \qquad P_{R}(t)/P_{T} = \frac{G_{R}G_{T}\lambda^{3}(qr_{e})^{2}}{32\pi^{2}R^{5}} \exp\left[-\frac{8\pi^{2}r_{i}^{2}}{\lambda^{2}}\right] \exp\left[-\frac{32\pi^{2}D(t-t_{i})}{\lambda^{2}}\right]$$

Forward scattering requires that the effective cross-sectional areas and the resultant transmission equations be modified from the back scatter relationships. As a result of the oblique geometry, the required length of the first Fresnel zone is greater than for back-scatter requirement by the usual secant factor for projecting to an inclined reference.

The greater length for the Fresnel zone means a larger number of electrons are contributing to the scattered energy. Thus, a larger signal and a signal of a longer duration than applicable for backscatter would be received for equivalent path distances. The penalty incurred for identical distances is the lower probability of a trail of sufficient length and at the appropriate geometrical position to satisfy the Fresnel zone requirements for a radio path.

ts for a radio path.

$$\frac{\beta}{\phi} = \text{angle between } \begin{cases}
\text{Trail and propagation plane} \\
\text{Normal to trail and } R_{\text{T}} \text{ or } R_{\text{B}} \text{ (Specular Reflection)}
\end{cases}$$

See Ref. (21)
$$\sigma_f = (r_e q)^2 \left[\left\{ \lambda R_T R_R / (R_T + R_R) \right\} (1 - \cos^2 \beta \sin^2 \Phi) \right]$$
 (Manning, L.A. and Eshleman, V.R., 1948)

Substituting a $\sin^2\alpha$ term as used by Eshleman, to account for rotation of the plane of polarization for linearly polarized antennas, the final transmission equation is:

Forward-Scatter-Underdense

$$\frac{10}{21, r_{i}=0} + (22) \quad P_{R}(t) = \frac{G_{T}G_{R}\lambda^{3} (qr_{e})^{2} \sin^{2}\alpha}{16\pi^{2} R_{T}R_{R} (R_{T}+R_{R}) (1 - \cos^{2}\beta \sin^{2}\phi)} \quad \exp\left[\frac{32\pi^{2} Dt}{\lambda^{2} \sec^{2}\phi}\right]$$

The duration of the forward scattered signal, based on a decay to exp [-1] of its initial amplitude is,

Sym def. (23)
$$t_{du}$$
 = Duration of an underdense trail

$$\frac{22}{P_R(t) = P_R}$$
 (24) $t_{du} = \frac{\lambda^2}{\sec^2 \phi / 16\tau^2}$ D (Amplitude Relationship)
$$\exp \left[-1\right]$$

Overdense Expressions

Since overdense trails by definition possess an electron volume density capable of supporting reflection in the usual sense, the trail must be considered to have a finite radius. Diffusion of the trail increases the radius of the volume until, for a given number of electrons, the volume density falls below the critical value for reflection.

When this condition is reached, the overdense trail has degenerated to an underdense distribution but the effective scattering as a result of the dispersed phase of contributions from the electrons is small. Conceptionally, the overdense medium can be visualized in terms of reflection from a cylindrical surface. The effective cross-sectional area for such an expanding trail for a Gaussian distribution of electrons is:

See Ref. (25)
$$\sigma_b = \frac{R}{2} \left(\text{Dtln} \left[r_e q \lambda^2 / 4\pi^2 \text{ Dt} \right] \right)$$
 (Eshleman, V.R., 1958)
$$\frac{5}{25} \qquad (26) \quad P_R(t) / P_T = \frac{G_T G_R \lambda^2}{64\pi^2 R^3} \qquad \left[4Dtln \left\{ r_e q \lambda^2 / 4\pi^2 Dt \right\} \right]^{1/2} \text{ (Back-scatter)}$$

$$\frac{Sym \ def}{T} \qquad (27) \quad \left\{ t_{do} \right\} = \begin{cases} Duration \ of \ overdense \ trail \\ Time \ after \ formation \ for \ MAX \ P_R \end{cases}$$

$$\frac{26}{27, \ P_R(t) = 0} \qquad (28) \quad t_{do} = r_e q \lambda^2 / 4\pi^2 \ D$$

$$\frac{26}{dP_R / dt = 0, \ 27} \qquad (29) \quad T = r_e q \lambda^2 / (4\pi^2 \ D \ exp \ [1])$$

The maximum received signal which occurs at time T is:

$$\frac{26}{t=T, 29} \qquad (30) \quad P_{R}(T) = P_{T}G_{T}G_{R}\lambda^{3} \quad \sqrt{r_{e}}q/(64\pi^{3} R^{3}) \quad \sqrt{\exp[-1]})$$

These relationships can be modified to cover the forward scatter case by applying the secant correction factor:

See Ref. (31)
$$\sigma_f = R \left[\frac{Dt}{\sec 2} \frac{2}{\Phi} \ln \left(r_{eq} \left(A \sec \Phi \right)^2 / 4\pi^2 Dt \right) \right]^{1/2}$$
 (Eshleman, V.R., 1958)

A transition line density of about 0.75 x
$$10^{14}$$
 electrons per meter exists between the overdense and underdense expressions for equivalent geometry. The maximum power received for the bistatic case from an overdense trail at a time, t = $7 \exp \left[-1\right]$, is:

$$\frac{32}{t=T \exp \left[-1\right]} (33) \quad P_R \text{ (T exp } \left[-1\right])/P_T = \frac{G_T G_R \lambda^3 \sin^2 \alpha \sqrt{r_e q \exp \left[-1\right]}}{32 \times^3 R_T R_R (R_T + R_R) (1 - \cos^2 \beta \sin^2 \phi)}$$

2.2 Availability Model

The radio propagation models for overdense and underdense trails requires a dependence on statistics or other models for predicting the availability of the medium. relationships presumed the presence of a favorable trail with an acceptable trail duration, but sufficient numbers of and suitable durations for useful events must exist for the medium to be satisfactory in all respects for communications purposes. The data of Table III, which is a tabulation of various order of magnitude properties of sporadic meteors can be used to derive the expected average rate of incidence of sporadic meteors:

Sym def (34)
$$\begin{cases} N^{/}(X \ge X_{O}) \\ N(X \ge X_{O}) \end{cases} = \begin{cases} Number of arrivals of argument X equal to or greater than a reference value X_{O} \end{cases}$$

$$\begin{cases} Per day at earth \\ Per square meter per second \end{cases}$$

Sym def (36)
$$\begin{cases} C_{i} \\ a \end{cases} =$$
Proportionality constant; $i = 1, 2,$ Exponential term

Table III (37)
$$N/(m \ge m_0) = c_1 m_0^a = 10^5 m_0^{-1}$$
 34, 35, 36

Table III (38)
$$N'(q \ge q_0) = C_2 q_0^a = 10^{22} q_0^{-1}$$
 (For m<10 grams) 34, 35, 36

1.7 x
$$10^{-22}$$
 N/ $(q \ge q_0)$

The actual arrival rate for a specific location is dependent upon the distribution of meteors, latitude of the observer, time of-year and time of the day; however, this generalized derivation correlates well with average statistics. Manning (Manning, L.A. and Eshleman, V.R., 1959) has shown that average values for C_2 and S, where S=-a+1, are 160 and 2 for medium latitudes and sporadic meteors. Manning's value of 160 for C_2 is used in subsequent derivations.

$$(40) \quad N \quad (q \ge q_0) = 160/q_0 \quad (\text{trails m}^{-2} \text{ sec}^{-1})$$

$$\frac{\text{Sym def}}{\text{N}(q_0,t)} \quad \begin{cases} N(q_0) \\ N(q_0,t) \end{cases} \quad \begin{cases} \text{Average number of useful trails per second} \\ \text{Rate of useful trails at a specific instant in time} \end{cases} \quad \text{With a line density} \ge the reference density, q_0.}$$

Sym def (42) W = Area of interest at trail heights in m²

$$\frac{41}{40, 42}$$
 (43) N(q \geq q₀) · W = 160 W/q₀

Not all of the trails within an area will be useful because of the previously referenced geometric constraints. Stanford personnel (Embry, U.R., 1962), during an investigation of the average rates of signal occurrence, determined this ratio to be between 3 and 5 percent for forward scatter from 0 to 1000 km. Sugar (Sugar, G.R., 1964) reports this ratio to be 5 percent for transmitter-receiver separations of 600 to 1000 km. These relationships apply for a point-to-point path whether it is an isolated path

km. These relationships apply for a point-to-point path whether it is an isolated path or one of the many paths of a network. It will subsequently be shown that practically all trails are useful for a central station that contacts any of a multitude of stations of a network as the opportunity occurs.

Sym def (44)
$$\eta$$
 = Ratio of useful trails to total trails through area W for a specified system geometry

(45) $N(q_0) = \eta \cdot N(q \ge q_0) \cdot W$

Figure 7 presents the results of a comprehensive collection of data by Stanford personnel to depict the hourly average rates for meteors at this latitude and for the entire year. The curves of mean daily and monthly variations in meteor rates, based on JANET (Forsyth, P.A. et al, 1957) and NBS (Sugar, G.R., 1964) measurements of Figure 8 exhibit the same basic relationships. Using this data and accepting the sinusoidal trends as being representative of the diurnal variations, the following terms and relationships can be introduced:

Sym def (46)
$$T = Local$$
 time of day in hours in terms of a 24-hour clock.

Sym def (47)
$$\begin{cases} \beta_p \\ \beta_{(T)} \end{cases} = \begin{cases} Peak \text{ daily arrival rate} \\ Arrival \text{ rate at time } T \end{cases}$$
Of useful trails above the average useful trail rate for the same day

$$\frac{47}{\text{Fig. 7-8, 46}}$$
(48) $\beta(T) = \beta_p \sin(2\pi T/24)$, For the day of interest

Sym def (49) $\beta(T) = \beta_p \sin(2\pi T/24)$, For the day of interest of interest to the annual average for a month from Figure 9

$$\frac{12}{47, 49}$$
(50) $N(q_0, t) = g \cdot N(q) + \beta(T)$,
$$\frac{50}{45, 48}$$
(51) $N(q_0, t) = g (160W\eta/q_0) + \beta_p \sin(\pi T/24)$

Measured data, including the information from Figure 7, without reference to detection thresholds, shows a general 5 to 1 correspondence between the hourly maximum and minimum rates for a day at latitudes near 40 to 50 degrees. The daily useful rate can accordingly be expressed in the following manner:

$$\frac{51}{\text{Restated}}$$
 (52) $N(q_0,t) = (160gW\eta/q_0)$ 1 + 0.67 sin ($\pi T/12$)

Equation 52 accordingly provides the generalized expressive for the average availability of total and useful trails for a point-to-point path for any area and period of time. This model satisfies the objectives of simple relationships, all input relationships can be satisfied, and it has general application to system requirements. It appears adaptable to change and special improvements, particularly by periods, when new data justifies the additional levels of sophistication. Compatibility for end path and other methods of illumination, as well as for midpath illumination techniques, has been preserved.

2.3 New System Techniques

The past efforts of using midpath illumination and moderately high powers in a brute-force like manner to maximize communications time or duty cycle, seems to have ignored the unusual potentials of this medium to cost-effectively handle some of our most challenging communications requirements. It offers capabilities for large-area networks of many small users and for special applications that have not heretofore been economically and technically practical. Intensive examination of the basic interrelationships, using the data developed herein and empirical data of others, have produced intriguing results (Sites, F.J., 1969, 1970 and 1976). These results include the advantages of end path illumination versus midpath illumination, exceptional frequency conservation, improved availability, optimal power relationships, cost-effective network provisions and other novel implications.

End path illumination instead of the usual illumination over the midpoint of the path results in several major improvements. A 3.8 dB advantage in path loss is gained with end path illumination. This is illustrated in Figure 10. The ratio of height-to-distance for a distance of 1000 km is 0.1 for end path illumination and 0.2 for midpath illumination. This result compares favorably with the conditions for a passive reflector for a radio microwave system. The requirement that the meteor trail must be tangent to one of the family of ellipsoids around the stations establishes that end path geometry increases the probability that a trail will be useful. Tests show a 1.5 to 2 increase in useful rates per unit area for this area (Embry, U.R., 1962; and Meeks, M.L., 1961). The larger area projected over the end point by a master station antenna with an

angular beamwidth, as opposed to the area that would be illuminated over the midpoint by the same antenna, results in a proportionate increase in the expected number of total trails and of useful trails per unit time. This, almost direct reflection that does not preclude use of minimum length trails, and other availability improvements increase the expected number of useful trails per unit time by at least an order of magnitude over the rate for midpath conditions. The disadvantages, which are not of importance for large-area networks, are a reduction in maximum system range for nominal provisions and a shorter duration in trail lifetime. Few trails will have useful lifetimes that approach or exceed two typical message times and, generally, a second message immediately following another message to the same station will not be needed. Figure 11 shows the loss over free space conditions as a function of distance for end path conditions, except that all distances from 0 to 100 km use end path illumination for a fictitious station distance of 100 km.

The instantaneous 3-dB bandwidth of this medium is nonsymmetrical and is about 7 MHz for a frequency of 30 MHz. However, the serial data rate is limited by multipath delays caused by two or more simultaneously useful trails within the common illuminated area. Such delays for typical system provisions limit the serial rate to about 5000 elements per second. Since the medium is not bandwidth limited, redundancy and/or frequency multiplexing of the serial channels can be used. Table IV shows the transmitter power requirement for a moderate system design at various serial binary rates and error probabilities. Only 20 watts of transmitter power is required for coherent phase-shift keying (CPSK) and convolution coding to transmit at 5000 bits per second with an error rate of less than ten errors per million to any station within several hundred kilometers. This average error rate is for the minimum useful signal and most meteor-burst signals will be above this threshold.

Figure 12 bounds the expected degree and duration of rutual interference between useful trails for a path for various useful trail rates. A maximum trail rate of 6 useful trails per minute for a specific path is considered to the. This maximum compares favorably with the rates possible with end path illumin, on and the related availability improvements. Figure 13 explores the implications of Figure 12 for useful trails rates in excess of this suggested maximum. It illustrates the ramifications of using too much power and of illuminating the lesser trails which, in turn, cause errors and a reduction in throughput as power is increased. The previously referenced Figure 4 illustrates the width of the footprints.

End path illumination permits the use of wide angle, zenith-looking antennas at remote stations. Such simple antennas offer important advantages for aircraft, portable, other mobile, unattended, and shielded stations. The zenith path is particularly suited for stations in jungles, high rise and mountainous areas, canyons, etc.

The random time-division like switching, by virtue of the random footprints, permit all remote stations to use a common response frequency. Judicious use of group and discrete addresses or codes to inhibit responses from some or all but one remote station is also implied. A second or multiple response frequencies, each with a 5000 bit per second channel, could be used at all or selected stations as needed to increase the effective information transfer rate from a remote station. The duty cycle of the response channel, observed at the input of a master station with a properly distributed network of remote stations, can approach 100% at each such master station.

An additional availability improvement technique, which also introduces a host of new operational potentials, is illustrated by Figure 14. If two master stations are located at a considerable distance on either side of a remote station, the trails useful to one master station can not, to a high probability, be used by the other master station. Thus, each master can work the remote station independently and on the same frequency without significant interference. Effectively, the throughput from the remote station on that frequency or channel would be or could be doubled. Judicious use of additional master stations, all on the same network frequencies, could further enhance such throughput from any or all of the stations covered without encountering serious interference. Numerous operational possibilities are represented. These include multiple mobile and fixed master stations, listen-only masters for a high probability of intercept of special remote area transmissions, redundant paths and hardware, etc. Such redundancy is capable of combating a variety of conditions, including general interference, diurnal distribution of radiants, jamming, nuclear blackouts, hardware failures, and general communications vulnerability. As few as five master stations, using the same interrogation frequency and the same response frequency, could cover the first 48 states of the USA and the contiguous border and ocean areas out to several hundred kilometers. A multitude of mobile, portable and fixed remote stations for either intra or interarea operations and on the same transmit and receive frequencies, could be accommodated.

3.0 CONCLUSIONS

The propagation and availability models, based on and supported by empirical results, are representative of what can be expected of this medium. Past efforts, however, have been predominately concerned with maximizing the communications time between two distant points and have not recognized the exceptional utility of these techniques for large-area networks. These models apply to a specific path and for useful trail rates for that path. Accordingly, network systems represent a new application of these proved models.

The suggested system techniques, which make natural use of the medium and its characteristics without forcing a particular result, should permit a host of new and cost-effective uses of meteor-burst technology. Developments, not fully covered in this paper, further confirm that fully automated systems and adaptive network features can be implemented. It appears that such automatic and manned networks could profitably complement communication satellite systems where small ground station costs are excessive, for polar coverage with relays via synchronous satellites, to avoid other intolerable low-angle or obstructed environments and for backup purposes. Such techniques should be of interest for applications not associated with current or planned satellite programs.

The proposed techniques make use of state-of-the-art designs and Nature's generosity. Most complementing functions and costly support features are essentially provided or performed by Nature. As a result, very cost-effective and simple provisions promise to accommodate what has been considered prohibitively costly and technically difficult tasks. The inherent reliability and dependability of these techniques by virtue of the simple system redundancy potentials seem to be of great significance for many applications.

BIBLIOGRAPHY

- Bailey, D.K., Bateman, R., Berkner, I.V., Booker, H.G., Montgomery, G.F., Purcell, E.M., Salisbury, W.W. and Wiesner, J.B., 1952, Phys. Rev., 86, A New Kind of Radio Propagation at Very High Frequencies Observable Over Long Distances
- Baldet, M.F., 1964, Flammarion Book of Astronomy, English Edition, pp. 251-397, Book VI: Planets
- Bartholome, P.J., 1967, TM-165, SHAPE Technical Centre, Results Obtained With The STC Meteor-Burst Communication System
- Bartholome, P.J. and Vogt, I.M., 1968, IEEE Trans., COM-16, pp. 268-278, COMET A New Meteor-Burst System Incorporating ARQ and Diversity Reception
- Bliss, W.H., Wagner, R.J., and Wickizier, G.S., 1957, Proc. Inst. Radio Engrs., 45, pp. 1934-1935, Experimental Facsimile Communication Utilizing Intermittent Meteor Ionization
- Booker, H.G., and Cohn, R., 1956, J Geophys. Res., Vol. 61, No. 4, pp. 707-733, A Theory of Long-Duration Meteor-Echoes Based On Atmospheric Turbulence With Experimental Confirmation
- Campbell, L.L., 1957, Proc. Inst. Radio Engrs., 45, pp. 1678-1684, Intermittent Communication With A Fluctuating Signal
- Chestnut, H., 1965, John Wiley and Sons, New York, pp. 310-311, Systems Engineering Tools
- Cottony, H.V. and Johler, J.R., 1952, Proc. Inst. Radio Engrs., 40, pp. 1053-1060, Cosmic Radio Noise Intensities In The VHF Band
- Crysdale, J.H., 1960, Inst. Radio Engrs. Trans., CS-8, pp. 33-40, Analyses of the Performance of the Edmonton-Yellowknife Janet Circuit
- 11. Davies, K., 1965, U.S. Government Printing Office, Washington, D.C., National Bureau of Standards Nomogram 80, Ionospheric Radio Propagation
- Ellyett, C.D., 1965, Spec. Supp. J Atmos. Terr. Phys., 2, pp. 198-199, Radar-Meteor Research in New Zealand
- 13. Embry, U.R., 1962, RADC-TDR-62-249 (SEL-62-012), Air Force Contract AF 30(602)-2398, The Probability of Intercepting Radio Signals Scattered By Meteor Trails
- Eshleman, V.R., 1958, AFCRC-TN-58-370, ASTIA AD 160819, Meteor Scatter
- Eshleman, V.R. and Manning, L.A., 1954, Proc. Inst. Radio Engrs., 42, pp. 530-536,
 Radio Communication By Scattering From Meteor Ionization
- Forsyth, P.A., Vogan, E.L., Hansen, D.R., and Hines, C.O., 1957, Proc. Inst. Radio Engrs., 45, pp. 1642-1657, The Principles of JANET-A Meteor-Burst Communications System
- 17. Greenhow, J.S. and Ne feld, E.L., 1959, J Atmos. Terr. Phys., 16, pp. 384-392, Turbulence At Altitudes Of 80-100 Km And Its Effects On Long-Duration Meteor Echoes
- Hannum, A.J., Evans, G.L., Chambers, J.T., and Otter, K., 1960, Inst. Radio Engrs. Trans., CS-8, pp. 113-133, Air-to-Ground Meteoric Scatter Communication System
- Hogg, D.C. and Mumford, W.W., 1960, Microwave J, 3, pp. 80-84, The Effective Noise Temperature of the Sky

- Manning, L.A., 1948, J. App. Phy., 19, pp. 689-699, The Theory of the Radio Detection of Meteors
- Manning, L.A. and Eshleman, V.R., 1959, Proc. Inst. Radio Engrs., 47, pp. 186-199, Meteors in the Ionosphere
- McKinley, D.W.R., 1961, McGraw-Hill Book Co., New York, Meteor Science and Engineering
- McKinley, D.W.R., 1969 Edition-Encyclopaedia Brittanica, Vol. 15, pp. 267-271, Meteor
- 24. Meeks, M.L. and James, J.C., 1957, Proc. Inst. Radio Engrs., 45, pp. 1724-1733, On The Influence Of Meteor-Radiant Distributions In Meteor-Scatter Communications
- 25. Meeks, M.L., 1961, Final Report Project A-241, Dept. of Navy Contract Nonr-991 (02), A Study Of Meteor Radiants And The Forward Scatter Of Radio Waves By Meteor Trails
- Mlodnosky, R.F. and Eshleman, V.R., 1960, AFCRC-TN-60-363, Air Force Contract AF 19(604)-2193, Radar Measurements Of Meteor Activity With Applications To Communications
- Montgomery, G.F. and Sugar, G.R., 1957, Proc. Inst. Radio Engrs., 45, pp. 1648-1693, The Utility of Meteor Bursts for Intermittent Radio Communications
- Richter, W.J., 1967, Technical Report ECOM 02181-F, Contract DA 36-029-AMC-02181
 (E), Multimode Propagation Communication System
- Robertson, D.S., Liddy, D.T., and Eldford, W.G., 1953, J. Atmos. Terr. Phys., 4, pp. 255-270, Measurements of Winds in the Upper Atmosphere By Means of Drifting Meteor Trains
- 30. Sites, F.J., 1969, Private Paper, Communications Via Meteor Trails
- 31. -----, 1970, Proprietary Document, Meteor Echo Adaptive Netting System (MEANS)
- -----, 1976, Proprietary Document, MEANS Transcontinental Vehicle Network (TVN)
- Skellet, A.M., 1931, Phys. Rev., 37, p. 1663, The Effect of Meteors on Radio Transmission through the Kennely-Heaviside Layer
- 34. -----, 1935, Proc. Inst. Radio Engrs., 23, pp. 132-149, The Ionizing Effect of Meteors
- 35. Sugar, G.R., 1964, Pdoc. IEEE., 52-2, pp. 116-136, Propagation Via Meteor Trails
- Vincent, W.R., Wolfram, R.T., Sifford, B.M., Jaye, W.E., and Peterson, A.M., 1957, Proc. Inst. Radio Engrs., 45, pp. 1963-1700. A Meteor Burst System For Extended Range VHF Communications
- 37. Whipple, F.L., 1951, Astrophys. J., 113, pp. 464-474, A Comet Model-11: Physical Relations For Comets and Meteors

TABLE I

Some Characteristics of Near Earth Space

Altitude km	Properties and Definitions	Electrical Properties	Mean Free Path - Meters	Meteor Particles
0 - 15	Troposphere 0–10km (negative temperature gradient, 290° to 220°K). Heat transport by convection.	Thunderstorms		Very rare Meteorites
15 - 30	Stratosphere 10–40km (Region of increasing temperature. Temperature 220 ^d to 265 ^o K). Winds/Turbulence (Jet Streams)	None	4,21X10 ⁻⁶	Very rare Meteorites
30 - 80	Mesosphere 40–80km (Region of decreasing temperature. Temperature 264 ^o – 200K) Lower lonospheric Region	D layer (daytime) NO [†] predominant ion	4,5X10 ⁻⁵	Most meteors dissipated - accumulation of meteor dust.
80 - 400	Thermosphere 80–700km (Region of strong heating). Hydromagnetic effects on dynamics. Free and near free molecular flow regimes. Pressure about 10–6 atmos. at 100 km	E, F ₁ , F ₂ layers 0 ⁺ , NO ⁺ , O ₂ , ions Photodissocia- tion of O ₂ . Photo- ionization of N, N ₂ , O.	4.25X10 ⁻³ (38m at 150km)	Meteor trials visible in lower region
400 - 1000	Thermosphere – Exosphere (Exosphere 700 – 5000km) Temperature 1610° – 1645°K (Day) and 1035° – 1045°K (Night) Pressure about 10-12 atmos, at 500 km.	O ⁺ ions, He ⁺ present Lower portion of Van Allen belts Lower edge of Magnetosphere over equator.	Hundreds of meters (Essentially infinite in Exosphere)	Unaffected entry - No effects
1000 - 3200	(Exosphere 700–5000km) Magnetosphere. Some particles escape from the earth's atmosphere	H ⁺ present Charged particles travel along magnetic force lines. Van Allen belts	Essentially infinite. (Particle at base of exosphere follow ballistic orbits returning to base or escaping)	Unaffected entry - No effects.

Composite of data from References 24 and 25, bibliography, and calculations

TABLE II

Meteor Streams: Observational Quantities

	U.T. Date	Extreme	Radiant 1950	V	Hourly	rate at mo	ximum	Radiant transit
Stream	at maximum	limits	R.A. Dec.	km/sec	visual	photo	radio	mianight - 001
Quadrantids	Jan, 3	Jan. 1 4	230 +48	42.7	30	1.9	95	08 ^k 28 ^m
Virginids	Mar. 13	Allar. 5 21	182 + 4	30.8	1	-	5	00 49
H (Whipple ²)		Mar. 13 Apr. 21	157 +56	15.2	-	-	-	20 49
Lyrids	Apr. 21	Apr. 20 23	270 +33	48.4	5	-	11	03 59
n Aquarids	May 4	May 2 6	336 + 0	64	5	-	15	07 36
Daytime Arietids	June 8	May 29 June 18	44 +23	39	-	-	66	09 51
Daytime & Perseids	June 9	June 1 16	62 +23	29	-	-	42	10 59
Daytime & Taurids	June 30	June 24 July 6	86 +19	32	-	-	27	11 12
Southern & Aquarids	July 30	July 21 Aug. 15	339 -17	43.0	1			02 14
Northern & Aquarids		July 14 Aug. 19	339 - 5	42.3	10		34	02 08
Southern · Aquarids		July 16 Aug. 25	338 -14	35.8	-	-	-	02 04
Northern + Aquarids		July 16 Aug. 25	331 - 5	31.2	-	-	-	01 36
a Capricomids	Aug. 1	July 17 Aug. 21	309 -10	25.5	-	-	10	00 00
Perseids	Aug. 12	July 29 Aug. 17	46 +58	60.4	37	2.5	49	05 43
X Cygnids		Aug. 19 22	289 +56	26.6	-	-	< 5	21 25
Draconids	Oct. 10	Oct. 10	264 +54	23.1	Periodic	, next retu	rn 1965-6	6 16 13
Orionids	Oct. 22	Oct. 18 26	94 +16	66.5	13	2.9	18	04 12
Southern Taurids	Nov. 1	Sept. 15 Dec. 15	51 +14	30.2	5	-1	<15	00 42
Northern Taurids	Nov. 1	Oct. 17 Dec. 2	52 +21	31.3	5	-	113	00 46
Andromedids	Nov. 7	Nov. 7	22 +27	21.3	-	-	< 5	22 23
Leonids	Nov. 17	Nov. 14 20	152 +22	72.0	6	-	<10	06 22
Geminids	Dec. 14	Dec. 7 15	113 +32	36.5	55	5.6	80	02 01
X Orionids		Dec. 9	87 +21	30.6	-	-	-	00 25
Monoceroitids		Dec. 13 15	103 + 8	44.0	-	-	-	01 21
Ursids	Dec. 22	Dec. 17	206 +80	35.2	15	-	13	08 24

Reproduced from Handbuch der Physik, vol. 52, by Sugar - NBS /18/

²F.L. Whipple, "Photographic Meteor Orbits and their Distribution in Space," Astron, J., vol. 59, p. 201; July, 1954.

TABLE III
Properties of Sporadic Meteors

	MASS (GRAMS)	RADIUS (SIZE)	NUMBER OF THIS MASS OR GREATER SWEPT UP BY THE EARTH EACH DAY	ELECTRON LINE DENSITY (ELEC- TRONS PER METER OF TRAIL LENGTH)
PARTICLES PASS THROUGH THE ATMOSPHERE AND FALL TO THE GROUND	104	8.0 CM	10	
PARTICLES TOTALLY DISINTEGRATED IN THE UPPER ATMOSPHERE LIMITS OF RADAR MEASUREMENTS	10 ³ 10 ² 10 1 10 ⁻¹ 10 ⁻² 10 ⁻³ 10 ⁻⁴ TO 10 ⁻⁸	4.0 CM 2.0 CM 0.8 CM 0.4 CM 0.2 CM 0.08 CM 0.04 CM 0.92 CM TO 8.0 MICRONS	10 ² 10 ³ 10 ⁴ 10 ⁵ 10 ⁶ 10 ⁷ 10 ⁸ 10 ⁹ 10 ¹³ (?)	10 ¹⁸ 10 ¹⁷ 10 ¹⁶ 10 ¹⁵ 10 ¹⁴ 10 ¹³ > 10 ⁹ (?)
MICRO METEORITES (PARTICLES FLOAT DOWN, CHANGED BY ATMOSPHERIC COLLISIONS)	10 ⁻⁹ TO 10 ⁻¹²	4.0 TO 0.4 MICRONS	TOTAL AS HIGH AS 10 ²⁰	PRACTICALLY NONE
PARTICLES REMOVED FROM THE SOLAR SYSTEM BY RADIATION PRESSURE	10 ⁻¹³	0.2 MICRONS	1	= =

TABLE IV

Potential Error Rates With and Without Coding

Typical Means Values - Lp≤ 163.5dB and 3dB Margin

		dB (UNCODED).		dB (UNCODED) DCPSK $> 7 \times 10^{-4}$	$E/N_o = 4.4 \text{ dB (CONVOLUTION)} \cdot$ $CPSK P_e > 10^{-5}$		
SYMBOL (BIT FOR BPSK) RATE IN BPS	REQUIRED PRING IN dB	REQUIRED TR POWER IN WATTS	REQUIRED PR/NO IN dB	REQUIRED TR POWER IN WATTS	REQUIRED P _R /N _O IN dB	REQUIRED TR POWER IN WATTS	
100	29.3	1.2	28.3	0.98	24.4	0.4	
200	32.3	2.5	31.3	. 1.95	27.4	0.8	
1,000	39.3	12.3	38.3	9.78	34.4	4.0	
2,000	42.3	24.6	41.3	19.50	37.4	8.0	
3,000	44.1	37 2	43.1	29.50	39.2	12.0	
4,000	45.3	49.0	44.3	39.00	40.4	15.8	
5,000	46.3	61.6	45.3	49.00	41.4	20.0	
6,000	47.1	74.1	46.1	59.00	42.2	24.0	
8,000	48.3	97.7	47.3	77.70	43.4	31.6	
10,000	49.3	123.1	48.3	98.80	44.4	39.8	

^{*}PRACTICAL IMPLEMENTATION E/No = 9.6 dB

5000 BPS is the maximum bit rate suggested for a basic MEANS channel. Single Channel per Carrier (SCPC) options with MEANS permit this rate for each of several channels at a station and a corresponding increase in the effective output rate.

^{**}ACTUAL MEASUREMENTS

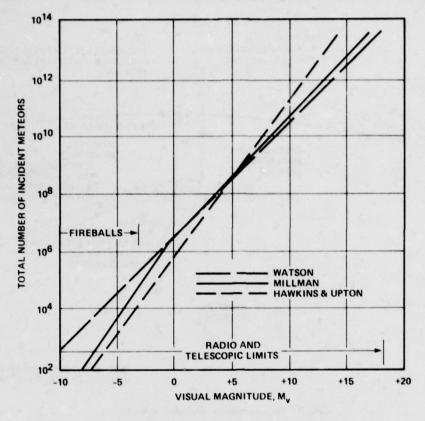


Fig.1 Number of meteor incident on earth in a 24-hour period

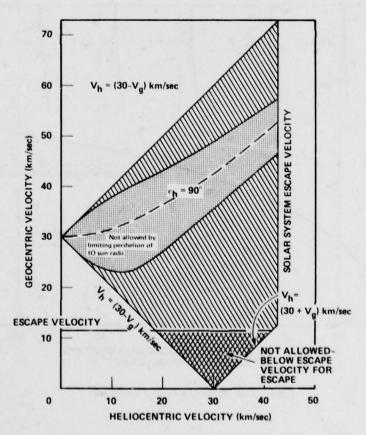


Fig. 2 Allowable Geocentric meteor velocities as a function of heliocentric velocity and a limiting orbit perihelion of 10 sun radii

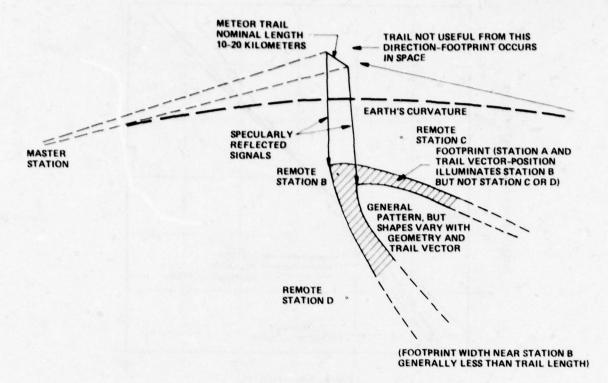


Fig.3 Representative footprint on earth

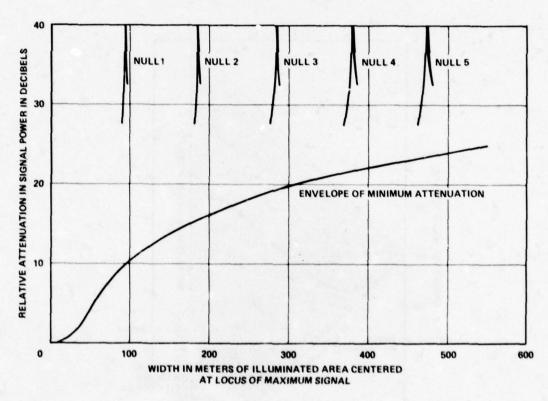


Fig.4 Trail width of a typical useful trail

Figure 5. Underdense Waveforms — (a) Theoretical, (b) Actual

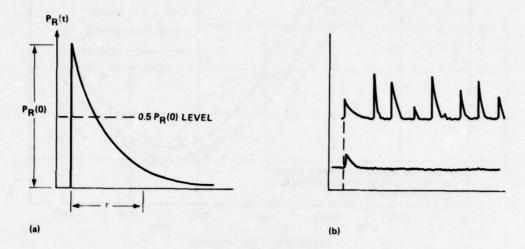


Fig.5 Underdense waveforms - (a) theoretical, (b) actual

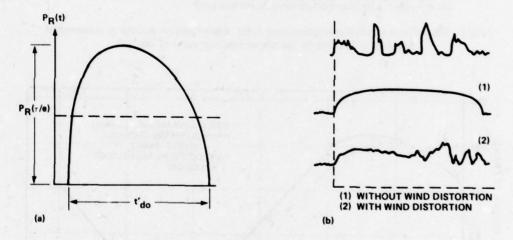
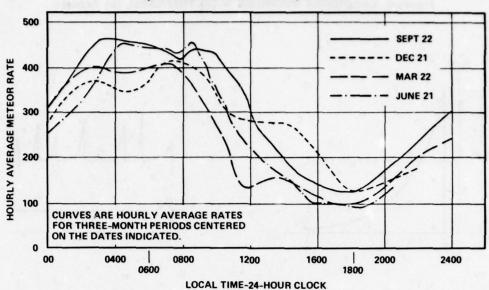


Fig.6 Overdense waveforms - (a) theoretical, (b) actual





"THE STATISTICAL PROPERTIES OF THE DATA ARE SUCH THAT IT CAN BE STATED WITH A PROBABILITY OF 0.95 THAT THE AVERAGE HOURLY RATES CALCULATED FROM SAMPLES DIFFER FROM THE TRUE AVERAGE HOURLY RATES BY LESS THAN 15% FOR SEPTEMBER, BY LESS THAN 26% FOR DECEMBER, BY LESS THAN 20% FOR MARCH, AND BY LESS THAN 25% FOR JUNE." MLODNOSKY (STANFORD ELECTRONICS LAB.)

Fig. 7 Diurnal and seasonal omnidirectional radar rates of meteor activity as measured at Stanford at 39 MHz by the rate-and-radiant radar of site 503

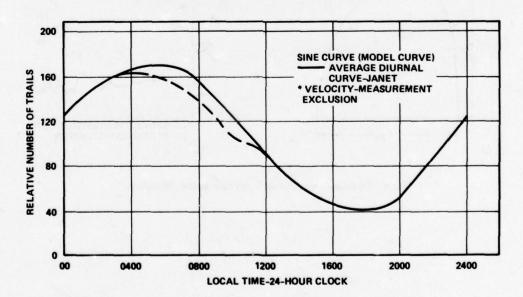


Fig. 8 Average diurnal rates – JANET system. Reproduced from Figure 5, page 13, of Reference 26

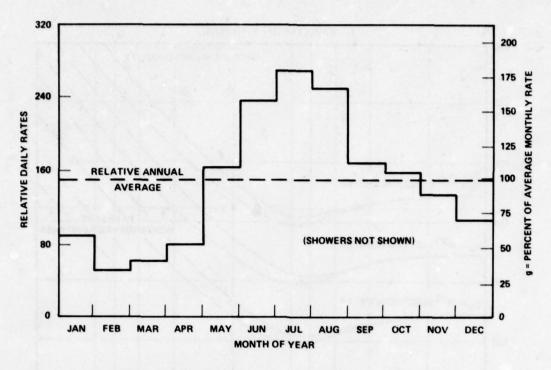


Fig.9 Relative diurnal rates for the various months of the year

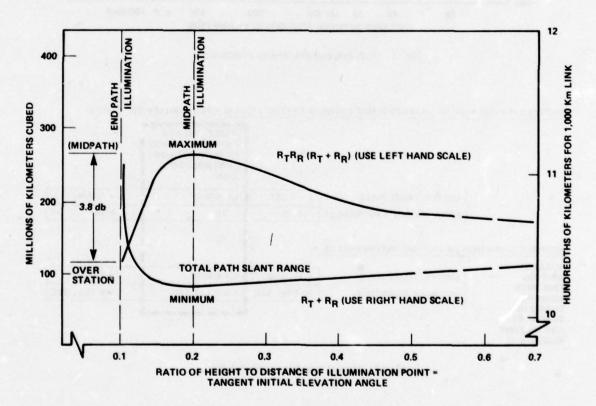


Fig. 10 A basic MEANS path loss advantage (3.8 db for 1000 Km path) over COMET-JANET illumination practices

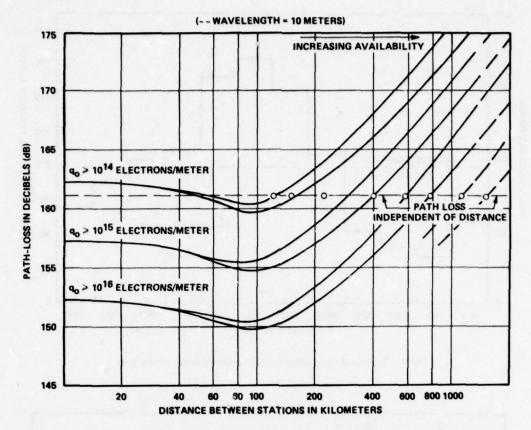


Fig.11 Path loss and availability relationships

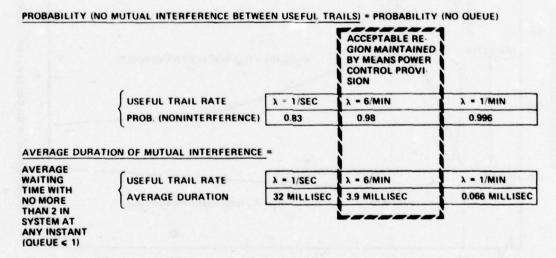


Fig.12 Mutual interference probabilities

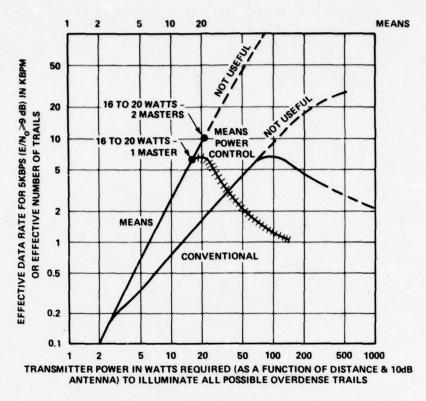


Fig.13 Optimum power utilization and effectiveness

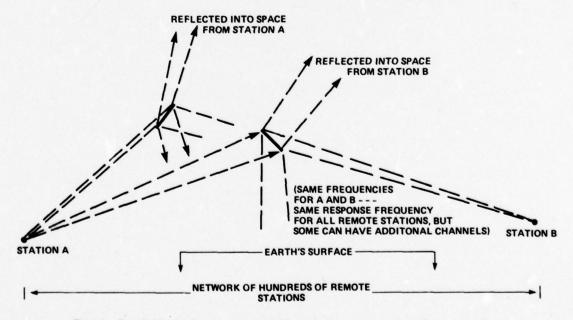


Fig. 14 Simple illustration of exclusive trails with two master stations for part or all of a network (more than two master stations approach such exclusive relationships)

PROPAGATION MEASUREMENTS ON THE ACE-HIGH TROPOSCATTER SYSTEM

by

A.N. Ince, I.M. Vogt SHAPE Technical Centre P.O. Box 174 The Hague Netherlands

SUMMARY

To predict the propagational reliability of the ACE High troposcatter system, extensive measurements were carried out over a period of two years (1963-1965) on several links which were selected to typify geographical and meteorological conditions in the system.

The measurement programme consisted of

- (a) long term measurements of the transmission loss on seven links, one in Norway, two in Germany, and four in the Mediterranean and
 - (b) measurement of the multipath intermodulation noise on five links

The paper discusses the measurement methods used, presents the results obtained, and compares them with theoretically predicted values.

1. INTRODUCTION

The ACE-High system (see Fig. 1) is a NATO-owned and NATO-operated communications system with 49 tropospheric scatter links and 41 line-of-sight microwave links. It provides high capacity transmission links from the most northern flank of NATO in Norway to the eastermost flank of NATO in Turkey.

When the ACE-High system planning began in 1958, data on the variability of the troposcatter transmission loss were not available in sufficient quantities to ensure a high degree of design accuracy.

It therefore became necessary to determine how the measured RF long-term distributions compared with theoretical calcultions, ie. to what extent theoretical calculations could be used to assess the propagational reliability of the system. Accurate knowledge of propagational characteristics was also needed because the capacity of some links was to be extended from 36 to 60 telephone channels.

In brief, the evaluation programme consisted of:

- (a) Long-term measurements to determine the RF signal level distribution for seven links, selected as representative of different geographical and meteorological conditions, and including some of the longest hops in the system. The links chosen were:
 - 1. Shetland Sola
 - 2. Emden M. Gladbach
 - 3. Paris N. M. Gladbach
 - 4. Athens Izmir
 - 5. Eskisehir Izmir
 - 6. Athens Kefallinia
 - 7. Kefallinia Catanzaro
 - (b) Calculation and measurement of the multipath intermodulation.

The measurements mentioned above were carried out during the years 1963 to 1965.

Chapter 2 summarises the results of the measurements of RF signal level distribution. The results of the multipath intermodulation noise measurements are presented in Chapter 3.

TRANSMISSION LOSS MEASUREMENTS

2.1 Long-term Transmission Loss Distribution

There are several empirical methods for the calculation of the long-term median tropospheric scatter loss L(50), but the most comprehensive one is that developed by the National Bureau of Standards (NBS) (Ref. 1). The essential parts of the work have been adopted by the International Radio Consultative Committee (CCIR) (Ref 2). The median transmission losses calculated by both methods for the seven links are shown in Table 1 together with the measured values.

Calculated and Measured Values of the Median
Transmission Loss

	Calcu	lated	Measured		
	LNBS	LCCIR	L _m	LNBS-Lm	LCCIR-Lm
1. Shetland-Sola	130	125	130	0	-5
2. Emden-M. Gladbach	125	125.5	126	-1	-0.5
3. Paris NM. Gladbach	127	126.5	125	+2	+1.5
4. Athens-Izmir	125	126.5	115	+10	+11.5
5. Eskisehir-Izmir	133	123.5	117.5	+15.5	+6
6. Athens-Kefallinia	125	118	117	+8	+1
7. Catanzaro-Kefallinia	121	117	108	+13	+9

The difference between predicted and measured median transmission loss can be as high as 15 dB. Figures 2 to 8 show for the seven links:

- (a) the calculated distribution of the short-term median signal level (curves marked C) including the estimated standard error
 - (b) the measured distribution of the 14-min median signal levels (curves marked M) and
- (c) the measured distribution of signal levels during the worst month (curves marked WM) of the recording period.

The characteristics valid for the great majority of the distribution curves are:

- (a) For high transmission loss the distributions, as expected, approximate the log-normal characteristic very closely. This region of high transmission loss is of utmost importance for the prediction of propagational reliability.
- (b) For the region of high signal strength, the distributions tend to deviate from the lognormal distribution in favour of still lower transmission loss. This seems to indicate that the propagation mechanism for high signal levels is different from that for low signal levels.
- (c) For four links (1, 3, 4 and 7), the standard deviation decreased as the median received signal strength decreased (Fig.9). For the remaining links (2, 5, and 6), the correlation between the monthly median and σ was nearly zero.
- (d) The standard deviation during the worst month varies between 3 and 7 dB on the different links.
- (e) From (c) and (d) above, it may be concluded that the signal level exceeded for a high percentage of the time during the worst month cannot be derived from the monthly median value. This is also indicated by Fig. 10, in which the 99.99% and the median signal levels are plottted.

2.2 Correlation Between The Median Transmission Loss and Atmospheric Parameters

Fig.11 gives the correlation coefficient, ρ , between the monthly median values of signal strength and those of N_S (surface refractive index) for links 1, 2, 3, and 7. For links 1, 2 and 3, ρ is higher than the value which might be expected from Ref. 3 where the correlation between N_S and ΔN measured near Emden during the years 1953 to 1958 is shown to be less than ρ . The meteorological data from the stations of links 4 and 5 were insufficient for the plotting of regression lines. Links 6 and 7 exhibit very low correlation (0.2 in both cases), but the meteorological data for links 6 and 7 were collected at only one station.

The correlation coefficients between the median (monthly, weekly and daily) RF signal level on one side and the surface refractivity, N_S , the temperature, and the dew-point temperature on the other side, for links 1 to 3 are compared in Table 2. As expected from CCIR (Ref. 4) the highest correlation is obtained between monthly medians rather than weekly values.

Table 2

Correlation between Median RF Received Signal Level and Meteorological Parameters

		Surface	e refrac	tivity*	Temper	ature	Dew F	oint	Average meteorological data
LINK		monthly	weekly	daily	monthly	weekly	monthly	weekly	
1 SHETLANDS-	ρ	0.86	0.77	0.4	0.88	0.5	0.91	0.63	April 64 - March 65 N _S = 322
SOLA	tga	0.81	0.75	0.52	0.94	0.31	1.0	1.0	t = 5.8°C D.P.= 4.3°C
2 EMDEN-	ρ	0.89	0.42	-0.07	0.79	0.4	0.79	0.26	May 64 - April 65 N _S = 318
M. GLADBACH	tga	0.37	0.27	-0.06	0.42	0.36	0.53	0.33	t = 10.5°C D.P.= 6.1°C
3 PARIS N.	ρ	0.78	0.4	0.04	0.74	0.46	0.67	0.25	Apr.:1 64 - March 65 N _S = 312
M. GLADBACH	tga	0.35	0.25	0.03	0.33	0.42	0.49	0.25	t = 11° C D.P.= 5.2°C

A Average of data from transmitting and receiving stations

p: correlation coefficient

tga: slope of regression line

Prediction of the distribution of the monthly median transmission loss from measured variations of the surface refractivity is possible only if high correlation between these parameters exists and the slope of their regression-lines is known. Reference 3 Eq. 14, reports a regression-line slope of 0.18 dB per unit of $N_{\rm S}$ derived from 37 American and 5 German links. This is considerably less than the figures obtained for links 1, 2, and 3, which are 0.81, 0.37, and 0.35 dB per unit of $N_{\rm S}$ respectively. Due to this wide spread in the slopes of the regression lines, reliable prediction of the monthly median transmission loss from measurements of the surface refractively is at present not possible, although the correlation between signal strength and $N_{\rm c}$ may be high.

2.3 Adjacent Links

The correlation between the transmission losses on adjacent links is of great interest in the assessment of the performance of systems such as ACE High, where circuits are routed over several troposcatter links in tandem. As might be expected, the monthly median values of the signal level on adjacent links were found to be correlated.

To determine whether it is likely that low values of the short-term median signal level will occur simultaneously on adjacent links, the correlation between the 14-min median values of signal level was determined on links 2 and 3. Correlation coefficients were calculated over periods of one day. These are plotted in Fig 12 against the average of the values of the daily median signal level measured on the two links.

For signal levels below the yearly median, the correlation coefficients are almost evenly spread between +0.5 and -0.5, which indicates that the correlation over longer periods, say one month, is zero. For high signal levels, which are of little importance for assessing the system performance, all correlation coefficients are positive (between 0 and 0.9);

3. MEASUREMENT OF MULTIPATH INTERMODULATION

3.1 General

The performance quality of a troposcatter radio link utilising frequency modulation (FM) is normally limited by basic thermal noise (BN) at low RF signal levels and by intermodulation noise (IM) at high RF signal levels. The total noise is always the sum of the BN and the IM, a fact which renders it impossible to make a direct measurement of intermodulation noise.

In the UHF band, EN is caused by additive thermal noise which originates at the input of the receiver and phase-modulates the carrier. Due to the automatic gain control (AGC) and the limiter used in the FM receivers, the basic noise in a channel is inversely proportional to the received carrier power above the FM threshold.

Intermodulation noise is caused by amplitude and phase non-linearities in the equipment and by multipath propagation. Intermodulation noise caused by multipath propagation - called multipath inter-

modulation for short - is dependent on system and path parameters. It is conceivable that in any troposcatter system where the path parameters are more or less fixed (e.g., the ACE High system) the multipath intermodulation presents a fundamental limitation on the attainable system performance and, with specified performance, on the system capacity.

In what follows we shall discuss the magnitude of multipath intermodulation as calculated theoretically and measured on the ACE High links 1 to 5 mentioned in Chapter 1.

3.2 Calculation

The calculations in this paper are based on Ref. 5 which describes a method of predicting the magnitude of inter-channel modulation due to multipath propagation on angle-modulated troposcatter radio systems. To predict the effect of multipath intermodulation, the path structure is assumed to be as shown in Fig 13. The main signal path is the shortest path following the beam centre line, the rest are echo paths. Calculation of the intermodulation requires (Ref. 5) the determination for each path of the loss, r, and the time delay, T, relative to the main signal. The relative loss, r, and the time delay, T, are tabulated in Table 3 for various echo paths taking into account the actual antenna patterns of the ACE High system.

	LANDS- DLA		DEN- NDBACH	PARI M.GLA	S N DBACH		ENS- MIR	ESKISI IZM	
r (dB)	T (µS)	r (dB)	Τ (μS)	r (dB)	T (µS)	r [®] (dB)	T (µS)	r (dB)	T (uS)
6.9	0.068	7	0.046	6.9	0.051	6	0.015	6.9	0.059
14.2	0.17	15	0.115	14.2	0.127	12.3	0.038	14.7	0.14
18.5	0.238	19	0.161	18.5	0.178	15.7	0.053	19.8	0.196
24	0.32	25	0.218	24	0.24	19	0.072	26.5	0.266
42	0.54	40	0.37	41	0.409	25.8	0.122	>40	0.45
-60	0.88	>60	0.6	>60	0.66	32.9	0.192	>60	0.72

Assuming Equal Antennas

A method of calculating the multipath intermodulation caused by a single echo is given in Ref. 6, with a set of curves showing the contours of constant interferences in the top channel of an FM system under equivalent noise loading conditions. With these data, a family of curves of signal-to-interference, S/I plotted against the echo delay, T, can be developed for a given base bandwidth and frequency deviation. The computed values of total echo reflection loss and time delay, which depend upon the path parameters and the free-space patterns of the antennas, are superimposed, and the maximum value of S/I caused by a single echo under propagation conditions corresponding to the standard atmosphere is thus found. The curves shown in Fig. 14 were derived for a channel deviation of 70 kHz. An empirical value of 9 dB has been added to the calculated noise power ratios listed in Table 2 to account for multiple echoes (page 24 of Ref. 5). In a similar manner, the maximum S/I for 60-channel operation (baseband bandwidth 60 to 300 kHz) for both pure FM and FM with pre-emphasis (curve B of Fig. 17) were computed and are shown plotted in Figs 15 and 16 respectively. Inspection of these figures shows that the multipath intermodulation may be decreased by more than 10 dB in the top channel if a pre-emphasis network is used.

3.3 Measurements

Intermodulation noise of radio systems is, a coording to CCIR recommendations, experimentally determined by the substitution of a "conventional load" for the multiplex input signal during the busy hour. The conventional load is a uniform-spectrum Gaussian noise signal, n, the mean absolute power of which at a point of zero relative transmission level is given by:

$$n(\overline{P}) = -1 + 4 \log_{e} N (dBmo)$$
 N< 240

where N is the total number of telephone channels. If the noise loading is eliminated by a band-stop filter from one of the telephone channels at the input of the modulator, the total noise (IM + BN) (i.e. equipment and multipath intermodulation, and basic thermal noise) in the same channel can be measured. If the conventional load were completely removed, what is measured at the channel output would be the basic noise, BN. Both measurements are expressed as noise-power-ratios, NPR, relative to the power measured in the same telephone channel under full conventional loading without the band-stop filter.

The intermodulation is then obtained as the difference between the (IM + BN) and then BN, assuming that both terms add on a power basis. To evaluate the multipath intermodulation the following conditions must be fulfilled:

- (a) the BN is not predominant, otherwise both measurements will be practically equal, and
- (b) the equipment intermodulation, including antenna feeder distortion, does not obscure the multipath intermodulation.

To minimise the equipment intermodulation, (b) above, the alignment of the transmitter and receiver under test was carefully checked and optimized and the bandwidth determining operational IF amplifier (3-dB bandwidth 1.1 MHz) was replaced by an IF amplifier with a 3-dB bandwidth in excess of 4 MHz.

The intermodulation originating in the equipment was measured by feeding the transmit signal into a receiver after appropriate frequency conversion and level adjustment.

The NPR test arrangement is shown schematically in Fig 18. The arrangement allows the simultaneous measurements of the RF signal strength and of the NPR of either the (BN + total IM) or the BN alone. The measurement procedure remains the same whether or not pre-emphasis is used.

The test results for links, 1, 2, 3, and 5 are summarised in Fig 19 to 22 wich show, for various channel deviations and different channels in the baseband, the NPR for BN, (BN + equipment IM), and the total intermodulation plus basic noise, as measured over the link. Pre-emphasis was used only for link 3. For link 4, multipath intermodulation could not be distinguished from (BN + equipment IM). This result was in agreement with the calculated data, which indicated that multipath intermodulation would be negligible.

The average level of the multipath intermodulation relative to the signal - expressed as the ratio S/I - at an RF signal level equal to the yearly median was calculated from measured data.

3.4 Comparison Between Calculations and Measurements

Very close agreement between the calculated and measured data could not be expected, mainly because:

- (a) The calculation of the single echo assumed an ideal antenna pattern and orientation, the latter greatly affecting the magnitude of multipath intermodulation.
- (b) To account for the multiplicity of echoes, a 9-dB adjustment was estimated, based on empirical data collected from four rather unusual links, three in the Arctic and one in the Caribbean, all of them over ice or water (pages 25 and 26 of Ref. 5).
- (c) There is a large spread (up to 12 dB) of values of median multipath intermodulation for a single median value of RF signal strength (Fig 13 of Ref 5). In addition, the slope of the regression-line relating median NPR and median RF signal strength is not constant, but has been reported (pages 23 of Ref. 5) to range from about 0.4 to 1.2 dB per dB or RF received signal power.

These limitations should be remembered when the calculated and measured results are compared (Table 4). All calculations are based on a standard atmosphere ($\bar{N}_S = 301$) and relate to the intermodulation in the highest baseband channel, which is assumed to be the worst. On average, link 1 was found to be 5 dB worse than calculated and appears to be the worst among the links examined for multipath intermodulation.

Link 2 and link 3 are respectively 1.5 dB and 4 dB better than estimated. This is not particularly significant because the equipment intermodulation is almost equal to, or worse than, the multipath IM, and any estimate of multipath IM is therefore liable to be considerably in error.

On link 5 where the measured RF median signal strength was found to be 6 dB higher than calculated the multipath IM is 4 dB worse than predicted. It is believed that the path geometry, which includes two high mountain ridges, is the cause of both abnormalities.

4. CONCLUSION

The measured long-term transmission loss on seven troposcatter links of the ACE High system is generally lower than the loss calculated by either the NBS or the CCIR method. Both methods provide comparable accuracy, but the CCIR method is easier to use.

The validity of the assumption of log-normal distribution for the short-term median transmission loss has been confirmed by the measurements for low-signal strengths.

For the worst month, the distribution of the short-term median transmission loss is more closely log-normal than for other months.

The standard deviation of the monthly distribution of the short-term transmission loss tends to decrease with the monthly median signal strength.

The measured values of the standard deviation of the yearly distribution are in fairly good agreement with the calculated values, except for two oversea paths.

The signal level exceeded for a high percentage of any month cannot be predicted from the monthly median values.

The correlation between the monthly median transmission loss and the surface refractivity is high on those links for which sufficient meteorological data were available (links 1, 2, and 3). However, the slope of the regression-line of link 1 differs considerably from those of links 2 and 3. All regression-line slopes determined are considerably higher than those reported in the literature.

Due to the wide spread in the slopes of the regression-lines, for which no explanation is available, reliable prediction of the monthly median transmission loss from measurements of the surface refractivity is not possible at present.

Limited measurements of the correlation between short-term median values on adjacent links indicate that for performance assessment it may be assumed that there is independent power fading during any one month.

The measured values of multipath intermodulation noise were found to be in reasonable agreement with the calculated values.

On link 5 where the measured median signal level was 6 dB higher than calculated the multipath IM was 4 dB worse than predicted. It is believed that the path geometry, which includes two high mountain ridges, was the cause for this discrepancy.

REFERENCES

- RICE, P.L., LONGLEY, A.G., NORTON, K.A., and BARSIS, A.P., "Transmission Loss Predictions for Tropospheric Communication Circuits" NBS Tech. Note 101.
- CCIR Report 238-2 (1974) "Propagation data required for trans-horizon radio relay systems" XIIIth Plenary Assembly, Vol. V, pp. 209-229, Geneva 1974.
- BEAN, B.R., FFHLABER, L., and GROSSKOPF, Jan 1962, "Die Radiometeorologie und ihre Bedeutung für die Ausbreitung der m-, dm- und cm- Wellen auf grosse Entfernungen". NTZ Vol. 15, pp. 9-16.
- CCIR Report 233-3 (1974), "Influence of the non-ionized atmosphere on wave propagation". XIIIth Plenary Assembly, Vol. V, pp. 66-79, Geneva 1974.
- BEACH, C.D., and TRECKER, J.M., January 1963, "A method for predicting interchannel modulation due to multipath propagation in FM and PM tropospheric radio systems" BSTJ pp. 1-36.
- BENNETT, W.R., CURTIS, H.E., and RICE, S.O., May 1955, "Interchannel interference in FM and PM systems under noise loading conditions". BSTJ, pp. 601-636.

Table 4: Summary of calculated and measured intermodulation noise

	1	2	3	4	1	5
LINK:	SHETLANDS -	EMDEN - M. GLADBACH	PARIS-N. ~ M. GLADBACH	ATHENS -	ESKIS	200000000000000000000000000000000000000
ANGULAR DISTANCE (mRAD.)	28.9	27.1	27.5	17.5	32	.6
1,67 L × θ ₁ × θ ₂ (μS)	0.141	0.096	0.106	0.0318	0.11	7
TEST PERIOD	MAY 1965	DEC. 1964	MARCH 1965	SEPT. 1964	ост.	964
MEASURED YEARLY MEDIAN / WORST MONTH MEDIAN (-dBm)	63/70	59/63	59/63.5	60/66	51.5/54	
N _S	300	310	300	290	27	5
CA	LCULATED AVI	ERAGE MULTIPATO MULTIPLE EC	TH INTERMODUL HOES (NS = 301)			
	dB	dB	dB	dB	d	В
36 CHANNELS: FM 152 kHz CHANNEL 70 kHz DEVIATION	45	50	49	63	5	0
60 CHANNELS: FM 290 kHz CHANNEL 63 kHz DEVIATION	39	46.5	44	57.5	43	.5
50 CHANNELS: PRE - EMPHASIS. 290 kHz CHANNEL 40 kHz AV. DEVIATION	51.5	58	56.5	70	54	5
		TERMODULATION STED FOR NS		ED AT MEDIAN F		
RF MEDIAN (-dBm) 63kHz DEVIATION	63	60	59		49 _M	64
	63	60		NOT -	т	640
63 kHz DEVIATION	63	60		NOT -	т	64
63 kHz DEVIATION 60 CHANNELS : FM		60 - 51.5	59	PRODULATION NOT	49 _M	-
63 KHZ DEVIATION 60 CHANNELS : FM 290 KHZ CHANNEL	34	_	59	INTERMODULATION NOT	49 _M	(42)
63 KHZ DEVIATION 60 CHANNELS : FM 290 KHZ CHANNEL 152 KHZ CHANNEL	34	51.5	59	INTERMODULATION NOT	49 _M	(42)
63 KHZ DEVIATION 60 CHANNELS : FM 290 KHZ CHANNEL 152 KHZ CHANNEL 105 KHZ CHANNEL	34	51.5	59	ODULATION NOT	49 _M	(42)
63 kHz DEVIATION 60 CHANNELS : FM 290 kHz CHANNEL 152 kHz CHANNEL 105kHz CHANNEL 56kHz CHANNEL 34kHz CHANNEL	34 39 41 —	51.5 54 —	59 48 54 — —	MULTIPATH INTERMODULATION NOT DISTINGUISHABLE FROM BN AND IM.	49 _M - 46 49.5	(42)

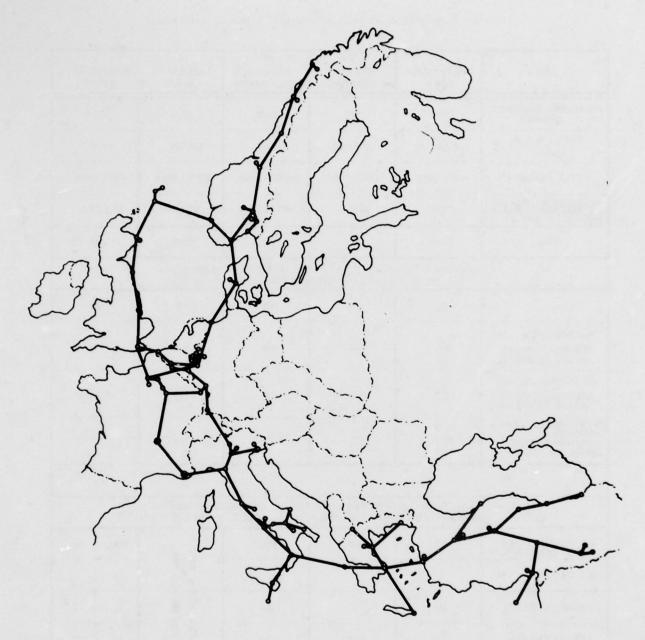


Fig. 1: Outline of the NATO ACE-High troposcatter system

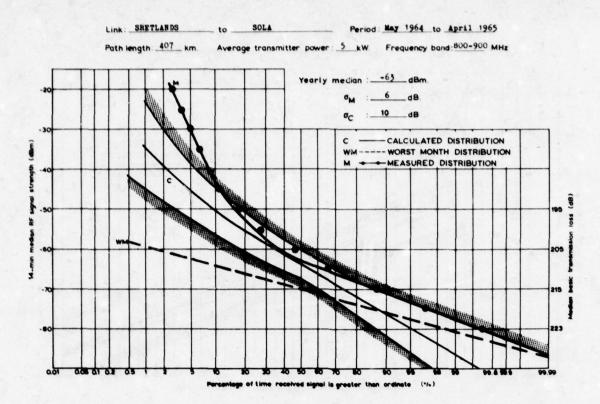


Fig. 2: Long-term distribution of 14-min median RF signal strength (SHETLANDS-SOLA)

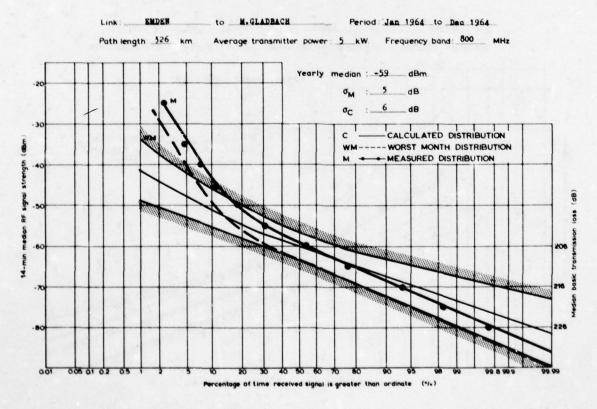


Fig. 3: Long-term distribution of 14-min median RF signal strength (EMDEN-M.GLADBACH)

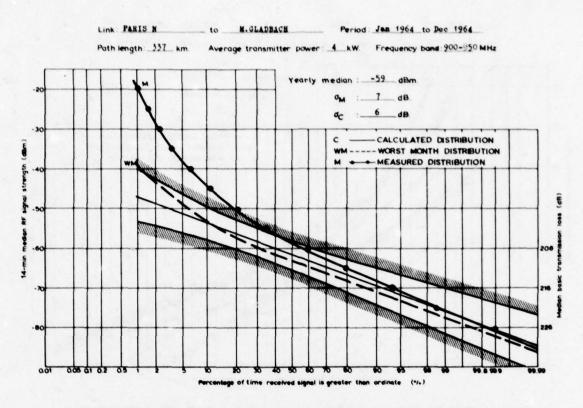


Fig. 4: Long-term distribution of 14-min median RF signal strength (PARIS N.-M.GLADBACH)

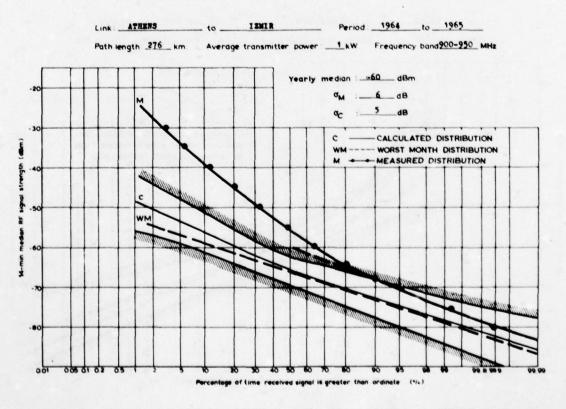


Fig. 5: Long-term distribution of 14-min median RF signal strength (ATHENS-IZMIR)

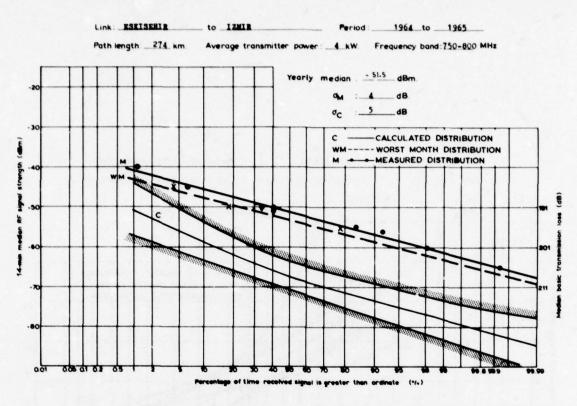


Fig. 6: Long-term distribution of 14-min median RF signal strength (ESKISEHIR-IZMIR)

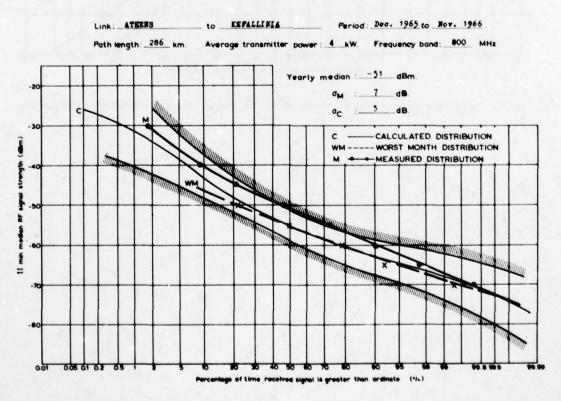


Fig. 7: Long-term distribution of 14-min median RF signal strength (ATHENS-KEFALLINIA)

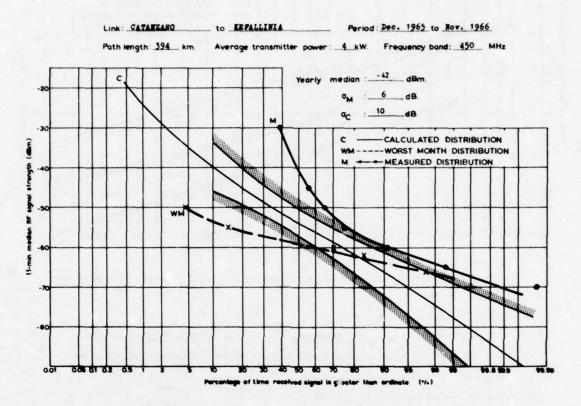


Fig. 8: Long-term distribution of 14-min median RF signal strength (CATANZARO-KEFALLINIA)

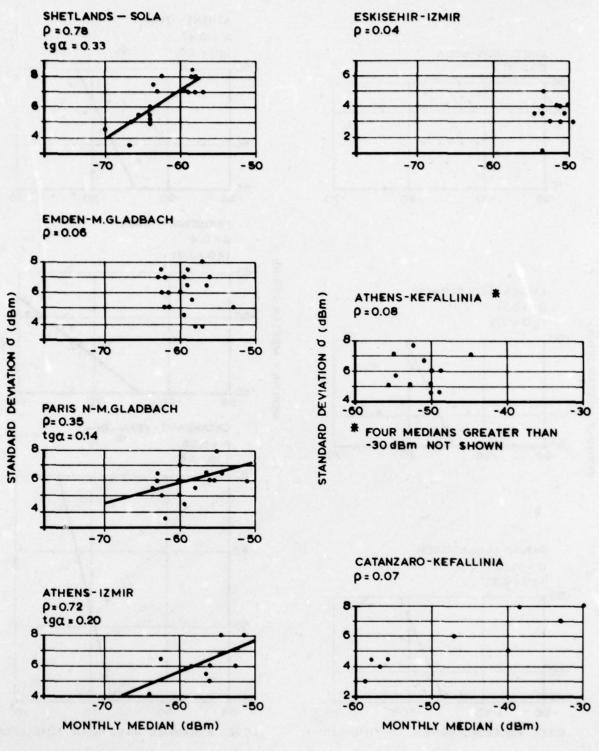


Fig. 9: Correlation between monthly median received RF signal level and its standard deviation

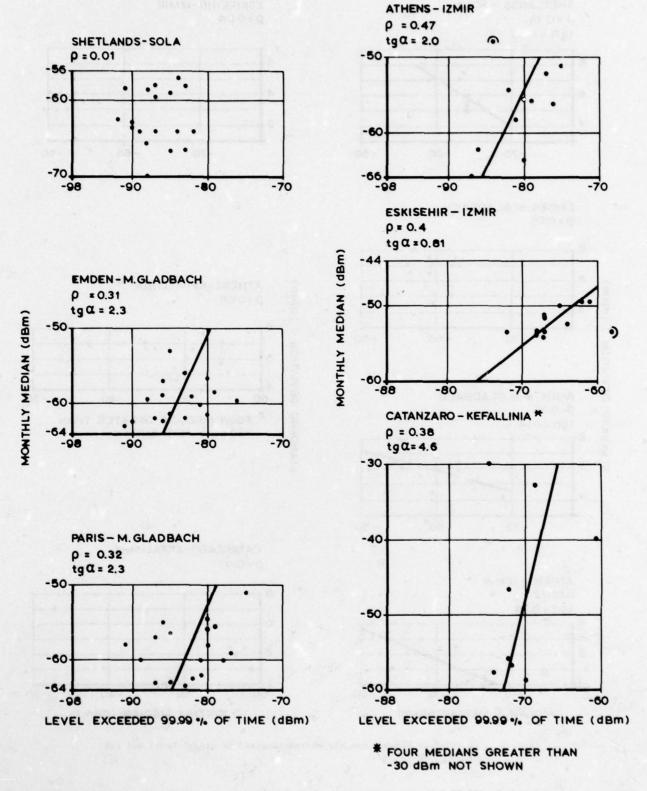


Fig. 10: Correlation between monthly medians and level exceeded 99.93% of the time

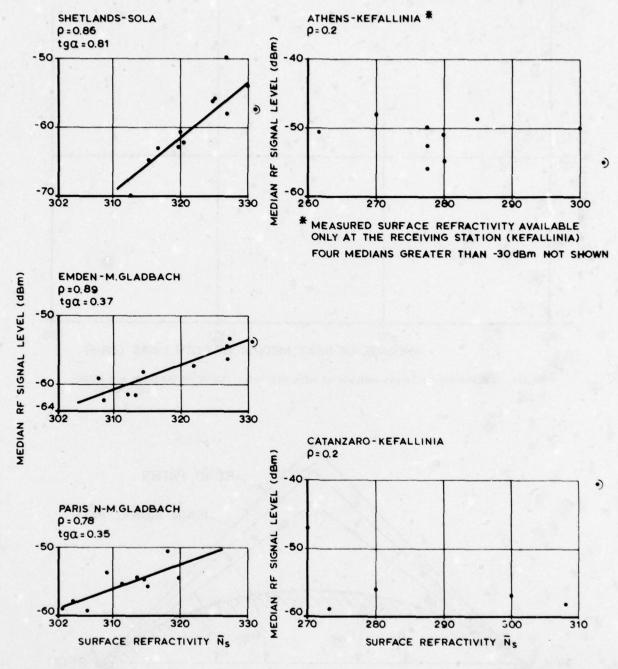


Fig. 11: Correlation between RF signal level and surface refractivity (monthly averages)

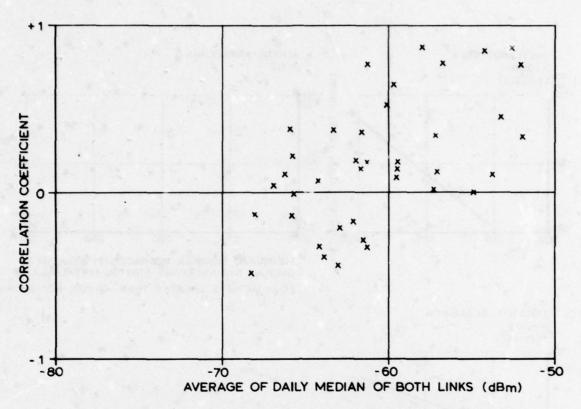
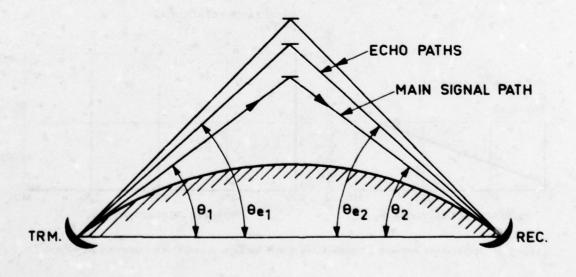


Fig. 12: Correlation of 14-min medians of adjacent links (EMDEN.-M.GLADBACH and PARIS-M.GLADBACH)



$$\frac{\theta_{e1}}{\theta_1} = \frac{\theta_{e2}}{\theta_2} = \rho$$

Fig. 13: Model of symmetrical tropospheric scatter path

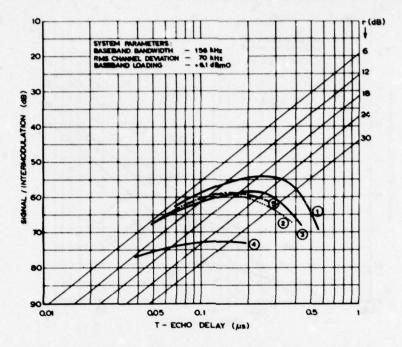


Fig. 14: Signal-to-intermodulation plotted against echo delay in top channel (single echo, FM without pre-emphasis)

Link 1: Shetlands - Sola

Link 2: Emden - M. Gladbach Link 3: Paris - M. Gladbach

Link 4: Athens - Izmir Link 5: Eskisehir - Izmir

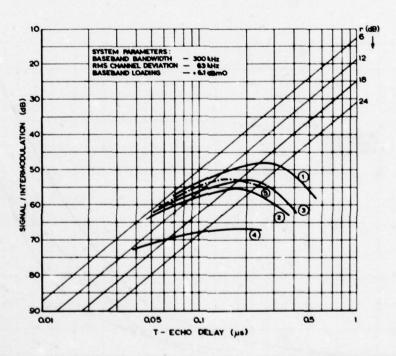


Fig. 15: Signal-to-intermodulation plotted against echo delay in top channel (single echo, FM without pre-emphasis)

Link 1: Shetlands - Sola Link 2: Emden - M. Gladbach Link 3: Paris - M. Gladbach

Link 4: Athens - Izmir Link 5: Eskisehir - Izmir

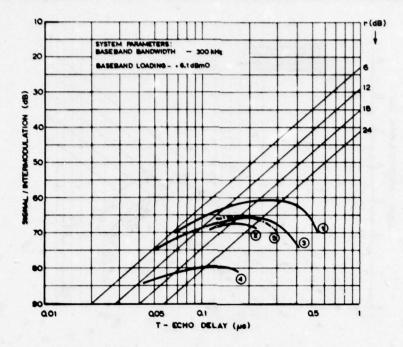


Fig. 16: Signal-to-intermodulation plotted against echo delay in top channel (single echo, FM with pre-emphasis according to Fig.17 Curve B)

Link 1: Shetlands - Sola Link 2: Emden - M. Gladbach Link 3: Paris - M. Gladbach Link 4: Athens - Izmir Link 5: Eskisehir - Izmir

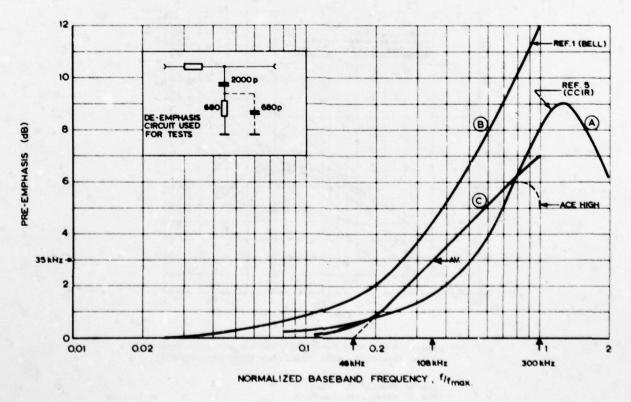


Fig. 17: Pre-emphasis characteristics

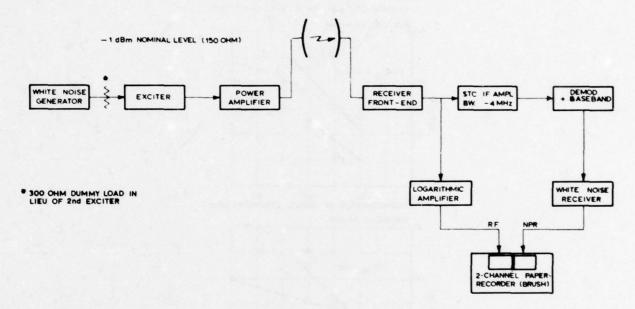
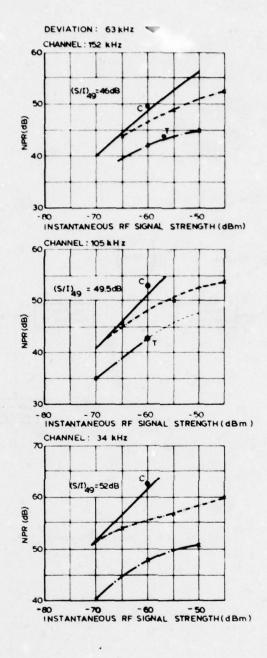


Fig. 18: N P R Test arrangement



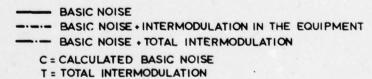
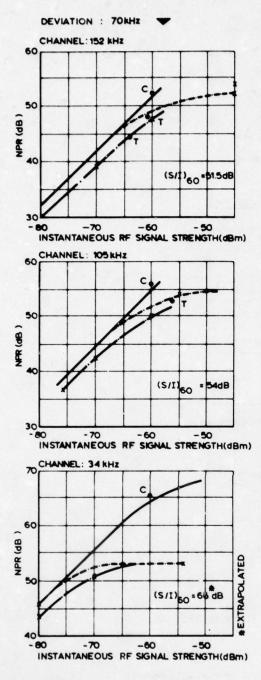


Fig. 19: Multipath intermodulation test results: Link Shetlands-Sola (May 1965) Conditions Conventional load 12 to 300 kHz, + 5.1 dBm0





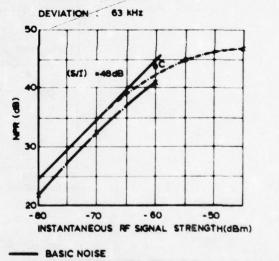
---- BASIC NOISE + INTERMODULATION IN THE EQUIPMENT

-- BASIC NOISE + TOTAL INTERMODULATION

C = CALCULATED BASIC NOISE

T = TOTAL INTERMODULATION

Fig. 20: Multipath intermodulations test results:
Link Emden-M.Gladbach (Dec 64)
Conditions: Conventional load 12 to 156 kHz
+ 5.2 dBm0



--- BASIC NOISE . INTERMODULATION IN THE EQUIPMENT

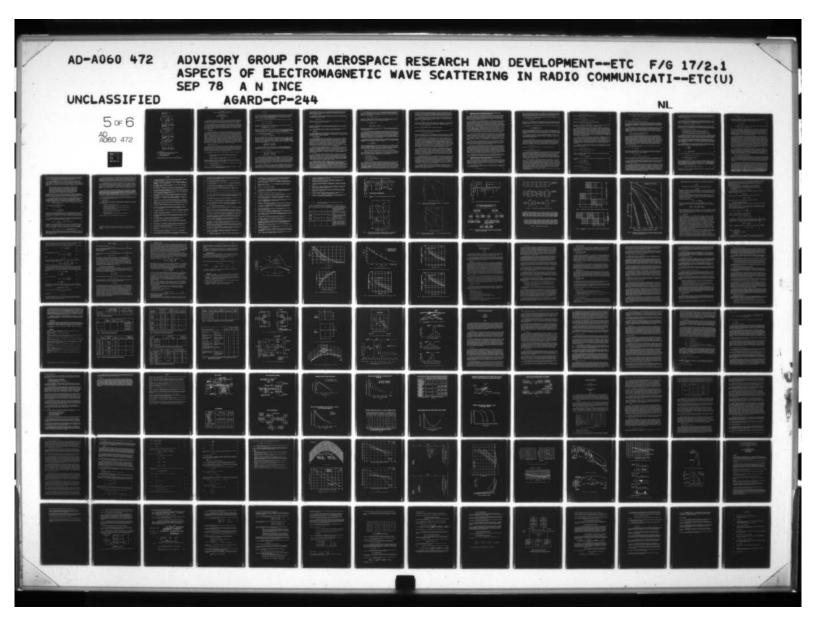
-- BASIC NOISE . TOTAL INTERMODULATION

C . CALCULATED BASIC NOISE

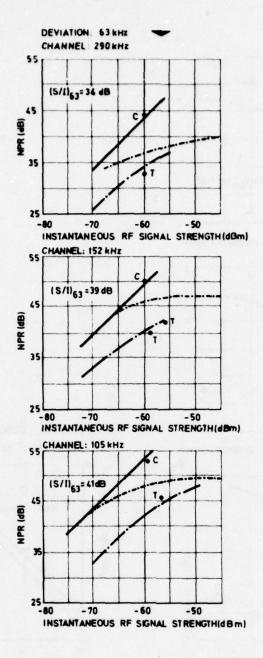
CHANNEL : 290 KHZ

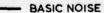
T . TOTAL INTERMODULATION

Fig. 21: Multipath intermodulation test results: Link Paris-M.Gladbach (Mar 65) Conditions: Conventional load 12 to 300 kHz, + 6.1 dBm0









- ---- BASIC NOISE + INTERMODULATION IN THE EQUIPMENT
- --- BASIC NOISE + TOTAL INTERMODULATION
 - C = CALCULATED BASIC NOISE
 - T = TOTAL INTERMODULATION

Fig. 22: Multipath intermodulation test results: Link Eskisehir-Izmir (Oct 64) Conditions: Conventional load 12 to 300 kHz, + 6.1 dBmo (no pre-emphasis)

A REVIEW OF SIGNAL PROCESSING FOR SCATTER COMMUNICATIONS

Phillip A. Bello CNR, Inc. 220 Reservoir Street Needham, Massachusetts 02194

ABSTRACT

This paper will review the state-of-the-art in effective communications techniques for fading multipath-distorted radio links. The system function parameters of important radio links will be defined and the relationship between the values of these parameters and the selection of appropriate modulation and demodulation techniques will be discussed.

Reliable communication over fading dispersive channels requires the utilization of diversity communications of some form. In addition to the conventional forms of diversity, such as space, frequency, angle, and polarization, advanced communication techniques make use of "signal" diversity which exists in the signal structure of the received digital modulation waveform by virtue of the time and frequency selectivity of the channel. Utilization of modem and coding techniques to exploit signal diversity will be discussed and error rate curves presented.

1. INTRODUCTION

The increasing demands for reliable digital data and digitized voice transmission have provided the motivation for the continuing research and development work on signal processing design for radio channels. In this paper the focus is on modem (modulator-demodulator) design techniques for fading dispersive channels, i.e., channels in which multipath and fading are the normal situation. While the discussion will focus on the techniques as general tools, consideration will be given to the application of these principles to specific channels. Before discussing modem techniques, we present a short background discussion on channel characterization and a list of some representative channel parameter values for radio channels of interest. The following section takes up modem techniques starting with design for flat fading situations and leading to a discussion of the impact of terminal equipment constraints on signal design. Considerable attention is given to modem techniques for radio channels using power amplifiers operating at constant peak power. Both, classes of techniques in which the pulses are slightly distorted by the channel, and those in which the pulses are highly distorted by the channel are considered. A following section discusses the considerable benefits to be achieved by coding on fading dispersive radio channels.

CHANNEL CHARACTERIZATION

The radio channels of interest here are linear and, as with all linear systems, the impulse response or transfer function provide the essential information for characterizing input-output behavior. However, such characterization is complicated by the fact that these system functions not only are random processes, but also at best quasi-stationary random processes. An idealized statistical model that has found general utility for fading dispersive radio channels when applied on a quasi-stationary basis is the Gaussian wide-sense stationary uncorrelated scattering channel (abbreviated GWSSUS) [1].

The defining characteristics of the GWSSUS model may be expressed in either of two equivalent forms:

- (a) The time-variant transfer function is a wide-sense stationary complex Gaussian process in both the time and frequency variables of the transfer function;
- (b) The impulse response is a burst of white noise which has complex Gaussian statistics on an ensemble basis.

The latter definition is useful for providing an interpretation in terms of a general independent-scatter model, while the former allows us to grasp directly the time and frequency selective distorting properties of the channel.

If we denote the time-variant transfer function of the channel by T(f,t), the WSSUS property of definition (a) becomes

$$\overline{T^*(f,t)T(f+\Omega,t+\tau)} = R(\Omega,\tau)$$
 (1)

where $R(\Omega,\tau)$ is called the <u>time-frequency correlation function</u> of the channel. In most cases of interest, the two correlation functions

$$q(\Omega) = R(\Omega, 0) \tag{2}$$

$$p(\tau) = R(0,\tau) \tag{3}$$

are sufficient to describe the frequency and time selectivity of the channel. The function $q(\Omega)$ is called the <u>frequency correlation function</u> of the channel since it is the correlation between two received carriers as a function of their frequency spacing Ω at transmission. The function $p(\tau)$ is just the autocorrelation function of a received carrier and, for symmetry, is called the <u>time correlation function</u>.

The time-variant impulse response $g(t,\xi)$ and transfer function T(f,t) are Fourier transform pairs

$$g(t,\xi) = \int T(f,t)e^{j2\pi f\xi} df$$
 (4)

$$T(f,t) = \int g(t,\xi)e^{-j2\pi f\xi} d\xi$$
 (5)

The equivalent definition (b) is a direct consequence of (a) and this Fourier transform relation [1]. In mathematical terms, (b) takes the form

$$\overline{g^{*}(t,\xi)g(t+\tau,\eta)} = Q(\tau,\xi)\delta(\eta-\xi)$$
 (6)

where $\delta(\cdot)$ is the unit impulse function. It is readily shown that $Q(\tau, \xi)$ and $R(\Omega, \tau)$ are Fourier transform pairs $(\tau \text{ fixed})$. $Q(\tau, \xi)$ has been called the <u>tap gain correlation function</u> because it is proportional to the autocorrelation function of the fluctuations for scatterers providing path delays in the range $(\xi, \xi + d\xi)$ in a tapped delay line channel model.

Of particular interest in applications is the intensity of scattering versus delay $\xi,Q(\xi)$, called the <u>delay power spectrum</u>

$$Q(\xi) = Q(0,\xi) = \int q(\Omega)e^{j2\pi\xi\Omega} d\Omega$$
 (7)

The delay power spectrum $Q(\xi)$ and frequency correlation function $q(\Omega)$ are Fourier transform pairs. From the width of $Q(\xi)$ we can directly determine the amount of intersymbol interference and the degree of frequency selectivity. This width is called the <u>multipath spread</u> of the channel. Clearly, one may define "width" in many ways. One definition that has found use in the literature (perhaps because it can be shown to characterize the onset of frequency selectivity in a limited bandwidth) is the rms multipath spread L. This parameter is defined in terms of $Q(\xi)$ as follows:

$$L = 2\sqrt{\int \xi^2 Q(\xi) d\xi} - \left[\int \xi Q(\xi) d\xi\right]^2$$

$$\int Q(\xi) d\xi - \left[\int Q(\xi) d\xi\right]^2$$
(8)

Also of particular interest in applications is the <u>Doppler power spectrum</u> and <u>Doppler spread</u> of the channel. The Doppler power spectrum $P(\nu)$ is the power spectrum of a received carrier and, thus, the Fourier transform of the time-correlation function $p(\tau)$

$$P(\nu) = \int p(\tau)e^{-j2\pi\nu\tau} d\tau \tag{9}$$

Analogous to (8) we have the definition of B, the rms Doppler spread,

$$B = 2\sqrt{\frac{\int \nu^2 P(\nu) d\nu}{\int P(\nu) d\nu}} - \left[\frac{\int \nu P(\nu) d\nu}{\int P(\nu) d\nu}\right]^2$$
(10)

The two power spectra $Q(\xi)$ and $P(\nu)$ and parameters B and L are the most used and most measured parameters for fading dispersive radio channels. It should be realized that, because of the quasi-stationary nature of the radio channels, $Q(\xi)$, $P(\nu)$, B, and L, and the other correlation functions discussed above must be regarded as slowly varying in time in addition to being somewhat dependent on operating frequency. Table 1 presents representative values of multipath and Doppler spread for several different fading-dispersive radio links, and includes some references so that the reader may obtain more detailed information. We have also listed the product BL, known as the spread factor, which has bearing on modem design, as will be discussed below.

To give the reader an intuitive picture relating multipath and Doppler spread to the distortion that may be produced on a signaling element of bandwidth W or time duration T, we show in Figure 1 a single record of the magnitude of a complex Gaussian process generated by computer simulation (a power spectrum equivalent to passing white noise through a double tuned filter was used). The horizontal axis can either be interpreted as time in units of

1/B or as frequency in units of 1/L. In the former case, the record would represent the received envelope of a fading carrier having the familiar Rayleigh distribution. In the latter case, the record would represent a "snapshot" of the magnitude of the transfer function of a GWSSUS channel.

Examination of Figure 1 shows, by inspection, that to achieve small distortion over the bandwidth W of a signaling element, the nonfrequency-selective or flat fading case, the following inequality must be satisfied:

$$\frac{\mathsf{W}}{1/\mathsf{L}} - \mathsf{WL} \ll 1 \tag{11}$$

Similarly, to have little distortion in a time interval T requires that the time duration of the signaling element satisfy the inequality

$$\frac{T}{1/B} - BT \ll 1 \tag{12}$$

The amount of distortion and system performance degradation suffered by a link for given values of BT and WL depend on the modem technique and, generally, the delay and Doppler power spectra shapes.

For a representative set of calculations on the degrading effects of time and frequency selective fading, the reader may consult references [38] through [46].

TECHNIQUES

We will gradually evolve the collection of available techniques for modem design by starting with simple cases and adding complexity. Most attention will be given to techniques applicable to channels having a power amplifier with a constant peak power constraint. The considerable benefits of coding are discussed.

3.1 Flat-Flat Fading

Let us assume first that we wish to communicate in such a way that our signaling elements suffer little distortion. This means that over the time duration and bandwidth of the signaling elements, the time-variant transfer function changes little, i.e., (11) and (12) must both be satisfied. Since the product WT has a lower bound for any meaningful definitions of W and T, it is possible to postulate channels for which both inequalities cannot be satisfied. In addition, there is a lack of precision in the strong inequalities (11) and (12). To clarify this situation by example; we have provided in Figure 2 some theoretical plots [46] of irreducible error probability, i.e., error probability due to signal distortion alone, for a binary phase-continuous FSK modem as a function of a normalized data rate $d = 1/T \sqrt{L/B}$, for different values of the spread factor BL.

Each of these curves exhibits a minimum. For data rates higher than the minimum, frequency-selective distortion predominates, while for data rates below this minimum, time-selective or fast fading predominates. Note that, as the spread factor decreases, the minimum error rate decreases. If the error rate due to additive noise alone is much larger than that due to selective fading alone, one may say that the inequalities (11) and (12) are satisfied to the extent required to represent performance on the basis of flat-flat fading or distortionless transmission. For brevity, we shall use the term flat fading to mean flat-flat fading.

It is instructive to compare, in Figure 3, the error rate performance of a binary PSK modem on a flat fading complex Gaussian channel with its performance on a nonfading channel for the same SNR. We note the ever-increasing SNR separation between these curves as the desired error rate decreases. Of course, the poor performance of the flat fading channel is due to the deep fades. To counteract these deep fades, one may employ diversity communications. This involves transmitting the same signal on a different channel from source to destination, selected so that the likelihood of both channels having deep fades is much smaller than either one separately having a deep fade.

A number of different methods of obtaining suitable diversity channels, and also a number of different methods of diversity combining, have been used in the past. The most common forms of diversity channels used are <u>space diversity</u> and <u>frequency diversity</u>. Channels separated sufficiently spatially (separated transmitters and/or separated receivers) tend to fade in an uncorrelated fashion as do channels with sufficiently separated operating frequencies. Additional forms of diversity channels, not infrequently discussed in the literature, are <u>polarization</u> and <u>angle</u>, corresponding to the usage of different polarizations and different antenna pointing angles. In the following sections we shall frequently refer to <u>signal diversity</u>, which is the diversity implicit in the received waveform by virtue of the time and frequency selective fading imposed by the channel on the received signal.

The optimal method of combining is called <u>predetection maximal ratio combining</u> [47] and involves weighting each diversity channel received signal by a complex gain which is proportional to the conjugate of the channel gain. Thus, for the k'th flat fading diversity channel, the received signal complex envelope $w_k(t)$ is related to the transmitted complex envelope z(t) by the equation

$$w_k(t) = g_k(t)z(t) + n_k(t)$$
 (13)

where $g_k(t)$ is a complex Gaussian process and $n_k(t)$ is an additive noise. For flat-flat fading, $g_k(t)$ changes very little over the duration of any signaling element in z(t). The diversity-combined signal w(t) for optimum combining takes the form

$$w(t) = \sum_{k=1}^{K} g_k^*(t) w_k(t)$$

$$= \left(\sum_{k=1}^{K} |g_k|^2\right) z(t) + \sum g_k^* n_k(t)$$
(14)

where K is the order of diversity. The term, $\Sigma |g_k|^2$, which represents the strength of the diversity combined signal, is just the k=1 sum of the instantaneous powers of the diversity channels.

Practical implementations attempting near-optimum combining have been carried out by industry (e.g., [48], [49]) utilizing decision-directed removal of the data modulation to recover an unmodulated carrier. Figure 4 shows the ideal performance of predetection maximal ratio combining for up to 8'th-order diversity. The solid lines are plots vs. the SNR per diversity channel while the dotted lines are plots vs. the total SNR, and the dashed line indicates the nonfading error rate curve. Note that as the order of diversity increases, the optimal diversity performance vs. total SNR approaches that of the nonfading channel, a satisfying result indeed. At 8'th-order diversity and error rates about 10⁻⁶, the approach is within 4 dB, decreasing to less than a dB at 10⁻².

Other forms of diversity combining are simpler to implement but suffer performance degradation relative to predetection maximal ratio combining. Thus, equal gain predetection combining which just phase weights the diversity channels, i.e.,

$$w(t) = \frac{K}{E} \frac{g_k^*}{|g_k|} w_k(t)$$
 (15)

suffers a degradation of around 0.6 dB for dual diversity and 1.0 dB for quadruple diversity at high SNR. Selection diversity, which involves selecting the channel with the largest strength and ignoring the rest, suffers 1.5 and 3.4 dB degradation for dual and quadruple diversity, respectively, relative to predetection maximal ratio combining at high SNR. (See [47] for a discussion of classical combining methods and their performances.)

3.2 Effect of Terminal Equipment Constraints and Selective Fading on Modem Design

It might appear from the preceding section that the problem of digital communications over fading dispersive channels is straightforward: use enough diversity with predetection maximal ratio combining and select signaling pulse durations and bandwidths for flat-flat fading. There are five important factors overlooked in this "solution":

- · Desired data rates
- · Power amplifier linearity
- · Channel allocation bandwidth
- · Channel measurement inaccuracies
- · Cost and complexity.

Adjusting the pulse duration for minimum distortion sets the data rate of the pulse train. This data rate will generally be far below the desired data rate. An increase in data rate can obviously be achieved by frequency-division-multiplexing additional pulse trains, taking due care not to allow significant interference between flat fading received pulse trains. To minimize the complexity of the modem, the number of parallel pulse trains should be kept as small as possible. To minimize the number of pulse trains, the technique of receiver time gating may be employed [39]. This technique is used on all advanced HF digital modems. Briefly, a synchronized time gate is placed over the received pulses to extract the central portion of the pulses and eliminate the intersymbol interference portion.

The separation frequency of adjacent pulse trains is set equal to the reciprocal of the time gate, so that an integrate-and-dump operation for each data stream produces orthogonality between all pulse trains if the intersymbol interference has been removed and if time-selective distortion is negligible. The multipath distorted energy which is excluded by the time gates is lost but, if the duty cycle of the gate is high, the loss in energy is small.

The utilization of optimal combining requires that the complex gains $\{g_k(t)\}$ in (13) be measured sufficiently accurately. Relatively small errors can introduce significant degradation [40]. Accurate measurement requires averaging over a time interval T_m long compared to a signaling element duration, i.e.,

$$T_{\rm m} \gg T$$
 (16)

in order for the resultant additive noise component of the measurement to have an effect on error rate small compared to that due to the additive noise components of the decision variables. To avoid time-selective fading distortion during the measurement requires

$$BT_m \ll 1 \implies BT \iff 1$$
 (17)

Moreover, for small degradation due to frequency-selective fading,

$$WL \ll 1$$
 (18)

Since the TW product has a lower bound, we find the above inequalities lead to the conclusion that the spread factor BL must satisfy the inequality:

if accurate measurement of $g_k(t)$ is to be attempted and predetection maximal ratio combining used. Since coherent detection, as in PSK demodulation, requires the extraction of a phase reference, the above arguments apply directly, and (19) is required if PSK modems are to be used.

We note from Table 1 that the spread factor of the troposcatter channel is very small, varying from 10⁻⁸ to 10⁻⁵, indicating that accurate channel measurements and coherent PSK operation should be possible without difficulty. On the other hand, the HF channel and the surface scatter channel, which can have spread factors as high as 10⁻², will present some difficulty in attempting channel measurements lasting many signaling elements. For such channels, one may use post-detection diversity combining coupled with differential PSK and incoherent FSK modems to good effect. In such a combining technique, the decision variables are added after filtering or integrate-and-dump operations. This procedure is standard on HF modems when diversity combining is used. At high SNR, the binary PSK modem is 3 dB better than binary DPSK, and the latter is 3 dB better than binary FSK. (See [47] for performance analysis.) The urban mobile and meteor burst channels lie somewhere between the above extremes, indicating that predetection combining may sometimes be possible.

The above discussion has centered on the use of frequency-division-multiplexed subcarriers combined with receiver gating to increase data rates beyond that of a single flat fading pulse train. Implicit in such an approach is the use of a linear power amplifier since such a multiplexed set of carriers has an instantaneous power with a large peak-toaverage value. For HF links this is not a problem, but for troposcatter links, for example, this linear power amplifier requirement cannot be met without large sacrifices in average radiated power. The Klystron used in troposcatter applications needs to run saturated and at constant peak power for high efficiency. In fact, for most radio links, constant peak power operation is the preferred mode.

To grasp the difficulty of the design problem, we repeat in Figure 5 the same transfer function "snapshot" shown in Figure 1. Superimposed on this random transfer function we show the bandwidth allocations for tropo and HF channels. Because of the normalized horizontal axis, these allocations are represented in units of the reciprocal multipath spread of the channel. Note that a signaling pulse which fully occupies the allocated bandwidth in a troposcatter channel will suffer severe frequency-selective distortion. Conventional modem techniques, described above for the flat fading channel, will clearly be inoperable. The typical HF channel has even larger selective fading distortion but, as described above, by using parallel transmission of low data rate streams coupled with receiver gating, the harmful effects of the selective fading are neutralized.

Despite the inability to use parallel transmission for increasing data rate on fading dispersive channels with constant envelope signal transmission constraints, we can use alternate approaches that have varying degrees of effectiveness. These techniques are categorized and discussed in the following section. Of course, these techniques may also be used when the power amplifier is linear.

3.3 Modem Techniques for Increased Bandwidth Utilization With Constant Envelope Transmission Constraint: Slightly Distorted Pulse Case

Figure 6 provides a categorization of modem techniques which are useful to varying degrees in increasing the data rate transmission beyond that of a flat fading transmission when the power amplifier limits the transmission to essentially constant envelopes. We first separate the techniques into two classes depending on whether the basic signaling elements or pulses are slightly or highly distorted by the channel. This section briefly considers the slightly distorted pulse case.

We consider first the case wherein the pulses are slightly distorted by the channel. In this case the highest data rates are achievable by the use of coherent detection, receiver time gating, and M'ary signaling in which several bits are represented by the frequency location and phase of a transmitted pulse. Constant envelope transmission occurs because only one pulse is used at any time. A performance analysis of this type of system is given in [44]. Such a system has been built and tested for troposcatter links [50] with on-the-air performance close to theoretical predictions. The maximum data rate achieved by this system was 3 Mb/s utilizing 4-FSK/2-PSK modulation, i.e., each pulse transmitted could have one of four frequencies and one of two phases corresponding to three bits of information. Seven other lower data rate modes of operation existed which allowed the utilization of a particular form of signal diversity, trading reduced data rate for increased performance. The availability of signal diversity arises from the observable fact (see Figure 5) that pulses at sufficiently different frequencies will fluctuate in an uncorrelated fashion. Predetection diversity combining of pulses with the same information on different frequencies then allows, in effect, the achievement of what might be called in-band frequency diversity.

Figure 7 illustrates the time gating concept with M'ary FSK. The four frequencies, f_1 , f_2 , f_3 , and f_4 , are utilized. Under flat fading conditions, the received envelope would be flat, as indicated in the top illustration. With selective fading, the received waveform, consisting of a sequence of pulses centered at a randomly-selected set of frequencies from f_1 , f_2 , f_3 , and f_4 would be received distorted, as shown in the middle illustration. The central portions of the pulses represent the strengths that a received carrier would have at the same transmitted frequency. After time gating, a set of rectangular pulses is obtained, as shown in the bottom illustration. The potentialities for signal diversity are clearly evident.

Another approach to achieving signal diversity is to use different time-frequency patterns of pulses to represent different symbols of a higher-order alphabet. If the patterns are chosen to have few pulses in common, the decision variables will be found to contain the sum of energies from pulses at several frequencies, providing in-band diversity. This has apparently not been implemented for coherent systems.

With noncoherent reception and slightly distorted pulses, M'ary FSK may be employed to increase data rate. As with coherent reception, signal diversity can be achieved by repeating the same information at different frequencies. Such a scheme has been implemented using incoherent binary FSK for troposcatter links [51]. The same binary FSK information was repeated at different frequencies until the allocated bandwidth was covered. The use of time-frequency patterns has also been implemented for troposcatter links with noncoherent detection [52], [53]. Maximum data rates of around 1 Mb/s were achieved with these techniques. Figure 8 shows the M'ary frequency time pattern used in [52]. Each pattern contains four pulses of different frequencies, and no two patterns overlap in more than one location, yielding a potential for third-order signal diversity (see the analysis in [15]).

A differentially-coherent modem approach is also possible with slightly distorted pulses. A reference pulse is needed for the differential PSK demodulation which reduces the data rate packing over FSK, but M'ary DPSK may be used to increase the data rate.

3.4 Modem Techniques for Increased Bandwidth Utilization With Constant Envelope Transmission Constraint: Highly Distorted Pulse Case

Instead of attempting to design signaling waveforms containing pulses that will be slightly distorted by the channel, one may attempt to use narrow pulses which will be highly distorted by the channel and devise demodulation procedures which can take advantage of this distortion. We demonstrate first that a highly distorted received pulse can potentially provide whatever signal diversity is implicit in the frequency selectivity existing over the frequency band occupied by the pulse.

For the techniques of interest, the energy in a received pulse has a dominant effect on the signal strength at the detector output. For a transmitted pulse s(t) with spectrum S(f), this energy is given by

$$s = \int |S(f)|^2 |T(f,t_0)|^2 df$$

where we have represented the channel by the "snapshot" of the time-variant transfer function applicable to the time of arrival of the received pulse. This approximation is valid provided the channel changes little in a time interval of the order of a pulse duration—a reasonable assumption for the channels in Table 1 for the data rates of interest.

Assuming $T(f,t_0)$ is a complex Gaussian process in f, standard orthogonal expansions [54] yield an alternate expression for δ as

$$s = \sum \lambda_k |g_k|^2 \tag{21}$$

where the $\{g_k\}$ are independent complex Gaussian variables of unit strength and λ_k are positive numbers equal to eigenvalues of an appropriate integral equation. The diversity action is evident by comparing this term with the signal term in predetection diversity combining in (14).

To proceed on a more intuitive basis, however, we may apply the sampling theorem to (20) to show that

$$s = \frac{1}{T_0} \sum_{n} \left| s\left(\frac{n}{T_0}\right) \right|^2 \left| T\left(\frac{n}{T_0}, t_0\right) \right|^2$$
(22)

where T₀ is the duration of the received pulse. We see from (22) that the energy of the received pulse is proportional to the sum of squared samples of the transfer function in the frequency domain weighted by the pulse energy density spectrum. From examination of Figure 5 we see that this gives a physical picture of the signal diversity as an "in-band" frequency diversity.

The use of pulses which become highly distorted implies that the received pulse becomes perceptibly lengthened by the impulse response of the channel. Thus, if L_{tot} is a multipath spread parameter defined as the "total" duration of the impulse response, and T is the transmitted pulse duration,

$$T_0 = T + L_{tot}$$
 (23)

is the received pulse duration. Consequently, if a sequence of pulses of duration T is to be transmitted continuously, there will be considerable intersymbol interference unless successive pulses occupy different frequency bands. Strictly speaking, not only is the pulse duration broadened, but also the received pulse bandwidth, because of the channel Doppler spread. Defining the Doppler spread parameter B_{tot} as the "total" bandwidth occupancy of a received carrier, we see that a received pulse will have the bandwidth

$$W_0 = W + B_{tot}$$
 (24)

where W is the transmitted pulse bandwidth. In most applications of interest,

$$W \gg B_{tot}$$
 (25)

so the pulse bandwidth broadening is small.

Returning to the categorization in Figure 6, we note that three reception techniques may generally be employed when highly distorted signaling pulses are used: coherent detection, energy detection, and differentially coherent detection. In the energy detection approach, the allocated bandwidth is conceived divided into frequency bands equal to the bandwidth of the received pulse W_0 , and time is divided into intervals of duration T_0 . However, it is clear that to avoid intersymbol interference with continuous transmission, constraints must be applied on the use of frequency slots for successive transmitted pulses. With due attention to this constraint, one may employ M'ary FSK or higher-order alphabets with time-frequency patterns of pulses.

Figure 9 illustrates the constraint problem with a simple example. It is assumed that $L_{\rm tot}$ = T so that T₀ = 2T. With a bandwidth allocation equal to $4W_0$, a continuous transmission in a binary FSK energy detection format is possible, as shown. The Mark and Space frequency bands for odd-numbered transmitted pulses are the lower two frequency bands of the four in the allocated bandwidth, while the even-numbered pulses use the upper two bands. The data sequence shown is MSS. Note that the data rate achieved with this approach is 1/T bits/sec with a bandwidth occupancy of $4W_0$. Assuming $W_0 \sim W$, this is a data rate packing of 1/4TW bits/sec/Hz. In detection, time gates of duration T₀ = 2T are applied following appropriate bandpass filters.* Computation of the energy in the gated waveform would provide the decision variables. Thus, for the first pulse in Figure 9, the Mark Filter time gate output would contain signal-plus-noise

*Any pulse stretching caused by the bandpass filters must be regarded as part of the channel and included in Ltot.

$$w_{M}(t) = r(t) + n_{M}(t)$$
 (26)

while the Space Filter output would contain noise alone,

$$w_{S}(t) = n_{S}(t) \tag{27}$$

An error would occur for the event

$$\int |r(t) + n_{M}(t)|^{2} dt - \int |n_{S}|^{2} dt < 0$$
 (28)

Expanding the square in the first term, this inequality becomes

$$\int |\mathbf{r}(t)|^2 dt + \text{noise terms} < 0$$
 (29)

which explicitly exhibits the signal diversity. Reference [42] examines theoretically the performance of an energy detection FSK modem for troposcatter links.

Provided the channel impulse response changes slowly enough, one may also use a differentially-coherent modem approach with highly distorted pulses. The available bandwidth is still divided up into frequency slots as described above, and the same constraints exist on the use of frequencies on successive time slots to avoid intersymbol interference. However, since the reference pulse for the differentially-coherent detection must operate on the same frequency, the described constraints on use of frequencies will result in the reference pulse being separated one or more time slots instead of being adjacent, as in the case of slightly distorted pulses. While two pulses are required to transmit information instead of one, as in the energy detection case, one may impress quaternary or higher-level DPSK modulation to increase the data rate. Also, FSK can be combined with the DPSK to make better use of the available bandwidth.

Figure 10 illustrates a simple format. The received pulse duration T_0 = 2T as in Figure 9, but now we assume half the available bandwidth = $2w_0$. Even-numbered data pulses use the bottom frequency slot, and odd-numbered pulses use the upper frequency slot. Referring to Figure 10 and the odd-numbered pulses, we note that received pulse 1 must act as a phase reference for received pulse 3, received pulse 3 must be a phase reference for received pulse 5, etc. An analogous procedure applies to the even-numbered pulses. If we assume quaternary DPSK, we see that (neglecting the initial reference pulses) the data rate is 2/T bits/sec for an occupied bandwidth of $2w_0 \approx 2w$, or a data rate packing of 1/Tw bits/sec/Hz.

In detection, received pulses are extracted as in the energy detection case, with a bandpass filter and a time gate. Thus, the received pulse corresponding to transmitted pulse 1 would take the form

$$w_1(t) = e^{j\gamma_1} r(t) + n_1(t)$$
 (30)

while that received due to pulse 3 would take the form

$$w_3(t) = e^{j\gamma_3}r(t) + n_3(t)$$
 (31)

where $n_1(t)$ and $n_3(t)$ are independent noises and γ_1 and γ_3 are the impressed data phase shifts. For quaternary DPSK,

$$e^{j(\gamma_3 - \gamma_1)} = \pm \frac{1}{\sqrt{2}} \pm \frac{j}{\sqrt{2}}$$
 (32)

The detection procedure involves the computation of real and imaginary parts of the complex integral

$$I_3 = \int w_3 w_1^*(t) dt$$
 (33)

To illustrate, suppose that

$$e^{j(\gamma_3 - \gamma_1)} = \frac{1}{\sqrt{2}} + j\frac{1}{\sqrt{2}}$$
 (34)

and error would occur if

Re
$$\{\int w_3(t)w_1^*(t) dt\} < 0$$
 (35)

or

Im
$$\{\int w_3(t)w_1^*(t) dt\} < 0$$
 (36)

Since the noises are randomly phased, we may rewrite the integral (33) in the form

$$I = e^{\int (\gamma_3 - \gamma_1)} \int [r(t) + n_3(t)][r^*(t) + n_1^*(t)] dt$$

$$= \left(\frac{1}{\sqrt{2}} + j \frac{1}{\sqrt{2}}\right) \int |r(t)|^2 dt + \text{noise terms}$$
(37)

which explicitly indicates the signal diversity effect.

We turn now to the use of coherent detection methods with highly distorted pulses. These methods are of considerable current interest for troposcatter links and several of the approaches have been implemented. The coherent detection techniques are first subdivided into those which combat intersymbol interference and those which do not. We consider the latter first.

In the latter case, the signal formats have the same general structure as for energy detection and differentially-coherent detection since the latter assumed no intersymbol interference. That is to say, the available bandwidth is assumed divided into slots of bandwidth W_0 and the time into intervals of duration T_0 . The main task here is the establishment of a good phase reference for the coherent detection. Two types of techniques have been used:

- · Decision-directed data modulation elimination
- · Pilot or sounding signal transmission.

In their troposcatter modem DAR-IV [55], Raytheon has used 4-PSK modulation. A phase reference was established by decision-directed removal of the 4-PSK modulation from the received pulses, followed by a recirculating delay line which averaged over enough pulses to produce a reference pulse with small enough noise not to affect error rate perceptibly by comparison to the noise on the data pulse. Their modem was not operated CW to avoid intersymbol interference. By using two frequency bands, however, in exactly the same format as shown in Figure 10 for the DPSK system, CW operation of the power amplifier can be used. However, separate channel measurements would be required for each frequency band. It is important to note that, when decision-directed extraction of a phase reference is used, a 90° ambiguity exists at the receiver which can be resolved by a differential encoding of the input bits in pairs. A penalty associated with differential encoding is a doubling of the error rate.

Assuming the format shown in Figure 10, the received waveforms have the same structure as in (30) and (31), but now

$$e^{\mathbf{j}\gamma_n} = \pm \frac{1}{\sqrt{2}} \pm \frac{\mathbf{j}}{\sqrt{2}} \tag{38}$$

since the recirculating delay line extracts the pulse r(t) which contains the phase reference. Assuming ideal extraction of r(t), the detection procedure involves computation of the Real and Imaginary parts of the complex integral

$$I_{1} = \int r^{*}(t)w_{1}(t) dt$$

$$= e^{j\gamma_{1}} \int |r(t)|^{2} dt + \int \gamma^{*}(t)n_{1}(t) dt$$
(39)

which, as in the previous cases, exhibits the signal diversity. The integral (39) is identical to the operation of the ideal "matched" filter received providing minimum error rate.

For the discussed signal structure (Figure 10), we have a data rate packing of 1/TW bits/sec/Hz. While we have illustrated a simple signal structure, it should be clear that more general structures can be used combining FSK and PSK in addition to higher alphabets with time-frequency patterns.

We turn now to techniques which operate in the presence of intersymbol interference. In these systems, the maximum data rate is achieved by allowing the received pulse to occupy the full bandwidth and using at least 4 PSK. The resulting data rate packing would be 2/TW bits/sec/Hz, assuming $W_0 \sim W$ as in the other cases. The smaller T is in relation to L_{tot} , however, the higher the complexity of the demodulator. In Figure 6 we have shown these techniques divided into three classes: adaptive maximum likelihood, adaptive equalizers, and (adaptive) hybrid schemes, combining both of the latter two approaches. We consider first the adaptive maximum likelihood receiver, which for additive white Gaussian noise provides minimum error probability in demodulating data sequences.

A brief theoretical discussion will be presented first. Assume, temporarily, that the channel is known, so that to each possible sequence of transmitted data $\mathbf{z}_n(t)$ there is a corresponding known received pulse train $\mathbf{w}_n(t)$. The actual received pulse train consists of the sum of signal and noise

$$w(t) = w_n(t) + \eta(t)$$
 (40)

Assuming equally likely transmitted sequences and white Gaussian noise, it is well-known that the receiver operation which minimizes the probability of selecting the wrong sequence of data as having been transmitted (also called the maximum likelihood receiver) involves the computation of the "distances" or "metrics":

$$M_{p} = \int |w(t) - w_{p}(t)|^{2} dt$$
 (41)

for all p, and selection of $z_m(t)$ as having been transmitted if $M_m < M_p$, for all p $\neq m$. Since there is a one-to-one correspondence between the information data sequence and each modulated signal $z_m(t)$, specification of $z_m(t)$ is equivalent to specifying the data sequence.

Two observations are in order here:

- ullet The complexity involved in direct computation of the distances $M_{\mbox{\scriptsize p}}$ grows exponentially with the length of the data sequence.
- If the channel is time-variant, it must be continually measured so that the correspondence between $z_n(t)$ and $w_n(t)$ is known at all times.

Forney [56] and Kobayashi [57] have shown that, in the case of a channel describable by a finite number of states, the complexity of the optimum receiver operation need not grow exponentially with the length of the data sequence if use is made of the Viterbi algorithm [58]. This algorithm is used in the MLT-1, a troposcatter modem built by CNR, Inc. [59], [60].

As discussed above, channel measurements may be obtained either by use of the received demodulated data signal alone in a decision-directed adaptive filter technique or else by direct use of a probing signal. In the MLT-1, a special probing signal is included in the transmitted signal structure for use in channel measurements and bit timing extraction at the receiver.

To gain insight as to the reason why signal diversity is achieved with the use of maximum likelihood demodulation, one notes that the probability of bit error for a minimum error probability receiver is closely approximated by the value [56]

$$P_{e} = C_{\phi} \left(\frac{d_{\min}}{2\sqrt{N_{0}}} \right) \tag{42}$$

where

$$\varphi(\alpha) = \int_{\alpha}^{\infty} \frac{1}{\sqrt{2\pi}} \exp\left(\frac{-y^2}{2}\right) dy \tag{43}$$

C is a constant, and dmin is the complex minimum distance between two received sequences,

$$d_{\min}^{2} = \min_{p,q} \int |w_{p}(t) - w_{q}(t)|^{2} dt; p \neq q$$
 (44)

Let the transmitted signal be given by

$$z(t) = \sum a_k s(t - kT)$$
 (45)

where a_k takes on a discrete set of values according to the information sequence, and s(t) is the transmitted pulse shape of duration T. As above, we assume a dispersive channel in which the transmission of s(t) produces the received pulse r(t). It is assumed that the channel is fading slow enough that this received pulse shape does not change significantly over the time interval required to implement a digital decision. With these definitions, the minimum distance can be expressed as

$$d_{\min}^{2} = \min_{p,q} \int |\Sigma [a_{k}^{(p)} - a_{k}^{(q)}] r(t - kT)|^{2} dt$$
 (46)

where $\{a_k^{(p)}\}$ is the set of transmitted pulse amplitudes for the p'th sequence, and $\{a_k^{(q)}\}$ is the set for the q'th sequence.

The sequence

$$e_k = a_k^{(p)} - a_k^{(q)}$$
 (47)

is called the error sequence. For a given channel pulse response r(t), there will be a worst-case error sequence which produces the minimum distance. We define the spectrum of the error sequence E(f) as the spectrum of the error impulse train e(t),

$$e(t) = \sum e_k \delta(t - kT)$$
 (48)

$$E(f) = \sum e_k e^{j2\pi fkT}$$
 (49)

The minimum distance can be expressed in the frequency domain by Parseval's theorem

as

$$d_{\min}^{2} = \int |E(f)|^{2} |S(f)|^{2} |T(f,t_{0})|^{2} df$$
 (50)

where S(f) is the spectrum of the transmitted pulse s(t), and $T(f,t_0)$ is the transfer function of the channel (snapshot). The signal diversity is evident by comparing (50) with (20). In the case where the minimum distance sequence corresponds to pulse trains differing only in one time slot, d_{\min} becomes directly proportional to δ in (20). As a matter of fact, simulations of MLT-1 and measured performance in troposcatter links indicate that the minimum distance sequence is usually of this form. Thus, a performance close to that of the technique described above, not having intersymbol interference, is achieved. However, the data rate packing is twice as much for the present technique.

An alternate technique to combat intersymbol interference is the adaptive equalizer, which has had considerable interest and application on telephone lines. More recently, is has been applied by Sylvania to the troposcatter channel [61], and some years ago it was applied to the HF channel [62]. Instead of trying to minimize the error rate, the adaptive equalizer approach attempts to minimize the mean-squared error between the received decision variables and the idealized noise-free decision variables. For difficult channels, a "tail cancellation" scheme is added to the normal equalizer configuration that attempts to remove intersymbol interference due to past decisions by assuming the latter were correct and using the current estimate of the channel impulse response. Systems which employ this cancellation scheme are called decision feedback or nonlinear feedback equalizers. Theoretical analysis of the performance of feedback equalizers on slowly fading dispersive channels has been carried out [63], and simulations [64] indicate that under ideal conditions of no feedback errors and perfect adaptation, the equalizer shows a performance close to that of the intersymbol interference-free case. However, there is no simple analytical argument demonstrating this equivalence as for the other systems described.

As the intersymbol interference expressed in units of transmitted pulse width increases, the complexity of the minimum error probability receiver increases exponentially while the adaptive equalizer receiver complexity only increases linearly. For this reason, there has been interest [65] in combining the two types of receivers for telephone lines. The equalizer would reduce the effective impulse response duration to an amount that could be handled without undue complexity by the Viterbi algorithm portion of the receiver. Apparently, such hybrid systems have not yet been applied to fading dispersive radio channels.

3.5 Application of Error-Correction Coding

One of the most promising new areas of signal design for fading dispersive channels of all types and radio channels in particular is the use of error-correction coding. Unfortunately, this fact appears to be little appreciated by system designers. In this concluding section of our review, we will provide an intuitive grasp of the reasons why error-correction coding can provide considerable benefits. Work in this area has been innovated mainly by David Chase [66] — [73]. Reference [69] provides a concise summary of some applications of this work.

The considerable performance improvements possible with coding may be traced primarily to the high orders of signal diversity achieved with no loss in data rate beyond the normal redundancy of the code, e.g., rate-1/2. The signal diversity achieved may be either of two types, (in-band) time or frequency diversity (or both). Normal application of time or frequency diversity, where the bandwidth allocation is fixed, results in a reduction in data rate proportional to the order of diversity achieved. Thus, for example, to achieve eighth-order time diversity straightforwardly involves repeating the same information eight times at sufficiently widely separated time instants that independent fading occurs. In such a case, the data rate is reduced by a factor of eight. With a sufficiently good code and decoding procedure, this eighth-order time diversity can be achieved with a data rate reduction of, at most, 1/2, corresponding to use of a rate-1/2 code. Even smaller rate reductions are possible. In an entirely dual sense, if data is being transmitted by

parallel frequency-division-multiplexed subcarriers, one may transmit the same information on eight subcarriers and achieve eighth-order diversity with an eightfold reduction in data rate. Or, properly using error-correction coding across the subchannels, eighth-order diversity can be obtained with a data rate reduction of, at most, 1/2.

From a <u>system design</u> point of view, an important byproduct of the high order of signal diversity is that irreducible error probability effects, due to whatever cause, become virtually eliminated in most cases, and the codem (coder-decoder-modem) produces very robust performance. Selection of modems or other system elements is then on the basis of preferring best uncoded performance at higher error rates than usual. This can significantly modify an overall system design. Examples of such impact are suggested by Chase in [69]. To quote:

"Once the benefits of coding are under consideration, several conventional communication concepts may be questioned. For the HF channel, operation just below MUF frequency (low multipath case) may no longer be the best operating frequency. For the troposcatter channel, the conventional use of quad diversity links may not be required in light of the possible coding performance gains. Similarly, for the aerosat channel, the design of a narrow beam antenna to eliminate the (detrimental) effects of scatter energy may not actually be required."

One point should be raised. The use of this coding approach to achieve time diversity introduces a time delay resulting from the interleaving of code bits. Each system must be examined to see if the time delay is tolerable. However, even a small amount of time delay relative to the fading correlation time can result in considerable benefits [60].

We now consider briefly the intuitive basis for the large signal diversity possible with error-correction coding. Consider a system in which error-correction coding in time is employed in conjunction with a PSK modem that uses highly distorted pulses and maximum likelihood decoding. For simplicity, we assume binary PSK. Interleaving of code bits is employed to provide as much independence of fading on these bits as possible. As in (45), the transmitted waveform for the q'th data sequence $\{a_k^{(q)}\}$ takes the form

$$z^{(q)}(t) = \sum a_k^{(q)} s(t - kT)$$
 (51)

The corresponding received waveform is given by

$$w^{q}(t) = \sum a_{k}^{(q)} r_{k}(t - kT)$$
 (52)

where

$$r_{k}(t) = \int s(t-\xi)g(kT,\xi) d\xi$$

$$= \int S(f)T(f,kT)e^{j2\pi ft} dt$$
(53)

is the received pulse shape corresponding to the k'th transmitted pulse shape. We have assumed that the channel changes little over a received pulse duration and replaced the impulse response and transfer function by snapshots. Assuming code bits far enough apart in time, $r_k(t)$ will be independent of $r_l(t)$ if $a_k^{(q)}$ and $a_l^{(q)}$ are connected with different code bits.

As discussed previously, the error rate is controlled by the minimum distance (44) as used in (42). To find the minimum distance, we can make all code blocks have the same code, except for one code block. Then, using (52) in (44),

$$d_{\min}^{2} = \min_{\substack{p,q \\ \text{(over a codeword)}}} \int |\Sigma[a_{k}^{(p)} - a_{k}^{(q)}] r_{k}(t-kT)|^{2} dt$$
 (54)

Coding places a lower bound on the number of places in which two codewords $a_k^{(p)}$ and $a_k^{(q)}$ can differ. If the codewords differ in at least d places, then there will be at least d places in (54) where $a_k^{(p)}$ - $a_k^{(q)}$ differs from zero. Noting that pulses corresponding to code bits will be separated in time due to the interleaving, we see that (54) becomes

$$d_{\min}^{2} = 4 \sum_{\text{(d terms)}} \int |r_{k}(t)|^{2} dt ; k \text{ selected from c places in which codewords differ}$$
 (55)

Equation (55) is exactly the form that the optimum matched filter receiver would have for distorted pulses if d'th-order time diversity were used. Note that the term $\int |\mathbf{r}_{\mathbf{k}}(t)|^2 dt$ supplies signal diversity also from the frequency selectivity of the channel, as discussed in the preceding section.

It has been implicit in the above discussion that optimum maximum likelihood decoding of the block codes was employed. In the past, such decoding has been of academic interest because of the impossible complexity involved. However, it has been one of the major achievements of Chase [73] that he has developed practical soft decoding algorithms (i.e., decoding procedures using decision variable information) which come close to maximum likelihood decoding. Hard decoding may also be used, but the diversity benefits are less [73].

In closing this section we present some theoretical error rate curves in Figure 11 to illustrate the benefits of error-correction coding. Error rate is plotted versus total SNR* for maximal ratio predetection combining of PSK with diversity ranging up to eighth order for an assumed flat fading channel. The error rate is also shown for an interleaved (24,12) Golay code (minimum distance 8) with conventional hard decoding applied to a single channel (i.e., nondiversity operation). With hard decoding, the performance has the asymptotic slope of the error rate vs. SNR which is the same as the fourth-order diversity curve.

Also shown is the soft decoding performance for the (24,12) code using nondiversity operation. The decoding technique is one developed by Chase [73, Algorithm 2]. Note that the performance of this error-correction coding arrangement with nondiversity operation is superior to eighth-order diversity operation without coding. It is also less than a dB worse than the error rate on a nonfading channel. Finally, a curve is also presented of the (24,12) code with channel measurement decoding over the nonfading channel. This is the limiting performance that would be achieved if the soft decision (24,12) coder-decoder were used in conjunction with enough in-band frequency diversity and space diversity.

CNR has implemented the (24,12) code with hard decision decoding [60] to work with their MLT-1 troposcatter digital modem. Future work for Rome Air Development Center will involve implementing soft decision decoding.

3.6 Items Neglected

Unfortunately, time limitations prevent this review from covering all of the topics of interest to signal processing in scatter communications. A complete list would include the following items:

- · Techniques employing feedback links
- Interaction of transmitter nonlinearities with signal design to minimize bandwidth occupancy
- Preamble design techniques for signal detection, Doppler acquisition, and frame sync acquisition
- Tracking techniques for frame sync and Doppler acquisition
- · Techniques to counter noise disturbances
- Spread spectrum systems
- Modem tradeoffs due to constraints implied by the existing inventory of radios.

Perhaps these topics will be covered elsewhere in this conference.

 $^{^{*}(}E_{b}/N_{0})_{TOTAL}$ corresponds to energy-per-bit over noise power density for all diversity channels. It is also the total signal power to noise power in a bandwidth equal to the bit rate.

REFERENCES

- P. A. Bello, "Characterization of Random Time-Variant Linear Channels," <u>IRE Trans.</u> on Communication Systems, Vol. CS-11, pp. 360 393, December 1963.
- [2] D. K. Bailey, "The Effect of Multipath Distortion on the Choice of Operating Frequencies for High-Frequency Communication Circuits," <u>IRE Trans. on Antennas and Propagation</u>, pp. 397 404, October 1959.
- [3] R. K. Salaman, "A New Ionospheric Multipath Reduction Factor (MUF)," <u>IRE Trans. on Communication Systems</u>, Vol. CS-10, June 1962.
- [4] R. A. Shepard, B. C. Tupper, and J. B. Lomax, "HF Data Compendium; Power Spectra and Oblique Ionograms," Stanford Research Institute, Menlo Park, California.
- [5] R. A. Shepard and J. B. Lomax, "Frequency Spread in Ionospheric Radio Propagation," <u>IEEE Trans. on Communications Technology</u>, Vol. 15, No. 2, pp. 268 - 275, April 1967.
- [6] L. W. Pickering, "The Calculation of Ionospheric Doppler Spread on HF Communication Channels," <u>IEEE Trans. on Communication</u>, May 1975.
- [7] J. B. Lomax, "Spread-F in the Pacific," in <u>Spread-F and Its Effect Upon Radiowave Communications</u>, P. Newman (ed.), Agardograph 95, p. 35, 1966.
- [8] C. C. Watterson, J. R. Juroshek, and W. D. Bensema, "Experimental Confirmation of an HF Channel Model," <u>IEEE Trans. on Communications Technology</u>, Vol. COM-18, No. 6, December 1970.
- [9] B. M. Sifford, et al., "HF Time- and Frequency-Dispersion Effects -- Experimental Validation of an FSK Error-Rate Model," Stanford Research Institute, Menlo Park, CA.
- [10] P. Beckmann and A. Spizzichino, The Scattering of Electromagnetic Waves from Rough Surfaces, Pergamon Press, 1963.
- [11] F. DuCastel, <u>Tropospheric Radiowave Propagation Beyond the Horizon</u>, Pergamon Press, p. 84, 1966.
- [12] P. A. Bello, "A Study of the Relationship Between Multipath Distortion and Wave Number Spectrum of Dielectric Noise in Radio Links," <u>Proc. IEEE</u>, Vol. 59, No. 1, pp. 47 75, January 1971.
- [13] P. A. Bello, "A Troposcatter Channel Model," <u>IEEE Trans. on Communications Technology</u>, Vol. COM-17, April 1969.
- [14] R. Branham, et al., "Correlation Bandwidth Measurements Over Troposcatter Paths," Technical Report ECOM-0251-F, June 1970.
- [15] P. A. Bello, L. Ehrman, and D. S. Arnstein, 'Modeling and Data Analysis Short and Medium Range Digital Troposcatter Tests," RADC Technical Report TR-69-233, Vol. 1, October 1969.
- [16] W. P. Birkmeir, et al., "A Comparison of Rake-Measurement Scattering Layer Signatures with Radiosonde Data," RADC-TR-74-17, February 1974.
- [17] L. G. Abraham, et al., "Tropospheric Scatter Multipath Tests," Technical Report No. 11, Communication Systems Lab., Sylvania Electronic Systems, Waltham, Mass., May 1967.
- [18] A. B. Crawford, D. C. Hogg, and W. H. Kammer, "Studies in Tropospheric Propagation Beyond the Horizon," Bell Telephone System Monograph 3340, 17 April 1959.
- [19] A. Sherwood and L. Suyemoto, "Multipath Measurements Over Troposcatter Paths," The Mitre Corp., Report MTP-170, April 1976.
- [20] L. Ehrman and J. W. Graham, "Digital Troposcatter Experiments," RADC-TR-72-350, January 1973.
- [21] H. Staras, "Rough Surface Scattering on a Communication Link," Radio Science, Vol. 3, No. 6, pp. 623 631, June 1968.
- [22] S. H. Durrani and H. Staras, "Multipath Problems in Communications Between Low-Altitude Spacecraft and Stationary Satellites," RCA Review, pp. 77-105, March 1968.

- [23] J. K. DeRosa, "On the Determination of the Delay Doppler Scattering Function for a Ground-to-Aircraft Link," <u>Symposium Digest</u>, 1970 Canadian Symposium on Communications, 12 - 13 November 1970.
- [24] K. L. Jordan, Jr., "Measurement of Multipath Effects in a Satellite-Aircraft UHF Link," Proc. IEEE, pp. 1117 - 1118, June 1967.
- [25] P. A. Bello, "Aeronautical Channel Characterization," <u>IEEE Trans. on Communication</u>, pp. 548 - 563, May 1973.
- [26] R. W. Sutton, et al., "Satellite-Aircraft Multipath and Ranging Experimental Results at L-Band," <u>IEEE Trans. on Communication</u>, pp. 639 - 647, May 1973.
- [27] J. F. Ossana, Jr., "A Model for Mobile Radio Fading Due to Building Reflection: Theoretical and Experimental Fading Waveform Power Spectra," <u>BSTJ</u>, Vol. 43, pp. 2935 - 2971, 1964.
- [28] R. H. Clarke, "A Statistical Theory of Mobile Radio Reception," <u>BSTJ</u>, Vol. 47, pp. 957 1000, 1968.
- [29] E. N. Gilbert, "Mobile Radio Diversity Reception," BSTJ, Vol. 48, pp. 2473 2492, 1969.
- [30] H. F. Schuld, "A Prediction Model for Multipath Propagation of Pulse Signals at VHF and UHF Over Irregular Terrain," <u>IEEE Trans. on Antennas and Propagation</u>, Vol. AP-18, pp. 253 - 258, 1970.
- [31] W. R. Young, Jr., and L. Y. Lacey, "Echoes in Transmission at 450 MHz from Land to Car Radio Units," Proc. IRE, Vol. 38, pp. 255 258, 1950.
- [32] G. L. Turin, et al., "A Statistical Model of Urban Multipath Propagation," Report on Grant H-1030 Project DC-D6-1, Teknekion, Inc., Berkeley, California, 1970.
- [33] P. C. Cox, "Correlation Bandwidth and Delay Spread Multipath Propagation Statistics for 910 MHz Urban Mobile Radio Channels," <u>IEEE Trans. on Communication</u>, Vol. COM-23, No. 11, November 1975.
- [34] W. C. Jakes, Microwave Mobile Communications, J. Wiley and Sons, 1974.
- [35] H. Suzuki, "A Statistical Model for Urban Radio Propagation," <u>IEEE Trans. on Communication</u>, Vol. COM-25, No. 7, pp. 673 680, July 1977.
- [36] M. D. Grossi and A. Jared, "Time and Frequency Spread in Meteor Burst Propagation Paths," Paper to be Presented at AGARD-Electromagnetic Wave Propagation Panel, 23rd Symposium on Aspects of EM Wave Scattering in Radio Communications, 3-7 October 1977.
- [37] F. Akram, et al., "Impulse Response of a Meteor Burst Communications Channel Determined by Ray-Tracing Techniques," <u>IEEE Trans. on Communication</u>, pp. 467-470, Apr. 1977.
- [38] P. A. Bello and B. D. Nelin, "The Influence of Fading Spectrum on the Binary Error Probabilities of Incoherent and Differentially-Coherent Matched Filter Receivers," IRE Trans. on Communication Systems, Vol. CS-10, No. 2, pp. 160-168, June 1962.
- [39] P. A. Bello, "Selective Fading Limitations of the Kathryn Modem and Some System Design Considerations," <u>IEEE Trans. on Communications Technology</u>, Vol. COM-13, No. 3, pp. 320 - 333, September 1965.
- [40] P. A. Bello and B. D. Nelin, "Predetection Diversity Combining With Selectively Fading Channels," <u>IRE Trans. on Communication Systems</u>, Vol. CS-10, No. 1, pp. 32-42, March 1962.
- [41] P. A. Bello and B. D. Nelin, "The Effect of Frequency-Selective Fading on the Binary Error Probabilities of Incoherent and Differentially-Coherent Match Filter Receivers," IEEE Trans.on Communication Systems, Vol. CS-11, No. 2, pp. 170 186, June 1963.
- [42] P. A. Bello and L. Ehrman, "Performance of an Energy Detection FSK Digital Modem for Troposcatter Links," <u>IEEE Trans. on Communications Technology</u>, Vol. COM-17, No. 3, pp. 368 - 379, June 1969.
- [43] P. A. Bello and L. Ehrman, "Error Rates in Diversity FDM-FM Digital Troposcatter Transmission," <u>IEEE Trans. on Communications Technology</u>, Vol. COM-17, No. 2, pp. 183 191, April 1969.
- P. A. Bello and T. Crystal, "A Class of Efficient High-Speed Digital Modems for Tropo Links," <u>IEEE Trans. on Comm. Tech.</u>, V. COM-17, No. 2, pp. 162 183, April 1969.

- [45] P. A. Bello and B. D. Nelin, "The Effect of Frequency-Selective Fading on Intermodulation Distortion and Subcarrier Phase Stability in Frequency Modulation Systems," IEEE Trans. on Communication Systems, pp. 87 101, March 1964.
- [46] P. A. Bello and B. D. Nelin, "Optimization of Subchannel Data Rate in FDM-SSB Transmission Over Selectively Fading Media," <u>IEEE Trans. on Communication Systems</u>, pp. 46 - 53, March 1964.
- [47] M. Schwartz, W. P. Bennett, and S. Stein, <u>Communication Systems and Techniques</u>, <u>Part III</u>, McGraw-Hill, 1966.
- [48] Raytheon Co., PDC-4 Predetection Combiner.
- [49] Motorola Co., reference not yet located.
- [50] P. A. Bello and J. W. Graham, "A High-Speed TDM Coherent FSK/PSK Digital Data Modem for Troposcatter Links," <u>Record of the IEEE 1971 International Conference on Communications</u>, pp. 20-18 to 20-24.
- [51] The Motorola Deltaplex System Reference not yet located.
- [52] A. S. Salin, D. Y. Prihar, and R. Werlink, "Frequency Time Modulation for Digital Troposcatter Transmission," Final Report, ECOM-02174-F, May 1967.
- [53] T. Lerner and D. L. Nicholson, "The Performance of Coded Diversity Systems on a Slowly Fading Rayleigh Channel," <u>IEEE Trans. on Communication</u>, Vol. COM-21, No. 2, pp. 1-9 - 110, February 1973.
- [54] P. A. Bello, "Some Results on the Problem of Discriminating Between Two Gaussian Processes," <u>IEEE Prof. Group on Information Theory</u>, Vol. IT-7, No. 4, pp. 224 233, October 1961.
- [55] M. Unkauf, R. Bagnell, and O. A. Tagliaferri, "Tactical Tropo Performance of an Adaptive Receiver," MTC Conference Record, pp. 28-10 to 28-14, 1-3 December 1975.
- [56] G. D. Forney, Jr., "Maximum-Likelihood Sequence Estimation of Digital Sequences in the Presence of Intersymbol Interference," <u>IEEE Trans. on Information Theory</u>, Vol. IT-18, No. 3, May 1972.
- [57] H. Kobayashi, "Correlative Level Coding and Maximum-Likelihood Decoding," <u>IEEE Trans. on Information Theory</u>, Vol. IT-17, No. 5, September 1971.
- [58] A. J. Viterbi, "Error Bounds for Convolutional Codes and an Asymptotically Optimum Decoding Algorithm," <u>IEEE Trans. on Information Theory</u>, Vol. IT-13, April 1967.
- [59] P. A. Beilo and D. Chase, "A Combined Coding and Modulation Approach for High-Speed Data Transmission Over Troposcatter Channels," NTC Conference Record, pp. 28-20 to 28-24, 1-3 December 1975.
- [60] D. Chase, et al., "Troposcatter Interleaver," Final Technical Report by CNR on Contract F30602-74-C-0133 with RADC, RADC-TR-76-213, July 1976.
- [61] D. R. Kern, P. Monsen, and C. J. Grzenda, "Megabit Digital Troposcatter Subsystem," NTC Conference Record, pp. 28-15 to 28-19, 1-3 December 1975.
- [62] M. J. DiToro, "A New Method of High-Speed Adaptive Serial Communication Through Any Time-Variable and Dispersive Transmission Medium," <u>First Annual Communication</u> <u>Convention Record</u>, Boulder, Colorado, pp. 763 - 767, 7-9 June 1965.
- [63] P. Monsen, "Adaptive Equalization of the Slow Fading Channel," <u>IEEE Trans. on Communication</u>, pp. 1064 1075, August 1974.
- [64] P. Monsen, "Digital Transmission Performance on Fading Dispersive Channels," <u>IEEE Trans. on Communication</u>, pp. 33 39, January 1973.
- [65] D. D. Falconer and F. R. Magee, "Evaluation of Decision Feedback Equalization and Viterbi Algorithm Detection for Voiceband Data Transmission Part I," <u>IEEE Trans.</u> on Communication, Vol. COM-24, No. 10, pp. 1130 1139, October 1976.
- [66] D. Chase and L. J. Weng, "Multiple-Burst Correction Techniques for Slowly Fading Channels," <u>IEEE Trans. on Information Theory</u>, September 1976.

- [67] D. Chase, "Digital Signal Design Concepts for a Time-Varying Rician Channel," IEEE Trans. on Communications, February 1976.
- [68] D. Chase, "The Application of Error Correcting Coding for Troposcatter Links," Paper Presented at the IEEE International Conference on Communications, San Francisco, California, June 1975.
- [69] D. Chase, "Improved Signal Design for Fading Channels by Coding," Paper Presented at the IEEE International Conference on Communications, San Francisco, California, June 1975.
- [70] D. Chase and L. J. Weng, "Multiple-Burst Correction Techniques for Slowly Fading Channels," Paper Presented at the IEEE International Symposium on Information Theory, South Bend, Indiana, October 1974.
- [71] D. Chase, "The Applications of Codem Concepts for Communications Over the Aeronautical Channel," Paper Presented at the International Telemetering Conference, Washington, D.C., October 1973.
- [72] D. Chase, "A Combined Coding and Modulation Approach for Communications Over Dispersive Channels," <u>IEEE Trans. on Communications</u>, March 1973.
- [73] D. Chase, "A Class of Algorithms for Decoding Block Codes With Channel Measurement Information," <u>IEEE Trans. on Information Theory</u>, Vol. IT-18, January 1972.

Table 1 Some Values of Multipath and Doppler Spread for Several Fading Dispersive Radio Channels

Channe 1	Multipath Spread L	Doppler Spread B	Spread Factor BL	Comments and References
HF	0.1 - 5.0 ms	0.1 - 2.0 Hz	10 ⁻⁵ - 10 ⁻²	[2] - [9]. Does not include trans- auroral paths for which Doppler spread can increase by a factor of 10 [5]. BL = 10 ⁻⁵ applies to a single ray path.
Troposcatter	0.1 - 0.5 µs	0.1 - 20.0 Hz	10 ⁻⁸ - 10 ⁻⁵	[10] - [20]. UHF - C-Band, antenna sizes for tactical and strategic links.
Surface Scatter with LOS	10.0 - 50.0 µв	250 - 400 Hz	25 x 10 ⁻³ - 2 x 10 ⁻²	[13], [21] - [26]. Aircraft speed 380 knots, 10-km altitude, elevation angle to satellite 10° - 30°, omni antenna, 1.6 GHz.
Urban Mobile	up to 5.0 µs	70 Hz	Up to 3.5 x 10 ⁻⁴	[27] - [35]. 60 mph vehicle, 450 MHz, New York probably worst case.
Meteor Burst	0.1 - 10.0 µs	0.1 - 10.0 Hz	10 ⁻⁸ - 10 ⁻⁴	[36],[37]. At the start of the ionization trail, the multipath and Doppler spreads take the low values, and with time the spreads increase to the large values. Values cover first ten seconds of trail.

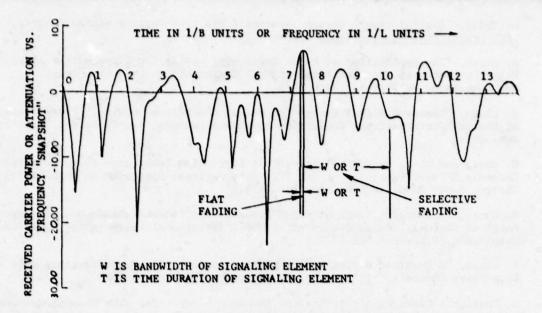


Figure 1 Illustration of Flat and Selective Fading in Time or Frequency Domain

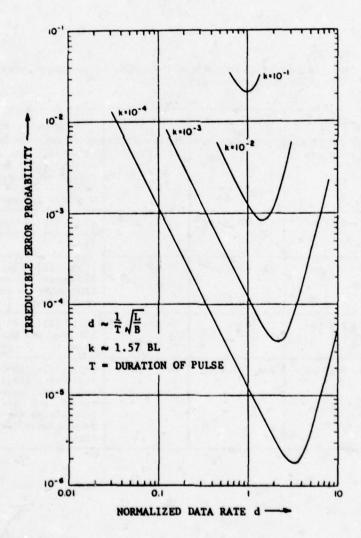


Figure 2 Irreducible Error Probability of Phase-Continuous FSK in the Presence of Multipath and Fast Fading (No additive noise and nondiversity operation; Gaussian shaped delay and Doppler power spectra)

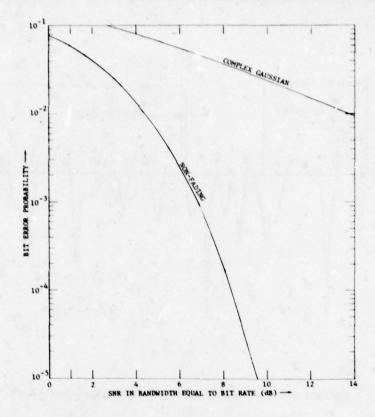


Figure 3 Error Rate vs. SNR of Ideal Binary PSK Modem for a Nonfading and a Complex Gaussian Fading Channel

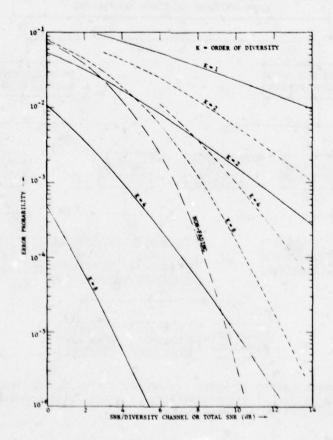


Figure 4 Error Rate vs. SNR per Diversity Channel for Predetection Maximal Ratio Diversity Combining of Binary PSK

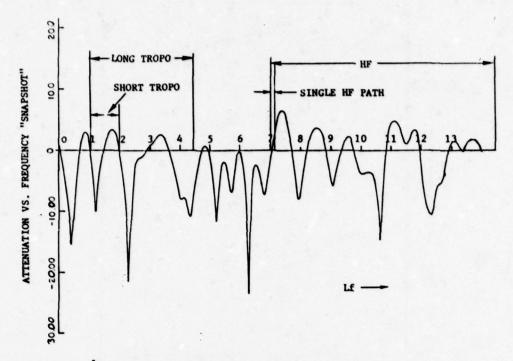


Figure 5 Channel Allocation in Units of Reciprocal Multipath Spread

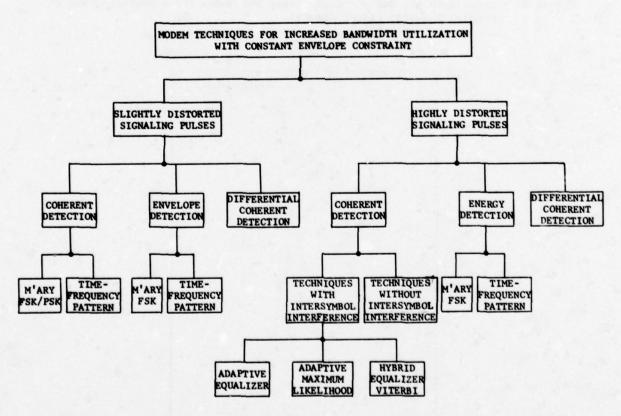


Figure 6 Categorization of Modem Techniques Useful for Increased Bandwidth Utilization of Dispersive Radio Channels with Constant Envelope Constraint on Radiated Power

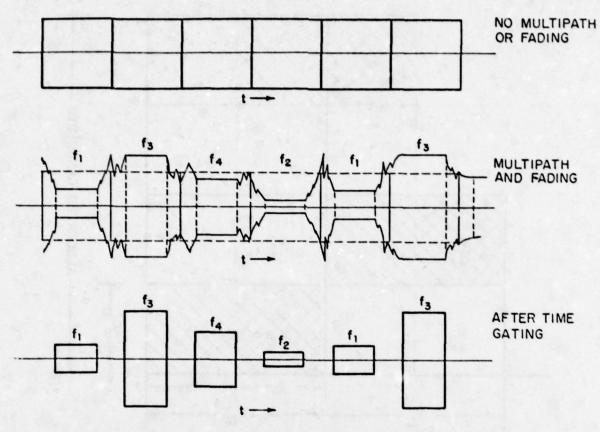


Figure 7 Illustration of Time Gating Concept with M'ary FSK

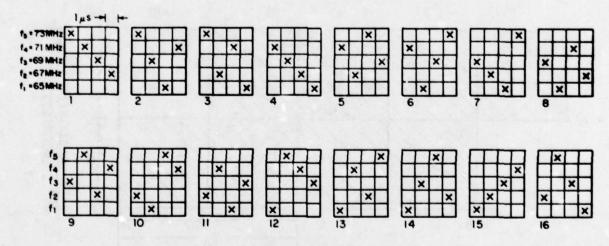


Figure 8 Martin Frequency-Time Pattern

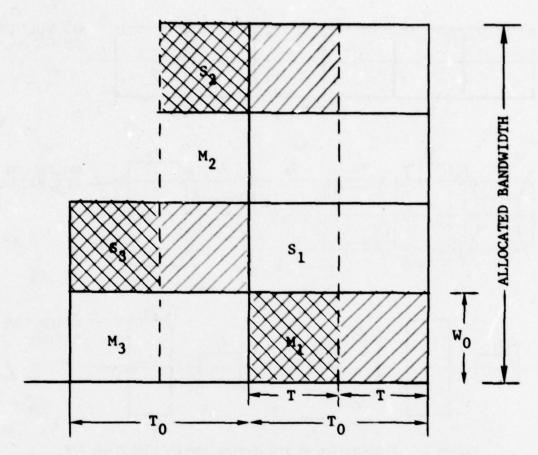


Figure 9 Illustration of Signal Format for Binary FSK with Energy Detection

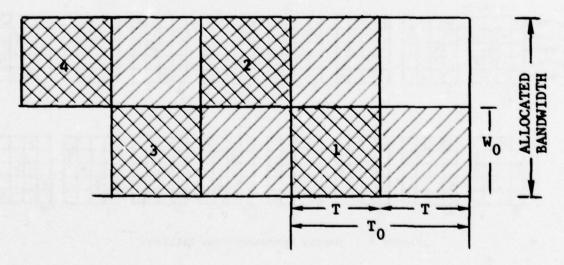


Figure 10 Illustration of a Signal Format for DPSK when Highly Distorted Pulses Are Used

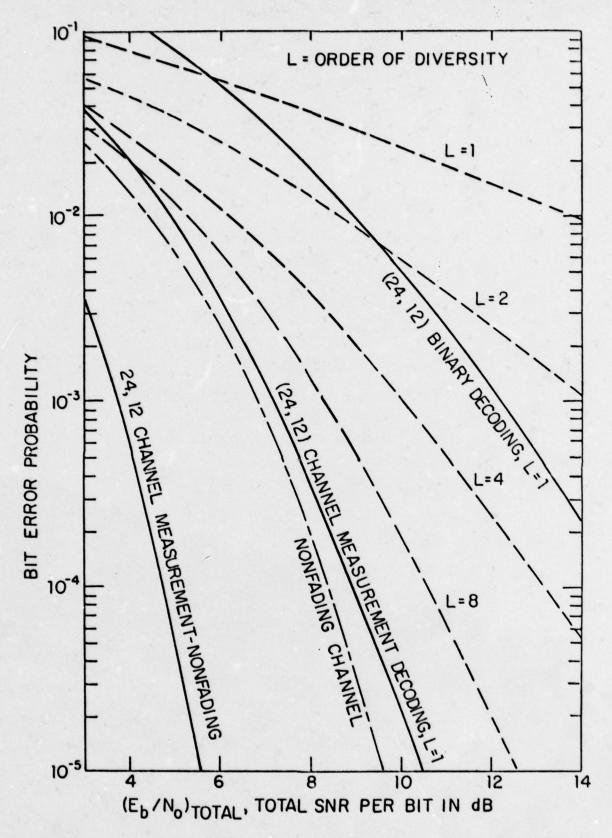


Figure 11 Comparison of the Interleaved (24,12) Golay Code with Binary and Channel Measurement Decoding to the Performance Possible by Predetection Maximal Ratio Combining (PSK Modulation)

MAXIMUM USABLE BANDWIDTH AND FREQUENCY DIVERSITY IN TROPOSCATTER COMMUNICATION

by

R. Valentin

Forschungsinstitut, Fernmeldetechnisches Zentralamt Darmstadt, Germany

ABSTRACT

Measurements concerning the maximum usable bandwidth as well as the frequency distance necessary for frequency diversity were performed on a 420-km tropospheric scatter path. A carrier frequency of 1.89 GHz and two side bands with variable frequency spacing up to 4 MHz were transmitted.

The received scatter-mode signals referring to the three different frequencies were correlated by means of an electronic correlator. Thus it was possible to obtain the frequency correlation function, which determines the maximum usable bandwidth and the frequency diversity spacing.

An analytic expression of the form

$$g(\Delta t) = N_{5/6} \left(\frac{\Delta t}{6 t} \right)$$

was fitted to the experimental results, where $N_{5/6}$ $\left(\frac{\Delta f}{\sigma f}\right)$ is the correlation function introduced into the scatter theory by Norton and defined for an arbitrary index γ by

$$N_{\gamma}\left(\frac{\Delta f}{\delta f}\right) = \frac{2}{\Gamma(\gamma)} \left(\frac{\Delta f}{\delta f}\right)^{\gamma} K_{\gamma}\left(\frac{\Delta f}{\delta f}\right)$$

 K_{γ} is the modified Bessel function of the order γ . δ_{f} is called frequency correlation width. It is dependent on the vertical correlation length l_{z} of the dielectric constant of the air in the common volume. The best agreement with the experimental results was obtained with a value of l_{z} of 9 m.

1. INTRODUCTION

In the frequency range of 1 to 10 GHz the operation of radio relay links far beyond the horizon depends mainly on the scattering of electromagnetic energy by the troposphere of the earth. The troposcatter is due to inhomogeneities in the dielectric constant of the air. The multipath propagation which is characteristic of the scatter mechanism results in statistical variations of the received radio field strength in space and time. Therefore the fade-out will rarely occur simultaneously if two receiving antennas are spaced at a certain distance. If two frequencies are transmitted and received by one receiving antenna, the fade-out of the signals referring to the two frequencies will also rarely happen simultaneously: the fading is frequency selective. This limits the bandwidth of a radio channel. The frequency correlation function is a measure of the unstable bandwidth of a fading radio channel. It also gives an indication how far apart inband frequency diversity channels must be spaced to obtain substantial diversity gain.

The two problems of finding the correlation of the field strength for two different receiving antennas spaced at a certain distance and the correlation for two different frequencies received with the same antenna are closely related to each other.

This paper is an enlargement of a former publication by Fehlhaber and Grosskopf dealing with the spatial structure of the scatter mode signal and the spatial correlation / 1 /. It is possible to obtain the frequency correlation from the spatial correlation on certain assumptions. Some qualitative conclusions about the extent of selec-

tive fading can already be drawn from the fact that multipath propagation is a characteristic of scatter. The greater the path differences due to the form and size of the common scatter volume are, the smaller will be the correlation of two signals at a fixed frequency separation.

That means: The fading at two different frequencies is the less correlated

- a) the larger the main lobes of the antennas (the smaller the diameter D)
- b) the larger the distance d between transmitter and receiver at a fixed scatter angle θ .
- c) the larger the scatter angle at a fixed distance d .

One can therefore expect, that the fading at two different frequencies is the less correlated the larger the value of

$$\frac{\theta \cdot d}{D}$$
 is.

That means that also the maximum usable bandwidth increases if the value of

$$\frac{D}{\theta \cdot d}$$
 increases.

More precise results for the frequency correlation should be given, now.

THE FREQUENCY CORRELATION FUNCTION

The similarity of the fading at two different frequencies is expressed by the frequency correlation function ρ (Δ f).

The general expression for the correlation function in the frequency domain is obtained from the fundamental expression for the scattered field E (k) resulting from the integral of elementary scattering elements / 1 /:

$$E(k) = -\frac{1}{4\pi} \int k^2 \cdot \xi' E_o \frac{e^{ikR_p}}{R_p} d^3 r \qquad (1)$$

where k is the wave number of the scattered field.

Then the non-normalized correlation function is

$$\rho_{c}(\Delta k) = E_{s}(k) \cdot E_{s}(k + \Delta k)$$
 (2)

The correlation of two fade signals at a frequency separation Δ f is closely related to the correlation of two signals received at two different antennas spaced at a vertical distance ζ / 2 /: In a range of frequency separations in which the inequality

$$\frac{\Delta f}{f} \ll 0.8 \frac{D^2}{\lambda \cdot d} \tag{3}$$

holds, the frequency separation Δ **f** is equivalent to a vertical antenna displacement of

$$\zeta = \frac{1}{2} \cdot \theta \cdot d \cdot \frac{\Delta f}{f}$$
 (4)

where D = antenna diameter

 λ = wave length

d = distance transmitter-receiver

f = frequency

 θ = scatter angle.

The quantity D^2/λ is the limit of the nearfield of the antenna. The ratio of the frequency difference Δ f to the frequency f must therefore be much smaller than the

ratio of the nearfield to the distance. Since D^2/λ is low for small antennas, the above equivalence theorem holds only for a narrow range of frequency spacings.

The spatial correlation function for small antennas was derived in /1/ and is given by

$$g_{c}(\zeta) = N_{5/6} \left(\frac{\zeta}{L_{z}}\right)$$
 (5)

with

$$L_z = 2 l_z. (5a)$$

For large antennas it is given by

$$\rho_{c} \left(\right) = \exp \left\{ -\frac{1}{2} \left(\frac{\zeta}{L_{z}} \right) \right\}$$
 (6)

with

$$L_{z} = 0.8 D$$
 (6a)

 $N_{5/6}$ is the correlation function introduced into the scatter theory by Norton and defined for an arbitrary index ν by

$$N_{\gamma} \left(\frac{\zeta}{L}\right) = \frac{2}{\Gamma(\gamma)} \left(\frac{\zeta}{L}\right)^{\gamma} K_{\gamma} \left(\frac{\zeta}{L}\right)$$
 (7)

where K_{γ} is the modified Bessel function of the order γ (Fig. 2).

 ${\bf L_Z}$ is the vertical correlation length of the received signal, which is given for small antennas by the vertical correlation length ${\bf l_Z}$ of the dielectric constant of the air in the common scatter volume, and for large antennas by the antenna diameter. Using the equivalence theorem, the frequency correlation function is then for small antennas given by

$$\theta_{c} (\Delta f) = N_{5/6} (\frac{\Delta f}{\delta f})$$
 (8)

with

$$^{6}f = \frac{4 f l_{z}}{\theta \cdot d}$$
 (8a)

and for large antennas by

$$g_c (\Delta f) = \exp \left\{ -\frac{1}{2} \left(\frac{\Delta f}{6 f} \right)^2 \right\}$$
 (9)

with

$$\delta_{\mathbf{f}} = \frac{1.6 \, \mathrm{D} \, \mathbf{f}}{9 \, \mathrm{d}} \qquad (9a)$$

The parameter δ_f is called the frequency correlation width. An interpolation formula for δ_f , which in the limit cases of small and large antennas goes over into formulas (8a) and (9a) is

$$\tilde{G}_{f} = \frac{0.8 \text{ f}}{9 \text{ d}} \sqrt{(2 \text{ D})^2 + (5 \text{ l}_{z})^2}$$
 (10)

As can be seen from (10) an antenna is to be considered small if

and large if

If the analytic expressions (8) or (9) hold, the frequency correlation function is fully characterized by the frequency correlation width $\mathcal{E}_{\mathbf{f}}$. As only $\mathcal{E}_{\mathbf{f}}$ is needed, the condition (3) can alternatively expressed by

$$\frac{\delta_f}{f} \ll 0.8 \frac{p^2}{\lambda \cdot d} \tag{11}$$

For small antennas this means

$$\theta > 0.8 \lambda / 1$$
 (12)

The equivalence theorem can therefore be applied to small antennas only if the scatter angle θ is sufficiently large.

For large antennas

$$e \gg \frac{1}{2} \lambda/D$$
. (13)

The right member of this inequality is approximately equal to half the antenna aperture angle $S_{\mathbf{A}}$:

$$\vartheta_{\Lambda} = 0.56 \cdot \lambda/D \tag{14}$$

The inequality thus requires that the scatter angle θ is much greater than $^{\mathfrak{R}}{}_{A}$. This condition is practically always satisfied in the case of large antennas. The correlation function given by (9) and (9a) agrees with that derived by S.O. Rice / 3 /. The only difference is that the value of $^{\mathfrak{G}}{}_{f}$ calculated according to (9a) is higher by the factor 1.4 than Rice's value. In his deviation Rice had assumed that the correlation length $^{1}{}_{z}$ of the dielectric constant of the air in the common volume is much smaller than the wavelength. This corresponds precisely to our case of large antennas as we have then practically always D >> 2.5 1.

PATH DESCRIPTION AND INSTRUMENTATION

The path over which measurements were made runs from Hamburg to a place near Darmstadt. The distance is about 418 km, and a path profile for k=4/3 is shown in Fig. 1. A 9-m-parabolic reflector antenna was used at the transmitting station so that the half value of the antenna beamwidth ϑ_A given by

$$\frac{A}{A} = 0.56 \frac{\lambda}{D} \text{ is}$$

$$\frac{A}{A} = 9.9 \text{ m rad}.$$

The receiving antenna had a diameter of D = 4.5 m, which results in a half beamwidth of

In a good approximation the height of the transmitting and receiving antennas can be assumed to be zero so that the scatter angle θ_0 is obtained from

The transmitting and receiving antennas had an elevation angle of about zero degree. The transmitter operated at 1.89 GHz and had an output power of 1 kW. Frequency modulation was provided up to 2 MHz, and the modulation index was chosen in such a way that the next two side lines of the transmitted spectrum differed from the main line at 1.89 GHz in amplitude by no more than 6 dB. The receiving instrumentation operated simultaneously at the three different frequencies having the same logarithmic characteristic. The signal strength received at the three frequencies was recorded by a multichannel magnetic tape recorder. The magnetic tapes were then processed with a BIOMAC correlator. The averaging time for measurements of the correlation function must be chosen to include many rapid fades. Therefore, the correlation was determined from 2-minute intervals of a tape recording.

4. EXPERIMENTAL RESULTS

The cross-correlation and the auto-correlation were evaluated. Care was taken to avoid reflections from aircrafts. It was also noticed that under high-pressure weather conditions, the kind of fading changed (the fade rate decreased markedly), which seemed to be due to a change from scattering to partial reflection from finite layers. For comparison with the theoretical expressions of the frequency correlation, the results obtained in this weather period were also neglected. The measured cross correlation between the signals referring to two different frequencies and the auto-correlation were used to determine the normalized amplitude cross correlation coefficients ρ_a .

This amplitude correlation refers to the output voltage of the receiver which has a logarithmic characteristic. Important to the scatter mechanism, however, is the rf correlation. It is therefore necessary to calculate the rf correlation coefficient from the measured amplitude correlation coefficient. For the case of Rayleigh distributed fading (pure scatter propagation) the problem is solved / 4/.

The amplitude correlation of 20 lg U is related to the rf correlation by

$$\beta$$
 (20 lg U) = $\frac{6}{\pi^2} \sum_{n=1}^{\infty} \frac{g_c^{2n}}{n^2}$ (15)

This dependence is plotted in Fig. 3. With the aid of the nomogram the rf cross correlation coefficient was determined for frequency spacings of 0.5, 1, 1.5, 2, 3 and 4 MHz. The measurements were performed over a period of about half a year. Only the events with real Rayleigh distributed fading were taken into account. This was checked by plotting the auto-correlation of the fading signal. The analytical expression for the auto-correlation function of Rayleigh-distributed fading

$$\beta(\tau) = e^{-\frac{1}{2}\left(\frac{\tau}{\tau_s}\right)^2} \tag{16}$$

was fitted to the measured auto-correlation function. Events with τ_s in the range of 0.1 s $\leq \tau_s \leq$ 1s were taken for further evaluation. The median value together with the standard deviation of the rf cross correlation coefficient are plotted in Fig. 4.

It is possible to fit the cross-correlation function discussed in chapter 2 to the experimental results. Although the inequality (3) is not quite fulfilled in our case, the analytic expression (8) is a fairly good approximation, if the value of the vertical correlation length of $l_z=9\,\mathrm{m}$ was chosen. The correlation function for $l_z=9\,\mathrm{m}$ is also plotted in Figure 4.

Assuming $l_z = 9$ m the frequency correlation width δ_f can be calculated from equation (10) as a function of the distance d and the antenna diameter D. This was done for 3 different frequencies. The scatter angle θ included in (10) was obtained in the following assumptions:

- a) between transmitter and receiver the earth has a smooth spherical surface,
- b) the transmitter and receiver heights are so low that they can practically be assumed to be zero,
- c) the antenna axes point towards the horizon.

One these assumptions we have

$$e = \frac{d}{kr_{\pi}} + 0.56 \text{ } 2/D \tag{17}$$

Here $kr_E = 8500$ km is the Equivalent radius of the earth $(k = \frac{4}{3}, r_E = 6375$ km). The results are shown in Figs. 5, 6 and 7.

The transmissible bandwidth

The frequency correlation width $\mathcal{E}_{\mathbf{f}}$ indicates how strongly the correlation runs towards zero with increasing Δ f. The usable bandwidth B is directly proportional to $\mathcal{E}_{\mathbf{f}}$:

$$B = \alpha \cdot \delta_{r} \tag{18}$$

The numerical value of α is determined by the requirements made on the reception quality and can therefore not be calculated or measured from the propagation point of view.

The relation and the figures show that $\mathcal{E}_{\mathbf{f}}$ and thus B are almost proportional to the frequency \mathbf{f} . If consequently a wide band is to be transmitted at given distance and antenna size one should choose the operating frequency as high as possible.

Frequency diversity

With space diversity the diversity separation Δ is that antenna spacing at which the correlation of the amplitudes has decreased to 1/e = 0.37. The L_z given in (5) and (6) are the correlation lengths of the rf voltage variations. This necessitates first a conversion to amplitudes. From / 1 / follows

The equivalence theorem thus supplies the frequency diversity separation $\Delta_{\mathbf{f}}$

$$\Delta_{\mathbf{f}} = 0.67 \, \epsilon_{\mathbf{f}} \tag{19}$$

or with (7)

$$\Delta_{f} = \frac{0.54}{\theta d} \text{ f} \sqrt{(2 D)^{2} + (5 1_{201})^{2}}$$
 (20)

To be safe it is advisable here to take instead of the mean or median value of l_z the value l_{z01} exceeded in 1% of the time.

References

- /1/ FEHLHABER, L. and GROSSKOPF, J., 1967, "Das elektromagnetische Feld am Empfangsort einer troposphärischen Scatterstrecke", NTZ 20, pp. 511-520 and 649-657.
- /2/ FEHLHABER, L., 1967, "Selektiver Schwund, übertragbare Bandbreite und Frequenzdiversity auf troposphärischen Scatterstrecken im Frequenzbereich zwischen 1 GHz und 10 GHz", Technischer Bericht FTZ Nr. 5589
- /3/ RICE, S.O., 1953, "Statistical fluctuations of radio field strength far beyond the horizon", Proc. IRE 41, pp. 274-281
- /4/ SOLLFREY, W. and BARLOW, E., 1965, Results published in Kerr, D.E., Propagation of short radio waves, New York, pp. 557-558

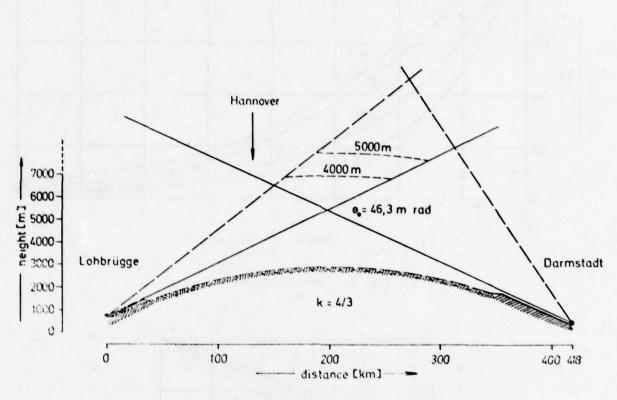
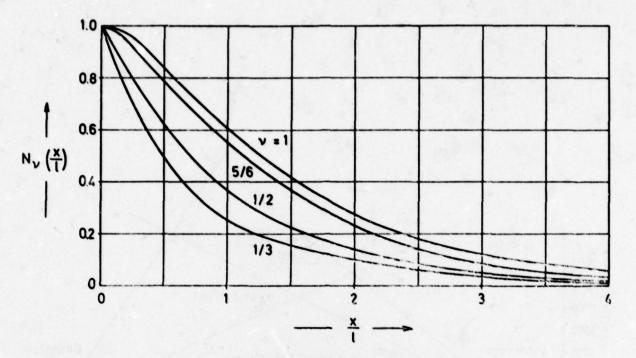


Fig. 1: Profile of the 1.89 GHz Transhorizon Path



, Fig. 2: Norton Function

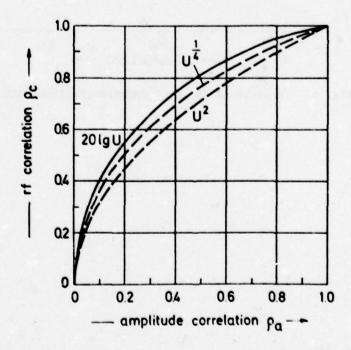


Fig. 3: Rf-Correlation versus Amplitude Correlation

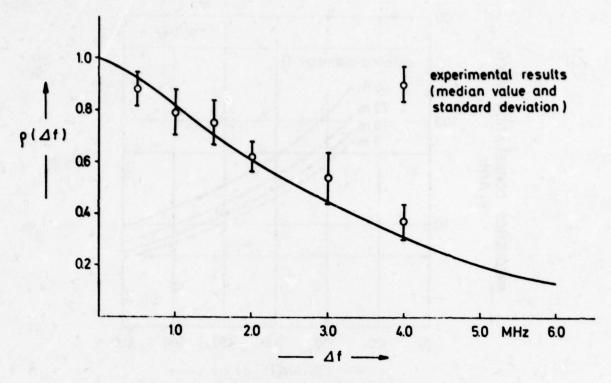


Fig. 4: Rf-Correlation versus Frequency Spacing

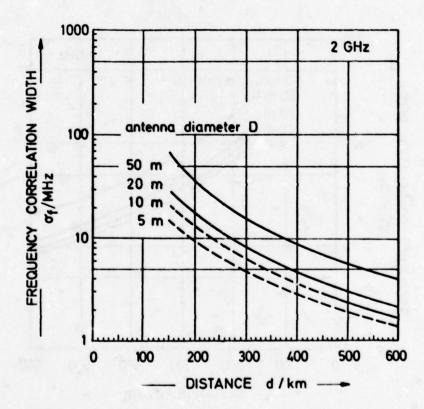


Fig. 5: Frequency Correlation Width as Function of the Distance at 2 GHz

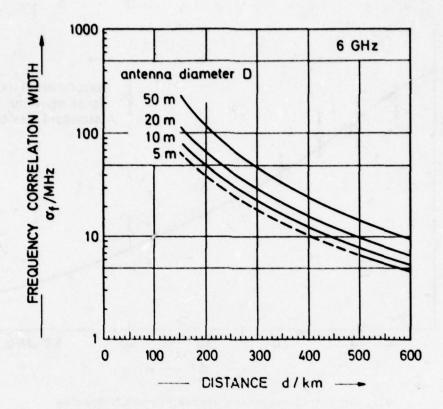


Fig. 6: Frequency Correlation Width as Function of the Distance at 6 GHz

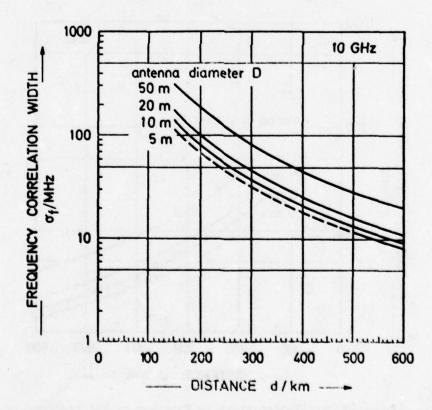


Fig. 7: Frequency Correlation Width as Function of the Distance at 10 GHz

TROPOSCATTER ANGLE DIVERSITY IN THEORY AND PRACTICE

M.W. Gough, G.C. Rider and R. Larsen

GEC-Marconi Electronics Limited, Marconi Research Laboratories, Great Baddow, Chelmsford, Essex, England.

SUMMARY

Background work on the behaviour of angle diversity in the troposcatter mode is briefly reviewed, together with some important applications. Favourable predictions of angle diversity behaviour, based on established theory and limited experimental validation, have encouraged confirmatory trials on an established oversea troposcatter link temporarily adapted for angle diversity working.

Trials at the U.K. terminal involved simultaneous comparison between a reference dual (angle/space) diversity system and optimised angle diversity systems involving firstly horizontally splayed beams and latterly vertically splayed beams. The horizontally offset system yielded channel cross-correlations and post-combiner relative efficiencies well in keeping with theoretical prediction, while the vertically offset system performed significantly better than predicted.

1. INTRODUCTION

The idea of using angle diversity in troposcatter systems is by no means new. (See CHISHOLM, J.H. et al., 1959, SURENIAN, D., 1965 and TRAVIS, G.W., 1968.) Ever since troposcatter circuits began to be engineered, it has been well known that diversity reception is essential to combat the deep and rapid Rayleigh fading inherent in this propagation mode. Formally, uncorrelated channels may be obtained by duplicating frequencies, by use of spaced paths, by consecutive transmission giving time diversity and by using different angles of arrival, i.e. angle diversity. The earlier links usually employed space/ frequency diversity since this system, with two antennas at each terminal, then represented the best compromise between the cost of antennes and equipment complexity. Latterly quadruple space diversity has been implemented by the polarization separation of paths. This is usually, but not quite accurately, termed space polarization diversity. Time diversity has never found favour, due largely to the long (approx. 1 second) time delays involved in transmission. More recently, as pressure on the radio spectrum has increased, alternative configurations have been explored, angle diversity included. The latter offers the considerable attraction of requiring, under certain conditions, only one antenna at each terminal of a long-haul link where the antennas are of course very costly. However with angle diversity it is inherently impossible for all of a group of diversity beams to have optimum signal alignment. equipment and cost advantages of angle diversity have therefore to be paid for with a small system loss in decibels. It is therefore of prime importance to ensure the best trade-off for each particular link, and the resulting system loss.

A good foundation for the necessary trade-off computations has been laid by theoretical work (KCONO, T., HIRAI, M. et al., 1962), which is well supported by beam-swinging and other tests. This work has been built upon (GOUGH, M.W., 1970), in order to establish diversity design implications for some typical cases, and was followed by experiments (GOUGH, M.W. and RIDER, G.C., 1975) to validate some of the predicted features. In particular, cross-correlation and squint loss measurements on angularly separated beams - data not previously available - agreed encouragingly with predictions. At that juncture two important phases of the angle diversity work were still outstanding. A test was needed on an operational troposcatter link, and the design principles already explored (GOUGH, M.W., 1970) needed embodiment in a composite computer program so that an optimum diversity configuration could be readily determined for specific links. The work on the first of these topics is described in this paper.

2. PATH GEOMETRY AND SYSTEM DETAILS

2.1. Introductory

The purpose of the trials to be described was to test the behaviour of two optimised dual angle diversity systems against a reference dual diversity system of known performance. Facilities for these trials were obtained by adapting an existing troposcatter terminal linking the U.K. with Germany. The link involved a conventional FM/FDM multi-channel telephony system. The relevant topographical and instrumental parameters are listed below.

Path length 352 km.

Scatter Angle 1.41° = 24.5 millired.

Operating Frequencies, 2 GHz band.

Frequency Diversity separation, 42 MHz.

Diversity System before modification, Quadruple Space/Frequency.

Diversity Systems after modification, Dual Space/Frequency and Dual Angle.

Diam. of Billboard Antennas, 18.3 m.

Antenna Spacing between centres, 21.3 m.

Antenna Plane-wave Beamwidth at half-power points, approx. 0.5° (applicable to splayed angle diversity beams as well as to unmodified antenna beams).

Polarization received at the U.K. terminal, vertical.

2.2. General Description

Fig. 1 shows the system as installed. For the purpose of the angle diversity trials, which were confined to the U.K. terminal, the installation there was modified according to Fig. 2, while the Germany terminal was unaltered. The conventional diplexer feed-horn at the North antenna at the U.K. terminal was replaced by twin feed-horns, giving a pair of splayed beams for angle diversity reception as detailed in Section 2.3. The transmitter on frequency f₃, which normally feeds the North antenna, was disconnected. The South antenna was unmodified, and involved a reference dual space/frequency diversity system against which the dual angle diversity system of the North antenna could be compared. The reference system had the diversity benefit of the differing frequencies f₁ and f₂ added to that due to the spacing of the distant transmitting antennas in Germany (Fig. 1). The arrangement subsequently proved to be an excellent dual diversity reference in that it gave a measured cross-correlation between diversity branches indistinguishable from zero (Section 6.2.3). The transmitter feeding the South antenna at a frequency f₄ was retained for communicating with the Germany terminal.

To avoid contamination by frequency diversity, the angle diversity system operated on frequency f_1 only and the receiver R_2 was not used. This necessitated using receivers R_1 and R_3 in the two angle-diversity branches, which entailed sharing R_3 between the reference and angle-diversity systems. This time-sharing was controlled by the coaxial switch S_1 , which switched receiver R_3 from one antenna to the other at 2-minute intervals (Fig. 2). The reference diversity system thus used receivers R_3 and R_4 , and the angle diversity system receivers R_3 and R_1 . Synchronously with the operation of switch S_1 , the switch S_2 connected alternately the baseband outputs of the angle and reference diversity systems to a maximal-ratio combiner. All switching operations were controlled by a Test Control Unit.

The object of the trials at the U.K. site was to compare dual angle diversity behaviour with reference diversity behaviour both before and after maximal-ratio diversity combining. To monitor pre-combiner behaviour, a d.c. control voltage available from each receiver provided analogue signals operating a chart recorder with two servo-pen drives and alternative chart speeds of 5 and 20 mm/minute. Recorder indication was approximately linear with receiver carrier level (dBm) over a 40 dB range. Regular calibrations were made.

The carrier levels generated in the respective dual-diversity branches could be simultaneously tape-recorded together with speech. The resulting calibrated and annotated tapes were subsequently sampled at a 20/second rate for the purpose of digitizing and transferring the data to a magnetic disc store. Statistical signal analysis was aided by a key-board operated computer graphics display. The carrier levels were also applied to a Data Logger, where they were digitized to provide one-minute-mean levels whose values were punched on paper tape.

To investigate post-combiner behaviour, a Noise Analyzer preceded by a Noise Receiver was used for measuring base-band output thermal noise power on a minute-mean basis. This output was quantized at 2 dB intervals and punched on tape. The equipment was periodically calibrated with the aid of a noise generator at the Germany transmitter. The system served to indicate changes in Basic Noise Power Ratio, and thereby assess the relative post-combiner performance of the angle diversity systems. It also provided timing pulses at minute intervals for operating the switches S₁ and S₂ via the Test Control Unit (Fig. 2).

2.3. Description and Properties of Angle Diversity Feed-horns

For the present trials two feed-horn assemblies were designed to provide alternative pairs of receiving beams splayed respectively horizontally and vertically. Their optimized design followed the application of classical scatter theory to angle-diversity behaviour (KOONO, T., HIRAI, M. et al.,1962). As developed, (GOUGH, M.W., 1970) it involves dimensioning contiguous rectangular feed-horns for the best compromise between :-

- (a) Squint Losses due to beam divergences from the conventional optimum direction of shoot,
- (b) Impairment of diversity efficiency due to finite cross-correlation arising from the overlapping skirts of the splayed beams and from unwanted coupling between feed-horns,
- (c) Antenna spillover loss due to reducing a feed dimension below the conventional optimum in the interests of controlling (a) and (b).

Due to the behaviour of (c), the optimum feed dimensions and overall system efficiency are somewhat affected by the plane of offsetting of the splayed beams relative to the plane of polarization of the received signal.

The respective feed-horn assemblies, constructed respectively for horizontally and vertically offset beams, were designed for the frequency f₁ and the path geometry of Fig. 4. From the aspect of optimizing efficiency with sole regard to the foregoing factors (a), (b) and (c), the constituent feed-horns should always touch. However, specialist advice dictated the insertion of an 8 mm gap between feed-horns in the vertically offset case, to reduce coupling between the feeds. This involved a small loss in theoretical efficiency. No gap was deemed necessary in the horizontally offset case. The laboratory-measured cross-coupling between adjacent feed-horns in the operating band amounted to 21 dB and 30 dB respectively for the horizontally offset and vertically offset assemblies. These unwanted couplings slightly impaired diversity efficiency by a calculable amount, (GOUGH, M.W., and RIDER, G.C., 1975) by adding to the trope-sphere-induced cross-correlation between the fading diversity signals. The basic feed-horn dimensions adopted for the two planes of offsetting during the present trials are sketched in Fig. 5.

Fig. 4 showing the path geometry defines the theoretical limits of the splayed receiving beams with vertical offsetting, as defined by their half-power points and, in the case of the lower beam, by a skyline cut-off adjusted theoretically to equalize the median levels from the respective beams. The hatched areas indicate the separated common scattering volumes generated by the intersection of the conventional transmitted beam with the two receiving beams.

FEEDER LOSS MEASUREMENTS

The RF switching arrangements (Fig. 2) introduced small imbalances in the feeder losses associated with the receivers. These losses were measured so that a true comparison could be made between diversity systems by comparing signals at the antenna terminals. A combination of preliminary measurements of losses in constituent lengths of waveguide and coaxial cable, followed by v.s.w.r. measurements on the assembled transmission lines short-circuited at the far end, led to the "best estimates" of the feeder losses listed in Table I.

4. PRELIMINARY ANTENNA ADJUSTMENTS

4.1. Horizontal Offsetting

Before starting the first phase of the trials the horizontally offset feed-horn assembly(Fig.3(a)) was mounted on a panning frame near the focus of the North antenna. Twin coaxial tails allowed flexible connections to the fixed waveguides used in the conventional system. After checking the elevation of the horizontally splayed beams the twin-feed assembly was panned horizontally in 25 mm steps, with the aim of equalizing as closely as possible the median signal levels from the two feeds. This was done by simultaneously recording the two Rayleigh-fading signals for about 2 minutes at each position, so as to compare their short-term median levels. Allowance was made for the measured 0.9 dB difference in the respective feeder losses (Table I). The observed rate of increase of median signal difference between the two feeds amounted to about 2 dB per cm shift of the feed-horns, testifying to the critical nature of the horizontal panning. This agrees well with theoretical expectation (KOONO, T., HIRAI, M. et al., 1962).

4.2. Vertical Offsetting

For the second phase of the trials the vertically offset feed-horn assembly (Fig. 3(b)) was installed in place of the horizontal one (Section 4.1). Vertical panning in 15 mm steps gave median signal differences approximating to the theoretical trend *, but showing four anomalous turning points and three balance points in the critical region (Fig. 5). Judged by its repeatability the effect seemed genuine, and probably resulted from the generation of subsidiary common scattering volumes by specular sea reflection. The effect is very evident on the left of Fig. 5, where in violation of the theoretical model, sea reflection contributes substantial energy from the over-dipped lower beam. The feed-horns finally were set at the most stable of the balance points as indicated by the arrow on Fig. 5.

5. MANAGEMENT OF TRIALS

After completing initial modifications and alignments (Sections 2, 5 and 4), the diversity trials were pursued intermittently for nearly 3 weeks. Most of the available time was devoted to the "vertically offset" angle diversity mode, as theory had predicted better performance with this mode than with horizontal offsetting. There was the further interest in discovering how the "vertically offset" performance would be affected by atmospheric layering involving significant departures from the theoretical model. During the trials the data logger, analogue recorder and noise analyzer (Section 2) were generally working continuously, apart from routine breaks for calibrations. However the diversity signal tape recordings, on which the accurate assessment of diversity performance mainly depended, comprised intermittent 20-minute measurement spells.

PRE-COMBINER PERFORMANCE

6.1. Introductory

The pre-combiner characteristics of the Reference Diversity System and the Angle Diversity System (vertically and horizontally offset varieties) were derived from computer-aided analysis of detailed magnetic tape records and from analysis of punched tape output from the data logger.

To make a fair comparison between the time-shared angle and reference diversity systems, the competing systems were measured alternately in 2-minute spells, with 0.5 sec. of lost time during each switchever by the Test Control Unit (Fig. 2). The latter also impressed one-minute time markers on the magnetic tape records, the analogue recorder and the data logger.

The results of the magtape and data logger records, embracing pre-combiner performance, are discussed in Sections 6.2 and 6.3.

6.2. Magnetic Tape Analysis

The magtape data, available in 20-minute spells, served to evaluate:-

- (a) The degree of inequality between the two branches of each diversity system,
- (b) The pre-combiner performance of each angle diversity system relative to the reference system, assessed on a median signal basis,
- (c) The cross-correlation between the constituent branches of each diversity system.

These three aspects will be considered in turn.

6.2.1. Diversity Branch Inequalities

The degree of equality maintained between the median levels from the respective branches of each diversity system was derived from minute-mean received levels (dBw) extracted from the stored magtape data.

* The marked asymmetry of the heoretical curve about the balance point results mainly from the assumption of progressive skyline cut-off of the lower beam as the twin beams are progressively dipped. Scatter angle dependence gives further asymmetry.

Calling the Branch Imbalance the difference (dB) between minute-mean levels from the two branches during a given minute, Table II lists the means of the Branch Imbalances (algebraic sign disregarded) for all tape-recorded minutes in the periods specified. Branch equality was satisfactory on all systems during the first two test periods, but rather large imbalances on both vertically offset and reference systems persisted throughout the final test period despite repeated calibrations.

The final test period was marked by a large drop in all signal levels, associated with the end of a spell of anti-cyclonic weather that had persisted throughout the earlier tests. Consequent changes in atmospheric stratification - assumed horizontal - could well have disturbed the balance of the vertically offset system (see Section 4.2), but not that of the reference frequency/space system. The reference system imbalance during the final test period remains unexplained.

6.2.2. Comparative Pre-combiner Median Signal Performance

A comparison between the angle and reference diversity systems on a median signal basis was a crucial element of the trials, because it evaluated the joint squint and spillover losses (Section 2.3) which are inherent features of angle diversity systems.

Each angle diversity system was initially adjusted to give equal median signal levels in its two branches (see Section 4). However to cater for the significant branch imbalances which subsequently developed in all the diversity systems (Section 6.2.1), the pre-combiner performance of each diversity system was based on the average of the median levels from the constituent diversity branches during each 20-minute magtape spell. Fig. 6 plots these branch average levels for the reference and angle diversity systems for all magtape spells. During the early periods the angle diversity branch averages generally fell short of their reference counterparts. However in the final (low signal level) period, vertically offset angle diversity substantially surpassed the reference system. This reversal of roles is discussed below.

The pre-combiner median efficiency of each angle diversity system is usefully expressed as the shortfall (dB) of its branch average level on that of the reference system, i.e. the interval between the traces on Fig. 6. Expressing a shortfall as a negative efficiency, Table III lists the median efficiencies measured during each magtape spell. For comparison with the period-mean efficiencies also tabulated, the table includes theoretical pre-combiner efficiencies evaluated as the sum of the antenna spillover losses and the antenna beam squint losses prevailing under average atmospheric conditions.

The measured angle diversity efficiencies emerge systematically, and in the last period substantially, better than theoretical expectation. Even after allowing \pm 2 dB for sampling and other experimental errors, vertically offset angle diversity showed a substantial advantage over the reference system under low signal conditions. During this phase the upper angle diversity beam collected more signal than the lower, and it also surpassed the stronger of the reference diversity branches by typically 5 dB. These effects are explainable in terms of Fig. 7, where the upper angle diversity beam collects a bonus signal from an intensified scattering region (or a weak inversion layer) to the exclusion of the weaker common scattering volume pertaining to the lower angle diversity beam or to a conventional troposcatter configuration.

More generally, it seems likely that the twin beams of a vertically offset angle diversity system, by straddling a large height interval in an erratically stratified atmosphere, will jointly in the long term capture more power - whatever the vertical disposition of the scatterers - than is obtainable via the vertically restricted beams of conventional systems.

6.2.3. Cross-correlation between Diversity Branches

The degree of short-term cross-correlation between Rayleigh-fading diversity branches governs the diversity advantage gained from maximal ratio combining of the respective signals. At the outset of the trials a computer analysis (Section 2.2) was performed on short runs of tape-recorded signal records to verify that short-term amplitude distributions closely followed the Rayleigh law. Successive one and two-minute runs on reference and angle diversity branches (including the upper beam of the vertically offset system) all gave satisfactory Rayleigh distributions down to the 0.1% fade level during low and high signal periods. The median auto-correlation time was 0.5 seconds, in good agreement with other troposcatter observations in the 2 GHz band which show fading rates of 1-2 positive median crossings per sec.

After transfer to the disc store for computer analysis, each 20-minute magtape recording yielded a series of cross-correlations derived from one-minute test spells, namely 10 cross-correlations from the reference diversity system interleaved with 10 from the angle diversity system. The recorded post-detection cross-correlations were measured via an approximately logarithmic amplifier to cope with a wide signal level range. Such correlations have been shown (GOUGH, M.W. and RIDER, G.C., 1975) to be significantly smaller than the envelope correlations that would have been measured via a linear amplifier. In Table IV the logarithmically measured cross-correlations, $\rho_{\rm L}$ for the angle diversity systems have been transformed to their linear envelope-correlation equivalents, $\rho_{\rm E}$, for direct comparison with theory based on average atmospheric conditions. The theoretical cross-correlations (last column) were computed (KOONO, T., HIRAI, M. et al., 1962) with allowance for the impairment (increase) in $\rho_{\rm E}$ due to the measured feed-horn cross-coupling noted in Section 2.3.

The Reference System cross-correlations listed in Table IV give mean values of virtually zero for all test periods, thus endorsing the system as a good dual diversity criterion. Horizontally offset angle diversity gives a mean envelope correlation in precise agreement with theory, while vertically offset diversity gives lower (i.e. better) values of $P_{\rm E}$ than predicted for both high and low signal periods. This betterment of theory with vertically splayed beams parallels previous troposcatter observations in the 2 GHz band with the 25 m steerable antenna at Chilbolton, U.K. (GOUGH, M.W. and RIDER, G.C., 1975). The reduced correlation compared with theory is thought to reflect the often erratic variation of scattering efficiency with height (see Fig. 7), as against the exponentially declining scattering parameter assumed in the theory.

Fig. 8 shows histograms of or for the three test periods, based on all the one-minute correlation samples from the magtapes corrected for logarithmic amplification. The arrowed measured medians are slightly below the measured means of Table V due to some skewness in the distributions. The indicated dispersion results partly from sampling errors stemming from a one-minute measuring interval, and partly from lack of statistical stationarity of the scatterers within the common volumes of the beams.

6.3. Data Logger Measurements

The data logger, connected in parallel with the magtape recorder, gave punched-tape outputs of minute-mean signal levels (dBw) from the diversity system being measured. In all, 55 data logger hours were secured. Though statistically more significant than the magtape data due to the longer sampling time, the data logger measurements were instrumentally less accurate because the daily calibrations had to be applied to minute-mean levels rather than to the near-instantaneous levels rapidly sampled during the magtape processing (Section 2.2).

6.3.1. Pre-combiner Relative Efficiencies

A check was made on the data logger's evaluation of pre-combiner relative efficiencies as analyzed for the magtape data of Section 6.2.2. The branch-average levels * for the reference and angle diversity systems were evaluated for each minute. Hourly medians of these quantities for the compared systems were then differenced to give a representative angle diversity relative efficiency for each data-logger hour. Finally these hourly efficiencies were averaged to give the period means listed in Table V.

For comparison purposes, Table V repeats the period-mean efficiencies (listed in Table III) that were derived during comparable test periods from the instrumentally more accurate magtape data. Due in part perhaps to the relatively short sampling time, the data logger appears to have exaggerated the efficiency of horizontally offset diversity, but for the vertically offset tests the data logger and magtape figures agree within 0.5 dB.

The data logger measurements unequivocally endorse the basic conclusion from the magtape analysis, namely the striking improvement of measured on predicted vertically offset diversity efficiency under low-signal conditions, to a degree that gives this system a very significant ascendancy over the reference system.

6.3.2. Cross-correlation between Minute-mean Signal Levels

Troposcatter link performance is usually estimated on the conservative assumption that the constituent diversity branches are completely correlated on a minute-mean or longer-term basis. This implies that relatively slow mean-level variations in the diversity branches keep in step and hence give no diversity advantage. However recent observations (MONSEN, F., 1972, GOUGH, M.W. and RIDER, G.C., 1975) have revealed some degree of long-term decorrelation between vertically splayed beams. This effect was pursued further in the present trials.

Table VI lists cross-correlations evaluated between pairs of minute-mean signal levels from the data logger during an aggregate test period of about 34 hours. The test spells varied from about one to four hours. The following broad conclusions can be drawn concerning the behaviour of the angle and reference diversity systems as regards cross-correlation between minute-mean signal levels in their respective branches:-

- (1) Under high-signal conditions all systems showed consistently high cross-correlations, thus endorsing the current practice of treating long-term variations as completely correlated in their constituent diversity branches.
- (2) The onset of low-signal conditions sometimes reduced the minute-mean correlations in the frequency/space diversity system, but not enough to justify waiving the rule in (1) above.
- (3) Low-signal conditions spasmodically reduced the minute-mean branch correlations in the vertically offset angle diversity system, sometimes very significantly.

The beneficial minute-mean signal decorrelations intermittently observed under condition (5) may be explained by postulating that gross differences occasionally occurred in the scatter patterns included in the respective common volumes (Fig. 4) associated with vertically splayed narrow receiving beams. The six days of low-signal data are insufficient to quantify the long-term benefits from this effect, but it is expected that it will significantly improve system efficiency during the "worst month", when improvement is of course most needed. The decorrelation benefit may be reinforced moreover by the pre-combiner efficiency bonus discussed in Section 6.2.2. in connection with vertically offset angle systems. Both benefits in fact accrue from the atmospheric model sketched in Fig. 7.

7. POST COMBINER PERFORMANCE

7.1. Introductory

A Noise Analyzer and Noise Receiver (Fig. 2 and Section 2.2) measured base-band cutput thermal noise power so as to assess, on a minute-mean basis, the post-combiner performance of each angle diversity system relative to the reference (frequency/space) system. Noise power in a 4 kHz bandwidth in each diversity system was sampled 15 times per hour, with a change-over every 2 minutes as for the previously described tests. 82 valid hours of test were obtained.

^{*} As with the magtape measurements, the imbalances between the respective diversity branches (both reference and angle diversity) significantly increased during the final test period.

7.2. Relative Post-combiner Efficiencies

Hourly median values of the sampled minute-mean noise power ratios (dB) from each angle diversity system were compared hour-for-hour with their reference system counterparts. The difference (dB) represents the angle diversity system overall relative efficiency for each hour. Table VII lists the mean of these hourly efficiencies and their standard deviation, for the three test periods shown. The last column gives the theoretical median efficiencies for the optimised angle diversity systems. The latter are based on maximal-ratio dual-diversity combining, average atmospheric conditions, and Rayleigh fading with branch correlations based on the tropospheric coupling between the overlapping skirts of the beams modified by the initially measured feed-horn cross-coupling (Section 2.3).

With horizontal offsetting the measured mean post-combiner efficiency is well in keeping with theory, while vertical offsetting betters theory slightly. Under low-signal conditions vertical offsetting exceeds prediction by more than 4 dB, confirming the trend exhibited by the pre-combiner measurements (Section 6).

Statistical significance tests were applied to the measured mean efficiencies of Table VII to gain assurance that the differences between them were unlikely to have arisen by chance. The tests showed that:-

- (1) The difference between the mean efficiency with horizontal offsetting and that with vertical offsetting is very significant under the high-signal conditions experienced during the test.
- (2) The difference between "vertically offset" mean efficiencies under respectively high and lowsignal conditions is highly significant, substantially surpassing the significance of test (1).

Hence there is good assurance that the observed differences in mean efficiency, stem (a) from changes in the direction of beam offsetting and (b) from substantial changes in mean signal level in the case of vertical offsetting.

8. EXTENSION TO EXTREME PERCENTAGE LEVELS AND QUADRUPLE DIVERSITY

Our trials of system behaviour were limited to assessing dual diversity performance at around the median level. While the results are very promising they do not indicate directly the relative angle diversity performance achieved for large time percentages, e.g. 99.%. This can nevertheless be deduced from the measured mean post-combiner efficiencies (Table VII) in conjunction with the measured mean cross-correlations (Table IV).

Troposcatter systems generally require quadruple diversity, and the foregoing test data are best applied, not to our experimental dual diversity reference system but rather to realisable quadruple diversity systems constructed from it. These could usefully take the form of 2 angle/2 frequency systems involving at each terminal a single billboard antenna with twin angle-diversity feed-horns. A polarized gr ting (ANDERSON, E.W., 1973), which is transparent or reflecting according to the wave polarization, permits two-way cross-polarized transmissions with independent adjustment of the transmit beams and the angle-diversity receive beams (RIDER, G.C. and GOUGH, M.W., 1973). In this way the angle diversity system can be optimised without compromising the transmit beam alignment.

In our conjectured 2 angle/2 frequency systems, equal median levels are assumed in all branches. The frequency-separated branches are independent and the angle-separated branches are taken to be correlated according to measured mean values of $\rho_{\rm E}$ listed in Table IV. System performance is compared with an idealised reference system comprising four equal and independent diversity branches.

Using representative results from the foregoing dual diversity trials, Table VIII illustrates the step-by-step derivation of the relative efficiencies expected from the postulated 2 angle/2 frequency systems at the 99.9% level. To ensure a conservative appraisal, the table excludes the use of the very favourable data for the final test period 12. 9.72 - 17. 9.72. To clarify the process, the diversity loss referred to is the amount (dB) by which the post-combiner performance of a partially correlated diversity system departs, at a specified time percentage, from that of the appropriate reference system due to finite correlation between diversity branches. Steps (d) and (f) in the table are based on the principle that the overall efficiency of angle diversity systems at a given time percentage is the sum of the diversity loss at that time percentage and the aggregated squint and spillover losses.

The final columns of Table VIII show how the efficiencies of the conjectural angle diversity systems founded on data from the present trials compare at the 99.9% level with theoretical expectation. Within the expected limits of uncertainty, the horizontally offset system conforms well to theory, while the vertically offset system betters theory by a significant 1.5 dBeven when the very favourable performance during the final test period has been excluded. Concerning the intrinsic efficiencies, it may be noted that the "horizontal offset" figures for the 99.9% level (lines (f) and (g)) are degraded by about 0.7 dB due to the rather poor isolation of 21 dB between the feed-horns (Section 2.3). Attention to feed-horn design would probably recover at least half of this deficit.

9. BROAD INFERENCES FROM THE TRIALS

The performance of two optimised dual-angle diversity systems has been weighed against a reference frequency/space system in several ways. While the pre-combiner (magtape) measurements of Table III interpret angle diversity performance rather more favourably than do the noise analyzer measurements of Table VII, the two groups of data have consistently established that :-

- Horizontally and vertically offset systems adequately followed theory under high-signal conditions, thus endorsing theoretical expectation that vertical offsetting is the better system.
- (2) Under low-signal conditions (with which horizontal offsetting was not involved) the vertically offset system not only substantially bettered theory but also surpassed the reference system.

The above findings require qualification in the light of the need for crossed polarizations in a two-way link. The present trials were restricted to vertical polarization, and it is estimated that, had horizontal polarization been available, it would have impaired our vertical offset performance at the 99.9% level (Table VIII, line (f)) by about 0.5 dB *, while improving horizontal offset performance by a like amount. This effect illustrates the principle that angle diversity systems perform best with the polarization which is aligned with the direction of offsetting. While this influence narrows the efficiency disparity between horizontal and vertical offsetting when applied to 2-way transmissions, we believe that the advantage remains unambiguously with the vertically offset system, having regard (a) to the notable enhancements on the reference system's signal level, (b) to the reduced short-term branch correlations and (c) to the intermittently reduced longer-term branch correlations.

Disregarding here any assessment of respective hardware losses and considering purely the evidence of the foregoing trials, it appears that a 2 angle/2 frequency system using a single antenna per terminal would compete well (at least under critical low-signal conditions) with the frequency/space system from which it was temporarily adapted.

ACKNOWLEDGEMENTS

Thanks are due to colleagues in the Antenna Department, Marconi Research Laboratories, for the design and realization of the twin feed-horn assemblies used in the trials, and also to colleagues in the Theoretical Sciences Laboratory, Marconi Research Laboratories, who carried out the computer analysis of the experimental data. Further acknowledgement is due to colleagues of Field Services, Marconi Communications Systems Ltd., who prepared test equipment, modified installations and executed the trials.

The authors wish to thank the Technical Director of GEC-Marconi Electronics Ltd for permission to publish this paper.

REFERENCES

ANDERSON, E.W., Sept. 1973. The application of angle diversity to tropospheric scatter links. Point-to-Point Communication, Vol. 17, No. 3.

BRENNAN, D.G., June 1959. Linear diversity combining techniques. Proc. IRE, Vol. 47, No. 6.

CHISHOLM, J.H., RAINVILLE, L.P., ROCHE, J.F. and ROOT, H.G., Sept. 1959. Angular diversity reception at 2290 MC over a 188-mile path. Trans. IRE Comms. Systems, Vol. CS-7, No. 3.

GOUGH, M.W., 1970. Angle diversity applied to tropospheric scatter systems. AGARD Conf. Proc. 70, paper 32.

GOUGH, M.W. and RIDER, G.C., July 1975. Angle diversity in troposcatter communications. Some confirmatory trials. Proc. IEE, Vol. 122, No. 7.

KOONO, T., HIRAI, M., INOUE, R. and ISHIZAWA, Y., Jan. 1962. Antenna-beam deflection loss and signal amplitude correlation in angle-diversity reception in UHF beyond-horizon communications. J. of the Radio Res. Labs., Tokyo, Japan, Vol. 9, No. 41.

MONSEN, P., April, 1972. Performance of an experimental angle diversity system. Trans. IEEE, Vol. COM-20. No. 2.

PIERCE, J.N. and STEIN, S., Jan. 1960. Multiple diversity with non-independent fading. Proc. IRE, Vol. 48, No. 1.

RIDER, G.C. and GOUGH, M.W., Sept. 1973. The case for angle diversity in troposcatter systems. Point-to-Point Communication, Vol. 17, No. 3.

SURENIAN, D., June 1965. Experimental results of angle diversity system tests. Trans. IEEE, Commun. Technol., Vol. COM-13.

TRAVIS, G.W., 1968. Angle diversity tests. Proceedings of the National Electronics Conference, Vol. XXIV.

^{*} Based on the assumption of re-optimized feed-horn dimensions to suit horizontal polarization.

		e Diversity quency/Space)	Dual Angle	Diversity
	Feeder Run serving R ₃	Feeder Run serving R ₄	Feeder Run serving R ₃	Feeder Run serving R
Total Branch Loss	3.8 dB	4.1 dB	4.1 dB	3.2 dB
Estimated Tolerance, dB	0.5 "	0.5 "	0.5 "	0.5 "

TABLE I BEST ESTIMATES OF FEEDER LOSSES

	N - > C	Mean of Branch	Imbalances, dB	
Period	Number of 20-minute Magtape runs	Reference Diversity System	Angle Diversity System	Comments
30. 8.72 - 1. 9.72	8	1.1	2.1	Horizontally Offset Angle Diversity. Signal levels high.
7. 9.72 - 8. 9.72	7	1.1	0.7	Vertically Offset Angle Diversity. Signal levels high.
13. 9.72 - 16. 9.72	6	4.7	4.6	Vertically Offset Angle Diversity. Signal levels low.

Note: The imbalances relate to the levels at the feed-horns.

TABLE II DIVERSITY BRANCH IMBALANCES FROM MAGTAPE DATA

Date	Start of Test Spell, Local Time	Angle Diversity Mode and Prevailing Signal Level	Pre-combiner Median Efficiency, dB	Mean for Test Period, dB	Theoretical Efficiency, dB (average atmospheric conditions)
30. 8.72	1700		- 3.4)		
31. 8.72	1200		- 1.1		
31. 8.72	1600	Horizontal	- 1.6		metal transfer
31. 8.72	2000	Offsetting	- 2.5	- 1.3	- 3.3
1. 9.72	0000		- 0.3		
1. 9.72	0400	High Signal	- 1.5		
1. 9.72	0800	Levels	+ 1.7		
1. 9.72	1200		- 1.3)		
7. 9.72	1200	Vertical	-0.9)		
7. 9.72	1600	Offsetting	+ 0.5	- 0.9	- 2.8
7. 9.72	2000	High Signal	- 2.5	- 0.9	- 2.0
8. 9.72	0000	Levels	- 0.5)		
13. 9.72	1200	Vertical	+ 8.0)		the second
13. 9.72	1600	Offsetting	+ 8.2		
14. 9.72	1000		+ 5.6	+ 6.0	- 2.8
14. 9.72	1400	Low Signal	+ 5.8		
16. 9.72	1600	Levels	+ 4.2		
16. 9.72	2000		+ 4.1)		

TABLE III MEASURED AND THEORETICAL PRE-COMBINER EFFICIENCIES - MAGTAPE DATA

Period, Angle Diversity Mode, and Prevailing Signal Level	ρ _L measu:	correlation, red via a amplifier Angle Diversity	Equivalent Envelope Correlation, PE (via linear amplifier) for Angle Diversity	Measured Period Mean P _E for Angle Diversity	Theoretical P _E for Angle Diversity (average atmos- pheric conditions)
30.8.72 - 1.9.72 Horizontal Offsetting High Signal Levels	- 0.13 - 0.01 + 0.02 - 0.15 - 0.13 + 0.13 - 0.05 + 0.03	+ 0.31 + 0.21 + 0.34 + 0.50 + 0.71 + 0.43 + 0.58 + 0.34	+ 0.42 + 0.29 + 0.45 + 0.63 + 0.63 + 0.81 + 0.55 + 0.70 + 0.45	+ 0•54	+ 0.54
7.9.72 - 8.9.72 Vertical Offsetting High Signal Levels	- 0.07 - 0.01 - 0.06 - 0.04 + 0.13 + 0.08 + 0.11	- 0.04 - 0.09 + 0.14 + 0.04 - 0.05 + 0.28 + 0.20	- 0.05 } - 0.13 } + 0.20 } + 0.05 } - 0.07 } + 0.38 } + 0.28 }	+ 0.10	+ 0.35
13.9.72 - 16.9.72 Vertical Offsetting Low Signal Levels	+ 0.14 + 0.05 + 0.08 - 0.04 + 0.03 - 0.05	+ 0.18 + 0.10 + 0.32 + 0.10 + 0.06 + 0.07	+ 0.25 } + 0.14 } + 0.42 } + 0.14 } + 0.08 } + 0.10 }	+ 0.19	+ 0.35

Note: The near-zero values of ρ_L for the reference (space/frequency) system made it unnecessary to compute equivalent envelope correlations, ρ_E , for this system.

TABLE IV DIVERSITY BRANCH CROSS-CORRELATIONS FROM MAGTAPE DATA

Data Logger			combiner Mean iciency, dB	Theoretical Efficiency, dB
Test Period	Comment	Data Logger	Magtape (See Table III)	(average atmos- pheric conditions)
4.9.72 4 hours	Horizontal Offset. High Signal Levels	+ 0.4	- 1.3	- 3.3
7.9.72 - 8.9.72 24 hours	Vertical Offset. High Signal Levels.	- 0.4	- 0.9	- 2.8
12.9.72 - 17.9.72 25 hours	Vertical Offset. Low Signal Levels	+ 5.6	+ 6.0	- 2.8

TABLE V PRE-COMBINER EFFICIENCIES - DATA LOGGER, MAGTAPE AND THEORETICAL RESULTS COMPARED

Date	Test Period, Local Time	Prevailing Signal Level	Type of Angle Diversity	MINUTE-MEAN Angle Diversity	CROSS-CORRELATIONS Reference Frequ/Space Diversity
31.8.72 4.9.72	1200-1400 1300-1600	} High	Horizontal Offset	+ 0.77 + 0.90	+ 0.74 + 0.70
7.9.72 7.9.72 8.9.72 8.9.72 8.9.72	1200-1600 2000-2200 0000-0200 0400-0550 1000-1200	High	Vertical Offset	+ 0.28 + 0.86 + 0.75 + 0.95 + 0.76	+ 0.64 + 0.93 + 0.88 + 0.98 + 0.87
12.9.72 13.9.72 14.9.72 15.9.72 16.9.72 17.9.72	1200-1500 1100-1400 1000-1400 1100-1200 1500-1800 1100-1400	Low	Vertical Offset	+ 0.46 + 0.07 + 0.04 + 0.47 + 0.70 + 0.40	+ 0.41 + 0.52 + 0.89 + 0.82 + 0.93 + 0.42

Test Period and Prevailing Signal Level	Type of Angle Diversity	Number of Hourly Samples	Standard Deviation of constituent Hourly Efficiencies, dB	Mean Relative Efficiency, dB	Theoretical Median Efficiency, dB
30.8.72 - 4.9.72 High Signal Levels	Horizontal Offsetting	33	1.45	- 3.5	- 3.8
7.9.72 - 8.9.72 High Signal Levels	Vertical Offsetting	19	1.25	- 2.0	- 3.1
12.9.72 - 17.9.72 Low Signal Levels	Vertical Offsetting	30	1.0	+ 1.5	- 3.1

TABLE VII ANGLE DIVERSITY POST-COMBINER RELATIVE EFFICIENCIES FROM THE NOISE ANALYZER

Dual Angle Diversity Measurements and inference therefrom	Origin	Line Identi- fication	Horizontally Offset Angle Diversity	Vortically Offset Angle Diversity
Measured Mean Cross-correlation between branches, $\rho_{\rm E}$	Table IV Periods 50.8.72-1.9.72 and 7.9.72-8.9.72	(a)	+ 0.54	+ 0.10
Inferred Median Diversity Loss associated with correlation measurements	BRENNAN, D.G. 1959, using the measured values of $\rho_{\rm E}$ in line (a)	(b)	0.4 dB	0.1 dB
Measured Post-Combiner Mean Loss with respect to the Reference System	Table VII, using Mean Relative Efficiencies from Periods 50.8.72-4.9.72 and 7.9.72-8.9.72	(e)	3.5 dB	2.0 dB
Inferred aggregated Squint and Spillover Losses	(c) minus (b) (See Section 8)	(d)	3.1 dB	1.9 dB
Inferred Diversity Loss not exceeded for 99.9% of the time for the conjectural 2 angle/ 2 frequency system	PIERCE, J.N. and STEIN, S., 1970, using the measured values of Pg in line (a)	(e)	1.4 dB	0.3 dF
Inferred Post-combiner Relative Efficiency achieved for 99.9% of the time with the 2 angle/ 2 frequency system	Minus (d) minus (e) (See Section 8)	(1)	- 4.5 dB	- 2.2 dB
Theoretical Efficiency achieved for 99.9% of the time with optimized 2 angle/2 frequency system	KOONO, T, HIRAI, M. et al., 1962, and GOUGH, M.W., 1970, using average atmospheric para- meters and idealised reference system	(g)	- 4.9 dB	- 3.7 dF

TABLE VIII STEPS IN PREDICTING THE 99.9% EFFICIENCIES OF 2 ANGLE/2 FREQUENCY DIVERSITY SYSTEMS
FROM THE DUAL ANGLE DIVERSITY TRIALS

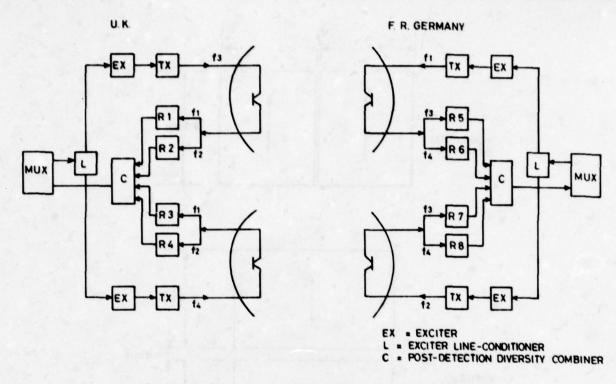


Fig. 1. U.K. - Germany troposcatter system as installed.

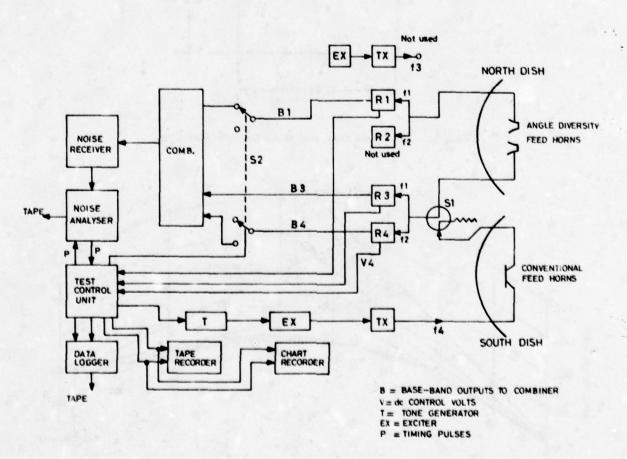


Fig. 2. U.K. terminal modified for angle diversity working.

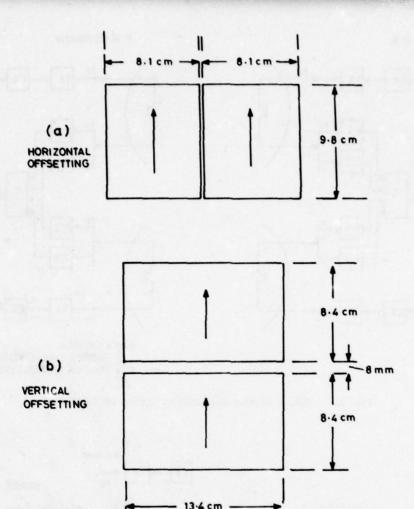


Fig. 3. Optimized feed-horn dimensions for test path.

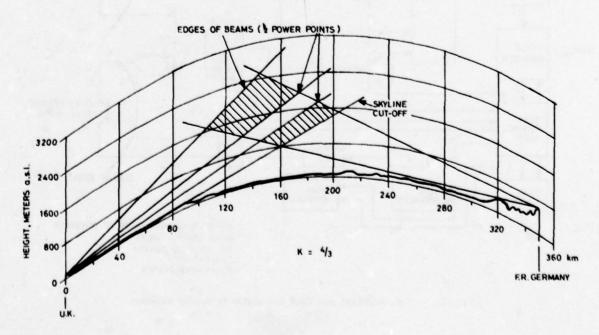


Fig. 4. Path profile with optimized vertically offset beams.

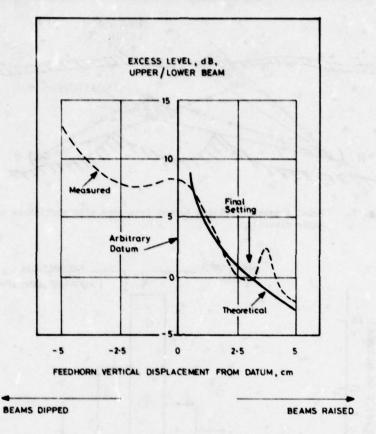


Fig. 5. Panning behaviour of vertically offset feed-horns.

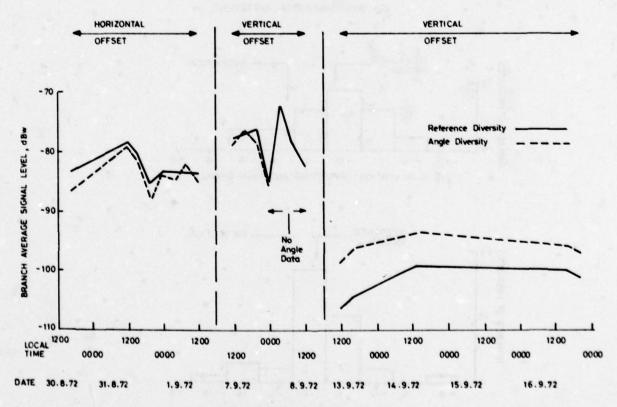


Fig. 6. Branch average pre-combiner levels for indicated diversity systems (20-min. magtape spells).

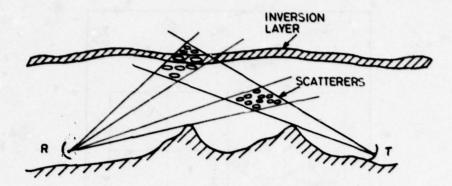
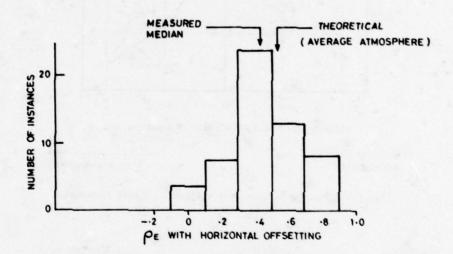
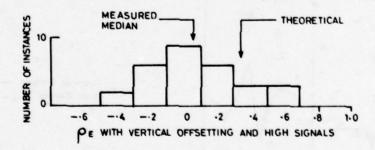


Fig. 7. Model atmosphere giving branch imbalance with vertically offset angle diversity.





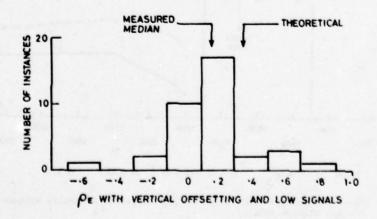


Fig. 8. Histograms of branch correlations with angle diversity.

AN EXPERIMENTAL PROGRAM LEADING TO DEVELOPMENT OF A TACTICAL DIGITAL TROPOSCATTER SYSTEM

A. Sherwood
S. Wenglin
J. Wick
The MITRE Corporation
Bedford, MA
USA

SUMMARY

The United States Air Force has the engineering responsibility for a new generation of all-digital troposcatter radio terminals for Tri-Service tactical application. No data base existed to establish the design requirements for the specialized adaptive signal processing equipment to be included in these terminals. Therefore, an extensive test program was undertaken to characterize the multipath nature of tactical troposcatter links. The data obtained was used to prepare the design specifications for the AN/TRC-170 troposcatter terminals. A performance prediction technique was derived which considers the variability in path loss and multipath spreading and the effect of this variability on modem performance to predict the usable range of this equipment. In any investigation where field data is reduced and modeling is attempted, questions are raised which can only be answered by additional investigation. Therefore, a suggested test plan inspired by this work concludes the paper.

1. INTRODUCTION

When the requirements for high speed digital troposcatter communication were first being established in 1973, hardware realizations of adaptive modem techniques were still laboratory curiosities and achievable performance was the subject of much conjecture. There were virtually no multipath measurements for troposcatter paths typical of tactical communication: 4.4 to 5.0 GHz, 50 to 200 mile range, and moderate gain antennas usually associated with readily transportable tactical systems. Although enough correlation bandwidth measurement data existed to suggest that data transmission at data rates of 2 MB/s would be plagued with dispersion and consequent intersymbol interference, the data base was not sufficient to establish design requirements for specialized adaptive signal processing techniques or even to fully justify their investigation.

It was obvious further work in this area was needed and a program of channel measurement and analysis was initiated. The measurement segment of the program concentrated on the multipath dispersion of two paths typical of those encountered in tactical military situations over a sufficiently long period of time that a reliable data base could be obtained. Also, the performance of several adaptive modem techniques was observed over the test paths and under controlled test situations using a troposcatter channel simulator. The analysis segment of the effort reduced the experimental data to a basis from which the performance of the AN/TRC-170 Radio Terminal Equipment could be specified. Also, a performance prediction model was derived based upon the experimental work. This model may be used, within the limitations imposed by a meager data base, to combine the statistical variations of both path loss and multipath spread to predict the performance of TRC-170 equipment in field deployments. The formulation of the prediction model clarified the areas in which further data would be advantageous.

2. TEST PROGRAM

The United States Air Force has engineering responsibility for a new generation of all-digital troposcatter radio terminals for Tri-Service tactical application. There are three terminals in this family which is designated as AN/TRC-170. The smallest terminal is similar in size to the analog AN/TRC-97 with expected deployment on paths of less than 100 miles. The intermediate terminal will serve paths beyond 100 miles while the range of the largest terminal will be in excess of 200 miles. Experimental data was required to identify the type of modem which would best serve the needs of these terminals. If the multipath spread was small, of the order of tens of namoseconds as predicted by the Bello model (Bello, P. A., 1969), relatively simple modem technology such as QPSK with fixed matched filter processing would be indicated. Intersymbol interference effects would be small and degrade performance only slightly. If the multipath spread were larger, use of conventional modulation would result in less than optimal system performance.

The design of the modem should be matched to the multipath characteristics of the channel. If the modem is overdesigned, its utility in a tactical communications environment is limited by undue cost, weight, and complexity. A modem which is inadequate for the multipath present not only suffers a degradation from its flat fading performance level due to intersymbol interference, but also it is unable to utilize the multitude of independently fading paths implicit in the medium to attain performance superior to that attainable for flat fading.

Therefore, the first objective of the test program was to obtain the necessary multipath statistics to allow the design of a modem optimized for the medium. A second objective of the program was to observe the relation between multipath spread effects and other observable path and meteorological parameters on the performance of digital troposcatter equipment. Prediction of the performance of such modems on postulated paths requires knowledge of not only the average magnitude but the statistics of the dispersion or multipath spread of the channel. Using twice the RMS multipath spread (2 σ) as a measure of dispersion, available data indicated that the multipath spread on troposcatter paths might be anywhere from tens to hundreds of nanoseconds. The wide range and attendant uncertainty of this data made engineering judgements

required in the development of digital troposcatter equipment difficult and the prediction of the performance of such equipment nearly impossible.

Design and evaluation of adaptive modems is greatly simplified if they can be tested under repeatable conditions. Such testing is very difficult and time consuming on over-the-air paths. Troposcatter multipath simulators have been constructed which provide valid and repeatable tests of modem performance. Another objective of the test program was to determine the necessary multipath parameters to effectively utilize the Quadrature Diversity Troposcatter Simulator (built for RADC by Signatron Inc.) for modem evaluation and performance specification. Part of the test effort included the comparison of the performance of several breadboard adaptive modems in over-the-air and simulator tests.

The experimental data required were gathered from October 1974 through August 1975 by personnel from the Rome Air Development Center (RADC) and The MITRE Corporation at the RADC test range in northwestern New York. This range has been in existence for more than 18 years and has been used for many types of tropospheric propagation measurements. It is one of the locations where extensive atmospheric structure probing activity has been conducted at L band over two paths as well as the site of many correlation bandwidth and diversity experiments.

The test paths used in this program are shown in Figure 1. Also shown on the figure are the locations at which routine meteorological measurements were made. The radio paths both are obstructed by tree lines which, at C band, effectively set the radio horizon. The resulting take-off angles ranged from one-third to one degree at the various sites as indicated in Table 1. These sites, then, are probably quite typical of sites where tactical communication equipment would be deployed and are not typical of carefully prepared hilltop sites which would more likely be found on permanent strategic troposcatter links. Comparison of the common volume geometry of troposcatter paths with high take-off angles with that of troposcatter paths operating over smooth earth or from selected sites with low or depressed take-off angles would tend to indicate that a greater degree of multipath spreading would be expected on the paths with the high take-off angles as long as the variation of atmospheric structure with height was the same for both situations.

2.1 Test Instrumentation

Multipath measurements were made using a "multipath analyzer" which is commonly known as a RAKE system as it uses a concept from the original RAKE communication system (Price, R., Green, Jr., P. E., 1958) for fading dispersive channels. The RAKE system in use at RADC was built by Sylvania, Inc. To isolate signal energy as a function of delay, the RAKE channel measurement technique (Barrow, B. B. et al, 1969) transmits a maximal-length binary sequence as a probe signal and the receiver cross-correlates locally generated sequences with the received signal. The auto-correlation function of such a sequence has a sharp peak at zero shift (relative delay) and then drops to nearly zero until the shift equals the sequence length, where it rises again. As shown in Figure 2, the RAKE receiver is made up of a bank of cross-correlators operating at progressively increasing delay increments. By comparing the relative output at successive delay increments or taps, the impulse response or delay power spectrum of the channel may be determined. If the overall radio system response is wide with respect to the rate of the probe sequence, the response at the various delays will be primarily due to multipath propagation in the medium. In the RAKE system used for the RADC tests, the bit rate was 10 MHz and the tap spacing was .1 microsecond.

Figure 3 is an overall block diagram of the equipment used in the field tests. The RAKE "multipath analyzer" transmitter and receiver interface with the radio system at a 70 MHz IF. For operation on the short path, the radio system was a modified AN/TRC-97 D. The power amplifier was tuned for broadband operation and produced about .9 Kw. On the longer path, the power amplifiers of the TRC-132 radio terminal were broadbanded and operated at about 5 Kw. In both terminals, the frequency synthesizers were replaced by stable laboratory equipment. At all sites, timing and frequency references were derived from a 5 MHz GR-1115-B standard oscillator with a frequency stability on the order of one part in 10¹⁰. Such high accuracy is necessary to reliably resolve delays on the order of hundreds of nanoseconds and Doppler shifts on the order of Hertz.

2.2 Propagation Test Results

Most of the tests were conducted during normal working hours local time, five days a week. Channel measurements were normally made once each hour to coincide with normal meteorological observations. This test schedule was altered to avoid data acquisition when aircraft were observed in the common volume. Unscheduled tests were conducted when sudden changes in path loss or multipath spread occurred or when an unusual condition such as layering was observed. On a few occasions, the test schedule was extended to late evening and/or around-the-clock operation.

From 1 October 1974 to 22 April 1975, all tests were conducted with the AN/TRC-97 on the short path. Various combinations of 8 and 15 foot antennas were utilized at the terminals. From 28 April through 12 May 1975, tests were conducted over the long path using the AN/TRC-132A using the standard 28 foot antennas. From 12 May through 10 July 1975, a long period of over-the-air modem testing was conducted on the TRC-97D short path. During these tests, normal RAKE testing was alternated with modem error rate tests. A final segment of tests was conducted over the TRC-132A long path from 17 July through 7 August 1975.

The USAF Environmental Technical Applications Center (USAFETAC) supplied three different types of meteorological data to the program: surface data from Rochester, Buffalo, Utica and Syracuse; wind shear data from Albany and Buffalo; and upper air data (rawinsonde data) from Albany and Buffalo.

A variety of meteorological parameters were computed and compared with the observed radio path behavior. The only significant correlation obtained was between the effective earth radius and median signal level.

diversity system was derived from minute-mean received levels (dBw) extracted from the stored magtape data.

* The marked asymmetry of the heoretical curve about the balance point results mainly from the assumption of progressive skyline cut-of of the lower beam as the twin beams are progressively dipped. Scatter angle dependence gives further asymmetry.

30-3

The primary statistic of interest in this investigation was the 2σ multipath spread parameter and hence, the available resources were concentrated on its characterization. The RAKE receiver determines the complex impulse response of the channel (i.e., the distribution of received power in the orthogonal multipath delay spreading and Doppler spreading domains). The delay power spectrum resulted when the mean value of the magnitude of the complex channel impulse response was computed. An example of such a spectrum is shown in Figure 4. Examples of the observed RMS Multipath Spread Distributions are given for Summer, Winter, and all data for all observations on the short path in Figure 5. Figure 6 compares the data obtained during the winter using the 28 foot antennas on the long path with that obtained using 8 foot and the combination of 8 and 15 foot antennas on the short path. Note that although there appears little difference in the mean values observed, the variance decreases with increasing antenna size. Although short term correlation was observed on a number of occasions between the variations of received signal level and multipath spread, no long term correlation was found.

Attempts to correlate the multipath spread variations with available meteorological data were hampered by the fact that the observation points were located at a significant distance from the common volume region of the path and also, the measurements were of more gross features of the troposphere than would be observed with the RAKE equipment. The only experiments in which high correlation has been found between meteorological and radio parameters measured with RAKE equipment have been those utilizing an aircraft equipped with a microwave refractometer and have been conducted at L band (Birkemeier, W. P. et al, 1973).

Although there are limitations on the test and meteorological data, the set of data obtained from the site at Verona over the duration of the test program is one of the most extensive currently available. It should be noted that equipment and time limitations precluded obtaining regular 24-hour data sufficient to characterize diurnal multipath variability. However, some general diurnal characteristics were noted. During the summer, the multipath spreading was greatest during the afternoon while during the winter, the reverse was true. Then the multipath spreading tended to be the greatest during the morning.

A general summary of the test data is given in Table 2. Here the high, low and spread between the values of RMS multipath spread and median RSL is given for various test conditions. The spread between the high and low values for the RMS multipath spread, in general, becomes less as the size of the antenna increases. This pattern is not evident for the spreads between the high and low values for the median RSL values.

2.3 Comparison With Other Results

Most of the earlier test results for short-to-medium range paths at C band have consisted of measurement of correlation bandwidth, an indirect measure of multipath. To make a comparison with earlier data, an approximation was developed which was used to translate correlation bandwidths into estimates of multipath spread. The derivation may be found in (ESD TR-77-252, 1977) and only the results are reproduced here.

One series of tests was conducted over a 100-statute-mile overland path in Florida (Gainsville to Orlando) during the period of 14 May to 15 June 1962 (Patrick, W. S., Wiggins, M. J., 1963). Tests were conducted at C band using 12-foot and 4-foot parabolic reflectors with takeoff angles of nearly zero degrees. The translated results of these tests are presented in Table 3. Most of the testing (100 hours) was conducted with the 12-foot reflectors. One day of the operation, tests were alternated between the 12-foot and 4-foot reflectors with essentially the same correlation bandwidth being observed. This tends to indicate that under the conditions of this test, it was the medium and not the antenna patterns which were limiting the multipath spread on the path.

During the period August 1969 through February 1970, a series of correlation bandwidth tests (Brown R. et al, 1970; Kennedy, D. J., 1972; Branham, R. 1961) were conducted over four paths at the RADC test through the conducted over four paths at the conducted over four paths at the RADC test through the conducted over four paths at the RADC test through the conducted over four paths at the RADC test through the conducted over four paths at the RADC test through the conducted over four paths at the RADC test through the conducted over four paths at the RADC

Another series of C band tests were conducted between Tobyhanna, Pennsylvania and Fort Monmouth, New Jersey from October 1966 through January 1967, and from February 1968 through July 1968 (Olson, W. A., 1971). During the first test period, 10-foot antennas were employed while 15-foot antennas were used during the second segment. More than 90 percent of the data was obtained using the smaller antennas. Results and path parameters of this experiment are also presented in Table 3.

From the very limited number of "test" paths included in the table, it appears that the overall range of multipath spreading is consistent with the range observed in the current test program. Also there appears to be an interrelation between observed multipath spread, takeoff angle, and path length as would be expected from geometric considerations. All paths, except for one, were over land and the majority were over relatively smooth terrain. Not included in this limited data base are: data for longer paths with antenna diameters in the 8 to 15-foot range; shorter range paths where diffraction effects predominate; terrain obstructed paths with large scatter angles; obstacle gain diffraction paths; and paths in other climatic regions. That is to say that data from direct or indirect measurement of multipath do not, for the most part, exist for the types of conditions expected in an operational deployment of tactical troposcatter radio equipment.

2.4 Comparison With Channel Models

The construction of a viable prediction technique for system performance requires a method of predicting the multipath statistics of a path. This prediction may either involve a large experimental data base or a theoretical channel model. Existing troposcatter channel models represent an attempt to predict average dispersion based upon path geometry, making certain assumptions relative to scattering efficiency as a function of scatter angle and common volume height. The detailed analysis of various models, their underlying physical assumptions and limitations has been beyond the scope of the effort to this point. It is felt that more data, of the type detailed in the proposed test plan, is needed to develop a new or modified model. However, there are some observations resulting from preliminary work which are worth mentioning.

The early Bello model (Bello, P. A., 1969) was formulated to fit data obtained on an L and path and involved a single integral which related the delay power spectrum to the geometry and antenna patterns of the troposcatter path. A later Bello model (Bello, P. A., 1968) predicts the delay power spectrum for troposcatter paths with arbitrary antenna orientation. The theoretical power spectrum is obtained by evaluating a double integral containing terms which account for the antenna patterns and path geometry, the tropospheric layering effects, and the spacial correlation between refractive index fluctuations at different points in the atmosphere.

The shape of the delay power spectrum obtained from the second Bello model is a good fit to the average delay power spectrum observed on the RADC path as is shown in Figure 4. This model agrees with the theory and experimental indications that the greatest scattering cross section generally exists in the lower portion of the common volume, near the great circle path.

Depending upon what values are selected for the parameters used to characterized the atmosphere, the second Bello model may be used to predict multipath spreads on the order of magnitude of those observed experimentally. There seems to be a reasonable agreement between the variations in takeoff angle, path length, and mean multipath spread as seen in the limited experimental data. It would appear that additional refinement of the atmospheric model used in the Bello model would be possible if additional propagation tests were supported with data from an airborne microwave refractometer probing the common volume.

2.5 Modem Test Results

The modems tested were all breadboard development models and hence, the data from these tests is in general, of proprietary nature. To illustrate the performance characteristics of an adaptive modem, a generalized modem curve is given in Figure 7. This plot indicates the ratio of energy per bit to noise spectral density ratio (Eb/No) required to maintain a fixed error rate as a function of multipath spread. Near zero multipath spread, such a modem approaches the performance of simple QPSK systems utilizing matched filter detection. As the multipath spread increases, the modem begins to realize the multipath diversity gain implicit in the propagating medium and, hence, the Eb/No ratio required to maintain the desired error rate decreases. Further increases in multipath spread begin to introduce significant intersymbol interference and cause the required Eb/No ratio to rise. An infinite slope would appear on this curve when the ISI causes the irreducible error rate to be higher than the desired error rate. Good modem engineering would produce a modem that requires minimum Eb/No near the mean expected multipath spread and does not exhibit significant ISI loss under the extreme multipath conditions to be expected on the path.

3.0 PERFORMANCE PREDICTION

The user of a communication link is ultimately interested in the percentage of the time that the link meets his requirements. To include in the performance prediction model the slow variation in multipath spread (the variation in delay power spectrum) as well as the slow variation in path loss (the long term fading), the concept of "generalized time-availability" has been formulated. This is an extension of the narrowband concept of time-availability which is defined as the percentage of hours for which the mean path loss is such that the desired grade-of-service is obtained. Generalized time-availability is then the percentage of hours for which the mean path loss and the mean multipath spread are jointly such that the desired grade-of-service is obtained.

Development of prediction techniques for service probability in the narrowband case has been the subject of a great deal of effort, most notably by the National Bureau of Standards. Emperical data from a great number of existing tropo links and special test links was combined to produce a method of predicting the time-availability and service probability of troposcatter links which takes into account their topological and climatological variables. This prediction technique, which is embodied in NBS Technical Note 101 (Rice, P. L. et al, 1967) has generally been accepted as a reliable tool for the characterization and prediction of troposcatter link performance.

In the high data rate case, performance of digital troposcatter modems is strongly influenced by multipath through the mechanisms of implicit diversity and intersymbol interference. From the results of the tests at RADC and other available data, it appears that the multipath behavior of the tropo medium is subject to a wide range of fluctuation with time. Little is currently shown about how these statistics vary with path geometry and climatology. Prediction of the performance of a high data rate troposcatter link must take this parameter into account even though there is comparatively little data upon which to base an empirical statistical model. Also lacking is a credible theoretical model which could utilize available climatological data to provide the necessary statistics. Nevertheless, an effort has been made to combine the data collected in the RADC tests on multipath variation with the NBS model of signal level variation to produce predictions of the generalized time availability (GTA) of a high data rate digital troposcatter link.

For a given set of path parameters, it is possible to determine from the NBS model the predicted mean and standard deviation of the log-normal probability density function (pdf) of the hourly median path losses. This pdf is for an average path with a given set of path parameters (distance, takeoff angles, climate, season or time block, and frequency), and hence, corresponds to a service probability of fifty percent. This pdf may be modified for other values of service probability and the modified form will be discussed later. Inclusion of the additional factors of aperture-to-medium coupling loss and the capabilities of the terminal equipment (i.e., transmitter power, noise figure, etc.) and the data rate, allows the density function of the hourly median Eb/No to be determined directly.

In the RADC tests, the multipath spread, as measured by the two sigma width of the delay power spectrum, has been found to vary with a distribution which may be approximated by a Gaussian pdf. The two quantities, Eb/No and the 2σ delay power spectrum width, were found to vary with low long term correlation. Thus, to simplify the analysis, they will be considered to be statistically independent.

The joint pdf of Eb/No and 2σ is then the product of their individual pdfs and may be treated as a two dimension Gaussian process. Geometrically, this is represented in Figure 8 as a "Gaussian dome." Also

shown in the figure is a generalized "modem curve"-the locus of the value of Eb/No required to maintain a constant bit error rate as the value of 2σ multipath spread is increased. The probability that the averages, over an hour, of the Eb/No and the 2σ multipath spread are such that the average bit error rate over the hour is less than the specified value is found by integrating the joint pdf over the portion of the X-Y plane that lies above the modem curve. (That is for values of Eb/No greater than the minimum given by the modem curve.) The value of this integral is defined to be the GTA. In the next section of this paper, the NBS statistical model of path loss will be discussed and the pdf of the variation in time hourly median path losses for service probabilities other than 50% will be stated. The use of the prediction model will be illustrated by the results of a computer numerical integration which shows the variation of GTA with range for one set of the family of three TRC-170 troposcatter terminals.

3.1 Path Loss Variability

The path loss observed on a given troposcatter link is not constant. There are rapid fluctuations, termed fast fading, with a period ranging from the order of a tenth to several seconds. For a CW or a narrowband signal, the envelope will have a Rayleigh type probability density function (Rayleigh fading) over an interval of several minutes. For a signal subject to fast frequency selective fading (i.e., signal bandwidth larger than the correlation bandwidth of the channel), the received power tends toward a log-normal distribution. That is to say that the power expressed in decibels follows a Gaussian distribution. Over longer intervals in the narrowband as well as the frequency selective case, fading is log-normally distributed.

The NBS model is expressed in terms of the statistics of the hourly medians of path loss. The variation of the median of the distribution of hourly medians for different climates and seasons as well as time blocks is given. Additionally, the random fluctuations in terms of the hourly medians is described in terms of a log-normal distribution with a standard deviation dependent upon range, frequency, climate, and time interval which may be a season, a defined time block, or the entire year. Usually the standard deviation for the upper and lower parts of the distribution are different, but as high time availabilities (above) 90% alone are of practical interest, only one side of the distribution will cross the modem curve. That is to say that the vast majority of the Gaussian dome of Figure 8 is above the modem curve. This distribution is meant to be representative of an average link with the stated parameters (distance, climate, etc.). Consider a given path over which, according to this distribution, the path loss is less than L for some fraction of the hours \mathbf{q}_t . This will be true only for 50% of the paths with the same parameters. One could say that the path loss was less than L (or the path gain was -L) with a time-availability of \mathbf{q}_t and a service probability of 50%. In order to achieve a greater confidence in the same value of time-availability, that is increase the service probability, it is necessary to accept a greater maximum path loss by adding a bias or safety factor. This may be expressed as $L(\mathbf{q}_t, \mathbf{q}_g) = A(0.5) + Y_{\mathbf{r}}(\mathbf{q}_t) + Y_{\mathbf{s}}(\mathbf{q}_t)$

 $L(q_t, q_s) = maximum path loss with:$

q, = time-availability

q service probability

A(0.5) = median path loss (q_t = 0.5, q_s = 0.5)

 $Y_r(q_t)$ = the bias of additional path loss to obtain the time-availability q_t

 $Y_s(q_t, q_s) = the bias of additional path loss to obtain the time-availability <math>q_t$ with a service probability of q_s .

As was previously mentioned, the distribution of the hourly medians of path loss in dB for a particular link is Gaussian. For the average link with the same parameters, the standard deviation of the hourly median path losses, $\sigma_{\rm t}$, can be found from the NBS model. For the purpose of evaluating the generalized time-availability, the probability density function for the hourly medians of Eb/No can be found from the NBS model but only for a service probability of .5. However, we are interested in using a service probability of .95 which is the value generally accepted in path performance prediction in the narrowband case. It is necessary to find, then, a probability density function for the fluctuation in time of the hourly medians, corresponding to an arbitrary and fixed service probability. This may be done formally as follows: Define a combined bias $Y(q_{\rm t}, q_{\rm s})$ as follows:

$$Y(q_t, q_s) = Y_r(q_t) + Y_s(q_t, q_s)$$

From this one can determine q_t as a function of Y and q_s or

This represents a cumulative distribution function, i.e., $q_{\underline{t}}$ is the probability that the path loss (with the median A(0.5) subtracted out) is less than Y. The desired pdf is obtained by differentiation,

$$P(Y, q_s) = \frac{d q_t(Y, q_s)}{dY}$$

with q playing the role of a parameter.

This pdf is found to be

$$P(Y, q_s) = \frac{1}{\sqrt{2\pi} \sigma_t (1-\beta)} \left[1 - \frac{\beta Y}{\sqrt{\beta Y^2 + (1-\beta)\alpha}} \right] \left[exp \left[-\frac{1}{2\sigma_t^2} \left[\frac{Y - \sqrt{\beta Y^2 + (1-\beta)\alpha}}{1-\beta} \right]^2 \right] \right]$$

where for smooth earth, or other case of known terrain parameters, and for 95% service probability

3.2 Sample Calculations of GTA vs. Range

There are three sets in the TRC-170 family of troposcatter terminals. The smallest of these terminals (Set 3) uses dual diversity, a 2 Kw power output, and 9.5 foot antennas. The intermediate terminal (Set 2) uses quad diversity, a 2 Kw power output and 9.5 foot antennas. The largest terminal also uses quad diversity, 6.6 Kw power output and 15 foot antennas. The generalized time availability as a function of range for these three sets for the maximum bandwidth and data rate (7. Mhz, 2.048 Mb/s) for an average error rate of 10^{-5} is given in Figure 9.

These curves were obtained by means of numerical integration of the joint pdf of Eb/No and the 2σ multipath spread over that portion of the plane above the modem curve – as previously described. The joint pdf of the hourly medians of Eb/No and the pdf of the 2σ width of the delay power are assumed to be independent processes, based upon the results of the RADC tests. The pdf of Eb/No was the form given above for a service probability of 95%. The pdf of the multipath spread is based upon the RADC tests. A Gaussian distribution was used with a standard deviation of .0586 microseconds for Set 1 (15 foot antennas). For Sets 2 and 3 (9.5 foot antennas) the standard deviation of .0725 microseconds. The median for all sets was .153 microseconds. As a simplification, these numbers were not varied with range although variation in path geometry (and atmospheric structure with changing common volume height) would be expected as path length increased.

For predicting path loss in this investigation, the 1972 update (Longley, A. G., 1973) of the 1968 Computer Method of Longley and Rice of ESSA (Longley, A. G., Rice, P. L., 1968) was used. This is essentially a computerization of NBS TN 101 (Rice, P. L. et al, 1968).

The path geometry used was smooth earth with antenna center heights of fifteen feet. Smooth earth was chosen as a general representation of troposcatter links. As the path loss prediction technique was the NBS TN 101, the NBS formulation of aperture-to-medium coupling loss was also used. This aperture-to-medium coupling loss formulation has no rigorous base in atmospheric physics and is not adequately supported by data in the range of path lengths typical of tactical troposcatter links. Also, there exists some question of how much interrelation exists between the path loss predictions and the predicted aperture-to-medium coupling loss due to a tendency for short paths to use small antennas and long paths to use large antennas. This possible ambiguity will be investigated in the test program to be detailed later in this paper.

3.3 Limitations of the Prediction Technique

The predictions made for the three TRC-170 sets are representative of the most accurate predictions possible at the present time with the physical measurements which have been made and the theoretical analysis which has been performed. There are several factors which are subject to uncertainty.

All of the multipath spread observations available to base the predictions come from two paths at RADC. As there is no broad empirical data base from which a valid multipath prediction model may be formulated, utilization of the prediction technique on a wide variety of paths is of limited validity.

It was assumed that the statistics of multipath spread width and path loss variability are independent. Initial experimental observations indicate that this assumption may not be particularly valid, especially on a short term basis. Reasonably high short term correlation between these fluctuations has been observed on the RADC path although the long term correlation appeared to be low. Additional data is needed to validate the assumption made in the model that the hourly median values of path loss and multipath spread are independent.

Also, questions exist concerning the magnitude of the aperture-to-medium coupling loss portion of the path loss present on path lengths of interest in the tactical situation. The NBS method predicts aperture-to-medium coupling loss which increases with path length while the CCIR method gives one value of loss, determined entirely by antenna gain, which is independent of path length (although there is a definite tendency for the size of antennas employed on a path to be related to the length of the path). Although both methods predict nearly the same loss for long paths, there exists a significant difference in their predictions at short range. The CCIR method predicts up to 5 dB more less for path lengths and antenna sizes typically encountered on tactical troposcatter links. This disagreement leads to about a 20 mile uncertainty in the predicted range of the equipment for path lengths in the vicinity of 100 miles.

4.0 PROPOSED EXPERIMENTAL PLAN

While complete specification of the above parameters for all path configurations and all climate types would require an extensive program of data collection, it is felt that certain specific data will allow reasonable preliminary predictions to be made using generalized prediction models. The most urgently needed data is for:

- 1. Long paths with small (8 and 15 foot) antennas
- 2. Short paths where diffraction effects predominate
- 3. Terrain obstructed paths with large scattering angles
- 4. Obstacle-gain diffraction paths
- 5. Paths of all types in other than continental temperate climate

The test program outlined in this paper is intended to illustrate the type and level of effort required to gather data pertinent to the AN/TRC-170 program as well as other programs involving high data rate digital troposcatter equipment. Currently, there are no plans to perform these tests. The test plan is offered rather to identify a need.

The necessary measurements may be performed using military troposcatter equipment in current inventory appropriately modified to accommodate RAKE measurements. A likely candidate for such modification would be an AN/TRC-132 which is a 10 Kw terminal. With appropriate modifications, it can be used to acquire multipath spread and aperture-to-medum coupling loss data on a variety of paths representative of tactical troposcatter links, in climate types typical of potential deployments. A suggested equipment configuration for this experimental work is shown in Figure 10. The equipment is not operated in its normal diversity configuration. Only two receivers are used. The IF output of one of these receivers feeds a narrowband CW receiver while the other output feeds either a RAKE multipath analysis receiver or a narrowband CW

Multipath spread measurements are made using the RAKE equipment. Aperture-to-medium coupling loss measurements are made by measuring the narrowband path loss using a small (3 foot) reference antenna on one frequency and a typical (8 or 15 foot) tactical troposcatter antenna on an adjacent frequency. The reference antenna is so small that it will suffer virtually no aperture-to-medium coupling loss. Therefore, the difference in the signal levels received on the two antennas may be used to characterize the effective gain of the larger antenna. Comparison of this effective gain with the free-space gain difference between the antennas gives an estimate of the aperture-to-medium coupling loss. Two closely spaced frequencies are used to allow measurement of two distinct paths simultaneously and are not intended to provide or measure any sort of diversity effects.

The data processing for this experiment would involve the calculation of the difference between the short term means of the signal levels on the large aperture link and the reference link when both links are operated in the CW mode. Statistics may be compiled on aperture-to-medium coupling loss based upon this difference in short term means. The RAKE equipment would be operated with the large aperture antennas to determine the multipath spread seen by such apertures. Relevant statistics will be generated to characterize the multipath and Doppler spreading as the data is acquired.

Desirable meteorological support would include observations of wind speed and atmospheric refractivity in the vicinity of the common volume. If possible, the use of an aircraft equipped with a microwave refractometer would provide fine scale atmospheric structure information which would be very useful in refining a multipath prediction model for troposcatter links.

To provide sufficient data to make a significant improvement in the data base, the following test program is suggested. As a minimum, measurements should be made on the following paths:

- 1. A long, average terrain, temperate test path
- A moderate, average terrain, temperate test path
 A short, diffraction, temperate test path
- 4. A short test path in mountainous terrain
- 5. A long test path in the desert
- 6. A short test path in the desert

These suggested test paths will provide data for a variety of conditions anticipated on operational troposcatter paths. These are a practical minimum of test paths - much more data would be helpful.

The three temperate climate test paths will provide the data for long paths with small antennas, for moderate length paths and for short paths where diffraction effects predominate. The intermediate length path is included to provide needed aperture-to-medium coupling loss data as well as reinforce the data base. The long and short paths will provide entirely new multipath and aperture-to-medium coupling loss information.

Data for terrain obstructed paths with large scattering angles and for obstacle-gain diffraction paths will be obtained on the specified short test path in mountainous terrain. The two desert paths will provide data for what is thought to be the most difficult climate type for digital transmission due to the expected wide variability in signal level and large multipath spread.

While measurements in other climatic regions, particularly those known for frequent surface and elevated duct formation, would provide significant and important information, it is felt that what has been described is a minimum measurement program. It is anticipated that data would be obtained at only one frequency and one polarization. The propagation characteristics under investigation are quite uniform across the band of interest and insensitive to antenna polarization.

As a minimum, measurements on these paths should be made both during summer and winter months and, for statistically significant data, observation periods should be at least 30 days long and should include sufficient observations to establish the diurnal behavior of the path.

5.0 CONCLUSION

In this paper, it has been shown how a test program was used to characterize the multipath characteristics of the troposcatter medium as an aid to the design of high data rate digital troposcatter equipment. Given the limitations of physically realizable modems, the question of predicting the performance of troposcatter communication systems utilizing them on postulated paths arises. While much experience in predicting performance of narrowband troposcatter links exists, the adaptive modems of high speed digital troposcatter equipment introduce the new variable of multipath spread width. Before accurate prediction models can be formulated, a representative data base is necessary. Given such a data base, it may be used to refine a multipath spread prediction model based upon observable physical and meteorological parameters of the path. Within these limitations, the prediction model described in this paper may be used as an aid in the selection of paths and appropriate equipment to provide reliable high speed digital transmission.

REFERENCES

Barrow, B. B., et al, April 1969, "Indirect Atmospheric Measurements Utilizing RAKE Troposcatter Techniques," Proceedings IEEE, Vol. 57, pp 537-551.

Bello, P. A., August 1968, "A Study of the Relationship Between Multipath Distortion and Wave Number Spectrum of Dielectric Noise in Radio Links," Signatron Inc., (AFCRL, Contract No. AF 19(628)-5931).

Bello, P. A., April 1969, "A Troposcatter Channel Model," IEEE Trans. Comm. Technology, Vol. COM-17, pp 130-137.

Birkemeier, W. P., et al, September 1973, "Wind Measurements Using Forward-Scatter CW Radar," Journal of Applied Meteorology, Vol. 12, No. 6, pp 1044-1053.

Branham, R., et al, June 1970, "Correlation Bandwidth Measurements Over Troposcatter Paths," Technical Report ECOM-0251-F (AD 871200L).

Branham, R. A., June 1961, "Experimental Observations of Correlation Bandwidth Over Troposcatter Paths," Proc. ICC.

Kennedy, D. J., April 1972, "A Comparison of Measured and Calculated Frequency Correlation Functions Over 4.6 and 7.6 GHz Troposcatter Paths," IEEE Trans. Comm., Vol. COM-20, pp 173-178.

Longley, A. G., Rice, P. L., July 1968, "Prediction of Troposcatter Radio Transmission Loss Over Irregular Terrain-A Computer Method," Institute for Telecommunication Sciences, Boulder, Colorado, Technical Report ERL 79-ITS-67.

Longley, A. G., (ESSA), 16 January 1973, Private Communication to S. M. Harris (MITRE).

Olson, W. A., May 1971, "Comparison Between Computer-Controlled Troposcatter Simulation and an Actual Link," Research and Development Technical Report ECOM-3423 (AD 728102).

Patrick, W. S., Wiggins, M. J., June 1963, "Experimental Studies of the Tropospheric Scatter Medium at Five Gigacycles," IEEE Trans. Aerosp. Navig. Electronics, Vol. ANE-10, pp 133-137.

Price, R., Green, Jr., P. E., March 1958, "A Communication Technique for Multipath Channels," Proc. IRE, Vol. 46, pp 555-570.

Rice, P. L., et al, 1 January 1967, "Transmission Loss Predictions for Troposcatter Communication Circuits," Institute for Telecommunication Sciences, Boulder, Colorado, NBS Technical Note 101 (Rev.), Vols. I & II.

Sherwood, A., Suyemoto, L., 1977, "Multipath Measurements Over Troposcatter Paths," ESD TR-77-252.

RADC TEST RANGE

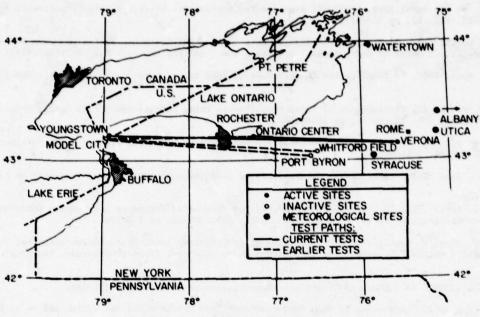


FIGURE 1

PATH PARAMETERS

TRANSMITTER LOCATION	0	NTARIO CENTE	R	YOUNGSTOWN
TRANSMITTER POWER (WATTS)	1,000	1,000	1,000	3,000
ANTENNAS: (TRANSMITTER, RECEIVER)				
SIZE (FT) GAIN (dB) 3 dB BEAMWIDTH (DEG)	8,8 39.1,39.1	8,15(OR 15,8) 39.1,44.5 1.9,1.0	15,15 44.5,44.5	28,28 49.8,49.8 0.54,0.54
ELEVATION ANGLE (DEG)	3/4,3/4	3/4 , 3/4	3/4,3/4	1/2,0
APERTURE - TO - MEDIUM COUPLING LOSS (dB)	5.2	6.9	9.4	16.8
DISTANCE (ST. MI)	86	86	86	168
FREQUENCY (MHz)	4,780	4,780	4,780	4,690

TABLE 1

RAKE SYSTEM FUNCTIONAL DIAGRAM

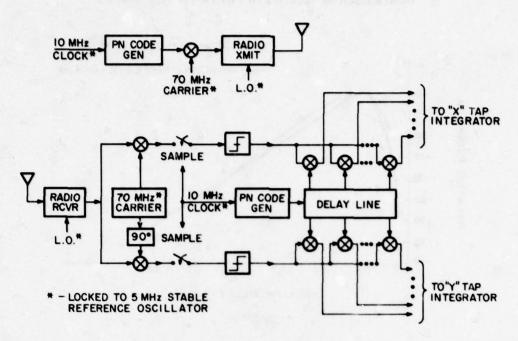
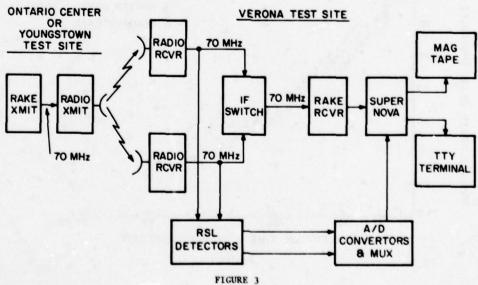
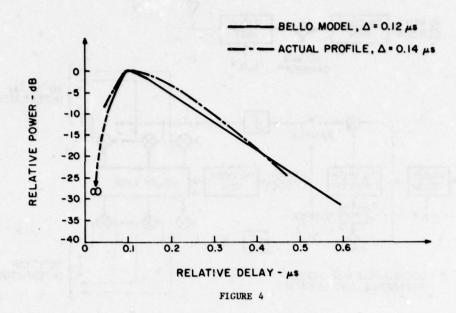


FIGURE 2

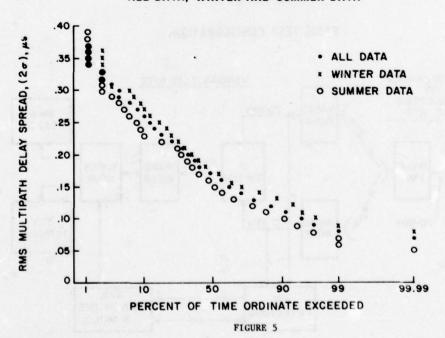
BASIC TEST CONFIGURATION



COMPARISON OF MULTIPATH POWER PROFILE SHAPES



RMS DELAY SPREAD DISTRIBUTIONS - 86 MILE PATH, XMIT 8 FT., RCVR 8 FT., ALL DATA, WINTER AND SUMMER DATA



RMS DELAY SPREAD DISTRIBUTIONS - 86 AND 168 MILE PATHS WINTER DATA

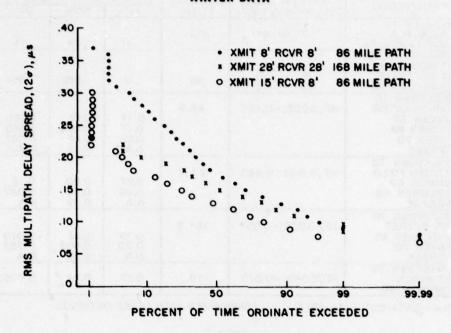


FIGURE 6

RMS DELAY AND MEDIUM RSL VALUES AT .10, .50, AND .90 PROBABILITY POINTS

ANTEN	NA SIZE	PATH LENGTH	RMS	DELAY	4.8	MED	IAN RSL	dBm
Tx	Rx (#)	MILES	10 %	50%	90%	10%	50%	901
∫ 8	8(1)	86	.27	.18	.12	-87	-96	-106
8 }	8(2)	86	. 22	.16	.12	-88	-97	-106
8	15	86	.19	.13	.09	-63	-91	-99
15	8	86	.17	.13	.09	-84	-91	-101
15	15	86	.15	.11	.09	-82	-86	-92
∫ 28	28(1)	168	.20	.15	.11	-90	-95	-102
28	28(2)	168	.21	.17	.11	-89	-93	-101

NOTE: TO ASSESS EXPERIMENTAL VARIABILITY, TWO RECEIVERS WERE USED FOR SOME TESTS. THESE RESULTS ARE BRACKETED AND THE RECEIVER NUMBER IDENTIFIED.

ESTIMATED MULTIPATH SPREADS FROM CORRELATION BANDWIDTH MEASUREMENTS

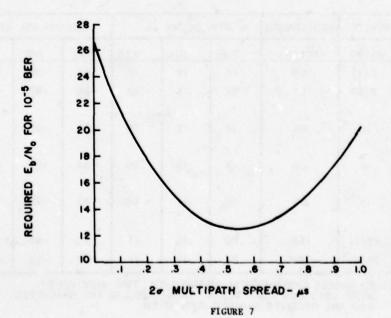
DATH (PERIOR	ANTENNA SIZE.	DISTANCE	ESTIMAT	ED 20 SP	READ AS
PATH/PERIOD	ELEVATION & (DEG)	ST. MI.	10%	50%	90%
GAINSVILLE TO ORLANDO, FLA 14 MAY-15 JUNE 62	12',0":0"	100	.41	.24	.14
TOBYHANNA, PA TO FORT MONMOUTH, NJ OCT 66 - JAN 67 FEB 68 - JULY 68	[5',}	93	.12	.082	.054
YOUNGSTOWN TO ONTARIO CENTER SUMMER 69 OCTOBER 69 WINTER 70 AVERAGE	10',0.025;-0.124	86.9	0.17 0.17 0.23 N.A.*	0.12 0.098 0.14 0.11	0.065 0.065 0.047 N.A.
YOUNGSTOWN TO WHITFORD FIELD SUMMER 69 NOVEMBER 69 AVERAGE	10',0.049; 0.865	123.7	0.27 0.26 N.A.	0.20 0.18 0.19	0.12 0.087 N.A.
YOUNGSTOWN TO POINT PETRE! SEPTEMBER 69 WINTER 70 AVERAGE	10',-0.034;-0.059	101.5	0.19 0.20 N.A.	0.11 0.093 0.10	0.069 0.069 N.A.
YOUNGSTOWN TO PORT BYRON FEBRUARY 70	10',0.049;-0.010	119	0.25	0.14	0.076

* N.A. - DATA NOT AVAILABLE

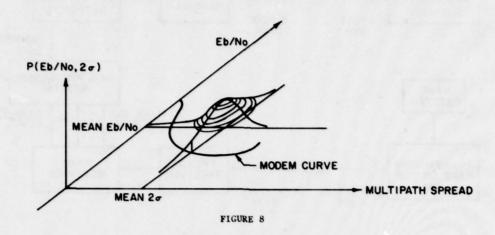
OVERWATER PATH (LAKE ONTARIO)

TABLE 3

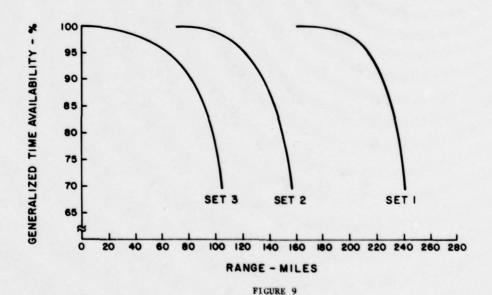
GENERALIZED MODEM CURVE DUAL DIVERSITY MODEM 7.0Mhz BW, 2.048Mb/s



REPRESENTATION OF MODEM CURVE AND JOINT PROBABILITY DENSITY FUNCTION P $\{Eb/No,2\sigma\}$ OF SIGNAL TO NOISE RATIO, Eb/No, and multipath spread, 2σ .



GENERALIZED TIME AVAILABILITY VS RANGE SETS 1, 2, AND 3 $10^{-5}\,\text{Ber}\,$ 2.048Mb/s, 7MHz BW



PROPOSED APERTURE-TO-MEDIUM COUPLING LOSS EXPERIMENT

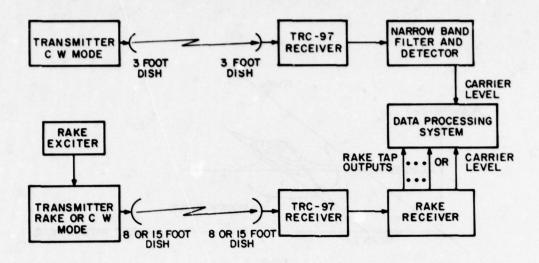


FIGURE 10

PROPAGATION MEASUREMENTS ON A TRANSALPINE OVER-THE-HORIZON PATH

by

J. Osterholz Defense Communications Engineering Centre Reston, Va. U.S.A.

and

P.T. Nielsen, E. Pusone, I. Vogt SHAPE Technical Centre The Hague Netherlands

SUMMARY

This paper presents the results of propagation measurements on a trans-horizon UHF path. The path was a 287 km forward scatter link between Southern Germany and Northern Italy, traversing the Swiss Alps. Measurements were carried out during the period January to June 1977. The results illustrate the large variation in propagation characteristics caused by a diurnally fluctuating mixture of troposcatter and diffraction propagation. Received signal level predictions based on a detailed topographic analysis of the test link, and measured data were shown to be in reasonable agreement. Frequent periods of rapid fading attributed to aircraft passage through the scatter volume were noted and data is presented which characterizes aircraft passage events according to their signal level and differential delay profiles.

1. INTRODUCTION

A long term test program was carried out as a cooperative effort between the Defense Communications Engineering Center (DCEC) and the SHAPE Technical Center (STC) for the purpose of obtaining performance data on multimegabit digital transmission systems operating over communications grade troposcatter links. Testing was accomplished between January and August 1977 over two NATO forward scatter links in Central Europe on which a prototype digital troposcatter transmission system was installed. (Ref. 1). This paper summarises the propagation data taken on one of the links and discusses the communications related aspects of UHF propagation over a highly mountainous transhorizon path.

Major design parameters of the UHF test link are given in Table 1 and a path profile, obtained from system installation records, is shown in Figure 1. Feldberg, the northern terminus of the link, is located on the highest mountain in the Black Forest about 24 km north-east of Todtnau, Germany. The actual site is located near the top of the mountain at an altitude of 1470 metres above sea level. Dosso dei Galli is the southern terminus and is located on one of the peaks in the Italian Alps, approximately 50 km north of Brescia, Italy. The altitude of Dosso dei Galli is 2175 metres above sea level.

	Feldberg	Dosso Dei Galli
Station Codes	AEFZ	IDGZ
Altitudes (m)	1470	2175
Horizon Angles (°)	-0.06	0.60
Antenna Sizes (m)	27	27
Great Circle Distance (km)		287
Nominal Power Output (kw)		4
Nominal Frequency (MHz)	900	
Diversity		quad /frequency)

Table 1. Major Test Link Characteristics

2. MEASURED PROPAGATION CHARACTERISTICS

2.1 Measured Received Signal Level (RSL) Statistics

The RSL of all active receivers was measured at 100 msec intervals with median values computed on the basis of 20 minute runs. Calibrations were made at least once per day to maintain a measurement

error of less than 1 dB and were referenced to the termination of the antenna feeds in the RF equipment room.

Distributions of 20-minute median RSLs for each of the four diversity receivers are presented in Figure 2. Figure 2 includes all data taken during three measurements periods - 24 January - 25 February, 2 April - 4 May and 15 May - 5 June. Although not shown in Figure 2, each of the three measurement periods produced slightly different cumulative RSL distributions. In Period 1, the largest difference was noted between the RSL distributions of the four receivers. The long term median RSL of Receiver 3 (RX3) was about 10 dB higher than those of RX1 and RX2 which, in turn, were 6 dB higher than the long term median RSL of RX4. It was also noted that the standard deviation of RX4 was considerably larger than those of the other receivers. The same general trend was observed in Period 2, but the spread of medians descreased. This development continued into Period 3 where the long term median RSLs of RX1 and RX3 became approximately equal while the median RSL of RX2 continued to be weaker and approached that of RX4. The median path loss for RX4 remained very nearly constant through the three periods, while the path loss for RX3 increased nearly 6 dB between February to May.

For all 20 minute runs, the short term distributions of 100 msec RSL samples were calculated for all receivers in use. Representative short term RSL distributions are shown in Figure 3(a) and 3 (b). Also shown for reference is a cumulative distribution for an ideal Rayleigh fading signal having the same mean power. In Fig. 3 (a), which was obtained during an active fading period, the distribution of the signal level measured in RX4 agrees moderately well with the Rayleigh distribution, except at the higher percentages. However, the fading range of the other receivers is much smaller than expected for a scatter signal. In Figure 3 (b), which was obtained during one of the more frequent shallow fading periods, the fading range of all four receivers is significantly less than that of the Rayleigh distribution which indicates the presence of specular components in the received signals, particularly in RX4.

To illustrate the long term variation of the fading range as well as the correlation between fading range and median RSL, two scatter plots were produced. These plots are shown in Figures 4 and 5 for RX3 and RX4, respectively, and include all data from the first measurement period. In these figures σ_n the standard deviation normalised to the mean of the RSL has been taken as a convenient measure for the fading range. For a Rayleigh fading signal σ_n is equal to zero dB.

From these figures, it is apparent that for both the highly specular channel (RX3) and the apparently Rician channel (RX4), the standard deviation $\sigma_{\mathbf{n}}$ was essentially uncorrelated with the median RSL measured in the appropriate receiver. Thus periods of strong fading were almost equally likely to occur at high or low median RSLs. Furthermore, with the exception of a few occasions, the RSLs of all diversity receivers proved to be essentially decorrelated.

2.2 Fade Rate

Mea fade rate data as measured over nominal 20 minute runs in the first period are shown in Figures 6 (a) and 6 (b) for all four receivers. Figure 6 (a) presents this data as a histogram which has been smoothed for illustrative purposes. Of interest in this figure are the observations that, for all receivers large periods of essentially no fading were measured and also that the distribution for RX2 and RX4 show two peaks. This is most apparent in the case of RX4. This distribution is seen to have a primary peak near 0.0 Hz and a secondary peak at approximately 0.2 Hz. This further supports other measured data which indicate that RX4 and possibly RX2 are composite channels with scatter and specular components. These components alternatively dominate at various times during the tests. The curves for RX1 and RX3 indicate that essentially specular signals were observed in these receivers throughout the first UMF measurement period. In Figure 6 (b), these measurements are presented as cumulative distributions. From this figure, it is seen that median values for the fade rate range from 0.2 Hz for RX4 to essentially 0.0 Hz for RX3. For Rayleigh fading channels it is possible to estimate the RMS doppler spread by multiplying the mean fade rate by 1.4, resulting in a median RMS doppler spread of 0.28 Hz for RX4. This value is consistent with the value of RMS doppler measured on other UHF troposcatter paths of similar length.

In addition to the normally observed fade rates, periods of faster fading occurred. These periods were ascribed to situations where reflected signals from aircraft traversing the scattering volume mixed with the normal propagation components. This area will be discussed in more detail later in this paper.

2.3 Measured Dispersion Statistics

The prediction and measurement of multipath dispersion is especially important on digital forward scatter links since multiplath dispersion can strongly affect the quality of communications. The model developed by Bello (Ref. 2) to estimate troposcatter multipath dispersion has been found to reasonably portray multipath dispersion on medium and long troposcatter paths. Bello postulates a function called the Delay Power Spectrum which he defines as the ensemble average of the time varying troposcatter channel impulse response. The basic shape of the delay power spectrum as derived by Bello is represented closely by a gamma function with climatic and topographic parameters accounting for the specific shape. As such, the model indicates a smooth decrease in received power as a function of increasing path delay. A quantity called $\delta_{\bf g}$, which represents the 2s or the double sided RMS width of the Delay Power Spectrum, is normally used to characterise the amount of dispersion on a troposcatter link.

$$\delta_{\mathbf{s}} = 2 \left[\int \tau^2 Q(\tau) d\tau - \left(\int \tau Q(\tau) d\tau \right)^2 \right]^{\frac{1}{2}}$$

where $Q(\tau)$ is the normalised Delay Power Spectrum and represents the mean received power due to excitation by an impulse function, evaluated at a specific delay, τ .

As the $Q(\tau)$ is, in itself, a long-term time varying quantity and a function of large scale meteorological changes, so is δ_S . In view of this, predictions were made for median and "worst case" values of δ_S . The median value of δ_S was estimated using a normalised effective earth radius (K) of 1.33 and a "worst case" δ_S was estimated using a K of .66, which was selected based upon data obtained from Panter (3) and from Grosskopf (4). Panter indicates that values of K on the order of .6 can be expected as a worst month median value in Europe whereas the measurements by Grosskopf show that a value K<1 does not occur more frequently than 0.1% of the time. The predicted values of δ_S are listed in Table 2.

K-FACTOR	ELEVATION ANGLE	δ _s
1.33 (median)	0	104 nsec
	.25	137 nsec
	.50	178 nsec
.66 (worst case)	0	185 nsec
	.25	242 nsec
	.50	304 nsec

Elevation angle in antenna beamwidths above the standard radio horizon

Table 2. Predicted Multipath Dispersion (δ_s)

Direct measurement of multipath dispersion was not possible due to the unavailability of a RAKE multipath analyser. However, a dispersion monitor derived from adaptation signals developed in the digital troposcatter modem used during the tests provided an approximate but real-time indication of the multipath spread. The dispersion monitor output voltage was translated into values of $\delta_{\rm S}$ using calibration curves obtained via a troposcatter channel simulator prior to the test. The dispersion monitor proved to have a usable dynamic range in $\delta_{\rm S}$ from 100 nsec to 500 nsec.

Since the dispersion monitor indicates total dispersion and is affected by contributions from all functioning diversity receivers, only data collected in a non-diversity configuration can unambiguously characterise the multipath dispersion of a single propagation channel. Single receiver $\delta_{\rm S}$ data was collected and compared with both median RSL and standard deviation $\sigma_{\rm R}$ as computed over 20 minute test runs. Negligible correlation was noted between either median RSL and $\delta_{\rm S}$ or $\sigma_{\rm R}$ and $\delta_{\rm S}$.

Figures 7 (a) and 7 (b) present cumulative distributions of δ obtained during the first measurement period for both single receiver, RX4, and dual space diversity configurations. As seen in Figure 7 (a), the median value of $\delta_{\rm S}$ measured in RX4 was approximately 155 nsec, with a 10 percentile value of 105 nsec and a 90th percentile value of 200 nsec. Dispersion data obtained from RX2 indicated much less dispersion, while data on RX1 and RX3 further confirmed their essentially specular nature. The dual diversity (RX2 + RX4) measurements indicated a measured median $\delta_{\rm S}$ that was approximately 85 nsec larger (240 nsec) than that measured with RX4 alone. The 10^{th} and 90^{th} percentile measured values for (RX2 + RX4) were 185 nsec and 320 nsec, respectively.

Short term (100 msec) correlations between dispersion monitor output and the diversity RSLs were calculated for each 20-minute run. Generally, this correlation was 0.3 or less. An exception, however, achieved during aircraft fading where much stronger correlations (.6 to .8) were measured.

Based on the measured RSL, fade rate, and $\delta_{\rm S}$ data, each of the four diversity receivers appeared to be dominated by different combinations of two distinct propagation modes where each combination is characterised by a different overall propagation delay. Knowing this, it is useful to explore the resultant multipath dispersion after diversity combining. This situation would be equivalent to the dispersion actually seen by a digital troposcatter modem in a diversity configuration on this path. From the measured data, it was concluded that for dual diversity, RX1 + RX3, the combined dispersion was only slightly larger than the dispersion of the individual receivers for most of the time whereas in dual diversity, RX2 + RX4, the combined dispersion was significantly higher. This observation further confirms that RX4 was heavily influenced by troposcatter propagation while RX2 only occasionally had a troposcatter component.

PROPAGATION ANALYSIS

3.1 Analysis of Received Signal Statistics

A comparison between the predicted RSL distribution and the corresponding measured results summarised in Figure 2 shows that, while there is good overall agreement between the predicted RSL distribution calculated using the method developed by the NBS (5) and measurements for RX4, significant differences exist between both the NBS method, and measured data for the other receivers. With the exception of RX4, the measured long term median RSLs for all other receivers tended to be higher than predicted and the standard deviations smaller. This effect is most pronounced for RX3. An interesting corollary observation is that the long term standard deviation of RSL is highest for RX4 and lowest for RX3. Short term RSL distributions, such as those previously shown in Figure 3 (a) and (b), support this observation. Fade rate data for the diversity receivers further confirms the nearly specular nature of RX1 and RX3 and the specular/scatter composition of RX2 and, most significantly, RX4.

It can be concluded from these observations that at least one specular or non-fading signal was present in addition to the troposcatter component in all four receivers. This specular signal was measured as having different and time varying intensities in the four receivers. For most of the time, RX3 was dominated by the specular signal, while RX4 tended to have the largest presence of the troposcatter signal. The other two receivers had about the same ratio of specular and scatter signal power which was slightly less than RX3 but much greater than RX4.

Estimation of the power ratio between the specular and scatter signal components in each of the diversity receivers is difficult since the wideband signal normally transmitted during the tests was subject to frequency selective fading. Frequency selective fading can cause the measured short term RSL distribution to display a fading range which is less than that which would be measured with flat fading.

However, if a narrowband signal (defined as having an effective bandwidth (BW) much less than the frequency correlation bandwidth) is transmitted instead on this link, the received signal would accurately reflect actual propagation conditions. In this case, the relative powers of the specular and fading components can be determined unambiguously from the ratio of standard deviation to mean of the received signal. The derivation of the separation procedure used is given in Appendix A.

To examine possible diurnal influences on the specular/scatter characteristic of this path, received signal levels in RX2 and RX4 using a 100 kHz BW FM transmitted signal instead of the wideband digital signal (7 MHz BW) were recorded for 20 consecutive hours on 6 and 7 May. This recording was processed using the procedure derived in the Appendix A to separate the specular and scatter component powers. The result, summarized in Figure 8, shows the received power for each signal component as a function of local time. The diurnal variation in scatter and specular powers measured in RX4 is the most interesting. As seen in this figure, the composition of RX4 was highly variable, with the scatter component ranging from 2 to 6 dB below the specular component for much of the day. However, between 0000-0200 and during the early morning hours of 0500-0730, the scatter component approached the intensity of the specular component and occasionally exceeded it.

The physical phenomenon responsible for this rather unusual propagation behaviour has not been positively identified. Part of the explanation may lie in the existence of a double diffraction propagation mode not previously expected. In fact, as seen in Figure 2, the largest RSLs of all four receivers approximate Millington's (Ref. 6) diffraction predictions based on double knife edge diffraction quite closely. However, knife edge diffraction alone does not explain the large differences in the median RSLs measured between the four diversity receivers.

In order to gain still further insight into the propagation characteristics of the test link, it was necessary that a more detailed description of the link topography be obtained. This was accomplished by using computerised LANDSAT topographic data. The result, a refined path profile, is shown in Figure 9. Figure 9 reveals a highly variable terrain structure not previously apparent in Figure 1 and confirms that double knife edge diffraction would likely be the dominant propagation mode for a significant percentage of time. It follows from inspection of Figure 9, that significant variations may also occur over a cross-section of terrain subtended by the main beam of the link antennas. To explore the significance of this, another path profile was constructed which indicates the minimum terrain altitude within the main beam of the link antennas. This profile is shown in Figure 10. A comparison with Figure 9, indicates that the propagation obstacles shown in Figure 10 are fewer and, more importantly, that the topographic structure is different. Given the narrow beamwidth of the link antennas, the precise path profile is expected to be very sensitive to antenna pointing. Thus, depending on the actual antenna pointing and prevailing meteomopgical conditions, the actual path profile is likely to be significantly different from the coarse profile shown in Figure 1. Further, off-boresight diffraction combined with possible reflections from near-vertical alpine mountain slopes could give rise to strong specular components which will differ in strength from one diversity path to another. Such specular components would have different transmission delays than the troposcatter component and, as discussed below, also contribute significantly to the overall multipath dispersion of the received signal in a diversity configuration.

3.2 Analysis of Multipath Dispersion Statistics

The analysis of the measured multipath data from the test link and the comparison with predicted values proved most interesting. The median value for the 2σ dispersion, or δ_S , which was measured in the nondiversity configuration utilising RX4 was 155 nsec. This value was higher than the 104 nsec predicted under median conditions at zero antenna elevation angle relative to the radio horizon. This larger value may have been due to one of the following causes:

- (a) The values assumed in the prediction for the effective earth radius and the slope of the refractive index spectrum may be different from the "median" values encountered during the measurements, which consist of only 17 points all taken in February.
- (b) The antenna may in fact have pointed slightly above the horizon, which increases the multipath dispersion (see Table 2).
- (c) The specular component also present in the signal of RX4 (although to a lesser degree than on the other receivers) may have caused an increase in dispersion. The measured increase of 50 ns could easily be explained by this effect if the specular component was due to double knife-edge diffraction; under nominal propagation conditions such a component was calculated to have a propagation delay that is 80 ns shorter than that of the shortest troposcatter path.

The fact that the 90th percentile of the dispersion was also larger than that predicted under worst conditions renders the explanation (a) above rather unlikely. However, no definite conclusion could be arrived at.

Figure 7 (b) shows cumulative distributions of the multipath dispersion measured in dual diversity

also recorded during the first UHF test period.

The measured median multipath dispersion of 230 ns for RX2 + RX4 was approximately 75 ns larger than that measured with RX4 alone. The 10th and 90th percentile measured values were 185 ns and 300 ns, respectively, i.e. 80 and 100 ns larger than for RX4 alone. The most likely explanation for the increase in dispersion is that the path delay of the strong specular component in the signal of RX2 differed markedly from the delay of the signal of RX4. However, it is apparent from Figures 5 and 8 that the signal of RX4 also contained a specular component which had approximately the same magnitude as and often exceeded the scatter component. If this specular component had encountered the same path delay as the specular component of RX2, one would expect a reduction in dispersion for dual diversity rather than an increase, since the power of the specular component in the combined signal would be expected to exceed the power of the scatter component (see Appendix B).

It therefore appears that at least two specular components with different path delays were received, one by RX4 and one by RX2. This conclusion is of course subject to the condition that the dispersion monitor voltage of the modem was a reasonably accurate indication of the $2\ \sigma$ multipath spread also for signals consisting of specular and scatter components. It should also be pointed out that the hypothesis presented above is based on less than 25 hours of measurement, and therefore remains somewhat questionable.

The dispersion measured in dual diversity on receivers 1 and 3 was normally much smaller (see Figure 7 (b)) with a median value of about 120 ns or less. However, values up to 310 ns were measured during a few periods, i.e. values approaching the larger values measured on RX2 and RX4.

The noticeably larger multipath dispersion measured in dual and quad diversity configurations over the non-diversity configuration is highly unusual and appears to be restricted to transhorizon propagation over a mountainous path. For pure troposcatter paths, the RMS multipath dispersion measured under multidiversity conditions should equate to single receiver measurements. However, on the UHF test link, the combination of additional diversity receivers added either a specular signal or a troposcatter signal, each possessing different transit times. Unlike a pure troposcatter path, a small increase in the elevation of the link antennas on this path would actually reduce the multipath dispersion since the received power of the specular components would be rapidly attenuated. Further increases in elevation angle would then result in more gradually increasing the RMS dispersion since the increasing elevation angle would cause greater differential troposcatter delay.

The above discussion concentrated on the prediction of the median $\delta_{\rm S}$. As seen in Figure 7, a relatively large spread about the median value of $\delta_{\rm S}$ was observed. Measurements made on other forward scatter links have also indicated similar spreads about the median $\delta_{\rm S}$ value. Therefore it is useful to compare the results obtained in this test program with the other measurements. Figure 11 contains both the δ distributions obtained from the nondiversity (RX4) and dual space (RX2 + RX4) diversity measurements taken under this proram as well as cumulative distributions of $\delta_{\rm S}$ measured on other test links (Ref. 7, 8). The distributions shown in Figure 11 have been normalised to their respective median values so that a direct comparison of variances can be made. As seen in Figure 11, the variability exhibited by each of the distributions is similar. As an example, the 90th and 99th percentile values of $\delta_{\rm S}$ are about 1.4 to 1.6 times the median (except for the case of receivers 1 and 3, which were dominated by specular components for most of the time).

3.3 Aircraft Passage Events

In addition to the major propagation modes displayed by the transalpine link, frequent periods of very rapid fading were overved. Mean fade rates measured during periods of rapid fading ranges from 12 to 50 Hz as opposed to the .01 to .1 Hz measured during normal fading. Figure 12 is a sample of data taken during the aforementioned periods of rapid fading. The lower trace in Figure 12 is the output of the logarithmic amplifier used to measure RSL. This output is linearly related to the diversity receiver RSL in dBm. The upper trace is the output of the dispersion monitor which is monotonically related to $\delta_{\rm S}$ in nsec. For aircraft fading events, the output of the dispersion monitor is actually an estimate of the differential delay between the normally incident signal and the signal reflected from the aircraft fusalage. Figure 12 is especially interesting since it portrays the three different modes of fast fading which were observed throughout the tests.

The first and most frequently observed fast fading mode, illustrated in Figure 12 (a), is characterised by a varied but elevated (10-20 dB) short term median RSL which is normally symmetrically distributed about a central epoch in the passage event. Fading about the median is relatively shallow (2.5 dB, peak to peak). This fast fading mode was denoted as A/C Mode I and results from a strong reflection from single aircraft as it passes through the scatter volume. As seen in Figure 12(a), during A/C Mode I the output of the dispersion monitor increases steeply as the aircraft enters the scatter volume, decreases as the aircract crosses the great circle path between transmitter and receiver and finally increases again as the aircraft leaves the scatter volume.

The second fast fading mode, denoted A/C Mode II, is typified in Figure 12 (b). A/C Mode II fading is characterised by a scintillation like appearance with no median RSL increase and generally less than 5 dB variation about the median. Multipath dispersion measurements made during A/C Mode II events generally indicate larger differential delays than those measured during A/C Mode I events. It is felt that A/C Mode II results from a single aircraft reflection entering by a side lobe of one of the antennas.

The third fast fading mode, called A/C Mode III, is seen in Figure 12 (c). A/C Mode III is characterised by fast, deep fading (10-20 dB, peak-to-peak) with a large increase in short term median RSL, (10-15 dB). Two explanations are suggested for this phenomena. The first explanation postulates the reception of two or more near equal intensity reflections, one arriving on boresight and the other reflecting from an intermediate region which is within line of sight of both the aircraft and the antenna. As an alternative explanation proposes reflections from multiple aircraft within the scatter volume, itself

As the common volume was located in the vicinity of Zurich International Airport, this explanation is considered more likely.

A comparison of the differential delay estimates measured during aircraft passages with estimates of the multipath dispersion measured under forward scatter conditions indicate that generally larger delays occur during aircraft events. On the UHF test link, differential delays of up to four times the median 20 multipath dispersion were noted and suggest that the performance of digital troposcatter systems will be limited by the occurance of aircraft passage events.

4. CONCLUSIONS

The measured received signal level statistics of the test link was influenced by a mode of propagation which was initially not expected. As a result of the highly variable terrain, strong specular signal components were found to coexist with a scatter component in all receivers and in fact, dominate certain diversity receivers for a substantial fraction of time. During periods when troposcatter was the dominant mode of propagation, good agreement was obtained between predicted and measured short term RSL statistics. However, during periods of mixed specular and scatter propagation, short term RSL statistics varied considerably from one diversity receiver to another and were consequently not predicted with any accuracy.

The existence of highly variable differential median diversity signal levels on the test link could cause a reduction of performance with digital transmission systems where a common control signal based on RSL is used to adjust diversity receiver gains. Since digital troposcatter performance is strongly related to both RSL and dispersion, adjusting receiver gains on the basis of RSL alone could reduce the effectiveness of lower power diversity paths having large amounts of implicit diversity due to dispersion.

The multipath spread, $\delta_{\rm S}$, for the UHF test link was measured for non and dual diversity, and was found to be larger than the values predicted initially. The larger measured values are, at least partially due to the mixed mode propagation encountered on the test link.

Since the increased multipath dispersion associated with mixed propagation modes can have significant influence on the transmission of wideband digital signals, it is extremely important to be able to predict the possible occurrence of such modes. In the case of the transalpine test link, the path profile used during engineering of the implace analog system proved inadequate for this purpose. The measured data could not be explained until after a detailed topographic analysis of the test link was accomplished. As a result, it is felt that a detailed topographic analysis and available analog link performance data are extremely valuable adjuncts to the design of digital troposcatter links that traverse large areas of mountainous terrain.

Aircraft passage events resulting in rapid fading occurred frequently throughout the test program. These events could be classified into three modes depending on the specific RSL and differential delays measured under normal forward scatter conditions were noted.

APPENDIX A

On The Separation of a Rice-Fading Channel into a Rayleigh-Fading and a Non-Fading Component

This appendix derives a relationship that permits the power ratio between the non-fading and the Rayleigh-fading components of a Rician fading-signal to be determined given a knowledge of the ratio of standard deviation to mean of the composite signal.

The output signal of a Rician channel may be thought of as consisting of two quadrature Gaussian signals plus a constant signal which for convenience may be taken to be in phase with one of the Gaussian components (Ref. 9). If the two quadrature components of the Rician signal are denoted \mathbf{X}_1 and \mathbf{X}_2 , it follows that \mathbf{X}_1 and \mathbf{X}_2 are independent random variables with density functions:

$$f_1(x_1) = \frac{1}{\sigma\sqrt{2\pi}} \exp\left[-\frac{|x_1|^2}{2\sigma^2}\right]$$
 (A1)

$$f_2(x_2) = \frac{1}{\sigma \sqrt{2\pi}} \exp \left[-\frac{(x_2 - m)^2}{2\sigma^2} \right]$$
 (A2)

where it can be assumed without loss of generality that $m \ge o$. The powers of the two quadrature signals, defined as $Z_1 = X_1^2$, are also satistically independent random variables. The total output power of the Rician channel is $Z = Z_1 + Z_2$.

By simple transformations, the density functions for \mathbf{z}_1 and \mathbf{z}_2 can be shown to be:

$$P_1(Z_1) = \frac{1}{\sigma \sqrt{2\pi Z_1}} \exp(-\frac{Z_1}{2\sigma^2}) U(Z_1)$$
 (A3)

$$P_{2}(Z_{2}) = \frac{1}{2\sigma\sqrt{2\pi}Z_{2}} \left[\exp\left(-\frac{(\sqrt{Z}_{2}-m)^{2}}{2\sigma^{2}}\right) + \exp\left(-\frac{(\sqrt{Z}_{2}+m)^{2}}{2\sigma^{2}}\right) \right] U(Z_{2})$$
 (A4)

where U(Z) is the unit step function,

$$\mathbf{U}(\mathbf{Z}) = \left\{ \begin{array}{ll} 0 & \mathbf{Z} \leqslant 0 \\ 1 & \mathbf{Z} > 0 \end{array} \right. \tag{A5}$$

From (A3), it is easy to show that

$$\mathbf{E}(\mathbf{Z}_1) = \sigma^2 \tag{A6}$$

$$Var \{Z_i\} = 2\sigma^4$$
 (A7)

The same results follow as special cases of the following calculations for \mathbf{Z}_2 .

Evaluation of the moments of \mathbf{Z}_2 involves the following integral:

$$I = \sigma^{\int_{0}^{\infty} \frac{\mathbf{z}^{\mathbf{n}}}{2\sigma\sqrt{2\pi}\mathbf{Z}^{\mathbf{n}}}} \left[\exp\left(-\frac{(\sqrt{\mathbf{z}}-\mathbf{m})^{2}}{2\sigma^{2}}\right) + \exp\left(-\frac{(\sqrt{\mathbf{z}}+\mathbf{m})^{2}}{2\sigma^{2}}\right) \right] d\mathbf{z}$$
 (A8)

which after substitution $t = \sqrt{z}$ becomes

$$I = \int_{0}^{\infty} \frac{t^{2n}}{\sigma^{2n}} \left| \exp\left(-\frac{(t-m)^{2}}{2\sigma^{2}}\right) + \exp\left(-\frac{(t+m)^{2}}{2\sigma^{2}}\right) \right| dt$$

$$= \int_{0}^{\infty} \frac{t^{2n}}{\sigma^{2n}} \exp\left(-\frac{(t-m)^{2}}{2\sigma^{2}}\right) dt$$

$$+ m^{\int_{\infty}^{\infty}} \frac{t^{2n}}{\sigma \sqrt{2\pi}} = \exp\left(-\frac{(t-m)^2}{2\sigma^2}\right) dt$$

$$+ \int_{0}^{\infty} \frac{t^{2n}}{\sigma\sqrt{2n}} \exp\left(-\frac{(t+m)^{2}}{2\sigma^{2}}\right) dt$$
 (A9)

After another substitution in which the arguments of the exponentials are denoted -u, the following expression results:

$$I = o^{\int_{0}^{\infty} \frac{(m + \sqrt{2\sigma^{2}u})^{2n} + (m - \sqrt{2\sigma^{2}u})^{2n}}{2\sqrt{\pi}\sqrt{u}}}$$
(A10)

This integral is easy to evaluate for n equal to 1 and 2. The results are:

$$\frac{n=1}{E\{z_2\} = m^2 + \sigma^2}$$
(All)

$$\frac{n=2}{E\{z_2^2\}} = m^4 + 6m^2\sigma^2 + 3\sigma^4$$
(A12)

so that

$$Var\{z_2\} = 2\sigma^4 + 4m^2\sigma^2$$
 (A13)

Since \mathbf{Z}_1 and \mathbf{Z}_2 are independent, the mean and variance of \mathbf{Z} are simply:

$$E(Z) = E(Z_1) + E(Z_2) = 2\sigma^2 + m^2$$
 (A14)

$$Var{z} = Var{z_1} + Var{z_2} = 4\sigma^4 + 4m^2\sigma^2$$
 (A15)

The ratio $\frac{1}{R}$ of standard deviation to mean of the Rician signal is therefore

$$\frac{1}{R} = \frac{20\sqrt{m^2 + \sigma^2}}{2\sigma^2 + m^2} \tag{A16}$$

or
$$\frac{1}{R} = \frac{\sqrt{1+2y}}{1+y}$$
 (A17)

where
$$y = \frac{m^2}{2\sigma^2}$$
 (A18)

is the desired power ratio between the non-fading and the Rayleigh-fading components. Solving for y, one finds

$$y = R^2 + R\sqrt{R^2 - 1} - 1 \tag{A19}$$

which is the desired result.

Fig. 13 shows two curves representing the power of the specular signal and the power of the Rayleigh signal in dB relative to the power of the composite signal. These curves correspond to the fractions y/(1+y) and 1/(1+y), respectively.

APPENDIX B

Multipath Dispersion for Mixed-Mode Propagation

On the UHF link the received signal was composed of a scatter component and a specular component. The path delay difference, τ , between the two components can be shown to be 79 ns.

The multipath dispersion, $\delta_{\rm g}$, (20 value of the delay power spectrum) for the combined signal depends on the ratio of specular to scatter component. $\delta_{\rm g}$ can be calculated, if a particular shape of the delay power spectrum is assumed for the scatter signal.

The delay power spectrum D(x), predicted by the Bello model can be approximated by:

$$D(x) = \frac{2x}{\sigma^2} e^{-\frac{\sqrt{2}x}{\sigma}}$$
(B1)

where 20 is the multipath dispersion of the scatter signal.

The mean m of x is given by:

$$\mathbf{m} = \int_{0}^{\infty} \frac{2\mathbf{x}^{2}}{\sigma^{2}} \mathbf{e}^{-\frac{\sqrt{2}\mathbf{x}}{\sigma}} d\mathbf{x} = \sqrt{2} \sigma$$
 (B2)

The delay power spectrum, $D_{c}(x)$, of the combined signal is composed of D(x) multiplied by the power, P_{sc} , of the scatter signal and a Delta function at $x = -\tau$ with the power, P_{sp} , of the specular component (with $P_{sc} + P_{sp} = 1$).

The mean, m_c , and the standard deviation, σ_c , are then given by:

$$\mathbf{m}_{\mathbf{C}} = \mathbf{p}_{\mathbf{SC}} \mathbf{m} - \mathbf{p}_{\mathbf{SD}} \mathbf{T} \tag{B3}$$

$$\sigma_c^2 = p_{sc}(\sigma^2 + m^2) + p_{sp}\tau^2 - m_c^2$$
 (B4)

combining equations B3 and B4 gives:

$$\sigma_c^2 = \sigma^2 (1+2P_{sp})P_{sc} + 2\sqrt{2} \sigma \tau P_{sp}P_{sc} + \tau^2 P_{sc}P_{sc}$$
 (B5)

Let
$$y = P_{sp}/P_{sc}$$
 (B6)

then
$$P_{sp} = y/(1+y)$$
 $P_{sc} = 1/(1+y)$ (B7)

With these values for the specular and the scatter components, σ^2 becomes:

$$\sigma_c^2 = \frac{1}{(1+y)^2} \{ (1+3y)\sigma^2 + 2\sqrt{2} \sigma \tau y + \tau^2 y \}$$
 (B8)

The multipath dispersion, $\delta = 2\sigma$, has been calculated for the range of multipath dispersion expected on the UHF-link and is shown in Fig. 14.

It can be seen that the maximum increase in multipath dispersion caused by the specular component is about 70 ns. As expected the multipath dispersion of the combined signal is actually less than that of the scatter component for large ratios of $P_{\rm SD}$ / $P_{\rm SC}$.

REFERENCES

- Defense Communications Engineering Center and SHAPE Technical Center, "Combined US/NATO Digital Troposcatter Test Plan", October 1976.
- BELLO, P.A., April 1969, "A Troposcatter Channel Model," IEEE Transactions on Communications Technology, Vol. COM 17, No. 2, pp. 130-137, April 1969.
- 3. PANTER, P.F., Communications System Design, New York, McGraw-Hill, pp. 390-392, 173.
- GROSSKOPF, K., April 1957, "Statistische Ermittlung des Krümmungsfaktors K im aquivalenten Erdradius aus Radiosondenaufstiegen, Fernmeldetechnisches Zentralamt der Deutschen Bundenspost", Technischer Bericht, Nr. 5528.
- RICE, P.L., et al., May 1965, "Transmission Loss Predictions for Tropospheric Communications Systems," National Bureau of Standards Tech Note 101, Vols. 1 and 2.
- MILLINGTON, G., et al., September 1962, "Double Knife-edge Diffraction in Field Strength Predictions", Proc. IEE, Vol 109, Part C, No. 16, pp. 419-429.
- 7. SIGNATRON INC., January 1973, "Digital Troposcatter Experiments", RADC-TR-72-350, pp. 11 to 56.
- SHERWOOD, A.R. and FANTERA, I; A., December 1975, "Multipath Over Troposcatter Paths with Application to Digital Transmission", NTC-75, pp. 28-1 to 28-9.
- 9. RICE, S.O., January 1948, "Statistical Properties of a Sine Wave plus Random Noise," BSTJ, Vol 27.

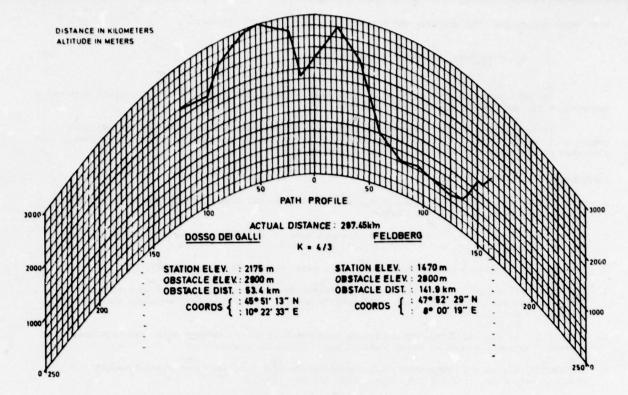


Fig. 1: Path profile

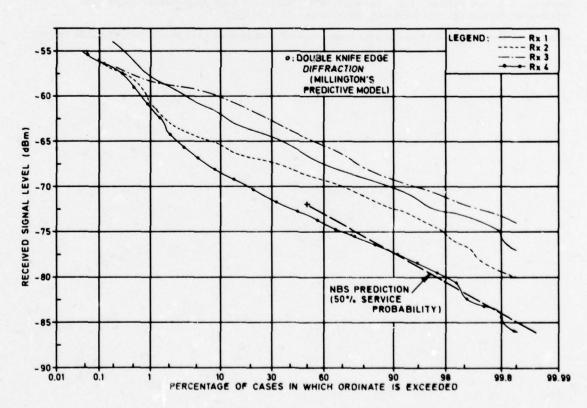
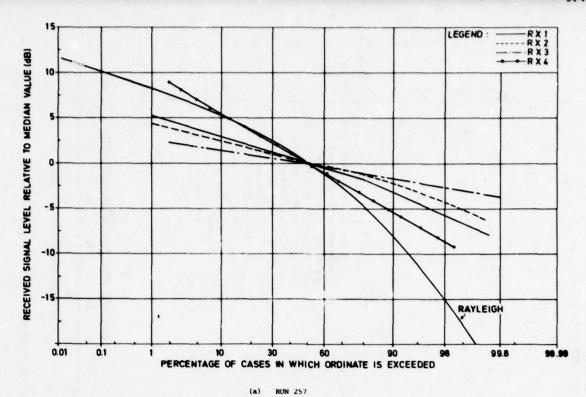


Fig. 2: Cumulative distribution function of received signal level (24 January - 5 June 1977)



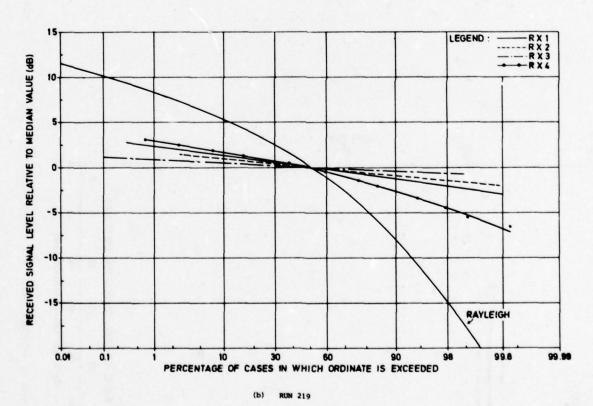
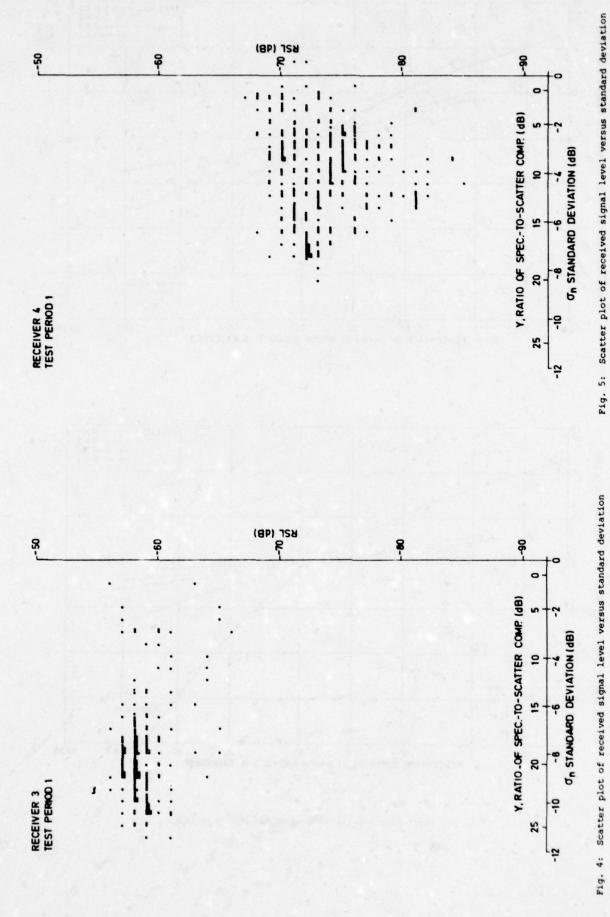
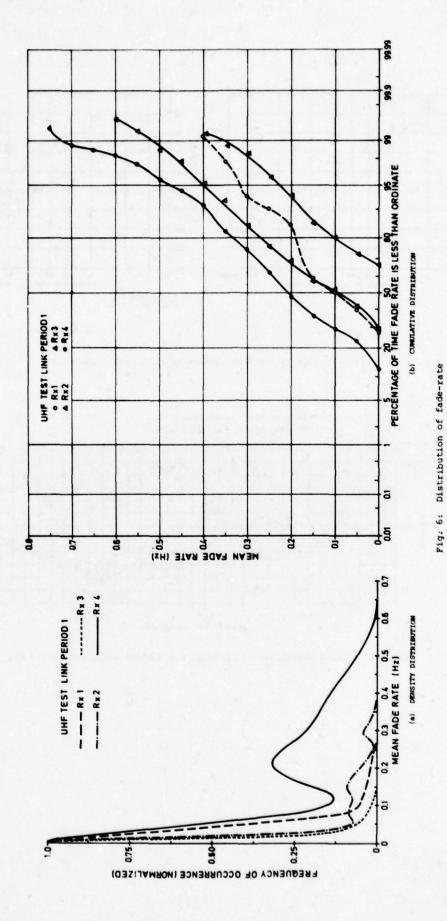


Fig. 3: Short-term distribution of received signal level





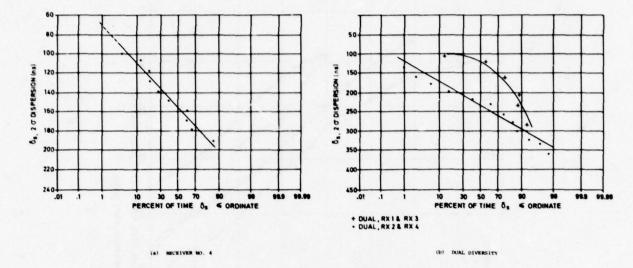


Fig. 7: Cumulative distribution of multipath dispersion

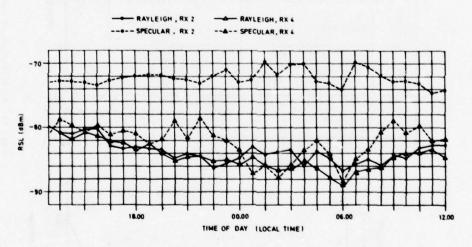


Fig. 8: Diurnal variations of specular and scatter components - 6-7 May

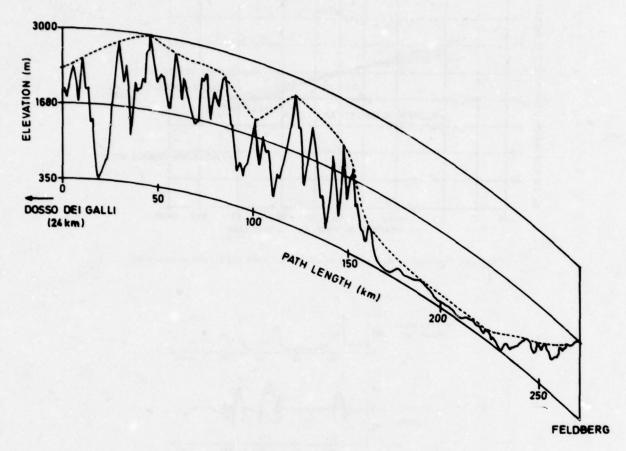


Fig. 9: Detailed great circle profile

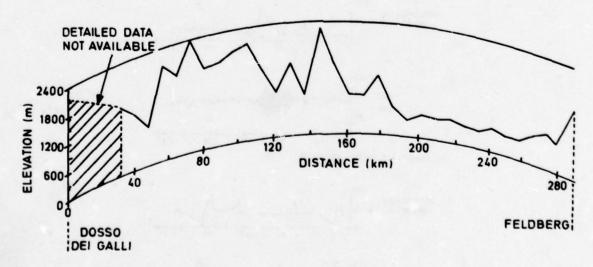


Fig. 10: Profile of lowest main beam elevation

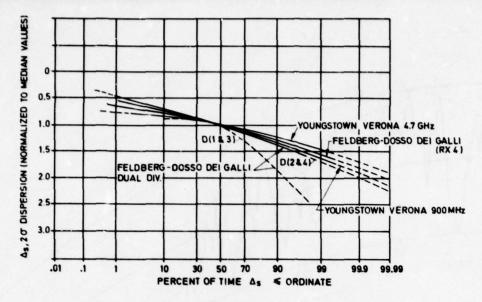


Fig. 11: Cumulative distribution of normalised multipath dispersion

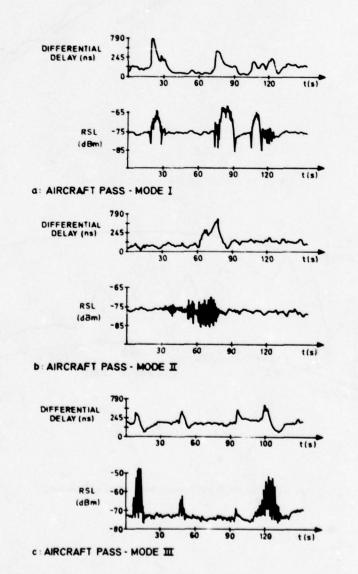


Fig. 12: Examples of RSL and dispersion measured during aircraft passes

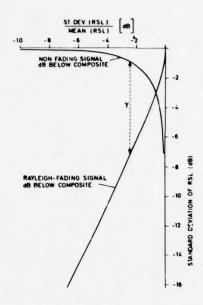


Fig. 13: Separation of scatter and specular components

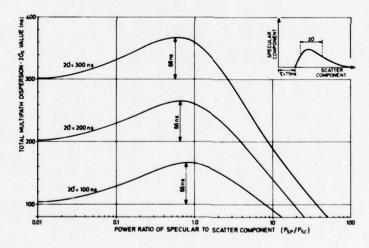


Fig. 14: Multipath dispersion for mixed mode propagation

UTILISATION DES CODES PSEUDO ORTHOGONAUX DANS LES CANAUX MULTITRAJETS NON STATIONNAIRES

USE OF PSEUDO-ORTHOGONAL CODES IN RANDOM MULTIPATH CHANNELS

par

F.Chavand, M.Gindre et C.Goutelard Laboratoire d'Etudes des Transmissions Ionosphériques Université Paris-Sud 9 avenue de la Division Leclerc 94230 Cachan, France

SUMMARY

Impulse response time in multipath channels such as ionospheric channel or VHF links, is an important limitation of bit rate in digital information transmissions. These transmission problems may be solved by use of information coding, code vectors being characterised by good aperiodic correlation. Such codes are called pseudo-orthogonal codes.

Use of pseudo-orthogonal codes allows to obtain increase of bit rate while a very low error ratio is guaranted.

The present paper has pseudo-orthogonal codes classification and codes construction algorithms.

These codes have been used in multipath ionospheric channel transmissions. Errors in particular path caused by interference of the other propagation modes are corrected for by the redundancy introduced by pseudo orthogonal codes. Furthermore the multiple paths can be considered to be functionning as sources repeating message and may be analysed by using the same codes.

Optimum receivers are selected according as one or more than one path are treated at reception: they are defined in studying the probability of error.

Probabilities of error are calculated in accordance with signal/noise ratio and propagation conditions.

Results show that for a required bit rate probability of error decreases considerably in comparison with classical systems.

A mode m has been developped and used in order to verify the theoritical study.

Experimental results demonstrate the validity of the principle and show the performances obtained.

RESUME

La durée de la réponse impulsionnelle des canaux multitrajets, tels que le canal ionosphérique où les liaisons VHF est une limitation importante du débit d'information.

L'utilisation des codes pseudo orthogonaux dont les vecteurs présentent des fonctions d' intercorrélation très faibles, permet d'envisager une augmentation importante du débit d' information tout en assurant des très faibles taux d'erreur.

Le présent article présente des classes de codes pseudo orthogonaux et montre qu'elles appartiennent à l'ensemble des codes les plus efficaces.

Des algorithmes de construction de codes sont développés et des exemples sont donnés. Ces codes ont été utilisés pour assurer des transmissions de données par le canal ionosphérique II est montré qu'il est possible d'optimiser le choix des codes pour un débit d'information désiré et que les codes pseudo orthogonaux autorisent l'utilisation des trajets multiples comme sources redondantes de l'information.

Plusieurs critères de décision peuvent être adoptés selon que l'onaccepte d'utiliser pour la transmission un ou plusieurs trajets.

Les critères optimum sont déterminés par l'étude des probabilités d'erreur.

A partir des critères optimum de décision, les probabilités d'erreurs sont calculées en fonction du rapport (Energie par bit d'information/ Densité spectrale de bruit) pour différentes configurations des conditions de propagation.

Les résultats obtenus montrent que pour un débit d'information donné, la probabilité d'erreurs est considérablement diminuée par rapport aux systèmes classiques. D'autre part, il est possible de réaliser des transmissions de données numériques à vitesse élevée.

Un modem a été développé et utilisé pour étayer l'étude théorique.

Les résultats expérimentaux sont très étroitement correlés avec les résultats théoriques.

Les applications de ce système apparaissent nombreuses tant dans les transmissions que la détection et la correction des erreurs ou dans les systèmes nécessitant des synchronisations automatiques.

La durée de la réponse impulsionnelle des canaux multitrajets, tels que les canaux ionosphériques ou VHF, limite le débit d'information dans les transmissions numériques.

Différentes solutions ont été proposées pour pallier cette limitation : utilisation de la diversité de fréquence [1], de systèmes adaptatifs [2] [3]

La solution présentée ici, repose sur l'utilisation de codes particuliers, dont les fonctions d'intercorrélation entre les vecteurs demeurent faibles [4] [5] [6]. Des codes répondant partiellement à ces conditions sont connus : codes pseudo-aléatoires (PN), codes orthogonaux et codes autosynchronisants [7], mais il n'existe pas à notre connaissance, de méthodes systématique permettant de déterminer les codes les plus performants. Une telle méthode de construction est proposée. Elle repose sur une généralisation de l'idée développée par GOLD [8] et aboutit à la construction des codes que nous avons appelés pseudo-orthogonaux.

Les performances de ce système sont évaluées, pour un degré d'interférence donné entre les trajets multiples comme sources redondantes répétant l'information. Plusieurs critères de décision sont applicables. Il est montré que pour une complexité donnée du récepteur le choix de ce critère peut être optimalisé pour obtenir le taux d'erreur le plus faible possèble.

I - PRINCIPE D'UNE TRANSMISSION PAR CODE PSEUDO-ORTHOGONAUX

La réponse impulsionnelle d'un canal multitrajet est constituée par une série d'impulsions. On appellera par la suite trajet principal, celui qui apporte l'affaiblissement minimum tandis que les autres seront appelés trajets secondaires.

Le principe de cette transmission consiste, à l'émission, à faire correspondre à chaque symbole du message un mot code binaire - ou vecteur code - v¹ de n éléments binaires (e,b,), d'un code V. A la réception le signal reçu est comparé par corrélation à tous les mots-code de V. Un circuit de décision du type à maximum de vraisemblance permet de restituer l'information (figure 1).

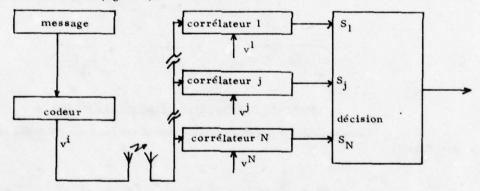


Figure 1 Schéma de principe de la liaison

Les interférences introduites par les différents trajets sont corrigées par la redondance du code.

II - DEFINITION DES CODES PSEUDO-ORTHOGONAUX

Dans le cas où la transmission se faitselon un mode synchrone, les signaux captés par le récepteur se présentent dans la configuration de la figure 2. La synchronisation étant faite sur le trajet principal, le corrélateur j, ayant le vecteur v comme signal de référence, fournirait en l'absence de bruit le signal Sj

 $S_{j} = \rho(0) + \sum_{r=1}^{2} \alpha_{r} \left[\rho_{j}(z_{r}) + \rho_{j}(-(z_{e}-z_{r}+z_{b})) \right]$ (1)

où

- &r désigne l'amplitude relative du l'ième trajet secondaire par rapport au trajet principal et q le nombre de trajets secondaires

- t_c est la durée d'un vecteur code et t_b l'espace entre deux vecteurs.

- la fonction de corrélation $\rho_{j_i}(\zeta_r)$ entre les vecteurs v^i et v^j décalés d'un temps n est dite apériodique car le signal reçu est apériodique. Cet adjectif permet de la différencier de la fonction de corrélation périodique $\rho_{j_i}(\zeta_r)$ qui serait obtenue avec un signal reçu périodique caractérisé par $t_b = 0$; par la suite ces notations désignent des fonctions de corrélations normées à l.

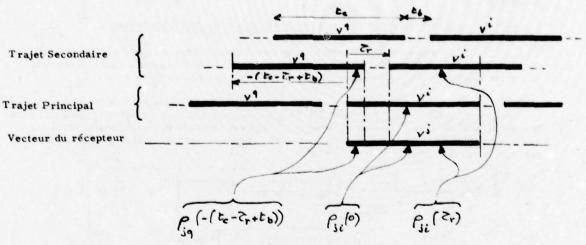


Figure 2
Structure du signal reçu à l'instant de décision

Le code adapté à ce type de transmission est celui qui minimise les termes parasites :

$$p = \rho_{ji}(0) + \sum_{r=1}^{q} \forall_r \left[\rho_{ji}(\vec{r}_r) + \rho_{jq} \left(-(t_c - \vec{r}_r + t_b) \right) p_{our} i \neq j \right]$$

$$p = \sum_{r=1}^{q} \forall_r \left[\rho_{jj}(\vec{r}_r) + \rho_{jq} \left(-(t_c - \vec{r}_r + t_b) \right) p_{our} i = j \right]$$
(1bis)

Anotre connaissance, il n'existe pas à l'heure actuelle de méthode de synthèse de codes permettant de minimiser le terme parasite p de Sj

Cependant les vecteurs du code peuvent être caractérisés par le fait que les valeurs prises par leurs fonctions d'autocorrélation, en dehors de leur maximum, et par leurs fonctions d'intercorrélation sont, en valeur absolue, bornées par une valeur faible devant 1, car cette propriété permet d'obtenir une forte atténuation du terme parasite p donc des trajets perturbateurs.

Il est possible de construire des ensembles dont les vecteurs sont caractérisés par des corrélations périodiques bornées.

$$|\rho(0)| \leq S_0 \quad \forall i \neq j$$
 (2)

$$\begin{aligned} |\rho_{ij}(0)| &\leq S_o & \forall i \neq j \\ |\rho_{ij}^{p}(2)| &\leq S_c^{p} & \forall i,j \quad \forall 2 \neq 0 \end{aligned}$$
 (2)

où So et Se sont des constantes strictement inférieures à l aussi faibles que possible et dont on peut déterminer les limites.

Cette approche du problème est intéressante, car elle permet d'effectuer un développement théorique complet. Cet exposé décrit une méthode de construction de codes caractérisés par les inégalités (2) et (3)

Pour un code V (n, k) constitué de vecteurs de n éléments binaires (e.b.) et de k bits d'information, on montre comment il est possible de déterminer le meilleur couple So et S_{ϵ}^{p} en déduisant le code pseudo orthogonal V (n, k) d'un code cyclique W (n, K).

Les codes sont ensuite testés pour déterminer la borne supérieure du terme parasite p.

III - CONSTRUCTION DES CODES BINAIRES V (n, k) PSEUDO ORTHOGONAUX

M. 1 Principe de la construction

Un vecteur
$$v^i$$
 de $V(n, k,)$ constitué par la suite des $a.b.$ $\begin{bmatrix} a_0^i, a_1^i, \dots, a_n^i, \dots, a_{n-1}^i \end{bmatrix}$

est défini par la matrice ligne
$$\begin{bmatrix} v^i \end{bmatrix} = \begin{bmatrix} 1 & 1 & 1 \\ 1 & 1 & 1 \end{bmatrix}$$
 où $j \in [0, n-1]$ $a_j^i \in [0, 1]$

Le symbole x v représente le vecteur obtenu après p permutations circulaires des composants de vi [xpvi] = [ain-p,ain-p+1, ---,ai,ai, ---ain-p-1]

La somme modulo deux entre deux vecteurs vⁱ et v^j est le vecteur dont chacune des composantes

est la somme modulo 2 des composantes de même rang de vⁱ et v^j

[vⁱ] \oplus [v^j] = [--, a_q \oplus a_q, --]

On montre [5] que la fonction de corrélation périodique

en fonction des distances extrêmes - au sens de HAMMING - entre les vecteurs du code, par la relation :

$$\rho_{ij}^{P(z)} = \left[m - 2d(v_i^i x^z v_i^j) \right] / n$$
(4)

où d (v, x v) est la distance entre les vecteurs vi et x v

Le problème de la recherche du minimum de $|\mathcal{P}_{ij}^{P}(\mathcal{E})|$ se trouve alors posé sous une forme classique qui est la recherche de codes linéaires caractérisés par certaines contraintes imposées à leur distance de HAMMING.

En effet, si d max (V) et d min (V) désignent les distances extrêmes entre les vecteurs d'un code V, l'inégalité (2) s'écrit :

 $d_{max}(V) \leq (1+5.) n/2$ (0)

 $d_{\min}(V) \gg (1-S_o)n/2$ (b) (5)

car pour $\overline{C} = 0$ la relation (4) ne fait intervenir que des vecteurs de V. Pour $\overline{C} \neq 0$ la relation (3) conduit à

 $d_{max}(W) < (1+S_c^*)n/2$ (6)

 $d_{min}(w) > (1 - S_c^P) n/2$ (b)

car v^i et $x \overset{\triangleright}{\sim} v^j$ sont des vecteurs du code cyclique W dans lequel V est inclus. De plus, l'inégalité (3) implique que $x \overset{\triangleright}{\sim} v^j$ et v^i soient différents, donc :

- lorsque i ≠ j on doit vérifier que vi≠x vi V≥ €[1,n:]ce qui implique que tout vecteur vi doit être d'ordre égal ou supérieur à n; c'est à dire que les n-l permutations circulaires qui peuvent être effectuées sur ses composantes conduisent à des vecteurs différents de vi.
- Lorsque i ≠ j on doit vérifier que vⁱ ≠ x ≥ v^j, ∀ i ≠ j , ∀ ≥ ∈ [1,n-1] ce qui implique que vⁱ et v^j n'appartiennent pas à une même classe du code cyclique W. Une classe d'un code cyclique étant constituée d'un vecteur et de tous ceux qui s'en déduisent par permutation circulaire de ses composantes.

Par conséquent, le code V (n, k) peut être composé de N = 2^k vecteurs d'ordre n tels que deux quelconques d'entre eux appartiennent à deux classes différentes d'un code cyclique W dans lequel les distances extrêmes entre deux vecteurs vérifient les inégalités (6)

Si le code cyclique W contient & classes résiduelles d'ordre n, le nombre de codes N' satisfaisant ces conditions est donné par :

où CN est le nombre de combinaisons de N éléments pris parmi a

Il est donc possible de trouver un grand nombre de codes, cependant, si la sélection des vecteurs est faite de façon aléatoire, les performances du code peuvent être inintéressantes.

La méthode de construction proposée conduit à un choix optimum et systèmatique de ces vecteurs.

III. 2 Méthode de construction des codes pseudo -orthogonaux.

Le choix d'un vecteur par classe d'ordre n de W peut être fait en effectuant une opération linéaire interne à W. Eneffet, soient

- V1 (n, k) un code cyclique inclus dans W (n, K)

- C un vecteur d'ordre n appartenant à W-V1, complèment de V1 dans W.

On montre [6] que le code V(n, k) définit par l'équivalence suivante :

$$v^i \in V(n,k) \Leftrightarrow [v^i] = [v_a^i] \oplus [c], [v_a^i] \in V_a(n,k)$$
 (7)

est tel que ses vecteurs sont d'ordre n, deux quelconques d'entre eux appartenant à deux classes différentes du code cyclique W.

Ce type de construction des codes pseudo-orthogonaux conduit à une expression simple des inégalités (5). En effet, v' et v^j étant deux vecteurs quelconques de V déduits de v^i_1 et v^j_2 par la relation (7), les distances d (v^i_1, v^j_2) et d (v^i_1, v^j_2) sont égales. Aussi, pour que les inégalités (5) soient vérifiées sur V, il faut et il suffit qu'elles le soient sur V_1

Cette propriété rend la méthode très intéressante car V₁ étant cyclique, on est ramené à un problème classique de détermination des distances extrêmes d'un code cyclique.

De plus, les codes pseudo-orthogonaux obtenus par cette méthode de construction appartiennent aux plus efficaces. En effet, il a été effectué une évaluation statistique [5] du nombre maximum de vecteurs d'une code pseudo orthogonal respectant les conditions (2) et (3) en fonction de R = Max (n | ?;). Les résultats obtenus par cette méthode de construction montre que l'on atteint, pour R donné, ce nombre maximum de vecteurs.

En conclusion, les codes optimaux V (n, k) peuvent être obtenus par une opération de translation interne dans un code cyclique W:

où W, V1 et c sont tels que :

V 1 (n, k,) code cyclique dont les distances extrêmesvérifient les inégalités (5)

W (n, k,) code cyclique dont les distances extrêmesvérifient les inégalités (6)

c vecteur d'ordre n appartenant au complément de V1 dans W

III. 3 Résultats

Cette méthode peut être appliquée à la construction des codes V (n, k) ayant n'importe quelle valeur impaire de n et n'importe quelle valeur de k [6]

On s'est contenté ici de reproduire les résultats les plus intéréssants concernant des codes qui sont orthogonaux (So =0) ou presque (So=1/n).

Les grandeurs reportées dans le tableau de la figure 3 sont :

$$E = \text{Max}[n|\rho_{ij}(0)|] \qquad \forall i \neq j$$

$$R = \text{Max}[n|\rho_{ij}(2)|] \qquad \forall i,j \quad \forall 2 \neq 0$$

$$R^{P} = \text{Max}[n|\rho_{ij}(2)|] \qquad \forall i,j \quad \forall 2 \neq 0$$

$$RR = \text{Max}[n|\rho_{ij}(2) + \rho_{iq}(-(t_{c}-2))|] \quad \forall i,j,q \quad \forall 2 \neq 0$$

Eel R^P sont liées à So et S_e par les relations

$$\mathcal{E} \leq n S_o$$
 $\mathbb{R}^P \leq n S^C$

et R la valeur maximale du terme parasite ρ (cf relation l bis) lorsque l'espace entre deux vecteurs est égal à la longueur d'un vecteur t_b = t_c

RR est la valeur maximale de ce même terme parasite lorsque th = 0 (émission continue).

On a reporté également les valeurs du paramètre de RR obtenus par des codes proposés par J. J. STIFFLER [7]. On constate que ces codes n'atteignent pas les conditions optimales.

codes	R ^P	ε	R	RR	RR 7
V (31, 5)	9	1	11	17	
V(32, 5)		0	12	20	20
V (63, 6)	15	1	17	29	
V (64,6)		0	18	30	36

Figure 3
Performance des codes pseudo-orthogonaux

Ces résultats montrent que les codes (32,5) autosynchéonisants et pseudoorthogonaux sont équivalents mais ont des performances inférieures aux codes V (31,5).

Le code autosynchronisant V (64,6) est moins performant que le code pseudoorthogonal V (64,6) qui est équivalent au code V (63,6).

IV - APPLICATION DES CODES PSEUDO-ORTHOGONAUX AUX TRANSMISSIONS [9]

IV. 1 Principe de la transmission

Le principe de la transmission a été résumé au premier paragraphe. Dans les essais expérimentaux qui ont été effectués, on a utilisé un codage binaire du type NRZ (non retour à zéro) et une modulation PSK à 2 états de phase. La réception a été faite selon un mode synchrone, et le critère de décision a été effectué sur les échantillons Z i des signaux de sortie des corrélateurs au terme de chaque corrélation.

IV. 2 Performances

Les performances de ce système sont examinées en fonction du bruit et des interférences apparaissant sur la liaison entre les différents trajets.

IV. 2.1. Influence du bruit

Le cas examiné ici correspond à celui d'une transmission à travers un canal monotrajet. Le critère de décision majoritaire consiste à rechercher la valeur maximum des échantillonnés Zi.

La probabilité d'erreur P_E calculée pour un bruit blanc Gaussien par la méthode de Viterbi [7] est donnée par l'expression :

$$P_{\epsilon}(\frac{NTP}{N_0}, \epsilon) = 1 - \int_{-\sqrt{2\pi}}^{+\infty} \left[ERF(v_4 + \sqrt{\frac{2NTP}{N_0}} (1 - \epsilon)) \right]^{N-1} dv_4$$

dans laquelle No = densité spectrale de bruit

.../...

NTP = enérgie du signal

 $\mathcal{E} = |\rho_{ij}(z=0)|$ Valeur de la fonction d'intercorrélation des vecteurs pour z=0

L'influence du bruit est traduite par la courbe de la figure 4 dans le cas d'un code V (32,5)

IV. 2. 2 Influence des signaux perturbateurs

Si vⁱ est le vecteur émis, l'action d'un signal perturbateur quelconque peut être évaluée à partir des valeurs :

- de sa fonction de corrélation S_1 avec le vecteur v^i et de sa fonction de distribution $P(S_1)$.

- de sa fonction de corrélation S_2 avec le vecteur v^i et de sa fonction de distribution $P(S_2)$.

La probabilité d'erreur est alors donnée par :

$$P_{E} = 1 - \iint_{D_{2}} P(S_{2}) \cdot P(S_{2}) dS_{3} dS_{2} \int_{-\infty}^{+\infty} \frac{\alpha^{2}}{\sqrt{2 \pi}} \left[ERF(v_{2} + \sqrt{\frac{2NTP}{N_{0}}} (1 + S_{2} - S_{2})) \right] dv_{2}$$
 (8)

expression dans laquelle D 1 et D2 représentent le domaine des variables S1 et S2

La relation (8) peut, en particulier être utilisée pour calculer l'influence des trajets multiples et des effets du filtrage du signal de réception ou du désynchronisme du récepteur.

IV. 2. 2. 1. Cas d'une propagation multitrajet

Dans le cas d'une propagation multitrajet, les signaux sont reçus dans une configuration relative quelconque. La figure 2 illustre la structure du signal de réception obtenu en présence des trajets multiples.

A l'instant de la décision le signal Z délivré par le corrélateur j est donné par la relation :

$$Z_{i} = \rho_{i}(0) + \sum_{r} \alpha_{r} \rho_{ri}(2) + N_{b}$$

où \mathcal{A}_r est l'amplitude relative du vecteur reçu v par rapport au vecteur v et N_b l'amplitude du bruit à la sortie du corrélateur j.

Dans ces conditions la probabilité d'erreur de détection peut s'exprimer par la

relation :

$$P_{E} = 1 - \int_{-S_{c}}^{+S_{c}} P(S_{1}) P(S_{2}) dS_{1} dS_{2} \int_{-\infty}^{+\infty} \frac{e^{-\frac{N_{1}^{2}}{2}}}{\sqrt{2\pi}} \left[ERF\left(v_{1} + \sqrt{\frac{2NTP}{N_{0}}} \left(1 + \sum_{r} \alpha_{r} (S_{1} - S_{2})\right) \right) \right] dv_{1}$$

Les résultats théoriques et expérimentaux sont illustrés sur la figure 5 pour un code V (32,5). Les courbes tracées pour un facteur $\sum \alpha_r$ constant montrent la détérioration inévitable de la probabilité d'erreur en fonction de l'amplitude des signaux perturbateurs.

IV. 2. 2. 2. Critère de décision

Dans une transmission à travers un canal à trajets multiples on peut considérer les trajets secondaires comme des perturbateurs ou comme des sources redondantes. On est alors conduit à deux types de critères de décision.

- le premier critère utilise le trajet principal pour effectuer la décision. Dans ce cas la valeur $\sum \alpha_r$ est minimale. Ce critère de décision, le plus simple, conduit aux performances illustrées par les courbes de la figure 5
- un second critère consiste à utiliser les trajets secondaires pour confirmer les résultats de détection obtenus sur le trajet principal.

On peut imaginer de choisir, pour effectuer la confirmation, l ou plusieurs trajets secondaires, mais la complexité du récepteur s'accroit d'autant. Nous nous sommes limités au cas où l'on utilise un seul trajet secondaire, celui donnant le signal de plus grande amplitude.

Pour chacun des deux trajets retenus, les signaux de sortie des corrélateurs sont alors classés par ordre décroissant de leurs valeurs et mis en mémoire. Il est possible d'établir de multiples critères de décision en comparant les 2 classements. Le critère de décision qui minimise la probabilité d'erreur dépend du nombre de valeurs des signaux Zi retenus pour effectuer la recherche de confirmation.

a) Prise en compte d'une valeur par trajet

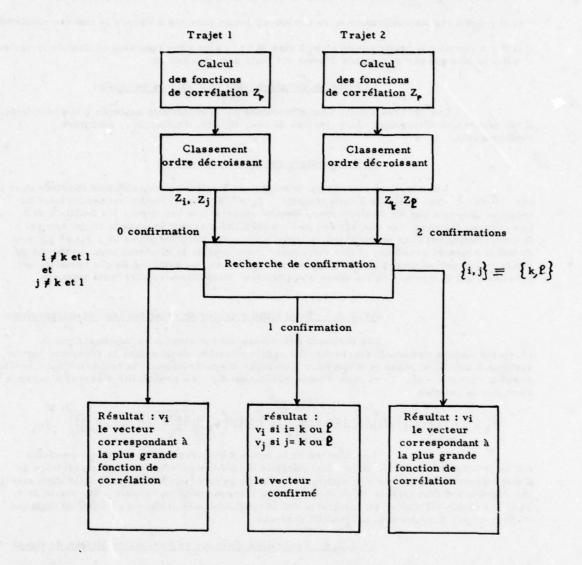
Ce critère de décision n'apporte aucune amélioration par rapport au cas de la détection sur le seul trajet principal.

b) Prise en compte de 2 valeurs par trajet

Soit Zi et Zj les 2 valeurs retenues pour le trajet l et Z ${f p}$ et Z ${f m}$ pour le trajet 2

trajet l	Zi	Zj	
			ordre décroissant
trajet 2	Ze	Z _m	

Le critère de décision optimum utilise l'algorithme de traitement suivant



CRITERE DE DECISION SUR 2 TRAJETS

AVEC PRISE EN COMPTE DE 2 VALEURS PAR TRAJET

La calcul des minima des probabilités d'erreur conduit aux critères suivants :

- si lou m sont différents de i ou j, il n'y a pas de confirmation. Le critère optimum consiste à retenir le numéro du corrélateur ayant le plus grand signal sur le trajet principal.
- si il y a une simple confirmation, le critère optimum consiste à retenir le numéro confirmé.
- si il y a une double confirmation c'est à dire si i et j sont simultanément confirmés le vecteur vi qui a la plus grande probabilité d'avoir été émis doit être retenu.

c) Prise en compte de plus de 2 valeurs par trajet

Les critères optima sont déterminés par une méthode analogue à la précédente. Il est nécessaire d'examiner alors les cas de non, simple, double..... multiples confirmations.

d) Comparaison des différents critères

Les résultats obtenus en retenant 2 ou 3 valeurs par trajet sont illustrés dans le cas $\mathbb{Z}\alpha_r=1$ sur la figure 6 dans laquelle $\mathbf{7}_1$ et $\mathbf{7}_2$ représentent respectivement les rapports (Energie par bit d'information/densité spectrale de bruit) pour les trajets 1 et 2. Ces courbes montrent une dégradation de la probabilité d'erreur lorsque le trajet servant à la confirmation est trop perturbé par le trajet principal. Dans les zones où $\mathbf{7}_1$ et $\mathbf{7}_2$ sont du même ordre de grandeur, il faut remarquer l'avantage de la détection avec recherche de confirmation par rapport à la détection sur un seul trajet. La synthèse de ces résultats est présentée sur la figure 7 où les zones d'application du meilleur critère sont reportés.

IV. 2. 2. 3. Probabilité d'erreur de détection avec désynchronisme

Les résultats précédents ont été obtenus en supposant que la réception était parfaitement synchrone. La synchronisation obtenue dans le récepteur par un système à boucle de phase peut conduire à un léger désynchronisme ; la fonction d'autocorrélation prend la valeur $1 - \mathcal{E}_o$ et celle d'intercorrélation \mathcal{E}_o . La probabilité d'erreur s'exprime alors par la relation

$$P_{E} = 1 - \iint_{D_{2}} P(\varepsilon_{\bullet}) P(\varepsilon_{i}) d\varepsilon_{\bullet} d\varepsilon_{i} \int_{-\infty}^{+\infty} \frac{v_{s}^{2}}{\sqrt{2\pi}} \left[ERF\left(v_{s} + \sqrt{\frac{2NTP}{N_{\bullet}}} \left(1 - \varepsilon_{\bullet} + \varepsilon_{i}\right)\right) \right]^{N-1} dv_{s}$$

Les courbes de la figure 8 montrent l'effet du désynchronisme sur la probabilité d'erreur. Il est ainsi possible de déduire qu'elle doit être la précision de l'asservissement du rythme des digits. On constate qu'un désynchronisme de 2/10 digit entraine une dégradation d'un facteur 10 de la probabilité d'erreur pour un rapport 1/2 voisin de 4. Dans les essais effectués, on enregistre des désynchronismes inférieurs à 1/10 de digit qui n'affectent pas gravement la probabilité d'erreur.

IV. 2. 2. 4. Probabilité d'erreur en fonction du filtrage du signal

Il est classique dans des transmissions numériques d'effectuer un filtrage du signal tel que

B = bande passante du signal en bande de base

B. T. = 1 T = durée digit

Il est possible d'augmenter le débit binaire en prenant BT 🗸 1

Cette opération est réalisée avantageusement par le filtrage du signal d'émission. Ce filtrage affecte cependant la probabilité d'erreur de détection à cause des trois effets suivants :

- il entraine un décalage temporel du maximum de la fonction d'autocorrélation
- il provoque une diminution de ce maximum
- il crée une intercorrélation non nulle (ou différente de ${\cal E}$) au moment de la détection

La figure 9 montre l'évolution de la probabilité d'erreur en fonction du rapport signal/bruit pour différente bande passante de filtrage.

On peut remarquer que la dégradation de la probabilité d'erreur est assez faible pour B.T. = 1 mais devient inacceptable pour B.T = $\frac{1}{2}$

IV. 3. Résultats

Deux types d'essais ont été réalisés : des essais en sondage zénithal qui est un cas d'exploitation particulièrement défavorable et des éssais à l'aide d'un simulateur de canal pouvant recréer les trajectoires multiples. Le code utilisé est un code pseudo orthogonal V (32,5)

La concordance observée entre les résultats a déjà été présentée [5]. L'avantage des essais en simulation est de rendre indépendants les phénomènes rencontrés simultanément en liaisons réelles.

Le cliché l représente un cas idéalisé de propagation sans perturbation. Sur la trace supérieure est représenté le signal reçu et sur la trace inférieure, l'exploration des 32 sorties des corrélateurs du récepteur. On peut constater qu'au moment de la détection (C=0) les valeurs sont toutes nulles exceptées celles correspondant au mot reçu (ici le mot n° 31).

Le cliché 2 illustre le cas d'une réception d'un signal en présence de bruit blanc. La valeur du rapport signal/bruit est de 0 dB à l'entrée du système de traitement. La qualité de la détection, apparente sur le cliché, est confirmé par le taux d'erreur mesuré (soit 4 x 10⁻⁶)

Le cliché 3 montre l'effet du désynchronisme sur la détection. La corrélation du mot reçu avec les mots de référence se faisant pour un décalage de 2/10 digits. La comparaison avec le cas idéal (cliché 1) montre l'apparition d'intercorrélation non nulle.

Dans l'expérience illustrée par le cliché 4, le spectre du signal brouilleur est réduit à une raie proche de la fréquence porteuse du signal émis. Son amplitude est égale à celle du signal utile.

L'effet de ce type de brouilleur est faible sur la détection car il est affaibli dans un rapport qui demeure toujours supérieur à $\frac{1}{\sqrt{N^2}}$

Les clichés 5 et 6 représentent une propagation à 2 trajets d'égale amplitude sans bruit et avec un rapport signal trajet 1/ bruit égal à 0 dB

La distinction de la valeur maximale des fonctions de corrélation est facile à réaliser dans ces conditions, ce qui justifie que la probabilité d'erreur de détection soit faible (7 x 10 - 2). La comparaison des clichés 5 et 6 montre que les trajectoires multiples introduisent plus de perturbations que le bruit.

IV - CONCLUSION

La transmission numérique de l'information par l'emploi de codes pseudoorthogonaux apparait avantageuse dans les canaux multitrajets non stationnaires.

Cet avantage est lié d'abord au fait que les codes pseudo orthogonaux se classent parmi les signaux à spectres étalés et en possèdent donc les propriétés de résistances aux bruits et aux perturbateurs.

La seconde raison vient du fait que la probabilité d'erreur de détection est une fonction très rapidement croissante de ces valeurs. Le gain obtenu avec ces codes est dû à la méthode de construction qui permet d'obtenir des codes optimaux dont les fonctions d'intercorrélation sont minimales.

L'application de ces codes a été faite à travers le canal ionosphèrique avec des critères de décision utilisant la redondance naturellement introduite par les trajectoires multiples.

L'application dans des transmissions à travers d'autres canaux multitrajets non stationnaires peut être envisagée par simple transposition.

BIBLIOGRAPHIE

- [1] M. L. DOELZ, E. T. HEALD, D. L. MARTIN

 Binary data transmission techniques for linear systems
- Proceeding of IRE mau 1957
- A new method of high speed adaptive serial communication through any time variable and dispersive medium

 First IEEE communication conv. June 1965. GC GA 2 et 3
- [3] G. DAVID, J.P. VAN HUFFELEN
 Description d'un dispositif autoadaptatif pour transmission de données sur liaisons ionosphèriques Agard Athènes May 1975
- C. GOUTELARD
 Système de transmission de données digitales à cadence rapide par voie ionosphèrique Rapport DRME Juillet 1969
- [5] F. CHAVAND, M. GINDRE, C. GOUTELARD

 Utilisation de codes pseudo orthogonaux adaptés aux transmissions ionosphèriques
 Agard Athènes May 1975
- [6] F. CHAVAND, M. GINDRE, C. GOUTELARD

 Les codes pseudo-orthogonaux. Constructions et applications. International meeting on data transmission Liège Nov 1977
- [7] S. W. GOLOMB

 Digital communications with space application Prentice Hall (1964)
- [8] R. GOLD

 Optimal binary sequence for spead spectrum multiplexing IEEE Trans. IT, USA (oct 1967) 13, n° 5, pp 619 -621
- [9] Brevet d'invention

[2]

M. J. DITORO

AD-A060 472

ADVISORY GROUP FOR AEROSPACE RESEARCH AND DEVELOPMENT—ETC F/6 17/2.1

ASPECTS OF ELECTROMAGNETIC WAVE SCATTERING IN RADIO COMMUNICATI—ETC(U)

SEP 78 A N INCE

UNCLASSIFIED

AGARD—CP—244

ADVISORY GROUP FOR AEROSPACE RESEARCH AND DEVELOPMENT—ETC F/6 17/2.1

ASPECTS OF ELECTROMAGNETIC WAVE SCATTERING IN RADIO COMMUNICATI—ETC(U)

BY THE COMMUNICATI—ETC(U)

ASPECTS OF ELECTROMAGNETIC WAVE SCATTERING IN RADIO COMMUNICATI—ETC(U)

BY THE COMMUNICATI—ETC(U)

ASPECTS OF ELECTROMAGNETIC WAVE SCATTERING IN RADIO COMMUNICATI—ETC(U)

BY THE COMMUNICATI—ETC(U)

ASPECTS OF ELECTROMAGNETIC WAVE SCATTERING IN RADIO COMMUNICATI—ETC(U)

BY THE COMMUNICATI—ETC(U)

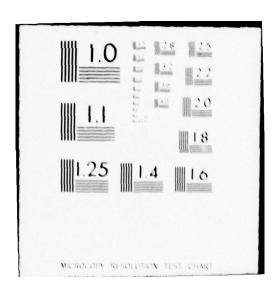
BY THE COMMUNICATI—ETC(U)

ASPECTS OF ELECTROMAGNETIC WAVE SCATTERING IN RADIO COMMUNICATI—ETC(U)

BY THE COMMUNICATI—ETC(U)

ASPECTS OF ELECTROMAGNETIC WAVE SCATTERING IN RADIO COMMUNICATI—ETC(U)

BY THE COMMUNICATI—ET



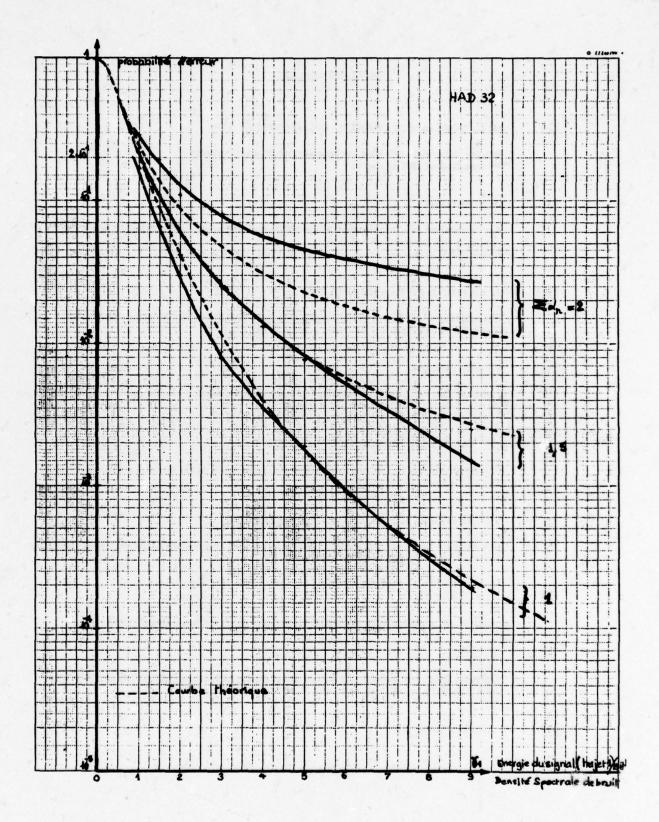


Figure 4

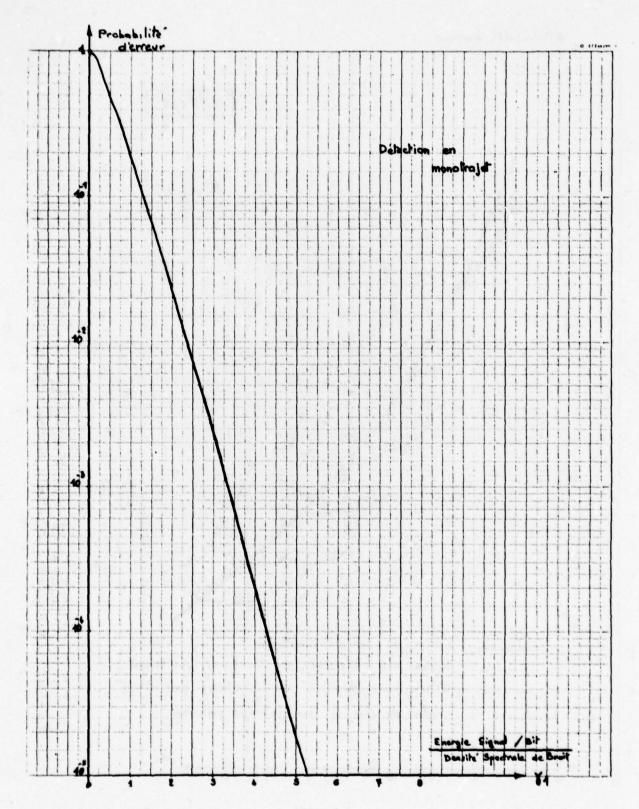


Figure 5

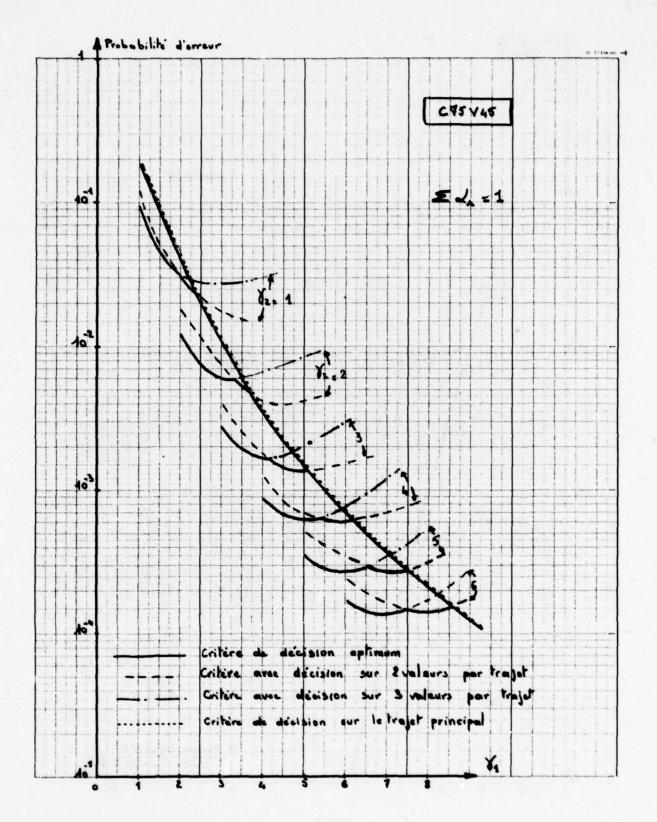


Figure 6

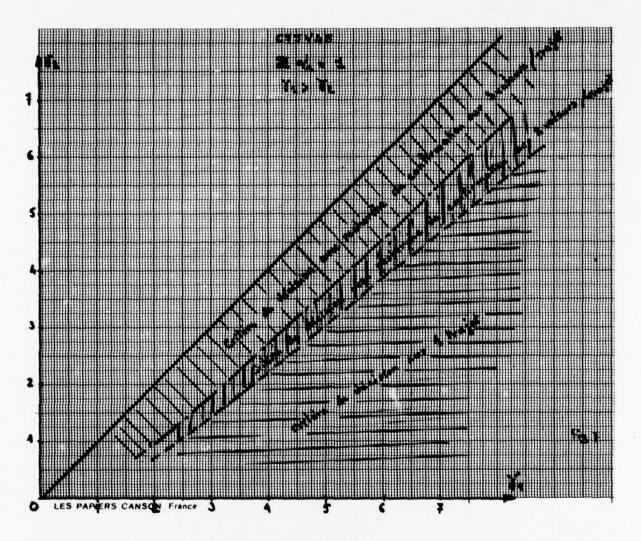


Figure 7

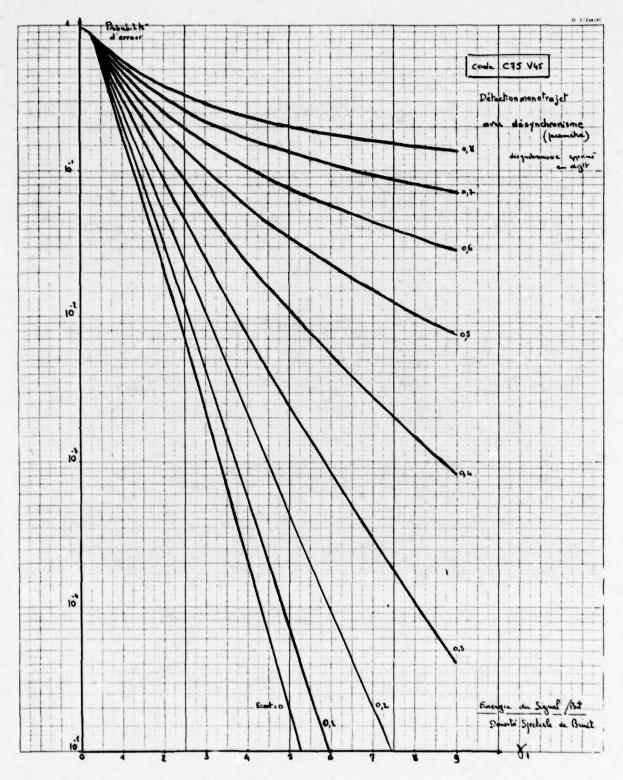


Figure 8

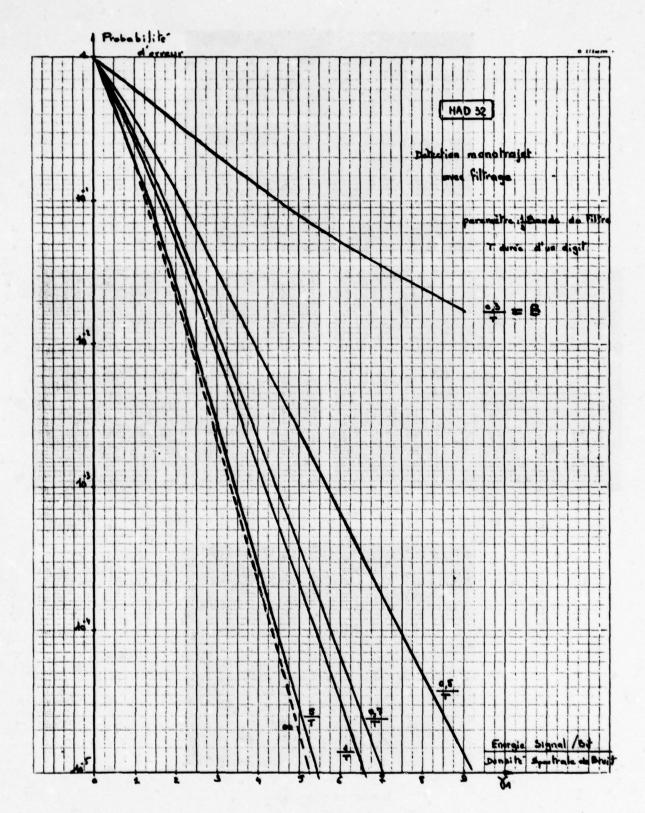
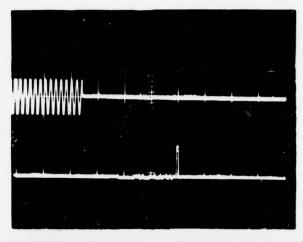
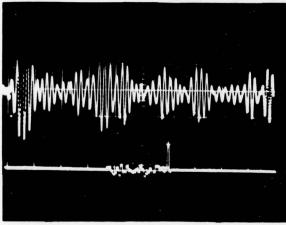
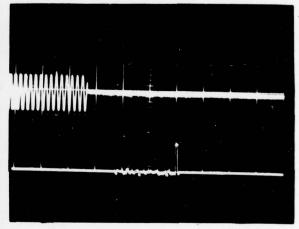


Figure 9

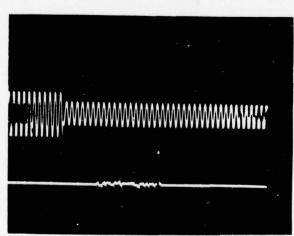


Cliché 1





Cliché 2



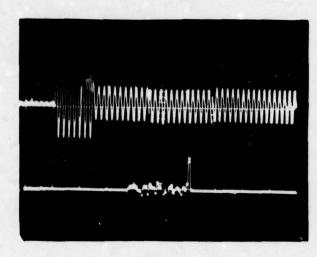
Cliché 3

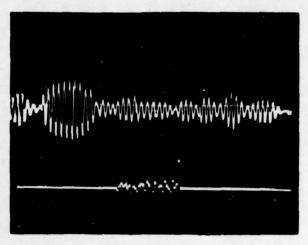
Cliché 4

Réception Monotrajet

- 1) Sans perturbation
- 2) En présence de bruit
- 3) Avec un désynchronisme constant
- 4) En présence d'un brouilleur cohérent

Clichés 1-4





Cliché 5

Cliché 6

Réception multitrajet

- 5) 2 trajets d'égale amplitude ($\sum d_n = 1$) sans bruit
- 6) Même condition avec bruit

Clichés 5 et 6

MLT-1 AN EXPERIMENTAL MODEM FOR TROPOSCATTER COMMUNICATIONS USING MAXIMUM LIKELIHOOD SEQUENCE ESTIMATION AND ERROR-CORRECTION CODING*

David Chase
Phillip A. Bello
CNR, Inc.
220 Reservoir Street
Needham, Massachusetts 02194

ABSTRACT

In this paper a new high-speed troposcatter digital modem, designated MLT-1, is discussed. This modem combines coding and modulation and achieves unprecedented reliability by exploiting the scatter properties of this channel to achieve "in-band" time and frequency diversity. Experimental results for a tactical single diversity troposcatter modem operating at uncoded data rates of 4.6 Mb/s and a coded data rate of 2.3 Mb/s are presented.

1. INTRODUCTION

The time-dispersive and time-varying properties of a troposcatter channel makes the problem of obtaining reliable high-speed data transmission quite interesting. In this paper a new modem, designated MLT-1, combines coding and modulation in an optimum manner to achieve unprecedented reliability by exploiting the scatter properties of this channel to achieve "in-band" time and frequency diversity.

The benefits of in-band frequency diversity, resulting from the channel's time-dispersion, is achieved by using signals with spectra occupying a bandwidth greater than the coherent bandwidth and employing a maximum likelihood sequence estimator (MLSE), based on the Viterbi algorithm, to demodulate in the presence of intersymbol interference. The benefits of in-band time diversity, resulting from the channel's time-variations, is achieved by the use of interleaved error correction codes.

This experimental modem is believed to represent the first application of a MLSE algorithm to a channel which is time-varying as well as time-dispersive. A measurement of the time-varying impulse response is achieved by a constant envelope phase modulation approach which contains a low-level PN probe sequence. By cross-correlating the received signal with a locally generated PN sequence, the receiver is able to obtain and maintain bit sync and continuously measure the channel's time-varying impulse response which is required for the MLSE algorithm. The implementation of this rather sophisticated demodulator is accomplished efficiently by early conversion of the received signal into its digital representation and by carefully optimizing (in a practical sense) the digital signal processing.

The fairly large time-varying error bursts prevalent on the troposcatter channel make conventional coding of successive digits ineffective. However, interleaving code digits for a short block code, such as a (24,12) Golay code, enables one to achieve a significant performance improvement due to in-band time diversity. These performance gains are achieved when code digits within a block code are significantly correlated, as demonstrated by operating with decoding delays in the order of 150 ms.

The effectiveness of these new signal processing concepts for scatter communications are demonstrated by theoretical results as well as by laboratory measured results obtained during testing at the RADC DICEF Facility over realistic simulators for troposcatter channels.

2. THEORETICAL CONSIDERATIONS

Consider the transmission problem depicted in Figure 1. A (complex) transmitted signal $\mathbf{z}_n(t)$, consisting of a modulated digital data stream, is fed to a channel which we assume initially to be time-invariant and known, such that for each possible transmitted waveform $\mathbf{z}_n(t)$ there is a known received waveform $\mathbf{w}_n(t)$ in the absence of noise. The actual received waveform $\mathbf{w}(t)$ consists of $\mathbf{w}_n(t)$ plus an additive white noise $\eta(t)$ of one-sided power density \mathbf{N}_0 watts/Hz:

^{*}Funds for this development were provided in part by the Air Force Systems Command, Rome Air Development Center, Griffiss Air Force Base, Rome, New York, under Contract No. F30602-74-C-0133 and by CNR, Inc., under its internal research and development programs.

$$w(t) = w_n(t) + \eta(t) \tag{1}$$

Assuming equally likely transmitted sequences, it is well-known that the receiver operation which minimizes the probability of selecting the wrong sequence of data as having been transmitted (also called the maximum likelihood receiver) involves the computation of the "distances" or "metrics":

$$M_{p} = \int |w(t) - w_{p}(t)|^{2} dt$$
 (2)

for all p, and selection of $z_m(t)$ as having been transmitted if $M_m < M_p$, for all p \neq m. Since there is a one-to-one correspondence between the information data sequence and each modulated signal $z_m(t)$, specification of $z_m(t)$ is equivalent to specifying the data sequence.

Two observations are in order here:

- The complexity involved in direct computation of the distances Mp grows exponentially with the length of the data sequence.
- If the channel is time-variant, it must be continually measured so that the correspondence between $\mathbf{z}_{\mathbf{n}}(t)$ and $\mathbf{w}_{\mathbf{n}}(t)$ is known at all times.

Forney [1] and Kobayashi [2] have shown that in the case of a channel describable by a finite number of states, the complexity of the optimum receiver operation need not grow exponentially with the length of the data sequence if use is made of the Viterbi algorithm [3]. This algorithm is used in the troposcatter modem discussed in this paper.

Channel measurements may be obtained either by use of the received demodulated data signal alone in a decision-directed adaptive filter technique or else by direct use of a probing signal. In the tropo modem discussed here, a special probing signal is included in the transmitted signal structure for use in channel measurements and bit signal extraction at the receiver.

To gain insight as to the reason why in-band time and frequency diversity is achieved with the use of interleaving codes and the use of maximum likelihood demodulation, one notes that the probability of bit error for a minimum error probability receiver is closely approximated by the value [1]

$$P_{e} = C\varphi\left(\frac{d_{\min}}{2\sqrt{N_{0}}}\right) \tag{3}$$

where

$$\varphi(\alpha) = \int_{\alpha}^{\infty} \frac{1}{\sqrt{2\pi}} \exp\left(\frac{-y^2}{2}\right) dy , \qquad (4)$$

C is a constant, and d_{min} is the complex minimum distance between two received sequences

$$d_{\min}^{2} = \min_{p,q} \int |w_{p}(t) - w_{q}(t)|^{2} ; p \neq q$$
 (5)

Considering coding first and, for simplicity, assume a flat fading channel with complex time-variant gain g(t). Let the transmitted signal be given by

$$z(t) = \sum a_{L}p(t - kT)$$
 (6)

where a_k takes on a discrete set of values according to the information sequence, and p(t) is the transmitted pulse shape of duration T. The received signal corresponding to a particular data sequence $a_k^{(p)}$ is thus given by

$$w_{p}(t) = \sum a_{k}^{(p)} p(t - kT)g(t)$$

$$\approx \sum a_{k}^{(p)} g(kT)p(t - kT)$$
(7)

where it has been assumed that the channel changes little for the duration of a pulse. The minimum distance becomes

$$d_{\min}^{2} = \min_{p,q} \sum |a_{k}^{(p)} - a_{k}^{(q)}|^{2} |g(kT)|^{2}$$
(8)

where we have normalized the energy of p(t) to be unity.

Coding places a lower bound on the number of places in which two code words $a_k^{(p)}$ and $a_k^{(q)}$ can differ. If the code words differ in at least d places, then d_{min} must be expressible as a weighted sum of d terms:

$$d_{\min}^2 = \sum \beta_k |g(kT)|^2$$
; k selected from d places in which code words differ (9)

Equation (9) is exactly the form that the minimum distance takes in the case of predetection time-diversity combining with the same symbol information repeated at the d time instants involved. By the use of interleaving, the code bits can be separated far enough apart to produce sufficient independence of fading for the maximum benefit of d'th-order diversity.

Equation (9) strictly applies to an optimum decoder which uses channel measurement (soft decision) information in determining the code word which yields the minimum error probability. The difference between a hard decoder and an optimum channel measurement decoder, for the (24,12) Golay code used in MLT-1, is illustrated on Figure 2 for the flat fading channel. Figure 3 illustrates how this coding approach compares to the performance possible when (time or frequency) diversity is utilized. The probability of a bit error is illustrated as a function of the total received energy per information bit, i.e., $E_{\rm b}/N_{\rm O}$, and thus the diversity and coding systems are compared fairly at a fixed data rate throughput and equal received power.

The attractiveness of even binary decoding of the interleaved (24,12) code is clear since this coding technique outperforms dual diversity (for Pe < 10^{-2}) and approaches the performance of fourth-order diversity. While only a hard decoder has been implemented in this experimental modem, plans are presently underway to incorporate a practical channel measurement decoder which has been shown by Chase [4], to closely approximate the performance of a complex optimum channel measurement decoder.

Consider now the case of in-band diversity. We assume a dispersive channel in which the pulse p(t) produces a response $w_0(t)$ which causes intersymbol interference. Then the minimum distance can be expressed as

$$d_{\min}^{2} = \min_{p,q} \int |\Sigma [a_{k}^{(p)} - a_{k}^{(q)}] w_{0}(t - kT)|^{2} dt$$
 (10)

The sequence

$$e_k = a_k^{(p)} - a_k^{(q)}$$
 (11)

is called the error sequence. For a given channel pulse response $w_0(t)$, there will be a worst-case error sequence which produces the minimum distance. We define the spectrum of the error sequence E(f) as the spectrum of the error impulse train e(t),

$$e(t) = \sum e_k \delta(t - kT)$$
 (12)

$$E(f) = \sum e_k e^{j2\pi fkT}$$
 (13)

The minimum distance can be expressed in the frequency domain by Parseval's theorem as

$$d_{\min}^{2} = \int |E(f)|^{2} |P(f)|^{2} |T(f)|^{2} df$$
 (14)

where P(f) is the spectrum of the transmitted pulse p(t), and T(f) is the transfer function of the channel. For T(f), a complex Gaussian process in f, it is well-known that the integral may be expressed rigorously as a sum of squared magnitudes of independent Gaussian variables,

$$d_{\min}^2 = \sum \lambda_i |g_i|^2 \tag{15}$$

where the λ_1 are eigenvalues of an appropriate integral equation. On a heuristic basis, one may apply the sampling theorem to the integral in (14) to convert the integral to a sum of

weighted samples of $|T(f)|^2$ at a set of frequencies. In either case, the in-band diversity becomes manifest whenever the bandwidth of P(f) exceeds the coherent bandwidth of the medium because then the terms in the sums do not fluctuate identically.

From the above brief discussion, it may be seen that optimum reception of block coded interleaved bits using pulses exceeding the coherent bandwidth of the channel allows the attainment of both time and frequency in-band diversity with minimum reduction in data rate packing.

SYSTEM DESCRIPTION

A block diagram of the system implemented is illustrated on Figure 4. The input data, at a rate of 2.3 Mb/s, is encoded with the rate-1/2 Golay code to yield an encoded data rate of 4.6 Mb/s. This coded data is combined with a PN probing sequence and fed to a complex modulator to produce the 70 MHz centered signal input to the troposcatter radio. At the receiving end, IF amplification and AGC are applied and, with the aid of a stable 70 MHz oscillator, the IF output is complex down-converted to baseband in-phase and quadrature channels. After sample-and-hold and analog-to-digital conversion, the remainder of the receiver implementation is entirely in digital form, aside from the VCXO used for bit synctiming.

In order to have a modem which is capable of applying maximum likelihood sequence estimations (MLSE) algorithms while communicating over a time-varying channel, one must develop a channel measurement technique which can adequately track the channel's impulse response. A certain minimum amount of time is required to measure an impulse response which is a function of the measurement technique and the channel noise. Furthermore, this measured time must be short compared to rate of change of the channel's impulse response. Needless to say, if the rate of change of impulse response is fast enough at MLSE algorithm would not be feasible. Fortunately, the measurement technique chosen for the troposcatter channel can adequately track the channel and furthermore, no start-up training sequence is required.

The key to successfully tracking the troposcatter channel has been the use of a pseudo-random (PN) probe embedded in the transmitted signal which is synchronized with the transmitted data. The receiver continuously measures the channel by cross-correlating the received signal with a stored replica of this PN probe.

A probe level of 1/4 the data level has been chosen to be imbedded in a quaternary phase shifted data signal. A probe of this level is of sufficient amplitude to accurately measure the channel's time-varying impulse response and yields only 1/4 dB loss in signal power.

The vector diagram corresponding to this QPSK signal is shown on Figure 5. In order to keep the probe in quadrature with the data, it must be data-dependent. From a complex notation point of view, the transmitted signal vector in Figure 5 would be represented as

$$v = r + js + \frac{1}{4} [p - jp \, sgn \, (rs)]$$
 (16)

The in-phase and quadrature NRZ data signals are $r=\pm 1$, $s=\pm 1$, respectively. The in-phase component of the probe signal is the same as for the binary PSK case discussed above, while the quadrature component of the probe - 1/4 p sgn (rs) is data-dependent. [sgn (x) yields the algebraic sign of x.] Since the probe and data are uncorrelated, one may show that the received signals corresponding to the in-phase and quadrature components of the transmitted probe are uncorrelated. Only the in-phase probe is used for channel measurement, the quadrature probe being supplied to keep the signal envelope constant. From (16) we see that the possible angles are computed from the formula,

$$\theta = \tan^{-1} \left\{ \frac{s - \frac{p}{4} \operatorname{sgn} (rs)}{r + \frac{p}{4}} \right\}$$
 (17)

and are found to be $\pm 14^{\circ}$, $\pm 76^{\circ}$, $\pm 104^{\circ}$, and $\pm 166^{\circ}$.

4. DISCUSSION OF THE EXPERIMENTAL RESULTS

The experimental laboratory test set-up is illustrated on Figure 6, where the troposcatter channel is modeled by a tapped delay line with complex Gaussian fluctuations and adjacent taps separated by 0.1 µsec delay [5]. These fading profiles were used in testing this system as discussed below.

- 1. Flat-Fading Channel A single fading path is simulated in this case to represent the limiting case where the multipath on a fading channel is such that only one significant fading path exists. RMS Doppler spreads of both 1 Hz and 10 Hz have been simulated for this case. It is expected that the actual RMS Doppler spread for tactical tropo will be within this range for a very high percentage of the time on the air.
- 2. Moderate Multipath This multipath profile represents a typical tactical channel. Seven paths spaced at 0.1 μsec with the following relative strength: 0 dB, -3 dB, -7 dB, -12 dB, -17 dB, -23 dB, and -29 dB, are used to represent this channel. Results are again obtained for RMS Doppler spreads of 1 Hz and 10 Hz.
- 3. <u>Severe Multipath</u> This severe multipath profile represents the high end of the expected multipath for tactical tropo. The profile is specified by nine paths spaced at .1 µsec with the following strengths: -3 dB, dB, -1 dB, -3 dB, -5 dB, -7 dB, -10 dB, -12 dB, -15 dB. Doppler spreads of both 1 Hz and 10 Hz were simulated.

Performance curves are obtained as a function of the ratio of the received power, P_r , to the product of the noise power density, N_0 , times the information rate R in bits/second. Defining the signal-to-noise ratio

$$E_b/N_0 = \frac{P_r}{N_0 R} \tag{18}$$

enables one to compare uncoded and coded systems as a function of the received power and at the same information data throughput. The modem without coding operates at a data rate of R = 4.6 Mb/s and the modem with coding operates at a data rate R = 2.3 Mb/s.

Figure 7 illustrates the performance for a flat-fading channel for decoding delays of 153.3 ms and 613.3 ms at an RMS Doppler spread of 1 Hz. The corresponding values of B τ and the correlator coefficient

$$\rho = e^{-\frac{\pi^2 B^2 \tau^2}{2}} \tag{19}$$

between code letters for these cases is obtained by noting that

$$B_T = (1/23)BT$$
 (20)

so that for

$$T = 153.3 \text{ ms}, B = 1 \text{ Hz}, B_T = .0067, \rho = .9997$$
 (21)

and for

$$T = 613.3 \text{ ms}, B = 1 \text{ Hz}, B_T = .026, \rho = .997$$
 (22)

Figure 8 illustrates the performance when we still have flat-fading but the RMS Doppler spread is increased to 10 Hz. Thus, for

$$T = 153.3 \text{ ms}, B = 10 \text{ Hz}, Br = .067, \rho = .978$$
 (23)

and for

T = 613.3 ms, B = 10 Hz, B_T = .26,
$$\rho$$
 = .716 (24)

Figures 9 and 10 are the corresponding results for moderate multipath, and Figures 11 and 12 give the same results for the severe multipath case.

For the flat-fading model an MLSE algorithm is not required since no significant multipath is introduced. Comparing the ideal coherent PSK modem results on Figure 2 to the experimental results on Figure 7, we note that for operating signal-to-noise ratios below 15 dB, the experimental results are within 2 dB of the ideal results. The difference is expected and can be directly attributed to the use of a practical four-pole Butterworth predetection filter of bandwidth 2.66 MHz and to the appropriate analog-to-digital conversions used in the implementation of the modem. Figure 8 indicates that for high signal-to-noise ratios, the irreducible error induced by the Doppler spread is evident. Reduction in the delay produced by the present channel measurement circuitry can eliminate this reduced performance at high Doppler spreads, including that produced by airplanes. However, for tactical tropo good performance is required at low SNR's and thus improved channel measurement circuits are not critical. Nevertheless, techniques exist for reducing the sensitivity

of this experimental modem to high Doppler spreads such as resulting from airplanes passing through the troposcatter's common volume. The in-band diversity available via the channel's multipath is evident in Figures 9 through 12, which illustrates the improved performance possible for multipath profiles which exceed the modems baud duration. For the severe multipath profile, the irreducible error results from both the effects of Doppler and multipath spread. It should be pointed out that when operating with diversity and/or error correction coding, the effects of these irreducible errors, which only appear at high signal-to-noise ratios, are minor.

Significantly improved performance is available by using an interleaved hard decision Golay code as illustrated in Figures 7 through 12. For the flat-fading channel, the required decoding delay is somewhat larger than that required for the multipath profiles considered. But, for all profiles with an RMS Doppler spread of 10 Hz, a decoding delay of .613 second is sufficient to achieve performance near the ultimate possible. However, it is important to note that even for an RMS Doppler spread of 1 Hz, significant coding gains are achieved. While it has been shown that when the correlation coefficient ρ = 1, no coding gain is possible [6], it is interesting to note that coding gains are possible even with values of ρ = .997 as in (22). The loss in performance due to the correlation between code bits is indicated on all these figures which include the performance possible when sufficient interleaving is used such that code digits can be assumed to be independent.

For a fixed decoding delay and Doppler spread, the correlation loss can be shown to decrease as the order of diversity increases and thus shorter decoding delays are possible when this single diversity unit, MLT-1, is extended to operate on dual or quad diversity tropo links. However, even for single diversity, the significant improvement of the experimental results on Figures 9 through 12, as compared to ideal flat-fading modem results on Figure 2, indicates the importance of in-band frequency and time diversity for obtaining reliable digital communications over troposcatter links. Table 1 illustrates the dB reduction in transmitter power resulting from in-band frequency diversity (modem without coding) and the dB reduction in transmitter power resulting from the combined effect of in-band frequency and time diversity (modem with coding). These results, obtained by comparing Figure 2 to Figures 9 through 12, are tabulated for a bit error rate of 10^{-3} and include the implementation losses present in the actual experimental unit. The reductions in transmitter power are even more impressive when error rates below 10^{-3} are considered.

All present experimental results for MLT-1 were obtained with no explicit diversity. Figure 13 illustrates the predicted performance on this modem for a range of multipath profiles when dual explicit diversity is available and the delay used in the channel measurement circuits is minimized. Under these conditions the performance is essentially the same for B = 1 and 10 Hz.

It is interesting to compare the MLT-1 performance with a coding delay of 1/2 second against a fourth-order diversity DAR-IV modem, because both would occupy around the same bandwidth and achieve the same data rate. By examining the measured results for the DAR-IV [7] the remarkable result is found that its error rate is comparable to the non-diversity MLT-1 codem with hard decoding when both have the same total received power available. With soft-decision decoding the MLT-1 codem would provide equivalent performance with considerably less received power than the total received power in quad-diversity operation of the DAR-IV.

In summation, our experimental results and hardware design indicate that the benefits of in-band diversity (resulting from the channel's multipath) can be obtained efficiently by a digital implementation modem based on an MLSE algorithm and the benefits of time diversity (resulting from the channel's time variations) can be obtained by interleaved coding techniques. Furthermore, even when a coded signal is transmitted, bandwidth utilization in the order of 1 bps per Hz of bandwidth can still be maintained.

REFERENCES

- [1] Forney, G. D., Jr., May 1972, "Maximum-Likelihood Sequence Estimation of Digital Sequences in the Presence of Intersymbol Interference," <u>IEEE Transactions on Information Theory</u>, Vol. IT-18, No. 3.
- [2] Kobayashi, H., September 1971, "Correlative Level Coding and Maximum-Likelihood Decoding," IEEE Transactions on Information Theory, Vol. IT-17, No. 5.
- [3] Viterbi, A. J., April 1967, "Error Bounds for Convolutional Codes and an Asymptotically Optimum Decoding Algorithm," <u>IEEE Transactions on Information Theory</u>, Vol. IT-13.

- [4] Chase, D., January 1972, "A Class of Algorithms for Decoding Block Codes With Channel Measurement Information," IEEE Transactions on Information Theory.
- [5] Chase, D., et al, July 1976, "Troposcatter Interleaver," Final Technical Report on Contract No. F30602-74-C-0133, RADC-TR-76-213, by CNR, Inc.
- [6] Chase, D., and Weng, L. J., September 1976, "Multiple Burst Correction Technique for Slowly Fading Channels," IEEE Transactions on Information Theory.
- [7] "Hybrid Tropo Transmission System," Final Technical Report by Raytheon Company, Prepared for Rome Air Development Center, Griffiss Air Force Base, New York, RADC-TR-76-250, August 1976.

Table 1 Comparison of Results for an Ideal PSK Modem With Flat-Fading to the Experimental Results* for MLT-1 (dB Reduction in Power Due to In-Band Diversity Illustrated at Bit Error Rates of 10⁻³)

		dem t Coding	Modem With (24,12) Golay Code and a Decoding Delay of 613 ms		
	B = 1 Hz	B = 10 Hz	B - 1 Hz	B = 10 Hz	
Moderate Multipath	6.5	3.7	9.2	12.3	
Severe Multipath	8.1	5.7	11.0	12.9	

^{*}The performance at 10 Hz is degraded relative to 1 Hz due to excessive delay in channel measurement circuits. This excessive delay can be removed by hardware modification.

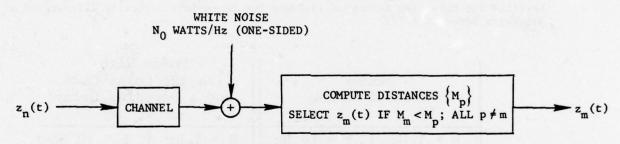


Figure 1 Optimum Reception for White Gaussian Noise

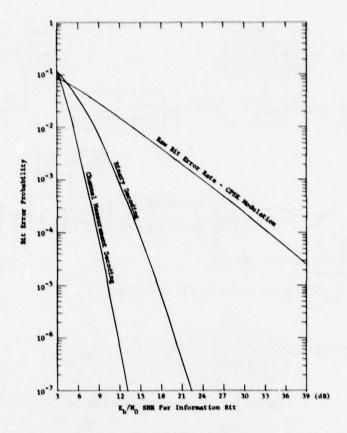


Figure 2 Coding Performance as a Function of the SNR Per Information Bit, Single Diversity, CPSK Modulation, Flat Rayleigh Fading

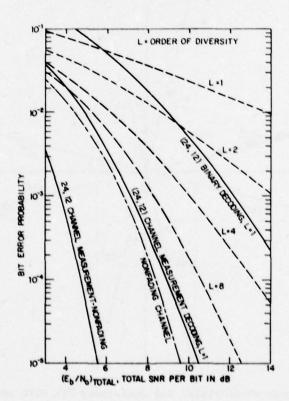


Figure 3 Comparison of the Interleaved (24,12) Golay Code With Binary and Channel Measurement Decoding to the Performance Possible by Diversity Combining (CPSK Modulation With Optimum Diversity Combining)

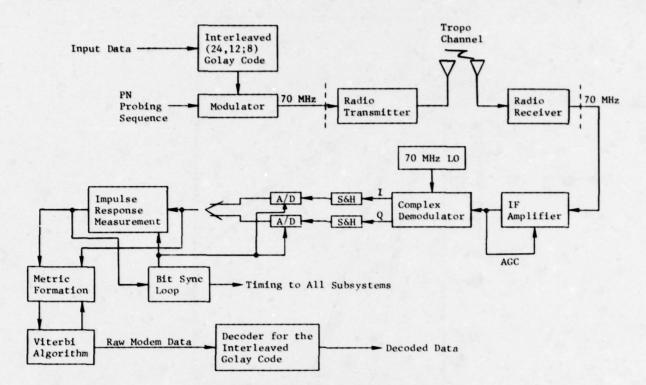


Figure 4 Block Diagram of MLT-1

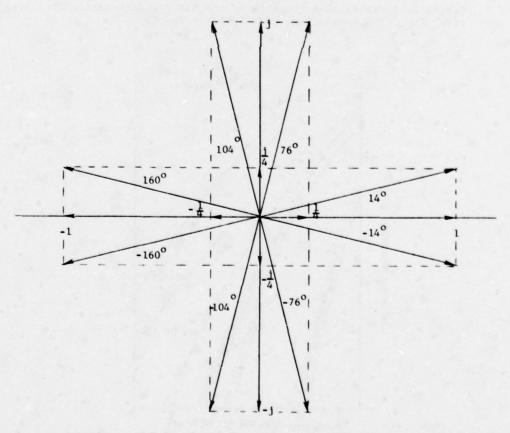


Figure 5 Vector Diagram of IF Signal for Quaternary PSK With an Imbedded Probe Signal

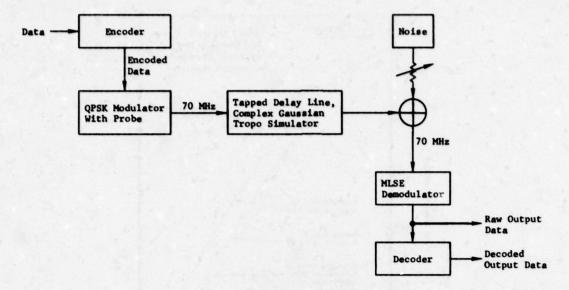


Figure 6 Laboratory Test Set-Up

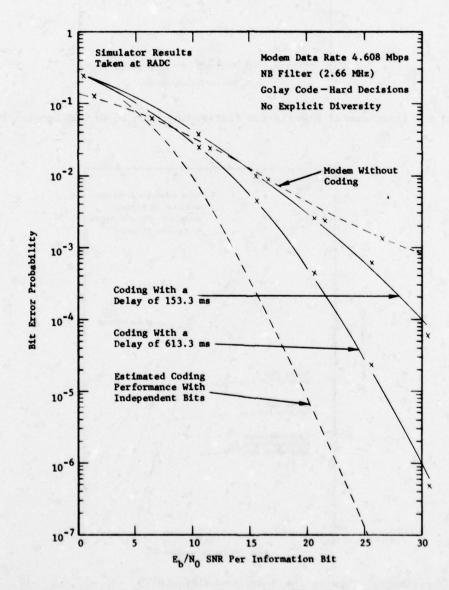


Figure 7 Experimental Results for Flat-Fading With 1 Hz RMS Doppler Spread

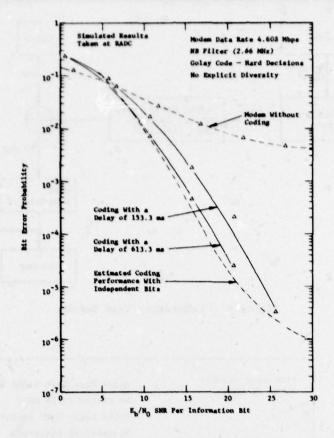


Figure 8 Experimental Results for Flat-Fading With 10 Hz RMS Doppler Spread

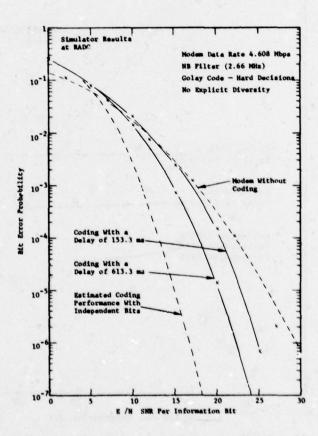


Figure 9 Experimental Results for Moderate Multipath (0, -3, -7, -12, -17, -23, -29 dB) at 1 Hz RMS Doppler Spread

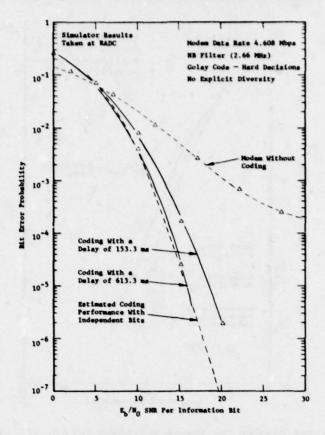


Figure 10 Experimental Results for Moderate Multipath (0, -3, -7, -12, -17, -23, -29 dB) at 10 Hz RMS Doppler Spread

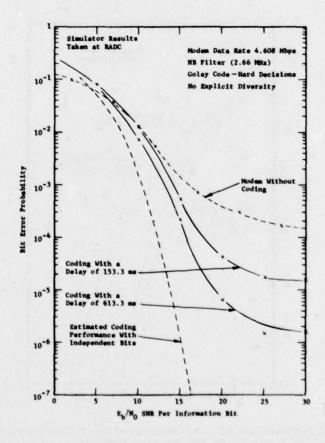


Figure 11 Experimental Results for Severe Multipath (-3, 0, -1, -3, -5, -7, -10, -12, -15 dB) at 1 Hz RMS Doppler Spread

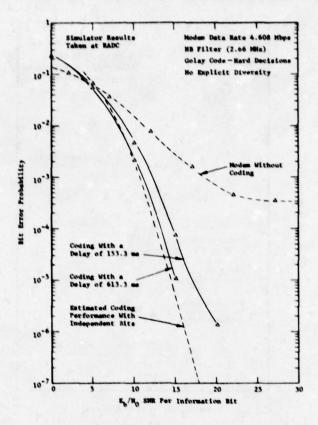


Figure 12 Experimental Results for Severe Multipath (-3, 0, -1, -3, -5, -7, -10, -12, -15 dB) at 10 Hz RMS Doppler Spread

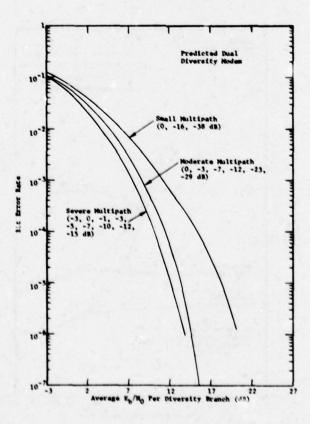


Figure 13 Predicted Performance of a Maximum-Likelihood Demodulator With Dual Explicit Diversity for 1 and 10 Hz RMS Doppler Spreads

AN EXPERIMENTAL MODEM FOR HF CHANNELS USING SPREAD-SPECTRUM AND BLOCK ENCODING

by

R.E. Schemel and A.N. Ince SHAPE Technical Centre, The Hague, Netherlands.

ABSTRACT: STC is currently carrying out an experimental programme to investigate the performance of a spread-spectrum HF modem designed to combat multipath and interference effects. The design of a prototype system is outlined and performance results are discussed. The features of the modem include automatic synchronization, diversity operation, provision for an ARQ mode and more elaborate coding methods.

1. Introduction

Multipath, interference and fading all significantly impair the transmission of digital signals in the HF band. Multipath is caused by a signal arriving at the receiver by two or more paths each with a different time delay; in disturbed ionospheric conditions multipath can consist of a continuum of echoes. Interference arises because too many transmitters are using the same channel, or frequencies immediately adjacent to it.

The HF spread spectrum modem (Ref 1) is designed to minimize the first two effects by the use of special modulation techniques and coding. The important characteristic of the technique is that the bandwidth of the signal transmitted is much greater than the information bandwidth and that the band spread is determined by a pseudo-noise (PN) sequence which gives protection against multipath, noise and interference of impulsive nature.

The coding employed gives a basic performance improvement of about 6 dB over uncoded FSK, but the modem employ, in addition to this basic coding, a form of error detection and re-transmission which reduces the errors caused by fading.

Fading can also be counteracted by the use of diversity, and this can be incorporated in the modem. In addition to the more usual forms of diversity, that between two received echoes can be exploited if required.

Modem Description

A functional block diagram of the SS HF modem is given in Fig. 1. The various sub-systems and the operation are described individually below.

2.1 Transmitter

Input data is encoded 5 bits at a time into one of 32 orthogonal waveforms. The total waveform set consists of 64 waveforms each 64 bits in length; 32 of the set are for data words, four are special characters for synchronization and re-transmission, and the remainder is unused. This first level of encoding is designed primarily to combat noise/interference and may be viewed as a simple block encoding scheme.

The first level encoded data stream is added modulo-2 to a long binary pseudorandom sequence (PN), the clock rate of which can be set in the range 1.3 to 85 Kbit/s. The composite signal then phase modulates a carrier prior to transmission. The maximum PN rate is set by the time dispersion of a single propagation mode. It appears (Ref. 2) that PN rates of more than about 200 Kbit/s may not be feasible without the use of more sophisticated adaptive equalizer techniques. It is this second level of encoding that allows the reception of a single propagation mode from a multipath set, the other modes giving rise to uncorrelated noise.

2.2 Receiver

Referring to Fig. 1(b), the receiver, which is described from an intermediate frequency onwards, first multiplies the input signal by a correctly timed version of the original PN sequence, thus recovering an RF signal whose phase modulation is the orthogonal waveform actually transmitted but corrupted by noise. Note that in practice the multiplication is performed on the local oscillator.

The IF signal is now brought down to baseband by in-phase and quadrature synchronous detectors. Each channel is digitized and is integrated for a time equal to one bit of the waveform. The result is stored, giving 64 samples over the waveform period. For the next period, a second store is switched into operation, leaving the first for processing.

The store is now read out and is correlated with each of the possible waveforms. To give an equivalent of the non-coherent correlation detector each correlation must be squared and added to its corresponding mate on the second channel, thus forming ${\rm In}^2 + {\rm Q_n}^2$. However, this is expensive in hardware; instead the modulus of each channel is added, giving a loss in performance of about 0.6 dB. As each correlation progresses, the two largest values are retained.

A second path, which normally comes from a second receiver but which can be locked into a different echo if required, also provides the largest two correlations as the output and a selection from the two paths is then made. The largest output represents the most likely waveform transmitted, and after decoding, yields the original input data. The difference between the largest and next largest outputs gives a measure of the error probability, and this is used to initiate a request for re-transmission if a pre-determined threshold is reached.

2.3 Synchronization

The receiver requires

- timing for the pseudo-noise sequence
- bit timing for the A/D converter/integrators
- waveform timing for the start of signal processing and for the output code

All these timing signals are derived from a master clock which is locked to the received PN sequence. Lock is maintained by a delay lock loop (Fig. 2). Initial synchronization of this is performed in both directions by resetting the PN sequence at the beginning of every character, thus producing a short sequence which can be quickly identified. The locking circuits conduct a drift search and when the signal has exceeded a pre-determined threshold for a given length of time, special control characters are used to inform the remote end of the circuit that acquisition has occured. When lock is achieved in both directions the PN sequence is no longer reset at every character.

Once locked all other timing is also in synchronization and will remain so, since character and bit timing are locked to the PN sequence at the transmitter. For point to point circuits the maximum drift rate of the received echoes is about 50 nanoseconds per second (due to ionospheric changes) and this is a small fraction of the minimum chip length of 10 microseconds. Thus the delay lock loop is essentially a slow acting device of narrow bandwidth. Short term fading is unlikely to affect it, but as a precaution the loop may be inhibited during fading. The clock has sufficient stability to cater for normal fading periods.

Operational considerations

One characteristic of the synchronization technique outlined above which should be noted is that, with the drift search mode, the receiver always locks to the first multipath component above some threshold value - this need not necessarily be the strongest or most stable component. If two separate processing paths are availabe, a different component can be selected for each and a mode diversity combining technique becomes a possibility.

Special circumstances will also arise when two echoes coalesce or when a multipath continuum exists. In the first case the delay lock loop tracks the stronger echo, which is in general advantageous. In the second, which happens only rarely, there will generally be specular components onto which lock can be obtained. In extreme cases tracking may not be possible.

Certain requirements of a minimal nature exist in order that signals can be correctly decoded. These are

- The chosen echo phase and amplitude do not vary significantly over the correlation period (e.g. about 150 msec for 50-Baud telegraph)
- (2) The chosen echo time delay remains reasonably constant over the chip period (10-100 microseconds)

Requirement (1) is met for point-to-point HF circuits. Fading and phase changes will generally be less than observed on a composite signal and thus the performance should be as good as or better than the commercially available "Piccolo" system (Ref. 3) which employs a detection process which is conceptually similar. That requirement (2) is satisfied follows from the phase stability. Under normal conditions, i.e. when a good specular echo is being received the performance of the equipment will be about 6 dB better than a simple FSK system would be if measured with gaussian noise interference. For the case of a multipath continuum this performance is reduced by the ratio of the chip length to the multipath spread.

Under practical conditions the simple FSK system will not achieve the theoretical performance because of intersymbol interference, other user interference, etc. In the case of bad multipath interference it might well fail completely. The transmission impairments to simple FSK become progressively more severe as the information rate is increased. There is no such limitation with the spread spectrum modem, but it must be realised that the echoes, which are not used, and interference appear as uncorrelated noise and this sets a limit to the information rate.

4. Test Results

In order to check the effectiveness of the particular implementation, the performance under laboratory conditions using an HF channel similator has been measured and compared with the theoretical performance figures. The measurements results given in Fig. 3 show that the measured performance is in the range 0.5 to 1 dB worse than the theoretical values.

The prototype SSHF modem is currently undergoing practical tests and only preliminary results are available. These indicate that the technique has considerable potential to merit further development.

References

- 1) DIXON, R.C., "Spread Spectrum Systems", Wiley 1976.
- LYNCH, J.T., et al "Measurement of the best time delay resolution obtained along E-W and N-S ionospheric paths" J. Radio Science, Vol. 7, Oct 1972.
- 3) BALEY, D., and RALPHS, J.D. "Piccolo 32-Tone Telegraph System in Diplomatic Communication" Proc IEE, Vol. 119, No. 9, September 1972.

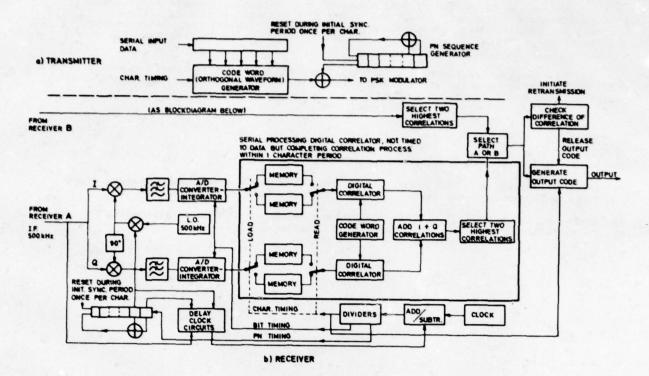


Fig. 1 Functional Block Diagram of STC SSHF Modem

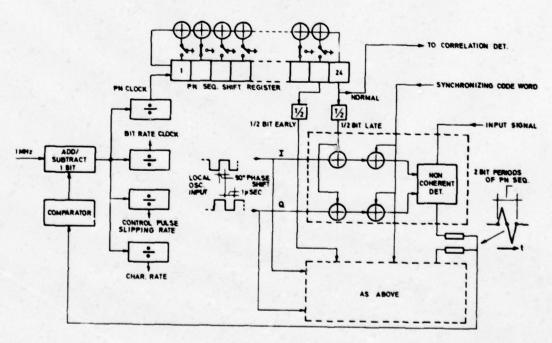


Fig. 2 Synchronizing circuits

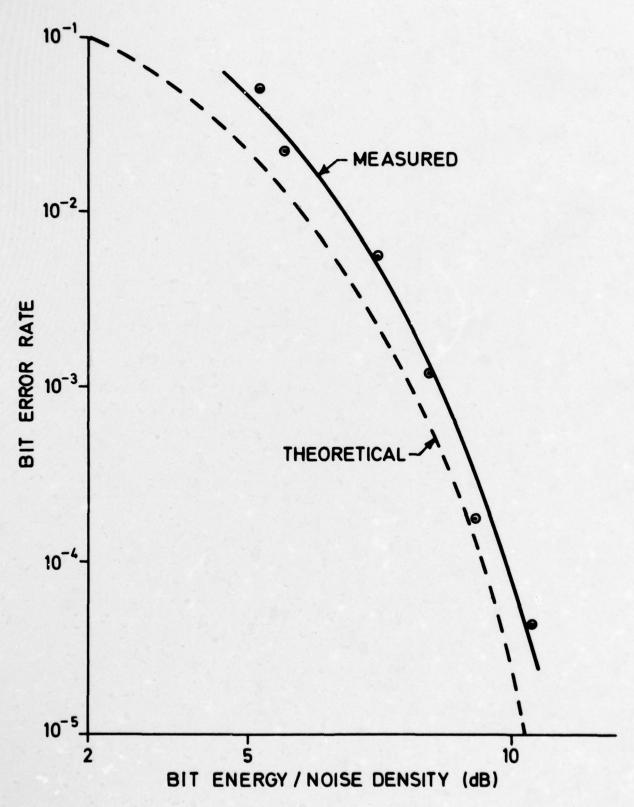


Fig. 3 Laboratory test results with SSHF modem

DISCUSSIONS AND COMMENTS

SESSION I:

SCATTER PROPAGATION_OF ELECTROMAGNETIC WAVES

Paper No: 1.1

A. N. Ince (STC): I would like to congratulate Dr. Gjessing on his lucid presentation of the various scatter mechanisms which affect communications channels. I would like to ask him why he omitted to deal, in his review, with signal-strength variability and to comment on the correlation, or lack of it, between signal-strength and the delay spectrum?

D. Gjessing (NO): Dr. Ince is, of course, raising a very important point, namely that of the factor of proportionality.

In the lecture I left this out for two main reasons. The first reason is that this has been studied by many very competent workers over many years. It has for instance been shown that the median value of the field strength on a transhorizon path is directly related to the standard deviation (r.m.s.) of the refractive index fluctuations. Similarly, the average or the median bandwidth is related to the average properties of the refractive index irregularity spectrum, and the average scattering cross-section σ is determined by the average properties of the scattering object. In my lecture I have stressed the factors which determine the variability of the parameters of interest. Specifically I have been addressing myself to the probability distributions of the pertinent radio circuit parameters and I have tried to relate this probability distribution to that describing the variability of the medium. I am therefore, basing my work on contributions from earlier scientists in the field.

The second reason for me not including the constant of proportionality, is that this requires very accurate and tedious calculations involving information about the constant factor (the DC term), around which the parameters of interest vary.

Then to your second question. Is there a correlation or a lack of it between signal-strength and the delay spectrum? This is not a very easy question unless we make very specific assumptions with regard to the atmospheric refractive index structure. If, for instance, we assume that the scattering is caused by a single layer in the atmosphere, then we know that the larger the refractive index variation is through the layer, the higher is the strength of the scattered wave. Similarly, the thicker the layer is, the wider is the delay spectrum. Hence, if we could assume that there is a direct correlation between layer thickness and the degree to which the refractive index varies through the layer, then clearly there would be a direct relationship between signal strength and the width of the delay spectrum. This, however, is not a very realistic situation. In a realistic model of the atmosphere we are dealing with more or less homogeneous isotropic turbulence super-imposed on a layered structure (to the extent that one can imagine isotropic homogeneous turbulence in a layered atmosphere). Under such conditions I see no direct relationship between signal strength and width of the delay spectrum.

D. Brodtkorb (NO): Can you comment on the aspect of phase response of the broadband radio communication channel?

D. Gjessing (NO): I understand your question as follows: In a communication system one is not only interested in the bandwidth properties of the channel, but one also needs information about the phase response. The point of Dr. Brodtkorb is well taken. For some applications, the frequency bandwidth function is of primary interest whereas in other applications the linearity of phase is the major factor. If you are dealing with a line-of-sight situation then I think this point is easily visualized. Referring for example, to the work by Lee and Harp from Stanford University, they give two sets of curves relating the atmospheric structure to parameters of direct interest to the radio communication engineer. They give the amplitude covariance function and also the covariance function of phase. From these, phase distortions as well as amplitude distortions may be calculated. If as an example, our problem is to map the surface of the ground by the use of a side-looking radar system, then both the amplitude covariance function and the phase covariance function is of importance, although perhaps the phase function playsa dominating role. This means that if you have two receiving elements measuring phase and amplitude at two different points in space, and if you correlate the phase, and the amplitude respectively as you move the two points away from each other, then you will find in general that the phase decorrelates before the amplitude does. When dealing with the over-the-horizon situation I think this phenomenon is far more difficult to visualize. Perhaps by inspecting what goes on in a RAKE troposcatter system, we can visualise what the atmospheric refractive index irregularity structure does to the phase. Perhaps Dr. Monsen who I see is present could comment on this.

P. Monsen (USA): I think the troposcatter channel is a complex Gaussian channel and the whole thing is described by second moment considerations.

Paper No: 1.2

- J. Blythe (UK): Could I just ask you how closely you think the spectrum of the turbulence in your model is like that which occurs in the troposcatter problem?
- W. Burrows (UK): Unfortunately there is a tendency to interpret the meaning of the word Turbulence in as many ways as there are disciplines in which it is used. We have created specific turbulence structures in the model, by using techniques familiar to the aerodynamicist. The elementary properties of these structures have also been measured, observed and confirmed by using techniques which, again, are familiar to the aerodynamicist.

However, in our search for correlation between the relatively fine scale structures and the fading or variations in the 'received signal' on the model system, we have concluded that their effects are of little consequence. Indeed, the comparisons that we have made between the 'received signal' spectra obtained from our full scale system and the identical spectra that have been obtained from the model, have lead us to the conclusion that we should pay more attention to the effects of the large scale air mass movements that are taking place in the lower atmosphere rather than to any fine scale structures.

- J. Blythe (UK): Dr. Burrows, this is most provocative.
- H. P. Williams (STC): I was wondering, how do you sort out the contributions to aerosols with turbulence factors? Do I get you right that you are using $2300 \ A^{\circ}$?
- W. Burrows (UK): No, I am using 6328 AO light in the visible red region.
- H. P. Williams (STC): Even there presumably it may have some effect, but if you went even further along in scale you would be having very distinct effects with aerosols wouldn't you? I thought at first you said 2300 A^O. The question still remains, but I think not so strongly.
- W. Burrows (UK): I think the simple answer to your question is that if aerosols have any effect, we have not seen it.
- L. Lewin (USA): Could you say something about the effect of dust in your model? Perhaps you could also elaborate a little more on your point of view relating to the common volume.
- W. Burrows (UK): Yes. The question of dust, although seemingly trivial, is very important in this type of modelling technique. We have, of course, seen both dust and its effects. We have also had problems with the occasional insect, which we have come to regard as a large particle of dust with predictable mobility!

The effects of dust particles on the fading signal observed on the 'model receiver' are quite recognisable and are very different from those due to air mass movements or so-called turbulence. As a result, data which has been recorded and subsequently found to contain 'dust responses' has been discarded prior to any further analysis in our programmes.

A similar situation exists in respect of the full scale 900 MHz link that has been used. With the transmitter situated on the South Coast of England, and the receiver terminal at Imperial College, London, there is frequent interference from air traffic in the vicinities of both Heathrow and Southampton airports. The effects of aircraft, which may be regarded as rather large "particles of dust", are readily recognisable and are well known. Again, close inspection of any raw data recorded from the full scale system will reveal the presence of aircraft along the path and the data sample is discarded in order to keep computer costs down to the minimum.

The Common Volume is perhaps a very controversial issue. The generally accepted common volume, atthe intersection of both transmitter and receiver beams in a terrestrial transhorizon tropospheric radio system, provides a very convenient physical model for analytical purposes. However, after considerable experimentation on the model, conducted in parallel with observations of the performance of a full scale system, it has been concluded that this traditional common volume has very little relevance to the real situation and is, therefore, an unacceptable concept.

The only common volume that we have come to recognise is that which exists between the two extreme boundaries at the two ends of the propagation path. The boundaries in the vertical direction are formed by the earth's surface and the tropopause with 'sides' many thousands of wavelengths on either side of the axis of the transmitter beam.

Our studies have shown that when a narrow beam is propagated through a gaseous medium, which is supporting a temparature gradient, the beam is subject to considerable time-varying distortion along its entire detectable length. The extent of this distortion is commulative along its length from the source and is the result of a progression of changes in the refractive index gradient profile 'surfaces', normal to the axis of the beam, at all points along the path of the beam. The overall effect of these changes gives rise to considerable changes in both the shape of its cross-section and, indeed,

the position of the effective axis which increases with distance from its source. These effects give rise to at least two simple conclusions. Firstly, that the traditional so-called common volume cannot be defined. Secondly, that the refractive index gradient properties of the $\frac{\text{whole}}{\text{sole}}$ of the propagation medium volume between the transmitter and receiver antennas should be considered in relation to the ultimate progress of a transmitted beam.

Many years ago I recorded these effects on ciné film which was shown at an $E.P.P.\ A.G.A.R.D.$ meeting in Ankara.

L. Lewin (USA): I would like most strongly to commend this paper to our attention. I believe it to be a very significant study, and one of whose results and methods we should take note. I think it should be extended in the direction of appropriate scaling, (something which I believe was not done) and also to accommodate a humidity gradient corresponding to what we believe happens in the real atmosphere. It is a substantial achievement to have obtained results that closely mimic typical measured results, but we should be careful about concluding too readily that the atmospheric conditions responsible for scatter phenomena have therefore been correctly simulated. There may well be finer scale structures, both in time and space, that occur in the real world but not in the model.

I would mention how the "Morphology of Physical Laws" first prepared by P. Belatini, in which the presence of various types of atmospheric disturbances, together with their scale, structures, velocity, etc., was predicted from very fundamental considerations, analogous to the theory of dimensions. These features may well be in evidence in Burrows' model, and the opportunity could possibly be taken to bring this unpublished (posthumous) material to light in the context of these experiments.

Paper No: 1.3

- J. Blythe (UK): Could I ask if you have attempted any experiments to validate any of the theory at all?
- K. Langenberg (FRG): No, as a matter of fact I did not. A theoretical investigation was stimulated by the original radio-wave propagation group of the late Professor Brotz at the University of Hamburg.
- J. Blythe (UK): Certainly a very interesting piece of work.
- S. N. Samaddar (USA): If the dimension (height) of the duct is many wavelengths, the representation of electromagnetic fields in terms of lateral waves may be suitable. However, if the dimension (height) of the duct is short so that it can allow only one or two modes (pole contributions), it may be necessary to include many lateral waves. In other words, for short dimension of the duct, modal representation appears to be convenient.
- K. Langenberg (FRG): It is not only a matter of direct height but also of the transmitter receiver distance; for small distances the lateral wave concept is the only one available whereas for large distances one does best to use a modal representation. The transition from one model to the other can be clearly investigated by the presented theory.

Paper No: 1.4

- J. A. Wick (USA): The conjecture contained in a series of papers by Bathias and Battesti indicates that climate type (and inherent variability in scatter cross-section with height) may have a significant influence upon the variation of coupling loss with distance, especially at shorter range. It would appear that consideration of the tendancy for high degrees of stratification in Maritime climate as opposed to subrefractive conditions found in desert climates would allow 1) better correlation of the major data case with theory and 2) allow a model to be formulated which would yield more accurate predictions in a given climatic region.
- L. Lewin (USA): This is an interesting comment. But any valid model must explain the behaviour over both sea and land. Conceivably it may be easier to put together the basis of a valid model by first working with maritime parameters. An alternative is the experimental laboratory model of Burrows (see paper 1.2).
- P. Gruber (USA): Why was the CCIR aperture medium coupling loss formula introduced? Would you recommend not to use the CCIR aperture to medium coupling loss formula since it is pessimistic, shows unrealistic losses for high gain antennaes and in particular disregards the scatter angle.
- L. Lewin (USA): I don't want to be finding myself in the position of damning any particular formula or author. I have not done the experiments that I have freely quoted here. I can't take responsibility for their accuracy. What I do find is that the majority of the calculations from many different sources do not give as high a loss as the CCIR formula and I think its probably an over simplification to have any formula that really doesn't depend on the scatter angle or distance. My impression, and it is purely a subjective impression, is that the curve was put together at a time when there was just not that much data known and somebody wanted something to put in and they put this in and maybe they wanted to see it merely as a historic attempt to deal with

it at an early stage and that it is now taken over by other data. I would tend to see it in that light.

- P. Gruber (USA): I believe that the CCIR approach is conservative and one can go wrong using this calculated coupling loss, since the CCIR formula could be in error by 10db especially if $G_1+G_2=100$ to 110db it would mean the difference between a 1kW or 10kW transmitter which is not acceptable, in the competitive commercial world. It appears that Fig. 1 & 2 (Paper 1.4) "Proposed Curve" might be more realistic.
- A. N. Ince (STC): Perhaps we all agree that more controlled experiments, including laboratory simulations of the kind Dr. Burrows talked about earlier (Paper 1.2) are required to address some of the issues raised here; experiments where one is concerned not only with signals at the input and output of the transmit and receive antennas but also with what really happens in between the two antennas. Having said this I would like to make two comments of practical interest in relation to antenna size and antenna-medium coupling loss. Referring to figures 1 and 2 in Prof. Lewin's paper you will observe that the coupling losses, as given by various authors, are almost all within 1-2 dB of the CCIR value when the range is in the interval 200-350 Kms which coversalmost all practical cases. Practically speaking 1-2 dB uncertainty due to this factor can be considered not to be very significant when this is compared with the overall performance prediction uncertainty which is often in the order of 10 dB (see paper 4.1). The second comment I would like to make is that when determining the antenna size for an application we should consider not only the coupling loss which affects the signal strength but also the dispersion which affects inter-modulation noise in analogue, and inter-channel interference in digital systems and which improves with increasing antenna size.

W. Burrows (UK): I can assure both Dr. Ince and Prof. Lewin that we have, in fact, conducted the type of exercise to which they refer. I didn't have the time, in my presentation, to give details of all my experimental work.

In both the $model\ {\it and}\ full\ {\it scale}\ links,\ firm\ relationships\ have\ been\ established\ between\ :$

- (i) Depth of fading and atmosphere lapse rate and
- (ii) Rates of fading and surface wind velocity normal to the path.

Also by using the model we have concluded that there is a preferred vertical 'angle of shoot' for a specific lapse rate along the path. There is also a preferred azimuthal 'angle of shoot' for a given surface wind velocity normal to the path.

Both of these results have been confirmed in reality on our full scale 900 MHz system. Fortunately, we were using 12ft. diameter 'Dish' antennas which were readily adjustable in both azimuth and elevation. An exercise of this type would be extremely difficult and costly with a 60ft. diameter antenna.

The effects of different size antenna apertures have also been the subject of modest investigation. Because of limited financial resources, the simple properties of only two different diameter antennas have been examined. From the results we obtained, it would appear that reducing the size of the aperture of a receiving antenna increases the magnitudes of the high frequency components present in the spectra of variations or fading in the received signal. The larger aperture antenna clearly integrates the complex incident wavefront to produce a smoothing effect.

Other results also show that increasing a receiver antenna aperture under the so-called very weak signal condition does not produce the increase in gain predicted by the plane-wave theory. Indeed, the "power collecting efficiency" of a receiving antenna would appear to be significantly related to the propagation conditions along a given path.

Both of these features have been examined and confirmed in the model for a wide range of "receiver antenna" apertures. The only expenses incurred being the cost of a range of "electron microscope apertures" and which was negligible.

It may be of interest to note that in the measurements made on both the full scale system and its model, Antenna to Medium coupling loss figures did not in any instance account for the discrepancies between theory and practice.

I. M. Vogt (STC): In your presentation you stated that narrowing the beamwidth of the antenna would result in zero additional gain if the scatter volume were to provide homogenious scattering efficiencies, as it would for very narrow beam antennas. Whereas this would be true if one beam were narrowed, however some gain would result if both transmitter and receiver antenna beam widths were reduced. Actually a gain of 3dB should result from increasing the gain of each antenna by 6dB. Is my understanding of your paper in this respect correct?

L. Lewin (USA): Yes, this feature is described in section 3.1 of the paper. It is a function of the size of the scatter volume relative to the beamwidth of the receiver antenna, but, of course, the <u>allocation</u> of the gain to only one antenna is quite arbitrary the received power is a function of the parameters of the entire link.

- S. Park (USA): I believe that one reason why there is so much confusion about the coupling loss is that it is very often not very well defined. There are really two ways of looking at it and I would like to know which is the way you look at it. One is to consider what happens if you double the aperture on an actual link: What would you gain by doing that? You can make experiments and you can get coupling loss that way. The other way would be to set up a model of path loss in the troposphere and associated with the model you associate a formula for the coupling loss. If you use a different model you get a different formula for the coupling loss, and that is why in the literature you find many different formulas for coupling loss because they use different scattering mechanisms. Now are you referring to a coupling loss through a specific model or are you considering the coupling loss as a concept of the fraction of scattered power to the available scattered power?
- L. Lewin (USA): Let me make it clear that my paper, to the extent that it is a valid survey, has looked at models from a number of different authors and has tried to reconcile their findings, and also their findings with experiments. Most of the authors do deal with a model which predicts various scattering laws, mostly amounting to an inverse power, and granted that that is happening what I have tried to understand for myself is "What is the meaning of this in terms of the physics of what is going on?" The best that I can describe it, and I would like to see it subject to an adequate experimental verification, is that there is a common volume and that when you increase the size of the antennas you are decreasing the availability of the common volume but you are also increasing your capacity to pick up from what common volume you are picking up from, and that to the extent that the scatterers would be uniform I believe that one would more or less balance the other. But when you narrow the antenna beam you can also point it lower down with advantage and this picks up the stronger scatterers. Therefore there is an improvement and it may or may not be the full amount of the extra antenna gain. If you don't get it you call it antenna coupling loss and I am not really sure that it is too helpful to do that. This is the best picture that I have, and as I said I would like to see it subject to confirmation experimentally. There is an additional feature which has been stressed here by Dr. Ince and that is that we shouldn't be hypnotized only with gain but, particularly when we are talking about digital systems, we are concerned with arrival times, and I think that quite generally as you get the larger antenna you narrow your acceptance range and you narrow the spread of arrival times, so from that point of view there may well be a gain even if there isn't a full aperture gain to be realized. This is the best I can do, I am afraid.

Paper No: 1.5

- P. Monsen (USA): A decision-feedback equalizer for troposcatter applications at data rates up to 12.6 Mb/s has been developed and tested on actual links both in Europe and the U.S. As pointed out in Mr. Schmitt's talk, airplanes in the common volume represent one of the most severe disturbances to the equalizer. Our tests show that the equalizer developed by Sylvania/Signatron in most cases could accommodate the airplane phenomenon. The link reported on my Mr. Schmitt also has rather severe multipath characteristics.
- F. Schmitt (FRG): Of course I know about the theoretical work that has been done by you, but until now I was not aware of any test results of the performance of your equalizer on a real troposcatter path. I am very interested in these results, because we are also designing an equalizer to be used on our path, which we feel to be an extremely difficult one to equalize.
- A. N. Ince (STC): I have two questions. The first relates to the correlation between transmission loss, or as you called it signal strength, and the time spread. If I understood you correctly you found between loss and time spread a positive correlation (or negative correlation between dispersion and signal strength). Could you please comment on whether or not you expected this or whether the opposite or no correlation at all might have been justified on theoretical grounds? I wonder, Mr. Chairman, if I may invite comments from the audience on this particular issue as well as on the second question that I have which relates to doppler spectrum. If Dr. Schmitt measured doppler could be comment if the spectrum was symmetrical or not and relate this to vertical or horizontal air motions giving rise to disturbances in the so-called common volume?
- F. Schmitt (FRG): In fact, we did not make measurements of the doppler on our test link as far as the correlation between the signal strength and the delay spread is concerned, we observed correlation in the case of night time measurements when there was a high degree of statistical stationarity.
- J. A. Wick (USA): The positive correlation between increasing path loss and increasing multipath spread was also observed by Bello on the RADC L-Band link and by Bukemeier on the Collins Radio University of Wisconsin Σ Band link.

Bukemeier processed the doppler spectrum and found that the width of these doppler spectra (corresponding to fade rate) was directly related to the cross-path component of wind speed in the common volume.

The interrelation between multipath spreading and path loss at L band can be strongly correlated to atmospheric stratification as was also shown by Bukemeier.

Paper No: 1.6

- L. Lewin (USA): Since the number observed is independent of frequency I would expect the number observed to be the number that actually enter the atmosphere and I don't see why this exhibits a minimum at a certain time of day. Should it not be the same throughout the 24 hours?
- G. H. Millman (USA): This question can best be answered by noting that meteors are for the most part travelling in the plane of the earth's orbit. On the night side of the earth, meteors which move in the same direction around the sun as the earth moves and with velocities greater than that of the earth only will be observed. In the morning hours, meteors travelling in both the same and opposite direction to that of the earth will be swept up by the earth. This results in a maximum and minimum rate of occurrence at approximately 0600 and 1800 hours local time, respectively.
- H. P. Williams (STC): I felt distinctly embarassed at the first figures that Dr. Millman showed because he was using 10^{14} electrons per meter as an over-dense case and I intend later on in my paper (4.4) to use it as an under-dense case. For the benefit of those who may not have looked into these things, the limits given depend upon the way you calculate it and they vary from 9.9 x 10^{14} to 2.2 x 10^{14} .
- G. H. Millman (USA): McKinley (D.W.R. McKinley, "Meteor Science and Engineering", McGraw-Hill Book Co., 1961) cites the transitional value of the line density of the meteor trail from the underdense to the overdense case as 2.4×10^{14} electrons/m. Manning and Eshleman (L.A. Manning and V.R. Eshleman, "Meteors in the Ionosphere", Proc. IRE, Vol. 47, pp 186-199, February 1959), on the other hand, define the transition point by 1.1×10^{14} electrons/m.

Paper No: 1.7

- J. Blythe (UK): May I enquire if you have attempted any experimental work?
- A. Javed (Canada): We have done some limited experimental work. We have received via meteor trails bursts of TV images from Channel 2 emitters (56-60 MHz) located well beyond line of sight. This has been done with a receiving station located in Pakistan (where I was before moving to Canada) and with another receiving station located in Illinois. From an estimate of the resolution of the received pictures (photographically recorded) and from the examination of the risetime of the received synch pulses we could conclude that the channel bandwidth, at the beginning of the trail formation, is equal to or larger than 4 MHz.
- N. M. Maslin (UK): Dr. Javed, your calculations consider great-circle propagation, is that correct? At the levels of transmitter power that you are considering (i.e., 100 kW), you will get interference from sporadic E and from ionospheric forward scatter. I believe that it is an experimental fact that you observe meteor trail reflections not exactly from great circle propagation but slightly to the side, from the so-called "hot spots". What would your reaction be to a communication system which tried to avoid these interfering modes of sporadic E and ionospheric forward scatter by using perhaps a split beam antenna which might try to pick up those "hot spots" and thus avoid some of the interfacing modes that you might get at the power levels that you are using?
- A. Javed (Canada): The answer to the first question is affirmative.

The answer to the second question, how to avoid interferences, is more difficult. By the way, airplanes also are a source of serious interference in many locations, such as the site in Illinois where we conducted part of our measurements. My inclination would be to approach the problem from a data processing standpoint. Meteor echoes have something peculiar: the Fresnel pattern at the beginning of their appearance. This pattern could be "recognized" and the link could be "enabled" only when the pattern is present. I know that some step in this direction has already been taken and meteor echo processors have already been built and used in the field, although they use "recognition" criteria other than Fresnel pattern monitoring. Apparently they have been proven quite effective against at least sporadic E and airplane interference.

Paper No: 1.8

- G. H. Millman (USA): Were you able to correlate the velocities of the irregularity patches with magnetic activity? What was the frequency dependency of the scintillation?
- J. Aarons (USA): Frequency dependence may range from f^O to f^{-2} , Rayleigh fading can be observed at two frequencies therefore we note an f^O dependence. With weak scattering the dependence is found to be most often $f^{-1} \cdot 5$.
- L. W. Barclay (UK): Dr. Aarons description of the post-sunset equatorial ionosphere was most interesting. Scatter propagation using these irregularities has been observed from the ground for many years. Perhaps the first report was by Orsborne and Humby in the early 1950's who noted pronounced signalling distortion on an HF telegraph channel between Singapore and UK. Trans-equatorial-propagation at frequencies up to 100 MHz has been observed in differing longitude zones: between North and South America; between Southern Africa and the Mediterranean and between Japan and Australia. These observations

may help in a study of the longitudinal and solar activity variations in the occurrence of the effect.

When this effect occurs HF north-south paths may depart substantially from the great circle. Oblique soundings between Tsumeb and Lindau have shown signals which arrive at up to 60° from the great circle.

- J. Aarons (USA): The patches I describe in our paper are 50-200 km EW and 500-1000 km NS. Each patch moves as a whole (EASTWARD) and therefore at times we would expect to see scattering off great circle. During some nights there are many patches and the best signal might be noted near great circle paths. We have used trans-equatorial scattering data to understand the phenomenon of the patch; see our paper recently accepted by the Journal of Geographical Research.
- A. N. Ince (STC): Could you comment on the electron density changes involved here and/or compare them with those obtained in artificial heatings of the ionisphere? (See paper 4.1)
- J. Aarons (USA): This first of all seems to be a depletion and the only thing that affects a scintillation is ΔN rather than $\Delta N/N$. The density that could account for this can be something of the order of 50% of the normal N in this region at this time with a depth of 50 to 100 kilometres, 10% to 50% (and at times almost 100%) could account for the very deep fading that we see.
- A. N. Ince (STC): 50% of N is a big change. That is almost a hole is it not!
- J. Aarons (USA): Well the data from the AE measurements are even more violent than that. What they say is that they have measured depletions of several orders of magnitude below N. In other words they come to a region in the F region where the electron density is several orders of magnitude below that of the surrounding region, but that is the big bubble rather than the small scale irregularities within the big bubble.

These are measurements that McClure made using the AE satellite information published two months ago in JGR.

- H. P. Williams (STC): Changes of that magnitude are so dramatic that I feel there must be some fairly straightforward explanation. What sort of explanations have been advanced so far?
- J. Aarons (USA): Well maybe some better theoreticians than I am would talk about it perhaps K.C. Yeh would like to do so.
- K. C. Yeh (USA): I think the current understanding is that in the underside of the F region sometimes the density can be very steep. Hence you have a situation of heavy fluid on top of light fluid which is intrinsically unstable and if you have any perturbation you have what is known as interchange instability and this would be manifested in the form of a bubble which would be rising up to the top of the F region where the ambient density is the same as the density where the region of instability occurred and is rising because of the process involved and might create small scale irregularities. So this is the current understanding of the problem.
- A. N. Ince (STC): You mean to say that this is the mechanism which gives rise to 50% change in N that Dr. Aarons referred to?
- K. C. Yeh (USA): This has been measured by in situe measurements and the theory does not have the sophistication to predict that yet because such a large change requires a non-linear theory to explain it and non-linear theories are hard to handle.
- S. N. Samaddar (USA): I have not seen your mathematical analysis. You mentioned that you had included the effect of some multiple scattering in your theory. How and by what method (mathematical) have you done that? Was it Rytor method?
- K. C. Yeh (USA): All the multiple scattering effects are included except the back scattering. The method is known as the parabolic equation method whereby a transport equation for the two-frequency two-position mutual coherence function is derived.
- S. N. Samaddar (USA): What do you mean by that? Are you talking about some differential equation?
- K. C. Yeh (USA): Yes, the differential equation satisfied by the mutual coherence function was projected. Details can be found in a paper which will appear in the forthcoming issue of Radio Science.

Paper No: 1.10

H. P. Williams (STC): I take it that the scale you had for visibility, when you referred to meteorological visibility, was the usual definition of a large black object on the horizon, was it? In the part of the world where I come from 3 miles is often regarded as fairly good visibility so that there

would be tremendous different feelings in the experiments done in California and what you would get, say, in the North Sea.

- M. Geller (USA): I hope that I did not give the impression that this is an all weather system. It is generally for those regions where the visibility is high. For instance the statistics show that in the Mediterranean you do have generally high visibility.
- I. M. Vogt (STC): I understood you to say that the scintillation on the ducted beams was considerably larger than the scintillation on the scattered beam. Do you have any explanation for this?
- M. Geller (USA): The apparent source size of the scatter beam is much larger so you get a lot of aperture averaging compared with the direct.
- I. M. Vogt (STC): I could understand it if you had a noncoherent source of radiation but you are using a lazer aren't you?
- M. Geller (USA): The coherence doesn't enter into the picture at all in the sense that our energy detection system is a non-coherent system. You can do the same experiments with an incoherent source, if you had a source that would emit, say, quarter of a megowatt power 10 nanno second pulses. The fact that we just use a lazer is because it is the only source available with those characteristics. We don't use the coherence at all.

End of Session I

SESSION II:

TECHNIQUES FOR PROPAGATION MEASUREMENTS AND CHANNEL SIMULATIONS

Papers 2.1 and 2.2

- A. N. Ince (STC): Simulators whether of the synthetic or the stored-channel type are being built basically for use in the performance comparison of various modems and yet it seems to me that the modem designers are seldom informed about the characteristics of the simulators which are eventually employed to test their modems. Do you think that there is adequate communication and feedback between the designers of simulators and modems?
- P. Bello (USA): I think the answer may be seen in Fig. 1 of Paper 2.1 which shows all the communications that should exist between the people doing the designing and building the simulators, the modems etc. However, as you said, there is a communication gap between the groups concerned; there is not enough feedback, there has never been enough feedback, there probably never will be, because of the diverse organizations involved in funding, contracting etc. One hopes that a conference such as this may help to establish some feedback between the designers of simulators and modems in different countries even in the same country. It is a problem we all have and I cannot offer a good solution.
- A. N. Ince (STC): An approach to this problem which might be taken by an organization wanting a new modem to be developed could be to have, first of all the simulator built and described and then give this to the modem manufacturer and tell him that this is the channel through which his modem is expected to work. If this is not done I feel that the time and effort taken to build a channel simulator, after the event as it were, would not help the desired modem to be produced.
- P. Bello (USA): I agree but what happens in reality is that everybody has got schedules and they want the modem delivered by a certain time. They do not want to wait till the channel model is developed, checked out and validated and a simulator built before they go ahead and design their modem. However, I concur; may be the whole world will slow down but they are all in too big a rush anyway!

End of Session II

SESSION III

PROPAGATION HAZARDS FOR COMMUNICATIONS

Paper No: 3.1

- L. Lewin (USA): Was the nature of the calculation of the field expansion expressions such as to require the assumption of the validity of the Raleigh hypothesis (which permits an external field expansion to be analytically contained inwards to the conductor suface)?
- K. Becker (FRG): The assumption is to replace the surface roughness by induced currents in the now inhomogeneous transition conditions for the electromagnetic field.

Paper No: 3.2

- L. Lewin (USA): Could you please answer the following questions:
- (i) What depolarization coefficients were assumed?
- (ii) How was I determined in relation to the comparison of theory and measurements?
- (iii) What would be the effect of more solid vertical structures such as stalks or tree trunks?
- (iv) Since the vegetation is semi-transparent, why is ground reflection considered unimportant?
- (v) Instead of t and t, could one contemplate L and ϕ where the statistics of ϕ relate to the leaf inclination? For corn, for instance, the leaves are more nearly vertical than horizontal would this not make $t_z \gg t$?
- A. K. Fung (USA): The answers to the questions above are as follows:
- (i) For Disc-shaped granules, the depolarization factors, \mathbf{A}_j , are 0, 0 and \mathbf{t} in the permittivity model.
- (ii) The parameter £, was determined by fitting data.
- (iii) Stalks and tree-trunks need be treated separately. In the case of dense leafy vegetation, the trunk is pretty much covered by leaves. Even if it is a vertical cylinder-type the model indicates that such a structure does not contribute to backscattering except at grazing incidence.
- (iv) This is because of attenuation within the vegetated medium. For sparse or thin layer of vegetation ground effect is certainly important within 30° of vertical.
- (v) Use of 1, $\mathbf{1}_{z}$ or L, appears to be equivalent. The main problem is that more adequate target-truth information is needed to verify what would be the best choice. My experience with data (scattering coefficient measurements) indicates that due to frequency filtering effect, 1, appears to be an effective parameter.

Paper No: 3.4

- K. Toman (USA): May I ask for the reasons, applications behind this study?
- L. Ladell (Sweden): The application is to mobilise radio links for army use.
- D. Brodtkorb (NO): Can you comment on the apparent significant difference between the measured and the theoretical curves?
- L. Ladell (Sweden): A statistical result based on only 16 individual measurements is very weak and may not be directly compared with a calculated result based on 500 simulations. However, it seems to me to be quite a good correspondence between the results, keeping this limitation in mind.
- J. H. Blythe (UK): How were your paths selected?
- L. Ladell (Sweden): The paths in this study were all diffractive paths spread over a $30 \times 50 \text{ km}^2$ region. Antenna sites were selected with respect to accessibility and suitability for this kind of radio link. That means open places, at least with a radius of 20m, not far from a road. The receiver equipment required power supply.

Paper No: 3.6

L. Lewin (USA): Is there a North-south or East-west bias in ducts and what is the

order of magnitude of duct sizes?

H. T. Dougherty (USA): For ducts associated with gradients at or near the surface, particularly the sea surface, I am not aware of any bias. From data derived from the AGY and BOMEX, I have the impression these gradients occur in patches, tens of kilometres across but of no particular orientation. However, these patches may be distributed so as to reflect ocean current directions. For ducts associated with elevated layers that are advective, there would be a tendency of the layers to extend along the wind directions possibly, roughly, east-west.

Duct widths can extend from meters (near the surface) to a few hundreds of meters (elevated layers and ducts) in the vertical direction and tens to hundreds of kilometers in the "horizontal" direction. That horizontal extent can, of course, be for thousands of kilometers (not continuous) in the trade wind regions of the world. Duct propagation has been observed between San Diego and Hawaii for example - and from Korea to Taiwan for example - via elevated layers and ducts that are not continuous; the layer heights, thickness, and gradients also tend to change (systematically) with horizontal distance.

End of Session III

SESSION IV

SYSTEM DESIGN AND APPLICATION

Paper No: 4.1

J. S. Belrose (Canada): Your paper was very comprehensive and a good review of the subject since it covered such a large number of types of scatter communications. You made one comment which caught my ear and I could not resist responding to it being an ionospheric physicist. I agree with your comment that at the same magnetic latitude in Europe geomagnetic phenomena were different than at the same magnetic latitude in Canada; this is why ionospheric and magnetrospheric physicists stopped long ago using geomagnetic latitude which is based on the dipole approximation of the earth's magnetic field. If you use corrected geomagnetic latitude of some form the anomalies, where one is looking at phenomena associated with the earth's magnetic field, disappear.

A comment more directly related to the topic of your paper concerns scatter or possibility of scatter communication associated with ionospheric heating. You described the field-aligned scatter which is very aspect sensitive but you did not mention the plasma wave scatter which will have aspect sensitivity in exactly the opposite way of the field-aligned scatter; it will work best at high latitude where one is looking along the field rather than orthrogonal to the field. This mode is probably much less aspect sensitive. It will probably scatter UHF waves better than the VHF waves but its utility is not yet proved. We are doing some exploratory experiments in the Ottowa region at the present moment but I have no results yet to report. In this mode of scatter reception takesplace at a frequency which is removed from the transmit frequency by plus or minus the heater frequency.

I. M. Vogt (STC): The first part of your comment does not call for an answer but the second point which is concerned with plasma wave scattering is covered in our paper.

Paper No: 4.3

- L. Lewin (USA): In one of your graphs at t=120 second, the interference went right down to zero. What was the cause of this?
- B. S. Skingley (UK): The cause of the destructive interference at t=120 seconds was in the choice of a fading scenario which gave an excessive rate of change in the up-fade direction together with a large change of level. This scenario was chosen for a practical system test to demonstrate that, for given control loop time constant, there can exist a combination of fade rate and level change, which can, briefly, defeat the system. It should be noted that if the up-fade at t=120 seconds had remained, there would have been significant improvements after only 5-10 seconds.
- P. Gruber (USA): May I ask if on the feedback transmission, whether you control the beam voltage or the drive?
- B. S. Skingley (UK): To date only RF power control has been found necessary. For low power (up to 50 watts) an output can be used whilst on high power klystron or twt systems it is necessary to change the drive power.
- A. N. Ince (STC): I agree that the transmitter power control is a useful technique which can save frequency spectrum; an important consideration in designing and implementing links. However, as we know, there are other techniques of achieving frequency conservation such as the use of multi-level modems which, on the other hand, require higher transmitter powers. A careful balance between power and spectrum occupancy which may depend on circumstances is therefore indicated.

Paper No: 4.4

N. M. Maslin (UK): Meteor scatter communications at shorter ranges of only a few hundred kilometers suffer the disadvantage of smaller time constants and smaller common areas of antenna illumination at meteor trail heights.

Do you believe that meteor scatter communications at lower frequencies, in the HF band, could help to overcome some of these difficulties?

H. P. Williams (STC): One would of course optimize antenna patterns for the range and frequency being used and I agree this would result in a smaller common area of illumination at a given height since the so-called "hot spots" are smaller in volume for a short link. This will certainly lead to a smaller duty cycle as will the smaller angle ϕ on a short link. There is a small compensating effect in that the overall path length is less.

If one were attempting to maximize the duty cycle on a short link one would

certainly wish to use a frequency below say 50 MHz to avoid "ceiling" effects so that trails at all heights within the "hot spot" volume would be effective. Of course the lower the frequency for a given antenna pattern, which is our situation, the higher the duty cycle, and this would indicate the use of the lowest frequency possible without encountering HF propagation for a substantial fraction of the time.

Of course for any path length one can use a split beam antenna to increase duty cycle. By this technique one concentrates power in the two hot spots which lie on either side of the great circle path and doesn't waste any in the barren zone in between.

End of Session IV

SESSION V

SIGNAL PROCESSING FOR SCATTER COMMUNICATIONS

Paper No: 5.1

- P. Monsen (USA): Could you comment on the parameters such as doppler rate and interleavings involved in the results shown in Fig. 11?
- P. Bello (USA): These error rate curves do assume that we are interleaving to have independent fluctuations in the bits. There is a penalty associated with using coding in the sense that you have to have a delay. For some systems that delay may or may not be tolerable. You can get quite a bit of improvement with a small amount of delay, but these curves do assume enough delay of the interleaved code to have independent fluctuations on each bit of the code. The paper by Dr. Chase on the MLT modem will give some results for small coding delay.

Paper No: 5.2

- P. Bello (USA): I object to the use of the term "maximum useable bandwidth". There is no maximum useable bandwidth with troposcatter in any sense as the way you have described it. You are limited entirely by your modulation techniques and your terminal equipment constraints. There is a maximum useable bandwidth in HF because you cannot transmit beyond a certain frequency but this is not an analogy at all and I would think that people not too familiar with the limitations imposed by a troposcatter channel would think that they could not transmit with bands exceeding what you are talking about. Do you have any comment on that?
- R. Valentin (FRG): I think I agree with you. The term "maximum useable bandwidth" or better "transmissible bandwidth" in my contribution refers only to the bandwidth limitations imposed by the scatter mechanism.
- J. Osterholz (USA): In most practical systems it is not, all of the time feasible, to use vertical antenna spacings. Would you care to comment on the relationships which we might be expected to see between the frequency separation and antenna separation for horizontal antenna spacings?
- R. Valentin (FRG): The equivalence theorem only holds for the vertical antenna displacement. Therefore I can't say anything about the relationship between frequency separation and antenna separation for horizontal antenna spacing.
- J. Osterholz (USA): Would your intuition tell you that the antenna spacings for horizontal diversity would be greater than for vertical?
- R. Valentin (FRG): Some time ago we performed measurements of the spatial correlation of the received scatter-mode signals. From these measurements the following was derived: The horizontal antenna spacing necessary to obtain substantial diversity gain in space diversity reception is a little larger than the vertical antenna spacing.

Paper No: 5.3

- P. Monsen (USA): I would like to make a brief comment. We are engaged in an angle diversity study ourselves. We have just entered our test phase so we don't have any test data but some of our theoretical work indicates some slight differences. For example, we have found that it is not such a good idea to make the powers in the two beams for the vertical angle diversity the same. Infact, the optimum pointing angle seems to be about a quarter of a beam width or half a beam width with central line elevated above the horizon. This leads to more squint loss but you make up for it with more power in the main beam. Under that constraint we are interested in comparing dual-space, dual-frequency with a conventional system with a dual-space, dual-angle in order to save the frequencies which is of some concern in some areas and what we find is that you actually end up better with the space angle configuration than with the conventional configuration. The advantage of this configuration is all the more because with dual frequency you need to have two power amplifiers; whereas with a dual-space dual-angle you can take the two power amplifiers and put them at the same frequency.
- J. Blythe (UK): I did comment that our theoretical calculations also support the fact that the equal signal case is not the optiumum working point for vertical angle diversity so I fully agree with that point and I am encouraged by your other remarks as well.
- J. Osterholz (USA): You mentioned that you did not notice any increase in path intermodulation noise in the elevated beam resulting from the elevated beam. Would you give me an idea what the bandwidth of the transmitted signal was?

- J. Blythe (UK): It was a conventional FDM system of 60 channels with a bandwidth of about 3 MHz.
- J. Wick (USA): Looking at your experimental data, I was wondering if there was any meteorological support going along with that. It would appear from what you saw that there was prevalence of high altitude layering and possibly some sub-refraction closer to the sea surface on this over-water path. I wonder if this is the case?
- J. Blythe (UK): We had no means of monitoring the detailed weather situation. There was a change from anticyclonic conditions to more disturbed weather at the middle of the test period as I indicated, but we lack any quantified met.data for the path.
- J. Wick (USA): I was concerned with these results where you showed the vertical separation vastly superior whether they would translate into other climate types or whether that was something that would be found primarily in over-water paths.
- J. Blythe (UK): Our initial planning tests indeed suggested that sea reflection was a disturbing factor, but only marginally so once the powers from the two beams had been equalized. I think that, regardless of foreground reflection, vertical beam separation will always show significant advantages over horizontal separation in climates where atmospheric layers habitually intercept the common volumes generated by either receiving beam. In addition, vertical angle diversity has a good chance of recovering its inherent losses in these circumstances, and thus equalling or out-performing conventional space-frequency and space-polarization systems. These conclusions are in line with the comments made just now by Monsen.
- A. N. Ince (STC): My question concerns your intermodulation measurement. Considering that the RF bandwidth occupied was fairly small how did you manage to measure the intermodulation, i.e. how were you able to separate path intermodulation from that of the equipment?
- J. Blythe (UK): We weren't basically. It was a comparison between the reference system and the angle diversity system. At least it showed that we weren't any worse off.

Paper No: 5.4

- A. N. Ince (STC): Please accept my congratulations on your very clear and objective exposition of the problems involved in the performance evaluation of troposcatter links. I would like to make a comment which is related to your statement that one deals with signal-to-noise ratios only in analog systems, and try to highlight the factors which lead to differences in the system design for analog and digital systems. The situation need not be fundamentally different in the two systems, particularly when the RF bandwidth occupied does not appreciably exceed the so-called correlation bandwidth and the channel performance (e.g. speech intelligibility) can be expressed as a function of the signal-to-noise ratio. As we know the multipath spread that causes intersymbol interference in digital systems produces intermodulation noise in analog systems but the magnitude of the design problem that the multipath phenomenon creates is much greater in digital systems mainly because these systems are designed, like the analog systems that they replace, on the basis of voice traffic often using 64 kb/s per voice channel thus leading, for the same traffic capacity, to much greater bandwidth requirements that often exceed the correlation bandwidth of the path. For example an analog system carrying 60 voice channels of near CCITT quality would typically require 1.5 MHz of RF bandwidth whereas a digital system of identical capacity would need a few times more bandwidth. As shown in our paper presented in Session IV (Paper 4.6) the multipath distortion in this example would not generally produce an unacceptable level of IM noise in the analog system using simple FM modems whereas the digital system would need expensive adaptive modems to cope with the same multipath and in addition would occupy more frequency spectrum. As long as we are dealing mainly with voice traffic we seem to be creating an unnecessary problem by going digital (I am excluding here the special requirements which one may have in military systems). In summary I would say that in deciding to go digital and in the design of the necessary system one should pay particular attention to the type of traffic to be carried by the system as well as to the requirements for transmission (including transmission of analog) and switching which at times, may allow the reduction of the voice digit rate (e.g. 32 kb/s Δ -mod) leading to smaller bandwidth occupancy and easier and cheaper modem design. Would you like to respond to my tongue-in-cheek comments above?
- J. Wick (USA): I have three comments. First of all, I am painfully aware of the multipath problem in analog systems. However, the prediction problem is generally handled differently. Generally, you treat the multipath as an additive noise term due to intermodulation noise so you don't have to get so intimately involved in the mechanics of a modem to make systems calculations. It is true that when somebody tells us to go digital on an analog system which carries primarily voice, one gets into a box, there is no question about that. We have to use clever modem techniques to exploit the medium to buy back some of the loss of going digital. Of course, you must realize that in the future, people aren't going to be talking to people as much as computers are going to be talking to computers, and a common communications format avoids system duplication. Also digital communications systems carrying analog voice can make

advantageous use of regenerative repeaters to keep noise low.

- S. Parl (USA): I have two comments. One thing that we have experienced is the equipment very often gives a considerable contribution to the measured delay spread. I wonder if you, in your measurements, tried to take this into account to separate the contributions of transmitter and receiver filters from the delay spread of the channel.
- J. Wick (USA): This problem ofwhich you are speaking occurs in RAKE probing where you have a distortion in the high power klystron amplifier, for instance, which would appear to be a multipath spread distortion. In the experimental program, I noted the fact that we were operating the equipment backed-off considerably from its maximum operating level, and back-to-back tests were made to determine that indeed what was being measured was the medium and not the nonlinearity of the klystron amplifiers whose transfer functions can create real problems when you are trying to do accurate RAKE probing.
- S. Parl (USA): The otherthing is the aperture-to-medium coupling loss measurement you are proposing. I have some reservation about the value of such a measurement because you can have variations in the upper atmosphere which would affect the signal level on the small antenna but which would not affect the signal level on the large antenna and what is really of value is the path loss. The real value is to be able to calculate the path loss you will get with a large antenna.
- J. Wick (USA): The question really is whether the term aperture-to-medium coupling loss is really meaningful at all. I think this has been discussed in another session. It is true that when you have a narrow beam antenna you may not see things, especially under anomalous propagation conditions, that you would see with a larger antenna beam. This may be involved in the quantity which has been observed and termed aperture-to-medium coupling loss and this is why I said that I thought the results of the experiment would be of a statistical nature rather than some magic number for all paths of a given length. I feel that there may be a great deal of variability associated with path geometry and climatology.

Paper No: 5.7

- J. Osterholz (USA): I would like to make a statement in reiterating what Dr. Ince had correctly pointed out earlier. We are talking about the application of troposcatter systems which, at least in the near-term, will have people talking to people rather than machines to machines. In a tandem connection where more than one tropo link is traversed, say, by a voice subscriber in the Autovon telephone system or a similar type of analog telephone system, the decoding delay can become important, infact it can become a significant factor in the system design. What I am addressing specifically is your curves which are representative of rms fade rates on the order of one Hertz or ten Hertz. A lot of the work that has been done on the troposcatter systems which use lower frequencies which are more typical for commercial as well as for long-distance military systems, show measured rms fade rates which are of the order of one tenth of your values. The question I have is, if, I wanted to estimate the coding delay for a particular performance, can I just multiply the coding delay by ten in the case of an rms fade rate of one tenth of a Hertz as opposed to one Hertz?
- D. Chase (USA): Two comments. The first is, for your application there is a good possibility that we don't need to bother with coding. Your data rate is higher your doppler spread is lower and consequently what you say is roughly true that your decoding delay for the same performance would be a factor of ten more. However, our results were for single diversity (i.e. no diversity) and we can therefore improve the system performance by using, say, dual diversity. In fact some studies which we have carried out in connection with a proposal show that this factor of ten may be recovered by using dual diversity, i.e. a system using dual diversity with coding could have the same kind of delays as those given in our paper for single diversity. I would like to make a further point here and that is that depending on the application it may not be necessary to use coding at all but simply employ our modem technique which is fairly efficient from the point of view of bandwidth utilization.
- J. Osterholz (USA): Referring to the modem block diagram in your paper where a sample/hold and A/D circuits are shown which appear as critical elements in the modem operation particularly at higher data rates can you state what quantization rate you use in the A/D conversion, in particular, for a system, say, of 9 mega bits/sec.
- D. Chase (USA): The modem we built had 6 bits per sample and we could probably get away with five or even lower. The loss at, say, four bits would be about a decibel.
- J. Osterholz (USA): I have one more question if I may. You mentioned the constraint of having to have a constant envelope carrier. Have you investigated backing-off the power amplifier obtaining something a little more linear, giving up the system gain, reducing the complexity of the modem but still obtaining the benefits you get from the adaptive processing without having to compensate for the constant envelope?
- D. Chase (USA): The simple answer to your question is no we have not investigated it.

- A. N. Ince (STC): You mentioned that complexity was an important issue in the modem design. Can you comment why this is considering that the cost of IC's and LSI produced in thousands is almost independent of complexity and that the modem cost may be a small fraction of the total system cost?
- D. Chase (USA): I wish more people would think the way you do. Unfortunately people still consider complexity in isolation rather than recognizing that complexity-cost relation is continuously changing and thanks to IC technology more complex circuits are being sold at prices to-day which are lower than those of less complex circuits of yester-years despite inflation.

End of Session V

SESSION VI

GENERAL DISCUSSION

The last session of the symposium was devoted to a general discussion and to comments on all the papers presented. The session concluded with a summary by The Chairman, Dr. A. N. Ince, of what he considered to be the significant data and techniques reported in the symposium which would be relevant to the planning and design of dedicated and switched networks which rely either totally or partly on scatter links. The questions, comments and discussions from the session are reported below.

L. W. Barclay (UK): Dr. Ince in his paper (Paper 4.1) only commented briefly on scatter from irregularities caused by aritifical ionospheric heating. However, he stated that the north-south extent of the communication zone was some tens of kilometers and that the technique could not be used at mid-European latitudes. This contrasts with the much more extensive communication zone described by Dr. Utlaut at the AGARD meeting last year in Brussels. Dr. Utlaut indicated a north-south extent of 100 km or more and he showed maps for the shape of the communications zone for heaters at various latitudes. Is this difference due to a more restricted assumption by Dr. Ince of the tolerable departure from specularity, or is it due to constraints on the location and configuration of the heating transmitter in Europe?

A. N. Ince (STC): First of all let me say that what is reported in our paper 4.1 on this subject is based on a survey of the literature and not on any real work done by STC. In case of discrepancy you should therefore refer to the literature referred to in our paper. Another point I would like to make is that research is active and there is quite a lot still to be learned on HF induced ionospheric modifications. In paper 4.1, referring to the zone of reception, or the footprint we mentioned that it would have, for field-aligned scattering (FAS), a width corresponding to deviations from mirror reflection of up to a degree or two. The exact width would depend on the geometry of the heated region, its altitude as well as on the path geometry. Dr. Utlaut in his article published in 1975. states that, assuming a modified ionosphere centered at 270 km altitude and a scattering region extending 100 km along the local magnetic field lines, scattering angles up to three degrees off normal for FAS and about five degrees for PLS (Plasma line scattering) would provide useful signals. It follows that, for FAS, the north-south extent of the reception zone would be upwards of 30 kms depending on the slant range and would be about 200 kms for a slant range of about 1000 kms. As far as the European coverage is concerned it should be noted that the angle of magnetic dip would be unsuitable for communications in Northern Europe as shown by Stathacopoulos and Barry in Ref 17 of Paper 4.1 to which reference should be made for more information.

L. W. Barclay (UK): Referring to the effect of sporadic-E on meteor-burst communication systems, I think it is important to be aware of the occurrence statistics of the various kinds of $E_{\rm S}$. Dr. Williams in his paper 4.4 was considering the effect of temperature latitude, 'flat', $E_{\rm S}$. This kind of $E_{\rm S}$ has a pronounced occurrence maximum in summer daytime so that interception probabilities, which are acceptable when based on annual occurrence statistics, may well be unsatisfactory during the summer. Dr. Sites in his paper 4.5 (as well as STC in paper 4.4) advocated the use of meteor-burst systems at high latitudes. Auroral $E_{\rm S}$, associated with geomagnetic storms, can support field-aligned scatter propagation which has substantial time and frequency dispersion. This is likely to prevent the use of a fast signalling burst mode during its occurrence.

A. N. Ince (STC): I shall answer the question since it refers mainly to interception. In Paper 3.5 what I reported were measured results, with theoretical interpretations, whose duration did, in fact, cover almost a full year including the summer months. The results which were obtained with a system operating at 40 MHz were, you will remember, expressed as cumulative distributions. For instance, referring to Fig. 8 or Paper 3.5 for the Santa-Marinella terminal in Italy, the median value of the interception ratio was only about 2%. Even in the case of Forest Moor the median value was only 7%, that is in 50% of all cases 7% of what I sent would be intercepted. Of course for a very small percentage of the time there would be full interception. As Mr. Barclay correctly pointed out, there was more interception in June and July, and in the afternoons, than at any other time. I recommended that the frequency of operation be increased to above 40 MHz in order to minimize interception generally. At higher frequencies the incidence of sporadic E is much less and therefore, the interception will decrease to levels below those measured at 40 MHz.

W. F. Utlaut "Ionospheric Modifications Induced by High-power HF transmitters" AGARD-CP-192, January 1977.

W. F. Utlaut "Ionospheric Modification Induced by High-power HF transmitters" Proc. IEEE. Vol. 63, July 1975.

Turning now to the second part of Mr. Barclay's comment, which concerned the phenomenon in northern latitudes, he pointed out the occurrence of competing modes of transmission such as FAS. Whether or not this can be a problem depends on the following three factors. First of all the aspect sensitivity of the competing mode is important. As we saw in the case of artificially created field-aligned irregularities, the aspect sensitivity is very great. In the case of the naturally created field-aligned modes the scattering probably occurs at lower heights, but the aspect sensitivity remains so that what I said for interception of meteor-burst signals would also apply here. Secondly, the relative levels of the signals are important. This, of course, is to some extent under the control of the system designer. If you do not use too high a power and if the level is below that of the meteor trails, for instance, then you will not even detect them. However, if other modes do occur and if the level is high then the results depend on the system design which is the third factor which affects the system performance. In the STC system, COMET, we use a transmission speed of 2000 Baud and ARQ which allows an automatic request to be sent to the sending terminal for re-transmission of data received in error. When the competing mode coincides with the meteor-burst signal non-destructively the information passed is not affected, it may even increase the duty cycle, and if the competing mode reduces the resultant signal to a level which causes the data to be received in error then the ARQ will ensure that the passage in error is ignored. If transmission took place via the competing mode and in between the meteor-burst signals then the throughput of the system would increase, provided of course, as Mr. Barclay said, the transmission rate is within the coherent bandwidth of the path.

- K. Toman (USA): What is adaptive equalization, how does it work in physical terms, and what limits the effectiveness of adaptive equalization techniques for troposcatter and HF channels?
- P. Bello (USA): The adaptive equalizer fits into the general framework of what might be called the class of "adaptive filters". An adaptive filter is a "black box" with a series of adjustable parameters, an input and output signal, and a desired output signal. With a desired output signal and an actual output signal, one may form an error signal. An algorithm can be found for adjusting the coefficients of this box to minimize the strength of the error signal.

As stated in this way, the definition is too general to be useful, and one has to reduce this box to some structure with identifiable parameters. In the case of adaptive equalizers, the most common basic structure is a tapped delay line with adjustable weights at the tap outputs and a summation of all weighted tap outputs. There are obviously other types of equalizers with adjustable coefficients. One may have a bank of filters with adjustable weights prior to summing, etc.

It was stated that the adaptive equalizer attempts to minimize the error between the actual output signal and the desired output signal. In the case of digital communications, the desired output signal is the transmitted data stream itself. Of course, this signal is not available and, instead, the actual output data stream is used as the desired signal. This output data stream is obtained by sampling and quantizing the output of the equalizer at the symbol rate. For binary data transmission, this quantizer would constitute a simple zero-threshold binary decision. The presence of errors on the output data stream causes a perturbation of the adaptive equalizer performance from ideal, but surprisingly high error rates can be tolerated.

The adaptive equalizers built for dispersive channels generally contain two "black boxes": a forward equalizer and a feedback equalizer (or tail canceller). Both the forward equalizer and tail canceller are tapped delay lines with adjustable weights. The objective of the tail canceller is to remove the intersymbol interference caused by the "tail" of the impulse response. This can be done if the tail of the impulse response and past data values are known. Neither of these are known exactly - past decisions are used as input to the tail canceller and, when the adaptive weights are automatically adjusted to minimize the error signal, the tail canceller impulse response approximates that of the tail of the channel impulse response. The forward equalizer attempts to minimize the intersymbol interference due to future data but can only do this on an average basis.

I would say the following about HF channels concerning how adaptive equalizers fit in and what the practical problems are. An averaging process is involved in adjusting the weights for minimum error. There is a delay in adaptation produced both by the averaging process and the length of the impulse response. If the adaptation delay is too long, it is not possible to "track" well the time variant channel fluctuations. If the averaging time is too short, the estimate of the adaptive coefficients becomes too noisy. It is my estimate that, for the average HF channel, the delay in adaptation due to the combined effects of necessary averaging time to keep the adaptive coefficient noise small and the length of the impulse response, is too large in relation to the channel fading time constant to give good performance for an adaptive equalizer. However, this argument is intuitive and remains to be established, or refuted, by analysis and/or simulation.

A. N. Ince (STC): As we have seen (e.g. Figs. 7 and 8 of Paper 5.4), when one plots the signal-to-noise ratio (SNR), required for a given BER against multipath delay spread (MDS), one sees that SNR decreases first before it rises with increasing MDS. The initial decrease in SNR is, of course, due to the so-called implicit diversity and the subsequent

increase in SNR must be the result of the modem not being capable of equalizing the channel. The question I have for Dr. Bello is, what are the physical and technological constraints which would limit the modem performance i.e., leaving aside the question of complexity and cost, what is the maximum MDS which can be equalized?

P. Bello (USA): There are two questions I think you want me to answer. One is - why does the curve go up? The other is - what do you want to do about it? The error rate goes up because the tapped delay line is not able any longer to cancel the intersymbol interference. Performance can be improved by making the line longer. However, there are some eventual limitations due to imperfections in signal processing which begin to accumulate with increasing length of the delay line. There will be some given practical limit to the length that you can use. But I suspect that, as far as troposcatter links are concerned, this limit has not been reached.

A. N. Ince (STC): I understand that no one has determined the actual limit set by physics for a given equalization method. Considering that to equalize greater and greater MDS requires effectively longer and longer delay lines and processing times, the limit to proper equalization is eventually set by the delay in the equalizer in relation to the channel fading rate, and in some modem implementations also by excess noise introduced into the processing of data by the additional taps.

As far as HF channels are concerned, the performance of adaptive equalizers could not be as good as for troposcatter channels because of the large differential path delays (milliseconds) which are of the order of the fade period in HF channels. The transmission rate required for HF is often modest and does not exceed a few kilobits/sec. However, because of the multipath effect compunded by noise and man-made interference of impulsive type it has not been possible to achieve economical transmission rates in excess of about 1 kilobits/sec with acceptable reliability and error rate. Since it does not seem likely that adaptive equalizers would perform too well and moreover they would not be able to cope with interference, spread-spectrum techniques could be used to separate the discrete HF paths (hops) and thus eliminate the effects of multipath. It is interesting to note that this same technique would also spread the energy of the impulsive noise and interference so that the signal-to-noise ratio in the detection bandwidth would improve (processing gain). While this technique allows the satisfactory transmission of data at rates not previously achievable at HF, its spectrum usage, not unlike the ionospheric sounder, is not quite consistent with internationally agreed channel allocations. However, it should be noted that it would, often, be possible to spread the transmit energy so much that the energy density would be lower than the noise of most receivers, thus causing no objectionable interference to others.

The technique above has been investigated by SHAPE Technical Centre theoretically and experimentally. The design of a prototype spread-spectrum HF modem including the performance results and future developments are discussed in a paper appended to the proceedings as Paper 5.8. The tests results, so far obtained, support the claimed advantages of the system.

End of Session VI

	REPOI	RT DOCU	MENTATION PAGE	
1. Recipient's Referen	ace 2. Originator's	Reference	3. Further Reference	4. Security Classification of Document
	AGARD-CF	2-244	ISBN 92-835-0219-1	UNCLASSIFIED
5. Originator	North Atlantic Tr	eaty Orga	ace Research and Developmization ly sur Seine, France	ment
6. Title	ASPECTS OF ELL	ECTROM	AGNETIC WAVE COMMUNICATIONS	
7. Presented at			Propagation Panel Symposi nusetts, USA, 3-7 October	
8. Author(s)	Various	Edited t	by: A.N.Ince*	9. Date September 1978
10. Author's Address		*SHAPE	Technical Centre	11. Pages
	Various	The Hag		550
12. Distribution Staten	policies an	d regulat	istributed in accordance wi ions, which are outlined on its of all AGARD publication	the
	wave transmission		Reflection	Signal processing
Radio communi Tropospheric sca Atmospheric sca	atter communicatio	on	Ionosphere Mathematical models Simulation	Meteor trails Ground clutter

14. Abstract

The Proceedings deal with the theory of scattering and reflection in the troposphere, the ionosphere, from meteor trails, and also scattering from ground environmental hazards such as hills, trees and buildings. Included in the propagation aspect are the prediction of long and short term signal characteristics and the modelling and simulation of radio channels using scatter mode of propagation. The proceedings also cover transmission and signal processing techniques for effective communications over such channels.

AGARD-CP-244	Electromagnetic wave transmission Radio communication	Tropospheric scatter communication Atmospheric scattering	Reflection Ionosphere Mathematical models Simulation Signal processing Meteor trails		AGARD-CP-244	Electromagnetic wave transmission Radio communication Tropospheric scatter communication	Atmospheric scattering Reflection Ionosphere Mathematical models Simulation Signal processing Meteor trails Ground clutter	
AGARD Conference Proceedings No.244 Advisory Group for Aerospace Research and	Development, NATO ASPECTS OF ELECTROMAGNETIC WAVE SCATTERING IN RADIO COMMUNICATIONS Edited by A.N.Ince	Published September 1978 550 pages	The Proceedings deal with the theory of scattering and reflection in the troposphere, the ionosphere, from meteor trails, and also scattering from ground environmental hazards such as hills, trees and buildings. Included in the propagation aspect are the prediction of long and short term signal characteristics and the modelling and short term signal characteristics and the modelling and short term signal characteristics and the	modelling and sindiation of fatio channels using	AGARD Conference Proceedings No.244 Advisory Group for Aerospace Research and	Development, NATO ASPECTS OF ELECTROMAGNETIC WAVE SCATTERING IN RADIO COMMUNICATIONS Edited by A.N.Ince Published September 1978 550 pages	The Proceedings deal with the theory of scattering and reflection in the troposphere, the ionosphere, from meteor trails, and also scattering from ground environmental hazards such as hills, trees and buildings. Included in the propagation aspect are the prediction of long and short term signal characteristics and the modelling and simulation of radio channels using	P.T.O.
AGARD-CP-244	Electromagnetic wave transmission	Tropospheric scatter communication Atmospheric scattering	Reflection Ionosphere Mathematical models Simulation Signal processing Meteor trails		AGARD-CP-244	Electromagnetic wave transmission Radio communication Tropospheric scatter communication	Atmospheric scattering Reflection Ionosphere Mathematical models Simulation Signal processing Meteor trails Ground clutter	
AGARD Conference Proceedings No.244 Advisory Group for Aerospace Research and	Development, NATO ASPECTS OF ELECTROMAGNETIC WAVE SCATTERING IN RADIO COMMUNICATIONS Edited by A.N.Ince	Published September 1978 550 pages	The Proceedings deal with the theory of scattering and reflection in the troposphere, the ionosphere, from meteor trails, and also scattering from ground environmental hazards such as hills, trees and buildings. Included in the propagation aspect are the prediction of long and short term signal characteristics and the production of prod	P.T.O.	AGARD Conference Proceedings No.244 Advisory Group for Aerospace Research and	Development, NATO ASPECTS OF ELECTROMAGNETIC WAVE SCATTERING IN RADIO COMMUNICATIONS Edited by A.N.Ince Published September 1978 550 pages	The Proceedings deal with the theory of scattering and reflection in the troposphere, the ionosphere, from meteor trails, and also scattering from ground environmental hazards such as hills, trees and buildings. Included in the propagation aspect are the prediction of long and short term signal characteristics and the modelling and simulation of radio channels using	P.T.O.

scatter mode of propagation. The proceedings also cover transmission and signal processing techniques for effective communications over such channels. Papers and discussions presented at the Electromagnetic Wave Propagation Panel Symposium held in Cambridge, Massachusetts, USA, 3-7 October, 1977.	scatter mode of propagation. The proceedings also cover transmission and signal processing techniques for effective communications over such channels. Papers and discussions presented at the Electromagnetic Wave Propagation Panel Symposium held in Cambridge, Massachusetts, USA, 3-7 October, 1977.
ISBN 92-835-0219-1	ISBN 92-835-0219-1
scatter mode of propagation. The proceedings also cover transmission and signal processing techniques for effective communications over such channels.	scatter mode of propagation. The proceedings also cover transmission and signal processing techniques for effective communications over such channels.
Papers and discussions presented at the Electromagnetic Wave Propagation Panel Symposium held in Cambridge, Massachusetts, USA, 3-7 October, 1977.	Papers and discussions presented at the Electromagnetic Wave Propagation Panel Symposium held in Cambridge, Massachusetts, USA, 3-7 October, 1977.
ISBN 92-835-0219-1	ISBN 92-835-0219-1